BULETINUL INSTITUTULUI POLITEHNIC DIN IASI

OF 1503/3
F F
8 000001 780477

Editat de
UNIVERSITATEA TEHNICĂ "GH. ASACHI" IASI

Tomul XLVII (LI)
Fasc. 1 - 2

ELECTROTEHNICĂ
ENERGETICĂ
ELECTRONICĂ

2001

BULETINUL INSTITUTULUI POLITEHNIC DIN IAŞI

BUDAPESTI MŰSZAKI ÉS GAZDASÁGTUDOMÁNYI EGYETEM
Műszaki Információs Központ és Könyvtár
2001
Országos

Tomul XLVII (LI)
Fasc. 1 - 2

Secţia

ELECTROTEHNICĂ. ENERGETICĂ. ELECTRONICĂ

2001

EDITORIAL STAFF

Prof. Dr. Eng. **MIHAI CREŢU** (President)
Prof. Dr. Eng. **VICTOR BULACOVSCHI** (Vice-President)
Prof. Dr. Eng. **ION GIURMA** (Vice-President)
Prof. Dr. Eng. **GHEORGHE ZET** (Secretary)
Prof. Dr. Doc. Eng. **ALFRED BRAIER** (Editor)
Prof. Dr. Eng. **HUGO ROSMAN** (Editor)
Prof. Dr. Eng. **MIHAIL VOICU** (Head of the Exchange Service)
Prof. Dr. Eng. **IOSIF BARTHA**
Prof. Dr. Eng. **ROMEN BUTNARU**
Prof. Dr. **ADRIAN CORDUNEANU**
Prof. Dr. Eng. **MIRCEA COZMÎNCĂ**
Prof. Dr. Eng. **ADRIAN DIMA**
Prof. Dr. Eng. **AURELIA GRIGORIU**
Prof. Dr. Eng. **MIRCEA GUŞĂ**
Prof. Dr. Eng. **DOREL LEON**
Prof. Dr. Eng. **MIHAI LUCANU**
Prof. Dr. Eng. **VALENTIN I. POPA**
Prof. Dr. Eng. **PAULICĂ RĂILEANU**

The **Bulletin of the Polytechnic Institute of Jassy** is edited by
the **Technical University "Gh.Asachi"** (the former Polytechnic Institute), Jassy.

TEXredaction:
Cristina Vasiliu, Adrian Rotaru
Technical University of Jassy

BULETINUL INSTITUTULUI POLITEHNIC DIN IAŞI
BULLETIN OF THE POLYTECHNIC INSTITUTE OF JASSY
Tomul XLVII (LI), Fasc. 1-2 2001

BUDAPESTI MŰSZAKI ÉS GAZDASÁGTUDOMÁNYI EGYETEM
Műszaki Információs Központ és Könyvtár
2001

ELECTROTEHNICĂ. ENERGETICĂ. ELECTRONICĂ

SUMAR

Pag.

HUGO ROSMAN, Câteva observaţii privind teorema reciprocităţii în câmpul electrostatic, şi în câmpul magnetic (franc., rez. rom.) 7

DORIN BELAUS, Două scheme de cuadripoli liniari neautonomi, cu impedanţele echivalente la gol şi în scurtcircuit egale în regim permanent armonic (engl., rez. rom.) 13

HUGO ROSMAN, Teorema lui Tellegen în sisteme mecanice (franc., rez. rom.) 19

VALENTIN BUZDUGA, OREST OLTU şi OVIDIU DRAGOMIRESCU, Asupra imunităţii circuitelor echilibrate la perturbaţii longitudinale (engl., rez. rom.) 25

AL.-M. AVASILOAIE, Regimul permanent al liniilor electrice omogene lungi excitate de semnale modulate în amplitudine cu purtătoarea suprimată. II. Formule tipice ale răspunsurilor în tensiune şi curent (engl., rez. rom.) 35

VALERIU MUNTEANU şi DANIELA TĂRNICERIU, Distribuţia ponderii codurilor ciclice binare (engl., rez. rom.) 51

VICTOR GRIGORAŞ şi CARMEN GRIGORAŞ, Descrierea sistemelor discrete aditive în domeniul timp (engl., rez. rom.) 57

ROMEO GHINEA, RADU BOZOMITU şi LIVIU GORAŞ, Asupra proiectării biquadului Kerwin-Huelsman-Newcomb. I. Condiţii de stabilitate a biquad-ului KHN cu integratoare neideale (engl., rez. rom.) 65

LUMINIŢA SCRIPCARIU şi PETRUŢ DUMA, Structuri Trellis sistematizate pentru coduri TURBO simetrice (engl., rez. rom.) 79

ADRIANA SÎRBU, Sistemele hibride – un cadru unificator pentru modelarea dinamicii convertoarelor de putere (engl., rez. rom.) 85

N. DAMEAN şi EMIL VREMERĂ, Metodă de măsurare a difuzivităţii termice a solidelor utilizând măsurări ale timpului. I. Abordare teoretică (engl., rez. rom.) 95

ADRIAN CREŢU, CARMEN COJOCARU-FILIPIUC şi ADRIANA-IOANA CREŢU, Consideraţii asupra funcţionării în regim tranzitoriu de scurtcircuit a divizorului inductiv de curent, liniar, compensat electronic cu convertor de curent (engl., rez. rom.) 105

I. SUCHAR şi RADU URSULEAN, Cupluri parazite în micromotoare de curent continuu cu comutaţie electronică (engl., rez. rom.) 115

Pag.

MIRCEA GOGU şi IRINA ATUDOREI, Aspecte privind modelarea simulink *s-function* a maşinii asincrone bifazate (engl., rez. rom.) 121

V. BAHRIN şi CARMEN COJOCARU-FILIPIUC, Asupra controlului optimal al sistemelor de acţionare cu servomotoare de curent continuu (engl., rez. rom.) 131

I. ANDRONE şi ADRIANA-ELENA PRISĂCARU, Conversia energiei în maşinile de inducţie bifazate nesimetrice (engl., rez. rom.) 139

V. BAHRIN şi CARMEN COJOCARU-FILIPIUC, Consideraţii asupra interdependenţei dintre materialele şi performanţele servomotoarelor electrice (engl., rez. rom.) 147

PETRUŢ DUMA, Implementarea unor algoritmi de calcul aritmetic pe microcontrolere din familia INTEL 8051 (engl., rez. rom.) 153

LAURENŢIU DIMITRIU şi LILIANA VORNICU, O abordare formală a sistemelor complexe de timp real în scopuri de diagnosticare (engl., rez. rom.) 163

LILIANA VORNICU şi LAURENŢIU DIMITRIU, O metodă de reducere a latenţei în sisteme de transmisie seriale (engl., rez. rom.) 169

RADU BURLICĂ, EUGEN HNATIUC şi BOGDAN HNATIUC, Evaluarea analitică a timpului de deconectare pentru aparatele electromagnetice de comutaţie de curent continuu (engl., rez. rom.) 175

VIOREL VARVARA şi GH. GEORGESCU, Analiza regimului şi calculul pierderilor suplimentare de putere în reţelele de distribuţie urbane funcţionând în regim permanent nesinusoidal (engl., rez. rom.) 181

C. ASAFTEI şi DORIN GROZA, Cazanele cu putere calorică – mai eficiente, mai economice (engl., rez. rom.) 189

VIOREL VARVARA, Regimuri de funcţionare nesimetrice ale unei reţele electrice de distribuţie (engl., rez. rom.) 197

RECENZII 209

BULETINUL INSTITUTULUI POLITEHNIC DIN IAŞI
BULLETIN OF THE POLYTECHNIC INSTITUTE OF JASSY
Tome XLVII (LI), Fasc. 1–2 2001

BUDAPESTI MŰSZAKI ÉS GAZDASÁGTUDOMÁNYI EGYETEM
Műszaki Információs Központ és Könyvtár
2001

ELECTROTECHNICS. ENERGETICS. ELECTRONICS

CONTENTS

Pp.

HUGO ROSMAN, Quelques observations concernant le théorème de la réciprocité en champ électrostatique et en champ magnétique (French, Romanian summary) ... 7

DORIN BELAUS, Two Schemes of the Linear General Four-Terminals which Realise, in the Harmonic Steady-State, the Equality between the Equivalent Impedances at the Idle and at Short Circuit (English, Romanian summary) 13

HUGO ROSMAN, Le théorème de Tellegen concernant les systèmes mécaniques (French, Romanian summary) 19

VALENTIN BUZDUGA, OREST OLTU and OVIDIU DRAGOMIRESCU, On the Immunity of the Balanced Circuits to Longitudinal Disturbing Signals (English, Romanian summary) 25

AL.-M. AVASILOAIE, The Steady-State of Electrical Homogeneous Long Lines, Excited by an Amplitude Modulated Signal with Suppressed Carrier. II. Typical Forms for Voltage and Current Responses (English, Romanian summary) 35

VALERIU MUNTEANU and DANIELA TĂRNICERIU, Weight Distribution of Binary Cyclic Codes (English, Romanian summary) 51

VICTOR GRIGORAŞ and CARMEN GRIGORAŞ, Time Domain Description of Additive Non-Linear Systems (English, Romanian summary) 57

ROMEO GHINEA, RADU BOZOMITU and LIVIU GORAŞ, On the Design of the Kerwin–Huelsman–Newcomb Biquad. I. Stability Conditions for the KHN Non-ideal Integrators Biquad (English, Romanian summary) 65

LUMINIŢA SCRIPCARIU and PETRUŢ DUMA, Systematic Trellis Structures for Symmetric TURBO Codes (English, Romanian summary) 79

ADRIANA SÎRBU, Hybrid Systems – an Unifying Framework for Power Converter Dynamics Modelling (English, Romanian summary) 85

N. DAMEAN and EMIL VREMERĂ, New Measurement Method of the Thermal Diffusivity in Solids Using Time Measurements. I. Theoretical Approach (English, Romanian summary) 95

ADRIAN CREŢU, CARMEN COJOCARU-FILIPIUC and ADRIANA-IOANA CREŢU, Considerations on the Short-Circuit Transient Operation of the Linear Current Inductive Divider, Electronically Compensated with a Current Converter (English, Romanian summary) 105

I. SUCHAR and RADU URSULEAN, Parasitic Torques in D.C. Micromotors with Electronic Switching (English, Romanian summary) 115

	Pp.
MIRCEA GOGU and IRINA ATUDOREI, Aspects Regarding the Two-Phase Induction Motor Simulink *s-Function* Modeling (English, Romanian summary)	121
V. BAHRIN and CARMEN COJOCARU-FILIPIUC, On the Optimal Control of Driving Systems with Direct Current Servomotors (English, Romanian summary)	131
I. ANDRONE and ADRIANA-ELENA PRISĂCARU, Energy Conversion in Unsymmetrical Two-Phase Induction Machines (English, Romanian summary)	139
V. BAHRIN and CARMEN COJOCARU-FILIPIUC, Considerations on the Interdependence Between Materials and Performances of Electrical Servomotors (English, Romanian summary)	147
PETRUŢ DUMA, Implementing Some Arithmetic Calculation Algorithms on Microcontrollers from INTEL 8051 Family (English, Romanian summary)	153
LAURENŢIU DIMITRIU and LILIANA VORNICU, A Formal Approach of Complex Real-Time Systems for Diagnosis Purposes (English, Romanian summary)	163
LILIANA VORNICU and LAURENŢIU DIMITRIU, A Method for Reducing the Latency in Serial Transmission Systems (English, Romanian summary)	169
RADU BURLICĂ, EUGEN HNATIUC and BOGDAN HNATIUC, The Analytical Evaluation of the Disconnecting Time for the DC Electromagnetic Commutation Apparatus with Contacts (English, Romanian summary)	175
VIOREL VARVARA and GH. GEORGESCU, Duty Analyse and Supplementary Power Losses in Distribution Electrical Networks Running under Non-Sinusoidal Steady State (English, Romanian summary)	181
C. ASAFTEI and DORIN GROZA, The Individual Heating Boiler – More Efficient, More Economic (English, Romanian summary)	189
VIOREL VARVARA, The Non-Symmetrical Steady State of a Three-Phase Distribution Network (English, Romanian summary)	197
BOOK REVIEWS	209

BULETINUL INSTITUTULUI POLITEHNIC DIN IAŞI
Tomul XLVII (LI), Fasc. 1–2, 2001
ELECTROTEHNICĂ. ENERGETICĂ. ELECTRONICĂ

C.D. 621.319.7; 621.3.013

QUELQUES OBSERVATIONS CONCERNANT LE THÉORÈME DE LA RÉCIPROCITÉ EN CHAMP ÉLECTROSTATIQUE ET EN CHAMP MAGNÉTIQUE

PAR
HUGO ROSMAN

On détermine les valeurs communes des égalités (1) et (2), qui représentent le théorème de la réciprocité en champ électrostatique, respectivement magnétique.

1. Introduction

On connaît depuis Maxwell que dans les systèmes linéaires est valable *le théorème de la réciprocité*. Evidemment l'énoncé de ce théorème est différent d'un système physique à l'autre. Par exemple, dans le cas d'un champ électrostatique, si on considère un système de n conducteurs chargés, situés dans un milieu linéaire, isotrope et nonpolarisé permanent, soient deux états de ce système caractérisés par les charges électriques libres q_j, q'_j et par les potentiels V_j, V'_j, $(j = 1, 2, ..., n)$. On peut prouver (par ex. [1, § **8.7**]) que, dans les conditions précisées ci-dessus, est valable la relation:

$$\sum_{j=1}^{n} q_j V'_j = \sum_{j=1}^{n} q'_j V_j, \tag{1}$$

établie par Green, répresentant *le théorème de la réciprocité en champ électrostatique*.

D'une façon analogue, si on considère, dans le cas d'un champ magnétique, un système de n conducteurs filiformes parcourus par des courants, situés dans un milieu linéaire, isotrope et nonmagnétisé permanent et deux états de ce système, caractérisés par les courants i_j, i'_j et les flux magnétiques ψ_j, ψ'_j, $(j = 1, 2, ..., n)$, qui traversent les surfaces delimitées par les contours des conducteurs, alors [1, § **12.4.1**]:

$$\sum_{j=1}^{n} i_j \psi'_j = \sum_{j=1}^{n} i'_j \psi_j, \tag{2}$$

relation qui est connue comme représentant *le théorème de la réciprocité en champ magnétique*. Il faut préciser que la relation (2) est valable seulement dans un régime quasistationnaire anélectrique.

Le but de cette Note est, surtout, d'établir la valeur commune des sommes (1), dans le cas du champ électrostatique et (2), dans celui du champ magnétique.

2. Cas du champ électrostatique

En ce qui concerne les charges q_j, q'_j, respectivement les potentiels V_j, V'_j, ($j = 1, 2, ..., n$), on peut écrire les relations évidentes:

$$q'_j = q_j + \Delta q_j, \quad V'_j = V_j + \Delta V_j, \tag{3}$$

avec $\Delta q_j \gtrless 0$, $\Delta V_j \gtrless 0$, de sorte que la relation (1) conduit à:

$$\sum_{j=1}^{n} q_j \Delta V_j = \sum_{j=1}^{n} V_j \Delta q_j. \tag{4}$$

On peut considérer cette dernière expression comme représentant un autre énoncé du théorème de la réciprocité en champ électrostatique. Une relation semblable à (4) a été établie, par une autre voie, par S i m o n y i [2].

Soient

$$W_e = \frac{1}{2} \sum_{j=1}^{n} q_j V_j, \quad W'_e = \frac{1}{2} \sum_{j=1}^{n} q'_j V'_j \tag{5}$$

les énergies emmagasinées dans le champ électrostatique du système de conducteurs dans les deux états considérés. Selon le modèle des relations (3) on peut admettre que

$$W'_e = W_e + \Delta W_e, \tag{6}$$

avec $\Delta W_e \gtrless 0$. Compte tenu de (3) et (5) il résulte:

$$\Delta W_e = \frac{1}{2} \sum_{j=1}^{n} q_j \Delta V_j + \frac{1}{2} \sum_{j=1}^{n} V_j \Delta q_j + \frac{1}{2} \sum_{j=1}^{n} \Delta q_j \Delta V_j, \tag{7}$$

ou, ayant en vue (4),

$$\Delta W_e = \sum_{j=1}^{n} q_j \Delta V_j + \frac{1}{2} \sum_{j=1}^{n} \Delta q_j \Delta V_j = \sum_{j=1}^{n} V_j \Delta q_j + \frac{1}{2} \sum_{j=1}^{n} \Delta q_j \Delta V_j. \tag{8}$$

Si on ajute aux deux membres de la relation (8) la quantité $2W_e = \sum_{j=1}^{n} q_j V_j$ on obtient, finalement

$$\sum_{j=1}^{n} q_j V'_j = \sum_{j=1}^{n} q'_j V_j = W_e + W'_e - \frac{1}{2} \sum_{j=1}^{n} \Delta q_j \Delta V_j, \tag{9}$$

où on a tenu compte de (6). Par cette voie on a pu évaluer la valeur commune des sommes (1).

Dans les cas particuliers où le passage d'un état à l'autre du système de conducteurs chargés est réalisé soit à des charges constantes ($\Delta q_j = 0$), soit à des potentiels constants ($\Delta V_j = 0$), les expressions (4) deviennent:

$$\sum_{j=1}^{n} q_j \Delta V_j = 0, \text{ respectivement } \sum_{j=1}^{n} V_j \Delta q_j = 0. \tag{10}$$

Dans la première situation la relation (9) conduit à:

$$\sum_{j=1}^{n} q_j V_j' = \sum_{j=1}^{n} q_j V_j = W_e + W_e', \tag{11}$$

tandis que dans la deuxième, à

$$\sum_{j=1}^{n} q_j V_j' = \sum_{j=1}^{n} q_j' V_j' = W_e + W_e'. \tag{12}$$

Il est évident que dans les deux cas ci-dessus:

$$W_e = W_e'. \tag{13}$$

Par conséquent dans deux états distincts d'un champ électrostatique, produit par un système de conducteurs chargés, situés dans un milieu linéaire, isotrope et nonpolarisé permanent, les énergies emmagasinées dans leurs champs électrostatiques sont les mêmes, si soit les charges électriques, soit les potentiels des conducteurs sont égales. Ce résultat doit être mis en connexion avec les théorèmes des forces électrostatiques généralisées [1, §§ **8.8.1**, **8.8.2**]; c'est dans un travail ultérieur qu'on va analyser d'une façon plus détaillée cet aspect.

3. Cas du champ magnétique

Si on utilise un procédé analogue à celui employé dans le § **2** on peut écrire les relations:

$$i_j' = i_j + \Delta i_j, \quad \psi_j' = \psi_j + \Delta \psi_j \tag{14}$$

et

$$\sum_{j=1}^{n} i_j \Delta \psi_j = \sum_{j=1}^{n} \psi_j \Delta i_j, \tag{15}$$

avec $\Delta i_j \gtrless 0$, $\Delta \psi_j \gtrless 0$.

On peut considérer que la relation (15) constitue une autre manière d'exprimer le théorème de la réciprocité dans la champ magnétique (v. (2)).

Si

$$W_m = \frac{1}{2}\sum_{j=1}^{n} i_j\psi_j, \quad W'_m = \frac{1}{2}\sum_{j=1}^{n} i'_j\psi'_j \tag{16}$$

représentent les énergies emmagasinée dans le champ magnétique du système de conducteurs considéré, dans les deux états ci-dessus, alors:

$$W'_m = W_m + \Delta W_m, \tag{17}$$

avec $\Delta W_m \gtrless 0$, où (v.(8)):

$$\Delta W_m = \sum_{j=1}^{n} i_j\Delta\psi_j + \frac{1}{2}\sum_{j=1}^{n}\Delta i_j\Delta\psi_j = \sum_{j=1}^{n}\psi_j\Delta i_j + \frac{1}{2}\sum_{j=1}^{n}\Delta i_j\Delta\psi_j. \tag{18}$$

Quant à la valeur commune des sommes (2) celle-ci est (v.(9)):

$$\sum_{j=1}^{n} i_j\psi'_j = \sum_{j=1}^{n} i'_j\psi_j = W_m + W'_m - \frac{1}{2}\sum_{j=1}^{n}\Delta i_j\Delta\psi_j. \tag{19}$$

Si on considère les cas particuliers où le passage d'un état du système de conducteurs parcourus par des courants à l'autre est réalisé soit à des courants constants ($\Delta i_j = 0$), soit à des flux constants ($\Delta\psi_j = 0$) les expressions (15) deviennent:

$$\sum_{j=1}^{n} i_j\Delta\psi_j = 0, \quad \text{respectivement} \quad \sum_{j=1}^{n}\psi_j\Delta i_j = 0. \tag{20}$$

Dans le premier cas (v. (11)):

$$\sum_{j=1}^{n} i_j\psi'_j = \sum_{j=1}^{n} i_j\psi_j = W_e + W'_m, \tag{21}$$

tandis que dans le deuxième:

$$\sum_{j=1}^{n} i'_j\psi_j = \sum_{j=1}^{n} i_j\psi_j = W_m + W'_m. \tag{22}$$

On observe aisément que dans les deux cas ci-dessus on a:

$$W_m = W'_m. \tag{23}$$

Par conséquent, dans deux états distincts d'un champ magnétique produit par un système de conducteurs parcourus par des courants et situés dans un milieu linéaire,

isotrope et nonmagnétisé permanent, les énergies emmagasinées dans leur champs magnétiques sont égales si, dans les états respectifs, soit les courants, soit les flux magnétiques, sont les mêmes.

Même dans ce cas, d'une façon sembable à une observation similaire concernant les transformations dans un champ électrostatique à charges électriques constantes ou à potentiels constants (v. § **2**), le résultat obtenu doit être corrélé au théorèmes des forces magnétiques généralisées [1, §§ **12.5.1**, **12.5.2**]; plus de détails concernant cet aspect vont être fournis dans un travail ultérieur.

4. Conclusions

1. On détermine les valeurs communes des égalités (1), (2), qui représentent, respectivement, le théorème de la réciprocité en champ électrostatique et en celui magnétique.

2. On aboutit à la conclusion que: a) dans deux états distincts d'un champ électrostatique produit par des conducteurs chargés, situés dans un milieu linéaire, isotrope et nonpolarisé permanent, les énergies emmagasinées dans leurs champs électrostatiques sont les mêmes si soit les charges électriques, soit les potentiels sont égales dans les deux états; b) dans deux états distincts d'un champ magnétique produit par des conducteurs parcourus par des courants, situés dans un milieu linéaire, isotrope et nonmagnetisé permanent, les énergies emmagasinées dans leurs champs magnétiques sont égales si soit les courants, soit les flux magnétiques sont les mêmes dans les deux états.

3. La conclusion précédente doit être mise en connexion avec les théorèmes des forces électrostatiques, respectivement magnétiques généralisées.

Reçue le 28 novembre 1999

Université Technique „Gh. Asachi", Jassy,
Chaire d'Electrotechnique

BIBLIOGRAPHIE

1. M o c a n u C.I., *Teoria câmpului electromagnetic*. Ed. Did. şi Pedag., Bucureşti, 1981.
2. S i m o n y i K., *Theoretische Elektrotechnik*. VEB Deutsche Verlag der Wissenschaften, Berlin, 1956.

CÂTEVA OBSERVAŢII PRIVIND TEOREMA RECIPROCITĂŢII IN CAMPUL ELECTROSTATIC, RESPECTIV MAGNETIC

(Rezumat)

Se determină valorile comune ale egalităţilor (1) şi (2), care reprezintă teorema reciprocităţii în câmpul electrostatic, respectiv magnetic.

BULETINUL INSTITUTULUI POLITEHNIC DIN IAŞI
Tomul XLVII (LI), Fasc. 1–2, 2001
ELECTROTEHNICĂ. ENERGETICĂ. ELECTRONICĂ

D.C. 621.392.5

TWO SCHEMES OF THE LINEAR GENERAL FOUR-TERMINALS WHICH REALISE, IN THE HARMONIC STEADY-STATE, THE EQUALITY BETWEEN THE EQUIVALENT IMPEDANCES AT THE IDLE AND AT SHORT CIRCUIT

BY
DORIN BELAUS

A concrete verification of the theoretical results obtained in [1], regarding the possibility to realize the equality between the idle equivalent impedance and the short-circuit one at input gate of a general four-terminals in harmonical steady-state is effected. The conditions of this equality and practical conclusions are derived.

1. Introduction

In a previous paper [1], the conditions of equality between equivalent impedances at idle and short-circuit were determined for a linear general four-terminals in a harmonic steady state. It asks the question, if theoretical results are verified by the real electrical circuits.

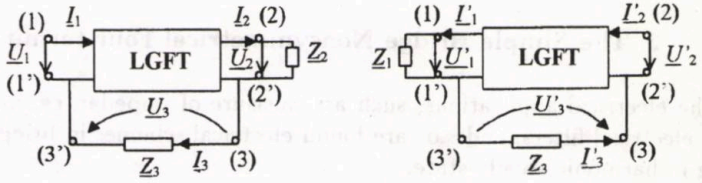

Fig. 1

Thus, for a linear general four-terminals (LGFT – Fig. 1 *a*), the equivalent impedance at input gate is:

$$(1) \qquad \underline{Z}_{e1} = \frac{(\underline{A}_{11}\underline{Z}_3 + \underline{A}_{13}\underline{A}_{31} - \underline{A}_{11}\underline{A}_{33})\underline{Z}_2 + \underline{A}_{12}\underline{Z}_3 + \underline{A}_{13}\underline{A}_{32} - \underline{A}_{12}\underline{A}_{33}}{(\underline{A}_{21}\underline{Z}_3 + \underline{A}_{23}\underline{A}_{31} - \underline{A}_{21}\underline{A}_{33})\underline{Z}_2 + \underline{A}_{22}\underline{Z}_3 + \underline{A}_{23}\underline{A}_{32} - \underline{A}_{22}\underline{A}_{33}},$$

with the equivalent impedances at idle and short-circuit:

$$(2) \quad \underline{Z}_{e10} = \frac{\underline{A}_{11}\underline{Z}_3 - \underline{A}_{11}\underline{A}_{33} + \underline{A}_{13}\underline{A}_{31}}{\underline{A}_{21}\underline{Z}_3 - \underline{A}_{21}\underline{A}_{33} + \underline{A}_{23}\underline{A}_{31}}, \quad (3) \quad \underline{Z}_{e1sc} = \frac{\underline{A}_{12}\underline{Z}_3 - \underline{A}_{12}\underline{A}_{33} + \underline{A}_{13}\underline{A}_{32}}{\underline{A}_{22}\underline{Z}_3 - \underline{A}_{22}\underline{A}_{33} + \underline{A}_{23}\underline{A}_{32}}.$$

This last two relations are equal if:

$$\underline{\tilde{Z}}_3' = \underline{A}_{33}, \quad \underline{\tilde{Z}}_3'' = \frac{|\underline{A}|}{|\underline{\tilde{A}}|}, \tag{4}$$

where $|\underline{A}| = \det\left[\underline{A}_{ij}\right]$, $(i, j = 1, 2, 3)$, and $|\underline{\tilde{A}}| = \underline{A}_{11}\underline{A}_{22} - \underline{A}_{12}\underline{A}_{21}$.

The solution (4_1) is not acceptable (s. [1]) and the solution (4_2) is satisfied only by *nonreciprocical general four-terminals*. In this case it results:

$$\underline{Z}_{e10}'' = \underline{Z}_{e1sc}'' = \frac{\underline{A}_{11}\underline{A}_{32} - \underline{A}_{12}\underline{A}_{31}}{\underline{A}_{21}\underline{A}_{32} - \underline{A}_{22}\underline{A}_{32}}, \quad (\underline{A}_{13}\underline{A}_{31} \neq \underline{A}_{11}\underline{A}_{23}), \tag{5}$$

and for energy supply at gate (*2*), (*2'*) (Fig. 1 *b*):

$$\underline{Z}_{e20}'' = \underline{Z}_{e2sc}'' = \frac{\underline{A}_{22}\underline{A}_{13} - \underline{A}_{12}\underline{A}_{23}}{\underline{A}_{21}\underline{A}_{13} - \underline{A}_{11}\underline{A}_{23}}, \quad (\underline{A}_{21}\underline{A}_{32} \neq \underline{A}_{22}\underline{A}_{31}). \tag{6}$$

The equality between the impedances at idle and short-circuit can be obtained for any impedance $\underline{Z}_3$ if (s. [1]):

$$\left|\underline{\tilde{A}}\right| = 0, \quad |\underline{A}| = 0, \tag{7}$$

so that it is necessary to exist directly proportionality between the coefficients of first two lines or columns of the matrix $[\underline{A}]$. In the paper [5] is proved that such a condition is valuable for *unidirectional* general four-terminals.

The conditions (7) were applied for many electrical schemes of general four-terminals cited in the speciality literature [3], [4] and the following schemes were obtained.

2. The Simple Bridge Nonsymmetrical Four-terminal

In the electrical applications, such as: measure of impedances, measure of frequency, electrical filters, and s.o. are found electrical schemes in bridge (Fig. 2 *a*, *b*) working in harmonic steady-state.

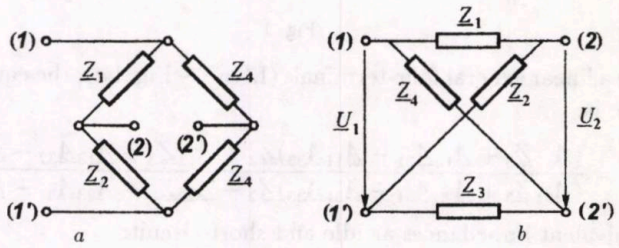

Fig. 2

The matrix $[\underline{A}_{ij}]$, $(i,j = 1,2,3)$, of the schemes, considered as general four-terminals, is:

$$[\underline{A}] = \frac{1}{\underline{Z}_2\underline{Z}_4 - \underline{Z}_1\underline{Z}_3} \times$$

$$\times \begin{bmatrix} (\underline{Z}_1+\underline{Z}_2)(\underline{Z}_3+\underline{Z}_4) & \underline{Z}_1\underline{Z}_2(\underline{Z}_3+\underline{Z}_4)+\underline{Z}_3\underline{Z}_4(\underline{Z}_1+\underline{Z}_2) & -\underline{Z}_3\underline{Z}_4(\underline{Z}_1+\underline{Z}_2) \\ \underline{Z}_1+\underline{Z}_2+\underline{Z}_3+\underline{Z}_4 & (\underline{Z}_1+\underline{Z}_4)(\underline{Z}_2+\underline{Z}_3) & -\underline{Z}_3(\underline{Z}_1+\underline{Z}_4) \\ \underline{Z}_3(\underline{Z}_1+\underline{Z}_2) & \underline{Z}_2\underline{Z}_3(\underline{Z}_1+\underline{Z}_4) & -\underline{Z}_2\underline{Z}_3\underline{Z}_4 \end{bmatrix}. \tag{8}$$

The rapport of terms of first line to second one:

$$\frac{\underline{A}_{11}}{\underline{A}_{21}} = \frac{\underline{A}_{12}}{\underline{A}_{22}} = \frac{\underline{A}_{13}}{\underline{A}_{23}}, \tag{9}$$

is, in this case

$$\frac{(\underline{Z}_1+\underline{Z}_2)(\underline{Z}_3+\underline{Z}_4)}{\underline{Z}_1+\underline{Z}_2+\underline{Z}_3+\underline{Z}_4} = \frac{\underline{Z}_1\underline{Z}_2(\underline{Z}_3+\underline{Z}_4)+\underline{Z}_3\underline{Z}_4(\underline{Z}_1+\underline{Z}_2)}{(\underline{Z}_1+\underline{Z}_4)(\underline{Z}_2+\underline{Z}_3)} = \frac{\underline{Z}_3\underline{Z}_4(\underline{Z}_1+\underline{Z}_2)}{\underline{Z}_3(\underline{Z}_1+\underline{Z}_4)}. \tag{10}$$

Performing the calculus, it results the known condition of equilibrium:

$$\underline{Z}_1\underline{Z}_3 = \underline{Z}_2\underline{Z}_4. \tag{11}$$

Indeed, the equivalent impedance at idle is:

$$\underline{Z}_{e10} = \frac{(\underline{Z}_1+\underline{Z}_2)(\underline{Z}_3+\underline{Z}_4)}{\underline{Z}_1+\underline{Z}_2+\underline{Z}_3+\underline{Z}_4}, \tag{12}$$

and the equivalent impedance at short-circuit is:

$$\underline{Z}_{e1sc} = \frac{\underline{Z}_1\underline{Z}_4}{\underline{Z}_1+\underline{Z}_4} + \frac{\underline{Z}_2\underline{Z}_3}{\underline{Z}_2+\underline{Z}_3}. \tag{13}$$

These last two impedances are equal if the impedance $\underline{Z}_1 = \underline{Z}_2\underline{Z}_4/\underline{Z}_3$, *e.g.*, is replaced in the relations (12) and (13),

$$\underline{Z}_{e10} = \underline{Z}_{e1sc} = \frac{\underline{Z}_2(\underline{Z}_3+\underline{Z}_4)}{\underline{Z}_2+\underline{Z}_3}. \tag{14}$$

O b s e r v a t i o n s.

1. The conditions (7) lead to get the relation of equilibrium (11). In this case, it results a potential difference $\underline{U}_2 = 0$ at the gate (*2*), (*2'*), so that this gate may be *at idle*, or *at short-circuit* without physical consequence on the equivalent impedance at the input gate (*1*), (*1'*).

2. The general bridge four-pole, used at equilibrium, may be considered as an *unidirectional four-terminals* because the energy transfer from input gate (1), $(1')$ to output gate (2), $(2')$ is blocked.

3. The *reciprocity* conditions, $|\underline{A}| = A_{33}$, $\underline{A}_{11}\underline{A}_{22} - \underline{A}_{12}\underline{A}_{21} = 1$ (s. [6]) as the conditions of symmetry, $\underline{A}_{11} = \underline{A}_{22}$, $\underline{A}_{13}\underline{A}_{31} = \underline{A}_{23}\underline{A}_{32}$ [6], are not satisfied.

3. The Complete Bridge Nonsymmetrical Four-terminal

The scheme of a complete bridge four-pole, with six impedances, is shown in Fig. 3 *a*, *b*.

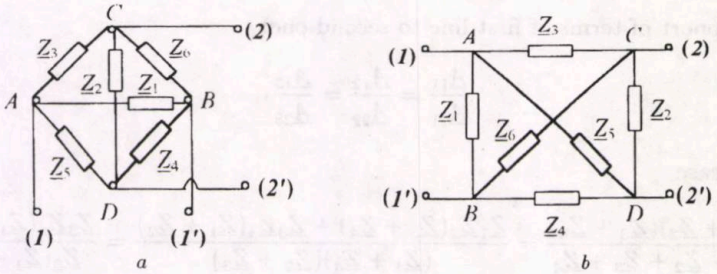

Fig. 3

These schemes can be considered in the theory of four-terminals as equivalent schemes of general four-terminals [4] and their characteristic matrix is:

(15)

$$[\underline{A}] =$$

$$= \begin{bmatrix} -\dfrac{\underline{Z}_2(\underline{Z}_3+\underline{Z}_6)(\underline{Z}_4+\underline{Z}_5)+\underline{Z}_3\underline{Z}_6(\underline{Z}_4+\underline{Z}_5)+\underline{Z}_4\underline{Z}_5(\underline{Z}_3+\underline{Z}_6)}{\underline{Z}_2(\underline{Z}_3\underline{Z}_4-\underline{Z}_5\underline{Z}_6)} & -\dfrac{\underline{Z}_4\underline{Z}_5(\underline{Z}_3+\underline{Z}_6)}{\underline{Z}_3\underline{Z}_4-\underline{Z}_5\underline{Z}_6} \\ -\dfrac{(\underline{Z}_4+\underline{Z}_5)[\underline{Z}_2(\underline{Z}_1+\underline{Z}_6)+\underline{Z}_3(\underline{Z}_2+\underline{Z}_6)]+\underline{Z}_1(\underline{Z}_4+\underline{Z}_6)(\underline{Z}_3+\underline{Z}_5)+(\underline{Z}_3+\underline{Z}_6)(\underline{Z}_4\underline{Z}_5+\underline{Z}_1\underline{Z}_2)}{\underline{Z}_1\underline{Z}_2(\underline{Z}_3\underline{Z}_4-\underline{Z}_5\underline{Z}_6)} & -\dfrac{\underline{Z}_3\underline{Z}_6(\underline{Z}_4+\underline{Z}_5)+\underline{Z}_4\underline{Z}_5(\underline{Z}_3+\underline{Z}_6)}{\underline{Z}_3\underline{Z}_4-\underline{Z}_5\underline{Z}_6} \\ -\dfrac{\underline{Z}_4[\underline{Z}_6(\underline{Z}_3+\underline{Z}_5)+\underline{Z}_2(\underline{Z}_3+\underline{Z}_6)]}{\underline{Z}_2(\underline{Z}_3\underline{Z}_4-\underline{Z}_5\underline{Z}_6)} & -\dfrac{\underline{Z}_3\underline{Z}_6(\underline{Z}_4+\underline{Z}_5)+\underline{Z}_4\underline{Z}_5(\underline{Z}_3+\underline{Z}_6)}{\underline{Z}_3\underline{Z}_4-\underline{Z}_5\underline{Z}_6} \end{bmatrix}$$

$$\begin{bmatrix} -\dfrac{\underline{Z}_3\underline{Z}_6(\underline{Z}_4+\underline{Z}_5)+\underline{Z}_4\underline{Z}_5(\underline{Z}_3+\underline{Z}_6)}{\underline{Z}_3\underline{Z}_4-\underline{Z}_5\underline{Z}_6} & \dfrac{\underline{Z}_4\underline{Z}_5(\underline{Z}_3+\underline{Z}_6)}{\underline{Z}_3\underline{Z}_4-\underline{Z}_5\underline{Z}_6} \\ -\dfrac{\underline{Z}_1(\underline{Z}_3+\underline{Z}_5)(\underline{Z}_4+\underline{Z}_6)+\underline{Z}_4\underline{Z}_6(\underline{Z}_3+\underline{Z}_5)+\underline{Z}_3\underline{Z}_5(\underline{Z}_4+\underline{Z}_6)}{\underline{Z}_1(\underline{Z}_3\underline{Z}_4-\underline{Z}_5\underline{Z}_6)} & \dfrac{\underline{Z}_4[\underline{Z}_6(\underline{Z}_3+\underline{Z}_5)+\underline{Z}_5(\underline{Z}_3+\underline{Z}_6)]}{\underline{Z}_1(\underline{Z}_3\underline{Z}_4-\underline{Z}_5\underline{Z}_6)} \\ -\dfrac{\underline{Z}_4\underline{Z}_6(\underline{Z}_3+\underline{Z}_5)}{\underline{Z}_3\underline{Z}_4-\underline{Z}_5\underline{Z}_6} & \dfrac{\underline{Z}_4\underline{Z}_5\underline{Z}_6}{\underline{Z}_3\underline{Z}_4-\underline{Z}_5\underline{Z}_6} \end{bmatrix}.$$

Conditions (7) being satisfied, the rapport (9) leads to the equality:

(16) $$\underline{Z}_3\underline{Z}_4 = \underline{Z}_5\underline{Z}_6.$$

In order to calculate the equivalent impedances $\underline{Z}_{e10}$ and $\underline{Z}_{e1sc}$, the triangle ACD of scheme (Fig. 3 *a*) will be transformed in star having the impedances $\underline{Z}_4$, $\underline{Z}_C$, $\underline{Z}_D$ (s. Fig. 4), where:

$$\underline{Z}_A = \frac{\underline{Z}_3\underline{Z}_5}{\underline{Z}_2+\underline{Z}_3+\underline{Z}_5},\quad \underline{Z}_C = \frac{\underline{Z}_2\underline{Z}_3}{\underline{Z}_2+\underline{Z}_3+\underline{Z}_5},\quad \underline{Z}_D = \frac{\underline{Z}_2\underline{Z}_5}{\underline{Z}_2+\underline{Z}_3+\underline{Z}_5}. \tag{17}$$

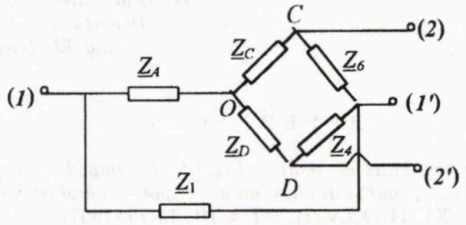

Fig. 4

The equivalent impedance at idle is:

$$\underline{Z}_{e10} = \frac{\underline{Z}_1\left[\underline{Z}_A + \dfrac{(\underline{Z}_C+\underline{Z}_6)(\underline{Z}_D+\underline{Z}_4)}{\underline{Z}_C+\underline{Z}_6+\underline{Z}_D+\underline{Z}_4}\right]}{\underline{Z}_1+\underline{Z}_A+\dfrac{(\underline{Z}_C+\underline{Z}_6)(\underline{Z}_D+\underline{Z}_4)}{\underline{Z}_C+\underline{Z}_6+\underline{Z}_D+\underline{Z}_4}}, \tag{18}$$

and the equivalent impedance at short-circuit:

$$\underline{Z}_{e1sc} = \frac{\underline{Z}_1\left(\underline{Z}_A + \dfrac{\underline{Z}_C\underline{Z}_D}{\underline{Z}_C+\underline{Z}_D} + \dfrac{\underline{Z}_4\underline{Z}_6}{\underline{Z}_4+\underline{Z}_6}\right)}{\underline{Z}_1+\underline{Z}_A+\dfrac{\underline{Z}_C\underline{Z}_D}{\underline{Z}_C+\underline{Z}_D}+\dfrac{\underline{Z}_4\underline{Z}_6}{\underline{Z}_4+\underline{Z}_6}}. \tag{19}$$

If the value of $\underline{Z}_4$ from relation (16) is introduced in the relations (18) and (19), it results the equality:

$$\underline{Z}_{e10} = \underline{Z}_{e1sc} = \frac{\underline{Z}_5\left[\underline{Z}_2\underline{Z}_3 + \underline{Z}_6(\underline{Z}_2+\underline{Z}_3+\underline{Z}_5)\right]}{(\underline{Z}_3+\underline{Z}_5)(\underline{Z}_2+\underline{Z}_3+\underline{Z}_5)}. \tag{20}$$

O b s e r v a t i o n s.

1. The conditions (7) lead to relation (16) of bridge equilibrium, where the impedances $\underline{Z}_1$ and $\underline{Z}_2$ of the bridge diagonals (Fig. 3 *a*) do not exist.

2. The potential difference $\underline{U}_2 = 0$, such as in the previous case and through the impedance $\underline{Z}_2$ does not flow an electrical current. The four-terminals is at equilibrium, power supply to gate (2), (2') is zero.

3. The condition (16) does not represent a reciprocity and symmetry one.

4. Conclusions

1. The equality of equivalent impedances $\underline{Z}_{e10}$ and $\underline{Z}_{e1sc}$ can be able, in the practical schemes, such as electrical bridges, if certain conditions are respected.

3. In this case, the general four-terminals is unidirectional and the power transfer is zero.

3. The equality of impedances $\underline{Z}_{e10} = \underline{Z}_{e1sc}$ does not impose the reciprocity or symmetry of the general four-terminals.

Received, June 15, 1999

Technical University "Gh.Asachi", Jassy,
Department of Electrotechnics
and Electrical Machines

REFERENCES

1. B e l a u s D., *Sur la possibilité de réaliser l'égalité des impédances équivalentes à la porte d'entrée, à vide et en court-circuit, d'un quadripôle général linéaire non-autonome.* Bul. Inst. polit., Iaşi, **XLIII (XLVII)**, *3-4*, s. III, 19-25 (1997).
2. R o s m a n H., *Le domaine d'existence de l'impédance équivalente à la porte d'entrée d'un quadripôle général en régime permanent harmonique.* Mem. secţ. şt., Acad. Rom., s. IV, **XI**, *1*, 193-206 (1988).
3. Ş o r a C., *Le quadripôle électrique.* Ed. Masson, Paris, 1969.
4. S i g o r s k y V.P., *Théorie générale des quadripôles* (en russe). Ed. Acad. Sci., Ukraïne, Kiev, 1955.
5. B e l a u s D., R o s m a n H., *Quadripôles généraux linéaires, non-autonomes, unidirectionnels, en régime permanent harmonique.* Bul. Inst. polit., Iaşi, **XLIV (XLVIII)**. *1-2*, s. III, 23-28 (1998).
6. R o s m a n H., *Sur les conditions de réciprocité et de symétrie d'un quadripôle général nonautonome en régime permanent harmonique.* Bul. Inst. polit., Iaşi, **XL (XLIV)**, *1-4*, s. III, 25-30 (1994).

DOUĂ SCHEME DE CUADRIPOLI LINIARI NEAUTONOMI, CU IMPEDANŢELE ECHIVALENTE LA GOL ŞI ÎN SCURTCIRCUIT EGALE ÎN REGIM PERMANENT ARMONIC

(Rezumat)

Se verifică, în practică, pe două scheme electrice, rezultatele generale, stabilite în [1], privitoare la existenţa unor cuadripoli pentru care impedanţele echivalente la poarta de intrare la gol şi în scurtcircuit sunt egale. Se determină condiţiile în care aceste egalităţi au loc şi se trag unele concluzii practice.

BULETINUL INSTITUTULUI POLITEHNIC DIN IAŞI
Tomul XLVII (LI), Fasc. 1–2, 2001
ELECTROTEHNICĂ. ENERGETICĂ. ELECTRONICĂ

C.D. 53; 621.3

LE THÉORÈME DE TELLEGEN CONCERNANT LES SYSTÈMES MÉCANIQUES

PAR
HUGO ROSMAN

On établit plusieurs variantes du théorème de Tellegen concernant les systèmes mécaniques ou électromécaniques. Le théorème est valable seulement pour certains systèmes mécaniques, capables à être modélés par un réseau électrique, qui constitue l'analogue du système mécanique considéré.

1. Introduction

Dans la théorie des réseaux électriques (linéaires, non-linéaires ou paramétriques) un rôle important est détenu par le théorème de T e l l e g e n [1], concernant les *pseudo-puissances* (instantanées, actives ou réactives). A savoir si on considère deux réseaux électriques, (I) et (II), actifs ou passifs, supposés, pour simplification, isolés, ayant des graphes topologiques orientés identiques, soient $u_k^{(\mathrm{I})}(t')$ (la tension entre les nœuds incidents à la branche k du réseau (I) au moment t' et $i_k^{(\mathrm{II})}(t'')$ – le courant qui circule par la branche k du réseau (II), au moment t'', avec $k = 1, 2, ..., B$, ou B est le nombre des branches du chaque réseau. Quant au régime de fonctionnement des réseaux respectifs il est considéré quasistationnaire, du type anélectrique. On peut prouver que, respectant les conditions ci-dessus, la relation

$$\sum_{k=1}^{B} u_k^{(\mathrm{I})}(t') i_k^{(\mathrm{II})}(t'') = 0 \tag{1}$$

est satisfaite. Toutefois, dans les même conditions est satisfaite et la relation

$$\sum_{k=1}^{B} u_k^{(\mathrm{I})}(t'') i_k^{(\mathrm{II})}(t') = 0. \tag{1'}$$

Les expressions (1) et (1′), qui se réfèrent aux sommes des pseuds-puissances instantanées dans les branches des deux réseaux considérés, représentent le théorème de Tellegen.

Dans ce qui suit on établit un théorème semblable valable pour certains systèmes mécaniques (ou électromécaniques).

2. Systèmes mécaniques. Analogies électromécaniques

Il est évident que, avant toute chose, les systèmes mécaniques pour lesquels on pourrait établir un théorème de type Tellegen, devront posséder la propriété d'être capables à être attachés à des graphes topologiques orientés. Or, tels systèmes mécaniques sont ceux qui permettent leur étude en se basant sur les analogies électromécaniques. Une telle étude des systèmes mécaniques a été effectuée, dans un cadre unitaire et, toutefois, très général, par D. S t a n o m i r [2]. Il est question, en premier lieu, des systèmes mécaniques constitués par des masses, des ressorts et des éléments de friction. On accepte l'hypotèse (simplificatrice) que les systèmes mécaniques étudiés ont des forces et des déplacements parallèles, les mouvements de rotation étant inexistants. Les graphes topologiques orientés, qui correspondent à de tels systèmes mécaniques, sont plans et on peut leur attacher deux liaisons olonomes-scléronomes linéaires à savoir:

a) Une première liaison représente *les équations des viteses relatives dans les cycles* (EVRC):

$$\sum_{m \in s} v_{rm} = 0, \quad (s = 1, 2, ..., C), \tag{2}$$

où C représente le nombre de cycles des graphes topologiques orientés considérés.

b) La deuxième liaison est constituée par *les équations des forces dans les nœuds* (EFN):

$$\sum_{n \in t} f_n = 0, \quad (t = 1, 2, ..., N), \tag{3}$$

où N est le nombre de nœuds des mêmes graphes. Ces forces sont positives si elles sont convergentes par rapport au nœud considéré et négatives dans le cas opposé.

Si on ajoute à ces conditions et celle que le système mécanique considéré contienne seulement des structures du type uniporte et des sources idéales, ainsi que celle visant la possibilité d'attacher au système mécanique considéré, d'une manière biunivoque, un graphe topologique orienté muni avec les liaisons mentionnées ci-dessus, on obtient les conditions nécessaires et suffisantes, formulées par D. Stanomir (*loc.cit.*), qui assûrent la possibilité d'établir une analogie entre un système mécanique et un réseau électrique (équivalent), à paramètres concentrés.

Une fois satisfaites ces conditions (nécessaires et suffisantes), D. Stanomir (*loc.cit.*) définit deux types possibles d'analogies entre un système mécanique et un réseau électrique équivalent:

a) Le type I, dans le cas où entre les liaisons du réseau électrique et celles du système mécanique on peut établir l'isomorphisme:

$$\text{EVRC} \Leftrightarrow \text{ETK I}, \quad \text{EFN} \Leftrightarrow \text{ETK II}, \tag{4}$$

où ETK I, ETK II représentent les équations obtenues par l'application du premier, respectivement du deuxième théorème de Kirchhoff au réseau électrique qui constitue le modèle du système mécanique considéré.

b) Le type II, si on peut établir entre les liaisons du réseau électrique et celles du système mécanique les isomorphismes:

$$\text{EFN} \Leftrightarrow \text{ETK I}, \quad \text{EVRC} \Leftrightarrow \text{ETK II}. \tag{5}$$

Comme conséquences de ces deux types d'analogies entre un système mécanique et un réseau électrique, en tant que modèle du premier d'entre ceux-ci, on peut établir, à leur tour, les analogies ci-dessous entre certaines paires de signaux à savoir:

$$f \rightleftarrows u, \quad v \rightleftarrows i, \quad \text{respectivement} \quad f \rightleftarrows i, \quad v \rightleftarrows u; \tag{6}$$

$$p \rightleftarrows u, \quad v \rightleftarrows i, \quad \text{respectivement} \quad p \rightleftarrows i, \quad v \rightleftarrows u; \tag{7}$$

$$p \rightleftarrows u, \quad q_v \rightleftarrows i, \quad \text{respectivement} \quad p \rightleftarrows i, \quad q_v \rightleftarrows u, \tag{8}$$

où v et f ont les significations ci-dessous (v. les relations (2) et (3)): i représente les courants dans les branches, u – les tensions des branches, p – les pressions, q_v – les moments sur chaque unité de surface.

3. Le théorème de Tellegen concernant les systèmes mécaniques

L'analogie électromécanique entre un système mécanique et un réseau électrique, présentée dans le § **2**, permet, aisément, à élargir le contenu du théorème de Tellegen, établi pour les réseaux électriques, en l'appliquant, aussi, aux système mécaniques.

Soient, donc, deux systèmes mécaniques, (I) et (II), qu'on peut mettre en correspondance, d'une manière biunivoque, avec des réseaux électriques. On admet que les systèmes mécaniques considérés sont, pour simplifier le raisonnement, isolés, ayant des graphes topologiques orientés identiques. Si on considère la correspondance (6_1) soit $f_s^{(\mathrm{I})}(t')$ la force qui correspond au nœud s du système (I) au moment t' et $v_m^{(\mathrm{II})}(t'')$ – la vitesse relative qui correspond à la branche m appartenant au graphe attaché au système (II), dans le moment t'', $(m = 1, 2, ..., B;\ s = 1, 2, ..., N)$. On amplifie la relation (v. (2)):

$$\sum_{m \in s} v_m^{(\mathrm{II})}(t'') = 0 \tag{9}$$

avec $\sum_{s=1}^{N} f_s^{(\mathrm{I})}(t')$ en obtenant

$$\sum_{s=1}^{N} f_s^{(\mathrm{I})}(t') \sum_{m \in s} v_m^{(\mathrm{II})}(t'') = 0. \tag{10}$$

Or, si on ordonne la somme double du membre gauche de la relation (10) par rapport aux indices des branches, il est possible à observer, aisément, que chaque vitesse,

$v_m^{(II)}(t'')$, intervient deux fois dans la somme $\sum_{m \in s} v_m^{(II)}(t'')$, une fois avec le signe plus et la deuxième fois avec le signe minus, de sorte que pour chaque paire de nœuds, p, q, incidents à la branche m, les termes qui contiennent, dans la relation (10), la vitesse (relative) $v_m^{(II)}(t'')$, ont la forme:

$$(11)\quad f_p^{(I)}(t')v_m^{(II)}(t'') - f_q^{(I)}(t')v_m^{(II)}(t'') = \left[f_p^{(I)}(t') - f_q^{(I)}(t')\right] v_m^{(II)}(t'') = \Delta f_m^{(I)}(t')v_m^{(II)}(t''),$$

où on a utilisé la notation

$$(12)\qquad f_p^{(I)}(t') - f_q^{(I)}(t') \overset{not}{=} \Delta f_m^{(I)}(t'),$$

de sorte qu'on peut écrire la relation (10) et sous la forme

$$(13)\qquad \sum_{m=1}^{B} \Delta f_m^{(I)}(t')v_m^{(II)}(t'') = 0.$$

D'une manière analogue on peut obtenir et les relations:

$$\sum_{m=1}^{B} \Delta v_m^{(I)}(t')f_m^{(II)}(t'') = 0, \quad \sum_{m=1}^{B} \Delta p_m^{(I)}(t')v_m^{(II)}(t'') = 0,$$

$$(14)\qquad \sum_{m=1}^{B} \Delta v_m^{(I)}(t')p_m^{(II)}(t'') = 0, \quad \sum_{m=1}^{B} \Delta p_m^{(I)}(t')q_m^{(II)}(t'') = 0,$$

$$\sum_{m=1}^{L} \Delta q_m^{(I)}(t')p_m^{(II)}(t'') = 0,$$

où

$$(15)\qquad \begin{gathered} v_p^{(I)}(t') - v_q^{(I)}(t') \overset{not}{=} \Delta v_m^{(I)}(t'), \quad p_p^{(I)}(t') - p_q^{(I)}(t') \overset{not}{=} \Delta p_m^{(I)}(t'), \\ q_{vp}^{(I)}(t') - q_{vq}^{(II)}(t') \overset{not}{=} \Delta q_{vm}^{(I)}(t'). \end{gathered}$$

Les relations (13) et (14) représentent autant de possibilités de formuler *le théorème de Tellegen pour les systèmes mécaniques.*

Il y a la possibilité de définir, dans le cas des système mécaniques, tout comme dans celui des réseaux électriques, des *pseudo-puissances instantanées* (évidemment mécaniques). Par exemple on peut définir de telles pseudo-puissances, en utilisant les notations:

$$(16)\qquad \begin{cases} p_m^{(I),(II)}(t', t'') \overset{not}{=} \Delta f_m^{(I)}(t')v_m^{(II)}(t''), \\ p_m^{(II),(I)}(t', t'') \overset{not}{=} \Delta f_m^{(II)}(t'')v_m^{(I)}(t'), \end{cases}$$

de sorte que les relations (12) et (13) deviennent

$$(17)\qquad \sum_{m=1}^{B} p_m^{(I),(II)}(t', t'') = 0, \quad \text{respectivement} \quad \sum_{m=1}^{B} p_m^{(II),(I)}(t', t'') = 0.$$

4. Conclusions

On démontre que pour les systèmes mécaniques qui admettent, en tant que modèle, un réseau électrique, répresentant l'analogue du système mécanique, on peut établir diverses variantes du théorème de Tellegen.

Reçue le 8 novembre 2000

Université Technique „Gh. Asachi", Jassy,
Chaire d'Electrotechnique

BIBLIOGRAPHIE

1. Tellegen B.D.H., *A General Theorem with Applications.* Phillips Res. Rev., 7, 259-262 (1952).
2. Stanomir D., *Teoria fizică a sistemelor electromecanice.* Ed. Acad., Bucureşti, 1982.

TEOREMA LUI TELLEGEN ÎN SISTEME MECANICE

(Rezumat)

Se stabilesc mai multe variante ale teoremei lui Tellegen referitoare la sisteme mecanice. Teorema este valabilă numai pentru acele sisteme mecanice care admit drept model o reţea electrică, reprezentand analogul sistemului mecanic.

BULETINUL INSTITUTULUI POLITEHNIC DIN IAŞI
Tomul XLVII (LI), Fasc. 1–2, 2001
ELECTROTEHNICĂ. ENERGETICĂ. ELECTRONICĂ

D.C. 621.392.5

ON THE IMMUNITY OF THE BALANCED CIRCUITS TO LONGITUDINAL DISTURBING SIGNALS

BY

VALENTIN BUZDUGA, *OREST OLTU and *OVIDIU DRAGOMIRESCU

An analytical approach regarding the immunity of the circuits that provide an *electrical* longitudinal symmetry, wherein are included the so-called *balanced* circuits, is proposed. First is proved that any *longitudinal symmetrical* circuit provides zero transversal response to certain *pairs* of excitation signals. Further on it is deduced that the immunity of such a circuit to a *longitudinally coupled* source may be improved by certain symmetry of the passive network that connects the source to the circuit's accessible terminals. As an application of the proposed approach, it is commented the immunity of a pair-wire transmission system to the disturbing signals supplied by a longitudinally coupled source.

1. Introduction

The usefulness of the balanced circuits in the symmetrical line transmission systems is well known from literature (s. [1], p. 191). A major property of the balanced circuits and symmetrical lines, resulting from their *geometrical* symmetry, consists in a high immunity to the longitudinal disturbances (s. [2], p. 68). As stated in *two*-port circuits modelling, "*if a horizontal center line can be drawn through the two-port in such a way as to make the two halves mirror images of each other, the two-port is said to be balanced*". In this understanding, "*any two-port that does not satisfy the condition for a balanced two-port, is an unbalanced two-port*" (s. [3], p. 653).

It is obvious that the geometrical symmetry of a circuit is not a perfect one, for example due to components' tolerance. Consequently, it can be accepted that only *quasi-balanced* circuits are used in practice. As interference phenomena may occur in some balanced transmission systems, it is of interest for Electromagnetic Compatibility analysis to relate such phenomena to the deviation of the balanced circuits from the desired geometrical symmetry. The present paper clarifies these aspects by expressing the response of certain *symmetrical* circuits to *longitudinal* excitations. The proposed modelling is based on the *three*-port characteristic equations of the *four*-terminal circuits (s. [4] and [5]).

In this paper are used the following conventions and results stated in [5]:

a) The *four*-terminal circuit is essentially characterized by systems

$$(1) \qquad U_1 = aI_1 + bI_2 + cI_3, \quad U_2 = bI_1 + dI_2 + eI_3, \quad U_3 = cI_1 + eI_2 + fI_3;$$

$$(2) \quad I_1 = AU_1 + BU_2 + CU_3, \quad I_2 = BU_1 + DU_2 + EU_3, \quad I_3 = CU_1 + EU_2 + FU_3,$$

representing linear expressions of the signals of three ports *in line*, connected to the circuit's accessible terminals as represented in Fig. 1 *a*.

b) The circuit within Fig. 1 *a* provides an *electrical* longitudinal symmetry if, in any external network, it equally responds either in the reference position or in the longitudinal inverted position (inverted around $l - l'$ axis). Obviously, any *balanced* circuit provides this electrical symmetry. The parameters of the *longitudinal symmetrical* circuits fulfil the conditions:

$$(3) \qquad c = -\frac{a+b}{2}, \quad e = -\frac{b+d}{2}, \quad C = E = \frac{F}{2},$$

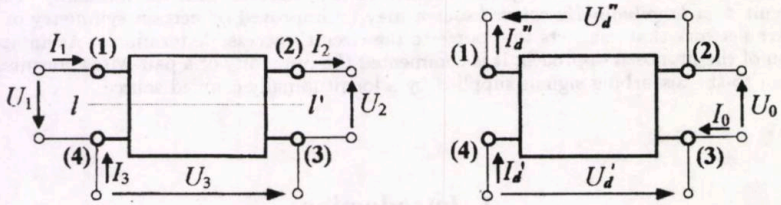

a *b*

Fig. 1.– A *four*-terminal circuit with miscellaneous systems of ports; *a* – the reference system of ports.

The analysis is performed taking into account only *non-degenerate* circuits. Consequently, excepting a finite number of frequencies in a finite frequency domain, equations systems (1) and (2) provide *non-singular* matrices. In certain applications, to the terminals of the circuit characterized by equation system (2), are connected y_g and y_L, as represented in Fig. 2.

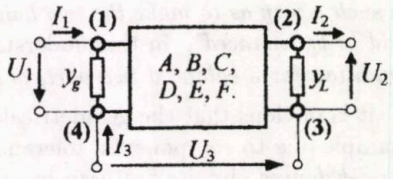

Fig. 2.– A *four*-terminal circuit in a parallel connection.

With help of (2) are easily deduced the following equations of the equivalent circuit within Fig. 2:

$$(4) \quad I_1 = (A+y_g)U_1+BU_2+CU_3, \quad I_2 = BU_1+(D+y_L)U_2+EU_3, \quad I_3 = CU_1+EU_2+FU_3.$$

2. The Response of the *Four*-Terminal Circuits to *Longitudinal* Excitations

Let be the circuit within Fig. 1 *a*, characterized by equations system (2). It is of interest to express the circuit's *transversal* response, U_0, on a load y_0, to the *longitudinal* excitations I'_d and I''_d represented in Fig. 1 *b*. For this purpose it is convenient to use the circuit's characteristic equations expressed as function of electrical signals within Fig. 1 *b*. These new equations result from (2), taking into account the signal relations concerning the same circuit represented in Fig. 1 *a* and, respectively Fig. 1 *b*:

$$I'_d = -I_1 + I_3, \quad I''_d = -I_1, \quad I_0 = -I_1 + I_2; \tag{5}$$

$$U_1 = -U'_d - U''_d - U_0, \quad U_2 = U_0, \quad U_3 = U'_d. \tag{6}$$

From (5), (2) and (6), may outcome the characteristic equations of the considered circuit, expressed in function of electrical signals of the ports represented in Fig. 1 *b*. In these new equations, the admittance parameters of the circuit are expressed in terms of the reference system (2), as follow:

$$\begin{cases} I'_d = (A - 2C + F)U'_d + (A - C)U''_d + (A - B - C + E)U_0, \\ I''_d = (A - C)U'_d + AU''_d + (A - B)U_0, \\ I_0 = (A - B - C + E)U'_d + (A - B)U''_d + (A - 2B + D)U_0. \end{cases} \tag{7}$$

For a transversal load, y_0, it can be written the relation $I_0 = -y_0 U_0$. In these conditions, the transversal response, U_0, to longitudinal excitations, I'_d and I''_d, is deduced from (7) by using Cramer's rule:

$$U_0 = \frac{\Delta'}{\Delta} I'_d + \frac{\Delta''}{\Delta} I''_d, \tag{8}$$

wherein:

$$\Delta' = \begin{vmatrix} -C & A \\ E & -B \end{vmatrix}, \quad \Delta'' = \begin{vmatrix} C - F & A - C \\ C - E & A - B \end{vmatrix},$$

$$\Delta = \begin{vmatrix} A - 2C + F & A - C & A - B - C + E \\ A - C & A & A - B \\ A - B - C + E & A - B & A - 2B + D + y_0 \end{vmatrix}. \tag{9}$$

2.1. The Response of a General *Four*-Terminal Circuit

It can be easily proved that, for any non-degenerate circuit, Δ' and Δ'' from (9) have not simultaneously zero values. In these conditions, taking into account

independent values for I'_d and I''_d, relation (8) reveals that the *four*-terminal circuits generally provide non-zero transversal response to the considered *longitudinal* disturbing excitations.

2.2. The Response of the *Longitudinal Symmetrical* Circuits

Let now a *longitudinal symmetrical* circuit, whose characteristic parameters fulfil the admittance conditions written in (3), $C = E = F/2$. In this case, from (8) and (9) it results:

$$U_0 = \frac{F}{2\Delta}(B - A)\left(I'_d + I''_d\right). \tag{10}$$

A non-degenerate circuit that provides a longitudinal symmetry, obviously fulfils admittance conditions $F \neq 0$ and, generally, $B \neq A$. Consequently, relation (10) reveals a *zero* transversal response if and only if:

$$I''_d = -I'_d. \tag{11}$$

Relation (11) corresponds to certain *symmetrical* longitudinal excitations (for example, two currents of same value flow into the circuit through the accessible terminals *1* and *4*).

If the analysis is performed w.r.t *voltage* excitations, it is convenient to use equations system (1), expressed in impedance parameters. Consequently, the considered circuit provides *zero* transversal response if the longitudinal excitations fulfil the dual condition w.r.t. (11):

$$U''_d = -U'_d. \tag{12}$$

R e m a r k s.

a) Relations (10) and (11) reveal a *high immunity* of the longitudinal symmetrical circuits to certain *pairs* of longitudinal excitations.

b) The values of longitudinal excitations represented in Fig. 1 *b*, either currents or voltages, result from the steady-state equations of the circuit. When these equations are established both the parameters of the given circuit and those of the external network are take into account.

c) If the longitudinal excitations, represented in Fig. 1 *b* proceed from *independent* sources, the relations expressed in (11) and (12) reveal *critical requirements* for zero transversal response. Such conditions cannot be practically fulfilled. Certain *symmetrical* excitations are provided if the two longitudinal excitations within Fig. 1 *b* proceed from the *same disturbing source* that is coupled to the circuit's accessible terminals, as shown in the following section.

3. The Response of the *Four*-Terminal Circuits to Certain *Longitudinally* Coupled Sources

It is of interest to express the response of the *four*-terminal circuits to certain disturbing sources that are *longitudinally coupled* to the accessible terminals of these circuits.

Let us consider that a disturbing source, characterized by equivalent parameters e_d and Z_5, is coupled to the *four* accessible terminals of certain circuits by means of Z_1, Z_2, Z_3 and Z_4, as represented in Fig. 3.

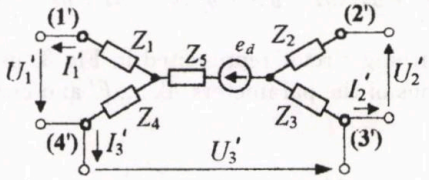

Fig. 3.– The modelling of a *longitudinal disturbing* circuit.

3.1. The Characteristic Equations of the Disturbing Circuit

The characteristic equations of the disturbing circuit represented in Fig. 3, expressed in impedance parameters, may be easily deduced by method of opened ports. These equations may be written as follow:

$$(13)\qquad \begin{cases} U_1' = -(z_1 + z_4)I_1' + 0 \cdot I_2' + z_4 I_3', \\ U_2' = 0 \cdot I_1' - (z_2 + z_3)I_2' + z_3 I_3', \\ U_3' = z_4 I_1' + z_3 I_2' - (z_3 + z_4 + z_d)I_3' + e_d. \end{cases}$$

R e m a r k s:

a) All the three ports within Fig. 3 are designated as *generating* ports, for easy writing of steady-state equations when an active circuit is connected with a passive one.

b) It is of interest to find out the conditions for the *longitudinal symmetry* of the passive network represented in Fig. 3 (that is for $e_d = 0$). Taking into account the impedance conditions written in (3), from (13) it results:

$$(14)\qquad z_1 = z_4 \quad \text{and} \quad z_2 = z_3.$$

The goal of the analysis is to find out the voltage response on given loads, in certain disturbed circuits. For this purpose it is convenient to use the characteristic equations expressed in admittance parameters. For the circuit represented in Fig. 3, these equations are the followings:

$$(15)\qquad \begin{cases} I_1' = A'U_1' + B'U_2' + C'U_3' + I_{01}', \\ I_2' = B'U_1' + D'U_2' + E'U_3' + I_{02}', \\ I_3' = C'U_1' + E'U_2' + F'U_3' + I_{03}'. \end{cases}$$

The admittance parameters $A', ..., F'$ and the currents $I_{01}', ..., I_{03}'$ from (15), may be deduced either by using the method of *short-circuited* ports, or by matrix inversion

from (13). In the following relations are used the admittance parameters of the components represented in Fig. 3, that is $y_j = 1/z_j$; also it is denoted by n the following expression:

$$n = (y_1 + y_4)(y_2 + y_3) + y_5(y_1 + y_2 + y_3 + y_4). \tag{16}$$

With regard to the disturbing circuit represented in Fig. 3, usual calculations lead to the following expressions of the parameters $A', ..., F'$ and currents $I'_{01}, ..., I'_{03}$ from (15):

$$\begin{aligned} A' &= -\frac{(y_2 + y_3)(y_4 + y_5) + y_4 y_5}{n} y_1, \quad B' = -\frac{y_1 y_2 y_5}{n}, \\ C' &= -\frac{y_1(y_2 + y_3)}{n} y_5, \quad D' = -\frac{(y_1 + y_4)(y_3 + y_5) + y_3 y_5}{n} y_2, \\ E' &= -\frac{y_2(y_1 + y_4)}{n} y_5, \quad F' = -\frac{(y_1 + y_4)(y_2 + y_3)}{n} y_5; \end{aligned} \tag{17}$$

$$I'_{01} = \frac{y_1(y_2+y_3)}{n} y_5 e_d, \quad I'_{02} = \frac{y_2(y_1+y_4)}{n} y_5 e_d, \quad I'_{03} = \frac{(y_1+y_4)(y_2+y_3)}{n} y_5 e_d. \tag{18}$$

3.2. The Response of the *Longitudinal Symmetrical* Circuits to *Longitudinally* Coupled Sources

Let be the circuit represented in Fig. 2, wherein the load y_L and the generator's admittance y_g are taken into account, and admit that the considered circuit provides a longitudinal symmetry. With admittance conditions within (3), from (4) are deduced the characteristic equations of such a circuit:

$$\begin{cases} I_1 = (A + y_g) U_1 + B U_2 + \dfrac{F}{2} U_3, \\ I_2 = B U_1 + (D + y_L) U_2 + \dfrac{F}{2} U_3, \\ I_3 = \dfrac{F}{2} U_1 + \dfrac{F}{2} U_2 + F U_3. \end{cases} \tag{19}$$

Let us consider that to the accessible terminals *1*, *2*, *3*, *4*, of the circuit characterized by equations system (19), are respectively connected the terminals *1'*, *2'*, *3'* and *4'*, of the disturbing circuit represented in Fig. 3. The steady-state conditions for this connection are the followings:

$$I'_1 = I_1, \; I'_2 = I_2, \; I'_3 = I_3, \; U'_1 = U_1, \; U'_2 = U_2, \; U'_3 = U_3. \tag{20}$$

With (20), from (15) and (19) the *steady-state* equations of the disturbed circuit may be established:

$$(21)\qquad \begin{cases} (A+y_g-A')\,U_1+(B-B')\,U_2+\left(\dfrac{F}{2}-C'\right)U_3=I'_{01}, \\ (B-B')\,U_1+(D+y_L-D')U_2+\left(\dfrac{F}{2}-E'\right)U_3=I'_{02}, \\ \left(\dfrac{F}{2}-C'\right)U_1+\left(\dfrac{F}{2}-E'\right)U_2+(F-F')\,U_3=I'_{03}. \end{cases}$$

The voltage response on the load y_L may be expressed from (21) as $U_2=\overline{\Delta}_2/\overline{\Delta}$, wherein:

$$(22)\quad \overline{\Delta}_2=\begin{vmatrix} A+y_g-A' & I'_{01} & F/2-C' \\ B-B' & I'_{02} & F/2-E' \\ F/2-C' & I'_{03} & F-F' \end{vmatrix},\quad \overline{\Delta}=\begin{vmatrix} A+y_g-A' & B-B' & F/2-C' \\ B-B' & D+y_L-D' & F/2-E' \\ F/2-C' & F/2-E' & F-F' \end{vmatrix}.$$

As regards to $\overline{\Delta}_2$ (s. (22)), the currents on the second column are expressed as in (18) and the admittance parameters C', E', F' within the third column are expressed as in (17). Usual calculations lead to the following expression of the voltage response:

$$(23)\qquad U_2=\frac{e_d y_5 F}{2n\overline{\Delta}}\begin{vmatrix} A+y_g-A' & y_1\,(y_2+y_3) & 1 \\ B-B' & y_2\,(y_1+y_4) & 1 \\ F/2-C' & (y_1+y_4)\,(y_2+y_3) & 2 \end{vmatrix}.$$

Relation (23) analytically reveals the demands for a high immunity of the longitudinal symmetrical circuits (inclusively *balanced circuits*) to longitudinal disturbing sources, as further on discussed. Each time it is considered that, excepting the named singular values, the components belonging to the disturbing circuit provide finite non-zero values.

R e m a r k s:

a) If $e_d \to 0$, the response U_2 is obviously zero. This requirement is known as *the decreasing of the emission level of the disturbing source.*

b) Another condition for a zero response U_2 is $y_5 \to 0$ (that is $z_5 \to \infty$). This requirement signifies *the decreasing of the disturbing source's available power.*

c) If the elements on the second column of the determinant within (23) are zero, then U_2 is also zero. Taking into account a whole frequency domain, this condition is fulfilled if $y_1=y_4=0$ (that is $z_1, z_4 \to \infty$), or if $y_2=y_3=0$ (that is $z_2, z_3 \to \infty$). These two requirements signify the *interrupt of the disturbing current's loop at the disturbed circuit's input or output.*

d) The response U_2 is also zero if the last two columns of the determinant within (23) are formed of proportional elements. This condition may be written as follows:

$$(24)\qquad y_1\,(y_2+y_3)=y_2\,(y_1+y_4)=\frac{1}{2}\,(y_1+y_4)\,(y_2+y_3).$$

From (24) it results:

$$y_1 = y_4, \quad y_2 = y_3. \tag{25}$$

The relations (25) are dual w.r.t. (14). They signify *the longitudinal symmetry of the passive network that connects the disturbing source to the disturbed circuit.*

R e m a r k:

If y_1, y_2, y_3 and y_4 physically belong to the electromagnetic environment, the conditions (25) cannot be generally achieved. In such situations, a common way for decreasing U_2 is to reduce the values of y_1, y_2, y_3 and y_4, as previously discussed. For this purpose, an *efficient separation* must be provided between the accessible terminals of the susceptible circuits and the terminals of the disturbing sources.

4. Application: The *Balancing* Requirement in Pair-Wire Transmission Systems

The pair-wire transmission line is a *longitudinal symmetrical* circuit. As stated in [6], this transmission line is characterized by the following three-port equations:

$$\begin{cases} U_1 = Z_c \operatorname{cth}\gamma l I_1 - \dfrac{Z_c}{\operatorname{sh}\gamma l} I_2 - \dfrac{Z_c}{2} \operatorname{th}\dfrac{\gamma l}{2} I_3, \\ U_2 = -\dfrac{Z_c}{\operatorname{sh}\gamma l} I_1 + Z_c \operatorname{cth}\gamma l I_2 - \dfrac{Z_c}{2} \operatorname{th}\dfrac{\gamma l}{2} I_3, \\ U_3 = -\dfrac{Z_c}{2} \operatorname{th}\dfrac{\gamma l}{2} I_1 - \dfrac{Z_c}{2} \operatorname{th}\dfrac{\gamma l}{2} I_2 + \dfrac{Z_c}{4} \left(\gamma l + 2 \operatorname{th}\dfrac{\gamma l}{2} \right) I_3. \end{cases} \tag{26}$$

In certain pair-wire transmission systems, the *longitudinal* disturbing paths often bind the *common nodes* within different equipment(s), as represented in Fig. 4.

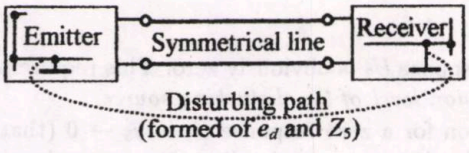

Fig. 4.– A *disturbs path*, often found in pair-wire transmission systems.

In these figure, the disturbing source formed by e_d and Z_5 is connected to the *longitudinal symmetrical* line by means of certain components that obviously belong to terminal equipment(s). They are identified within emitting equipment's output impedance and receiving equipment's input impedance, as represented in Fig. 5.

The steady-state equations within § **3** may now be written in the following conditions:

a) the disturbed circuit consists in the pair-wire transmission line, characterized by system (26);

b) the disturbing circuit is just represented in Fig. 3, wherein y_1, y_2, y_3 and y_4 are:

$$y_1 = \frac{1}{Z_{g1}},\quad y_2 = \frac{1}{Z_{r1}},\quad y_3 = \frac{1}{Z_{r2}},\quad y_4 = \frac{1}{Z_{g2}}. \tag{27}$$

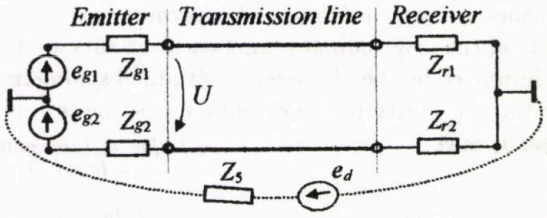

Fig. 5.– A *balanced* transmission system's schematics diagram.

For a high immunity of the considered transmission system, condition (25) must be fulfilled. Thus, from (25) and (27) may be analytically deduced the well-known balancing requirement with respect to electrical ground, both in the emitting and the receiving equipment:

$$Z_{g1} = Z_{g2} \quad \text{and} \quad Z_{r1} = Z_{r2}. \tag{28}$$

R e m a r k s:

a) With regard to signal's transmission, the essential constrains in Fig. 5 proceed from circuits' adapting and the desired voltage level, U, at the transmission line's input. By denoting Z_c the characteristic impedance of the transmission line, these constrains may be written as:

$$Z_{g1} + Z_{g2} = Z_c,\quad Z_{r1} + Z_{r2} = Z_c,\quad e_{g1} + e_{g2} = 2U. \tag{29}$$

b) In certain balanced equipment's service, a special attention is paid to the *symmetry* of the output signal with regard to emitter's common ground (that is $e_{g1} = e_{g2} = U$). Obviously, this adjusting requirement has no connection with the transmission systems' immunity.

c) Taking into account the adapting requirements within (29), from (28) it results:

$$Z_{g1} = Z_{g2} = Z_{r1} = Z_{r2} = \frac{Z_c}{2}. \tag{30}$$

For a suitable immunity of the pair-wire transmission system, these relations must be fulfilled in the whole frequency domain wherein the system's equipment(s) may be disturbed.

d) In the proposed modelling, the disturbing source is connected to *well-specified* common nodes. In certain situations, depending on electromagnetic environment, only adequate *shielding* and *grounding* of the considered equipment(s) achieve this assumption.

5. Conclusions

The analysis of the *four*-terminal circuits' behaviour with regard to conduced disturbing signals may be completely performed using the circuits' *three*-port characteristic equations. The so-called *balanced* circuits provide a high immunity only to certain pairs of disturbing signals. This property equally belongs to any *four*-terminal circuit that provides an *electrical* longitudinal symmetry.

The immunity of the longitudinal symmetrical circuits w.r.t. certain longitudinal disturbances is improved by the *electrical* longitudinal symmetry of the network that connects the disturbing source to the circuits' accessible terminals.

Received, September 11,2000

Technical University "Gh.Asachi", Jassy, Department of Telecommunications and
* *"Politehnica" University, Bucharest*

REFERENCES

1. M a t e e s c u Ad., *Analiza si sinteza circuitelor electrice*. Ed. Did. şi Pedag., Bucureşti, 1975.
2. A n t o n e s c u M., *Linii şi sisteme de transmisiuni telefonice*. Inst. polit. Iaşi, 1981.
3. M a d h u S., *Linear Circuit Analysis*. Prentice Hall, Englewood Cliffs, New Jersey, 1988.
4. Ş o r a C., *Cuadripolul electric*. Ed. Tehnică, Bucureşti, 1964.
5. B u z d u g a V., *On Four-terminal Circuits Modelling*. Bul. Inst. polit., Iaşi, **XLV(IL)**, *1-2*, s. Electrot., Energ., Electron., 27-37 (1999).
6. B u z d u g a V., *Contribuţii privind compatibilitatea electromagnetică în sisteme electronice cu transmisii de semnale prin cablu*. Ph.D.Diss., "Politehnica" Univ., Bucharest, 2000.

ASUPRA IMUNITĂŢII CIRCUITELOR
ECHILIBRATE LA PERTURBAŢII LONGITUDINALE

(Rezumat)

Se studiază imunitatea circuitelor care prezintă simetrie electrică *longitudinală*, în această clasă fiind incluse şi aşa-numitele circuite *echilibrate*. Pentru început se demonstrează că oricare circuit cu simetrie *electrică* longitudinală prezintă răspuns transversal nul la anumite *perechi* de excitaţii perturbatoare. Se stabileşte că imunitatea acestor circuite la perturbaţii cuplate *longitudinal* poate fi îmbunătăţită considerabil prin simetrizarea reţelei pasive care conectează sursa perturbatoare la terminalele de acces ale circuitelor. Ca aplicaţie este cercetată imunitatea la perturbaţii longitudinale a unui sistem de transmisie prin cablu bifilar.

BULETINUL INSTITUTULUI POLITEHNIC DIN IAŞI
Tomul XLVII (LI), Fasc. 1-2, 2001
ELECTROTEHNICĂ. ENERGETICĂ. ELECTRONICĂ

D.C. 621.316.1; 621.396.619

THE STEADY-STATE OF ELECTRICAL HOMOGENEOUS LONG LINES, EXCITED BY AN AMPLITUDE MODULATED SIGNAL WITH SUPPRESSED CARRIER

II. TYPICAL FORMS FOR VOLTAGE AND CURRENT RESPONSES

BY
AL.M. AVASILOAIE

By means of a symbolic representation of the Amplitude Modulated Signal with Suppressed Carrier (AMSC) at the input of an Electrical Homogeneous Long Line (EHLL), it is possible to get the voltage an current responses, in steady-state, as a sum of two AMSC oscillations, both for the general case of EHLL and for the EHLL without losses or distortions.

1. Introduction

In [3], we proved, using a symbolic method [1], (s. § **2**), that for an Electrical Homogeneous Long Line (EHLL), which has the *primary* (natural) parameters R_l, L_l, G_l, C_l, the following symbolic forms of equations w.r.t. the input of the line can be written:

$$(1)\qquad \begin{cases} \hat{U} = \hat{U}_1 \dfrac{e^{\hat{\gamma}(l-x)} + e^{-\hat{\gamma}(l-x)}}{2} - \hat{Z}_c \hat{I}_1 \dfrac{e^{\hat{\gamma}(l-x)} - e^{-\hat{\gamma}(l-x)}}{2}, \\ \hat{I} = -\dfrac{\hat{U}_1}{\hat{Z}_c} \cdot \dfrac{e^{\hat{\gamma}(l-x)} - e^{-\hat{\gamma}(l-x)}}{2} + \hat{I}_1 \dfrac{e^{\hat{\gamma}(l-x)} + e^{-\hat{\gamma}(l-x)}}{2}, \end{cases}$$

where $\hat{U}$, $\hat{I}$ are the symbolic expressions for voltage and current in a point of the EHLL, situated at a distance x from the output of the line, l – the length of the line, $\hat{U}$, $\hat{I}$ – the symbolic expressions for voltage and current at the input of the line, $\hat{\gamma}$ – the *hypercomplex constant of propagation* and $\hat{Z}_c$ – the *hypercomplex characteristic impedance.*

The expressions for $\hat{\gamma}$, $\hat{Z}_c$, obtained in [5], can be also, written as follows:

$$(2)\qquad \hat{\gamma} = \Gamma e^{i\varphi_1} e^{j\psi_1} e^{ij\chi_1} = \alpha_1 + i\beta_1 + j\beta_2 + ij\alpha_2,$$

where

$$(3)\qquad \begin{cases} \alpha_1 = \Gamma(\mathrm{ch}\chi_1 \cos\varphi_1 \cos\psi_1 + \mathrm{sh}\chi_1 \sin\varphi_1 \sin\psi_1), \\ \beta_1 = \Gamma(\mathrm{ch}\chi_1 \sin\varphi_1 \cos\psi_1 - \mathrm{sh}\chi_1 \cos\varphi_1 \sin\psi_1), \\ \beta_2 = \Gamma(\mathrm{ch}\chi_1 \cos\varphi_1 \sin\psi_1 - \mathrm{sh}\chi_1 \sin\varphi_1 \cos\psi_1), \\ \alpha_2 = \Gamma(\mathrm{ch}\chi_1 \sin\varphi_1 \sin\psi_1 + \mathrm{sh}\chi_1 \cos\varphi_1 \cos\psi_1), \end{cases}$$

$$(4)\qquad \Gamma=\sqrt[8]{[R_l+(\omega-\Omega)^2L_l^2][R_l^2+(\omega+\Omega)^2L_l^2][G_l^2+(\omega-\Omega)^2C_l^2][G_l^2+(\omega+\Omega)^2C_l^2]},$$

$$(5)\qquad \varphi_1=\frac{1}{4}\operatorname{arccotan}\frac{[R_lG_l+(\Omega^2-\omega^2)L_lC_l]^2+\Omega^2(R_lC_l-L_lG_l)^2-\omega^2(R_lC_l+L_lG_l)^2}{2\omega(R_lC_l+G_lL_l)[R_lG_l+(\Omega^2-\omega^2)L_lC_l]},$$

$$(6)\qquad \psi_1=\frac{1}{4}\operatorname{arccotan}\frac{[R_lG_l-(\Omega^2-\omega^2)L_lC_l]^2-\Omega^2(R_lC_l+L_lG_l)^2+\omega^2(R_lC_l-L_lG_l)^2}{2\Omega(R_lC_l+G_lL_l)[R_lG_l-(\Omega^2-\omega^2)L_lC_l]}+\frac{\pi}{2},$$

$$(7)\qquad \chi_1=\ln\sqrt[8]{\frac{[R_l^2+(\omega-\Omega)^2L_l^2][G_l^2+(\omega-\Omega)^2C_l^2]}{[R_l^2+(\omega+\Omega)^2L_l^2][G_l^2+(\omega+\Omega)^2C_l^2]}},$$

and

$$(8)\qquad \hat{Z}_c=Z_c\mathrm{e}^{\mathrm{i}\theta}\mathrm{e}^{\mathrm{j}\tau}\mathrm{e}^{\mathrm{ij}\xi}=z_{c1}+\mathrm{i}z_{c2}+\mathrm{j}z_{c3}+\mathrm{ij}z_{c4},$$

where

$$(9)\qquad \begin{cases} z_{c1}=Z_c(\mathrm{ch}\xi\cos\theta\cos\tau+\mathrm{sh}\xi\sin\theta\sin\tau),\\ z_{c2}=Z_c(\mathrm{ch}\xi\sin\theta\cos\tau-\mathrm{sh}\xi\cos\theta\sin\tau),\\ z_{c3}=Z_c(\mathrm{ch}\xi\cos\theta\sin\tau-\mathrm{sh}\xi\sin\theta\cos\tau),\\ z_{c4}=Z_c(\mathrm{ch}\xi\sin\theta\sin\tau+\mathrm{sh}\xi\cos\theta\cos\tau), \end{cases}$$

$$(10)\qquad Z_c=\ln\sqrt[8]{\frac{[R_l^2+(\omega+\Omega)^2L_l^2][R_l^2+(\omega-\Omega)^2L_l^2]}{[G_l^2+(\omega+\Omega)^2C_l^2][G_l^2+(\omega-\Omega)^2C_l^2]}},$$

$$(11)\qquad \theta=\frac{1}{4}\arctan\frac{2\omega(G_lL_l-R_lC_l)[R_lG_l-(\Omega^2-\omega^2)L_lC_l]}{[R_lG_l-(\Omega^2-\omega^2)L_lC_l]^2+\Omega^2(R_lC_l+L_lG_l)^2-\omega^2(R_lC_l-G_lL_l)^2},$$

$$(12)\qquad \tau=\frac{1}{4}\arctan\frac{2\Omega(G_lL_l-R_lC_l)[R_lG_l+(\Omega^2-\omega^2)L_lC_l]}{[R_lG_l+(\Omega^2-\omega^2)L_lC_l]^2-\Omega^2(R_lC_l-L_lG_l)^2+\omega^2(R_lC_l+G_lL_l)^2},$$

$$(13)\qquad \xi=\ln\sqrt[8]{\frac{[R_l^2+(\omega-\Omega)^2L_l^2][G_l^2+(\omega+\Omega)^2C_l^2]}{[R_l^2+(\omega+\Omega)^2L_l^2][G_l^2+(\omega-\Omega)^2C_l^2]}},$$

the voltage (an AMSC one) at the input of the EHLL being

$$u(t)=U_1\sin(\omega t+\varphi)\sin(\Omega t+\psi).$$

In [5], we have established that for input signals:

$$(14)\quad u_1(t) = U_1 \sin(\omega t + \varphi_U)\sin(\Omega t + \psi_U),\quad i_1(t) = I_1 \sin(\omega t + \varphi_I)\sin(\Omega t + \psi_I),$$

which may be symbolically represented by *special elements* (s. § **2**)

$$(15)\qquad \hat{U}_1 = U_1 e^{j\varphi_U} e^{j\psi_U},\quad \hat{I}_1 = I_1 e^{j\varphi_I} e^{j\psi_I},$$

the steady-state response for voltage and current can be considered, respectively, as a sum of eight colinear amplitude modulated signals, namely:

$$\begin{aligned}
&u(x,t) = \\
&= U_1 \frac{e^{(\alpha_1+\alpha_2)(l-x)} + e^{(\alpha_1-\alpha_2)(l-x)}}{4} \sin[\omega t + \beta_1(l-x) + \varphi_U] \sin[\Omega t + \beta_2(l-x) + \psi_U] + \\
&+ U_1 \frac{e^{(\alpha_1+\alpha_2)(l-x)} - e^{(\alpha_1-\alpha_2)(l-x)}}{4} \cos[\omega t + \beta_1(l-x) + \varphi_U] \cos[\Omega t + \beta_2(l-x) + \psi_U] + \\
&+ U_1 \frac{e^{-(\alpha_1-\alpha_2)(l-x)} + e^{-(\alpha_1+\alpha_2)(l-x)}}{4} \sin[\omega t - \beta_1(l-x) + \varphi_U] \sin[\Omega t - \beta_2(l-x) + \psi_U] - \\
&- U_1 \frac{e^{-(\alpha_1-\alpha_2)(l-x)} - e^{-(\alpha_1+\alpha_2)(l-x)}}{4} \cos[\omega t - \beta_1(l-x) + \varphi_U] \cos[\Omega t - \beta_2(l-x) + \psi_U] - \\
&- Z_c I_1 \frac{e^{(\alpha_1+\alpha_2)(l-x)+\xi} + e^{(\alpha_1-\alpha_2)(l-x)-\xi}}{4} \sin[\omega t + \beta_1(l-x) + \theta + \varphi_I] \times \\
&\times \sin[\Omega t + \beta_2(l-x) + \tau + \psi_I] - Z_c I_1 \frac{e^{(\alpha_1+\alpha_2)(l-x)+\xi} - e^{(\alpha_1-\alpha_2)(l-x)-\xi}}{4} \times \\
&\times \cos[\omega t + \beta_1(l-x) + \theta + \varphi_I] \cos[\Omega t + \beta_2(l-x) + \tau + \psi_I] + \\
&+ Z_c I_1 \frac{e^{-(\alpha_1-\alpha_2)(l-x)-\xi} + e^{-(\alpha_1+\alpha_2)(l-x)+\xi}}{4} \sin[\omega t - \beta_1(l-x) + \theta + \varphi_I] \times \\
&\times \sin[\Omega t - \beta_2(l-x) + \tau + \psi_I] - Z_c I_1 \frac{e^{-(\alpha_1-\alpha_2)(l-x)-\xi} - e^{-(\alpha_1+\alpha_2)(l-x)+\xi}}{4} \times \\
&\times \cos[\omega t - \beta_1(l-x) + \theta + \varphi_I] \cos[\Omega t - \beta_2(l-x) + \tau + \psi_I],
\end{aligned} \tag{16}$$

respectively

$$i(x,t) =$$

$$= I_1 \frac{e^{(\alpha_1+\alpha_2)(l-x)} + e^{(\alpha_1-\alpha_2)(l-x)}}{4} \sin[\omega t + \beta_1(l-x) + \varphi_I] \sin[\Omega t + \beta_2(l-x) + \psi_I] +$$

$$+ I_1 \frac{e^{(\alpha_1+\alpha_2)(l-x)} - e^{(\alpha_1-\alpha_2)(l-x)}}{4} \cos[\omega t + \beta_1(l-x) + \varphi_I] \cos[\Omega t + \beta_2(l-x) + \psi_I] +$$

$$+ I_1 \frac{e^{-(\alpha_1-\alpha_2)(l-x)} + e^{-(\alpha_1+\alpha_2)(l-x)}}{4} \sin[\omega t - \beta_1(l-x) + \varphi_I] \sin[\Omega t - \beta_2(l-x) + \psi_I] -$$

$$- I_1 \frac{e^{-(\alpha_1-\alpha_2)(l-x)} - e^{-(\alpha_1+\alpha_2)(l-x)}}{4} \cos[\omega t - \beta_1(l-x) + \varphi_I] \cos[\Omega t - \beta_2(l-x) + \psi_I] -$$

$$- \frac{U_1}{Z_c} \cdot \frac{e^{(\alpha_1+\alpha_2)(l-x)-\xi} + e^{(\alpha_1-\alpha_2)(l-x)+\xi}}{4} \sin[\omega t + \beta_1(l-x) - \theta + \varphi_U] \times \tag{17}$$

$$\times \sin[\Omega t + \beta_2(l-x) - \theta + \psi_U] - \frac{U_1}{Z_c} \cdot \frac{e^{(\alpha_1+\alpha_2)(l-x)-\xi} - e^{(\alpha_1-\alpha_2)(l-x)+\xi}}{4} \times$$

$$\times \cos[\omega t + \beta_1(l-x) - \theta + \varphi_U] \cos[\Omega t + \beta_2(l-x) - \tau + \psi_U] +$$

$$+ \frac{U_1}{Z_c} \cdot \frac{e^{-(\alpha_1-\alpha_2)(l-x)+\xi} + e^{-(\alpha_1+\alpha_2)(l-x)-\xi}}{4} \sin[\omega t - \beta_1(l-x) - \theta + \varphi_U] \times$$

$$\times \sin[\Omega t - \beta_2(l-x) - \tau + \psi_U] - \frac{U_1}{Z_c} \cdot \frac{e^{-(\alpha_1-\alpha_2)(l-x)+\xi} - e^{-(\alpha_1+\alpha_2)(l-x)-\xi}}{4} \times$$

$$\times \cos[\omega t - \beta_1(l-x) - \theta + \varphi_U] \cos[\Omega t - \beta_2(l-x) - \tau + \psi_U].$$

We will try to get the typical form of the responses, as a sum of two AMSC oscillations, dephased by $\pi/2$.

2. Symbolical Representation of AMSC

The symbolical method, proposed by A. B r a i e r [1], is based on the main idea to establish a correspondence between real functions of scalar argument and the elements of some algebra over the real field. In this way, a signal of type:

$$u(t) = e^{\delta t}[U' \sin(\omega t + \varphi) \sin(\Omega t + \psi) + U'' \cos(\omega t + \varphi) \cos(\Omega t + \psi)], \tag{18}$$

can be symbolically represented by an element $\hat{U}$ of a four order, associative and commutative, with unity element algebra, $\mathcal{A}_4$, over the real field $\mathbb{R}$, called P-Polynions Algebra (PPA), which can be written as:

$$\hat{u} = u_1 + iu_2 + ju_4 + iju_4, \quad u_1, ..., u_4 \in \mathbb{R}, \tag{19}$$

with:

$$\mathrm{i}^2 = \mathrm{j}^2 = -1, \qquad (\mathrm{ij})^2 = (\mathrm{ji})^2 = 1, \tag{20}$$

i, j, ij, being the elements of an arbitrary basis of PPA, and 1 – the unity element.

So, by means of the symbolical method, to the derivative $\mathrm{d}u/\mathrm{d}t$, which has a form similar to (18), corresponds the element $\hat{u}^* \in$ PPA, obtained with the relation:

$$\hat{u}^* = \hat{u}\hat{d} = \hat{d}\hat{u} = u_1^* + \mathrm{i}u_2^* + \mathrm{j}u_3^* + \mathrm{ij}u_4^*, \quad u_1^*, ..., u_4^* \in \mathbb{R}, \tag{21}$$

where element

$$\hat{d} = \delta + \mathrm{i}\omega + \mathrm{j}\Omega, \quad \delta, \omega, \Omega \in \mathbb{R}, \quad \hat{d} \in \mathrm{PPA}, \tag{22}$$

plays the rôle of a derivation operator.

There are taking place the relations:

$$\begin{cases} u_1 = U' \cos\varphi\cos\psi + U'' \sin\varphi\sin\psi, & u_2 = U' \sin\varphi\cos\psi - U'' \cos\varphi\sin\psi, \\ u_3 = U' \cos\varphi\sin\psi - U'' \sin\varphi\cos\psi, & u_4 = U' \sin\varphi\sin\psi + U'' \cos\varphi\cos\psi; \end{cases} \tag{23}$$

$$U' = \frac{1}{2}\left[\sqrt{(u_1+u_4)^2 + (u_2-u_3)^2} + \sqrt{(u_1-u_4)^2 + (u_2+u_3)^2}\right] > 0, \tag{24}$$

$$U'' = \frac{1}{2}[\mathrm{sign}(u_1u_4 - u_2u_3)]\left|\sqrt{(u_1+u_4)^2 + (u_2-u_3)^2} - \sqrt{(u_1-u_4)^2 + (u_2+u_3)^2}\right|; \tag{25}$$

$$\begin{aligned} \tan\varphi &= \frac{u_4U' - u_1U''}{u_3U' + u_2U''} = \frac{u_2U' + u_3U''}{u_1U' - u_4U''}, \\ \tan 2\varphi &= \frac{2(u_1u_2 + u_3u_4)}{u_1^2 - u_2^2 + u_3^2 - u_4^2} = \frac{(u_1+u_4)(u_2+u_3) + (u_1-u_4)(u_2-u_3)}{(u_1-u_4)(u_1+u_4) - (u_2-u_3)(u_2+u_3)}, \end{aligned} \tag{26}$$

$$\begin{aligned} \tan\psi &= \frac{u_4U' - u_1U''}{u_2U' + u_3U''} = \frac{u_3U' + u_2U''}{u_1U' - u_4U''}, \\ \tan 2\psi &= \frac{2(u_1u_3 + u_2u_4)}{u_1^2 + u_2^2 - u_3^2 - u_4^2} = \frac{(u_1+u_4)(u_2+u_3) - (u_1-u_4)(u_2-u_3)}{(u_1-u_4)(u_1+u_4) + (u_2-u_3)(u_2+u_3)}. \end{aligned} \tag{27}$$

The element (18) can be written under an exponential form:

$$\hat{u} = (U' + \mathrm{ij}U'')\mathrm{e}^{\mathrm{i}\varphi}\mathrm{e}^{\mathrm{j}\psi} = U\mathrm{e}^{\mathrm{i}\varphi}\mathrm{e}^{\mathrm{j}\psi}\mathrm{e}^{\mathrm{ij}\chi}, \tag{28}$$

where:

$$U = \sqrt{U'^2 - U''^2}, \qquad \tanh\chi = \frac{U''}{U'}. \tag{29}$$

If $U'' = 0$, $\delta = 0$, $u(t)$ is a non distortioned AMSC:

$$u(t) = U' \sin(\omega t + \varphi)\sin(\Omega t + \psi), \tag{30}$$

and the element $\hat{u}_s \in$ PPA, which represents the signal (30), is called *special polynion*, $u_1, ..., u_4$ becoming:

$$(31)\qquad \begin{cases} u_1 = U' \cos\varphi \cos\psi, & u_2 = U' \sin\varphi \cos\psi, \\ u_3 = U' \cos\varphi \sin\psi, & u_4 = U' \sin\varphi \sin\psi, \end{cases}$$

taking place the relations:

$$(32)\qquad u_1 u_4 = u_2 u_3, \qquad (33)\qquad \tan\varphi = \frac{u_4}{u_3} = \frac{u_2}{u_1}, \quad \tan\psi = \frac{u_3}{u_1} = \frac{u_4}{u_2},$$

$$(34)\qquad \frac{1}{\hat{u}} = \frac{1}{U'} e^{-i\varphi} e^{-j\psi}, \quad \hat{u} = U' e^{i\varphi} e^{j\psi}, \qquad (35)\qquad U' = \sqrt{u_1^2 + u_2^2 + u_3^2 + u_4^2}.$$

The exponential form (34) show that a special polynion results only by dividing or multiplying two special ones.

3. Determination of Typical Forms of Voltage and Current Steady-State Responses to an AMSC at the Input of an EHLL

3.1. General Case

Let be an EHLL, having the *natural* parameters R_l, L_l, G_l, C_l, the *secondary* ones, $\hat{\gamma}$, $\hat{Z}_c$, given by relations (2),...,(7), respectively (8),...,(13), excited by the input signals (14) symbolically represented by special elements (15) of PPA (20).

For determining the voltage steady-state response, let introduce the expressions (2_2), (8_2), (15) in the first equation of system (1). After some computations it results:

$$\begin{aligned} \hat{U} = \frac{1}{2}\Big\{ & U_1 e^{\alpha_1(l-x)} e^{i[\beta_1(l-x)+\varphi_U]} e^{j[\beta_2(l-x)+\psi_U]} e^{ij\alpha_2(l-x)} + \\ & + U_1 e^{-\alpha_1(l-x)} e^{-i[\beta_1(l-x)-\varphi_U]} e^{-j[\beta_2(l-x)-\psi_U]} e^{-ij\alpha_2(l-x)} - \\ & - Z_c I_1 e^{\alpha_1(l-x)} e^{i[\beta_1(l-x)+\theta+\varphi_I]} e^{j[\beta_2(l-x)+\tau+\psi_I]} e^{ij\alpha_2(l-x)+\xi} + \\ & + Z_c I_1 e^{-\alpha_1(l-x)} e^{-i[\beta_1(l-x)-\theta-\varphi_I]} e^{-j[\beta_2(l-x)-\tau-\psi_I]} e^{-ij\alpha_2(l-x)-\xi} \Big\} = \\ & = u_1 + iu_2 + ju_3 + iju_4. \end{aligned} \qquad (36)$$

For $u_1, ..., u_4$ are resulting the relations:

$$
\begin{aligned}
u_1 = \frac{1}{2}\Big\{ & U_1 e^{\alpha_1(l-x)} \mathrm{ch}\alpha_2(l-x)\cos[\beta_1(l-x)+\varphi_U]\cos[\beta_2(l-x)+\varphi_U]+ \\
& +U_1 e^{\alpha_1(l-x)} \mathrm{sh}\alpha_2(l-x)\sin[\beta_1(l-x)+\varphi_U]\sin[\beta_2(l-x)+\varphi_U]+ \\
& +U_1 e^{-\alpha_1(l-x)} \mathrm{ch}\alpha_2(l-x)\cos[\beta_1(l-x)-\varphi_U]\cos[\beta_2(l-x)-\psi_U]- \\
& -U_1 e^{-\alpha_1(l-x)} \mathrm{sh}\alpha_2(l-x)\sin[\beta_1(l-x)-\varphi_U]\sin[\beta_2(l-x)-\psi_U]- \\
& -Z_c I_1 e^{\alpha_1(l-x)} \mathrm{ch}[\alpha_2(l-x)+\xi]\cos[\beta_1(l-x)+\theta+\varphi_I]\cos[\beta_2(l-x)+\tau+\psi_I]- \\
& -Z_c I_1 e^{\alpha_1(l-x)} \mathrm{sh}[\alpha_2(l-x)+\xi]\sin[\beta_1(l-x)+\theta+\varphi_I]\sin[\beta_2(l-x)+\tau+\psi_I]+ \\
& +Z_c I_1 e^{-\alpha_1(l-x)} \mathrm{ch}[\alpha_2(l-x)-\xi]\cos[\beta_1(l-x)-\theta-\varphi_I]\cos[\beta_2(l-x)-\tau-\psi_I]- \\
& -Z_c I_1 e^{-\alpha_1(l-x)} \mathrm{sh}[\alpha_2(l-x)-\xi]\sin[\beta_1(l-x)-\theta-\varphi_I]\sin[\beta_2(l-x)-\tau-\psi_I]\Big\},
\end{aligned}
\tag{37}
$$

$$
\begin{aligned}
u_2 = \frac{1}{2}\Big\{ & U_1 e^{\alpha_1(l-x)} \mathrm{ch}\alpha_2(l-x)\sin[\beta_1(l-x)+\varphi_U]\cos[\beta_2(l-x)+\psi_U]- \\
& -U_1 e^{\alpha_1(l-x)} \mathrm{sh}\alpha_2(l-x)\cos[\beta_1(l-x)+\varphi_U]\sin[\beta_2(l-x)+\psi_U]- \\
& -U_1 e^{-\alpha_1(l-x)} \mathrm{ch}\alpha_2(l-x)\sin[\beta_1(l-x)-\varphi_U]\cos[\beta_2(l-x)-\psi_U]- \\
& -U_1 e^{-\alpha_1(l-x)} \mathrm{sh}\alpha_2(l-x)\cos[\beta_1(l-x)-\varphi_U]\sin[\beta_2(l-x)-\psi_U]- \\
& -Z_c I_1 e^{\alpha_1(l-x)} \mathrm{ch}[\alpha_2(l-x)+\xi]\sin[\beta_1(l-x)+\theta+\varphi_I]\cos[\beta_2(l-x)+\tau+\psi_I]+ \\
& +Z_c I_1 e^{\alpha_1(l-x)} \mathrm{sh}[\alpha_2(l-x)+\xi]\cos[\beta_1(l-x)+\theta+\varphi_I]\sin[\beta_2(l-x)+\tau+\psi_I]- \\
& -Z_c I_1 e^{-\alpha_1(l-x)} \mathrm{ch}[\alpha_2(l-x)-\xi]\sin[\beta_1(l-x)-\theta-\varphi_I]\cos[\beta_2(l-x)-\tau-\psi_I]- \\
& -Z_c I_1 e^{-\alpha_1(l-x)} \mathrm{sh}[\alpha_2(l-x)-\xi]\cos[\beta_1(l-x)-\theta-\varphi_I]\sin[\beta_2(l-x)-\tau-\psi_I]\Big\},
\end{aligned}
\tag{38}
$$

$$
\begin{aligned}
u_3 = \frac{1}{2}\Big\{ & U_1 e^{\alpha_1(l-x)} \mathrm{ch}\alpha_2(l-x)\cos[\beta_1(l-x)+\varphi_U]\sin[\beta_2(l-x)+\psi_U]- \\
& -U_1 e^{\alpha_1(l-x)} \mathrm{sh}\alpha_2(l-x)\sin[\beta_1(l-x)+\varphi_U]\cos[\beta_2(l-x)+\psi_U]- \\
& -U_1 e^{-\alpha_1(l-x)} \mathrm{ch}\alpha_2(l-x)\cos[\beta_1(l-x)-\varphi_U]\sin[\beta_2(l-x)-\psi_U]- \\
& -U_1 e^{-\alpha_1(l-x)} \mathrm{sh}\alpha_2(l-x)\sin[\beta_1(l-x)-\varphi_U]\cos[\beta_2(l-x)-\psi_U]- \\
& -Z_c I_1 e^{\alpha_1(l-x)} \mathrm{ch}[\alpha_2(l-x)+\xi]\cos[\beta_1(l-x)+\theta+\varphi_I]\sin[\beta_2(l-x)+\tau+\psi_I]+ \\
& +Z_c I_1 e^{\alpha_1(l-x)} \mathrm{sh}[\alpha_2(l-x)+\xi]\sin[\beta_1(l-x)+\theta+\varphi_I]\cos[\beta_2(l-x)+\tau+\psi_I]- \\
& -Z_c I_1 e^{-\alpha_1(l-x)} \mathrm{ch}[\alpha_2(l-x)-\xi]\cos[\beta_1(l-x)-\theta-\varphi_I]\sin[\beta_2(l-x)-\tau-\psi_I]- \\
& -Z_c I_1 e^{-\alpha_1(l-x)} \mathrm{sh}[\alpha_2(l-x)-\xi]\sin[\beta_1(l-x)-\theta-\varphi_I]\cos[\beta_2(l-x)-\tau-\psi_I]\Big\},
\end{aligned}
\tag{39}
$$

$$u_4 = \frac{1}{2}\Big\{U_1 e^{\alpha_1(l-x)} ch\alpha_2(l-x)\sin[\beta_1(l-x)+\varphi_U]\sin[\beta_2(l-x)+\psi_U]+$$

$$+U_1 e^{\alpha_1(l-x)} sh\alpha_2(l-x)\cos[\beta_1(l-x)+\varphi_U]\cos[\beta_2(l-x)+\psi_U]+$$

$$+U_1 e^{-\alpha_1(l-x)} ch\alpha_2(l-x)\sin[\beta_1(l-x)-\varphi_U]\sin[\beta_2(l-x)-\psi_U]-$$

$$-U_1 e^{-\alpha_1(l-x)} sh\alpha_2(l-x)\cos[\beta_1(l-x)-\varphi_U]\cos[\beta_2(l-x)-\psi_U]-$$

(40)

$$-Z_c I_1 e^{\alpha_1(l-x)} ch[\alpha_2(l-x)+\xi]\sin[\beta_1(l-x)+\theta+\varphi_I]\sin[\beta_2(l-x)+\tau+\psi_I]-$$

$$-Z_c I_1 e^{\alpha_1(l-x)} sh[\alpha_2(l-x)+\xi]\cos[\beta_1(l-x)+\theta+\varphi_I]\cos[\beta_2(l-x)+\tau+\psi_I]+$$

$$+Z_c I_1 e^{-\alpha_1(l-x)} ch[\alpha_2(l-x)-\xi]\sin[\beta_1(l-x)-\theta-\varphi_I]\sin[\beta_2(l-x)-\tau-\psi_I]-$$

$$-Z_c I_1 e^{-\alpha_1(l-x)} sh[\alpha_2(l-x)-\xi]\cos[\beta_1(l-x)-\theta-\varphi_I]\cos[\beta_2(l-x)-\tau-\psi_I]\Big\}.$$

Utilizing the relations (24),...,(27) we get for U', U'', φ, ψ the expressions:

$$U',U'' = \frac{1}{2\sqrt{2}}\Big[(U_1^2+Z_c^2 I_1^2 e^{2\xi})ch2(\alpha_1+\alpha_2)(l-x)+(U_1^2-Z_c^2 I_1^2 e^{2\xi})\cos 2(\beta_1-\beta_2)(l-x)-$$

$$-2U_1 Z_c I_1 e^{\xi}[sh2(\alpha_1+\alpha_2)(l-x)\cos(\varphi_U-\psi_U-\theta+\tau-\varphi_I+\psi_I)+$$

$$+\sin 2(\beta_1-\beta_2)(l-x)\sin(\varphi_U-\psi_U-\theta+\tau-\varphi_I+\psi_I)]\Big]^{1/2} \pm$$

(41)

$$\pm\Big[(U_1^2+Z_c^2 I_1^2 e^{-2\xi})ch2(\alpha_1-\alpha_2)(l-x)+(U_1^2-Z_c^2 I_1^2 e^{-2\xi})\cos 2(\beta_1+\beta_2)(l-x)-$$

$$-2U_1 Z_c I_1 e^{-\xi}[sh2(\alpha_1+\alpha_2)(l-x)\cos(\varphi_U+\psi_U-\theta-\tau-\varphi_I-\psi_I)+$$

$$+\sin 2(\beta_1+\beta_2)(l-x)\sin(\varphi_U+\psi_U-\theta-\tau-\varphi_I-\psi_I)]\Big]^{1/2},$$

(42)
$$2\varphi = \arctan\frac{(u_1+u_4)(u_2+u_3)+(u_1-u_4)(u_2-u_3)}{(u_1-u_4)(u_1+u_4)-(u_2-u_3)(u_2+u_3)},$$

(43)
$$2\psi = \arctan\frac{(u_1+u_4)(u_2+u_3)-(u_1-u_4)(u_2-u_3)}{(u_1-u_4)(u_1+u_4)+(u_2-u_3)(u_2+u_3)},$$

$$\operatorname{sign} U'' = \operatorname{sign}(u_1u_4 - u_2u_3) = \operatorname{sign}\Big\{U_1^2 \operatorname{sh}2\alpha_1(l-x)\operatorname{sh}2\alpha_2(l-x)+$$

$$+Z_c^2 I_1^2 \mathrm{e}^{2\xi}[\operatorname{ch}^2(\alpha_1+\alpha_2)(l-x) - \cos^2(\beta_1-\beta_2)(l-x)]+$$

$$+Z_c^2 I_1^2 \mathrm{e}^{-2\xi}[\cos^2(\beta_1+\beta_2)(l-x) - \operatorname{ch}^2(\alpha_1-\alpha_2)(l-x)]\Big\}+$$

$$+U_1 Z_c I_1 \mathrm{e}^{\xi}\Big\{\sin 2(\beta_1-\beta_2)(l-x)\sin[(\psi_U-\psi_I-\tau)-(\varphi_U-\varphi_I-\theta)]- \tag{44}$$

$$-\operatorname{sh}2(\alpha_1+\alpha_2)(l-x)\cos[(\psi_U-\psi_I-\tau)-(\varphi_U-\varphi_I-\theta)]\Big\}+$$

$$+U_1 Z_c I_1 \mathrm{e}^{-\xi}\Big\{\sin 2(\beta_1+\beta_2)(l-x)\sin[(\tau-\psi_U+\psi_I)-(\varphi_U-\varphi_I-\theta)]-$$

$$-\operatorname{sh}2(\alpha_1-\alpha_2)(l-x)\cos[(\tau-\psi_U+\psi_I)-(\varphi_U-\varphi_I-\theta)]\Big\},$$

where are taking place the relations (for $x' = l - x$):

$$(u_1+u_4)(u_2+u_3)+(u_1-u_4)(u_2-u_3) =$$

$$=\frac{1}{4}\Big\{U_1^2[\mathrm{e}^{2\alpha_1 x'}\sin 2(\beta_1 x'+\varphi_U) - \mathrm{e}^{-2\alpha_1 x'}\sin 2(\beta_1 x'-\varphi_U)-$$

$$-\mathrm{e}^{2\alpha_2 x'}\sin 2(\beta_2 x'-\varphi_U)+\mathrm{e}^{-2\alpha_2 x'}\sin 2(\beta_2 x'+\varphi_U)]+$$

$$+U_1 Z_c I_1[-\mathrm{e}^{2\alpha_1 x'-\xi}\sin(2\beta_1 x'+\theta+\varphi_I+\tau+\psi_I+\varphi_U-\psi_U)+$$

$$+\mathrm{e}^{-2\alpha_1 x'-\xi}\sin(-2\beta_1 x'+\theta+\varphi_I+\tau+\psi_I+\varphi_U-\psi_U)-$$

$$-\mathrm{e}^{2\alpha_1 x'+\xi}\sin(2\beta_1 x'+\theta+\varphi_I-\tau-\psi_I+\varphi_U+\psi_U)- \tag{45}$$

$$-\mathrm{e}^{-2\alpha_1 x'+\xi}\sin(2\beta_1 x'-\theta-\varphi_I+\tau+\psi_I-\varphi_U-\psi_U)-$$

$$-\mathrm{e}^{2\alpha_2 x'-\xi}\sin(2\beta_2 x'-\theta-\varphi_I-\tau-\psi_I-\varphi_U+\psi_U)-$$

$$-\mathrm{e}^{-2\alpha_2 x'-\xi}\sin(2\beta_2 x'+\theta+\varphi_I+\tau+\psi_I+\varphi_U-\psi_U)-$$

$$-\mathrm{e}^{2\alpha_2 x'+\xi}\sin(-2\beta_2 x'+\theta+\varphi_I-\tau-\psi_I+\varphi_U+\psi_U)+$$

$$+\mathrm{e}^{-2\alpha_2 x'+\xi}\sin(2\beta_2 x'+\theta+\varphi_I-\tau-\psi_I+\varphi_U+\psi_U)]+$$

$$+Z_c^2 I_1^2[\mathrm{e}^{2\alpha_1 x'}\sin 2(\beta_1 x'+\theta+\varphi_I) - \mathrm{e}^{-2\alpha_1 x'}\sin 2(\beta_1 x'-\theta-\varphi_I)+$$

$$+\mathrm{e}^{2\alpha_2 x'}\sin 2(\beta_2 x'-\theta-\varphi_I) - \mathrm{e}^{-2\alpha_2 x'}\sin 2(\beta_2 x'+\theta+\varphi_I)]\Big\},$$

$$(u_1+u_4)(u_2+u_3)-(u_1-u_4)(u_2-u_3)=$$

$$=\frac{1}{4}\Big\{U_1^2[\mathrm{e}^{2\alpha_1 x'}\sin 2(\beta_2 x'+\varphi_U)-\mathrm{e}^{-2\alpha_1 x'}\sin 2(\beta_2 x'-\psi_U)-$$

$$-\mathrm{e}^{2\alpha_2 x'}\sin 2(\beta_1 x'-\psi_U)+\mathrm{e}^{-2\alpha_2 x'}\sin 2(\beta_1 x'+\psi_U)]+$$

$$+U_1 Z_c I_1[-\mathrm{e}^{2\alpha_1 x'+\xi}\sin(2\beta_2 x'-\theta-\varphi_I+\tau+\psi_I+\varphi_U+\psi_U)-$$

$$-\mathrm{e}^{2\alpha_1 x'-\xi}\sin(2\beta_2 x'+\theta+\varphi_I+\tau+\psi_I-\varphi_U+\psi_U)-$$

$$-\mathrm{e}^{2\alpha_1 x'+\xi}\sin(2\beta_2 x'+\theta+\varphi_I-\tau-\psi_I-\varphi_U-\psi_U)-$$

$$-\mathrm{e}^{-2\alpha_1 x'-\xi}\sin(2\beta_2 x'-\theta-\varphi_I-\tau-\psi_I+\varphi_U-\psi_U)-$$

$$-\mathrm{e}^{2\alpha_2 x'-\xi}\sin(2\beta_1 x'-\theta-\varphi_I-\tau-\psi_I+\varphi_U+\psi_U)-$$

$$-\mathrm{e}^{-2\alpha_2 x'-\xi}\sin(2\beta_1 x'+\theta+\varphi_I+\tau+\psi_I-\varphi_U+\psi_U)+$$

$$+\mathrm{e}^{2\alpha_2 x'+\xi}\sin(2\beta_1 x'+\theta+\varphi_I-\tau-\psi_I-\varphi_U-\psi_U)+$$

$$+\mathrm{e}^{-2\alpha_2 x'+\xi}\sin(2\beta_1 x'-\theta-\varphi_I+\tau+\psi_I+\varphi_U+\psi_U)]+$$

$$+Z_c^2 I_1^2[\mathrm{e}^{2\alpha_1 x'}\sin 2(\beta_2 x'+\tau+\psi_I)-\mathrm{e}^{-2\alpha_1 x'}\sin 2(\beta_2 x'-\tau-\psi_I)+$$

$$+\mathrm{e}^{2\alpha_2 x'}\sin(2\beta_1 x'-\tau-\psi_I)-\mathrm{e}^{-2\alpha_2 x'}\sin 2(\beta_1 x'+\tau+\psi_I)]\Big\}, \tag{46}$$

$$(u_1+u_4)(u_1-u_4)+(u_2-u_3)(u_2+u_3)=$$

$$=\frac{1}{4}\Big\{U_1^2[\mathrm{e}^{2\alpha_1 x'}\cos 2(\beta_2 x'+\psi_U)+\mathrm{e}^{-2\alpha_1 x'}\cos 2(\beta_2 x'-\psi_U)+$$

$$+\mathrm{e}^{2\alpha_2 x'}\cos 2(\beta_1 x'-\psi_U)+\mathrm{e}^{-2\alpha_2 x'}\cos 2(\beta_1 x'+\psi_U)]+$$

$$+U_1 Z_c I_1[-\mathrm{e}^{2\alpha_1 x'-\xi}\cos(2\beta_2 x'-\varphi_U+\psi_U+\theta+\varphi_I+\tau+\psi_I)-$$

$$-\mathrm{e}^{2\alpha_1 x'+\xi}\cos(2\beta_2 x'-\theta-\varphi_I+\tau+\psi_I+\varphi_U+\psi_U)+$$

$$+\mathrm{e}^{2\alpha_2 x'-\xi}\cos(2\beta_1 x'+\varphi_U-\psi_U-\theta-\varphi_I-\tau-\psi_I)-$$

$$-\mathrm{e}^{2\alpha_2 x'+\xi}\cos(2\beta_1 x'+\theta+\varphi_I-\tau-\psi_I-\varphi_U-\psi_U)+$$

$$+\mathrm{e}^{-2\alpha_1 x'-\xi}\cos(2\beta_2 x'+\varphi_U-\psi_U-\theta-\varphi_I-\tau-\psi_I)+$$

$$+\mathrm{e}^{-2\alpha_1 x'+\xi}\sin(2\beta_2 x'+\theta+\varphi_I-\tau-\psi_I-\varphi_U-\psi_U)-$$

$$-\mathrm{e}^{-2\alpha_2 x'-\xi}\cos(2\beta_1 x'-\varphi_U+\psi_U+\theta+\varphi_I+\tau+\psi_I)+$$

$$+\mathrm{e}^{-2\alpha_2 x'+\xi}\cos(2\beta_1 x'-\theta-\varphi_I+\tau+\psi_I+\varphi_U+\psi_U)]+$$

$$+Z_c^2 I_1^2[\mathrm{e}^{2\alpha_1 x'}\cos 2(\beta_2 x'+\psi_I+\tau)+\mathrm{e}^{-2\alpha_1 x'}\cos 2(\beta_2 x'-\psi_I-\tau)-$$

$$-\mathrm{e}^{2\alpha_2 x'}\cos 2(\beta_1 x'-\psi_I-\tau)-\mathrm{e}^{-2\alpha_2 x'}\cos 2(\beta_1 x'+\psi_I+\tau)]\Big\}, \tag{47}$$

$$
\begin{aligned}
&(u_1+u_4)(u_1-u_4)-(u_2-u_3)(u_2+u_3)= \\
&=\frac{1}{4}\Big\{U_1^2[\mathrm{e}^{2\alpha_1 x'}\cos(2\beta_1 x'+\varphi_U)+\mathrm{e}^{-2\alpha_1 x'}\cos(2\beta_1 x'-\varphi_U)+ \\
&+\mathrm{e}^{2\alpha_2 x'}\cos 2(\beta_2 x'-\varphi_U)+\mathrm{e}^{-2\alpha_2 x'}\cos 2(\beta_2 x'+\psi_U)]+ \\
&+U_1 Z_c I_1[-\mathrm{e}^{2\alpha_1 x'-\xi}\cos(2\beta_1 x'+\varphi_U-\psi_U+\theta+\varphi_I+\tau+\psi_I)- \\
&-\mathrm{e}^{2\alpha_1 x'+\xi}\cos(2\beta_1 x'+\theta+\varphi_I-\tau-\psi_I+\varphi_U+\psi_U)+ \\
&+\mathrm{e}^{2\alpha_2 x'-\xi}\cos(2\beta_2 x'-\varphi_U+\psi_U-\theta-\varphi_I-\tau-\psi_I)- \\
&-\mathrm{e}^{2\alpha_2 x'+\xi}\cos(2\beta_2 x'-\theta-\varphi_I+\tau+\psi_I-\varphi_U-\psi_U)+ \\
&+\mathrm{e}^{-2\alpha_1 x'-\xi}\cos(2\beta_1 x'-\varphi_U+\psi_U-\theta-\varphi_I-\tau-\psi_I)+ \\
&+\mathrm{e}^{-2\alpha_1 x'+\xi}\sin(2\beta_1 x'-\theta-\varphi_I+\tau+\psi_I-\varphi_U-\psi_U)- \\
&-\mathrm{e}^{-2\alpha_2 x'-\xi}\cos(2\beta_2 x'+\varphi_U-\psi_U+\theta+\varphi_I+\tau+\psi_I)+ \\
&+\mathrm{e}^{-2\alpha_2 x'+\xi}\cos(2\beta_2 x'+\theta+\varphi_I-\tau-\psi_I+\varphi_U+\psi_U)]+ \\
&+Z_c^2 I_1^2[\mathrm{e}^{2\alpha_1 x'}\cos 2(\beta_1 x'+\theta+\varphi_I)+\mathrm{e}^{-2\alpha_1 x'}\cos 2(\beta_1 x'-\theta-\varphi_I)- \\
&-\mathrm{e}^{2\alpha_2 x'}\cos 2(\beta_2 x'-\theta-\varphi_I)-\mathrm{e}^{-2\alpha_2 x'}\cos 2(\beta_2 x'+\theta+\varphi_I)]\Big\}.
\end{aligned}
\tag{48}
$$

In relations (36),...,(48), α_1, α_2, β_1, β_2, Z_c, θ, τ, ξ, are given, respectively, by the expressions (3_1), (3_4), (3_2), (3_3), (10),...,(13).

According to the mentioned symbolic method, to the element (36_2) corresponds a function which has a form similar to (18), for $\delta = 0$:

$$
\begin{aligned}
u(x,t) &= U'(x)\sin[\omega t+\varphi(x)]\sin[\Omega t+\psi(x)]+ \\
&+U''(x)\cos[\omega t+\varphi(x)]\cos[\Omega t+\psi(x)] = u_1(x,t)+u_2(x,t),
\end{aligned}
\tag{49}
$$

where $U'(x)$, $U''(x)$, $\varphi(x)$, $\psi(x)$ are given by relations (41),...,(44).

That means that in every point, at distance x from the output of an EHLL, excited at the input by an AMSC, the voltage steady-state response is a modulated and distortioned signal which is a sum of two signals namely, the *main component*, $u_1(x,t)$ and the *distortioned component*, $u_2(x,t)$, that are amplitude modulated signals with suppressed carrier, having the phases of the modulation (terms in ω) and of the oscillation (terms in Ω) dephased by $\pi/2$.

The current steady-state response has a form similar to (48), (because of the similarity between the second equation of the system (1) and the first one). Consequently:

$$
i(x,t) = I'(x)\sin[\omega t+\varphi'(x)]\sin[\Omega t+\psi'(x)]+I''(x)\cos[\omega t+\varphi'(x)]\cos[\Omega t+\psi'(x)],
\tag{50}
$$

where $I'(x)$, $I''(x)$, $\varphi'(x)$, $\psi'(x)$ have expressions similar to (41),...,(44) in which U_1, Z_cI_1, φ_U, ψ_U, φ_I, θ, τ, ξ must be replaced with I_1, U_1/Z_c, φ_I, ψ_I, φ_U, ψ_U, $-\theta$, $-\tau$, $-\xi$, respectively.

The same substitution must to be accomplished in the relations (37),...,(40), (45),...,(48), for obtaining $i_1, ..., i_4$ instead of $u_1, ..., u_4$.

3.2. Particular Cases

a) *EHLL without Losses*

In the case of EHLL without losses, we proved [3], [5], that $\hat{\gamma}$, $\hat{Z}_c$ have the expressions:

$$\hat{\gamma} = \hat{d}\sqrt{L_lC_l} = \mathrm{i}\omega\sqrt{L_lC_l} + \mathrm{j}\Omega\sqrt{L_lC_l}, \quad R_l = G_l = 0, \tag{51}$$

$$\hat{Z}_c = \sqrt{\frac{L_l}{C_l}} = Z_c, \tag{52}$$

that means:

$$\alpha_1 = \alpha_2 = 0, \quad \beta_1 = \omega\sqrt{L_lC_l}, \quad \beta_2 = \Omega\sqrt{L_lC_l}, \tag{53}$$

$$z_{c1} = Z_c = \sqrt{\frac{L_l}{C_l}}, \quad z_{c2} = z_{c3} = z_{c4} = 0, \quad \theta = \tau = \xi = 0. \tag{54}$$

The relations (37),...,(40) become more simple:

$$\begin{aligned} u_1 = \frac{1}{2}\Bigg(& U_1\Big\{\cos[\omega\sqrt{L_lC_l}(l-x)+\varphi_U]\cos[\Omega\sqrt{L_lC_l}(l-x)+\psi_U]+ \\ & +\cos[\omega\sqrt{L_lC_l}(l-x)-\varphi_U]\cos[\Omega\sqrt{L_lC_l}(l-x)-\psi_U]\Big\}- \\ & -\sqrt{\frac{L_l}{C_l}}I_1\Big\{\cos[\omega\sqrt{L_lC_l}(l-x)+\varphi_I]\cos[\Omega\sqrt{L_lC_l}(l-x)+\psi_I]- \\ & -\cos[\omega\sqrt{L_lC_l}(l-x)-\varphi_I]\cos[\Omega\sqrt{L_lC_l}(l-x)-\psi_I]\Big\}\Bigg), \end{aligned} \tag{55}$$

$$\begin{aligned} u_2 = \frac{1}{2}\Bigg(& U_1\Big\{\sin[\omega\sqrt{L_lC_l}(l-x)+\varphi_U]\cos[\Omega\sqrt{L_lC_l}(l-x)+\psi_U]- \\ & -\sin[\omega\sqrt{L_lC_l}(l-x)-\varphi_U]\cos[\Omega\sqrt{L_lC_l}(l-x)-\psi_U]\Big\}- \\ & -\sqrt{\frac{L_l}{C_l}}I_1\Big\{\sin[\omega\sqrt{L_lC_l}(l-x)+\varphi_I]\cos[\Omega\sqrt{L_lC_l}(l-x)+\psi_I]+ \\ & +\sin[\omega\sqrt{L_lC_l}(l-x)-\varphi_I]\cos[\Omega\sqrt{L_lC_l}(l-x)-\psi_I]\Big\}\Bigg), \end{aligned} \tag{56}$$

$$u_3 = \frac{1}{2}\Bigg(U_1\Big\{\cos[\omega\sqrt{L_lC_l}(l-x)+\varphi_U]\sin[\Omega\sqrt{L_lC_l}(l-x)+\psi_U]-$$
$$-\cos[\omega\sqrt{L_lC_l}(l-x)-\varphi_U]\sin[\Omega\sqrt{L_lC_l}(l-x)-\psi_U]\Big\}-$$
$$-\sqrt{\frac{L_l}{C_l}}I_1\Big\{\cos[\omega\sqrt{L_lC_l}(l-x)+\varphi_I]\sin[\Omega\sqrt{L_lC_l}(l-x)+\psi_I]+ \tag{57}$$
$$+\cos[\omega\sqrt{L_lC_l}(l-x)-\varphi_I]\sin[\Omega\sqrt{L_lC_l}(l-x)-\psi_I]\Big\}\Bigg),$$

$$u_4 = \frac{1}{2}\Bigg(U_1\Big\{\sin[\omega\sqrt{L_lC_l}(l-x)+\varphi_U]\sin[\Omega\sqrt{L_lC_l}(l-x)+\psi_U]+$$
$$+\sin[\omega\sqrt{L_lC_l}(l-x)-\varphi_U]\sin[\Omega\sqrt{L_lC_l}(l-x)-\psi_U]\Big\}-$$
$$-\sqrt{\frac{L_l}{C_l}}I_1\Big\{\sin[\omega\sqrt{L_lC_l}(l-x)+\varphi_I]\sin[\Omega\sqrt{L_lC_l}(l-x)+\psi_I]- \tag{58}$$
$$-\sin[\omega\sqrt{L_lC_l}(l-x)-\varphi_I]\sin[\Omega\sqrt{L_lC_l}(l-x)-\psi_I]\Big\}\Bigg),$$

and also the relation (s. (41)):

$$U', U'' =$$
$$= \frac{1}{2}\Bigg(\Bigg\{U_1^2\cos^2[(\omega-\Omega)\sqrt{L_lC_l}(l-x)] - \sqrt{\frac{L_l}{C_l}}U_1I_1\sin[2(\omega-\Omega)\sqrt{L_lC_l}(l-x)]\times$$
$$\times\sin(\varphi_U-\psi_U-\varphi_I+\psi_I)+\frac{L_l}{C_l}I_1^2\sin^2[(\omega-\Omega)\sqrt{L_lC_l}]\Bigg\}^{1/2}\pm \tag{59}$$
$$\pm\Bigg\{U_1^2\cos^2[(\omega+\Omega)\sqrt{L_lC_l}(l-x)] - \sqrt{\frac{L_l}{C_l}}U_1I_1\sin[2(\omega+\Omega)\sqrt{L_lC_l}(l-x)]\times$$
$$\times\sin(\varphi_U+\psi_U-\varphi_I-\psi_I)+\frac{L_l}{C_l}I_1^2\sin^2[(\omega+\Omega)\sqrt{L_lC_l}]\Bigg\}^{1/2}\Bigg)$$

and (s. (44)):

$$\operatorname{sign}U'' = \operatorname{sign}\Bigg(\Bigg(\sqrt{\frac{L_l}{C_l}}I_1\Bigg)^2\Big\{-\sin[2\omega\sqrt{L_lC_l}(l-x)]\sin[2\Omega\sqrt{L_lC_l}(l-x)]\Big\}+$$
$$+U_1I_1\sqrt{\frac{L_l}{C_l}}\Big\{\sin[2(\omega-\Omega)\sqrt{L_lC_l}(l-x)]\sin(\psi_U-\psi_I-\varphi_U+\varphi_I)+ \tag{60}$$
$$+\sin[2(\omega+\Omega)\sqrt{L_lC_l}(l-x)]\sin(-\psi_U+\psi_I-\varphi_U+\varphi_I)\Big\}\Bigg).$$

b) *EHLL without Distortions*

For this case, taking in account Heaviside's condition:

$$\frac{R_l}{L_l} = \frac{G_l}{C_l},$$

the expressions for $\hat{\gamma}$ and $\hat{Z}_c$ become:

$$\hat{\gamma} = R_l\sqrt{\frac{C_l}{L_l}} + \mathrm{i}\omega\sqrt{L_lC_l} + \mathrm{j}\Omega\sqrt{L_lC_l}, \quad \alpha_1 = R_l\sqrt{\frac{C_l}{L_l}}, \quad \beta_1 = \omega\sqrt{L_lC_l}, \tag{61}$$

$$\beta_2 = \Omega\sqrt{L_lC_l}, \quad \alpha_2 = 0,$$

respectively:

$$\hat{Z}_c = \sqrt{\frac{L_l}{C_l}} = Z_c, \quad z_{c1} = Z_c, \quad z_{c2} = z_{c3} = z_{c4} = 0, \quad \theta = \tau = \xi = 0. \tag{62}$$

The expressions (37),...,(48) change, corresponding to the substitution of α_1, β_1, β_2, α_2, Z_c, by the values given in (61), (62).

4. Conclusions

1. By means of a symbolic representation (s. § **2**) are obtained the voltage or current steady-state response of an EHLL to an AMSC input excitation, both in the general case and in the particular cases of EHLL without losses or distortions, considering the EHLL as a linear system.

2. The steady-state response results as a composition of two AMSC, *the main* and *the distortioned* components, dephased by $\pi/2$; this form of the response, (49), (50), are denoted as the *typical forms of voltage or current responses.*

3. There are established the expressions (37),...,(44) of the components of the polynion (element of PPA) which represents symbolically the voltage response. All of them are depending, finally, of the natural parameters R_l, L_l, G_l, C_l of EHLL, as well as of the length, l, of the EHLL and of the point x (as distance from the output) where the response is determined.

4. In general, in every point of the EHLL (excepting the input point $x = l$), the responses (49), (50) will be distortioned. The particular cases (if possible) when the signals will be not distortioned, as well as the study of signs of relations (42), (43), (44), will be the subject of a next paper.

Received, December 8, 2000

Technical University "Gh.Asachi", Jassy,
Department of Electrotechnics

REFERENCES

1. B r a i e r A., *Utilizarea algebrelor pe corpul real în mecanica vibraţiilor.* Ph. D. Diss., Polyt. Inst., Jassy, 1968.
2. B r a i e r A., R o s m a n H., *A Symbolic Study of Linear Systems Responses to Amplitude Modulation Inputs.* Bul. Inst. polit., Iaşi, **XLI (XLV)**, *3-4*, s.III, 25-36 (1995).
3. A v a s i l o a i e A., *Contributions to the Study of Propagation of Amplitude Modulation Signals Along Homogeneous Electrical Long Lines, in Steady-State.* Bul. Inst. polit., Iaşi, **XLV (IL)**, *1-2*, s.III, 51-61 (1999).
4. A v a s i l o a i e A., *Hypercomplex Expressions of Secondary Parameters of an Homogeneous Electrical Long Line, Excited by an Amplitude Modulated Signal with Suppressed Carrier (AMSC).* Bul. Inst. polit., Iaşi, **XLV (IL)**, *3-4*, s.III, 53-61 (1999).
5. A v a s i l o a i e A., *The Steady-State of Electrical Homogeneous Long Lines, Excited by an Amplitude Modulated Signal with Suppressed Carrier.* I. *Voltage and Current Waves.* Bul. Inst. polit., Iaşi, **XLVI (L)**, *3-4*, s. Electrot., Energ., Electron. (2000).

REGIMUL PERMANENT AL LINIILOR ELECTRICE OMOGENE LUNGI EXCITATE DE SEMNALE MODULATE ÎN AMPLITUDINE CU PURTĂTOAREA SUPRIMATĂ

II. Formule tipice ale răspunsurilor în tensiune şi curent

(Rezumat)

Cu ajutorul unei reprezentări simbolice a semnalelor modulate în amplitudine, cu purtătoarea suprimată [1], este posibil să se obţină forme ale răspunsului în curent şi tensiune, în regim permanent, ca o sumă de două semnale modulate în amplitudine cu purtătoarea suprimată, având fazele modulaţiei şi oscilaţiei în cuadratură. Se studiază cazul general ca şi cazurile particulare ale liniilor electrice lungi omogene fără pierderi sau fără distorsiuni.

BULETINUL INSTITUTULUI POLITEHNIC DIN IAŞI
Tomul XLVII (LI), Fasc. 1–2, 2001
ELECTROTEHNICĂ. ENERGETICĂ. ELECTRONICĂ

D.C. 621.394.9

WEIGHT DISTRIBUTION OF BINARY CYCLIC CODES

BY
VALERIU MUNTEANU and DANIELA TĂRNICERIU

Let s and k be integers such that s is a divisor of $2^k - 1$. Let $g(x)$ be a divisor of $x^s - 1$ over GF(2). The binary cyclic code C of length $N = 2^k - 1$ generated by $(x^N - 1)/g(x)p(x)$ is considered. For special cases, the weight distribution of C is determined by using the weights of the cyclic code of length s generated by $(x^s - 1)/g(x)$.

1. Introduction

The classical definitions and results for coding theory can be found in [1]. The words of a cyclic code are described by the polynomial representation. A binary cyclic code is called *primitive* if its length is $N = 2^k - 1$ for any integer k. In this paper we consider the case when the check polynomial of such a code is the product of two special irreducible divisors of $x^N - 1$ over GF(2).

Let s and k be integers such that s is a divisor of $2^k - 1$. Let $g(x)$ be a divisor of $x^s - 1$ over GF(2), and let $p(x)$ be a primitive polynomial of degree k over GF(2).

We consider the binary cyclic code C of length $N = 2^k - 1$ generated by $(x^N - 1)/g(x)p(x)$.

For special cases we determine the weight distribution of C by using the weights of the cyclic code of length s generated by $(x^s - 1)/g(x)$.

2. Preliminaries

2.1. Notations

If GF(q) is the finite field of order q and h is any integer, $h \geq 1$, we recall that the trace of GF(q^k) over GF(q) is defined by $\mathrm{tr}(z) = z + z^q + ... + z^{q^i} + ... + z^{q^{k-1}}$. If i divides j, then the trace of GF(2^j) over GF(2^i) is denoted by tr_i^j. If γ is in a extension field of GF(2), its minimal polynomial is denoted by $m_\gamma(x)$.

If $a(x) = \sum_{i=0}^{n} a_i x^i \in \mathrm{GF}_q[x]$, then:

a) the reciprocal polynomial of $a(x)$ is denoted by $a(x)$, that is, $a(x) = x^d a(x^{-1})$, where d is the degree of $a(x)$;

b) the support of $a(x)$ is $\text{supp}[a(x)] = \{i \varepsilon N : 0 \leq i \leq r \text{ and } a_i \neq 0\}$;

c) the weight of $a(x)$ is $w[a(x)] = |\text{supp}[a(x)]|$.

If $\underline{a} = (a_j)_{j \in J} \in (\text{GF}(q^k))^j$, then $f_{\underline{a}}(x)$ is the polynomial over GF (q^k) defined by $f_{\underline{a}}(x) = \sum_{j \in J} a_j x^j$.

In the following we consider a fixed integer k and we denote $F = \text{GF}(2^k)$ and $F^* = \text{GF}(2^k) \setminus \{0\}$.

2.2. The Trace Function Description of a Cyclic Code

If C is a cyclic code of length L over GF(2) generated by $g(x)$, then the check polynomial $h(x)$ of C is classically defined by $x^L - 1 = g(x)h(x)$ over GF(2). Also recall that the generator polynomial of $C^\perp$ (orthogonal code of C), is $\tilde{h}(x)$.

The following proposition is a version of the main property of the M a t t s o n - S o l o m o n transform [2], and was introduced by several authors:

P r o p o s i t i o n 1. *Let C be a cyclic code of length L over* GF(2), *with L odd. Let* GF(2^h) *be the splitting field of $x^L - 1$ over* GF(2) *and let tr denote the trace of* GF(2^h) *over* GF(2). *Let β be a primitive L^{th} root of unity over* GF(2) *and let $\tilde{h}(x)$ be the generator polynomial of $C^\perp$.*

If J is a subset of $\{0, 1, \ldots, L-1\}$ such that $\tilde{h}(x) = \prod_{j \in J} m_{\beta^j}(x)$, then C is the set of words

$$c_{\underline{a}}(x) = \sum_{i=0}^{L-1} \text{tr}(f_{\underline{a}}(\beta^i))x^i, \quad \textit{where } f_{\underline{a}}(x) = \sum_{j \in J} a_j x^j, \ \underline{a} = (a_j)_{j \in J} \in (\text{GF}(2^h))^J.$$

D e f i n i t i o n 1. With the notations of Proposition 1, if

$$h(x) = \prod_{j \in J} m_{\beta^j}(x),$$

then J is called a check set of C relatively to β.

2.3. Presentation of the Codes

Let n, s and k be integers such that $ns = 2^k - 1$. Let $g(x)$ be a divisor of $x^s - 1$ over GF(2) and let $p(x)$ be a primitive polynomial of degree k over GF(2). Let α be in GF(2^k) such that α^{-1} is a root of $p(x)$. In this way, $p(x)$ is the minimal polynomial of α^{-1}. Define $\delta = \alpha^s$ and $\gamma = \alpha^n$. We consider the following binary codes: a) the cyclic code, C, of length $N = 2^k - 1$ generated by $(x^N - 1)/g(x)p(x)$; b) the cyclic code, Γ, of length s generated by $(x^s - 1)/g(x)$; c) the cyclic code, Δ, of length n, generated by $(x^n - 1)m_\varepsilon(x)$ with $\varepsilon = \delta^{-1}$.

Let GF(2^γ) be the splitting field of $x^s - 1$ over GF(2) and let GF(2^m) be the splitting field of $x^n - 1$ over GF(2).

From Proposition 1, we deduce the following description of Γ, Δ and C, and their weights:

1° C o d e Γ. If

$$\tilde{g}(x) = \prod_{j \in J} m_{\gamma^j}(x) = \prod_{j \in J} m_{\alpha^{nj}}(x)$$

then

$$\Gamma = \left\{ \mu_{\underline{u}}(x) = \sum_{i=0}^{s-1} \left[\mathrm{tr}_1^r \left[f_{\underline{u}}(\gamma^j) \right] \right] x^i : \underline{u} \in (\mathrm{GF}(2^\gamma))^J \right\}, \tag{1}$$

where

$$f_{\underline{u}}(x) = \sum_{j \in J} u_j x^j, \text{ with } \underline{u} = (u_j)_{j \in J} \in (\mathrm{GF}(2^\gamma))^J,$$

$$w\left[\mu_{\underline{u}}(x)\right] = \zeta \left\{ 0 \leq i \leq s-1 : \mathrm{tr}_1^\gamma \left[f_{\underline{u}}(\gamma^i) \right] = 1 \right\}, \tag{2}$$

where ζ denotes the size.

2° C o d e Δ, with:

$$\Delta = \left\{ v_b(x) = \sum_{i=0}^{n-1} \left[\mathrm{tr}_1^m (b\delta^i) \right] x^i : b \in \mathrm{GF}(2^m) \right\}, \tag{3}$$

$$w\left[v_b(x)\right] = \zeta \left\{ 0 \leq i \leq n-1 : \mathrm{tr}_1^m \left(b\delta^i \right) = 1 \right\}. \tag{4}$$

3° C o d e C. If J is the γ-check set of Γ, then the *alpha*-check set of C is $\{1\}U(nJ)$. Therefore,

$$C = \left\{ m_{(a,\underline{v})}(x) = \sum_{i=0}^{2^k-2} \left[\mathrm{tr}_1^k \left[a\alpha^i + f_{\underline{v}}(\alpha^{in}) \right] \right] x^i : a \in \mathrm{GF}(2^k) \text{ and } \underline{v} \in \mathrm{GF}(2^k))^J \right\}, \tag{5}$$

where

$$f_{\underline{v}}(x) = \sum_{j \in J} v_j x^j \text{ if } \underline{v} = (v_j)_{j \in J} \in (\mathrm{GF}(2^k))^J.$$

Denote the weight $w[m_{(a,\underline{v})}(x)]$ by $w[a, \underline{v})$. Then

$$\begin{aligned} ww[a, \underline{v}] &= \zeta \left\{ 0 \leq i \leq 2^k - 2 : \mathrm{tr}_1^k(a\alpha) + \mathrm{tr}_1^k[f_{\underline{v}}(\alpha^{in})] = 1 \right\} = \\ &= \zeta \left\{ x \in F^* : \mathrm{tr}_1^k(ax) + \mathrm{tr}_1^k(zx^n)] = 1 \right\}. \end{aligned} \tag{6}$$

3. The Weight of C

The following theorem gives a description of weights of C by means of the weights of Γ and certain weights of Δ.

T h e o r e m. *Let* $\delta \doteq \alpha^s$. *Let* $\mathrm{GF}(2^m)$ *be the splitting field of* $x^n - 1$ *over* $\mathrm{GF}(2)$ *and let be* $\mathrm{GF}(2^m)$. *Define*

$$\underline{v}_b(x) = \sum_{i=0}^{n-1} \mathrm{tr}_1^m(b\delta^i)x^i$$

Then the set of nonzero weights of C *is the set of all integers of the kind:*

a) $2^k - 1$;

b) $nw[\mu(x)]$, *where* $\mu(x) \in \Gamma\backslash\{0\}$;

c) $2^{k-1} + nw[\mu(x)] - 2\sum_{e\in S} w[\underline{v}_{b_e}(x)]$, *where* $\mu(x) \in \Gamma\backslash\{0\}$;

d) $S = \mathrm{supp}[\mu(x)]$, $b_e = \mathrm{tr}_m^k(a, \alpha^e)$, *and* $a \in \mathrm{GF}(2^k)$.

In other words, the characteristic function in F^* of $\overline{H}_a$ is $h(x) = \mathrm{tr}(ax)$ and the characteristic function in F^* of $E(\underline{v})$ is $\mathrm{tr}_1^k[f_{\underline{v}}(x^n)]$.

It comes from (6) that $w(a, \underline{v})$ is the number of solutions in F^* of $\mathrm{tr}_1^k(ax) + \mathrm{tr}_1^k[f_{\underline{v}}(x^n)]$, which is also the cardinality of the symmetric difference $\overline{H}_a \delta E(\underline{v})$. Then,

$$w(a, \underline{v}) = \left|\overline{H}_a \Delta E(\underline{v})\right| = \left|\overline{H}_a\right| + |E(\underline{v})| - 2\left|\overline{H}_a \cap E(\underline{v})\right|. \tag{7}$$

Now, we need to calculate the cardinalities of the sets: $\overline{H}_a$, $E(\underline{v})$ and $\overline{H}_a \cap E(\underline{v})$. The case $\underline{v} = 0$ is a trivial one and we now assume $\underline{v} \neq \underline{0}$. Obviously:

$$\text{if } a = 0, \text{ then } \left|\overline{H}_a\right| = 0; \text{ if } a \neq 0, \text{ then } \left|\overline{H}_a\right| = 2^{k-1}. \tag{8}$$

3.1. Calculation of $|E(\underline{v})|$

From the definition of α and γ, we know that $\gamma^i = (\alpha^i)^n$. Let us consider the multiplicative subgroup G_n of the n^{th} roots of unity in F^*. Because $ns = 2^k - 1$, the distinct classes mod G_n are equals to $\alpha^e G_n$ with $0 \leq e \leq s-1$. From the definition, if z belongs to $E(\underline{v})$ alike behave the members of zG_n. Consequently, $E(\underline{v})$ is a disjoint union of classes mod G_n. If $x = \alpha^e g$, with $g \in G_n$ and $0 \leq e \leq s-1$, then $g^n = 1$ and $x^n = \alpha^{en}(g^n) = (\alpha^n)^e = \gamma^e$, and therefore $\mathrm{tr}_1^k[f_{\underline{v}}(x^n) = \mathrm{tr}_1^k[f_{\underline{v}}(\gamma^e)]$.

If

$$f_{\underline{v}}(x) = \sum_{j\in J} v_j x^j, \quad \text{with } \underline{v} = (v_j)_{j\in J} \in (\mathrm{GF}(2^k))^J,$$

then

$$\mathrm{tr}_1^k[f_{\underline{v}}(\gamma^e)] = \mathrm{tr}_1^k\left(\sum_{j\in J} v_j \gamma^{ej}\right) = \sum_{j\in J} \mathrm{tr}_1^k(v_j\gamma^{ej}).$$

Using the transitivity property of the trace function and because γ belongs to $\mathrm{GF}(2)$

$$\mathrm{tr}_1^k(v_j\gamma^{ej}) = \mathrm{tr}_1^\gamma \mathrm{tr}_1^k(v_j)] = \mathrm{tr}_1^k(u_j\gamma^{ej}), \text{ where } u_j = \mathrm{tr}_\gamma^k(v_j).$$

Finally

$$\mathrm{tr}_1^k[f_{\underline{v}}(\gamma^e)] = \mathrm{tr}_1^k\left(\sum_{j\in J} u_j\gamma^{ef}\right).$$

In other words,

$$\mathrm{tr}_1^k[f_{\underline{v}}(\gamma^e)] = \mathrm{tr}_1^k[f_{\underline{u}}(\gamma^e)], \text{ where } \underline{u} = (u_j)_{j\in J} \text{ and } u_j = \mathrm{tr}_\gamma^k(v_j).$$

We conclude that $x = \alpha^c \in E(\underline{v})$ if and only if $\mathrm{tr}_1^\gamma[f_{\underline{u}}(\gamma^c)] = 1$, which means from (1) that $e \in \mathrm{supp}[\mu_{\underline{u}}(x)]$. Therefore,

$$E(\underline{v}) = \bigcup_{e\in S}(\alpha^c G_n), \text{ where } S = \mathrm{supp}[\mu_{\underline{u}}(x)], \tag{9}$$
$$\underline{u} = (u_j)_{j\in J} \text{ and } u_j = \mathrm{tr}_\gamma^k(v_j).$$

It follows that $|E(\underline{v})| = n\,[\mathrm{supp}[\mu_n(x)]|$, that is:

$$|E(\underline{v})| = nw[\mu_{\underline{u}}(x)], \text{ where } S = \mathrm{supp}[\mu_{\underline{u}}(x)], \tag{10}$$
$$\underline{u} = (u_j)_{j\in J} \text{ and } u_j = \mathrm{tr}_\gamma^k(v_j).$$

3.2. Calculation of $\left|\overline{H}_a \cap E(\underline{v})\right|$

a) If $a = 0$, $\overline{H}_a =$, and $\left|\overline{H}_a \cap E(\underline{v})\right| = 0$.

b) If $a \neq 0$, using (9)

$$\overline{H}_a \cap E(\underline{v}) = \overline{H}_a \cap \left(\bigcup_{e\in S}\alpha^e G_n\right) = \bigcup_{e\in S}\left(\overline{H}_a \cap \alpha^e G_n\right),$$

which implies

$$\left|\overline{H}_a \cap E(\underline{v})\right| = \sum_{e\in S}\left|\overline{H}_a \cap \alpha^e G_n\right|. \tag{11}$$

The definition of G_n implies that $G_n = \{1, \delta, ..., \delta^i, ..., \delta^{n-1}\}$, with $\delta = \alpha^s$. Consequently,

$$\left|\overline{H}_a \cap \alpha^e G_n\right| = \zeta\left\{0 \le i \le n-1 : \mathrm{tr}_1^k\left(a\alpha^e\delta^i\right) = 1\right\}.$$

If $b_e = \mathrm{tr}_m^k(a\alpha^e)$ then $\mathrm{tr}_1^k(a\alpha^e\delta^i)\mathrm{tr}_m^k[a\alpha^e] = \mathrm{tr}_f^m(b_e\delta^j)$. We obtain from (3)

$$\left|\overline{H}_a \cap \alpha^e G_n\right| = w[v_{b_e}(x)] \text{ with } b_e = \mathrm{tr}_m^k(a\alpha^e). \tag{12}$$

Finally, from (11), it results

$$\left|\overline{H}_a \cap E(\underline{v})\right| = \sum_{e\in S} w[v_{b_e}(x)], \text{ where } S = \mathrm{supp}[\mu_{\underline{u}}(x)]. \tag{13}$$

4. Conclusion

Starting from (7) and using (8), (10) and (13), we are now able to calculate $w(a, \underline{v})$.

a) If $a \neq 0$ and $\underline{v} = \underline{0}$, then

$$w(a, \underline{0}) = 2^{k-1}.$$

b) If $a = 0$ and $\underline{v} \neq \underline{0}$, then

$$w(a, \underline{v}) = 2^{k-1} + nw[\mu_{\underline{u}}(x)] - 2\sum_{e \in S} w[v_{b_e}(x)],$$

with

$$\underline{u} = (u_j)_{j \in J} \text{ and } u_j = \mathrm{tr}_\gamma^k(v_j), \quad S = \mathrm{supp}[\mu_{\underline{u}}(x)] \text{ and } b_e = \mathrm{tr}_m^k(a\alpha^e).$$

Received, March 17, 2000

Technical University "Gh.Asachi", Jassy,
Department of Telecommunications

REFERENCES

1. Mc Williams F.J., Sloane N.J.A., *The Theory of Error-correcting Codes.* North-Holland, Amsterdam, 1977.
2. Mattson H.F.Jr., Solomon G., *A New Treatment of Bose-Chaudhuri Codes.* J. Soc. Indust. Appl. Math., **9**, 654-669 (1961).

DISTRIBUŢIA PONDERII CODURILOR CICLICE BINARE

(Rezumat)

Fie întregii s şi k astfel încât s să fie un divizor al lui $2^k - 1$. Fie $g(x)$ un divizor al lui $x^s - 1$ în GF(2) şi fie $p(x)$ un polinom primitiv de grad k în GF(2). Se consideră codul ciclic binar C de lungime $N = 2^k - 1$ generat de $(x^N - 1)/g(x)p(x)$. Pentru cazuri speciale se determină distribuţia ponderii lui C folosind ponderea codului ciclic de lungime s generat de $(x^s - 1)/g(x)$.

BULETINUL INSTITUTULUI POLITEHNIC DIN IAŞI
Tomul XLVII (LI), Fasc. 1–2, 2001
ELECTROTEHNICĂ. ENERGETICĂ. ELECTRONICĂ

D.C. 681.5; 621.316

TIME DOMAIN DESCRIPTION OF ADDITIVE NON-LINEAR SYSTEMS

BY
VICTOR GRIGORAŞ and *CARMEN GRIGORAŞ

A special class of discrete-time non-linear systems that observe the additivity property is proposed. Algebraic and dynamic additive systems properties are presented. Due to additivity, a special type of convolution product can be introduced, that structures the set of additive systems as an algebra. The proposed convolution product allows characterizing additive non-linear discrete-time systems, from the input–output point of view, and response computation in a simpler way, similar to linear ones.

1. Introduction

Linear discrete-time systems are characterized by two main properties, namely *additivity*: if $\forall\, e_1[k],\ e_2[k],\ y_1[k] = Ae_1[k],\ y_2[k] = Ae_2[k]$ then $A(e_1[k] + e_2[k]) = y_1[k] + y_2[k]$ and *homogeneity*: if $y[k] = Ae[k]\ \forall\, e[k]$ then $A(ae[k]) = ay[k]\ \forall\, a \in \mathbb{R}$. In order to rigorously define *Additive Non-linear Discrete-time Systems*, denoted in the following as ANDS, we will first consider the general, operator form of a system, $y[k] = Su[k]$, where the operator S is not yet restricted to a particular class, the input signal, $u[k]$, takes values in the input domain D_u and the output signal, $y[k]$, takes values in the output domain D_y, $S : D_u^Z \longrightarrow D_y^Z$, $u[k] \in D_u$, $y[k] \in D_y$. The two domains may or may not be equal, but, to allow the possibility of cascading systems, it is implicitly assumed that the input domain includes the output one, $D_y \subset D_u$. We denote the summation in D_u as $+$ and the summation in D_y as $\oplus$.

ANDS models several discrete-time non-linear systems, such as *algorithmic analog to digital converters, sigma-delta modulators* and *two's complement non-linear digital filters*, lack only the homogeneity property to be linear. They have both similarities and dissimilarities when compared to linear systems. The ANDS being similar to linear ones, most of the system elements they are composed of are linear, namely summers, amplifiers and delay elements. The only different elements are the non-linear algebraic functions, obeying additivity. This is why, in the following section we will concentrate only on *memory-less systems*, giving rigorous definitions for additive non-linear algebraic functions and giving some examples of such non-linearities. The next section deals with *dynamic (memory) ANDS*. Convolution-like time-domain formulae are presented allowing to compute the response of an additive system in a

similar way to linear ones. Some final remarks on the ANDS properties and response calculation formulae conclude the paper.

2. Algebraic Additive Systems

2.1. Defining Additivity

D e f i n i t i o n 1. *We define* self additive algebraic functions, $r(\cdot)$, *as those obeying the relation*:

$$r : D_u \longrightarrow D_y r(u_1 + u_2) = r(r(u_1) + r(u_2)). \tag{1}$$

By means of the defined function, we can give a definition for the summation in D_y as:

D e f i n i t i o n 2. *Define summation in* D_y, $\oplus$, *as the self additive function of the sum in* D_u, $+$:

$$y_1 \oplus y_2 = r(y_1 + y_2). \tag{2}$$

With this new definition we may rewrite the equation in the definition as:

$$r(u_1 + u_2) = r(u_1) \oplus r(u_2). \tag{3}$$

D e f i n i t i o n 3. *An algebraic function,* $p(\cdot)$, *is* additive with respect to a self additive function, $r(\cdot)$, *if it satisfies the relation*:

$$p : D_u \longrightarrow D_y; \quad p(u_1 + u_2) = r(p(u_1) + p(u_2)) = p(u_1) \oplus p(u_2). \tag{4}$$

2.2. The Symbolic Residue Function

As a useful example, the sum modulo a fixed real number $a \in \mathbb{R}$ can be defined over a properly structured set. Taking as a reference the fixed real interval $I = [-a, a)$ we can formulate:

D e f i n i t i o n 4. *The real congruence modulo a fixed real number* $a \in \mathbb{R}$, *denoted by* $\equiv$, *is*:

$$\forall x, y \in \mathbb{R} : x \equiv y \Leftrightarrow \exists k(\cdot) \in \mathbb{Z} : x - y = k(x - y)a. \tag{5}$$

The function $k(\cdot)$, that appears as a by-product in the previous definition, is called the *symbolic quotient function*, due to its direct relation to the symbolic dynamics of discrete-time chaotic systems encountered later.

D e f i n i t i o n 5. *The residue* equivalence class *mod a is the set of the real congruent* $\equiv$ *real numbers*:

$$\overline{x} = \{x \in \mathbb{R} | x \equiv x_0, x_0 \in I\}. \tag{6}$$

For each $x \in \mathbb{R}$ the representative element of its residue class, $x_0 \in I$, as in the previous definition, is unique, thus we can formulate

D e f i n i t i o n 6. *The symbolic residue function* $r(x)$ *is*:

$$r : \mathbb{R} \longrightarrow I, r(x) = x_0 = x - k(x)a \ \forall x \in \mathbb{R}. \tag{7}$$

Under these circumstances it is easy to demonstrate the following

P r o p o s i t i o n 1. *For each* $x \in \mathbb{R}$ *there is only one value for the symbolic quotient function and for the symbolic residue function, and they obey to*

$$\forall x \in \mathbb{R} : x = k(x)a + r(x). \tag{8}$$

Thus, the analytical relations are:

$$k(x) = \text{round}\left(\frac{x}{a}\right) = \left\lfloor \frac{x + 0.5}{a} \right\rfloor \tag{9}$$

for the symbolic quotient function, while for the symbolic residue:

$$r(x) = x - a\left\lfloor \frac{x + 0.5}{a} \right\rfloor, \tag{10}$$

or, in another notation:

$$\forall x \in \mathbb{R} : r(x) = x(\text{mod}\, a), \tag{11}$$

leading to the graphical representations (made for $a = 1$ for simplicity) in Figs. 1 and 2.

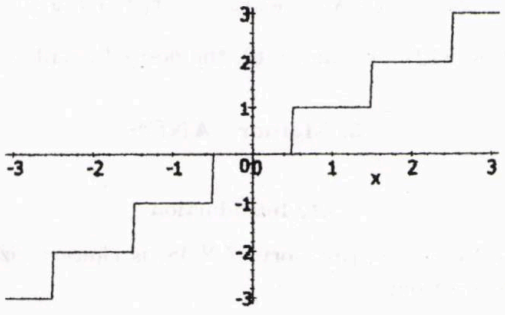

Fig. 1.– The symbolic quotient function.

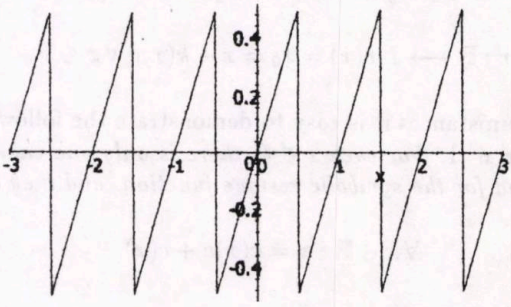

Fig. 2.– The symbolic residue function.

P r o p o s i t i o n 2. *The symbolic residue function is self additive.*
The left hand side of the self additivity definition is:

$$r(x+y) = (x+y) - ak(x+y), \tag{12}$$

while the right hand side of the same definition is:

$$r(r(x)+r(y)) = (r(x)+r(y)) - ak(r(x)+r(y)). \tag{13}$$

But, by definition:

$$r(x) = x - ak(x); \quad r(y) = y - ak(y). \tag{14}$$

Taking (13) and (14) into account, it results:

$$r(r(x)+r(y)) = (x+y) - a[k(r(x)+r(y)) + k(x) + k(y)]. \tag{15}$$

We must notice that:

$$k(x+y) = k(x) + k(y) + k(r(x)+r(y)). \tag{16}$$

By comparing Eqs. (12), (15) and (16), the desired result is obvious.■

3. Memory ANDS

3.1. Introduction

The most general dynamic (memory) ANDS, is characterized by an order, N, additive, difference equation:

$$\bigoplus_{n=0}^{N} a[n]y[k-n] = \bigoplus_{m=0}^{M} b[m]u[k-m]. \tag{17}$$

for time invariant systems and, for the time variant case:

$$\bigoplus_{n=0}^{N} a[n,k]y[k-n] = \bigoplus_{m=0}^{M} b[m,k]u[k-m]. \tag{18}$$

In the following we will concentrate on time-invariant systems. The additivity property of the proposed class of systems leads to *convolution-like formulae* for computation of the time response.

D e f i n i t i o n 7. *We can define the set of nod a signals*:

$$I^Z = \{x : Z \longrightarrow I | k \in Z : x[k] \in I\}. \tag{19}$$

It is easy to demonstrate that I^Z has the structure of a modulus over the ring of integers Z.

P r o p o s i t i o n 3. *The signal set I^Z is a modulus over the ring of integers:*

1. *I^Z is an additive group.*
2. *Z is a ring.*
3. *I^Z is a scalar multiplicative semi-group over the ring of integers Z.*

Due to the fact that in I^Z we cannot introduce an internal product compatible with the sum, we define the set of integer valued signals, used as multipliers for the mod a signals.

D e f i n i t i o n 8. *The set of integer valued signals is*

$$Z^Z = \{h : Z \longrightarrow Z | k \in Z; h[k] \in Z\}. \tag{20}$$

This new set of signals has the algebraic structure of a modulus over the ring of integers Z.

P r o p o s i t i o n 4. *The signal set Z^Z has the following properties*:

1. *Z^Z is an additive group.*
2. *Z is a ring.*
3. *Z^Z is a scalar multiplicative semi-group over the ring of integers Z.*

3.2. Convolution Definitions

D e f i n i t i o n 9. *Inside the set of causal signals from Z^Z*:

$$\forall h_c \in Z^Z : h_c[k] = \sigma[k]h_c[k],$$

we can define the *integer convolution product*:

$$\forall h_1, h_2 \in Z^Z : (h_1 *_z h_2)[k] = \sum_{m=0}^{k} h_1[m]h_2[k-m]. \tag{21}$$

With this new operation, the set of integer valued signals, Z^Z, has the algebraic structure of a ring.

P r o p o s i t i o n 5. *The signal set Z^Z is a ring*:

1. *Z^Z is an additive group.*

2. Z^Z *is a* $*_z$ *multiplicative semi-group.*

D e f i n i t i o n 10. *Inside the ordered set pair* (I^Z, Z^Z), *for causal signals*:

$$\forall u_c \in I^Z : u_c[k] = \sigma[k]u_c[k], \quad \forall h_c \in Z^Z : h_c[k] = \sigma[k]h_c[k],$$

we can define the (outer) additive (mod a) convolution product:

$$\forall u_c \in I^Z, \ \forall h_c \in Z^Z : u_c[k] *_a h_c[k] = \bigoplus_{l=0}^{k} u_c[l]h_c[k-l]. \tag{22}$$

Based on this outer convolution product, it is easy to demonstrate:

P r o p o s i t i o n 6. *The mod a set of signals,* I^Z, *has the structure of an algebra over the ring of integer valued signals,* Z^Z:

1. I^Z *is an additive group;*
2. Z^Z *is a ring;*
3. I^Z *is a* $*_a$ *multiplicative semi-group;*
4. $*_a$ *is distributive over the integer signals summation.*

3.3. Time Response Formulae

We characterize a general non-linear discrete-time system by the difference equation:

$$\bigoplus_{n=0}^{N} a[n]y[k-n] = \bigoplus_{m=0}^{M} b[m]u[k-m], \tag{23}$$

where $a[n], b[m] \in Z$, $\forall n = 0, ..., M$, $\forall u[\cdots]y[\cdots] \in I^Z$ and $a[0] = 1$, without any loss of generality.

D e f i n i t i o n 11. *The following recursive definition for the integer valued weight function,* $h[k]$, *can be formulated*:

$$h[k] = b[k](\sigma[k] - \sigma[k-M]) - \sigma[k] \sum_{n=1}^{N} a[n]h[k-n], \tag{24}$$

where $\sigma[\cdots]$ denotes the discrete-time Heaviside step function and the initial value for the integer valued weight function is chosen $h[0] = 1$.

R e m a r k 1. We should notice that in the additive case, $h[k]$ is not the response of the system to a discrete-time unit pulse. It was obtained imposing $h[0] = 1$, not $u[0] = 1$. This is due to the lack of homogeneity (non-linearity) of the systems, that leads to the response to different amplitude input pulses not to be proportional to one-another.

Based on definition 11, the following property can be demonstrated:

P r o p o s i t i o n 7. *For any causal, mod a, input signal,* $u[k] \in I$, *iteratively solving the difference equation (23) in order to obtain the time response* $y[k]$ *is equivalent to computing an outer convolution*:

$$u, y \in I^Z, \ h \in Z^Z, \ y[k] = u[k] *_a h[k]. \tag{25}$$

Applying the discrete outer convolution (22) to an arbitrary input signal, $u[k] \in I$, and the integer weight function of the ANDS (24), it results:

$$\overline{y}[k] = \bigoplus_{l=0}^{k} u[k-l]\left[b[l](\sigma[l] - \sigma[l-M]) - \sum_{n=1}^{N} a[n]h[l-n]\right]$$

and

$$\overline{y}[k] = \bigoplus_{m=0}^{M} u[k-m]b[m] - \sum_{n=1}^{N} a[n] \bigoplus_{l=1}^{n} u[k-l]h[l-m]. \tag{26}$$

For $k = 0$, it is obvious that:

$$\overline{y}[0] = (u *_a h)[0] = u[0]b_0 = y[0]$$

and, if we admit that, for $l = 0, 1, ..., k-1$, we have $\overline{y}[l] = y[i]$, it follows:

$$\overline{y}[k] = \bigoplus_{m=0}^{M} u[k-m]b[m] - \bigoplus_{n=1}^{N} a[n]y[k-n] = y[k],$$

this result completing the induction.■

R e m a r k 2. It is important to note that the essential property that permits us to demonstrate the theorem is the additivity of the mod a sum, allowing to interchange the order of summation over l and n in equation (26) with the appropriate change of summation type.

4. Conclusions

The present paper is an overview of a particular class of discrete-time non-linear systems, namely the additive non-homogeneous ones. This study is enforced not only by powerful theoretical results, but also by possible applications in the study of useful non-linear circuits, such as digital filters with 2's complement overflow non-linearity.

Due to the similarity of ANDS with discrete-time linear systems, time response formulae similar to the convolution product were found. They give profound insight on the dissimilarities between linear systems and ANDS, highlighting the fact that ANDS may be regarded as being "on the edge of linearity". Differences between the algebraic properties of the linear convolutional algebra and additive convolutional modulus can be better understood this way. The difficulty of calculating the additive weight function is one of the limitations in practical applying the proposed method.

Received, March 28, 2000

Technical University "Gh.Asachi", Jassy,
Department of Electronics
and
**ITC, Jassy*

REFERENCES

1. C h u a L.O., L i n T., *Chaos in Digital Filters.* IEEE Trans. on Circuits and Systems, **CAS-35**, *6*, 648-658 (1988).

2. Chua L.O., Parker T.S., *Chaos: a Tutorial for Engineers.* Proc. of IEEE, **75**, *8*, 982-1008 (1987).
3. Davies A.C., Petkov G.P., *Computing Basis of Attraction of Limit-Cycles in Non-Linear Discrete-Time Systems.* Proc. of Internat. Symp. on Circuits and Systems, ISCAS'96, Atlanta, GA, USA, 1996, II-469-II-472.
4. Dachselt F., Gotz M., Schwartz W., *Discrete-Time Chaotic Systems Homomorph on Modules.* Proc. of the Internat. Specialist Workshop on Nonlinear Dynamics in Electronic Systems, NDES'99, Ronne, Denmark, July 15-17, 1999, 17-20.
5. Feldmann U., Hasler M., Schwarz W., *On the Design of a Synchronizing Inverse of a Chaotic System.* Proc. of the Europ. Conf. on Circuit Theory and Design, ECCTD'95, Istambul, Turkey, August 30 – September 1, 1995, 479-482.

DESCRIEREA SISTEMELOR DISCRETE ADITIVE ÎN DOMENIUL TIMP

(Rezumat)

Se prezintă o clasă specială de sisteme discrete neliniare, care respectă proprietatea de aditivitate. Sunt prezentate proprietăţile sistemelor aditive algebrice şi cu memorie. Datorită aditivităţii, pot fi introduse forme speciale de convoluţie, cu ajutorul cărora se poate structura mulţimea sistemelor aditive ca o algebră. Produsul de convoluţie introdus permite caracterizarea sistemelor discrete, aditive, neliniare din punct de vedere intrare–ieşire şi calculul răspunsului într-un mod simplificat, similar celui pentru sisteme liniare.

BULETINUL INSTITUTULUI POLITEHNIC DIN IAŞI
Tomul XLVII (LI), Fasc. 1–2, 2001
ELECTROTEHNICĂ. ENERGETICĂ. ELECTRONICĂ

D.C. 621.3.016.35

ON THE DESIGN OF THE KERWIN–HUELSMAN–NEWCOMB BIQUAD

I. STABILITY CONDITIONS FOR THE KHN NONIDEAL INTEGRATORS BIQUAD

BY

ROMEO GHINEA, RADU BOZOMITU and LIVIU GORAŞ

The stability of a three-amplifier biquad is analyzed considering a dominant pole and a finite d.c. gain, for the integrators active devices. An analytical condition for the passive feedback network to ensure filter stability for nonideal operational amplifiers, transconductance amplifiers and transresistance amplifiers based integrators is derived.

1. Introduction

Analysis of active filters stability taking into consideration the nonideal character of the components and devices is an important issue, especially when high quality factors are needed. Computer simulation are the ultimate tool before physical experiment; however, analytical methods using (rather) simple (macro)models for the devices may be useful during the early stages of the design process.

The aim of this paper is to present several analytical results concerning the KHN (Kerwin–Huelsman–Newcomb) biquad stability using the Nyquist criterion. The general topology is depicted in Fig. 1 where the integrators can be implemented in various ways.

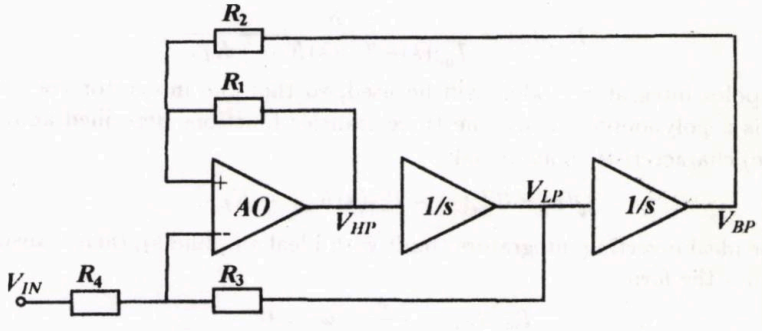

Fig. 1.– Electrical schematic of the KHN biquad.

The following discussion is made under the simplifying assumption that the integrator cells are identical and are modeled at the system level by the transfer and transmission functions, $H_{\text{int}}(s)$ and $T_{\text{int}}(s)$, respectively ($T_{\text{int}}(s) = 1/H_{\text{int}}(s)$).

Moreover, the coupling effects of the integrators and of the operational amplifier used in the adder cell are neglected.

Under the above conditions, the schematic in Fig. 1 can be described by the configuration shown in Fig. 2, which emphasizes the system level aspects of the filter structure.

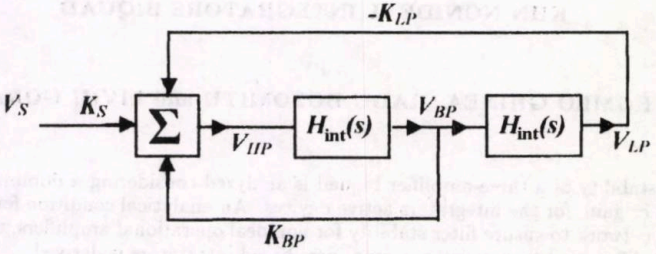

Fig. 2.– Equivalent schematic for the KHN biquad.

The coefficients K_S, K_{BP}, K_{LP} appearing in Fig. 2 are:

$$K_S = \left(1 + \frac{R_1}{R_2}\right)\left(\frac{R_4}{R_3 + R_4}\right) > 0, \quad K_{BP} = \left(1 + \frac{R_1}{R_2}\right)\left(\frac{R_3}{R_3 + R_4}\right) > 0,$$

$$K_{LP} = \frac{R_1}{R_2} > 0. \tag{1}$$

The KHN biquad can be used to synthesize three types of filters and transfer functions (low-pass, band-pass or high-pass), according to the terminal the output voltage is considered: V_{LP}, V_{BP}, or V_{HP},

$$H_{HP}(s) = \frac{K_S T_{\text{int}}^2(s)}{T_{\text{int}}^2(s) - T_{\text{int}}(s)K_{BP} + K_{LP}}, \quad H_{BP}(s) = \frac{K_S T_{\text{int}}(s)}{T_{\text{int}}^2(s) - T_{\text{int}}(s)K_{BP} + K_{LP}},$$

$$H_{LP}(s) = \frac{K_S}{T_{\text{int}}^2(s) - T_{\text{int}}(s)K_{BP} + K_{LP}}. \tag{2}$$

Only poles integrator models will be used, so that the integrator transmission function is a polynomial. Thus, the three transfer functions described above have the (same) characteristic polynomial:

$$Q(s) = T_{\text{int}}^2(s) - T_{\text{int}}(s)K_{BP} + K_{LP}, \tag{3}$$

where, for ideal inverting integrators (built with ideal amplifiers), their transmission function has the form:

$$T_{\text{int}\,0}(s) = -\frac{s}{\omega_0}, \quad \omega_0 > 0, \tag{4}$$

In these conditions, the three transfer functions and their common characteristic polynomial are, respectively:

$$H_{HP_0}(s) = \frac{K_S s^2}{s^2 + K_{BP}\omega_0 s + K_{LP}\omega_0^2},$$

$$H_{BP_0}(s) = \frac{K_S s\omega_0}{s^2 + K_{BP}\omega_0 s + K_{LP}\omega_0^2}, \tag{5}$$

$$H_{LP_0}(s) = \frac{K_S \omega_0^2}{s^2 + K_{BP}\omega_0 s + K_{LP}\omega_0^2},$$

$$Q_0 = s^2 + K_{BP}\omega_0 s + K_{LP}\omega_0^2. \tag{6}$$

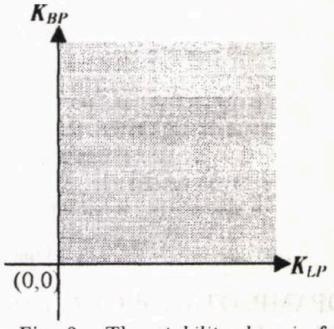

Fig. 3.– The *stability domain* for the ideal biquad (shaded area).

According to the Routh-Hurwitz criterion the stability of the ideal biquad is ensured for the entire first quadrant of the parameter plane (K_{LP}, K_{BP}), as shown in Fig. 3.

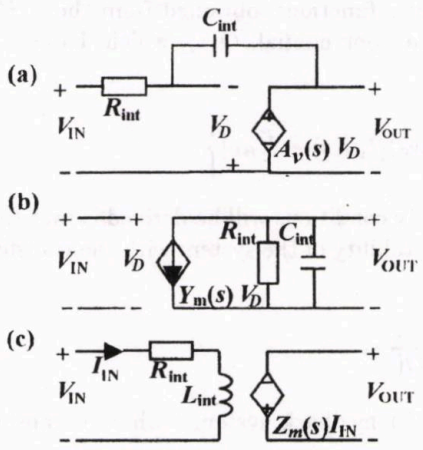

Fig. 4.– Nonideal integrators based on OPAMP (*a*), OTA (*b*), ORA (*c*).

2. Nonideal Integrators

In the following, the integrator nonidealities will be considered as a consequence of the active devices nonidealities only. We will take into account three integrators topologies, one based on voltage operational amplifier (OPAMP) and the other two on transconductance (OTA) and transresistance amplifier (ORA) (Fig. 4).

The OPAMP based integrator has a feedback topology (*a*), while the OTA and ORA ones have a feedforward one ((*b*) and (*c*)). Their transmission functions have the following forms:

$$\begin{cases} T_{\text{int}}(s)\big|_{\text{OPAMP}} = -\left[\dfrac{1}{A(s)B(s)} + \dfrac{1}{B(s)} - 1\right], \\ T_{\text{int}}(s)\big|_{\text{OTA}} = -\dfrac{1}{A(s)B(s)}, \\ T_{\text{int}}(s)\big|_{\text{ORA}} = -\dfrac{1}{A(s)B(s)}, \end{cases} \tag{7}$$

where the significances of $A(s)$ and $B(s)$, for the three types of amplifiers, are:

$$A(s) = A_v(s), \quad A(s) = Y_m(s)R_{\text{int}}, \quad A(s) = \frac{Z_m(s)}{R_{\text{int}}} \tag{8}$$

and

$$B(s) = \frac{s + \omega_i}{\omega_i}, \tag{9}$$

with

$$\omega_i = \frac{1}{R_{\text{int}}C_{\text{int}}}, \quad \omega_i = \frac{1}{R_{\text{int}}C_{\text{int}}}, \quad \omega_i = \frac{R_{\text{int}}}{L_{\text{int}}}, \tag{10}$$

for OPAMP, OTA and ORA, respectively.

When the amplifiers are modeled with only poles (a typical case), from the above relations results that the integrator transmission functions, $T_{\text{int}}(s)$, are polynomials, confirming the hypothesis made in the end of the previous section.

3. Stability Analysis Based on Nyquist Criterion

As shown above, the three types of transfer functions, obtained from the KHN biquad topology, have the same characteristics polynomial, $Q(s)$, which, based on (3), can be written in the form:

$$Q(s) = K_{LP}\left\{1 + \frac{1}{K_{LP}}T_{\text{int}}(s)[T_{\text{int}}(s) - K_{BP}]\right\}. \tag{11}$$

The basic observation on which the stability conditions will be derived is that the stability of the biquad is equivalent with the stability of the system with the transfer function

$$H_{\text{CL}}(s) = \frac{1}{Q(s)}, \tag{12}$$

which can be regarded as a closed loop (CL) feedback system with the transfer function

$$H_{\text{CL}}(s) = \frac{1/K_{LP}}{1 + H_{\text{OL}}(s)}, \tag{13}$$

with the open loop (OL) transfer function

$$H_{\text{OL}}(s) = \frac{1}{K_{LP}}T_{\text{int}}(s)[T_{\text{int}}(s) - K_{BP}], \tag{14}$$

which is a polynomial, since $T_{\text{int}}(s)$ is a polynomial too.

Thus, the biquad stability can be studied using the Nyquist criterion for the closed loop transfer function, $H_{CL}(s)$.

When s circles clockwise the Nyquist contour (Fig. 5), the $H_{OL}(s)$ hodograph circles clockwise Z times the point $(-1, 0)$, where Z is the number of zeros in the left half s-plane of the function $1 + H_{OL}(s)$. Based on (13), the zeros of the function $1 + H_{OL}(s)$ are also the poles of the closed loop transfer function $H_{CL}(s)$. Thus, the stability of the biquad is ensured if and only if $Z = 0$, which means the $H_{OL}(s)$ hodograph should not circle the point $(-1, 0)$.

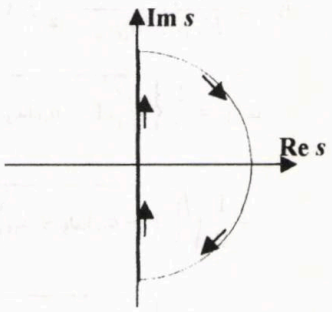

Fig. 5.– The Nyquist contour.

3.1. OPAMP Based Integrator

In the following we will suppose that the voltage operational amplifier used to build the integrator cells has finite D.C. gain and a single (dominant) pole:

$$A_V(s) = \frac{a_0\omega_p}{s + \omega_p}. \tag{15}$$

Using (7),...,(10) and (15), the integrator transmission function becomes:

$$T_{int}(s) = -\frac{s^2 + s[(1 + a_0)\omega_p + \omega_i] + \omega_p\omega_i}{a_0\omega_p\omega_i}. \tag{16}$$

From (14) and (16) the equivalent open loop transfer function may be obtained:

$$H_{OL}(s) = \frac{1}{K_{LP}(a_0\omega_p\omega_i)^2}\left\{s^2 + [(1 + a_0)\omega_p + \omega_i]s + \omega_p\omega_i\right\} \times$$
$$\times\left\{s^2 + [(1 + a_0)\omega_p + \omega_i]s + \omega_p\omega_i(1 + a_0K_{BP})\right\}. \tag{17}$$

For $s = j\omega$, the real and imaginary parts of $H_{OL}(j\omega)$ are, respectively:

$$\Re e H_{OL}(j\omega) = \frac{1}{K_{LP}} \cdot \frac{1}{(a_0\omega_p\omega_i)^2} \times$$
$$\times\left(\omega^4 - \omega^2\left\{[(1 + a_0)\omega_p + \omega_i]^2 + \omega_p\omega_i(2 + a_0K_{BP})\right\} + (\omega_p\omega_i)^2(1 + a_0K_{BP})\right), \tag{18}$$

$$\Im m H_{OL}(j\omega) = -\frac{1}{K_{LP}} \cdot \frac{2[(1 + a_0)\omega_p + \omega_i]}{(a_0\omega_p\omega_i)^2}\omega\left[\omega^2 - \frac{1}{2}\omega_p\omega_i(2 + a_0K_{BP})\right],$$

or, in condensed form,

$$\Re e H_{OL}(j\omega) = K_x(\omega^2 - \omega_{x1}^2)(\omega^2 - \omega_{x2}^2), \quad \Im m H_{OL}(j\omega) = K_y\omega(\omega^2 - \omega_y^2), \tag{19}$$

where K_x, K_y, ω_{x1}, ω_{x2}, ω_y are:

$$K_x = \frac{1}{K_{LP}} \cdot \frac{1}{(a_0\omega_p\omega_i)^2} > 0, \quad K_y = -\frac{1}{K_{LP}} \cdot \frac{2[(1+a_0)\omega_p + \omega_i]}{(a_0\omega_p\omega_i)^2} < 0,$$

$$\omega_{x1} = \frac{1}{2}\left\{\sqrt{\left[(1+a_0)\omega_p + \omega_i\right]^2 + \omega_p\omega_i\left(1+\sqrt{1+a_0K_{BP}}\right)^2} - \right.$$

$$\left. -\frac{1}{2}\sqrt{\left[(1+a_0)\omega_p + \omega_i\right]^2 + \omega_p\omega_i\left(1-\sqrt{1+a_0K_{BP}}\right)^2}\right\} > 0,$$

(20)

$$\omega_{x2} = \frac{1}{2}\left\{\sqrt{\left[(1+a_0)\omega_p + \omega_i\right]^2 + \omega_p\omega_i\left(1+\sqrt{1+a_0K_{BP}}\right)^2} + \right.$$

$$\left. +\frac{1}{2}\sqrt{\left[(1+a_0)\omega_p + \omega_i\right]^2 + \omega_p\omega_i\left(1-\sqrt{1+a_0K_{BP}}\right)^2}\right\} > 0,$$

$$\omega_y = \frac{1}{2}\sqrt{2\omega_p\omega_i(2+a_0K_{BP})} =$$

$$= \frac{1}{2}\sqrt{\omega_p\omega_i\left[(1+\sqrt{1+a_0K_{BP}})^2 + (1-\sqrt{1+a_0K_{BP}})^2\right]} > 0.$$

It can be easily proved that:

(21)

$$\omega_{x2} > \omega_y > \omega_{x1}.$$

Indeed:

$$\omega_{x2} > \omega_y \quad i.e. \quad \omega_{x2}^2 > \omega_y^2$$

and consequently:

$$\left[(1+a_0)\omega_p + \omega_i\right]^2 +$$

$$+\sqrt{\left\{\left[(1+a_0)\omega_p + \omega_i\right]^2 + \omega_p\omega_i(1+\sqrt{1+a_0K_{BP}})^2\right\}} \times$$

$$\times\sqrt{\left\{\left[(1+a_0)\omega_p + \omega_i\right]^2 + \omega_p\omega_i(1-\sqrt{1+a_0K_{BP}})^2\right\}} > 0;$$

also:

$$\omega_y > \omega_{x1} \quad i.e. \quad \omega_y^2 > \omega_{x1}^2$$

and consequently:

$$[(1+a_0)\omega_p+\omega_i]^2 -$$

$$-\sqrt{[(1+a_0)\omega_p+\omega_i]^2+\omega_p\omega_i(1+\sqrt{1+a_0K_{BP}})^2}\times$$

$$\times\sqrt{[(1+a_0)\omega_p+\omega_i]^2+\omega_p\omega_i(1-\sqrt{1+a_0K_{BP}})^2}<0,$$

that is

$$[(1+a_0)\omega_p+\omega_i]^2 <$$

$$<\sqrt{[(1+a_0)\omega_p+\omega_i]^2+\omega_p\omega_i(1+\sqrt{1+a_0K_{BP}})^2}\times$$

$$\times\sqrt{[(1+a_0)\omega_p+\omega_i]^2+\omega_p\omega_i(1-\sqrt{1+a_0K_{BP}})^2}.$$

The Nyquist diagram is formed by two parts, one for $s=\mathrm{j}\omega$ and the other one for s lying on the infinite semicircle.

Due to the fact that the real part of $H_{\mathrm{OL}}(s)$ is an even function and the imaginary part of $H_{\mathrm{OL}}(s)$ is odd, the $H_{\mathrm{OL}}(\mathrm{j}\omega)$ polar diagram crosses the real axis in two points, A_{1+}, A_{2-}, and the imaginary axis in four points, B_{1+}, B_{1-}, B_{2+}, B_{2-}, with the coordinates:

$$A_{1+}=\Big(0,\ \Re eH_{\mathrm{OL}}(\mathrm{j}0)\Big),\quad A_{2-}=\Big(0,\ \Re eH_{\mathrm{OL}}(\pm\mathrm{j}\omega_y)\Big) \tag{22}$$

and

$$\begin{cases} B_{1+}=\Big(+\Im mH_{\mathrm{OL}}(\mathrm{j}\omega_{x1}),\ 0\Big), & B_{2+}=\Big(-\Im mH_{\mathrm{OL}}(\mathrm{j}\omega_{x2}),\ 0\Big), \\ B_{1-}=\Big(-\Im mH_{\mathrm{OL}}(\mathrm{j}\omega_{x1}),\ 0\Big), & B_{2-}=\Big(+\Im mH_{\mathrm{OL}}(\mathrm{j}\omega_{x2}),\ 0\Big); \end{cases} \tag{23}$$

(the points B_{1+}, B_{1-} and B_{2+}, B_{2-} are symmetrical relative to the origin).

Taking into consideration the signs of K_x, K_y, ω_{x1}, ω_{x2} and ω_y from (20) and inequality (21) we obtain:

$$\Re eH_{\mathrm{OL}}(\mathrm{j}0)=K_x\omega_{x1}^2\omega_{x2}^2>0,\quad \Re eH_{\mathrm{OL}}(\pm\mathrm{j}\omega_y)=K_x(\omega_y^2-\omega_{x1}^2)(\omega_y^2-\omega_{x2}^2)<0, \tag{24}$$

and

$$\begin{aligned} \Im mH_{\mathrm{OL}}(+\mathrm{j}\omega_{x1})&=+k_y\omega_{x1}(\omega_{x1}^2-\omega_y^2)>0, \\ \Im mH_{\mathrm{OL}}(-\mathrm{j}\omega_{x2})&=-k_y\omega_{x2}(\omega_{x2}^2-\omega_y^2)>0, \end{aligned} \tag{25}$$

showing that A_{1+}, B_{1+}, B_{2+} are situated on the positive semiaxes, while A_{2-}, B_{1-}, B_{2-}, on the negative ones.

The general shape of the $H_{OL}(j\omega)$ polar diagram is sketched in Fig. 6 and shows the positions of the six points relative to the origin.

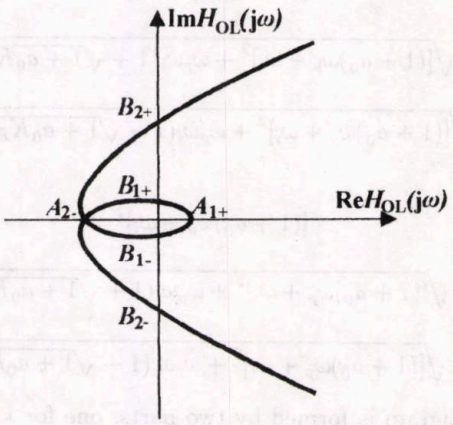

Fig. 6.– The general shape of $H_{OL}(j\omega)$.

Before tracing the hodograph of $H_{OL}(s)$, we note that when s is following clockwise the semicircle of the Nyquist contour, $|s| \to \infty$ and $\arg s \in [-\pi/2, +\pi/2]$, where the upper arrow indicates the direction of variation. Based on the expression of $H_{OL}(s)$ we can write that $\lim_{|s|\to\infty} \frac{H_{OL}(s)}{s^4} = \frac{1}{K_{BP}(a_0\omega_p\omega_i)^2} > 0$ which allows, making the approximation $H_{OL}(s) \cong \frac{1}{K_{BP}(a_0\omega_p\omega_i)^2} s^4$, to write $|H_{OL}(s)| \cong \frac{1}{K_{BP}(a_0\omega_p\omega_i)^2} |s^4| \to$ $\to \infty$ and $\arg H_{OL}(s) \cong 4 \arg s \in [-\pi/2, +\pi/2]$.

The biquad stability is ensured if and only if the $H_{OL}(s)$ hodograph does not circle clockwise the point (–1, 0), when s is following clockwise the Nyquist contour, *i.e.* the stability is ensured if and only if the point (–1, 0) is placed between the points A_{1+}, A_{2-} (Fig. 7).

In terms of the coordinates (21) of the points A_{1+}, A_{2-} the stability condition becomes:

$$\Re e H_{OL}(j\,0) > -1 > \Re e H_{OL}(j\omega_y). \tag{26}$$

The first inequality is always satisfied because $\Re e H_{OL}(j\,0) > 0$ as shown in (24) and the second one, in conjunction with (24), can be rewritten in the form:

$$K_x(\omega_y^2 - \omega_{x1}^2)(\omega_y^2 - \omega_{x2}^2) < -1. \tag{27}$$

Based on the expressions of the parameters K_x, ω_y, ω_{x1}, ω_{x2} the final form of the *stability condition* is:

$$K_{LP} < \frac{1}{4}K_{BP}^2 + \frac{1}{2}a_0 K_{BP}\left[\frac{(1+a_0)\omega_p + \omega_i}{a_0\sqrt{\omega_p\omega_i}}\right]^2 + \left[\frac{(1+a_0)\omega_p + \omega_i}{a_0\sqrt{\omega_p\omega_i}}\right]^2, \tag{28}$$

and the equation of the *stability frontier* in the plane $(K_{BP},\ K_{LP})$ is the parabola:

$$K_{LP} = \frac{1}{4}K_{BP}^2 + \frac{1}{2}a_0\left[\frac{(1+a_0)\omega_p + \omega_i}{a_0\sqrt{\omega_p\omega_i}}\right]^2 K_{BP} + \left[\frac{(1+a_0)\omega_p + \omega_i}{a_0\sqrt{\omega_p\omega_i}}\right]^2. \tag{29}$$

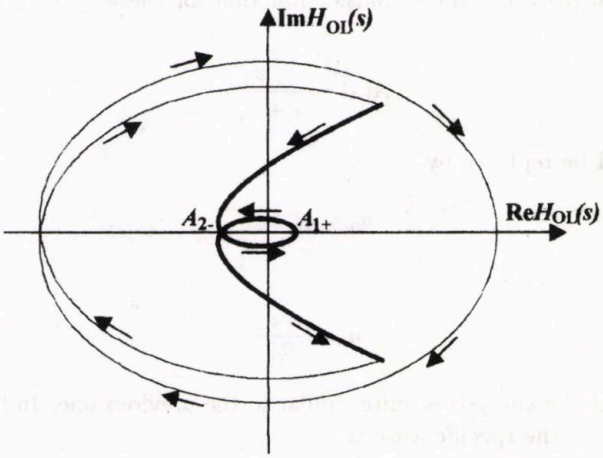

Fig. 7.– The general shape of the hodograph of $H_{OL}(s)$ ($H_{OL}(j\omega)$ represented with thick line).

In Fig. 8 the stability frontier and the stability domain were plotted for $a_0 = 10^5$, $\omega_p = 10^6$ and $\omega_i = 10^5$.

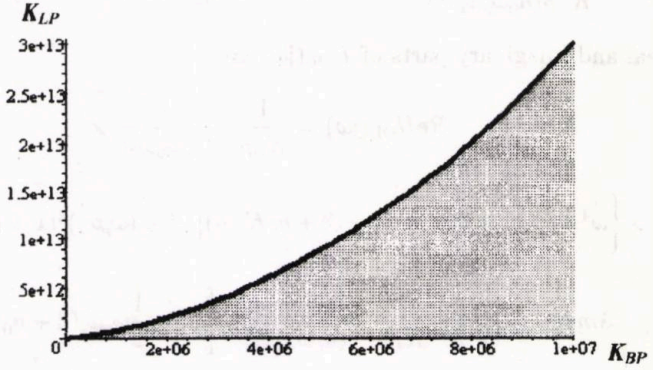

Fig. 8.– The *stability frontier* (thick line) and *stability domain* (shaded area) in the $(K_{BP},\ K_{LP})$ plane.

3.2. OTA and ORA Based Integrators

The transconductance and transresistance amplifiers are supposed to have finite D.C. gain and a single pole:

$$Y_m(s) = \frac{g_m\omega_p}{s+\omega_p} \quad \text{and} \quad Z_m(s) = \frac{r_m\omega_p}{s+\omega_p}. \tag{30, 31}$$

According to (8) the voltage transfer function for these types of amplifiers has the same form:

$$A(s) = \frac{a_0\omega_p}{s+\omega_p}, \tag{32}$$

where a_0 should be replaced by

$$a_0 = g_m R_{\text{int}} \tag{33}$$

for OTA and

$$a_0 = \frac{r_m}{R_{\text{int}}} \tag{34}$$

for ORA, so that the analysis is quite similar to the previous one. In the follwing we will point out only the specific aspects.

The integrator transmission function has the form:

$$T_{\text{int}}(s) = -\frac{s^2+(\omega_p+\omega_i)s+\omega_p\omega_i}{a_0\omega_p\omega_i}, \tag{35}$$

so that the equivalent open loop transfer function is:

$$H_{\text{OL}}(s) = \frac{1}{K_{LP}(a_0\omega_p\omega_i)^2}\left[s^2+(\omega_p+\omega_i)s+\omega_p\omega_i\right]\left[s^2+(\omega_p+\omega_i)s+\omega_p\omega_i(1+a_0K_{BP})\right]. \tag{36}$$

The real and imaginary parts of $H_{\text{OL}}(\text{j}\omega)$ are:

$$\Re e H_{\text{OL}}(\text{j}\omega) = \frac{1}{K_{LP}} \cdot \frac{1}{(a_0\omega_p\omega_i)^2} \times$$

$$\times\left\{\omega^4 - \left[(\omega_p+\omega_i)^2+\omega_p\omega_i(2+a_0K_{BP})\right]\omega^2 + (\omega_p\omega_i)^2(1+a_0K_{BP})\right\}, \tag{37}$$

$$\Im m H_{\text{OL}}(\text{j}\omega) = -\frac{1}{K_{LP}} \cdot \frac{2(\omega_p+\omega_i)}{(a_0\omega_p\omega_i)^2}\omega\left[\omega^2 - \frac{1}{2}\omega_p\omega_i(2+a_0K_{BP})\right],$$

or, equivalently:

$$\Re e H_{\text{OL}}(\text{j}\omega) = K_x(\omega^2-\omega_{x1}^2)(\omega^2-\omega_{x2}^2), \qquad \Im m H_{\text{OL}}(\text{j}\omega) = K_y(\omega^2-\omega_y^2), \tag{38}$$

where the parameters K_x, K_y, ω_{x1}, ω_{x2}, ω_y have the expressions:

$$K_x = \frac{1}{K_{LP}} \cdot \frac{1}{(a_0\omega_p\omega_i)^2} > 0, \quad K_y = \frac{1}{K_{LP}} \cdot \frac{2(\omega_p + \omega_i)}{(a_0\omega_p\omega_i)^2} < 0,$$

$$\omega_{x1} = \frac{1}{2}\left[\sqrt{(\omega_p + \omega_i)^2 + \omega_p\omega_i(1 + \sqrt{1 + a_0K_{BP}})^2} - \right.$$

$$\left. - \sqrt{(\omega_p + \omega_i)^2 + \omega_p\omega_i(1 + \sqrt{1 - a_0K_{BP}})^2}\right] > 0,$$

(39)

$$\omega_{x2} = \frac{1}{2}\left[\sqrt{(\omega_p + \omega_i)^2 + \omega_p\omega_i(1 + \sqrt{1 + a_0K_{BP}})^2} + \right.$$

$$\left. + \sqrt{(\omega_p + \omega_i)^2 + \omega_p\omega_i(1 + \sqrt{1 - a_0K_{BP}})^2}\right] > 0,$$

$$\omega_y = \frac{1}{2}\sqrt{2\omega_p\omega_i(2 + a_0K_{BP})} =$$

$$= \frac{1}{2}\sqrt{\omega_p\omega_i\left[(1 + \sqrt{1 + a_0K_{BP}})^2 + (1 - \sqrt{1 + a_0K_{BP}})^2\right]} > 0,$$

so that:

(40) $$\omega_{x2} > \omega_y > \omega_{x1}.$$

The $H_{\mathrm{OL}}(\mathrm{j}\omega)$ polar diagram crosses the real axis and respectively, the imaginary axis in the points

(41) $$A_{1+} = (0, \Re e H_{\mathrm{OL}}(\mathrm{j}\,0)), \quad A_{2-} = (0, \Re e H_{\mathrm{OL}}(\pm \mathrm{j}\omega_y)),$$

and

(42) $$\begin{cases} B_{1+} = (+\Im m H_{\mathrm{OL}}(\mathrm{j}\omega_{x1}),\ 0), & B_{2+} = (-\Im m H_{\mathrm{OL}}(\mathrm{j}\omega_{x2}),\ 0), \\ B_{1-} = (-\Im m H_{\mathrm{OL}}(\mathrm{j}\omega_{x1}),\ 0), & B_{2-} = (+\Im m H_{\mathrm{OL}}(\mathrm{j}\omega_{x2}),\ 0). \end{cases}$$

As in the previous case,

(43) $$\Re e H_{\mathrm{OL}}(\mathrm{j}\,0) = K_x\omega_{x1}^2\omega_{x2}^2 > 0, \quad \Re e H_{\mathrm{OL}}(\pm \mathrm{j}\omega_y) = K_x(\omega_y^2 - \omega_{x1}^2)(\omega_y^2 - \omega_{x2}^2) < 0,$$

and

(44) $$\Im m H_{\mathrm{OL}}(+\mathrm{j}\omega_{x1}) = +k_y\omega_{x1}(\omega_{x1}^2 - \omega_y^2) > 0,$$
$$\Im m H_{\mathrm{OL}}(-\mathrm{j}\omega_{x2}) = -k_y\omega_{x2}(\omega_{x2}^2 - \omega_y^2) > 0,$$

so that A_{1+}, B_{1+}, B_{2+} are situated on the positive semiaxes, while A_{2-}, B_{1-}, B_{2-}, on the negative ones.

The shapes of the $H_{\mathrm{OL}}(\mathrm{j}\omega)$ polar diagram and of the $H_{\mathrm{OL}}(s)$ hodograph are identical to those in the previous section (Figs. 6 and 7), thus the stability is ensured if and only if the point (–1, 0) is placed between the points A_{1+}, A_{2-}.

In terms of the coordinates of the points A_{1+}, A_{2-} the stability condition can be expressed as:

$$\Re e H_{\mathrm{OL}}(\mathrm{j}\,0) > -1 > \Re e H_{\mathrm{OL}}(\pm \mathrm{j}\omega_y), \tag{45}$$

where the first inequality is always satisfied because $\Re e H_{OL}(\mathrm{j}0) > 0$, as shown in (43), and the second one, in conjunction with (43), can be rewritten in the form:

$$K_x(\omega_y^2 - \omega_{x1}^2)(\omega_y^2 - \omega_{x2}^2) < -1, \tag{46}$$

leading to the final form of the *stability condition*:

$$K_{LP} < \frac{1}{4}K_{BP}^2 + \frac{1}{2}a_0 K_{BP}\left(\frac{\omega_p + \omega_i}{a_0\sqrt{\omega_p\omega_i}}\right)^2 + \left(\frac{\omega_p + \omega_i}{a_0\sqrt{\omega_p\omega_i}}\right)^2. \tag{47}$$

The equation of the *stability frontier*, in the plane (K_{BP}, K_{LP}), is again a parabola

$$K_{LP} = \frac{1}{4}K_{BP}^2 + \frac{1}{2}a_0\left(\frac{\omega_p + \omega_i}{a_0\sqrt{\omega_p\omega_i}}\right)^2 K_{BP} + \left(\frac{\omega_p + \omega_i}{a_0\sqrt{\omega_p\omega_i}}\right)^2; \tag{48}$$

the stability frontier and the stability domain are similar to those in Fig. 8.

4. Concluding Remarks

The stability of a three amplifier biquad was analyzed considering a dominant pole and a finite D.C. gain, for integrators based on operational amplifiers, transconductance and transresistance amplifiers. Analytical conditions for the dependence of the feedback resistances on the integrators parameters to ensure stability were derived. Further results concerning the design of the bandwidths and central frequencies of bandpass active filters will be presented in the second part of this paper.

Received, July 12, 2000

Technical University "Gh.Asachi", Jassy,
Department of Electronics

REFERENCES

1. Huelsman L.P., Allen P.E., *Introduction to the Theory and Design of Active Filters.* McGraw-Hill Inc., New York, 1980.
2. Toumazou C., Lidgey F.J., Haigh D.G. (Eds.), *Analogue IC Design: The Current-Mode Approach.* Peter Peregrinus Ltd., London, 1990.
3. Bakken T., Choma J. Jr., *Stability of a Continuous-Time State Variable Filter with OPAMP and OTA-C Integrators.* Great Lakes Symposium on VLSI, Febr. 1998.

4. B a k k e n T., C h o m a J. Jr., *Stability of a Continuous-Time State Variable Filter with ORA-L and Current Amplifiers Integrators.* Great Lakes Symposium on VLSI, Febr. 1998.

ASUPRA PROIECTĂRII BIQUAD-ULUI KERWIN–HUELSMAN–NEWCOMB
I. Condiţii de stabilitate a biquad-ului KHN cu integratoare neideale

(Rezumat)

Se studiază stabilitatea unui biquad implementat cu trei amplificatoare (biquad-ul KHN), considerând că dispozitivele active ale integratoarelor au câştig de c.c. finit şi un singur pol (dominant). Se determină legătura dintre rezistenţele de reacţie şi parametrii integratoarelor pentru a asigura stabilitatea. Relaţia este utilă pentru asigurarea condiţiilor necesare de stabilitate ale unui filtru activ cu integratoare cu parametri precizaţi.

BULETINUL INSTITUTULUI POLITEHNIC DIN IAŞI
Tomul XLVII (LI), Fasc. 1–2, 2001
ELECTROTEHNICĂ. ENERGETICĂ. ELECTRONICĂ

D.C. 621.394.9

SYSTEMATIC TRELLIS STRUCTURES FOR SYMMETRIC TURBO CODES

BY

LUMINIŢA SCRIPCARIU and PETRUŢ DUMA

Symmetrical TURBO codes based on systematic error-correcting codes are studied. A comparison between block-codes (Hamming, Reed-Solomon) and tree-codes (Trellis) is made. A method for convolutional codes systematization is proposed. The convolutional coding rate of 2 : 3 used for symmetrical half-rate Turbo-Trellis coding algorithms is considered. Optimal convolutional coding systematic structures for Turbo codes are deduced.

1. Introduction

Digital communications systems such as terrestrial or satellite mobile communications are hardly affected by additive Gaussian noise and envelope fading phenomenon, so that random errors and error-burst appear in the received decoded signal [1]. These effects are more powerful if the signal-to-noise ratio is decreased using lower power supply or if the receiver is placed in a "shadow" region reported to the transmitter. Some obstacles, with fixed or mobile position, could produce radio signal attenuation for shorter or longer time intervals and the data could be lost if a powerful error-correcting code is not used [2].

TURBO codes used for error-correction are applied on some interleaved data symbols (Fig. 1).

First of all, the serial data sequence is partitioned into blocks of symbols or bits. Every block is converted into a matrix, D. On the next step, a systematic error-correcting code is used to encode the rows of D; in this way the horizontal parity matrix, P_H, results. Then, another code is applied on each column of the merged matrices D and P_H. The vertical and auxiliary parity matrices P_V and P_A are obtained.

The coding rates of the codes are denoted: $k_1 : n_1$ and $k_2 : n_2$.

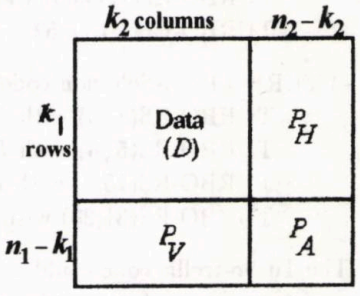

Fig. 1.– TURBO Code Principle.

Combining two codes on a data matrix a TURBO code results and the coding rate is computed as:

$$R = \frac{k_1 k_2}{n_1 n_2}. \tag{1}$$

If the same code with a coding rate $k : n$ is applied on the rows and the columns, then a symmetric TURBO code is obtained with the coding rate

$$R = \frac{k^2}{n^2}. \tag{2}$$

The basic code must be systematic in position to keep unmodified the data matrix D.

If this code is organized on bits, such as Hamming or binary Trellis codes, then a binary TURBO code results.

If the basic code is designed on a non-binary Galois Field (GF), such as Reed-Solomon or multilevel Trellis codes, the TURBO code will be defined on the same numerical field with multibit symbols.

The TURBO code name must specify the basic code name used and the coding parameters, in particular the coding rate.

The global coding rate of a TURBO code could have very different values. In order to compare the redundancy of the codes, the coding rate is approximate to a standard value, 1 : 2 (half-rate), 1 : 3, 2 : 3, etc.

For example, there are:

a) TURBO Hamming codes:
TURBO-H(7;4) with $R = 16 : 49 \cong 1 : 3$.
TURBO-H(15;11) with $R = 121 : 225 \cong 1 : 2$.
TURBO-H(31;26) with $R = 676 : 961 \cong 2 : 3$.

b) TURBO binary Trellis (convolutional) codes:
TURBO-C(31;13;12) [3] with $R = 4 : 9 \cong 1 : 2$.
TURBO-C(71;53;35) with $R = 4 : 9 \cong 1 : 2$.
TURBO-C(11;18;6;52) with $R = 9 : 16 \cong 1 : 2$.

c) TURBO Reed-Solomon codes:
TURBO-RS(7 ; 5) with $R = 25 : 49 \cong 1 : 2$.
TURBO-RS(5 ; 3) with $R = 9 : 25 \cong 1 : 3$.
TURBO-RS(15;9) with $R = 81 : 225 \cong 1 : 3$.
TURBO-RS(31;23) with $R = 529 : 961 \cong 1 : 2$.

The Turbo-trellis code could have higher dimensions of the data matrix, in order to ensure minimum L steps of the Viterbi Decoding Algorithm for each row and column of the received matrix. L represents the decision-length of the trellis code.

2. Trellis Code Systematization

A block error-correcting code is easily designed as a systematic one which could be used for a TURBO code.

The "tree" codes (trellis or convolutional) are obtained first with non-systematic and non-recursive coding structures. In order to apply a trellis code for a TURBO encoding technique, a recursive systematic coding (RSC) structure must be used. This is easily done for the half-rate convolutional codes but these ones could not be used in a TURBO code because the redundancy increased by 300%. Therefore for TURBO codes we have to choose a convolutional code with a coding rate of $2:3$ or $3:4$. The systematization of a convolutional code with higher dimensions (coding rate or constraint length) becomes difficult and the Viterbi decoding algorithm is too complicated for a real-time application.

So we are interested to obtain $2:3$ or $3:4$ systematic convolutional codes with only one memory cell for each input, which generate half-rate TURBO codes ($R=1:2$).

The initial trellis code ($R=k:n$) is generated by a non-recursive and non-systematic structure described by the generating matrix:

$$G = [g_{ij}(x)]_{i=\overline{1,k},j=\overline{1,n}}. \tag{3}$$

The elements of G are constant or first order polynomials. The polynomial variable is the delay operator, D (for binary case) or x (in the general case of the GF symbols). The code will be denoted based on the coefficients of the generating polynomials, decreasing the variable powers.

There are a lot of $2:3$ binary symmetric convolutional codes with two memory cells. We have to find out the noncatastrophic codes which admit unique decoded output and to select the optimum one, deduced on the basis of the minimum Hamming distance criteria (Table 1).

Table 1

Optimum Binary Convolutional Code with Maximum Four State Variables

Convolutional Code	State-variables number	Coding rate	Free Hamming distance	Correctable error number
C(3,1)	1	1:2	3	1
C(11;01;31)	1	2:3	3	1
C(31;13;12)	2	2:3	4	$1+d$
C(7;11)	3	1:2	6	$2+d$
C(71;53;35)	4	2:3	5	2
C(11;18;6;52)	3	3:4	7	3

These optimal codes are non-recursive and non-systematic excepting the first one. The half-rate codes are not interesting for TURBO codes.

The $2:3$ codes must be systematized if they are used in TURBO coding algorithm.

The generating matrices of some codes and the square determinants are given in what follows:

1. C(31;13;12)

$$G1(x) = \begin{bmatrix} 1+x & 1 & 1 \\ 1 & 1+x & x \end{bmatrix}; \tag{4}$$

$$\Delta 12 = x^2;\ \Delta 13 = 1 + x + x^2;\ \Delta 23 = 1; \tag{5}$$

$g.c.d.\{\Delta 12;\ \Delta 13;\ \Delta 23\} = 1$, the code is non-catastrophic.

2. C(71;53;35)

$$G2(x) = \begin{bmatrix} 1+x+x^2 & 1+x^2 & 1+x \\ 1 & 1+x & 1+x^2 \end{bmatrix}; \tag{6}$$

$$\Delta 12 = x^3 + x^2;\ \Delta 13 = x^3 + x^4;\ \Delta 23 = x^2 + x^4; \tag{7}$$

$g.c.d.\{\Delta 12;\ \Delta 13;\ \Delta 23\} = x^2$; the code is non-catastrophic.

3. C(11;18;6;52)

$$G3(x) = \begin{bmatrix} 0 & 1 & 0 & 1+x \\ 1 & 0 & x & 1 \\ 1+x & 1 & 1 & 0 \end{bmatrix}; \tag{8}$$

the polynomial coefficients are given by:

$$C = \begin{bmatrix} 00 & 01 & 00 & 11 \\ 01 & 00 & 10 & 01 \\ 11 & 01 & 01 & 00 \end{bmatrix}. \tag{9}$$

Reading the transpose of C row-by-row and converting it into decimal, it results the coefficients of the code (11;18;6;52):

$$\Delta 123 = x + x^2 + x^3;\ \Delta 124 = 1 + x + x^2;\ \Delta 134 = 1;\ \Delta 234 = x; \tag{10}$$

$g.c.d.\{\Delta 123;\ \Delta 124;\ \Delta 134;\ \Delta 234\} = 1$; the code is non-catastrophic.

The generating matrices of the non-systematic non-recursive 2:3 trellis codes could be generally expressed as:

$$G_{\mathrm{NNC}} = \begin{bmatrix} a & b & c \\ b & a & d \end{bmatrix} \tag{11}$$

and its square determinants computed mod 2 are:

$$\Delta 12 = a^2 + b^2;\ \Delta 23 = bd + ac;\ \Delta 13 = ad + bc. \tag{12}$$

The recursive systematized code will have the generating matrix:

$$G_{\text{RSC}} = \begin{bmatrix} 1 & 0 & m \\ 0 & 1 & n \end{bmatrix}, \tag{13}$$

where

$$m = \frac{\Delta 23}{\Delta 12} x^p \qquad \text{and} \qquad n = \frac{\Delta 13}{\Delta 12} x^p;$$

here p is a value chosen to ensure the causality of the system.

So the RSC(31;13;12) has the modified generating matrix delayed by two bits in order to be causal and non-recursive:

$$G1_{\text{RSC}}(x) = \begin{bmatrix} 1 & 0 & \dfrac{1}{x^2} \\ 0 & 1 & \dfrac{1+x+x^2}{x^2} \end{bmatrix} x^2 = \begin{bmatrix} x^2 & 0 & 1 \\ 0 & x^2 & 1+x+x^2 \end{bmatrix}. \tag{14}$$

The RSC(71;53;35) has the generating matrix:

$$G2_{\text{RSC}} = \begin{bmatrix} \dfrac{x+x^2}{1+x^2} & 1 & 0 \\ \dfrac{1+x}{1+x^2} & 0 & 1 \end{bmatrix}. \tag{15}$$

Based on relations (14) and (15) the systematic coding structures result with minimum number of state variables (Figs. 2 and 3).

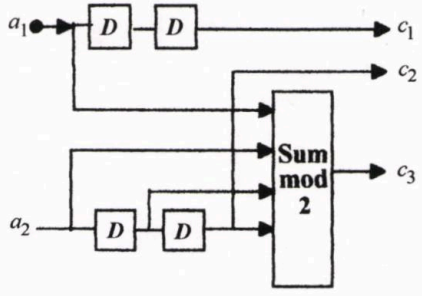

Fig. 2.– NSC(31;13;12) encoder.

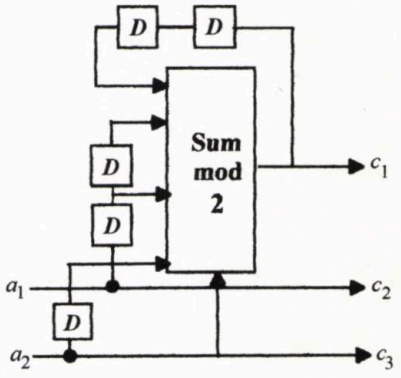

Fig. 3.– RSC(71;53;35) encoder.

3. Conclusions

Digital communication systems performances are improved using error-correcting codes. "Block" codes and "trellis" codes behaviour on TURBO coding is analysed

and compared. Symmetric TURBO algorithms are based on systematic coding structures. A method for 2:3 trellis coding systematization is proposed and optimum cases are deduced and processed.

Received, October 29, 2000

Technical University "Gh.Asachi", Jassy,
Department of Telecommunications

REFERENCES

1. Blahut R.E., *Digital Transmission of Information.* Addison-Wesley Publishing Co., 1990.
2. Berlekamp E.R., Peile R.E., Pope S.P., *The Application of Error Control to Communications.* IEEE Comm. Mag., **25**, *4*, 44-57 (1987).
3. Alexandru N.D., Scripcariu L., *About a NEW Algorithm for Minimum Hamming Distance Estimation of Convolutional Codes.* Proc. Internat. Conf. on "Development and Application Systems", **07**, Suceava, May 1996, 7-10.
4. Sklar B., *A Primer on Turbo Code Concepts.* IEEE Comm. Mag., **35**, *12*, 94-102 (1997).

STRUCTURI TRELLIS SISTEMATIZATE PENTRU CODURI TURBO SIMETRICE

(Rezumat)

Se studiază codurile corectoare de erori utilizate pentru codare TURBO simetrică. Sunt comparate codurile de tip „bloc" (Hamming, Reed-Solomon) cu cele de tip „arbore" (Trellis, convenţionale) în ceea ce priveşte posibilitatea utilizării lor pentru implementarea algoritmilor TURBO. Se propune o metodă de sistematizare a codurilor convenţionale cu rată de codare 2:3, generatoare de coduri TURBO de tip 1:2. Sunt deduse codurile convoluţionale binare optime şi structurile de codare sistematice ale acestora în câteva cazuri particulare.

BULETINUL INSTITUTULUI POLITEHNIC DIN IAŞI
Tomul XLVII (LI), Fasc. 1–2, 2001
ELECTROTEHNICĂ. ENERGETICĂ. ELECTRONICĂ

D.C. 621.314.5

HYBRID SYSTEMS – AN UNIFYING FRAMEWORK FOR POWER CONVERTER DYNAMICS MODELLING

BY
ADRIANA SÎRBU

Based on a previously proposed hybrid model for power converters, the dynamics of these particular electronic systems is described. Within this framework, the accurate description of the system trajectories and the control function of a power converter, the steady-state and the transient regime could be analytically approached. A comparative study with other existing models (differential equations based multi-models, Petri Nets – or bond graph – based models) is performed, investigation aimed to underline the adequacy of the proposed model both from the physical/electronic point of view and the mathematical rigor. The aspects of using the proposed model in simulation based quantitative analysis of power converters are finally commented.

1. Introduction

In a previous paper, [1], we have presented a new approach to power converter modelling from the hybrid dynamical systems point of view, [2],...,[8]. The proposed structural definition differentiated three sections: a discrete-time dynamics part, a continuous-time dynamics part, connected by means of a continuous–discrete interface. Each individual component of every section was explicitly detailed for the particular case of the power converter as a hybrid dynamic system.

In order to analytically describe the components of the model, we have introduced and we will use in the next sections the following notations: the input alphabet for the finite automaton (F) is defined by Σ, given in [1], equation (10), σ_c is the vector of controlled symbols, with elements in the alphabet Σ_c, given by relation (6) in [1] and modelling the gate signals applied to the controllable switches of the converter, while z is the augmented state-vector, introduced in [1], equation (22).

2. Power Converter Dynamics in Terms of the Hybrid Model

One of the benefits of the hybrid model is its capacity to allow, unlike other existing models, a rigorous definition of the control function of the power converter. Thus, this function has to be of discrete type, being produced by external events (signals), which have generated the forced commutations of the switching devices.

The control function of the converter is implemented by means of a sequence of time instants, $\overline{T}$:

$$\bar{t}_0 < \bar{t}_1 < \ldots < \bar{t}_i < \ldots, \tag{1}$$

at which vectors of controllable symbols σ_c, which have at least one nonvoid symbol, are delivered.

So, the control function appears as a succession of pairs:

$$(\bar{t}_0, \sigma_{c_0}),\ (\bar{t}_1, \sigma_{c_1}),\ \ldots,\ (\bar{t}_i, \sigma_{c_i}),\ \ldots \tag{2}$$

defined on the cartesian product $\overline{T} \times (\Sigma_c \setminus [b])$, where $[b]$ denotes the r_G dimensional vector with all symbols equal to the void symbol and r_G is the number of controlled switching devices.

One can notice that (2) formulates the most general possibility to command the converter by means of the signals applied on the gates of the power devices. However, from a practical point of view, in the control sequence (2) several restrictions are to be imposed both on the time instants, $\bar{t}_i$, and on the delivered vectors of symbols, σ_{c_i}.

So, the usual operation can be related to continuous disjoint segments of time $I_\rho = (a_\rho, a_\rho + 1]$, which is a covering of $\mathbf{R}_+ = \bigcup_{\rho=0}^{\infty} I_\rho$. Let us consider that $\overline{T}$ in equation (1) refers explicitly to the interval I_ρ. This partitioning of the continuous time semiaxis results from the practical way of establishing the sequence $\overline{T}$ in (1) for each I_ρ, which is related to certain time periods denoted generically by T_ρ. Within each period, T_ρ, the same vectors of controllable symbols are delivered, in the same order:

$$\sigma^\rho_{c_0},\ \sigma^\rho_{c_1},\ \ldots,\ \sigma^\rho_{c_{\nu_\rho - 1}}. \tag{3}$$

The number ν_ρ, the structure of the vector of symbols and the order of delivering are specific to the chosen application and are used during the same interval I_ρ.

In accordance to (2), the control function on the interval I_ρ is realized by specifying the time instants when the symbols are to be delivered, ordered as in (3) within the interval I_ρ by:

$$\overline{t^\rho_{p\nu_\rho + i}} = a_\rho + pT_\rho + \theta^\rho_i(T_\rho),\quad (i = 0, \ldots, \nu_\rho - 1;\ p = 0, 1, \ldots, p^\rho_{\max}), \tag{4}$$

where the shift duration, $\theta^\rho_i(T_\rho)$, with respect to the period T_ρ, depend on T_ρ and satisfy the ordering relation:

$$0 < \theta^\rho_0 < \theta^\rho_1 < \ldots < \theta^\rho_{\nu_\rho - 1} < T_\rho, \tag{5}$$

with the possibility of equality at one extremity.

As compared with the general notation proposed in [1], equation (32), we explicitly used the superscript ρ to emphasize the belonging to I_ρ. Usually, for the upper extremity of the interval, I_ρ, the following condition is fulfilled:

$$a_{\rho+1} = a_\rho + (p^\rho_{\max} + 1)T_\rho. \tag{6}$$

So, during the circuit operation, the intervals I_0, I_1,..., I_ρ follow one another, each of them being a multiple of the period used to construct the control sequence.

It is to be noticed that the individuality of each interval I_ρ is given by the period T_ρ and by the vectorial function

$$\Theta_\rho(T_\rho) = [\,\theta_0^\rho \quad \theta_1^\rho \quad \ldots \quad \theta_{\nu_\rho-1}^\rho\,], \tag{7}$$

the components of which satisfy (5). In what follows the vector Θ_ρ will be referred to as the command vector.

Practically, by means of the time instants θ_i^ρ (when the symbols $\sigma_{c_i}^\rho$ are delivered) one models the pulse width modulation function, T_ρ. This function can be defined by means of a control parameter vector π, m_π-dimensional, which can include modulation indices, firing angles, phase displacement angles. The application which expresses Θ_ρ as a function of the vector π, on the interval I_ρ, will be denoted

$$\eta_\rho : \mathbf{R}^{m_\pi} \to \mathbf{R}^{\nu_\rho}. \tag{8}$$

Generally, the definition of η can be modified as a function of ρ.

Based on the above discussion, one can easily conclude that the control function of the converter is implemented by means of the period T_ρ and of the map η_ρ which provide the vector-valued function $\Theta_\rho(T_\rho)$ (possibly with variable number of elements ν_ρ), $\Theta_\rho(T_\rho)$ being referred to as gating time instants vector.

Depending on the type of energy conversion (AC/AC, DC/AC, DC/DC), from one interval to another, both T_ρ and Θ_ρ may be varied, or only T_ρ, or only Θ_ρ. For example, for the AC/DC converters, $T_\rho = T$ remains unchanged (equal to the period of the AC power supply), and the control is implemented exclusively by means of Θ_ρ. For certain resonant DC/DC converters, [11], only T_ρ is changed (θ_i^ρ keeping the same definition as a function of T_ρ, that is $\theta_i^\rho(T_\rho) = \theta_i(T_\rho)$, $\forall\, \rho$).

The operation of the converter during the I_ρ interval will be referred to as the ρ functioning cycle.

We are now in the position to rigorously formulate the problematic of the transient and steady-state dynamics for the operation of a power converter. For the sake of simplicity we suppose that the dynamics is analyzed on the whole semiaxis of time, that is we consider an interval of form $I_0 = [0,\ \infty)$. The time instants at which the gating signal are applied are defined by means of the period T_0 and of the ν_0-dimensional vector Θ_0. (Obviously these values remain unchanged as we refer to the interval I_0-real positive semiaxis and this fact is equivalent to stating that the map η is unchanged and so the vector π is constant). Under the assumption that there exist a steady-state, the transient evolution of the continuous state $z \in \mathbf{R}^n$, corresponding to a certain initial conditions and to the control parameters T_0, Θ_0, is described by

$$z_{(T_0,\theta_0)}(t) = z^{\mathrm{pe}}_{(T_0,\theta_0)}(t) + z^{\mathrm{tr}}_{(T_0,\theta_0)}(t), \tag{9}$$

where

$$\lim_{t\to\infty} z^{\mathrm{tr}}_{(T_0,\theta_0)}(t) = 0 \tag{10}$$

and

$$z^{pe}_{(T_0,\theta_0)}(t+T_0) = z^{pe}_{(T_0,\theta_0)}(t), \quad t \in [0,\infty), \tag{11}$$

is a periodic function, with period T_0.

The steady-state is described by the trajectory $z^{pe}_{(T_0,\theta_0)}(t)$ which represents a closed asymptotically stable (at least locally) orbit in $\mathbf{R}^n$. It is obvious that choosing other control parameters T_0 and/or Θ_0 will determine another closed orbit. Generally, the transfer from one steady-state to another is accomplished by changing T_k and/or Θ_k, the transient regime being described by (10).

We must emphasize that the existence of steady-state hypothesis is supported only by practice, meaning that power converters operation exhibit this property. The results available until now in hybrid system theory can not handle the complexity of the proposed structure, more specific, the following aspects: the mixture between internal and external discrete events and the deliverance of non void symbols which influence only the physical state of the devices, but are ineffective for the open/closed state of the switch (as it is the case for the thyristors or GTOs).

The proposed model was successfully used in simulation for different power converter topologies, [2], [9]. One of the most profitable results obtained using this approach was devising a new and extremely efficient method to determine the steady-state of the power converter, [10].

3. The Compatibility Between the Hybrid Model and Other Power Converter Models

Starting from the hybrid model proposed for the power converters, one can perform a comparative study with other existing models (differential equations based multi-models, Petri Nets – or bond graph – based models), investigation aimed to underline the adequacy of the proposed model both from the physical/electronic point of view and the mathematical rigor.

3.1. The Compatibility with Differential Equation Based Multi-Models

For this case the mathematical abstraction refers to the solutions of differential equations on the sets on which this solutions are defined. In fact, these solutions are (possibly after some linear transformations) just the transition functions of the dynamical functions belonging to the family $\{S_k\}$ of smooth time-invariant functions, [1], which belong to the structure of the dynamical system. But while in the commutation time instants the existence of the solution is guaranteed only by means of intuitive arguments for the case of differential equations based multi-models, the mechanism of commutation for the dynamic systems from the structure of the hybrid system, (M_s), rigorously ensures the transfer of the state of one mode in the initial state of the next mode. In this way the hybrid model guarantees the existence of the trajectories for the entire positive real semi-axis of time, $\mathbf{R}_+$.

Moreover, based on the structural representation of the hybrid model and on the details in previous section, the control of the converter by means of discrete

events and the switching of the linear dynamics are fully consistent from the system theory point of view. In the multi-model description these elements appear only as simple analytical conditions necessary to specify the domains of definition for each differential equation, or, in other words, the discontinuity points of the vector fields.

Based on these assessments we assert that any differential equation based multi-models can be transposed in the hybrid dynamical system framework, with an adequate construction of the continuous–discrete interface (I) and of the finite automaton (F), [1]. This unifying characteristic of the hybrid model results from the geometrical foundation of the approach namely: the hybrid system is defined directly in the global terms of the trajectories, while the differential equation expressed local correlations between the trajectories and certain vector fields. Consequently, all the descriptions of multi-models type, built with circuit theory specific methods, [13], can be transposed in the transition functions form which enter in the structure of the continuous part of the hybrid system.

3.2. The Compatibility with Petri Nets Based Models

To concatenate the differential equation based models associated to the functioning modes of the converters several authors used Petri Nets (as for example [14], [15]). Through this approach a rigorous discrete dynamics was created which interacts with the continuous one in a manner specific to the hybrid systems. The similarity results from the fact that the finite automaton (F) from the hybrid structure proposed in [1] is equivalent to the particular type of Petri Nets used to sequentiate the models (state-automaton network, in which each transition has only one input arch and only one output arch, the transitions Modeling events). What is still inconsistent in these approaches is the rigorous analytical definition of the mathematical objects which implement the interface as a distinct element in the hybrid system structure and implicitly the behavior of the differential equations at the switching time instants.

3.3. The Compatibility with Bond Graph Models

Processing the bond graph which models the energy transfer in a power converter, one gets differential equations type descriptions. A significant progress towards the hybrid Modeling is ensured by the energetic approach it self which allows deriving a unique acausal graph, [16]. This incorporates both the continuous dynamics of the passive elements as resistors, inductors and capacitors, and the discrete dynamics (open–closed) of the switching devices. Moreover, by appropriate gathering of the "0" junctions, all the switches can be grouped together into a cell responsible for the occurrence of all the commutations. Although the commutation mechanism has an energetic essence, it is capable to provide all the binary combinations of the switches and at the same time is structurally isolated from the continuous part.

For a graphical suggestive image one can examine the diagram in Fig. 1 in which by means of multiple arrows the global energetic transfer originated by the sources is suggested. In this way two different dynamical entities are delimited, which unlike

discrete–continuous interface in the hybrid model, are interfaced based on energetic principles.

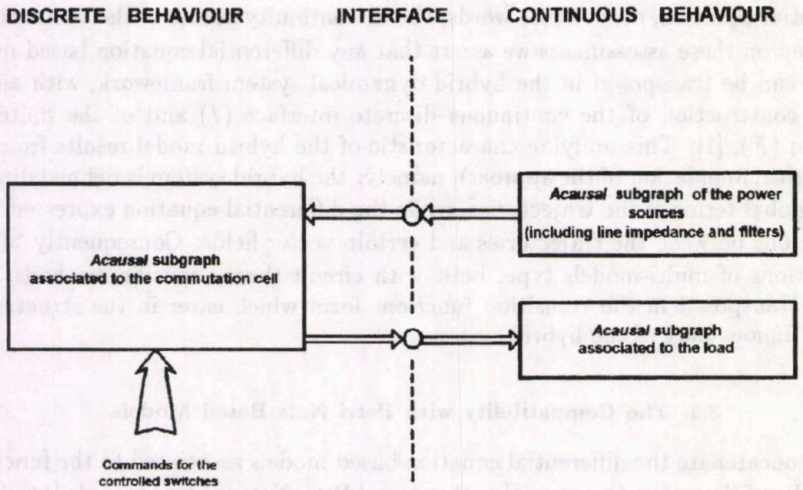

Fig. 1.– Diagram of the connections between acausal bond subgraphs associated to the sources (including lines and filters), the switches and the load.

However, the acausal graph which reveals the hybrid structure is an incomplete model. Thus the time-variable assignment of the integral causality [16], [17], induces several causal graphs (that is several differential equations based models), the chaining of which creates problems as described above. In other words, the existing structure of the hybrid system in the stage of the acausal graph disappears. In this context it is worth mentioning the idea in [18], to define the sequence of the associated causal graphs by means of a Petri Net, solving in this way the problems commented in the previous sections.

On the other hand, the time-invariant assignment of the causality keeps the uniquenesss of the causal graph and, at the same time, the separation, in the final model, between the commutation cell, with discrete behaviour and the continuous dynamics.

Based on the causality assignement in the diagram depicted in Fig. 1 one establishes the input and output signals originating from the two multiple connection points of the interface, with respect to the three constitutive blocks. For the case of integral causality assignment, for each configuration of the switches in the commutation cell, the whole ensemble can be modeled as a linear dynamic system, equivalent (applying, if necessary, some linear transformations in $\mathbf{R}^n$) with a member of the family $\{S_k\}$ from the structure of the hybrid system presented in [1]. The commutation cell (by means of the switch characteristics) has the role of mode sequentiator played by the automaton (F) from the hybrid system structure, [1].

The main difference when comparing to (F) consists in the fact that the commutation cell is crossed just by the signals which characterize the continuous dynamic systems, that is signals with energetic content. That is why, from the mathematical point of view, the discontinuities in the switch characteristics appear in the vector field of the attached differential equation, at the commutation time instants, fact which generates the problems indicated in the previous section.

4. Hybrid Modelling in Simulation Based Quantitative Analyze of Power Converter Dynamics

We showed that complex analytical form of the signals which characterizes the operation of a power converter can be rigorously modeled based on the concept of hybrid system. This fact is directly reflected in the quantitative analysis area by means of the possibility offered to build simulation models which accurately and efficiently exploit the commutation problem from the algorithmic point of view (commutation instants and definition of the transition function in these instants).

As there are very few theoretical results for the qualitative analysis of the complex power converter dynamics, simulation plays a central role in the quantitative analysis.

The topic of this section must be regarded in the context of the existence in the scientific community, for over a decennium, of many approaches to the simulation of power converters. During this period a lot of notable results concerning the devising and exploitation of adequate software products have been reported.

We want to stress that the simulation effectively consists in the construction of a trajectory in $\mathbf{R}^n$, the existence of which is subsidiary presumed. For the hybrid model, the existence of the trajectory associated with any initial state is theoretically guaranteed by the structural dynamic definition, detailed in the previous section, while for other types of models, as we commented above, the existence is not rigorously guaranteed and is accepted from physical considerations invoked for the commutation time instants. Thus, one can ascertain that these problems of punctual nature, which in the analytical approach rise serious difficulties concerning the existence and uniqueness of the solution, in the numerical approach they do not represent an impediment, and the simulation can be performed based on an *ad-hoc* procedure which allows for the construction of the transition function in the vicinity of the commutation instants.

In the spirit of this clear distinction between the rigor of the analytical formulation and the possibility to numerically exploit a model, it becomes obvious that the reviewed models in the previous sections can be used in simulation. After all, we proved that there is a full compatibility, from the dynamics local description point of view, as long as the vector field has no discontinuities.

The proposed hybrid model offers a systematic procedure to handle internal or external discrete events which specify the switching of the continuous dynamics and can use for the numerical generation the transition functions φ_k, [1], equation (17), any differential equation type model equivalent to [1], equation (20), provided either

by system energy processing methods, or by circuit theory specific methods. This fact is directly reflected in the quantitative analysis area by means of the possibility offered to built simulation models which efficiently exploit the commutation problem from the algorithmic point of view (commutation instants and definition of the transition function in these instants).

We have successfully used the differential equation based multi-model and the bond graph model in the analysis and simulation of different power converters, as reported for example in [9], [10], [19], [20].

5. Conclusions

The main goal of the paper is to demonstrate the viability of the hybrid dynamical system based model for power converters, model proposed in a previous paper, [1]. Thus, the approach of power converters modelling from the hybrid systems point of view proves to be adequate and rigorous. The most important result is the possibility offered by this type of model to analytically describe the control function of a power converter, incorporating in a rigorous framework engineering concepts as gate-signals, modulation and so on.

It was also proved that different simulation models reported in the literature had in fact as algorithmic support models possessing hybrid structure characteristics, incompletely substantiated as concerns the behavior at the commutation instants, but presenting practical strategies for the calculus of the trajectory, while assigning additional properties in order to define it at the commutation instants. This is the reason why we consider that the proposed model is the main nucleus, which by adequate mathematical formulation, provides compatibility between different existent techniques of modelling power converters, practically, incorporating them and offering the most general framework in this field.

Received, December 12, 2000

Technical University "Gh.Asachi", Jassy,
Department of Telecommunications

REFERENCES

1. Păstrăvanu A., *A New Point of View Concerning the Power Converter Modelling.* Bul. Inst. polit., Iaşi, **XLIV (XLVIII)**, *3-4*, s.III, 97-109 (1998).
2. Păstrăvanu A., *Contribuţii la proiectarea, modelarea şi simularea acţionărilor electrice de curent continuu.* Ph. D. Diss., Tech. Univ. "Gh. Asachi", Jassy, 1996.
3. Branicky M.S., Bokar V.S., Mitter S.K., *A Unified Framework for Hybrid Control: Background, Model and Theory.* Proc. of the 33rd Conf. on Decision and Control, Lake Buena Vista, Florida, Dec. 1994, 4228-4234.
4. Antsaklis P.J., Lemmon M., Stiver J.A., *Modeling and Design of Hybrid Control Systems.* Proc. of 2nd IEEE Mediter. Symp. on New Directions in Control & Automation, Creta, Greece, June 19-22, 1994, 440-447.
5. Lennartson B., Egardt B., Tittus M., *Hybrid Systems in Process Control.* Proc. of the 33rd Conf. on Decision and Control, Lake Buena Vista, Florida, December 1994, 3587-3592.
6. Dogruel M., Ozguner U., *Modelling and Stability Issues in Hybrid Systems.* Lecture Notes in Computer Science – Hybrid Systems II, *999*, 148-165 (1995).

7. Ye H., Michel A., Antsaklis P., *A General Model for the Qualitative Analysis of Hybrid Dynamical Systems.* Proc. of the 34th Conf. on Decision and Control, New Orleans, Dec. 1995, 1473-1477.
8. Ye H., Michel A., Hou L., *Stability Theory for Hybrid Dynamical Systems.* Proc. of the 34th Conf. on Decision and Control, New Orleans, Dec. 1995, 2679-2684.
9. Păstrăvanu A., *Simulation of Power Converters as Hybrid Systems with Continuous Semigroups of Linear Operators.* Proc. of the 5th Conf. of Internat. Assoc. for Math. a. Comp. in Simulation, IMACS'96, Saint-Nazaire, September 17-19, 1996, 529-534.
10. Păstrăvanu A., *A Direct Approach to Steady-State Dynamics of Power Converters.* Proc. of the 7th Internat. Power Electronics & Motion Control Conference, Budapest, Sept. 2-4, 1996, 3/536-539.
11. Verghese G., Elbuluk M., Kassakian J., *A General Approach to Sampled-Data Modeling for Power Electronic Circuits.* IEEE Trans. on Power Electronics, **PE-1**, *2*, 76-88 (1986).
12. Visser H.R., van den Bosch P.P.J., *Modelling of Periodically Switching Networks.* IEEE Power Electronic Specialists Conf. Rec., 67-73 (1991).
13. Balabanian N., Bickart T., *Teoria modernă a circuitelor*, (transl. from English). Ed. Tehnică, Bucureşti, 1974.
14. Yao P., Glao S., Manese G.M., *Extension of the Hybrid Analysis Method for Numerical Simulation with Variable Topology of Switched Power Converters.* Proc. of IMACS'TCI-93, Montreal, July 7-9, 1993, 385-391.
15. Yan F., Shi L., Manese G.M., *Automatic Modelling of Power Static Converters by Parallel Petri Nets.* Proc. of IMACS'TCI-93, Montreal, July 7-9, 1993, 477-482.
16. Buisson J., *Analysis and Characterization of Hybrid System with Bond-Graphs.* IEEE Syst. Man and Cybernetics Conf. Proc., Lille, October 17-20, 1993, 264-269.
17. Borne P., Dauphin-Tanguy G. *et al., Modélisation et Identification des Processus.* Edition Technip, Paris, 1995.
18. Michel P., Masche B., Manesse G., *Bond Graph Enumeration of the Configurations of Power Static Converters.* IEEE Syst. Man and Cybernetics Conf. Proc., October 17-20, 1993, 251-256.
19. Păstrăvanu A., Gogu M., *Block Diagram Modeling and Simulation in a Bond Graph Framework.* Proc. of BEC'96, the 5th Biennial Conf. on Electronics and Microsystems Technology, Tallinn, October 7-11, 1996, 221-224.
20. Sîrbu A., Alexa D., Cleju I., *Robust Fourier Analysis of Variable Topology Systems in a Switched Bond-Graph Framework.* Proc. of 16th IMACS World Congress, Lausanne, Switzerland, 2000.

SISTEMELE HIBRIDE – UN CADRU UNIFICATOR PENTRU MODELAREA DINAMICII CONVERTOARELOR DE PUTERE

(Rezumat)

Folosind un model hibrid pentru convertoarele de putere, se descrie dinamica acestui tip particular de sisteme electronice. În acest cadru se pot aborda riguros: descrierea traiectoriilor sistemului, funcţia de control, regimul permanent şi cel tranzitoriu. Se efectuează, de asemenea, un studiu comparativ cu alte modele existente în literatură (multi-modele bazate pe sisteme de ecuaţii diferenţiale, modele ce folosesc reţele Petri sau grafuri Bond), investigaţie menită să sublinieze adecvanţa modelului propus, atât din punct de vedere fizic/electronic, cât şi din punct de vedere riguros analitic. Se comentează, în final, câteva aspecte legate de folosirea modelului propus în analiza cantitativă, bazată pe simulare, a convertoarelor electronice de putere.

BULETINUL INSTITUTULUI POLITEHNIC DIN IAŞI
Tomul XLVII (LI), Fasc. 1–2, 2001
ELECTROTEHNICĂ. ENERGETICĂ. ELECTRONICĂ

D.C. 621.317.39

NEW MEASUREMENT METHOD OF THE THERMAL DIFFUSIVITY IN SOLIDS USING TIME MEASUREMENTS

I. THEORETICAL APPROACH

BY

N. DAMEAN and EMIL VREMERĂ

A new method for the measurement of the thermal diffusivity in solids using transient conditions is proposed. This method utilizes the principle of superposition of thermal loads. Only time measurements are required, and no accurate temperature and heat flow rate measurements are needed. The method utilizes the Seebeck effect for the measurement of the time dependence on the temperature. A solution of the heat transfer equation for the model pertinent to the described method is derived, and a practical approach is proposed for developing.

1. Introduction

The thermal conductivity of solids is an intrinsic physical property of the material, and is of great importance in determining heat flow rates and temperature distribution in the solid.

Many experimental methods for the measurement of the thermal conductivity of solids are described in the literature. Most of these methods are based on the conductive heat transfer equation solution, with well-defined boundary conditions. All the measurements are performed by applying a thermal load to the sample, and monitoring the resulting temperature distribution in the sample. The measurements are performed under either steady-state or transient conditions approximating the boundary conditions used in the analytical solution. The temperatures and heat transfer rates are measured at selected locations from which the thermal conductivity can be deduced.

In the steady-state measurements, a constant heat flux is driven through a sample of fixed cross-section. The temperatures at a few points along the sample are measured, and the thermal conductivity is calculated using Fourier's equation [1].

Other methods are performed in transient conditions [2], where the physical property measured is the thermal diffusivity rather than the thermal conductivity; each of these methods is based on a geometrical model on which specific thermal load and boundary conditions are induced. The differential equation describing the thermal conditions is integrated using the chosen boundary conditions. The solution yields a

relation between the measured temperature values and the thermal diffusivity [3].

All those methods are based on accurate heat flow rate and temperature measurements using thermocouples, thermistors or infrared detectors; the accuracy of the temperature measurements is of major importance regarding the accuracy of the thermal diffusivity values obtained.

A new method for the thermal diffusivity measurement in solids in transient conditions is proposed in what follows. It uses the principle of superposition of thermal loads. In this method, an arbitrary thermal load (*e.g.* a continuous line source) is applied to a sample of a given shape for a time $t = t_0$. This interrupted thermal load may be treated as a superposition of a continuous line source applied at $t > 0$, together with another continuous line source of the same magnitude but of negative sign, which is applied for times $t > t_0$. The solution of the differential equation for the temperature distribution at the given thermal loads and boundary conditions shows a maximum temperature as a function of time at any point in the sample. The time at which the maximum is obtained can be accurately measured, and the accuracy of the time measurement is independent of the accuracy of the temperature measurement.

The thermoelectric effect, by which an electric EMF is generated in a conductor as a result of a difference of temperatures at its two ends, is instrumented as an additional means (like thermocouples, thermistors, etc.) for measuring the thermal signal.

In this paper, the above mentioned new method for measuring the thermal diffusivity of solids is developed. The thermal load is a one-dimensional uniform heat flux and the response signal is detected using the Seebeck effect in the sample. The ratio of the time, τ, when the signal goes through a maximum, to the applied thermal load time, t_0, relates the thermal diffusivity of the sample to its dimensions, but is independent of the Seebeck coefficient or the magnitude of the thermal disturbance.

A solution of the heat transfer equation for the model pertinent to the described method is presented. An apparatus approximating the model assumptions and using the new method is also proposed for measuring the thermal diffusivities of solids.

2. Thermal Model

The thermal model chosen for the measurement of the thermal diffusivities of electrical conductors is a one-dimensional infinite slab of thickness L.

One surface of the infinite slab is maintained at a constant temperature, T_∞, while at other surface a uniform heat flux is applied for a time $t = t_0$, (s. Fig. 1).

Let be

$$\theta = T - T_\infty \tag{1}$$

the difference of temperatures. The differential equation with partial derivatives and boundary conditions for this problem are:

$$\frac{\partial^2 \theta}{\partial x^2} = \frac{1}{\alpha} \cdot \frac{\partial \theta}{\partial t}, \tag{2}$$

respectively

$$(3)\quad \theta(x,0)=0;\quad \theta(L,t)=0;\quad \left(\frac{\partial\theta}{\partial x}\right)_{(0,t)}=-\frac{q_0}{k},\ t_0\geq t>0;\quad \left(\frac{\partial\theta}{\partial x}\right)_{(0,t)}=0,\ t>t_0.$$

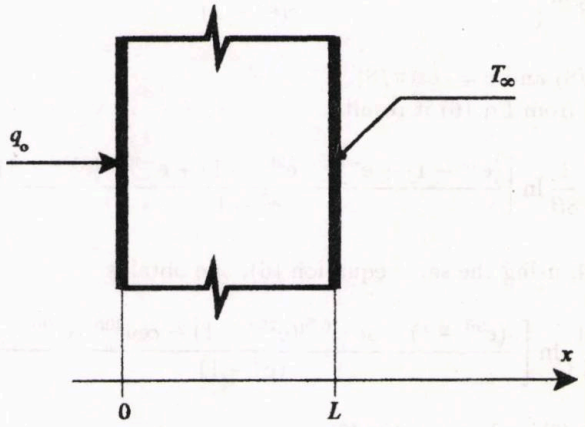

Fig. 1.– The thermal model.

The detailed solution of differential equation (2) and boundary conditions (3) is given in Appendix A. The solution yields an expression for the temperature as a function of time and location in the sample, for time $t > t_0$ (s. equation (A.8)):

$$(4)\quad \theta(x,t)=\frac{8q_0L}{\pi^2k}\sum_{n=0}^{\infty}\frac{\cos\dfrac{(2n+1)\pi x}{2L}}{(2n+1)^2}\left[e^{-(2n+1)^2\pi^2\alpha(t-t_0)/(4L^2)}-e^{-(2n+1)^2\pi^2\alpha t/(4L^2)}\right].$$

Inspection of expression (4) shows that the temperature goes through a maximum at different times for different x values. The time $t = \tau$ at which the temperature reaches a maximum is obtained by differentiating this expression with respect to time and setting the derivative to 0 (s. Appendix A). The dimensionless parameters:

$$(5)\qquad \beta=\frac{\pi^2\alpha t_0}{4L^2},\quad \eta=\frac{\tau}{t_0},$$

are defined, where the expression for β includes material properties, sample dimensions and the thermal disturbance duration. In contrast, η is the ratio of the measured time, τ, for the signal in the sample to reach a maximum to the applied thermal load time, t_0. One obtains

$$(6)\qquad \sum_{n=0}^{\infty}\cos\frac{(2n+1)\pi x}{2L}\left[e^{-(2n+1)^2\beta\eta}-e^{-(2n+1)^2\beta(\eta-1)}\right]=0.$$

The conditions at $x = L/4$, $x = L/2$ and $x = 3L/4$ are of special interest. It is found that truncating expression (6), after the first four members, yields an inaccuracy of less than 0.001%.

For $x = L/4$, using Eq. (6), one obtains

$$\eta = \frac{1}{8\beta} \ln \left[\frac{-s(e^{9\beta} - 1) + se^{-16\beta\eta}(e^{25\beta} - 1) + ce^{-40\beta\eta}(e^{49\beta} - 1)}{c(e^{\beta} - 1)} \right], \tag{7}$$

where $s = \sin(\pi/8)$ and $c = \cos(\pi/8)$.

For $x = L/2$, from Eq. (6) it results:

$$\eta = \frac{1}{8\beta} \ln \left[\frac{(e^{9\beta} - 1) + e^{-16\beta\eta}(e^{25\beta} - 1) + e^{-40\beta\eta}(e^{49\beta} - 1)}{e^{\beta} - 1} \right]. \tag{8}$$

For $x = 3L/4$, using the same equation (6), one obtains

$$\eta = \frac{1}{8\beta} \ln \left[\frac{s(e^{9\beta} - 1) - se^{-16\beta\eta}(e^{25\beta} - 1) - ce^{-40\beta\eta}(e^{49\beta} - 1)}{c(e^{\beta} - 1)} \right], \tag{9}$$

where $s = \sin(3\pi/8)$ and $c = \cos(3\pi/8)$.

Equations (7),...,(9) represents the relations between the measured times (appearing in η), and the material properties (in β) as shown in Fig. 2.

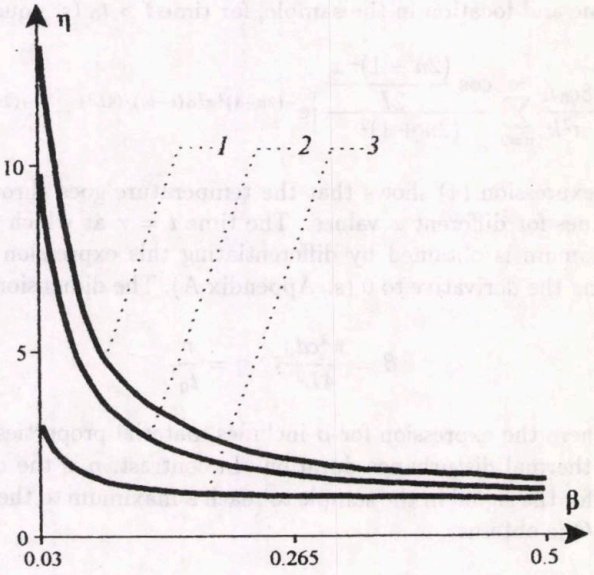

Fig. 2.– η values as a function of β: *1* – $x = 3L/4$; *2* – $x = L/2$; *3* – $x = L/4$.

3. Apparatus

The apparatus used for the measurements and the principle of measurement described in the present work are shown in Fig. 3.

During the measurement, the rod-shaped sample *2* is covered by a very good insulator *3* ($k \approx 3 \times 10^{-2}$ $Wm^{-1}K^{-1}$). This arrangement approximates the one-dimensional model used here. One end face of the sample is in good thermal contact with a cylindrical copper block (*4*) which serves as a heat sink at the temperature,

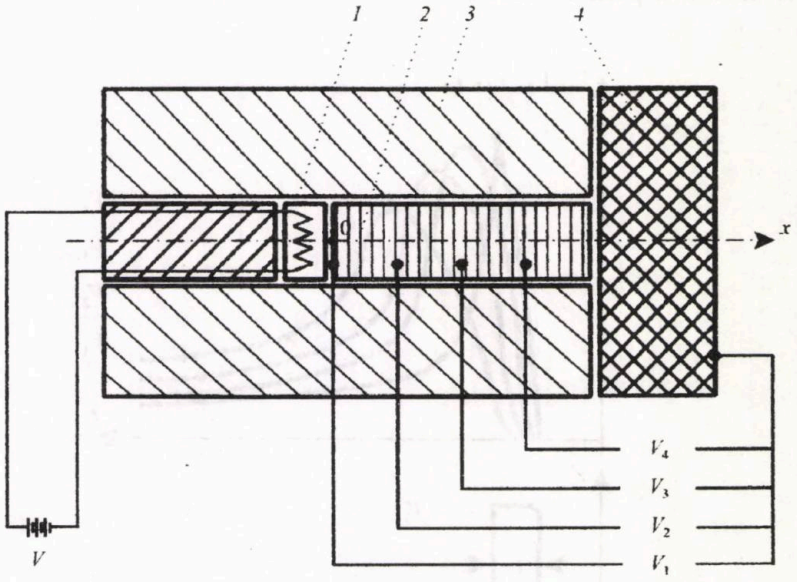

Fig. 3.– Experimental apparatus and measurement principle: *1* – heater; *2* – sample; *3* – thermal insulation; *4* – heat sink (cooper block).

T_∞. The thermal contact is assured by applying thermal conductive paste to the copper block at the contact surface. The other end face is in contact with a very low heat capacity heater (*1*) which is pressed against the rod by a spring-loaded holder. The tension of the spring can be controlled by a tightening screw. The heater is electrically insulated from the sample by a thin electrical insulator. The thermal signal from the sample is obtained *via* four thin copper wires touching the sample and a wire attached to the copper block. One copper wire is in contact with the sample face at the heater end, and the others at the exact places of $L/4$, $L/2$ and $3L/4$ on the sample's cylinder face. Four thermoelectric EMFs are measured (V_1, V_2, V_3, V_4) for each copper wire with respect to the copper block which is maintained at a constant temperature. The sample and insulation are encased in a PVC housing

for structural stability.

The measurement is performed by applying a constant voltage, V, to the heater for a definite time, t_0 (a square pulse heat load). The signals V, V_1, V_2, V_3, V_4 are stored in a memory. A representative measurement showing the obtained five curves is represented in Fig. 4. From the square heating pulse, V, the exact heat pulse duration, t_0, is measured. The thermoelectric response, V_1, at the face of the sample which is in contact with the heater, is synchronous with the heater pulse. It starts immediately at the rise of the heater pulse, and its rise is abruptly stopped at the end of the heater pulse. On the other hand, the others thermoelectric EMFs (V_2, V_3, V_4) are delayed, and are rising slowly until they reach a maximum at time τ well after the heater pulse V is over.

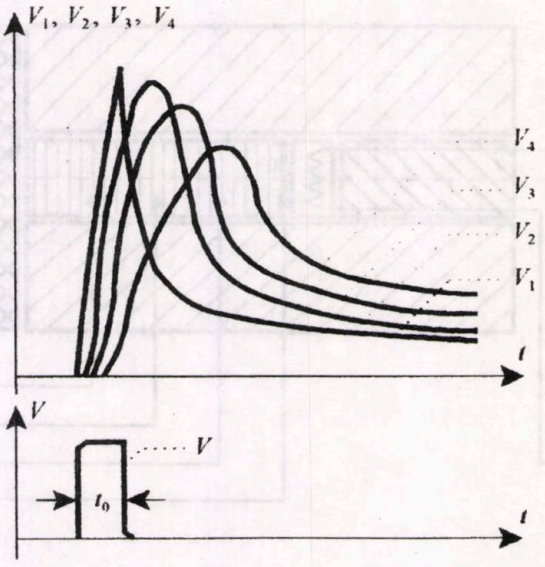

Fig. 4.– Signal dependences *vs.* time: V – signal applied to the heather; V_1, V_2, V_3, V_4 – measured signals.

The described here method utilizes the thermoelectric EMF generated by the Seebeck effect. This EMF is measured between four copper contacts with a sample and the heat sink. This method is used for the measurement of the thermal diffusivity of various metals.

Therefore, the values of t_0 and τ are derived by the measurements. The values of β are found from equations (7),...,(9), depending on the copper wire used. Finally, the thermal diffusivity is calculated using Eq. (5).

When preparing the sample and during the optimization of measurement parameters the following considerations had to be taken into account:

a) The power rating of the small heater element is very limited, and therefore is

the magnitude of the thermoelectric EMFs obtained for a given thermal load duration t_0 in the measurement is very limited too.

b) The thermal load duration has to be small with respect to the thermal disturbance transition time in the sample. This means that increasing the height of the signals by making the thermal disturbance longer is possible only up to a limit.

c) The using of a high thermal load implies the dependence of the thermal diffusivity on temperature.

d) Due to the heat dissipation along the sample, the longer the sample length the weaker the obtained thermoelectric EMF signal.

e) Depending on the obtained values of $\eta = \tau/t_0$, the values of β can be obtained from the Eqs. (7),...,(9), in accordance with the corresponding copper wire (s. Fig. 2). The fourth wire is used for materials having high thermal diffusivity, but the second wire is used for materials having small thermal diffusivity.

f) The proposed method involves only time measurements and does not require temperature measurement. Thus, it is considered to yield more accurate results than methods using temperature measurement.

Concerning the error analysis, there are two kind of errors which must be considered: errors ralated to the chosen model and errors related to the measurement process.

The using of the unidimensional heat equation is justified if a good thermal isolator on the sample surface is applied.

The most important source of errors is determinated by the positioning error of the copper wires. It is considered that a $\pm 2\%$ positioning error can determine a $\pm 4\%$ thermal diffusivity error.

Also, some other errors can appear at the measurements of t_0 and τ; operating time of thermal load, t_0, can be determinated precisely. The measurement error of τ depends on the level of the EMFs signals. It is considered that a $\pm 2\%$ error for τ can determine a $\pm 2\%$ thermal diffusivity error. As an overall estimation, the total error for thermal diffusivity measurement is of $\pm 5\%$, in comparison with 10...15% when the classical methods are used (s. [4]).

4. Conclusions

The new diffusivity measurement method, proposed in this paper, implies time measurement and does not require temperature or heat flux measurement, as it is the case of the classical methods. An immediate consequence of this characteristic is the small measurement error for the new method in comparison with the usual methods.

The theoretical approach of the method is detailed, and an experimental apparatus is proposed. Some recommendations for further improvements of the practical approach are included.

Apendix A

Derivation of the Equations

A.1. Uniform Heat Flux

The thermal model is shown schematically in Fig. 1. We define θ as in relation (1), where T_∞ is the ambient temperature at $t=0$ and also the constant temperature at the cold side of the sample ($x=L$), which is in good contact with the heat sink.

The differential equation with partial derivatives and the boundary conditions are done, respectively, by (2) and (3).

The solution of this problem is given in [3]:

$$\theta(x,t)=\frac{q_0 L}{k}\left[\left(1-\frac{x}{L}\right)-\frac{8}{\pi^2}\sum_{n=0}^{\infty}\frac{\cos\dfrac{(2n+1)\pi x}{2L}}{(2n+1)^2}e^{-(2n+1)^2\pi^2\alpha t/(4L^2)}\right], \tag{A.1}$$

where $n=0,1,2,3,\ldots$.

Relation (A.1) shows the temperature distribution as a function of time and location in the sample.

A.2. The Superposition of Thermal Loads

The principle of superposition of thermal loads may be applied for the solution of the problem presented above. The thermal load in the plane $x=0$ is given by (A.1) together with the boundary conditions (3_3), (3_4).

The principle of superposition of thermal loads may be realized by superimposing two thermal loads as shown in Fig. 5.

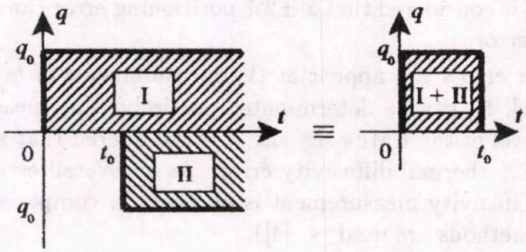

Fig. 5.– The principle of superposition of thermal loads.

The resulting temperature distribution in the sample at time $t > t_0$ is the sum of the two temperature distributions obtained in expression (A.1), taking into account the time lag and opposite sign of the two loads:

$$\theta(x,t)=\frac{q_0 L}{k}\left[\left(1-\frac{x}{L}\right)-\frac{8}{\pi^2}\sum_{n=0}^{\infty}\frac{\cos\dfrac{(2n+1)\pi x}{2L}}{(2n+1)^2}e^{-(2n+1)^2\pi^2\alpha t/(4L^2)}\right]- \tag{A.2}$$

$$-\frac{q_0 L}{k}\left[\left(1-\frac{x}{L}\right)-\frac{8}{\pi^2}\sum_{n=0}^{\infty}\frac{\cos\dfrac{(2n+1)\pi x}{2L}}{(2n+1)^2}e^{-(2n+1)^2\pi^2\alpha(t-t_0)/(4L^2)}\right].$$

Rearranging the terms of this equation, one obtains

$$\theta(x,t) = \frac{8q_0L}{\pi^2 k}\sum_{n=0}^{\infty}\frac{\cos\dfrac{(2n+1)\pi x}{2L}}{(2n+1)^2}\left[e^{-(2n+1)^2\pi^2\alpha(t-t_0)/(4L^2)} - e^{-(2n+1)^2\pi^2\alpha t/(4L^2)}\right]. \tag{A.3}$$

Notations

C – specific heat, [J kg^{-1}K^{-1}];
k – thermal conductivity, [W m^{-1}K^{-1}];
L – slab length, [m];
n – integer;
q_0 – uniform heat flux, [W m^{-2}];
t – time, [s];
t_0 – operating time of thermal load, [s];
T – temperature, [K];
T_∞ – heat sink temperature, [K];
x – axial coordinate, [m];
α – thermal diffusivity, [m^{2}s^{-1}];
β – parameter (s. Eq. (5));
η – parameter (s. Eq. (5));
$\theta(x,t)$ – temperature difference $T - T_\infty$ in the point x at the time t, [K];
ρ – density, [kg m^{-3}];
τ – time to reach maximum temperature, [s].

Received, December 30, 2000

The University of Twente, The Netherlands
Laboratory for Measurement
and Instrumentation
and
** Technical University "Gh. Asachi", Jassy,*
Department of Electrical Measurements

REFERENCES

1. * * * *Standard Method of Test for Thermal Conductivity of Materials by Means of the Guarded Hot Plate.* American National Standard, ASTM Comm., **C-16**, designation C177-71, 15-28 (1971).
2. Parker W.J., Jenkins R.J., Butler C.P., Abbott G.I., *Flash Method of Determining Thermal Diffusivity, Heat Capacity and Thermal Conductivity.* J. Appl. Phys., **9**, *32*, 82-95 (1961).
3. Carslaw H.S., Jaeger J.C., *Conduction of Heat in Solids.* Oxford University Press, London, 1959.
4. Touloukian Y.S., *Thermophysical Properties of Matter.* The TPRC data series, vol.**10**, *Thermal diffusivity*, IFI Plenum, NY, 1973.

METODĂ DE MĂSURARE A DIFUZIVITĂŢII TERMICE A SOLIDELOR UTILIZÂND MĂSURĂRI ALE TIMPULUI

I. Abordare teoretică

(Rezumat)

Se prezintă o nouă metodă pentru măsurarea difuzivităţii termice a solidelor utilizându-se starea termică tranzitorie. Această metodă utilizează principiul suprapunerii încărcărilor termice. Este necesară numai măsurarea timpului şi nu este necesară măsurarea precisă a temperaturii sau a vitezei de propagare a căldurii. Metoda utilizează efectul Seebeck pentru măsurarea dependenţei de timp a temperaturii. Se prezintă modelul matematic corespunzător metodei descrise, precum şi o posibilitate de realizare practică.

BULETINUL INSTITUTULUI POLITEHNIC DIN IAŞI
Tomul XLVII (LI), Fasc. 1–2, 2001
ELECTROTEHNICĂ. ENERGETICĂ. ELECTRONICĂ

D.C. 621.317.727

CONSIDERATIONS ON THE SHORT-CIRCUIT TRANSIENT OPERATION OF THE LINEAR CURRENT INDUCTIVE DIVIDER, ELECTRONICALLY COMPENSATED WITH A CURRENT CONVERTER

BY
ADRIAN CREŢU, CARMEN COJOCARU-FILIPIUC and ADRIANA-IOANA CREŢU

It is studied the short-circuit transient state of a linear current inductive divider (CID) automatically compensated with a current converter. With this aim, one determines and solves the differential equations of this regime, for the CID non-compensated, respectively the compensated one, with current converter.

Comparing the error currents, $i_0(t)$, of the CID compensated, respectively non-compensated, it results that after connecting the current converter it is obtained a diminution of the aperiodical component of alternating component, accompanied by a corresponding decrease of the CID errors.

Consequently, as long as the magnetic core of the CID is not saturated (in practice, saturation can be avoided in the same manner as in case of the current transformer with air-gaps), in applications that does not require the galvanic insulation of the primary circuit with respect to the secondary one, the ratio metrological performance/cost achieved by utilization of an electronically compensated CID is superior to that obtained by use of electronically compensated current transformers, both in the sinusoidal steady-state and in the transient short-circuit states.

1. Introduction

The current inductive divider (CID) electronically compensated [1], [2] assures, in sinusoidal steady-state, extremely high measurement accuracy in a wide variation range of the measured current and it successfully replaces the current transformer in cases when the galvanic insulation of the primary circuit with respect to the secondary one is not necessarily required.

With the aim to extend the utilization of a CID for the measurement of asymmetrical short-circuit currents of the form:

$$I_1 = I_{1m}(\mathrm{e}^{-t/T_1} - \cos \omega t), \tag{1}$$

where $T_1 = L_1/R_1$ represents the time constant of the primary circuit, it is necessary to determine and to solve the differential equations that characterize the short-circuit transient operation of the linear CID in both variants: non-compensated, respectively

electronically compensated with current converter. The analysis of these equations emphasizes the possibilities, the advantages, and the limitations in the utilization of the CID electronically compensated with current converter, in the case of the precise measurement of the short-circuit currents.

2. The Differential Equation of the Non-Compensated CID

In order to determine the differential equation of the linear CID (Fig. 1 *a*) one uses the system resulted from writting the ampere-turns equation of a CID and the Kirchhoff voltage equation applied to the secondary circuit:

$$(2) \qquad \begin{cases} N_1 i_0 = N_1 i_1 + N_2 i_2, \\ e_2 + e_{d_2} + e_{d_1} + e_S = (R_2 + R_S) i_2 + R_1 i_1, \end{cases}$$

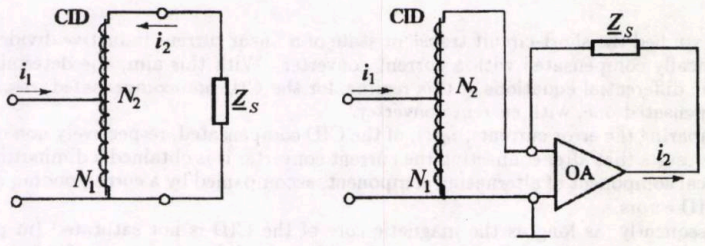

Fig. 1

where: N_1 and N_2 represents the number of turns of the ratio windings; i_0 – the no-load operation current of the CID; i_1, i_2 – the currents flowing in the primary, respectively in the secondary circuit; R_1 – the resistance of the primary winding; R_2 – the resistance of the secondary winding; R_S – the resistance of the load $\underline{Z}_S = R_S + \mathrm{j}\omega L_S$;

$$(3) \qquad e_2 = -N_2 \frac{\mathrm{d}\varphi}{\mathrm{d}t} = -N_2 \frac{\mathrm{d}}{\mathrm{d}t}\left(\frac{N_1 i_0}{R_m}\right) = -\frac{N_1 N_2}{R_m} \cdot \frac{\mathrm{d}i_0}{\mathrm{d}t}$$

– the e.m.f. induced in the secondary winding by the useful flux $\varphi = N_1 i_0 / R_m$, where $R_m = l/\mu S$ is the reluctance of the magnetic circuit of the CID, depending on its length, l, on its sectional area, S, and on the magnetic permeability, μ, of the material from which the core is made of;

$$(4) \qquad e_{d_2} = -L_{d_2} \frac{\mathrm{d}i_2}{\mathrm{d}t}$$

– the e.m.f. corresponding to the leakage inductivity L_{d_2} of the secondary winding;

$$(5) \qquad e_{d_1} = -L_{d_1} \frac{\mathrm{d}i_1}{\mathrm{d}t}$$

– the e.m.f. corresponding to the leakage inductivity L_{d_1} of the primary winding;

$$e_S = -L_S \frac{\mathrm{d}i_2}{\mathrm{d}t} \tag{6}$$

– the e.m.f. corresponding to the self-inductivity L_S of the load $\underline{Z}_S$.

Replacing, in the voltage equation of the system (2), the e.m.f. by their values given by relations (3),...,(6) and taking into account that from the ampere-turns equation it results:

$$i_2 = \frac{N_1}{N_2}(i_0 - i_1), \tag{7}$$

one obtains:

$$-\frac{N_1 N_2}{R_m} \cdot \frac{\mathrm{d}i_0}{\mathrm{d}t} - \frac{N_1}{N_2} L_{d_2} \frac{\mathrm{d}i_0}{\mathrm{d}t} + \frac{N_1}{N_2} L_{d_2} \frac{\mathrm{d}i_1}{\mathrm{d}t} - L_{d_1} \frac{\mathrm{d}i_1}{\mathrm{d}t} -$$

$$-\frac{N_1}{N_2} L_S \frac{\mathrm{d}i_0}{\mathrm{d}t} + \frac{N_1}{N_2} L_S \frac{\mathrm{d}i_1}{\mathrm{d}t} = \frac{N_1}{N_2}(R_2 + R_S) i_0 - \frac{N_1}{N_2}\left(R_2 + R_S - \frac{N_2}{N_1} R_1\right) i_1. \tag{8}$$

If it is denoted by:

$$L_\mu = \frac{N_2^2}{R_m}, \tag{9}$$

the magnetizing inductivity of the CID, the differential equation (8) becomes:

$$(L_\mu + L_{d_2} + L_2)\frac{\mathrm{d}i_0}{\mathrm{d}t} + (R_2 + R_S) i_0 = \left(L_{d_2} - \frac{N_2}{N_1} L_{d_1} + L_S\right)\frac{\mathrm{d}i_1}{\mathrm{d}t} + \left(R_2 - \frac{N_2}{N_1} R_1 + R_S\right) i_1. \tag{10}$$

Constructing the CID winding so that the resistance and the leakage inductivity of turn be the same, then [7]:

$$\frac{R_1}{R_2} = \frac{L_{d_1}}{L_{d_2}} = \frac{N_1}{N_2}, \tag{11}$$

the effect of the *internal load* of the CID becomes zero $\left(R_2 - \frac{N_2}{N_1} R_1 = 0,\ L_{d_2} - \frac{N_2}{N_1} L_{d_1} = 0\right)$ and the equation (10) becomes:

$$(L_\mu + L_{d_2} + L_2)\frac{\mathrm{d}i_0}{\mathrm{d}t} + (R_2 + R_S) i_0 = L_S \frac{\mathrm{d}i_1}{\mathrm{d}t} + R_S i_1. \tag{12}$$

Because:

$$L_{d_2} + L_S \ll L_\mu \tag{13}$$

and denoting by:

$$T_2 = \frac{L_\mu + L_{d_2} + L_S}{R_2 + R_S} \approx \frac{L_\mu}{R_2 + R_S}, \tag{14}$$

the time constant of the secondary circuit of the CID *corresponding to the resistance* $R_{i_2} = R_2 + R_S$, with:

$$T_{2(1)} = \frac{L_\mu + L_{d_2} + L_S}{R_S} \approx \frac{L_\mu}{R_S}, \tag{15}$$

the time constant of the secondary circuit *corresponding to the load resistance*, R_s, and with:

$$k_{L(1)} = \frac{L_S}{L_\mu + L_{d_2} + L_S} \approx \frac{L_S}{L_\mu}, \tag{16}$$

the ratio of the self-inductivities of the CID, from (12) one obtains the differential equation that characterizes the operation of the linear CID in the short-circuit state:

$$\frac{\mathrm{d}i_0}{\mathrm{d}t} + \frac{I_0}{T_2} = k_{L(1)}\frac{\mathrm{d}i_1}{\mathrm{d}t} + \frac{i_1}{T_{2(1)}}. \tag{17}$$

Equation (17) has the same form as that of a current transformer [4], [9], [10], the only difference being given by the values of the coefficients. In the case of a current transformer, the coefficient $k_L = (L_{d_2} + L_S)/L_\mu$ of the term that contains $\mathrm{d}i_1/\mathrm{d}t$ is bigger ($k_L > L_{L(1)}$) and the time constant of its secondary circuit is smaller:

$$T_2 = \frac{L_\mu}{R_2 + R_S} < T_{2(1)} = \frac{L_\mu}{R_S}.$$

The modification of the values of the coefficients in equation (17) from k_L to $k_{L(1)}$ and from T_2 to $T_{2(1)}$ is a consequence of the fact that, by observing the condition (11) (by a careful construction of the CID), the effect of the *internal load* of the CID is cancelled, *i.e.* the effect of the resistance and of the leakage inductivity of its winding.

In order to estimate quantitatively the operation of the linear CID, in the short-circuit transient state, it is necessary to determine the value $i_0(t)$ of the error current. As equation (17) represent a linear differential one of the first order, after performing all calculations one obtains:

$$i_0(t) = I_{1m}\left\{\frac{T_1 - k_{L(1)}T_{2(1)}}{T_1 - T_2}\cdot\frac{T_2}{T_{2(1)}}\left(\mathrm{e}^{-t/T_1} - \mathrm{e}^{-t/T_2}\right) + \right.$$

$$\left. + \frac{1}{1 + T_2^2\omega^2}\left[T_2\omega\left(k_{L(1)} - \frac{T_2}{T_{2(1)}}\right)\sin\omega t + \left(k_{L(1)}\omega^2 T_2^2 + \frac{T_2}{T_{2(1)}}\right)\left(\mathrm{e}^{-t/T_2} - \cos\omega t\right)\right]\right\}. \tag{18}$$

Under the practical assumptions:

$$T_2^2\omega^2 \gg 1, \quad k_{L(1)}T_{2(1)} \ll T_2, \quad k_{L(1)}T_{2(1)} \ll T_1, \tag{19}$$

it results:

$$i_0(t) \approx I_{1m}\left[\frac{T_1}{T_1-T_2}\cdot\frac{T_2}{T_{2(1)}}\left(e^{-t/T_1}-e^{-t/T_2}\right)-\right.$$

(20)

$$\left.-\frac{T_2}{T_{2(1)}}\cdot\frac{1}{T_2\omega}\sin\omega t+k_{L(1)}\left(e^{-t/T_2}-\cos\omega t\right)\right].$$

Replacing in (20) $k_{L(1)}$ by k_L and considering $T_{2(1)}=T_2$ one obtains the value, $i_0(t)$, of magnetizing current corresponding to the operation in the short-circuit transient state of a *current transformer*:

$$(21)\quad i_0(t) \approx I_{1m}\left[\frac{T_1}{T_1-T_2}\left(e^{-t/T_1}-e^{-t/T_2}\right)-\frac{1}{T_2\omega}\sin\omega t+k_L\left(e^{-t/T_2}-\cos\omega t\right)\right].$$

By comparison of expressions (20) and (21) of the error currents $i_0(t)$, in the case of a CID, respectively of a current transformer, one finds a slight decrease of the current $i_0(t)$ of the CID, determined by the rise from T_2 to $T_{2(1)}$ of the time constant $(T_2/T_{2(1)}<1)$ and by the decrease from k_L to $k_{L(1)}$ of the self-inductivies ratio, at the same time with the annulment of the internal load effect. Thus, as far as the core of the inductive divider is not saturated, like in the case of a current transformer [10], (by the construction of linearized CID's, with air-gaps), it can also be utilized for the measurement of short-circuit transient currents, finding a shift decrease of its errors with respect to those of the *current transformer*.

3. The Differential Equation of the Linear CID Electronically Compensated with Current Converter

In the technical literature there are presented various schematics for the automated compensation of errors in a CID, including electronic amplifiers rated at the power corresponding to the error current or to the load current, operating as a current converter or current–voltage, as a repeater or as a voltage amplifier [1], [2]. From these diagrams, in what follows we shall consider the compensation schematic with current converter [1], represented in Fig. 1 *b* that allows the correction *from outside* of the CID errors without any constructive modifications. In the sinusoidal steady-state, by this procedure the CID errors can be reduced at less than 0.1 p.p.m. in a large range of measured current values, of the load impedance and of the working frequency. The electronic compensation device is dimensioned at the power corresponding to the secondary load current so that the method is advantageous in the case when i_2 has small values.

The differential equation of the linear CID compensated with current converter is obtained from the system resulted by writing the ampere-turns equation of the CID and the Kirchhoff voltage equation applied to the secondary circuit (Fig. 1 *b*):

$$(22)\quad \begin{cases} N_1 i_0 = N_1 i_1 + N_2 i_2, \\ e_2 + e_{d_2} + e_{d_1} + e_S = \left(R_2 + \dfrac{R_S}{A}\right) i_2 + R_1 i_1, \end{cases}$$

where A represents the voltage amplification of the operational amplifier, OA, utilized for the construction of the current converter, and:

$$e_S = -\frac{L_S}{A} \cdot \frac{\mathrm{d}i_2}{\mathrm{d}t} \tag{23}$$

– the e.m.f. corresponding to the self-inductivity L_S of the load $\underline{Z}_S$.

Substituting, in the voltage equation of the system (22), the e.m.f.s by their expressions, (3),...,(5), respectively (23), and taking into account that from the ampere-turns equation it results:

$$i_2 = \frac{N_1}{N_2}(i_0 - i_1), \tag{24}$$

one obtains the differential equation:

$$\begin{aligned} &-\frac{N_1 N_2}{R_m} \cdot \frac{\mathrm{d}i_0}{\mathrm{d}t} - \frac{N_1}{N_2} L_{d_2} \frac{\mathrm{d}i_0}{\mathrm{d}t} + \frac{N_1}{N_2} L_{d_2} \frac{\mathrm{d}i_1}{\mathrm{d}t} - L_{d_1} \frac{\mathrm{d}i_1}{\mathrm{d}t} - \frac{N_1}{N_2} \cdot \frac{L_S}{A} \cdot \frac{\mathrm{d}i_0}{\mathrm{d}t} + \frac{N_1}{N_2} \cdot \frac{L_S}{A} \cdot \frac{\mathrm{d}i_1}{\mathrm{d}t} = \\ &= \frac{N_1}{N_2}\left(R_2 + \frac{R_S}{A}\right) i_0 - \frac{N_1}{N_2}\left(R_2 + \frac{R_S}{A} - \frac{N_2}{N_1} R_1\right) i_1. \end{aligned} \tag{25}$$

Considering the relation (9), equation (25) can be written under the form:

$$\begin{aligned} &\left(L_\mu + L_{d_2} + \frac{L_S}{A}\right) \frac{\mathrm{d}i_0}{\mathrm{d}t} + \left(R_2 + \frac{R_S}{A}\right) i_0 = \\ &= \left(L_{d_2} - \frac{N_2}{N_1} L_{d_1} + \frac{L_S}{A}\right) \frac{\mathrm{d}i_1}{\mathrm{d}t} + \left(R_2 - \frac{N_2}{N_1} R_1 + \frac{R_S}{A}\right) i_1. \end{aligned} \tag{26}$$

Having in view the condition (11), the equation (10) becomes:

$$\left(L_\mu + L_{d_2} + \frac{L_S}{A}\right) \frac{\mathrm{d}i_0}{\mathrm{d}t} + \left(R_2 + \frac{R_S}{A}\right) i_0 = \frac{L_S}{A} \cdot \frac{\mathrm{d}i_1}{\mathrm{d}t} + \frac{R_S}{A} i_1. \tag{27}$$

Denoting by:

$$T_{2\alpha} = \frac{L_\mu + L_{d_2} + \dfrac{L_S}{A}}{R_2 + \dfrac{R_S}{A}} \approx \frac{L_\mu}{R_2 + \dfrac{R_S}{A}}, \tag{28}$$

the time constant of the secondary circuit of the CID electronically compensated, *corresponding to its total resistance*, $R_{2i} = R_2 + R_{S\alpha} = R_2 + R_S/A$, with:

$$T_{2\alpha(1)} = \frac{L_\mu + L_{d_2} + \dfrac{L_S}{A}}{R_S} \approx A\frac{L_\mu}{R_S} = AT_{2(1)}, \tag{29}$$

the time constant of the secondary circuit CID electronically compensated, *corresponding to the load resistance*, $R_{S\alpha}$ ($T_{2(1)}$ being the time constant of the secondary

circuit of the *non-compensated* CID, corresponding to the load resistance, R_S, given by (15)), and with:

$$k_{L\alpha(1)} = \frac{\dfrac{L_S}{A}}{L_\mu + L_{d_2} + \dfrac{L_S}{A}} \approx \frac{L_S}{AL\mu} = \frac{k_{L(1)}}{A}, \tag{30}$$

the ratio of self-inductivities of the CID electronically compensated ($k_{L(1)}$ being given by relation (16)), from (27) one obtains the differential equation that characterizes the operation of the linear CID *electronically compensated, in the short-circuit transient state*:

$$\frac{\mathrm{d}i_0}{\mathrm{d}t} + \frac{i_0}{T_{2\alpha}} = k_{L\alpha(1)}\frac{\mathrm{d}i_1}{\mathrm{d}t} + \frac{i_1}{T_{2\alpha(1)}}. \tag{31}$$

The time constant $T_{2\alpha}$ can be written in the form:

$$T_{2\alpha} = \frac{L_\mu}{R_2 + \dfrac{R_S}{A}} = \frac{R_2 + R_S}{R_2 + \dfrac{R_S}{A}}T_2 = nT_2, \tag{32}$$

where T_2 results from (14), and:

$$n = \frac{R_2 + R_S}{R_2 + \dfrac{R_S}{A}} < 1 + \frac{R_S}{R_2}.$$

The differential equations (17) and (31) of the linear CID *non-compensated*, respectively *compensated with current converter*, have the same form, but their coefficients have different values. For the linear electronically compensated CID it is found a slight increase of the time constant of the secondary circuit corresponding to its total resistance, namely from $T_2 = L_\mu/(R_2 + R_S)$ to $T_{2\alpha} = L_\mu/(R_2 + R_S/A)$, an important increase of the time constant of the secondary circuit corresponding to the load resistance, from $T_{2(1)}$ to $T_{2\alpha(1)} = AT_{2(1)}$, and a significant decrease of the self-inductivities ratio of the CID, from $k_{L(1)}$ to $k_{L\alpha(1)} = k_{L(1)}/A$, as a consequence of the effect of "external load" annulment in the secondary circuit, produced by the electronic compensation device.

In order to analyse quantitatively the operation of the linear electronically compensated CID in the short-circuit transient state, it is necessary to determine the value $i_0(t)$ of its error current. As the equation (31) represents a linear differential equation of the first order, starting from the general solution of this type of equation [8], after performing all calculations, one obtains:

$$i_0(t) = I_{1m}\left\{\frac{T_1 - k_{L\alpha(1)}T_{2\alpha(1)}}{T_1 - T_{2\alpha}} \cdot \frac{T_{2\alpha}}{T_{2\alpha(1)}}\left(\mathrm{e}^{-t/T_1} - \mathrm{e}^{-t/T_{2\alpha}}\right) + \frac{1}{1 + T_{2\alpha}^2\omega^2} \times \right.$$

$$\left. \times \left[T_{2\alpha}\omega\left(k_{L\alpha(1)} - \frac{T_{2\alpha}}{T_{2\alpha(1)}}\right)\sin\omega t + \left(k_{L\alpha(1)}\omega^2 T_{2\alpha}^2 + \frac{T_{2\alpha}}{T_{2\alpha(1)}}\right)\left(\mathrm{e}^{-t/T_{2\alpha}} - \cos\omega t\right)\right]\right\}. \tag{33}$$

Under the practical assumptions:

$$T_{2\alpha}^2\omega^2 \gg 1, \quad k_{L\alpha(1)}T_{2\alpha(1)} \ll T_2, \quad k_{L\alpha(1)}T_{2\alpha(1)} \ll T_1, \tag{34}$$

it results:

$$i_0(t) \approx I_{1m}\left[\frac{T_1}{T_1 - T_{2\alpha}} \cdot \frac{T_{2\alpha}}{T_{2\alpha(1)}}\left(e^{-t/T_1} - e^{-t/T_{2\alpha}}\right) - \right.$$
$$\left. - \frac{T_{2\alpha}}{T_{2\alpha(1)}} \cdot \frac{1}{T_{2\alpha}\omega}\sin\omega t + k_{L\alpha(1)}\left(e^{-t/T_{2\alpha}} - \cos\omega t\right)\right]. \tag{35}$$

Considering (29), (30) and (32), the expression (35) becomes:

$$i_0(t) \approx I_{1m}\left[\frac{T_1}{T_1 - nT_2} \cdot \frac{nT_2}{AT_{2(1)}}\left(e^{-t/T_1} - e^{-t/nT_2}\right) - \right.$$
$$\left. - \frac{T_2}{AT_{2(1)}} \cdot \frac{1}{T_2\omega}\sin\omega t - \frac{k_{L(1)}}{A}\left(e^{-t/nT_2} - \cos\omega t\right)\right]. \tag{36}$$

Comparing the expression of the error currents, $i_0(t)$, in the case of a *non-compensated* CID (rel. (20)) and respectively, in that of an *electronically-compensated one* (rel. (36)), it is found a very important decrease, by A times, of the alternating component (owing to the increase of the time constant $T_{2\alpha(1)}$ and to the decrease of the ratio $k_{L\alpha(1)}$ of the self-inductivities of the compensated CID), that implies as consequence a corresponding decrease of CID errors. Similarly to the case of an electronically compensated current transformer [4], here, as well in case of a CID, it is more difficult to estimate the effect of the correction electronic device on the aperiodical component of the error current, $i_0(t)$, its diminution being smaller (by $\frac{A}{n} \cdot \frac{T_1 - nT_2}{T_1 - T_2}$ times), owing to the n times increase ($n < 1 + R_S/R_2$) of the time constant $T_{2\alpha}$ of the secondary circuit (s. (32)). That is why, in such conditions as well, the CID compensated with current converter can be utilized for the measurement or for sensing the short-circuit transient currents, because in this case, also, the compensatory role of the correction electronic device is maintained as long as it does not occur the saturation of the magnetic core.

4. Conclusions

It is studied the short-circuit transient state of a linear CID compensated with current converter, determining the differential equation of the CID in this state and its corresponding solution.

Comparing the error currents, $i_0(t)$, of a non-compensated CID and respectively of a compensated with current one, it results that after connecting the correction electronic device, it takes place a decrease of the aperiodical component of the error

current and an important decrease of its alternating component, accompanied by the corresponding decrease of errors, what indicates the possibility to utilize the electronically compensated CID for the measurement or for sensing the short-circuit transient currents.

In applications that does not require the galvanic insulation of the primary circuit with respect to the secondary one, the ratio metrological performances/cost, achieved by utilization of the electronically compensated CID, is superior to that obtained by utilization of electronically compensated current transformers, both in sinusoidal steady-state and in short-circuit transient state.

Received, June 19, 2000

Technical University "Gh.Asachi", Jassy,
Department of General Electrotechnics
and Electrical Machines

REFERENCES

1. Creţu El., Lucanu M., Creţu A., Filipiuc C., *Electronically Compensated Inductive Current Divider.* Bul. Inst. polit., Iaşi, **XXXVII (XLI)**, *3-4*, s.III, 27-33 (1991).
2. Creţu A., Creţu El., *About an Electronic Method for the Compensation of the Inductive Current Divider.* Bul. Inst. polit., Iaşi, **XLV (IL)**, *3-4*, s. Electrot., Energ., Electron., 87-93 (1999).
3. Creţu El., Creţu A., *About a Diagram for the Automatic Error Compensation in Voltage Transformers.* Bul. Inst. polit., **XLII (XLVI)**, *1-2*, s.III, 77-81 (1996).
4. Lucanu El., Creţu A., *Consideraţii asupra funcţionării în regim tranzitoriu de scurtcircuit a transformatorului de curent liniar, compensat electronic.* Bul. Inst. polit., Iaşi, **XXII (XXVI)**, *1-2*, s.III, 57-62 (1976).
5. Beard G., *Single-Stage Amplifier-Aided Current Transformers Possesing Small Ratio Errors at 60Hz.* IEEE Trans., **IM-28**, *2*, 141-146 (1979).
6. Millea A., *Măsurări electrice.* Ed. Tehnică, Bucureşti, 1980.
7. Millea A., *Divizorul inductiv de curent.* Metrologia aplicată, **14**, *11*, 491-496 (1967).
8. Corduneanu A., *Ecuaţii diferenţiale cu aplicaţii în electrotehnică.* Ed. Facla, Timişoara, 1981.
9. Manolescu P., *Analiza lineară a funcţionării transformatorului de curent în regim tranzitoriu de scurtcircuit.* Electrotehnica, **16**, *5*, 189-198 (1968).
10. Musy Cl., *Les transformateurs de courant linéarisés.* Assoc. des Ing. Electr. de Montefiore, Aim, Belgique, **82**, *2*, 47-58 (1969).

CONSIDERAŢII ASUPRA FUNCŢIONĂRII ÎN REGIM TRANZITORIU DE SCURTCIRCUIT A DIVIZORULUI INDUCTIV DE CURENT, LINIAR, COMPENSAT ELECTRONIC CU CONVERTOR DE CURENT

(Rezumat)

Se studiază regimul tranzitoriu de scurtcircuit al unui divizor inductiv de curent, liniar (DIC), compensat automat cu convertor de curent. Se stabilesc şi se soluţionează ecuaţiile diferenţiale ale DIC, necompensat, respectiv, compensat cu convertor de curent, corespunzătoare acestui regim.

Din compararea curenţilor de eroare, $i_0(t)$, ai DIC compensat şi, respectiv, necompensat, rezultă că în urma cuplării convertorului de curent se produce o diminuare a componentei aperiodice a curentului $i_0(t)$ şi o puternică micşorare a componentei alternative a acestuia, însoţite de micşorarea corespunzătoare a erorilor DIC. Prin urmare, atât timp cât miezul divizorului inductiv nu se saturează magnetic (în practică acest fenomen se poate înlătura, ca şi în cazul transformatorului de curent [10], prin construirea unor DIC liniarizate, cu întrefieruri), în aplicaţiile în care nu se impune

cost realizat prin utilizarea DIC, compensat electronic, este superior celui obţinut prin folosirea transformatoarelor de curent, compensate electronic, atât în regim permanent cât şi în regim tranzitoriu de scurtcircuit.

BULETINUL INSTITUTULUI POLITEHNIC DIN IAŞI
Tomul XLVII (LI), Fasc. 1–2, 2001
ELECTROTEHNICĂ. ENERGETICĂ. ELECTRONICĂ

D.C. 621.313.2-9

PARASITIC TORQUES IN D.C. MICROMOTORS WITH ELECTRONIC SWITCHING

BY
I. SUCHAR and RADU URSULEAN

The main causes that led to the parasitic torques in D.C. micromotors with a permanent magnet as rotor and electronic switching are studied. The parasitic torques that are created by the nonsinusoidal voltage and current in the winding are also emphasized.

1. Introduction

The study refers to the D.C. micromotor with electronic switching described in [1]. The principle electrical diagram, in a simplified version, is presented in Fig. 1.

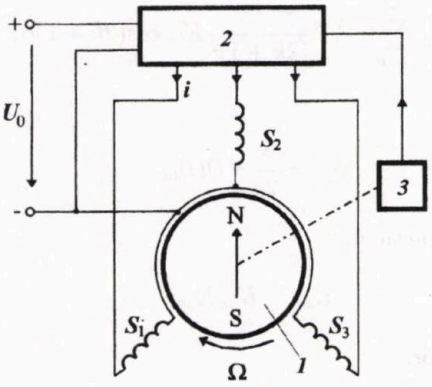

Fig. 1

This type of motor has the rotor as inductor and is built by means of a cylindrical magnet with one pair of poles diametrically magnetized.

The stator contains the induced winding consisting of three identical sections, S_1, S_2 and S_3, each one having N windings. The active sides of the winding are placed in notches of length L which exist on the interior surface of the cylinder of diameter D of the core. The core is made by sheet plates of electrotechnic steel. The notches are parallel to the generators of the cylindrical surface.

The current i flows through each section during one third of period of a complete rotation of the inductor, so that the magnetomotor voltage create with the magnetic flux of the inductor an electromagnetic torque.

Switching on and off the D.C. voltage U_0 that powers the sections is achieved by means of the electronic switch (*2*), according to the drive signals generated by the transducer (*3*). The transducer detects the position of the N–S axis of the rotor with respect to the magnetic field axis produced by the section of the powered winding.

2. Theoretical Background

For each section of $N_s = 3$ ones the electromagnetical processes are identical during each conduction period ($T_c = 2\pi/pN_s$ radians). Only the section that is in electrokinetic regime will be the one of interest in what follows.

The D.C. micromotor in our study is characterized by a rectangular magnetic induction, B, across the circumference of the gap, $\alpha \in [0, 2\pi]$, so that the Fourier series of the induction is

$$B(\alpha) = \frac{4}{\pi} B_m \sum_{k=0}^{\infty} (-1)^k \frac{1}{2k+1} \cos(2k+1)\alpha, \tag{1}$$

where B_m is the amplitude of the magnetic induction in the gap.

It was shown, [2], that the overall magnetic flux through the surface of the N windings, when the inductor rotates by an angle α, is given by:

$$\psi = \psi_m \sum_{k=0}^{\infty} (-1)^k \frac{1}{(2k+1)^2} K_{bk} \cos(2k+1)\alpha, \tag{2}$$

where

$$\psi_m = \frac{\pi}{2p} N D l B_m \tag{3}$$

represents the overall magnetic flux;

$$K_{bk} = K_{zk} K_{yk} \tag{4}$$

– the overall winding factor;

$$K_{zk} = \frac{\sin(2k+1)\dfrac{\beta}{2}}{(2k+1)\dfrac{\beta}{2}}, \quad k \in \mathbb{N}, \tag{5}$$

– the zone (repartition) factor of the winding;

$$K_{yk} = \sin(2k+1)\frac{\tau}{2} \tag{6}$$

– the shorten factor of the step of the winding, β – the breadth of the zone in which the active conductors of a coil are placed and τ – the step of the winding.

In the case of the studied micromotor $\tau = 2\beta = 2\pi/3$ radians and therefore, considering (2), it results:

$$\psi = \frac{3\sqrt{3}}{2\pi}\psi_m \left[\sum_{k=0}^{\infty} \frac{1}{(6k+1)^3}\cos(6k+1)\alpha - \sum_{k=0}^{\infty} \frac{1}{(6k-1)^3}\cos(6k-1)\alpha\right]. \tag{7}$$

During the rotation of the inductor a sum of periodical voltages are induced in the winding:

$$\sum_{\nu=1}^{\infty} e_\nu = -\frac{\mathrm{d}\psi}{\mathrm{d}t}. \tag{8}$$

Taking into account (7) and the equality $\alpha = \Omega t$, we get:

$$\sum_{\substack{\nu=1 \\ \nu\neq k}}^{\infty} e_\nu = E_m \left[\sum_{k=0}^{\infty} \frac{1}{(6k+1)^2}\cos(6k+1)\alpha - \sum_{k=0}^{\infty} \frac{1}{(6k-1)^2}\cos(6k-1)\alpha\right], \tag{9}$$

where

$$E_m = \frac{3\sqrt{3}}{2\pi}\Omega\psi_m \tag{10}$$

represents the amplitude of the fundamental of the induced voltage and Ω – the angular speed of the rotor.

The sum $\sum_{\nu} e_\nu$, in formula (9), lacks the even and the multiple of three harmonics. It also can be noticed that amplitude of the other harmonics are far less than the fundamental. Computing the first twelve harmonics and comparing them to the amplitude of the fundamental led to the results presented in Table 1.

Table 1

k	1		2		3		4		5		6	
ν	5	7	11	13	17	19	23	25	29	31	35	37
weight, [%]	4	2.04	0.826	0.591	0.346	0.277	0.189	0.16	0.119	0.104	0.082	0.073

In Fig. 2 one section of the winding, which is powered by the voltage U_0, is presented; the winding is characterized by the resistance R_S and the inductance L_S.

The driving block *4* and the power transistor T, which plays the role of the switch, are the constitutive elements of the contactless switch *2*, driven by the position transducer of the rotor, *3*.

The electrokinetic regime may be characterized by the following equation, written for voltages:

$$U_0 + \sum_{\nu=1}^{\infty} e_\nu = u_T + u_S = (R_S + R_{EC})i + L_S\frac{\mathrm{d}i}{\mathrm{d}t}, \tag{11}$$

where u_S and u_T represent, respectively, the voltage on the section of the winding and on the collector–emitter resistance of the transistor.

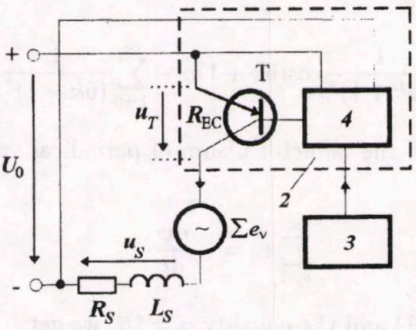

Fig. 2

Because during the functioning the resulting voltage, the one in the active section of the winding, varies periodically according to a nonsinusoidal law:

$$u = U_0 + \sum_{\nu=1}^{\infty} e_\nu, \tag{12}$$

it is obvious that the current is a nonsinusoidal signal too:

$$i = I_0 + \sum_{\nu=1}^{\infty} i_\nu. \tag{13}$$

The value of the electromagnetic torque of the motor is

$$m = \frac{1}{\Omega} ui = \frac{1}{\Omega} \left(U_0 + \sum_{\nu=1}^{\infty} e_\nu \right) \left(I_0 + \sum_{\nu=1}^{\infty} i_\nu \right). \tag{14}$$

During a complete rotation of the inductor, the mean value of the electromagnetic torque is given by

$$M = \frac{1}{\Omega} \left(U_0 I_0 + \sum_{\nu=1}^{\infty} E_\nu I_\nu \cos \varphi_\nu \right) = \frac{1}{\Omega} \left(P_0 + \sum_{\nu=1}^{\infty} P_\nu \right), \tag{15}$$

where $P_0 = U_0 I_0$ is the D.C. power and $\sum_{\nu=1}^{\infty} P_\nu = \sum_{\nu=1}^{\infty} E_\nu I_\nu \cos \varphi_\nu$ represents the sum of the active powers of each harmonic.

The last formula may be written as

$$M = M_0 + \sum_{\nu=1}^{\infty} M_\nu. \tag{16}$$

Therefore, because the current and the voltage are nonsinusoidal, the shaft of the micromotor in Fig. 1 is driven by a main torque and a sum of parasitic torques, $\sum_{\nu} M_{\nu}$.

The torque M_0 is created exclusively by the D.C. components of the voltage and the current. This torque is the only one that rotates the inductor in the desired direction.

The pulsating torques $\sum_{\nu} M_{\nu}$, due to the harmonics of the voltage induced during rotation, are breaking torques and they perturb the uniformity of the rotation speed of the D.C. micromotors with electronic switching.

The study carried out on the micromotor presented in [1] proves that in $\sum_{\nu} M_{\nu}$ the parasitic torques corresponding to the even and multiples of three harmonics are missing and the weight of the harmonics becomes negligible for $\nu > 7$.

Breaking torques are produced on the internal periphery of the core of the induced, especially in micromotors with small gap and open notches, due to the dental harmonics, *i.e.* the pulsatory variation of the permeance as a function of the rotation angle of the rotor. These torques are as important as the speed of rotation, n, of the rotor becomes greater, therefore as the frequency $f = Zn/60$ of the teeth harmonics becomes greater; Z is the number of the teeth of the stator.

The parasitic torque which appears due to the teeth harmonics, according to [4], is given by

$$M_Z = k_0 \frac{\pi}{2p} D l B_m \frac{\mathrm{d}\Lambda}{\mathrm{d}\alpha}, \tag{17}$$

where k_0 is a proportionality factor, [A/H], B_m – the value of the mean magnetic induction, [T], Λ – the permeance, [H] and α – the rotation angle, [rads.].

The pulsatory variations of the permeance caused by the alternative presence of the iron of the teeth and of the nonmagnetic medium from the notches can be lowered rising the gap of the micromotor, utilizing the closed notches or inclining the notches of the induced with a dental step. To diminish the parasitic torques due to the dental harmonics it is recommended to choose the length of the pole arch as an integer multiple of the dental step, the number of the teeth must have an odd value and the length of the opening of the notch must be the lowest possible.

Some parasitic torques may be generated by the constructive imperfections of the micromotors as the asymmetries of the magnetic circuit and the nonuniformities of the gap.

3. Conclusions

The main causes which determine the parasitic torques in D.C. motor with electronic switching were presented. A special attention was given to the parasitic torques generated due to the nonsinusoidal voltage and current in the windings.

The parasitic torques, M_{ν}, due to the harmonics of rank $\nu = 6k+1$, $(k = 1, 2, 3, \ldots)$, of the voltage and the current act in the same way as the one of the fundamental.

The parasitic torques, M_ν, due to the harmonics of rank $\nu = 6k - 1$ act contrary. For $\nu > 7$ the weight of the parasitic torques may be neglected.

In the micromotor built as described in [1] the parasitic torques, M_ν, of even and multiple of 3 harmonics are not generated.

Some hints to lower the parasitic torques and to rise the efficiency of the D.C. micromotors with electronic switching were also given.

Received, July 10, 2000

Technical University "Gh. Asachi", Jassy,
Department of General Electrotechnics
and Electrical Machines

REFERENCES

1. Suchar I., Creţu A., *D.C. Motor with Contactless Commutation* (in Romanian). Romanian Patent, *74350* (1980).
2. Suchar I., *Contributions to the Study of the Functioning of the D.C. Motors without Collector* (in Romanian). Ph. D. Diss., Polyt. Inst., Jassy, 1981.
3. Suchar I., *On the Transducers Used in D.C. Motors with Static Switching.* Bul. Inst. polit., Iaşi, **XLIV (XLVIII)**, *1-2*, s.III, 79-90 (1998).
4. Vasiliu Gh., Suchar I., Şerban Gh., *D.C. Micromotors with Static Commutation* (in Romanian). Ed. Tehnică, Bucureşti, 1976.

CUPLURI PARAZITE ÎN MICROMOTOARE DE CURENT CONTINUU CU COMUTAŢIE ELECTRONICĂ

(Rezumat)

Se studiază principalele cauze care determină apariţia cuplurilor parazite în micromotoare cu rotorul magnet permanent şi cu comutaţie electronică (statică). Se insistă asupra acelor cupluri parazite generate de faptul că tensiunea rezultată şi curentul din înfăşurare variază nesinusoidal în timp.

BULETINUL INSTITUTULUI POLITEHNIC DIN IAŞI
Tomul XLVII (LI), Fasc. 1–2, 2001
ELECTROTEHNICĂ. ENERGETICĂ. ELECTRONICĂ

D.C. 621.313.333.021/2

ASPECTS REGARDING THE TWO-PHASE INDUCTION MOTOR SIMULINK *s-FUNCTION* MODELING

BY
MIRCEA GOGU and *IRINA ATUDOREI

A two-phase induction machine SIMULINK *s-function* modeling method is proposed, using one supply operating equation, in a stationary reference frame. The authors choosed the two-phase induction machine for modeling because the same equations describe both one-phase induction machine with auxiliary phase and the three-phase induction machine after *d-q* transformations dynamic operation. So, one can use presented models in order to study some three-phase or one-phase induction machine adjustable speed drivers, with an adequate data file for the electrical machine parameters.

1. Introduction

The electrical drive systems using two-phase induction motors cover a large range of powers, reason for which, the whole machine – convertor – regulator system design is very difficult. As a consequence, one needs a modeling – simulating instrument, which should take into account the particularities of each subsystem, to determine the stability and the dynamic performances of the system, to verify the control method used, to establish the regulator parameters, in order to obtain a most propitious dynamic answer.

Meant to simulate dynamic systems, the SIMULINK package provides, in order to make models, besides a number of intrinsic functions contained, an excellent graphic interface, using the MATLAB environments as mathematical support.

Ever since the fifth decade of the century, the state variables method has become very used for nonlinear systems analyses. In the state-space, a nonlinear system (power electronic circuit, electric machine), may be described using the equations:

$$(1) \qquad \frac{\mathrm{d}}{\mathrm{d}t}[x] = [A][x] + [B][u], \qquad (2) \qquad y = [C][x] + [D][u],$$

where: $[u] = m \times 1$ is a vector representing m inputs (independent quantities); $[y] = p \times 1$ – a vector representing p outputs (important quantities); $[x] = n \times 1$ – a vector which contains a set of n independent auxiliary variables; $[A]$, $[B]$, $[C]$, $[D]$ – matrices containing real constants, called the *state-space equations matrices* and having suitable dimansions. It is remarkable the fact that matrix $[A]$ is always an n order square matrix.

2. The Two-phase Induction Machine *s-function* Model in a Stationary Reference Frame

Under single supply conditions, the two-phase induction machine operates according to the following equations, in a stationary reference frame:

$$(3)\quad \begin{cases} u_{ds} = R_s i_{ds} + \dfrac{\mathrm{d}}{\mathrm{d}t}\Psi_{ds}, & \Psi_{ds} = L_{ss} i_{ds} + L_m i_{dr}, \\ u_{qs} = R_s i_{qs} + \dfrac{\mathrm{d}}{\mathrm{d}t}\Psi_{qs}, & \Psi_{qs} = L_{ss} i_{qs} + L_m i_{qr}, \\ 0 = R_r i_{dr} + \dfrac{\mathrm{d}}{\mathrm{d}t}\Psi_{dr} + \omega_r \Psi_{qr}, & \Psi_{dr} = L_{rr} i_{dr} + L_m i_{ds}, \\ 0 = R_r i_{qr} + \dfrac{\mathrm{d}}{\mathrm{d}t}\Psi_{qr} - \omega_r \Psi_{dr}, & \Psi_{qr} = L_{rr} i_{qr} + L_m i_{qs}. \end{cases}$$

The system (3) let us write the following relations for currents:

$$(4)\quad i_{ds} = \frac{L_{rr}}{L_{ss}L_{rr} - L_m^2}\Psi_{ds} - \frac{L_m}{L_{ss}L_{rr} - L_m^2}\Psi_{dr}, \quad i_{qs} = \frac{L_{rr}}{L_{ss}L_{rr} - L_m^2}\Psi_{qs} - \frac{L_m}{L_{ss}L_{rr} - L_m^2}\Psi_{qr},$$

$$(5)\quad i_{dr} = \frac{L_{ss}}{L_{ss}L_{rr} - L_m^2}\Psi_{dr} - \frac{L_m}{L_{ss}L_{rr} - L_m^2}\Psi_{ds}, \quad i_{qr} = \frac{L_{rr}}{L_{ss}L_{rr} - L_m^2}\Psi_{qr} - \frac{L_m}{L_{ss}L_{rr} - L_m^2}\Psi_{qs}.$$

From (3),...,(5) the flux derivatives expressions may be obtained:

$$(6)\quad \begin{cases} \dfrac{\mathrm{d}}{\mathrm{d}t}\Psi_{ds} = -\dfrac{R_s L_{rr}}{L_{ss}L_{rr} - L_m^2}\Psi_{ds} + \dfrac{R_s L_m}{L_{ss}L_{rr} - L_m^2}\Psi_{dr} + u_{ds}, \\ \dfrac{\mathrm{d}}{\mathrm{d}t}\Psi_{qs} = -\dfrac{R_s L_{rr}}{L_{ss}L_{rr} - L_m^2}\Psi_{qs} + \dfrac{R_s L_m}{L_{ss}L_{rr} - L_m^2}\Psi_{qr} + u_{qs}, \\ \dfrac{\mathrm{d}}{\mathrm{d}t}\Psi_{dr} = -\dfrac{R_r L_m}{L_{ss}L_{rr} - L_m^2}\Psi_{ds} + \dfrac{R_r L_{ss}}{L_{ss}L_{rr} - L_m^2}\Psi_{dr} - \omega_r \Psi_{qr}, \\ \dfrac{\mathrm{d}}{\mathrm{d}t}\Psi_{qr} = -\dfrac{R_r L_m}{L_{ss}L_{rr} - L_m^2}\Psi_{qs} + \dfrac{R_r L_{ss}}{L_{ss}L_{rr} - L_m^2}\Psi_{qr} + \omega_r \Psi_{dr}. \end{cases}$$

In accordance to equations (6), we can define the $[A]$, $[x]$, $[B]$ and $[u]$ matrices, in order to write the *s-function* program:

$$(7)\quad [A] = \begin{bmatrix} -\dfrac{R_s L_{rr}}{L_{ss}L_{rr} - L_m^2} & 0 & \dfrac{R_s L_m}{L_{ss}L_{rr} - L_m^2} & 0 \\ 0 & -\dfrac{R_s L_{rr}}{L_{ss}L_{rr} - L_m^2} & 0 & \dfrac{R_s L_m}{L_{ss}L_{rr} - L_m^2} \\ \dfrac{R_r L_m}{L_{ss}L_{rr} - L_m^2} & 0 & -\dfrac{R_r L_{ss}}{L_{ss}L_{rr} - L_m^2} & -\omega_r \\ 0 & \dfrac{R_r L_m}{L_{ss}L_{rr} - L_m^2} & \omega_r & -\dfrac{R_r L_m}{L_{ss}L_{rr} - L_m^2} \end{bmatrix},$$

$$(8) \qquad [x] = \begin{bmatrix} \Psi_{ds} \\ \Psi_{qs} \\ \Psi_{dr} \\ \Psi_{qr} \end{bmatrix}, \quad \frac{\mathrm{d}}{\mathrm{d}t}[x] = \begin{bmatrix} \frac{\mathrm{d}}{\mathrm{d}t}\Psi_{ds} \\ \frac{\mathrm{d}}{\mathrm{d}t}\Psi_{qs} \\ \frac{\mathrm{d}}{\mathrm{d}t}\Psi_{dr} \\ \frac{\mathrm{d}}{\mathrm{d}t}\Psi_{qr} \end{bmatrix}, \quad [B] = \begin{bmatrix} 1 & 0 \\ 0 & 1 \\ 0 & 0 \\ 0 & 0 \end{bmatrix}, \quad [u] = \begin{bmatrix} u_{ds} \\ u_{qs} \end{bmatrix}.$$

So, equations (6),...,(8) allow to write the two-phase induction machine model *s-function* program, in a stationary d–q reference frame.

s-Function Motbif Program

```
Function [sys,x0] = motbif(t,x,,flag)
% Two-phase induction machine s-function model,
in a stationary reference frame.
%                    by Mircea Gogu
if flag == 0
Sys = [4 0 5 3 0 0];
    x0 = [0 0 0 0];
elseif flag == 1
    wr = u(3);  % rotor angular speed;
    motdat;
    sys(1:4) = Aim*x(1:4) + Bim*u(1:2);
elseif flag == 3
motdat;
        y(1:4) = Cim*x(1:4) + Dim*u(1:2);
        sys(1) = y(1);
        sys(2) = y(3);
sys(3) = Lrr*x(1)/k - Lm*x(3)/k;
        sys(4) = Laa*x(3)/k - Lm*x(1)/k;
        sys(5) = km*(-x(1)*x(4) + x(2)*x(3));
else
        sys = [];
end; % End of program.
```

Motbif program opens the *motdat* file, where the machine parameters are mentioned and the state-space matrices $[A]$, $[B]$, $[C]$, $[D]$ are defined.

Motdat File

```
% motdat – Induction machine parameters data file;
%                    by Mircea Gogu
J1 = 0.004;      % inertia moment;
Rs = 2.045;      % stator resistance;
Rr = 1.435;      % rotor resistance;
P = 2;           % numbers of pairs of poles;
Lss = 0.156;     % stator leakage inductance;
Lrr = 0.156;     % rotor leakage inductance;
Lm = 0.147;      % magnetizing inductance;
Lm2 = Lm*Lm;
k = Lss*Lrr-Lm;
km = p*Lm/(Lss*Lrr-Lm);
%          A, B, C, D matrix definition
%          - Matrix A -
Aim(1,1) = -Lrr*Rs/k;
Aim(1,2) = 0;
Aim(1,3) = Lm*Rs/k;
Aim(1,4) = 0;
Aim(2,1) = 0;
Aim(2,2) = -Lrr*Rs/k;
Aim(2,3) = 0;
Aim(2,4) = Lm*Rs/k;
Aim(3,1) = Lm*Rr/k;
Aim(3,2) = 0;
Aim(3,3) = -Lss*Rr/k;
Aim(3,4) = -wr;
Aim(4,1) = 0;
Aim(4,2) = Lm*Rr/k;
Aim(4,3) = wr;
Aim(4,4) = -Lss*Rr/k;
%      - Matrix B -
Bim(1,1) = 1;
Bim(1,2) = 0;
Bim(2,1) = 0;
Bim(2,2) = 1;
Bim(3,1) = 0;
Bim(3,2) = 0;
Bim(4,1) = 0;
Bim(4,2) = 0;
%      - Matrix C -
% by constructing an unit matrix
Cim = eye(4);
%      - Matrix D -
Dim = zeros(4,2);
% End of program;
```

The Pulse Wide Modulated (PWM) two-phase inverter – induction motor system model is presented in Fig. 1 and the two-phase induction machine *s-function* model, in Fig. 2.

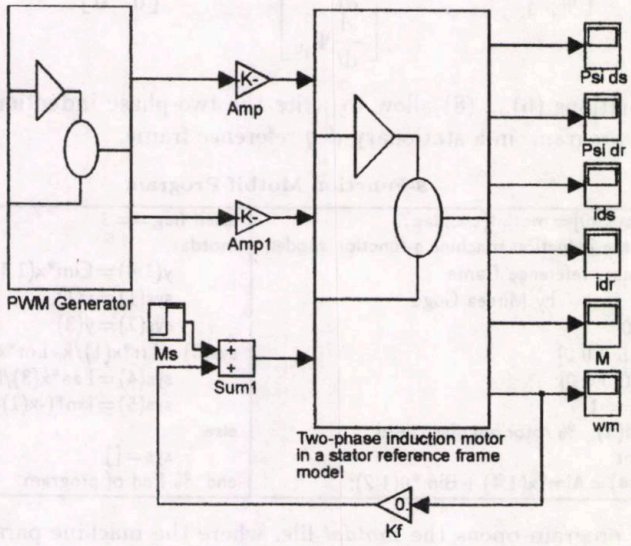

Fig. 1.– PWM inverter – motor system model.

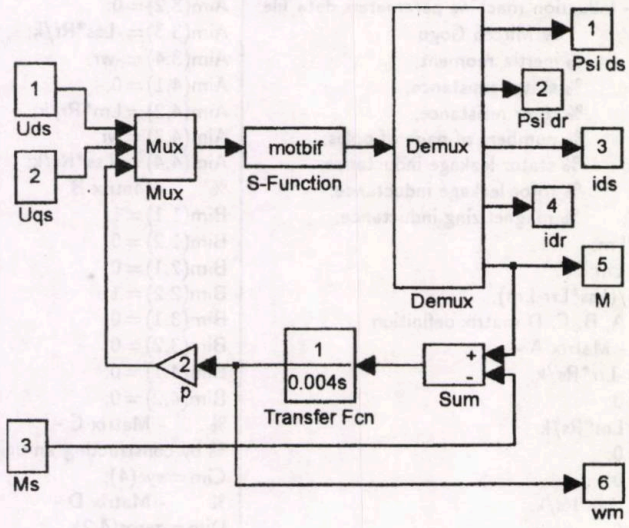

Fig. 2.– Induction motor *s-function* model in a stationary reference frame.

The model illustrated in Fig. 2 is a variant in which *s-function* does not calculate mechanical rotor speed, ω_m, and therefore does not calculate the electric speed, ω_r, either. So, mechanical speed is calculated outside of *s-function* block, using the relations:

$$(9) \qquad M - M_s = \frac{J}{p} s\omega_r; \quad \frac{\omega_r}{p} = \omega_m \text{ and consequently } \omega_m = (M - M_s)\frac{1}{J_s}$$

and constitutes one of the input sizes for this. "PWM Generator" block is a two-phase PWM generator model. One obtains at his outputs two PWM command waves, 90 electrical degrees shifted. This block configuration may be followed in Fig. 3.

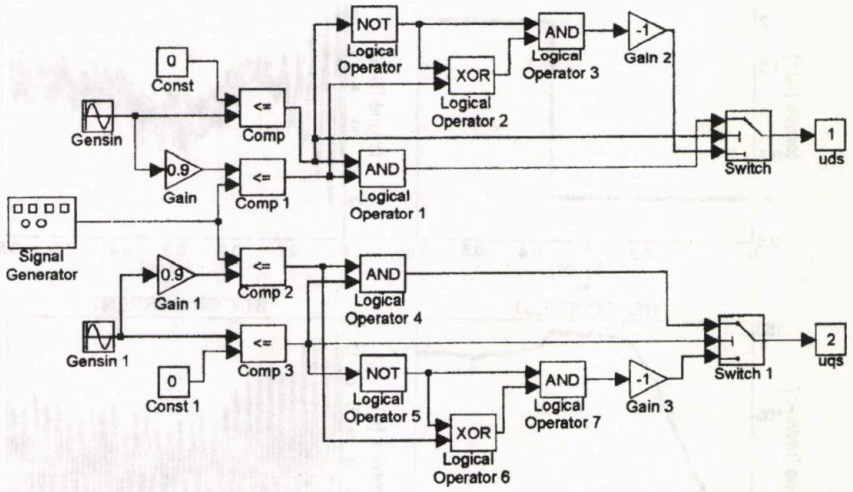

Fig. 3.– SPWM generator model.

Based on the model presented in Fig. 3, we has studied the open loop motor starting conditions at step load torque evolution and the obtained simulation results are shown in Fig. 4.

Mechanical and electrical rotor speed calculus may be done inside of the *s-function* model. In this case, the machine model in Fig. 2 simplifies, becoming more compact. With that end in view we can write a new *s-function* program, which opens nevertheless the same data file *modat*, if we study with the same machine at $f = 50$ Hz, $U_{cc} = 120$ V, $k_f = 0.016$ (friction coefficient).

s-Function Motbif1 Program

```
Function [sys,x0] = motbif(t,x,u,flag)
% Two-phase induction machine s-function model,
in a stationary reference frame.
%                    by Mircea Gogu
if flag == 0
        sys = [5 0 5 3 0 0];
        x0 = [0 0 0 0]';
elseif flag == 1
        wr = x(5);
        motdat;
    M = km*(-x(1)*x(4)+x(2)*x(3));
    isd = Lrr*x(1)/k - Lm*x(3)/k;
    ird = Lss*x(3)/k - Lm*x(1)/k;
    sys(1:4) = Aim*x(1:4) + Bim*u(1:2);
    sys(5) = p*(M-u(3))/J1;
elseif flag == 3;
    wr = x(5);
    motdat;
    y(1:4) = Cim*x(1:4) + Dim*u(1:2);
    sys(1) = y(1);
    sys(2) = y(3);
    sys(3) = Lrr*x(1)/k - Lm*x(3)/k;
    sys(4) = Lss*x(3)/k - Lm*x(1)/k;
    sys(5) = x(5)/2;
    sys(6) = km*(-x(1)*x(4) + x( )*x(3));
else
    sys = [];
end; % End of program.
```

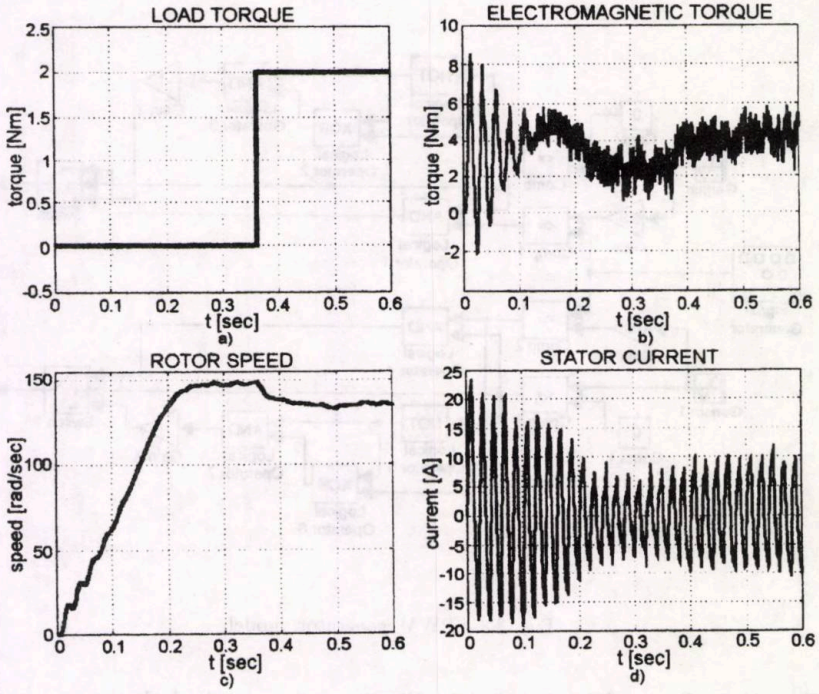

Fig. 4.– Results of the motor operation study, using the model shown in Fig. 1.

Structure of PWM inverter – two-phase induction motor system model will be identical with the one in Fig. 1. Instead, the two-phase induction machine model in a stationary reference frame structure, will be modified as shown in Fig. 5.

Both *motbif* and *motbif1* use the same *motdat* data file. *Motbif1* calculates the rotor angular speed in accordance with mechanical equation, in which, the inertia

moment J_1 interferes. This parameter is presented in *motdat* file, but is used only by *motbif1*.

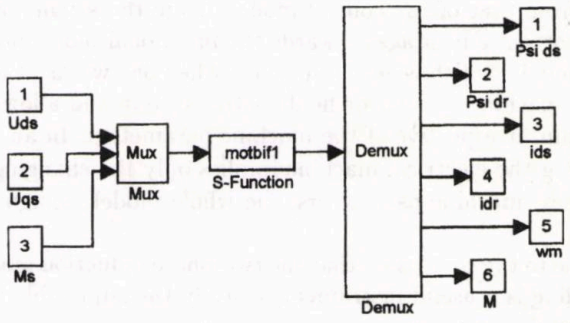

Fig. 5.– *s-function* speed calculation model.

Fig. 6 shows the results of the motor's behavior under the same conditions, obtained on this model.

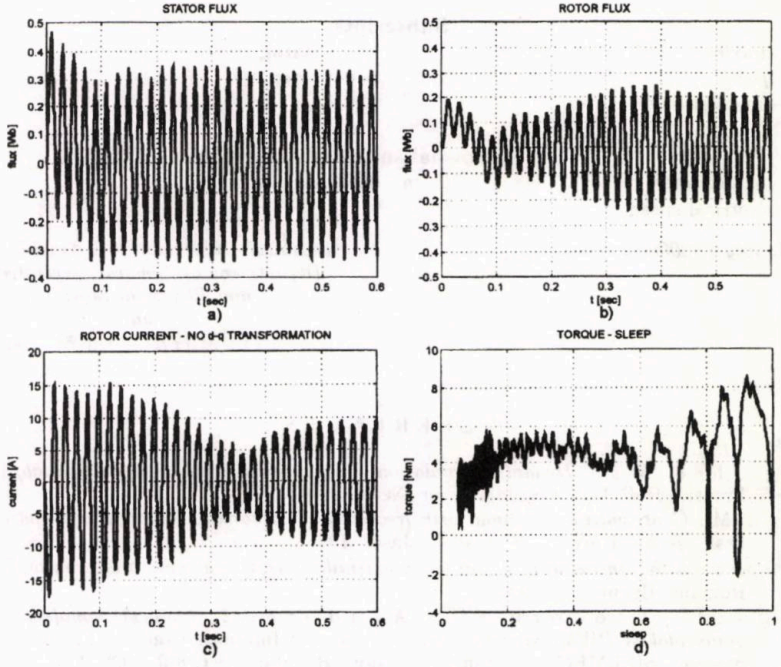

Fig. 6.– Results of the motor operation mode study, using the model shown in Fig. 5.

3. Conclusions

Two-phase induction machine modeling in MATLAB/SIMULINK environments offers large possibilities to study its behavior, both from viewpont of the command techniques and from that of the control mode. Using the *s-function* model, we can enjoy of two important advantages towards the functional bloks model. It realizes a more compact model – which is very important when one works at a whole assembly PWM inverter – machine – scalar or field control system and allows using the same *s-function* program, irrespective of the machine parameters. In an already modeled assembly, changing the electrical machine implies only the changing of the data file which contains new machine parameters, the whole model configuration remaining the same.

Thus, we come to the conclusion that the two-phase induction machine SIMULINK *s-function* modeling is a useful instrument to study the adjustable two-phase induction motors speed drives systems.

Notations

u – instantaneous voltage, [V];
i – instantaneous current, [A];
R – resistance, [Ω];
f – fundamental frequency, [Hz];
M – torque, [Nm];
L – inductance, [H];
Ψ – flux, [Wb];
d/dt – rate of change;
J – inertia moment, [Nm/(rad/sec)];
ω – angular speed, [rad/sec].

Subscripts

d – d axis;
q – q axis;
m – magnetizing quantity;
s – stator;
r – rotor.

Special subscripts

s – load torque;
r – electrical speed;
m – mechanical speed.

Received, July 4, 2000

Technical University "Gh.Asachi", Jassy,
Department of General Electrotechnics
and Electrical Machines
and
**S.C. MATRIX S.R.K, Jassy*

REFERENCES

1. Ong Chee-Mun, *Dynamic Simulation of Electric Machinery Using Matlab/Simulink.* Prentice Hall, Upper Saddle River, New Jersey, 1998.
2. Gogu M., *Contribuţii la comanda prin frecvenţă a motaorelor de curent alternativ.* Ph. D. Diss., Techn. Univ., „Gh. Asachi", Jassy, 1998.
3. Câmpeanu A., *Introducere în dinamica maşinilor electrice de curent alternativ.* Ed. Acad. Române, Bucureşti, 1998.
4. Gogu M., Teodoru E.C., Atudorei I., *Motorul monofazat în regim sinusoidal şi PWM, modelat Simulink.* Second Internat. Conf. of Electromechanical Systems, SIELMEC'99, Chişinău, Moldova Republic, Oct. 8-9, 1999, **I**, 111-114.
5. * * *Matlab User Guide.* The MathWorks, Prentice Hall Inc., Englewood Cliffs, NJ, 1992.
6. * * *Simulink User Guide.* The MathWorks, Prentice Hall Inc., Englewood Cliffs, NJ, 1992.

ASPECTE PRIVIND MODELAREA SIMULINK *s-FUNCTION* A MAŞINII ASINCRONE BIFAZATE

(Rezumat)

Se prezintă o metodă de modelare SIMULINK *s-function* a maşinii asincrone bifazate, utilizând ecuaţiile de funcţionare în regim de simplă alimentare, scrise într-un referenţial solidar cu statorul. S-a preferat motorul asincron bifazat, deoarece maşina asincronă trifazată, după transformările d–q şi maşina asincronă monofazată cu fază auxiliară, funcţionează conform aceloraşi ecuaţii. Astfel, se poate utiliza modelul maşinii bifazate şi pentru studiul sistemelor de acţionare reglabile cu maşini asincrone trifazate sau monofazate cu fază auxiliară.

BULETINUL INSTITUTULUI POLITEHNIC DIN IAŞI
Tomul XLVII (LI), Fasc. 1–2, 2001
ELECTROTEHNICĂ. ENERGETICĂ. ELECTRONICĂ

D.C. 621-526

ON THE OPTIMAL CONTROL OF DRIVING SYSTEMS WITH DIRECT CURRENT SERVOMOTORS

BY

V. BAHRIN and CARMEN COJOCARU-FILIPIUC

Some considerations concerning the solution of the optimal control problem of driving systems with d.c. servomotors are presented.

Some aspects are emphasized regarding the linear-square optimization with finite final time.

There are highlighted the steps of the optimal control determination and it is given an exemple of an optimal control algorithm implementation.

1. Introduction

In the last years, the activity aiming to assure the additional functions of control and supervision (optimal, adaptive, robust, or fuzzy control, identification of parameters, remote diagnoses and communication, etc.) has enjoyed a special attention. These functions imply utilization of a performant controller and rise a notable software problem, caused by restrictions imposed by the real time operation. The real time system ensures the control of a process, and the correct operation of the system depends on the values of the control quantities and on the moment at which these values are imposed.

The present stage is characterized by a remarkable performance increase of technological processes, based on the progress achieved in such domains as: design and constrcution of electrical machines (servomotors), electrical driving systems, power electronics, calculus techniques, systems theory and automated control.

The obtaintion of driving systems with superior performances requires application of the modern theory regarding the optimal and adaptive control strategies, the state regulation, the multivariable control, for whose implementation of the most recent achievements of microelectronics are utilized.

The presence of multiprocessor systems in the structure of modern electrical drives determines the improvement of the control performances by consideration of certain functional non-linearities and by introduction of certain regulation criteria imposed by the operation regime. The multiprocessor systems allow the utilization of artificial intelligence in electrical drives control, with the facility of assuming certain tasks of the human operator. These computation systems have the capability to take

certain decisions on basis of information received, and to initiate new jobs.

The formulation of the optimal control problem [2] of electrical driving systems is dictated by the working characteristics of the driven mechanism, as well as by the technological process requirements.

2. The Linear-square Optimization with Finite Final Time

The optimization problem taken into consideration refers to the dynamic multivariable processes [3] that can be described by linear models and that can occur in the operation of electrical driving systems.

It is considered the problem of the state optimal control for the invariant linear systems described by the equation:

$$\dot{x}(t) = Ax(t) + Bu(t), \tag{1}$$

where $x(t) \in \mathbb{R}^n$, $u(t) \in \mathbb{R}^m$, and A and B are matrices of adequate dimensions.

It is adopted a quality indicator of the expression [2]:

$$I = \frac{1}{2}[x_d - x(t_f)]^T S[x_d - x(t_f)] + \tag{2}$$
$$+\frac{1}{2}\int_0^{t_f} [x_d(t) - z_d]^T Q\left[x(t) - z_d + u^T(t)Pu(t) + x^T(t)Lu(t) + u^T(t)L^T x(t)\right],$$

where the matrices S, Q, P and L are:

$$S = \operatorname{diag}(s_1 \;\; 0), \quad Q = \operatorname{diag}(q_1 \;\; q_2), \quad P = p > 0, \quad L = l \geq 0, \tag{3}$$

with s_1, q_1, $q_2 > 0$, and $x_d = z_d = [w_d \;\; 0]^T$ the vector that defines the desired values for the state magnitudes.

When the variation of the resistant torque, $m(t)$, has a certain known expression, the following equations can be attached to the driving systems:

$$\dot{x}(t) = Fx(t) - Nv(t) + w(t), \quad \dot{v}(t) = -F^T v(t) - Rw(t) + Qz_d(t), \tag{4}$$

where v is the correction vector, whose terminal condition has the expression:

$$v(t_f) = (S - R)x(t_f) - Sx_d. \tag{5}$$

By differentiation of the adjunct vector $p(t) = Rx(t) + v(t)$, and substituting the result in the linear model of the driving system described by the state equations where the perturbation vector $w(t)$ was introduced as well, one obtains:

$$\left(-RNR + RA + A^T R + Q\right)x(t) + \dot{v}(t) + \left(A^T - NR\right)v(t) + Rw(t) - Qz_d(t) = 0. \tag{6}$$

The equation (5) is satisfied for any $x(t)$ and $v(t)$ if the conditions

$$RNR - RA - A^T R - Q = 0, \tag{7}$$

$$\dot{v}(t) = -\left(A^T - RN\right) v(t) + z(t), \tag{8}$$

are fulfilled, where the relation $z(t) = -Rw(t) + Qz_d(t)$ was utilized.

Matrix R is a solution of a matricial Ricatti [2] equation, and the correction vector $v(t)$ satisfies the non-homogeneous linear equation:

$$\dot{v}(t) = -Fv(t) + z(t), \tag{9}$$

where $F = A - NR$.

With equations (4) and (5), the system:

$$\begin{bmatrix} \dot{x}(t) \\ \dot{v}(t) \end{bmatrix} = \begin{bmatrix} F & -N \\ 0 & -F^T \end{bmatrix} \begin{bmatrix} x(t) \\ v(t) \end{bmatrix} + \begin{bmatrix} w(t) \\ z(t) \end{bmatrix}, \tag{10}$$

can be written, which has the solution:

$$\begin{bmatrix} x(t) \\ v(t) \end{bmatrix} = \begin{bmatrix} \Psi(t,t_f) & \Omega_{12}(t,t_f) \\ 0 & \Phi(t,t_f) \end{bmatrix} \begin{bmatrix} x(t_f) \\ v(t_f) \end{bmatrix} + \int_0^{t_f} \begin{bmatrix} \Psi(t,\tau) & \Omega_{12}(t,\tau) \\ 0 & \Phi(t,\tau) \end{bmatrix} \mathrm{d}\tau, \tag{11}$$

where $\Omega(t,t_f)$ is the transition matrix.

Under such conditions, the state vector $x(t)$ has the expression:

$$x(t) = \Psi(t,t_f)x(t_f) + \Omega_{12}(t,t_f)v(t_f) + \int_{t_f}^{t} \left[\Psi(t,\tau)w(\tau) + \Omega_{12}(t,\tau)z(\tau)\right] \mathrm{d}\tau, \tag{12}$$

which, considering the end condition (5), becomes:

$$\begin{aligned} x(t) = {} & \left[\Psi(t,t_f) + \Omega_{12}(t,t_f)(S-R)\right] x(t_f) - \Omega_{12}(t,t_f)Sx_d(t) + \\ & + \int_{t_f}^{t} \left[\Psi(t,\tau)w(\tau) + \Omega_{12}(t,\tau)z(\tau)\right] \mathrm{d}\tau. \end{aligned} \tag{13}$$

Having in view that the solution of equation (9) has the expression:

$$v(t) = \Phi(t,t_f)v(t_f) + \int_{t_f}^{t} \Phi(t,\tau)z(\tau)\,\mathrm{d}\tau, \tag{14}$$

where the correction vector is defined by (5), one can derive the state vector at the final moment, $x(t_f)$, from relation (13).

Introducing the notation $M(t,t_f)=\Psi(t,t_f)+\Omega_{12}(t,t_f)(S-R)$, the state vector $x(t)$ can be written as:

$$x(t)=M(t,t_f)x(t_f)-\Omega_{12}(t,t_f)Sx_d(t)+\int_{t_f}^{t}[\Psi(t,\tau)w(\tau)+\Omega_{12}(t,\tau)z(\tau)]\,\mathrm{d}\tau. \tag{15}$$

The initial and the final state vectors, $x(t_0)$ and $x(t_f)$ have, respectively, the following expressions:

$$x(t_0)=M(t_0,t_f)x(t_f)-\Omega_{12}(t_0,t_f)+\int_{t_f}^{t_0}[\Psi(t_0,\tau)w(\tau)+\Omega_{12}(t_0,\tau)z(\tau)]\,\mathrm{d}\tau, \tag{16}$$

$$x(t_f)= \tag{17}$$

$$=M^{-1}(t_0,t_f)\left\{x(t_f)+\Omega_{12}(t_0,t_f)Sx_d-\int_{t_f}^{t_0}[\Psi(t_0,\tau)w(\tau)+\Omega_{12}(t_0,\tau)z(\tau)]\,\mathrm{d}\tau\right\}.$$

Replacing the vector $x(t_f)$ in relation (14), one obtains:

$$v(t)=\Phi(t,t_0)\Phi(t_0,t_f)\left\{(S-R)M^{-1}(t_0,t_f)x(t_0)+(S-R)M^{-1}\Omega_{12}(t_0,t_f)Sx_d-\right. \tag{18}$$

$$\left.-Sx_d-(S-R)M^{-1}(t_0,t_f)\int_{t_f}^{t_0}[\Psi(t_0,\tau)+\Omega_{12}(t_0,\tau)z(\tau)]\mathrm{d}\tau\right\}+\int_{t_f}^{t}\Phi(t,\tau)z(\tau)\mathrm{d}\tau.$$

With the matrix $V(t_0,t_f)=(S-R)M^{-1}(t_0,t_f)$, the relation (18) can be written as:

$$v(t)=\Phi(t,t_0)\Phi(t_0,t_f)\left\{V(t_0,t_f)x(t_0)+V(t_0,t_f)\Omega_{12}(t_0,t_f)Sx_d-Sx_d-\right. \tag{19}$$

$$\left.-V(t_0,t_f)\int_{t_f}^{t_0}[\Psi(t_0,\tau)w(\tau)+\Omega_{12}(t_0,\tau)z(\tau)]\,\mathrm{d}\tau\right\}+\int_{t_f}^{t}\Phi(t,\tau)z(\tau)\,\mathrm{d}\tau.$$

Because $z(t)$ does not depend on τ for constant resistant torque, the last term of relation (19) can be redefined in a shape more convenient for its implementation:

$$\int_{t_f}^{t}\Phi(t,\tau)z(\tau)\,\mathrm{d}\tau=e^{-F^{T}t}\int_{t_f}^{t}e^{F^{T}\tau}z\,\mathrm{d}\tau=e^{-F^{T}t}\left(e^{F^{T}\tau}-I\right)F^{-T}\int_{t_f}^{t}z\,\mathrm{d}\tau=[I-\Phi(t,t_f)]\,F^{-T}z. \tag{20}$$

With these considerations, for constant exogenetical quantities the correction vector (19) becomes:

$$v(t)=\Phi(t,t_0)\Phi(t_0,t_f)\left\{V(t_0,t_f)x(t_0)+V(t_0,t_f)\Omega_{12}(t_0,t_f)Sx_d-Sx_d-\right.$$

(21)

$$\left.-V(t_0,t_f)\int_{t_f}^{t_0}[\Psi(t_0,\tau)w+\Omega_{12}(t_0,\tau)z(\tau)]\mathrm{d}\tau-F^{-T}z\right\}+F^{-T}z.$$

3. Determination of the Optimal Command

For the determination of the optimal command in closed loop, in a first stage, one aims to solve the Riccati differential equation by utilising numerical procedures, or an adequate command of the MATLAB library.

After establishing the transition matrices Ψ and Φ for F and F^T respectively, the constant matrices $\Omega_{12}(0,t_f)$, $M(0,t_f)$ and V (from relation (19)) can be calculated.

Knowing the variation law of the resistant torque, $m(t)$, and consequently knowing the expression of the perturbation vector:

$$W(t)=\begin{bmatrix}-1/J_r\\0\end{bmatrix}m(t), \tag{22}$$

one can calculate the constant vectors that occur in the relation (21).

The off-line calculus can be achieved according to an algorithm having the following development [1]:

a) introduction of data reffering to the system, to the criterion and the variation law of the resistant torque, $m(t)$;

b) solving of the Riccati matrix equation;

c) calculation of the F matrix, then calculation of the transition matrices Ψ and Φ for F and F^T respectively;

d) calculation of the constant matrices $\Omega_{12}(0,T)$, $M(0,T)$, V and the constant vectors that occur in relation (21).

Calculi referring to the real time control process will have the following sequence:

α) introduction of data established in stages a), b), c) and d);

β) determination (reading) of the initial value $m(0)$, or estimation of the resistant torque amplitude;

γ) reading of the $x(t_i)$ (*i.e.* $w(t_i)$ and $i(t_i)$) for every moment $t_i\in[0,t_f]$ making use of the appropriated periferic device;

δ) calculation of $v(t_i)$ for every moment $t_i\in[0,t_f]$;

ε) repetition of steps γ) and δ) for $t_i\in[0,t_f]$.

4. Implementation of the Optimal Control Algorithms

The implementation of the optimal control algorithm [1] proposed in § **3** as well as the obtention of certain results by numerical simulation for the case of constant

resistant torque are based on simulation programs written in MATLAB. For the parameters of the d.c. permanent magnet servomotor the following values have been considered: $U_N = 110$ V, $I_N = 3.3$ A, $R_A = 3.1\ \Omega$, $L_A = 0.16$ H, $K_E = 0.58$ Vs/rad, $K_M = 0.58$ Nm/A, $J_r = 0.028$ Nms^2/rad.

Under these assumption, the linear model described by the state equations for the considered servomotor is of the shape:

$$(23) \qquad \begin{bmatrix} \dot{\omega}(t) \\ \dot{i}(t) \end{bmatrix} = \begin{bmatrix} 0 & 20 \\ -3.5 & -19.375 \end{bmatrix} \begin{bmatrix} \omega(t) \\ i(t) \end{bmatrix} + \begin{bmatrix} 0 \\ 6.25 \end{bmatrix} u(t) + \begin{bmatrix} -35.71428 \\ 0 \end{bmatrix} m(t).$$

For the quality indicator (2) we have considered the matrices $S = \mathrm{diag}(1,0)$, $Q = \mathrm{diag}(1,3,1)$ and $P = p = 2$, and the final moment of the value $t_f = 0.9$ s.

The answers of the servomotor with optimal control, for the state quantity (the rotatioal speed) at the initial moment $x_0 = 25$ rad/s and for the imposed value $x_d = 50$ rad/s for a zero disturbance torque, and respectively for $x_d = x_0 = 50$ rad/s with a disturbance torque $m = 0.78$ Nm are represented in Fig. 1, respectively in Fig. 2.

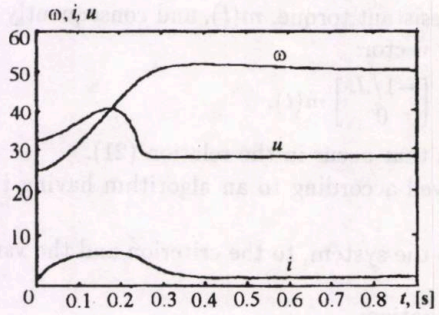

Fig. 1

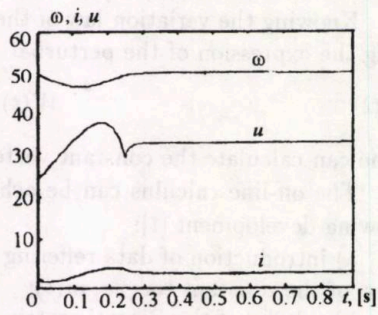

Fig. 2

5. Conclusions

The optimal control must assure certain quality conditions that mainly concern the average deviations of the state quantities with respect to the desired values.

The optimal control problems have in view both the energetic and the quality aspects referring to the dynamic behaviour of the electrical drive systems.

Initializing the optimizing process implies the initial knowing of vectors x_d and z_d, as well as of the disturbance $w(t)$. If only the shape of the disturbance $w(t)$ is known (and its amplitude is not known), in the off-line calculation, a normal variation $w(t)/||w(t)||$ will be considered and, at the beginning of the process, one should measure the amplitude of the components of the vector $w(0)$, after which the quantities shall be multiplied by the constant matrices.

The optimal control aims to ensure good system behaviour at the end of the optimization interval by imposing the steady state values $u_s = \omega_d/K_e - mR_A/K_M$.

The increase of the sampling period of the optimal control correction component determines the reduction of the calculus volume for solving the optimization problem.

Received, July 4, 2000

Technical University "Gh.Asachi", Jassy,
Department of General Electrotechnics
and Electrical Machines

REFERENCES

1. B a h r i n V., *Algoritmi pentru conducerea optimală a sistemelor de acţionare cu servomotoare de curent continuu.* Sci Sess. SECOMAR, *16*, Constanţa, 1999, 151-156.
2. B a h r i n V., T u l e a ş c ă I., *Consideraţii privind conducerea optimală a sistemelor de acţionare cu motoare de curent continuu.* Internat. Conf. of Electromech. Syst. SIELMEC '99, Chişinău, **II**, 1999, 55-58.
3. B a h r i n V., C o j o c a r u - F i l i p i u c C., *Consideration on the Optimization of Electrical Driving Systems.* Proc. of the Internat. Conf. on Applied and Theor. Electr., ICATE 2000, Craiova, May 2000, 464-465.

ASUPRA CONTROLULUI OPTIMAL AL SISTEMELOR DE ACŢIONARE CU SERVOMOTOARE DE CURENT CONTINUU

(Rezumat)

Sunt prezentate unele aspecte legate de soluţionarea problemei de conducere optimală a sistemelor de acţionare cu servomotoare de curent continuu.

Se fac unele precizări privind optimizarea liniar-pătratică cu timp finit.

Se pun în evidenţă etapele determinării comenzii optimale şi se exemplifică implementarea algoritmilor de conducere optimală.

BULETINUL INSTITUTULUI POLITEHNIC DIN IAŞI
Tomul XLVII (LI), Fasc. 1–2, 2001
ELECTROTEHNICĂ. ENERGETICĂ. ELECTRONICĂ

D.C. 621.313.333.021/2

ENERGY CONVERSION IN UNSYMMETRICAL TWO-PHASE INDUCTION MACHINES

BY
I. ANDRONE and ADRIANA-ELENA PRISĂCARU

Based on the so-called "equivalent numbers of phases" of the unsymmetrical two-phase induction machine, the energy conversion in such type of electrical machine is examined. The machine torques as functions of the equivalent numbers of rotor phases were obtained.

1. Introduction

In some previous papers [1],...,[3] a new approach of the unsymmetrical two-phase induction machine theory was developed. The equivalent numbers of phases of such machines were introduced. These equivalent numbers of phases are global coefficients which take into account the main reasons for a two-phase induction machine to be or to became unsymmetrical: the two m.m.f.'s of the two different phases are different in magnitudes, the phase shift and the space angle between the magnetic induction, set up by the two windings, are different from $\pi/2$.

Let us consider an unsymmetrical two-phase induction motor having the connections diagrams as in Fig. 1. The stator of the machine has two different phases, u and v, and a symmetrical rotor, squirrel-cage, for example. The two stator windings have, respectively, $w_u k_{uyq}$ and $w_v k_{vyq}$ effective turns and α_{1uv} space angle between them. The actual rotor is replaced by an equivalent stand still one [1], [2] (Fig. 2). The equivalent rotor has two different phases, u' and v', having the same effective turns as the stator. The two rotor phases have α'_{2uv} space angle between them.

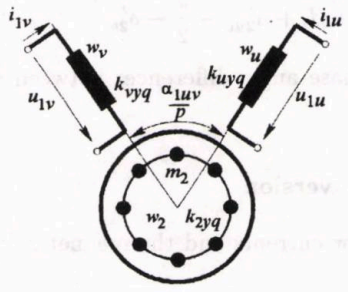

Fig. 1

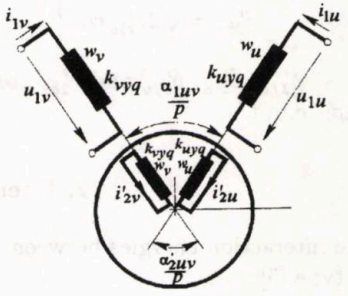

Fig. 2

The magnetic fluxes received by the phase windings of the equivalent rotor due to the opposite revolving magnetic fields are:

$$(1)\quad \Psi'_{2fu} = w_u k_{uyq} \Phi_f \cos(sp\Omega_1 t + \beta_f), \quad \Psi'_{2bu} = w_u k_{uyq} \Phi_b \cos[(2-s)p\Omega_1 t + \beta_b)]$$

for the u rotor phase, and

$$(2)\quad \begin{aligned} \Psi'_{2fv} &= w_v k_{vyq} \Phi_f \cos(sp\Omega_1 t + \beta_f - \alpha'_{2uv}), \\ \Psi'_{2bv} &= w_v k_{vyq} \Phi_b \cos[(2-s)p\Omega_1 t + \beta_b + \alpha'_{2uv})], \end{aligned}$$

for the v rotor phase. The total, per phase, magnetic fluxes are:

$$(3)\quad \Psi'_{2u} = \Psi'_{2fu} + \Psi'_{2bu}, \qquad (4)\quad \Psi'_{2v} = \Psi'_{2fv} + \Psi'_{2bv}.$$

In relations (1),...,(4) u and v denote the phase windings, f and b – the forward and backward revolving magnetic fields [1], [2]. The per pole magnetic fluxes in (1) and (2) are [3]:

$$(5)\quad \Phi_f = \frac{2}{p} LRB_f, \qquad (6)\quad \Phi_b = \frac{2}{p} LRB_b,$$

where B_f and B_b are the magnitude of the forward, f, and the backward, b, revolving magnetic fields.

The equivalent currents through equivalent rotor are [3], [4]:

$$(7)\quad i'_{2u} = i'_{2fu} + i'_{2bu}, \qquad (8)\quad i'_{2v} = i'_{2fv} + i'_{2bv},$$

where:

$$(9)\quad \begin{aligned} i'_{2fu} &= \sqrt{2} I'_{2fu} \cos\left(sp\Omega_1 t + \beta_f - \frac{\pi}{2} - \delta'_{2fu}\right), \\ i'_{2bu} &= \sqrt{2} I'_{2bu} \cos\left[(2-s)p\Omega_1 t + \beta_f - \frac{\pi}{2} - \delta'_{2bu}\right], \\ i'_{2fv} &= \sqrt{2} I'_{2fv} \cos\left(sp\Omega_1 t + \beta_f - \alpha'_{2uv} - \frac{\pi}{2} - \delta'_{2fv}\right), \\ i'_{2bv} &= \sqrt{2} I'_{2bv} \cos\left[(2-s)p\Omega_1 t + \beta_b + \alpha'_{2uv} - \frac{\pi}{2} - \delta'_{2bv}\right]. \end{aligned}$$

In (9) δ'_{2fu}, δ'_{2bu}, δ'_{2fv} and δ'_{2bv} are the phase angle differences between currents and their e.m.f.'s.

2. Energy Conversion

The interaction energies between the rotor currents and the magnetic fluxes are of the type [5]:

$$(10)\quad w_{2u} = \Psi'_{2u} i'_{2u} = (\Psi'_{2fu} + \Psi'_{2bu})(i'_{2fu} + i'_{2bu})$$

for the u rotor phase and

$$w_{2v} = \Psi'_{2v} i'_{2v} = (\Psi'_{2fv} + \Psi'_{2bv})(i'_{2fv} + i'_{2bv}) \tag{11}$$

for the v rotor phase.

If the following notations are made:

$$w_{2ffu} = \Psi'_{2fu} i'_{2fu}, \quad w'_{2fbu} = \Psi'_{2fu} i'_{2bu}, \quad w_{2bfu} = \Psi'_{2bu} i'_{2fu}, \quad w_{2bbu} = \Psi'_{2bu} i'_{2bu}; \tag{12}$$

$$w_{ffv} = \Psi'_{2fv} i'_{2fv}, \quad w'_{2fbv} = \Psi'_{2fv} i'_{2bv}, \quad w_{2bfv} = \Psi'_{2bv} i'_{2fv}, \quad w_{2bbv} = \Psi'_{2bv} i'_{2bv}, \tag{13}$$

the energies (10) and (11) become:

$$w_{2u} = w_{2ffu} + w_{2fbu} + w_{2bfu} + w_{2bbu}, \quad w_{2v} = w_{2ffv} + w_{2fbv} + w_{2bfv} + w_{2bbv}. \tag{15}$$

The instantaneous electromagnetic torques due to the magnetic energies are given by:

$$m_{2u} = \left(\frac{\partial w_{2u}}{\partial \theta_2}\right)_{i'_{2u}=\text{ct.}}, \tag{16}$$

for the u phase and

$$m_{2v} = \left(\frac{\partial w_{2v}}{\partial \theta_2}\right)_{i'_{2v}=\text{ct.}}, \tag{17}$$

for the v phase. In (16) and (17):

$$\theta_2 = \Omega t \tag{18}$$

is the rotor coordinate at any instant t and Ω is the angular speed of the rotor.

If Ω_1 denote the angular speed of the forward revolving magnetic field,

$$\Omega_1 = \frac{\omega_1}{p} = \frac{2\pi f_1}{p}, \tag{19}$$

and the relation between the angular speeds is

$$\Omega_1 = \Omega + s\Omega_1, \tag{20}$$

it follows that:

$$sp\Omega_1 t = p\Omega_1 t - p\theta_2, \quad (2-s)p\Omega_1 t = p\Omega_1 t + p\theta_2. \tag{21}$$

The components of the instantaneous torques (16) and (17) are given by:

$$m_{ffu} = \left(\frac{\partial w_{2ffu}}{\partial \theta_2}\right)_{i'_{2fu}=\text{ct.}}, \tag{22}$$

$$m_{fbu} = \left(\frac{\partial w_{2fbu}}{\partial \theta_2}\right)_{i'_{2bu}=\text{ct.}}, \tag{23}$$

$$(24)\qquad m_{bfu}=\left(\frac{\partial w_{2bfu}}{\partial\theta_2}\right)_{i'_{2fu}=\text{ct.}},\qquad (25)\qquad m_{bbu}=\left(\frac{\partial w_{2bbu}}{\partial\theta_2}\right)_{i'_{2bu}=\text{ct.}},$$

for the u rotor phase, and

$$(26)\qquad m_{ffv}=\left(\frac{\partial w_{2ffv}}{\partial\theta_2}\right)_{i'_{2fv}=\text{ct.}},\qquad (27)\qquad m_{fbv}=\left(\frac{\partial w_{2fbv}}{\partial\theta_2}\right)_{i'_{2bv}=\text{ct.}},$$

$$(28)\qquad m_{bfv}=\left(\frac{\partial w_{2bfv}}{\partial\theta_2}\right)_{i'_{2fv}=\text{ct.}},\qquad (29)\qquad m_{bbv}=\left(\frac{\partial w_{2bbv}}{\partial\theta_2}\right)_{i'_{2bv}=\text{ct.}},$$

for the v rotor phase.

Taking into account (21) the partial derivatives (22),...,(29) are:

$$(30)\qquad \begin{aligned} m_{2ffu}&=\frac{1}{\sqrt{2}}pw_uk_{uyq}\Phi_fI'_{2fu}\sin\left(\frac{\pi}{2}+\delta'_{2fu}\right)+\\ &+\frac{1}{\sqrt{2}}pw_uk_{uyq}\Phi_fI'_{2fu}\sin\left(2sp\Omega_1t+2\beta_f-\frac{\pi}{2}-\delta'_{2fu}\right),\end{aligned}$$

$$(31)\qquad \begin{aligned} m_{2fbu}&=\frac{1}{\sqrt{2}}pw_uk_{uyq}\Phi_fI'_{2bu}\sin\left[2(s-1)p\Omega_1t+\beta_f-\beta_b+\frac{\pi}{2}+\delta'_{2bu}\right]+\\ &+\frac{1}{\sqrt{2}}pw_uk_{uyq}\Phi_fI'_{2bu}\sin\left(2sp\Omega_1t+\beta_f+\beta_b-\frac{\pi}{2}-\delta'_{2bu}\right),\end{aligned}$$

$$(32)\qquad \begin{aligned} m_{2bfu}&=-\frac{1}{\sqrt{2}}pw_uk_{uyq}\Phi_bI'_{2fu}\sin\left[2(1-s)p\Omega_1t+\beta_b-\beta_f+\frac{\pi}{2}+\delta'_{2fu}\right]-\\ &-\frac{1}{\sqrt{2}}pw_uk_{uyq}\Phi_bI'_{2fu}\sin\left(2sp\Omega_1t+\beta_f+\beta_b-\frac{\pi}{2}-\delta'_{2fu}\right),\end{aligned}$$

$$(33)\qquad \begin{aligned} m_{2bbu}&=-\frac{1}{\sqrt{2}}pw_uk_{uyq}\Phi_bI'_{2bu}\sin\left(\frac{\pi}{2}+\delta'_{2bu}\right)-\\ &-\frac{1}{\sqrt{2}}pw_uk_{uyq}\Phi_bI'_{2bu}\sin\left[2(2-s)p\Omega_1t+2\beta_b-\frac{\pi}{2}-\delta'_{2bu}\right],\end{aligned}$$

for the u phase, and:

$$(34)\qquad \begin{aligned} m_{2ffv}&=\frac{1}{\sqrt{2}}pw_vk_{vyq}\Phi_fI'_{2fv}\sin\left(\frac{\pi}{2}+\delta'_{2fv}\right)+\\ &+\frac{1}{\sqrt{2}}pw_vk_{vyq}\Phi_fI'_{2bv}\sin\left(2sp\Omega_1t+2\beta_f-2\alpha'_{2uv}-\frac{\pi}{2}-\delta'_{2fv}\right),\end{aligned}$$

$$m_{2fbv} = \frac{1}{\sqrt{2}} p w_v k_{vyq} \Phi_f I'_{2bv} \sin\left[2(s-1)p\Omega_1 t + \beta_f - 2\alpha'_{2uv} + \frac{\pi}{2} + \delta'_{2bv}\right] +$$

(35)

$$+ \frac{1}{\sqrt{2}} p w_v k_{vyq} \Phi_f I'_{2bv} \sin\left(2p\Omega_1 t + \beta_f + \beta_b - \frac{\pi}{2} - \delta'_{2bv}\right),$$

$$m_{2bfv} = -\frac{1}{\sqrt{2}} p w_v k_{vyq} \Phi_b I'_{2fv} \sin\left[2(1-s)p\Omega_1 t + \beta_b - \beta_f + 2\alpha'_{2uv} + \frac{\pi}{2} + \delta'_{2fv}\right] -$$

(36)

$$- \frac{1}{\sqrt{2}} p w_v k_{uyq} \Phi_b I'_{2fv} \sin\left(2p\Omega_1 t + \beta_b + \beta_f - \frac{\pi}{2} - \delta'_{2fv}\right),$$

$$m_{2bbv} = -\frac{1}{\sqrt{2}} p w_v k_{vyq} \Phi_b I'_{2bv} \sin\left(\frac{\pi}{2} + \delta'_{2bv}\right) -$$

(37)

$$- \frac{1}{\sqrt{2}} p w_v k_{vyq} \Phi_b I'_{2bv} \sin\left[2(2-s)p\Omega_1 t + 2\beta_b + 2\alpha'_{2uv} - \frac{\pi}{2} - \delta'_{2bv}\right],$$

for the v phase.

The average values of the torques are of the type:

$$M = \frac{1}{nT} \int_{t_0}^{t_0+nT} m \, dt. \tag{38}$$

Consequently the average values of the forward and backward torques due to the u phase are, respectively:

$$M_{fu} = M_{2ffu} = \frac{1}{nT} \int_{t_0}^{t_0+nT} m_{2ffu} \, dt = \frac{1}{\sqrt{2}} p w_u k_{uyq} \Phi_f I'_{2fu} \sin\left(\delta'_{2fu} + \frac{\pi}{2}\right), \tag{39}$$

$$M_{bu} = M_{2bbu} = \frac{1}{nT} \int_{t_0}^{t_0+nT} m_{2bbu} \, dt = -\frac{1}{\sqrt{2}} p w_u k_{uyq} \Phi_b I'_{2bu} \sin\left(\delta'_{2bu} + \frac{\pi}{2}\right), \tag{40}$$

because the average values of m_{2fbu} and m_{2bfu} are zero and also:

$$\frac{1}{nT} \int_{t_0}^{t_0+nT} \frac{1}{\sqrt{2}} p w_u k_{uyq} \Phi_f I'_{2fu} \sin\left(2sp\Omega_1 t + 2\beta'_f - \frac{\pi}{2} - \delta'_{2fu}\right) dt = 0, \tag{41}$$

$$\frac{1}{nT} \int_{t_0}^{t_0+nT} \frac{1}{\sqrt{2}} p w_u k_{uyq} \Phi_b I'_{2bu} \sin\left[2(2-s)p\Omega_1 t + 2\beta_b - \frac{\pi}{2} - \delta'_{2bu}\right] dt = 0. \tag{42}$$

For the v phase, similarly:

$$M_{fv} = M_{2ffv} = \frac{1}{nT}\int_{t_0}^{t_0+nT} m_{2ffv}\,\mathrm{d}t = \frac{1}{\sqrt{2}} p w_v k_{vyq} \Phi_f I'_{2fv} \sin\left(\delta'_{2fv} + \frac{\pi}{2}\right), \tag{43}$$

$$M_{bv} = M_{2bbv} = \frac{1}{nT}\int_{t_0}^{t_0+nT} m_{2bbv}\,\mathrm{d}t = -\frac{1}{\sqrt{2}} p w_v k_{vyq} \Phi_b I'_{2bv} \sin\left(\delta'_{2bv} + \frac{\pi}{2}\right), \tag{44}$$

because the average values m_{2fbv} and m_{2bfv} are zero and also:

$$\frac{1}{nT}\int_{t_0}^{t_0+nT} \frac{1}{\sqrt{2}} p w_v k_{vyq} \Phi_f I'_{2fu} \sin\left(2sp\Omega_1 t + 2\beta_f - 2\alpha'_{2uv} - \frac{\pi}{2} - \delta'_{2fv}\right) \mathrm{d}t = 0, \tag{45}$$

$$\frac{1}{nT}\int_{t_0}^{t_0+nT} \frac{1}{\sqrt{2}} p w_v k_{vyq} \Phi_b I'_{2bu} \sin\left[2(2-s)p\Omega_1 + 2\beta_b + 2\alpha'_{2uv} - \frac{\pi}{2} - \delta'_{2bv}\right] \mathrm{d}t = 0. \tag{46}$$

The resultant torques (forward and backward) are, respectively,

$$M_f = M_{fu} + M_{fv}, \tag{47}$$

$$M_b = M_{bu} + M_{bv}. \tag{48}$$

3. Observations and Conclusions

1. The torques having zero average values (m_{2fbu}, m_{2bfu}, m_{2fbv}, m_{2bfv}) and those given by (41), (42) and (45), (46) are acting on the machine axis if the machine has low inertia.

2. If the machines is a symmetrical one:

$$m_{2fbu} + m_{2fbv} = 0, \tag{49}$$

$$m_{2bfu} + m_{2bfv} = 0, \tag{50}$$

because they are opposite and

$$m_{2bbu} = m_{2bbv} = 0, \tag{51}$$

because there are not backward components of the magnetic fluxes and currents. Consequently

$$m_2 = m_{2ffa} + m_{2ffb} = 2m_{2f}. \tag{52}$$

3. The r.m.s. values of the e.m.f. in the equivalent rotor windings are:

$$\begin{aligned} E'_{2fu} &= \sqrt{2}\pi s f_1 w_u k_{uyq} \Phi_f, \quad E'_{2fv} = \sqrt{2}\pi s f_1 w_v k_{vyq} \Phi_f, \\ E'_{2bu} &= \sqrt{2}\pi(2-s) f_1 w_u k_{uyq} \Phi_b, \quad E'_{2bv} = \sqrt{2}\pi(2-s) f_1 w_v k_{vyq} \Phi_b. \end{aligned} \tag{53}$$

Consequently, the torques become:

$$M_{fu} = \frac{E'_{2fu} I'_{2fu}}{s\Omega_1} \cos \delta'_{2fu}, \quad M_{fv} = \frac{E'_{2fv} I'_{2fv}}{s\Omega_1} \cos \delta'_{2fv},$$

(54)

$$M_{bu} = \frac{E'_{2bu} I'_{2bu}}{(2-s)\Omega_1} \cos \delta'_{2bu}, \quad M_{bv} = \frac{E'_{2bv} I'_{2bv}}{(2-s)\Omega_1} \cos \delta'_{2bv}.$$

4. The torques may be expressed as functions of the machine's parameters and of the equivalent number of rotor's phases:

$$M_f = M_{fu} + M_{fv} = \frac{R'_{2fu} I'^2_{2fu}}{s\Omega_1} + \frac{R'_{2fv} I'^2_{2fv}}{s\Omega_1} =$$

(55)

$$= \frac{l_{fu} R'_{2fu} I'^2_{2fu}}{s\Omega_1} = \frac{l_{fv} R'_{2fv} I'^2_{2fv}}{s\Omega_1} = \frac{m_2 R_2 I^2_{2f}}{s\Omega_1},$$

because [4]:

$$\frac{1}{l_{fu}} + \frac{1}{l_{fv}} = 1 \tag{56}$$

and

$$M_b = M_{bu} + M_{bv} = \frac{R'_{2bu} I'^2_{2bu}}{(2-s)\Omega_1} + \frac{R'_{2bv} I'^2_{2bv}}{(2-s)\Omega_1} =$$

(57)

$$= \frac{l_{bu} R'_{2bu} I'^2_{2bu}}{(2-s)\Omega_1} = \frac{l_{bv} R'_{2bv} I'^2_{2bv}}{(2-s)\Omega_1} = \frac{m_2 R_2 I^2_{2b}}{(2-s)\Omega_1},$$

since

$$\frac{1}{l_{bu}} + \frac{1}{l_{bv}} = 1. \tag{58}$$

In (55),...,(58) l_{fu}, l_{fv}, l_{bu} and l_{bv} are the equivalent numbers of rotor phases.

Received, July 6, 2000

Technical University "Gh.Asachi", Jassy,
Department of General Electrotechnics
and Electrical Machines

REFERENCES

1. Androne I., Prisăcaru A., *On the Equivalent Circuits Diagram of the Two-phase Unsymmetrical Induction Motors.* Bul. Inst. polit., Iaşi, **XLII (XLVI)**, *1-2*, s.III, 95-104 (1996).
2. Androne I., Prisăcaru A., Pavel V., Verdeş M., Lozonschi T.L., *Voltages Equations of the Unsymmetrical Two-phase Electrical Induction Motors.* Proc. Internal.Conf. on Power Engineering'97, ICOPE'97, Tokyo, Vol. **2**, 297-300.
3. Prisăcaru A., Androne I., Pavel V., Verdeş M., Radu G., *The Magnetizing Currents of the Unsymmetrical Two-phase Induction Motors.* ICATE'98,

Proc. of the Internat. Conf. on Appl. a. Theoret. Electr., Vol. **III**, Electrical Machines, Electrical Drives and Electromechanical Equipment, Craiova, România, June 4-6, 1998, 127-132.

4. A n d r o n e I., P r i s ă c a r u A., *Secondary Parameters of the Unsymmetrical Two-phase Induction Motors.* Bul. Inst. polit., Iaşi, **XLIII (XLVII)**, *1-2*, s.III, 97-106 (1997).
5. G h e o r g h i u I.S., F r a n s u a Al.S., *Tratat de maşini electrice.* Vol. **III**, Ed. Acad., Bucureşti, 1971.

CONVERSIA ENERGIEI ÎN MAŞINILE DE INDUCŢIE BIFAZATE NESIMETRICE

(Rezumat)

Pe baza noţiunii de „numere echivalente de faze" ale maşinii de inducţie bifazate nesimetrice, introdusă de autori, a fost examinată conversia electromecanică a energiei în asemenea tipuri de maşini. Au fost obţinute relaţiile cuplurilor dezvoltate în maşină în funcţie de numerele echivalente de faze ale rotorului.

BULETINUL INSTITUTULUI POLITEHNIC DIN IAŞI
Tomul XLVII (LI), Fasc. 1–2, 2001
ELECTROTEHNICĂ. ENERGETICĂ. ELECTRONICĂ

D.C. 621.318.22

CONSIDERATIONS ON THE INTERDEPENDENCE BETWEEN MATERIALS AND PERFORMANCES OF ELECTRICAL SERVOMOTORS

BY
V. BAHRIN and CARMEN COJOCARU-FILIPIUC

In the paper there are made certain specifications regarding the relationship between the utilized materials and the achieved performances of electrical servomotors.

One emphasizes the fact that the utilization of the insulating materials of a superior temperature class determines the improvement of the electrical servomotors performances.

A comparative analysis is made on the relative characteristics of a permanent excited servomotor and a servomotor with electromagnetic excitation. This analysis makes evident the advantages of the permanent excited servomotors.

1. Introduction

The electrical servomotors are fundamental components of the driving systems, that must satisfy requirements regarding the energetical indicators, the operation reliability, the accuracy of the command execution, the extension ranges of speed and torque value they are capable to develop [2].

The rapid progress achieved in the domain of materials utilized in the electrical machines construction and particularly in that of permanent magnets used for the excitation of electrical servomotors, have led to a spectacular evolution of their performances.

For the designers of electrical servomotors a first priority problem is represented by the adequate choice of materials for the construction of the machine, correlated with the performances imposed to the driving system as an ensemble, and with the final cost limit that must be observed [1]. In the context of the present competition conditions, the electrical machine designer is compelled to assume the last achievements both in the domain of the electrical engineering materials and in the range of the power semiconductor devices and integrated control circuits.

2. The Electrical Insulation of Servomotors

The electrical insulation of an electrical servomotor influences the value of the slot space utilization factor; on the other hand, the temperature that can be endured by the insulation and the coefficient of thermal dissipation on the insulated conductors surface influence the values of the specific amperturns and of the admissible current density [1].

The electrical servomotors made in Romania are constructed with insulation materials of the insulation class F (having the limit temperature of 155°C). The utilization of the insulating materials of the temperature class H (with the limit temperature of 180°C) allows the realization of high performance servomotors, characterized by increased values of the power/volume ratio [2].

The 190 SRD 1000 servomotor, made by IFMA-Bucharest, is equipped [3] with a disk rotor and the insulation is impregnated with epoxide resin of the temperature class F. By modification of the rotor insulation it was constructed the servomotor SRD 191C (191 SRD 1300) with a 30% higher rated power, with unmodified condition of mass and overall dimensions.

For the servomotor SRD 191C the utilized insulation is based on glass fabric impregnated in hismaleimidic resin (made at the "Petru Poni" Institute, Jassy) complying with the insulation class H, hot pressed (at 170°C) for 30 min. The disk rotor of the servomotor is made of punched copper, the thin sheets are hot soldered (owing to the glass fabric impregnated with hismaleimidic resin) and then electron beam welded. The such achieved rotor has a high mechanical rigidity (because the glass fabric with hismaleimidic resin is not enough flexible) and a less electrical rigidity than in case of utilization of epoxide resins.

Table 1 centralizes the electromechanical parameters [3] of the servomotors 190 SRD 1000 and 191 SRD 1300; it emphasizes the fact that utilization of the insulating materials of the class H determines the improvement of the electrical servomotors performances.

Table 1

Characteristics and electrotechnical parameters	Symbol	190 SRD 1000	191 SRD 1300
Rated power, [W]	P_n	1,000	1,300
Rated torque, [N cm]	M_n	320	413
Rated speed, [rpm]	n_n	3,000	3,000
Rated voltage, [V]	U_n	82	82
Rated current, [A]	I_n	15	20
Low speed maximum current, [A]	I_{sc}	16.5	18
Electromotive voltage at 1,000 rev/min., [V]	K_E	25	24.3
Terminal resistance at 20°C, [Ω]	R_b	0.45	0.45
Rotor self induction, [μH]	L	100	100
Rotor inertia moment, [kg cm^2]	J	12	12
Mechanical time constant, [m s]	τ_m	11	12.5
Maximum pulse torque, [N cm]	M_{imp}	2,440	2,670
Maximum pulse current, [A]	I_{imp}	100	100
Maximum speed, [rpm]	n_{max}	5,000	5,000
Viscous friction torque at 1,000 rev/min., [N cm]	M_F	15	15
No-load lose torque constant, [N cm]	K_D	15	15.3
Torque per Ampère, [N cm/A]	K_T	24.2	23.2
Constant voltage load speed drop, [rpm/N cm]	K_N	0.88	1
No-load current, [A]	I_0	2	2.5

3. Permanent Magnets for the Excitation of Servomotors

The permanent magnets utilized in the construction of electrical servomotors are made of metals or alloys that present a high remanent magnetic density, practically constant for a long time [1]. Utilization of permanent magnets facilitated the construction of servomotors characterized by a high efficiency, small dimensions, superior dynamic performances and lower operation costs.

The introduction of permanent magnets in the electromechanical structure of electrical servomotors led to reduction of restrictions of thermal and mechanical nature, what facilitated the obtention of higher values for the airgap magnetic flux density as compared to those obtained by a winding excitation.

The permanent magnets utilized for the servomotors excitation have to comply with the following requirements [3]:

a) to have a long time stability of the magnetic characteristics, to withstand mechanical shocks and the action of chemical agents, and to present a high enough electrical resistivity;

b) modifications of the excitation magnetic flux determined by over currents occurred in the servomotor operation must be reversible;

c) the maximum admissible operation temperature of the permanent magnet must be higher than that of the magnetic circuit of the servomotor; modifications of the inductor magnetic flux introduced by over-temperatures occured during the servomotor operation must be reversible and the temperature coefficients of the magnetic materials must have small values.

None of the permanent magnet materials have ideal magnetic properties, but by a judicious design some critical parameters can be improved.

To emphazise the positive aspects brought by utilization of permanent magnet excitation it is given a comparative analysis regarding the characteristics of the relative power, P/P_n, relative torque, M/M_n and relative speed, n/n_n, as functions of the relative current, I/I_n, for a permanent excited servomotor (Fig. 1) and for a servomotor with electromagnetic excitation (Fig. 2), respectively [3].

From the variations of the relative power as a function of the relative current the following conclusions can be drawn [3]:

a) for smaller than unity relative currents the relative power of the permanent excited servomotor is increasing in a larger domain than in case of the electromagnetic excitation servomotor;

b) for the relative current $I/I_n = 1$ the relative power of the permanent excited servomotor (owing to absence of the excitation losses), has greater values then for the servomotor with electromagnetic excitation;

c) for higher than unity relative currents the relative power of the permanent excited servomotor still present a (small) rise, while with the electromagnetically excited servomotor, the relative power decreases.

Regarding the relative torque characteristics as function of the relative current we can note the following observations [3]:

a) the relative torque increases faster in case of the servomotor with electromagnetic excitation for the same increase of the relative current;

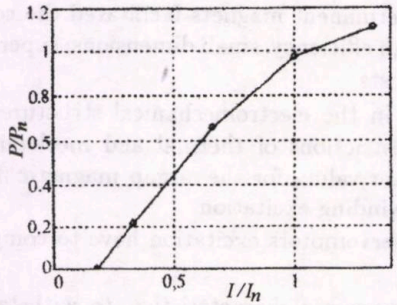

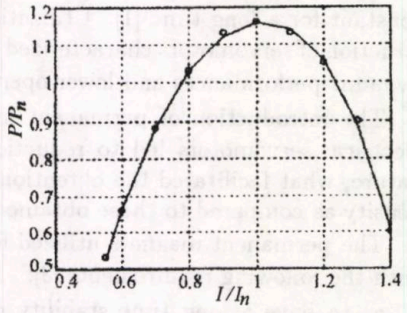

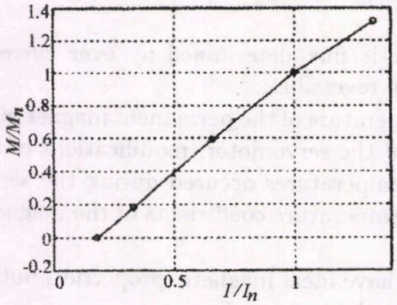

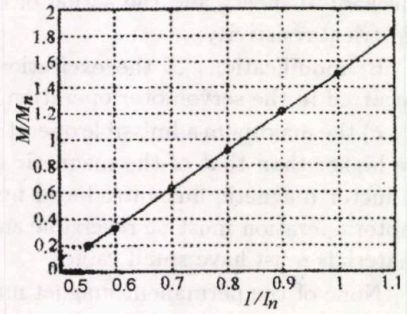

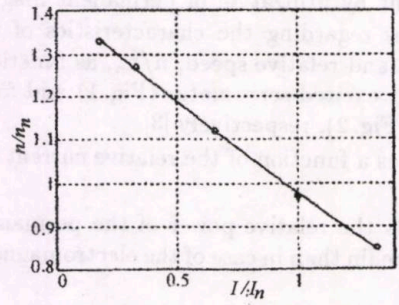

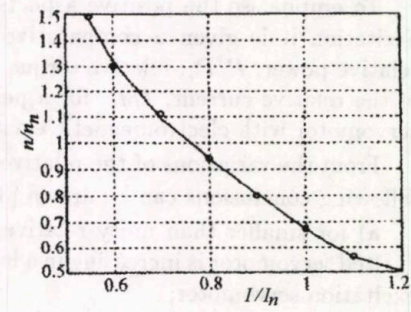

Fig. 1 Fig. 2

b) for the relative current $I/I_n = 1$ the value of the relative torque is superior when using an electromagnetic excited servomotor.

The aspect of relative speed characteristic in function of the relative current emphasizes the following conclusions:

a) the linearity of these characteristics is maintained for a larger range of values in case of the permanent excited servomotor;

b) for the relative current $I/I_n = 1$ the relative speed of the permanent excited servomotor is superior to the relative speed of the electromagnetically excited servomotor;

c) in case of the electromagnetically excited servomotor the characteristic has important deviations from linearity.

4. Observations and Conclusions

The quality of materials utilized for realization of the electrical insulation, of the ferromagnetic core and of the permanent magnets, influences the design, the construction and the performances of the electrical servomotors.

The servomotors insulation must to have an as high as possible dielectric rigidity, with the goal of reducing its thickness and with advantageous effects on heat transmission as well as a high thermal conductibility [1].

The ferromagnetic core has to be made of materials with an as high as possible relative magnetic permeability and low specific losses.

The brushes of servomotors are made of graphited brass or graphited silver with high metal content, in order to reduce the voltage drops. Materials with more than 50% metal allow an operation life up to 5,000 hours for usual applications and up to 600 hours in aeronautic applications where the small atmospherical pressure leads to premature wear [1].

The performances of the small power permanent excited servomotor become comparable with the ones of the relative big power servomotors with electromagnetic excitation.

Received, November 13, 2000

Technical University "Gh.Asachi", Jassy,
Department of General Electrotechnics
and Electrical Machines

REFERENCES

1. S t o i a D., *Motoare de curent continuu excitate cu magneţi permanenţi.* Ed. Tehnică, Bucureşti, 1983.
2. B o l d e a I., *Parametrii maşinilor electrice.* Ed. Acad Române, Bucureşti, 1991.
3. B a h r i n V., *Servomotoare de curent continuu cu magneţi permanenţi.* Ed. Performantica, Iaşi, 1999.

CONSIDERAŢII ASUPRA INTERDEPENDENŢEI DINTRE MATERIALELE ŞI PERFORMANŢELE SERVOMOTOARELOR ELECTRICE

(Rezumat)

Se fac unele precizări privind relaţia materiale–performanţă pentru servomotoarele electrice.

Se pune în evidenţă faptul că utilizarea materialelor izolante de clasă superioară determină îmbunătăţirea performanţelor servomotoarelor electrice.

Se efectuează o analiză comparativă a caracteristicilor relative ale unui servomotor excitat permanent cu cele ale unui servomotor cu excitaţie electromagnetică. Această analiză evidenţiază avantajele servomotoarelor excitate cu magneţi permanenţi.

BULETINUL INSTITUTULUI POLITEHNIC DIN IAŞI
Tomul XLVII (LI), Fasc. 1–2, 2001
ELECTROTEHNICĂ. ENERGETICĂ. ELECTRONICĂ

D.C. 511; 518.8

IMPLEMENTING SOME ARITHMETIC CALCULATION ALGORITHMS ON MICROCONTROLLERS FROM INTEL 8051 FAMILY

BY

PETRUŢ DUMA

The calculus algorithms for the operation of addition, subtraction, increment, decrement, multiplication, the n power, division and extraction of square root for signed and unsigned multi-byte binary numbers are described. For each particular arithmetic operation, the author wrote the program sequences which can be run on any microcontroller from INTEL 8051 family. The binary numbers used in these calculations can be 16, 32, 48 or 64-bit long and with slight adjustments in the program sequences, various other number of bytes can be used in these calculations.

1. Introduction

The INTEL 8051 microcontroller has arithmetic calculation instructions for unsigned 8-bit numbers, as shown in Table 1. The abbreviations have the following meaning: A – accumulator, B – special function register, s – source, d – destination, Ri – general purpose register $R0$, $R1$,...,$R7$, (a8H) – the contents of the internal data memory location with address a8H, (Ri) – the contents of the internal data memory location with the address stored in the general purpose register $R0$ or $R1$, d8H – immediate data, DPTR – register used for addressing external memory, $[A : B]$ – the quotient of dividing A to B, $\{A : B\}$ – the remainder of the division.

Table 1

Operation	Symbolic form	Mnemonic	Observation
Addition	$A \leftarrow A + s$	ADD A, s	$s = Ri$, $(i = \overline{0,7})$
Addition with carry	$A \leftarrow A + s + C$	ADDC A, s	$s =$ (a8H)
Subtraction	$A \leftarrow A - s - C$	SUBB A, s	$s = (Rj)$, $(j = \overline{0,1})$
			$s =$ d8H
Increment	$d \leftarrow d + 1$	INC d	$s = A, Ri$, (a8H), (Rj), DPTR
Decrement	$d \leftarrow d - 1$	DEC d	$s = A, Ri$, (a8H), (Rj)
Multiplication	$BA \leftarrow A \cdot B$	MUL AB	$B =$ high $A \cdot B$; $A =$ low$A \cdot b$
Division	$AB \leftarrow A : B$	DIV AB	$A = [A : B]$; $B - \{A : B\}$

For signed arithmetic calculations, the most significant bit holds the sign, and in the rest of the bits is stored the number's value. The positive numbers have in the most significant bit the binary value of logical "0", while the negative numbers have in that bit the binary value of logical "1".

The signed arithmetic calculations determine at first the sign of the result, then the required calculation is made using the absolute value of the operands. After the

absolute value of the result is determined, if the sign bit is affected, the overflow flag is set in order to signalize this error.

2. The Addition and the Subtraction of Binary Numbers

The command program for adding two multi-byte unsigned binary numbers consists basically of a program loop where the bytes of the numbers are added starting with the less significant ones and concluding with the most significant ones. During this loop, the current rank byte of the first number is transferred in accumulator A and the corresponding byte of the second number is transferred in a general purpose register, *e.g.* $R0$. Afterwards, the contents of the accumulator A is added to the contents $R0$ and to the carried bit (C) from the inferior rank, the result being loaded in the corresponding rank of a memory buffer. The program loop is repeated for as many times as the number of bytes included in the binary numbers.

The subtraction of two multi-byte unsigned binary numbers is performed in a similar manner, except that instead of calculating the sum of the bytes from a certain rank when is performed their subtraction (the "loan" from the previous rank is also subtracted).

In both these operations, the command programs are simple and do not require the description of a logic chart or any other details.

Assume the signed binary numbers X and Y for calculating the algebraic sum (addition/subtraction). In this case, the sign of the algebraic sum is determined according to Table 2; the absolute values of the two numbers are used for calculating the sum or the difference of the binary numbers.

Table 2

X sign	Y sign	Operation	Result sign	Algebraic sum
+	+	$X+Y$	+	$\|X\|+\|Y\|$
+	−	$X+Y$	+ if $\|X\| \geq \|Y\|$	$\|X\|-\|Y\|$
			− if $\|X\| < \|Y\|$	$\|Y\|-\|X\|$
−	+	$X+Y$	+ if $\|X\| \leq \|Y\|$	$\|Y\|-\|X\|$
			− if $\|X\| > \|Y\|$	$\|X\|-\|Y\|$
−	−	$X+Y$	−	$\|X\|+\|Y\|$
+	+	$X-Y$	+ if $\|X\| \geq \|Y\|$	$\|X\|-\|Y\|$
			− if $\|X\| < \|Y\|$	$\|Y\|-\|X\|$
+	−	$X-Y$	+	$\|X\|+\|Y\|$
−	+	$X-Y$	−	$\|X\|+\|Y\|$
−	−	$X-Y$	+ if $\|X\| \leq \|Y\|$	$\|Y\|-\|X\|$
			− if $\|X\| > \|Y\|$	$\|X\|-\|Y\|$

Incrementing or decrementing binary multi-byte numbers consist of adding or subtracting a unit, respectively, to /from the less significant byte of the binary number and of updating the carry or "loan" respectively regarding the higher rank byte. This is nothing else but a particular case of the addition and subtraction operations when X is any binary number and Y is unitary ($X+1$ and $X-1$, respectively).

3. The Multiplication of Binary Numbers

Manual multiplication of two unsigned binary numbers consists of computing the

sum of partial products. Assuming the binary numbers 11101011_2 and 10101001_2 one can calculate the product:

$$
\begin{array}{r}
11101011 \\
\underline{10101001} \\
11101011 \\
11101011 \\
11101011 \\
11101011 \\
\hline
1001101100100011_2
\end{array}
$$

The command program for multiplying two unsigned multi-byte binary numbers uses a left-shifting and adding algorithm.

The multiplier is tested bit by bit from the less significant bit to the most significant one. Every time when the current bit of the tested multiplier is logical "1", the partial result of the product is added to left-shifted multiplicand, while if the tested bit is logical "0", the partial result remains unaltered. At the beginning, the partial result is added the multiplicand, then the multiplicand doubled by left-shifting, insuring in this manner the adequate partial values.

Assume the multiplicand X has n bits and the multiplier Y has m bits. The product $X \cdot Y$ generates a result, P, which has a maximum of $n+m$ bits. Therefore, for multiplicand X, it must be reserved a working area $n+m$ bits, in order to calculate the values $2^i X$, $(i = 0, 1, ..., m-1)$.

The basic organigram of the program which performs the multiplication of two binary numbers is shown below.

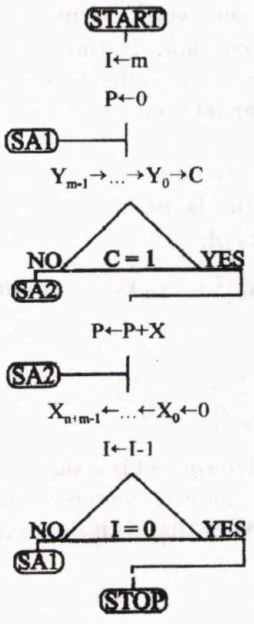

Initialize iteration counter in variable I with value m.

Initialize product P with 0.

Bit-by-bit transfer in the carry flag C, the binary values of multiplier Y starting with the less significant bit.

Current bit of the multiplier Y is tested.

Current bit of the multiplier Y is logical "1".

The partial result of the product P is added the value stored in the multiplicand (2^IX, I = 0,1,...).

The multiplicand is doubled; the value of 2^IX is determined.

Decrement iteration counter.

Test if the product P of the binary numbers is calculated. The product is calculated.

If the binary numbers are signed, then the sign of the product P is calculated as mod 2 sum between the signs of the multiplicand X and the multiplier Y, the absolute values of the two numbers being determined, and the calculus algorithm of the product is called.

The instruction set of the INTEL 8051 microcontroller includes the instruction MULAB which performs the multiplication between the contents of accumulator A and register B (the high part of the result is loaded in register B, while the low part is loaded in accumulator A). Using this instruction, an easier calculation algorithm can be designed for multiplying two binary numbers.

Assume the 16-bit binary numbers A and B which can be written as follows:

$X = X_3X_2X_1X_0$, where X_3, X_2, X_1 X_0 are the four hexadecimal numbers of number X;

$Y = Y_3Y_2Y_1Y_0$, where Y_3, Y_2, Y_1, Y_0, are the four hexadecimal numbers of number Y;

$X = X_3 \cdot 10^3H + X_2 \cdot 10^2H + X_1 \cdot 10^1H + X_0 \cdot 10^0H$ (H indicates the hexadecimal numeration base);

$Y = Y_3 \cdot 10^3H + Y_2 \cdot 10^2H + Y_1 \cdot 10^1H + Y_0 \cdot 10^0H$.

Binary numbers X and Y consist of 8-bit numbers:

$$X = X_3X_2 \cdot 10^2H + X_1X_0, \quad Y = Y_3Y_2 \cdot 10^2H + Y_1Y_0.$$

The result of multiplying X and Y is the following:

$$P = X \cdot Y = (X_3X_2 \cdot 10^2H + X_1X_0)(Y_3Y_2 \cdot 10^2H + Y_1Y_0) =$$
$$= X_3X_2 \cdot Y_3Y_2 \cdot 10^4H + X_1X_0 \cdot Y_1Y_0 + X_3X_2 \cdot Y_1Y_0 \cdot 10^2H + X_1X_0 \cdot Y_3Y_2 \cdot 10^2H.$$

The above described algorithm is reduced to a linear one, which calculates four partial products (using the instruction MULAB) and their sum. In this way, the calculus time is reduced with about an order of magnitude. In order to multiply longer binary numbers, it is necessary to calculate more partial products and to sum them up.

Calculating the power $n = 2, 3, \ldots$ of multi-byte binary numbers represents a simpler multiplication case, if an adequate grouping of terms is used.

Calculating the square of the 16-bit number X consists of:

$$X^2 = (X_3X_2 \cdot 10^2H + X_1X_0)^2 = (X_3X_2)^2 \cdot 10^4H + (X_1X_0)^2 + 2X_3X_2 \cdot X_1X_0 \cdot 10^2H.$$

Calculating the cube of the 16-bit number X is:

$$X^3 = (X_3X_2 \cdot 10^2H + X_1X_0)^3 = (X_3X_2)^3 \cdot 10^6H + (X_1X_0)^3 +$$
$$+3[(X_3X_2)^2 \cdot X_1X_0 \cdot 10^2H + X_3X_2 \cdot (X_1X_0)^2] \cdot 10^2H.$$

If the binary number for which the power n must be determined is a signed one, then the sign of the result must be found. This sign is plus for even powers while for the odd powers, it equals the sign of the binary number. After that, it is determined the power of the absolute value.

4. The Division of Binary Numbers

Manually dividing two unsigned binary numbers is made as described in the following example. Considering the binary numbers 10101101_2 and 1100_2, the quotient and the remainder are calculated as follows:

$$\begin{array}{l} 10101101_2 \; \underline{1100_2} \\ \underline{1100} \qquad 1110_2 \\ =10011 \\ \underline{1100} \\ ==1110 \\ \underline{1100} \\ ==101_2 \end{array}$$

The command program for dividing two multi-byte unsigned binary numbers uses a left shifting (rotation) and subtraction algorithm.

The divisor is subtracted from the most significant bits of the dividend. If the subtraction does not generate carry ($C = 0$), then the corresponding bit of the quotient is 1; if the result of the subtraction generates "loan" ($C = 1$), then the corresponding bit of the quotient is 0 and the subtraction is no longer performed. The remainder is added to the following binary digit and the algorithm is continued.

When dividing two random binary numbers, the first not-null significant bit of the dividend and of the divisor can be placed on any position. Therefore it is required a working area where the dividend is entered bit-by-bit using left shifting and from which the divisor is subtracted in order to determine the bit from the quotient of the respective rank; at the end, the working area includes the remainder of the division.

Assume that the dividend X is n bits long while the divisor Y is m bits long. The division $X : Y$ generates a quotient of maximum n bits and a remainder R, of maximum m bits. Before starting the calculation algorithm, it is necessary to test the divisor; if Y equals 0, the error is signalized.

The basic organigram of the program which performs the division of two binary numbers is shown below (the quotient is inserted bit-by-bit into the dividend X):

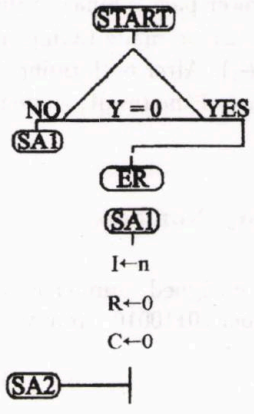

Test if the divisor Y is zero.

The divisor Y is zero.

Error and algorithm cancelled.

Divisor Y is other than zero.

Initialize iteration counter in variable I with value n.

Initialize working area R with zero (remainder).

Reset carry flag.

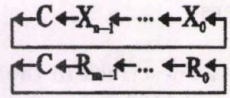

The most significant bit of dividend X is inserted in the working area R; the quotient of the division is updated in X.

$t \leftarrow C$

The carry flag is transferred in bit t.

$AUX \leftarrow tR - Y$

The divisor Y is subtracted from the most significant bits of dividend X stored in the working area R; the result of the subtraction is stored in the auxiliary variable AUX ($tR=2^m t+R$).

$C \leftarrow \bar{C}$

The current bit of the quotient is updated.

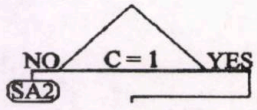

The current binary value of the quotient is tested.

The subtraction tR−Y did not generate "load".

$R \leftarrow AUX$

The working area R is updated with the result of the previous subtraction

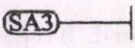

$I \leftarrow I-1$

Decrement the iteration counter.

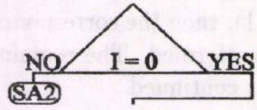

Test if the division between the two binary numbers is finished.

The division is concluded.

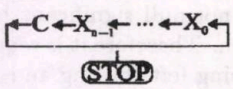

The quotient is updated with the last computed binary value; the quotient is stored in X and the remainder in R.

If the binary numbers are signed, then the sign of the quotient is calculated as the mod 2 sum of the dividend X sign and the divisor Y sign, while the sign of the remainder R is the sign of the dividend. Afterwards, the absolute values of the two numbers are determined and the division calculation algorithm is called.

Using this algorithm, the integer part of the quotient is determined. It may be also determined a number of p bits of the result after the decimal point. In this case, it is necessary to initialize the iteration counter, I, with the value $n+p$ while the n-bit dividend X is extended to $n+p$ bits adding to its lower part p binary values of logical "0". Also, the left-shifting of the dividend X must be made taking into account its length of $n+p$ bits ($\underbrace{\leftarrow C \leftarrow X_{n+p-1} \leftarrow \ldots \leftarrow X_0 \leftarrow}$). After performing the algorithm, the most significant n bits include the integer part of the result, while the less significant p bits include the decimal part.

5. Extracting the Square Root of a Binary Number

Manually extraction of the square root from a binary unsigned number is performed as in the following example; assume the binary number 10110010_2 from which we wish to extract the square root:

$$\begin{array}{l|l} \sqrt{10.11.00.10} & 1101_2 \\ \underline{01} & \underline{1 \cdot 1 = 1} \\ =111 & \underline{101 \cdot 1 = 101} \\ \underline{101} & \underline{1100 \cdot 0 = 0} \\ =100010 & 11001 \cdot 1 = 11001 \\ \underline{11001} & \\ =11001_2 & \end{array}$$

The command program for extracting the square root from an unsigned multi-byte binary number uses a subtraction and left-shifting (rotating) algorithm.

The binary digits of the numbers are grouped by two and in bytes, starting with the less significant part. From the most significant byte of the binary number, the immediate data $40H$ is subtracted. If the result of the previous subtraction did not generate a "loan" ($C = 0$), then the binary digit of the result is logical "1", while if the result of the subtraction did generate a "loan" ($C = 1$), then the binary digit of the result is logical "0" and the subtraction is no longer performed. The rest of the binary number from which the square root is to be extracted, left after the subtraction, is left-shifted twice. At each left-shifting, the less significant bit is set to logical "0".

Afterwards, from the transport of the left-shifting and the most significant byte of the number are subtracted the result and the immediate data $40H$. Similar to the previous case, the result is given by reversing the carry flag. The algorithm continues with the left-shifting of the number and so on.

In order to perform the algorithm in the manner described above, it is required a working area Z where to insert the most significant two bits of the binary number after the subtraction operation.

Assume that the binary number from which the square root is to be extracted is $2n$ bits long. Result R has maximum n bits while the required working area, Z, must be also of n bits. The result of the operation is stored at the end in the carry flag and in the working area.

The basic organigram which performs the square root from a binary number is presented below.

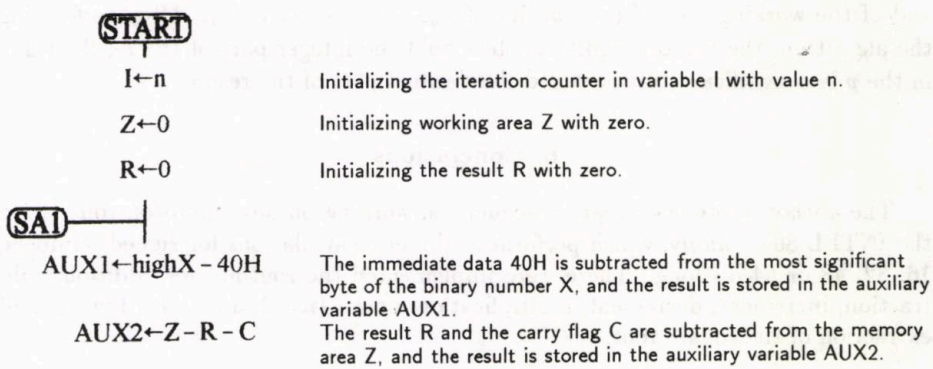

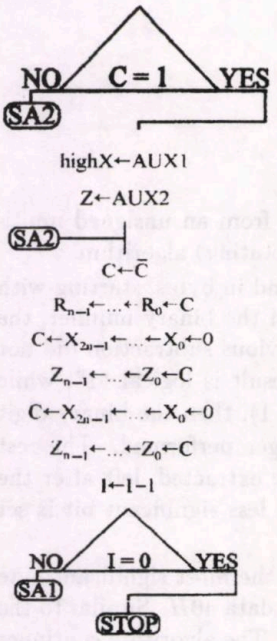

Test if the previous subtraction generated a "loan".

The subtraction did not generate a "loan".

The result of the previous subtraction is transferred from AUX1 and AUX2 in the most significant bit of the binary number X and in the working area Z respectively.

The current bit of the result is updated.

The current bit of the result is stored in R using a left-shifting.

The binary number X is left-shifted twice, so that its two most significant bits are inserted into variable Z, while the two less significant bits of number X are set to logical "0".

Decrement iteration counter.

Test if the extraction of the square root is concluded.

The square root is determined.

The square root is extracted only from positive numbers. In the case of signed binary numbers, it is compulsory that the sign is tested. If the sign is positive, the algorithm described above can be used in order to extract the square root, while if the sign is negative, an error is signalized.

Using this algorithm, the integer part of the square root can be calculated. A number of p bits from the decimal places can also be determined. In this case, the iteration counter I must be initialized with $n+p$, the $2n$ bits binary number is extended to $2n+2p$ bits adding $2p$ binary values of logical "0" at its lower part, while the result R and the working area Z have $n+p$ bits. Also, the left-shifting must be made taking into account the lengths of the result R ($n+p$ bits; $R_{n+p-1} \leftarrow ... \leftarrow \leftarrow R_0 \leftarrow C$), of the binary number X ($2n+2p$ bits; $C \leftarrow X_{2n+2p-1} \leftarrow ... \leftarrow X_0 \leftarrow 0$) and of the working area Z ($n+p$ bits; $Z_{n+p-1} \leftarrow ... \leftarrow Z_0 \leftarrow C$). After performing the algorithm, the n most significant bits hold the integer part of the result, while in the p less significant bits is stored the decimal part of the result.

6. Conclusions

The author wrote the program sequences, working on any microcontroller from the INTEL 8051 family, which perform arithmetic calculations for signed numbers, 16, 32, 48 or 64-bit long. There were implemented the routines for addition, subtraction, increment, decrement, multiplication, power ($n=2$, 3 and 4), division and extraction of the square root.

The division and square root extraction generate a result which includes the integer part but also a number of bits from the decimal part.

All these arithmetic calculation routines are included in an interactive program sequence and are stored in a memory area no larger than 4 kbytes.

Received, October 12, 2000

Technical University "Gh.Asachi", Jassy,
Department of Telecommunications

REFERENCES

1. Căpăţînă O., *Proiectarea cu microcalculatoare integrate.* Ed. Dacia, Cluj-Napoca, 1992.
2. Leventhal L.A., *Programmation en langage assembleur.* Ed. Radio, Paris, 1989.
3. * * * *INTEL 8051 Microcontroller.* Data Book, 1990.
4. Rony P.R., Larsen D.G., Titus J.A., *Microcomputer Interfacing and Programming.* Howard W. Sams & Co. Inc., NY, 1987.
5. Allworth S.T., *Introduction to Real-Time Software Design.* MacMillan Press, NY, 1982.
6. Davidoviciu A., Barbat B., *Limbaje de programare pentru sisteme de timp real.* Ed. Tehnică, Bucureşti, 1986.

IMPLEMENTAREA UNOR ALGORITMI DE CALCUL ARITMETIC PE MICROCONTROLERE DIN FAMILIA INTEL 8051

(Rezumat)

Se descriu algoritmii de calcul pentru operaţiile de adunare, scădere, incrementare, decrementare, înmulţire, împărţire, ridicare la putere şi extragere de rădăcină pătrată pentru numerele binare cu şi fără semn. Pentru fiecare operaţie aritmetică în parte sunt elaborate, de către autor, segmentele de program corespunzătoare pentru a fi executate pe orice microcontroler din familia INTEL 8051. Numerele binare utilizate în calcule au 16, 32, 48 sau 64 biţi, iar cu modificări minore în segmentele de program se pot realiza calcule şi pentru un alt număr de biţi.

BULETINUL INSTITUTULUI POLITEHNIC DIN IAŞI
Tomul XLVII (LI), Fasc. 1–2, 2001
ELECTROTEHNICĂ. ENERGETICĂ. ELECTRONICĂ

D.C. 681.5

A FORMAL APPROACH OF COMPLEX REAL-TIME SYSTEMS FOR DIAGNOSIS PURPOSES

BY
LAURENŢIU DIMITRIU and LILIANA VORNICU

A formal approach of complex real-time systems to obtain some possibilities of errors detection useful for diagnosis purpose is studied. We propose a formal analysis based on strings and vectors. To study state reachability we have introduced and defined reachabilty pattern vectors, reachability vectors and reachability-comparing vectors. Then the problem of value satisfiabilty is approached. Finally some diagnosis properties are presented.

1. Introduction

In many technical domains, *e.g.* automotive, more and more systems were added and are more difficult to determine the actual condition in case of a defect. Soon a multitude of connecting cables and adapters were required to reach the necessary measuring points. Moreover there was an increasing amount of information needed to make an effective diagnosis [1]. An important place play in modern control the real-time systems. Sometimes these systems are very complex and are more and more difficult to diagnose without some support. In classic approach of diagnosis, because of the permanently increasing amount of electronics functions, it is necessary to develop connectors with an increased number of contacts. Modern electronics diagnosis uses self-diagnosis capabilities, and with the help of an interconnection and standardization of the interface leading to the external tester, the many different complex and expensive adapters have become superfluous.

In this paper we develop an analysis for real-time complex systems to monitor the state reachability and value satisfiabilty, as necessary steps in diagnosis.

2. Timed Transition Systems and Timed Traces

We shall consider a complex system, S, formed by n subsystems. Let denote them by: S_1, S_2,...,S_n. The subsystems are connected so that the complex system could be described as a function:

$$S = S(S_1, S_2, ..., S_n) \quad \text{and} \quad S = \bigcup_{i=1}^{n} S_i. \tag{1}$$

For each subsystem we consider the *timed transitions*. A *timed transition system* is a labeled transition system with two types of labels: atomic actions and delay actions (positive reals), representing discrete and continuous changes of real-time systems [2].

For a subsystem, S_i, a trace, σ^j, of a timed transition system is an *infinite* sequence of transitions of the form:

$$\sigma^i = s_0^i \xrightarrow{\alpha_0^i} s_1^i \xrightarrow{\alpha_1^i} s_2^i \xrightarrow{\alpha_2^i} \ldots s_k^i \xrightarrow{\alpha_k^i} s_{k+1}^i \cdots \tag{2}$$

Let Act be a finite set of actions. We use $\mathbb{R}$ to stand for the set of non-negative real numbers, D for the set of delay actions $\{\varepsilon(d) | d \in \mathbb{R}\}$.

We denote $\delta^i(s^i \xrightarrow{\alpha^i} s'^i)$ the duration of a transition in a subsystem S_i defined by:

$$\delta^i(s^i \xrightarrow{\alpha^i} s'^i) = 0 \quad \text{if} \quad \alpha^i \in \text{Act}, \tag{3}$$

$$\delta^i(s^i \xrightarrow{\alpha^i} s'^i) = d^i \quad \text{if} \quad \alpha^i \in \varepsilon^i(d^i). \tag{4}$$

We obtain the following strings of duration of transitions for the n subsystems:

$$\begin{cases} \Delta^1 = \{\delta_0^1, \delta_1^1, \delta_2^1, ..., \delta_k^1, ...\}, & \text{for the } 1^{\text{st}} \text{ subsystem;} \\ \Delta^2 = \{\delta_0^2, \delta_1^2, \delta_2^2, ..., \delta_k^2, ...\}, & \text{for the } 2^{\text{nd}} \text{ subsystem;} \\ \ldots\ldots\ldots\ldots\ldots\ldots\ldots\ldots\ldots\ldots\ldots\ldots\ldots\ldots\ldots\ldots\ldots\ldots \\ \Delta^n = \{\delta_0^n, \delta_1^n, \delta_2^n, ..., \delta_k^n, ...\}, & \text{for the } n^{\text{th}} \text{ subsystem.} \end{cases} \tag{5}$$

We denote $\Delta^i(\sigma^i, j, k)$ the accumulated delay of σ^i between the positions j, k defined by:

$$\Delta^i(\sigma^i, j, k) = \sum_{j \le p < k} \delta^i(\sigma^i(p)). \tag{6}$$

In the expression (6), we shall consider only *non-zero* traces. A trace σ^i is *non-zero* if for all natural numbers, N, there are a position k so that $\Delta^i(\sigma^i, 0) > N$.

Let consider the same initial moment t_0^i, $(i = 1, 2, ..., n)$, for all subsystems. For simplicity, we admit $t_0^i = 0$. Having in mind all accumulated delay of σ^i related to the initial state moment, for every subsystem, we obtain a string having the form:

$$T^i = \{0, \Delta^i(\sigma^i, 0, k)\}_{k=1,2,...} = \left\{0, \sum_{0 \le p < k} \delta^i(\sigma^i(p)), ...\right\}_{k=1,2,...} \tag{7}$$

Writing more detailed the strings for the all n subsystems, we obtain:

$$(8)\quad \begin{cases} T^1 = \left\{ t_0^1 = 0, t_1^1 = \delta_0^1, t_2^1 = \delta_0^1 + \delta_1^1, ..., t_k^1 = \sum\limits_{0 \le j < k} \delta_j^1, ... \right\}, \\ T^2 = \left\{ t_0^2 = 0, t_1^2 = \delta_0^2, t_2^2 = \delta_0^2 + \delta_1^2, ..., t_k^2 = \sum\limits_{0 \le j < k} \delta_j^2, ... \right\}, \\ \cdots\cdots\cdots\cdots\cdots\cdots\cdots\cdots\cdots\cdots\cdots\cdots\cdots\cdots\cdots\cdots \\ T^n = \left\{ t_0^n = 0, t_1^n = \delta_0^n, t_2^n = \delta_0^n + \delta_1^n, ..., t_k^n = \sum\limits_{0 \le j < k} \delta_j^n, ... \right\}. \end{cases}$$

These strings mark the moments when the subsystems change their states. Now we can define a string to mark the moments of changes in the complex system:

$$(9)\qquad T = \bigcup_{i=1}^{n} T^i = \left\{ 0, \bigcup_{i=1}^{n} \left\{ t_1^i = \delta_0^i, t_2^i = \delta_0^i + \delta_1^i, ..., t_k^i = \sum_{0 \le j < k} \delta_j^i, ... \right\} \right\}.$$

The elements of the string T are arranged, having the form:

$$(10)\qquad T = \left\{ t_0 = 0, t_1, t_2, ..., t_k, t_{k+1}, ... \right\}, \quad \text{with} \quad \left\{ T_{k+1} > t_k \right\}_{k=0,1,2,...}.$$

We can consider the trace of timed transition system for the complex system:

$$(11)\qquad \sigma = s_0 \xrightarrow{\alpha_0} s_1 \xrightarrow{\alpha_1} s_2 \xrightarrow{\alpha_2} ... s_k \xrightarrow{\alpha_k} s_{k+1} ...$$

To describe the state of the complex system for each $t_i \in T$ moment, we use a string of vectors as it follows:

$$(12)\quad s_0 = \begin{Vmatrix} s_0^1 \\ s_0^2 \\ \cdots \\ s_0^n \end{Vmatrix}, \; s_1 = \begin{Vmatrix} s_1^1 = s^1\langle t_1 \rangle \\ s_1^2 = s^2\langle t_1 \rangle \\ \cdots\cdots\cdots \\ s_1^n = s^n\langle t_1 \rangle \end{Vmatrix}, \; s_2 = \begin{Vmatrix} s_2^1 = s^1\langle t_2 \rangle \\ s_2^2 = s^2\langle t_2 \rangle \\ \cdots\cdots\cdots \\ s_2^n = s^n\langle t_2 \rangle \end{Vmatrix}, \; ..., \; s_k = \begin{Vmatrix} s_k^1 = s^1\langle t_k \rangle \\ s_k^2 = s^2\langle t_k \rangle \\ \cdots\cdots\cdots \\ s_k^n = s^n\langle t_k \rangle \end{Vmatrix}, \; ...$$

A state $s_k^i = s^i\langle t_k \rangle$ of i^{th} subsystem at the moment $t_k \in T$, when a timed transition occurs in the complex system, is defined as:

$$(13)\quad s_k^i = s^i\langle t_k \rangle = \begin{cases} s^i(t_k), \;\; t_k \in T^i, \\ s^i(t_k - \Delta t_k^i), \; t_k \notin T^i, \; \Delta t_k^i = \min(t_k - t_j^i), \; t_j^i \in T^i, \; t_j^i < t_k. \end{cases}$$

3. State Reachability

Now we introduce *state reachability timed transition criterion.* We consider that a subsystem *reaches a state* in a *timed transition* if:

$$(14)\qquad s^i\langle t_k \rangle = s^i(t_k).$$

The complex system reaches a state if for $t_k \in T$ there is at least a subsystem that reaches a state. If at the moment t_k more than one subsystem reaches a state, we consider that the complex system reaches a state only if *all* subsystems mentioned above reach their states. We assign the logic value r_k^i to denote that the subsystem S_i reaches a state in the moment t_k of timed transitions of the complex system S. The assignment is the following:

$$r_k^i = r^i(t_k) = \begin{cases} 1, \text{ if } s^i\langle t_k\rangle = s^i(t_k), \\ 0, \text{ if } s^i\langle t_k\rangle \neq s^i(t_k). \end{cases} \tag{15}$$

We can observe the reachability properties of the complex system studying the *reachability vector*, r_k, defined as:

$$r_k = r(t_k) = \begin{Vmatrix} r_k^1 \\ r_k^2 \\ \cdots \\ r_k^n \end{Vmatrix}. \tag{16}$$

The complex system that reaches the state s_k is described by a non-zero reachability vector, $r_k \neq 0$. The number "1" in this vector depends upon the number of subsystem satisfying the reachability criterion at the moment t_k.

To study the behaviour of the complex system from reachability point of view imposes to compare reachability vectors with *reachability pattern vectors*, r_k^*, defined as:

$$r_k^* = r^*(t_k) = \begin{Vmatrix} r_k^{*1} \\ r_k^{*2} \\ \cdots \\ r_k^{*n} \end{Vmatrix}. \tag{17}$$

The reachability pattern vectors could be software generated using the information on individual traces of the subsystems. Let now compare the reachability vectors to the corresponding reachability pattern vectors. The results is a *reachability-comparing vectors*, r_k^C, defined by:

$$r_k^C = r^C(t_k) = \begin{Vmatrix} r_k^1 \oplus r_k^{*1} \\ r_k^2 \oplus r_k^{*2} \\ \cdots\cdots \\ r_k^n \oplus r_k^{*n} \end{Vmatrix}, \tag{18}$$

where $\oplus$ is EXCLUSIVE OR operator.

The complex system has a correct behaviour from timed transitions system point of view if the comparing vector is zero ($r_k^C = 0$).

4. Assignment of Values Vectors

For every subsystem we could assign values to the different states. In the moment t_k we denote the value corresponding to the state s_k^i with $V_k^i \sim v_k^i$, where

$\sim \in \{\leq, \geq, =, \in\}$, and $v_k^i = v^i\langle t_k\rangle$ represent a numerical value, a logical value or an interval. The complex system is described using *values vector*, V_k:

$$V_k = \left\| \begin{matrix} V_k^1 \\ V_k^2 \\ \dots \\ V_k^n \end{matrix} \right\| = \left\| \begin{matrix} \sim v^1\langle t_k\rangle \\ \sim v^2\langle t_k\rangle \\ \dots\dots\dots \\ \sim v^n\langle t_k\rangle \end{matrix} \right\|, \quad \text{where} \quad \sim \in \{\leq, \geq, =, \in\}. \tag{19}$$

The assignment of the $\sim$ condition must satisfy the following condition:

$$V_k^i \sim v^i\langle t_k\rangle \rightarrow \begin{cases} \sim v^i(t_k), \quad t_k \in T^i, \\ \\ \sim v^i(t_k - \Delta t_k^i), \ t_k \notin T^i, \ \Delta t_k^i = \min(t_k - t_j^i), \ t_j^i \in T^i, \ t_j^i < t_k. \end{cases} \tag{20}$$

The elements of the vector could be numerical values, logical values or intervals. Having in view that assigned elements are not homogenous we can use a more suggestive vector based on the satisfiabililty of $\sim$ condition.

Let consider an *actual values vector* V_{ak} for the complex system. The elements of this vector are obtained from the physical system, having the form:

$$V_{ak} = \left\| \begin{matrix} v_a^1\langle t_k\rangle \\ v_a^2\langle t_k\rangle \\ \dots\dots \\ v_a^n\langle t_k\rangle \end{matrix} \right\|, \tag{21}$$

and $v_a^i\langle t_k\rangle$ assign the value based on the following condition:

$$v_a^i\langle t_k\rangle = \begin{cases} v_a^i(t_k), \quad t_k \in T^i, \\ \\ v_a^i(t_k - \Delta t_k^i), \ t_k \notin T^i, \ \Delta t_k^i = \min(t_k - t_j^i), \ t_j^i \in T^i, \ t_j^i < t_k. \end{cases} \tag{22}$$

In this way, we denote by V_{sk}^i the logical value defined with the relation:

$$V_{sk}^i = \begin{cases} 0, & \text{if} \quad v^i\langle t_k\rangle \sim v_a^i\langle t_k\rangle \\ \\ 1, & \text{if} \quad v^i\langle t_k\rangle \not\sim v_a^i\langle t_k\rangle \end{cases}, \quad \text{and} \quad V_{sk} = \left\| \begin{matrix} V_{sk}^1 \\ V_{sk}^2 \\ \dots \\ V_{sk}^n \end{matrix} \right\|, \quad \text{with} \quad V_{sk}^i \in \{0,1\}\Big|_{i=1,2,\dots,n}. \tag{23}$$

V_{sk} represents the *satisfiability values vector* for the complex system. To obtain this vector is necessary to know *values vectors*. This could be software generated, and using the satisfiability condition, the satisfiability values vectors could be determined. The behaviour at the moment t_k of the system is correct if $V_{sk} = 0$.

T h e o r e m. *If for a complex real-time system the reachability-comparing vector r_k^C is non-zero, the satisfiability values vector V_{sk} is not necessary non-zero.*

P r o o f. Let consider that a sub-system fails to reach the state s_k^i at the moment t_k. For this reason, the assigned value V_k^i will be $v^i\langle t_{k-p}\rangle$ and not $v^i\langle t_k\rangle$, where string

for that reachability state condition is valid. At the moment t_k the actual value will be $v_a^i\langle t_k\rangle = v_a^i(t_k)$, because $t_k \in T^i$. It is possible that $v_a^i\langle t_{k-p}\rangle \sim v_a^i\langle t_k\rangle$ or not. So, the satisfiability values vector is not necessary zero.

Finally, we could conclude that the complex system has a correct behaviour at a moment t_k only if $r_k^C \vee V_{sk} = 0$. The global behaviour could be defined as correct if:

$$r_k^C \vee V_{sk} = 0\Big|_{k=1,2,\ldots}. \tag{24}$$

5. Conclusions

The behaviour of a complex real-time system looking for state reachability and value satisfiability is studied. The analysis uses arranged strings and vectors to detect the problems. The vectors monitor the system and are utilized to point the moments when the system fails. The algorithm of our analysis could be easily software implemented. Using an appropriate memory, it is possible to record the non-zero *reachability-comparing vectors* and non-zero *satisfiability values vectors* and their assigned moments. Reading this helpful information from the memory of the system, the diagnosis will be improved and more rapid. An internal processing could provide a high level structured diagnosis information, useful to repair or even to auto-repair the complex system.

Received, February 12, 2000

Technical University "Gh.Asachi", Jassy,
Department of Applied Electronics

REFERENCES

1. Jurgen R., *Automotive Electronics Handbook.* McGraw Hill, Inc., New York, 1995, 22.1-22.6.
2. Lindahl M., Petterson P., Yi W., *Formal Design and Analysis of a Gear Controller: an Industrial Case Study Using UPPAAL.* Proc. of the 4th Internat. Workshop on Tools and Algorithms for the Construction and Analysis of Systems, Gulbenkian Foundation, Lisbon, Portugal, March 31 – April 2, 1998, LNCS 1384, B. Steffen (Ed.), 281-297.

O ABORDARE FORMALĂ A SISTEMELOR COMPLEXE DE TIMP REAL ÎN SCOPURI DE DIAGNOSTICARE

(Rezumat)

Se prezintă o metodă de abordare formală pentru analiza funcţionării sistemelor de timp real, urmărindu-se obţinerea unor rezultate ce pot fi utilizate practic pentru diagnosticare. Pornind de la caracteristicile de timp real ale subsistemelor componente, se construiesc şirul întârzierilor cumulate ale sistemului complex şi vectorii de atingere a stărilor şi de satisfacere a valorilor. La fiecare moment din şirul întârzierilor cumulate se efectuează compararea vectorilor din sistem cu cei obţinuţi prin proiectare şi analiză. Eventualele deosebiri între vectorii prelevaţi din sistem şi vectorii şablon pun în evidenţă defecţiuni ale sistemului complex. Memorarea rezultatelor comparării şi a momentelor de timp asociate poate fi utilă în diagnosticarea sistemului în vederea depanării, sau, într-o abordare mai evoluată, pentru auto-depanare.

BULETINUL INSTITUTULUI POLITEHNIC DIN IAŞI
Tomul XLVII (LI), Fasc. 1–2, 2001
ELECTROTEHNICĂ. ENERGETICĂ. ELECTRONICĂ

D.C. 621.397.26

A METHOD FOR REDUCING THE LATENCY IN SERIAL TRANSMISSION SYSTEMS

BY
LILIANA VORNICU and LAURENŢIU DIMITRIU

In a real-time transmission system it is very important to minimize latency when message or data are transmitted in packets on the communication channel. Latency is a very important parameter in time critical applications. The transmission system has to manage timing constraints, which can be satisfied by choosing a proper algorithm and also has to satisfy the latency requirements. Latency can be sometimes inadmissible if a lot of messages or data had been corrupted. A solution, which minimize latency by using a correction block on the transmission channel, is proposed.

1. Introduction

Real-time signal transmission applications are commonly designed using dataflow software architecture. To understand fundamental real-time properties of such architecture, we must analyze the transmission conditions and constraints.

The correctness of real-time distributed systems solutions depends not only of the used algorithms, but especially of the "real" time at which these solutions have been calculated. To obtain significant results, the tempered calculation and linear programming support algorithms are used. Finally, a correct analysis for all the system priority levels is obtained. Because the real-time distributed system time constraints, the algorithms used allow arbitrary guarantees. The real-time system guarantees the time response for the implemented process.

In a real time communication system, the transmission of messages or data on the channel is allowed by the priority of each message, in order to assure a fast flowing rate and to minimize the latency [1]. Because latency is defined to be the time required to transfer a message from the transmitting source, measured from the moment it is prepared to send the message until it is correctly received by the targeted receiver, it may include a retry strategy if the initial exchange is not successful.

Messages with a lower period (a higher monolitic rate) will have higher priorities, so that it is solved the microprocessor's priority. The highest priority data flow information is allocated to the processor.

The messages are transmitted through a real time channel, between two application entity levels: a source (the transmitter) and an output device (the receiver).

Once a message on the communication bus is accepted, it will be transmitted in a limited time. To get an optimization and a correct reception, first the messages are fragmented into smaller parts (with the same length) so they have a lower length than the maximum one. The timing constraints are now distributed to these smaller parts of messages. The necessary time for this messages reordering is very low.

The standard timing constraints with a great importance in the system solutions are the deadlines and periods. These two constraints can be limited by choosing a proper algorithm and reducing the length of the transmission channel. In what follows, we propose a method to reduce the length of the transmission channel by reducing the messages correction time. A very important system constraint is *latency*, defined as the time delay between the sampling of the signal and the presentation of the processed signal to the output device (*e.g.* which may be a screen, speaker, or another computer in multimedia) [2]. We can use this definition with a clarification. Since we can only measure time in period units of the source, we consider the messages delivered each period by the source to the "one sample"; each pulse in the transmission constitutes one sample. Hence, under the strong synchronical hypothesis, latency is the delay between the enqueuing of all messages on the channel by the receiver.

Latency is a function of the scheduling algorithm [3] and also has a structural component. There is a pattern of executions that result in various latency values for the input messages.

If all the messages have the same length but smaller than the maximum service time (the minimum laxity), it will be choosen the FIFO order (First-In-First-Out); the message that first arrives on the data bus will be transmitted first.

We consider a message transmission between a transmitter, T, and a receiver, R. Denote m_1, m_2,...,m_n, messages to be transmitted on the communication channel. If all the messages are correct (not corrupted), than the latency of the real-time system will be the time for transmission (since the first message is transmitted on the communication channel until the last one is received). The latency is defined in this case, by:

$$\text{Latency} = t_{t_1} + t_{t_2} + \ldots + t_{t_n} = \sum_{i=1}^{n} t_{t_i}, \tag{1}$$

where t_{t_1}, t_{t_2},...,t_{t_n} are the transmission times for messages m_1, m_2,...,m_n, respectively.

In the case when all the messages have the same length, the transmission time will be for each message the same. Denoting it with t_t we can write:

$$t_{t_1} = t_{t_2} = \ldots = t_{t_n} = t_t. \tag{2}$$

So, in this particular case, latency will be:

$$\text{Latency} = \sum_{i=1}^{n} t_{t_i} = nt_t, \tag{3}$$

where n is the number of equal length messages.

The messages are transmitted in packets with a smaller length than the maximum service time. So, at the end of the transmission a correction is necessary. If errors are detected, the transmission had to be restarted with the correction made by the control frame.

The relations (1) and (3) are correct if there is a no corrupted message. By applying the recent results in real-time system's latency theory, if there is one or more corrupted messages in the transmitted packet, the latency will be much higher because it will be necessary to retransmit the whole packet. For example, if there is one corrupted message, the system's latency will be:

$$\text{Latency} = \sum_{i=1}^{n} t_{t_i} + \sum_{i=1}^{n} t_{t_i} = nt_t + nt_t = 2nt_t. \tag{4}$$

As the previous relation shows, the latency is twice higher than when all the messages are correct. The transmission will be repeated until the messages arriving at the receiver are correct.

2. Method's Principle

In the classical procedures, the transmission is made as it is shown in the Fig. 1. The system's latency will be as relation (3) if there is no corrupted message, and as relation (4) if it is one or more corrupted messages.

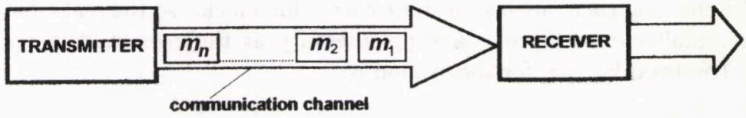

Fig. 1

The latency is defined as the time measured between the moment when the message is ready to be transmitted on the communication channel and the moment when it is correctly received. In order to optimize the transmission channel performance and to minimize the latency, in the following we propose a transmission with a correction block, as it is shown in the Fig. 2.

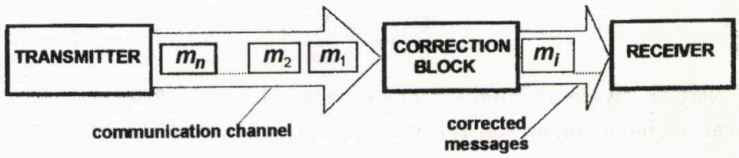

Fig. 2

The procedure is as follows: a packet of messages, denoted m_1, m_2,...,m_n, is transmitted on the communication channel between the transmitter, T and the receiver, R. We consider a correction block on the communication channel, which must

to correct the transmitted messages using a correction code (which is the same for all the messages). So, only the corrupted messages are corrected, the rest of them being transmitted further, to the receiver. In this case, the latency will increase but smaller than in the previous case (Fig. 1). The correction time doesn't have importance because it is very small. The corrupted messages are transmitted again after the corrections have been made. So, the system's latency will be reduced even a supplementary latency is added for correction. The presence of this block has a major importance in reducing the real time system's latency [3].

The solution is useful for the multiplexed buses, using long lines presence of significant disturbances, as it is shown in Fig. 3.

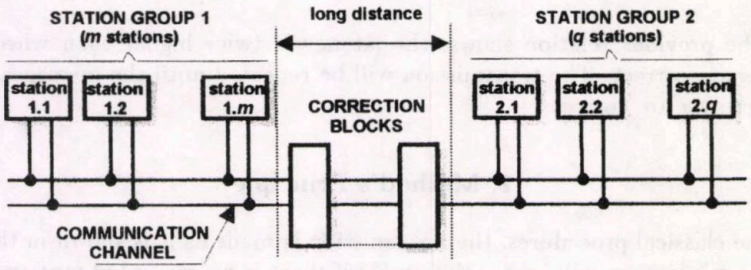

Fig. 3

On the channel, there are one or more correction blocks, so the real-time system's latency is smaller even there is a supplementary at the correction blocks on the channel. The total latency for the system is:

$$\text{Latency}_{\text{system}} = \sum_{i=1}^{n} t_{t_i} + \sum_{k=1}^{l} t_{t_k}, \tag{5}$$

where t_{t_k} is the time for message m_k correction, and k – the number of messages to be corrected.

The correction time has a reduced importance. The correction is made on the channel, with correction codes, and only for the corrupted messages that are transmitted again on the communication channel, after the corrections have been made. We can write:

$$\sum_{k=1}^{l} t_{t_k} \ll \sum_{i=1}^{n} t_{t_i}. \tag{6}$$

In these way the system's total latency is reduced.

We can define a corruption ratio:

$$C_r = \frac{N_{cm}}{N_m}, \tag{7}$$

where: N_{cm} is the number of corrupted messages and N_m – the number of transmitted messages.

Adding the number N_{cm1} of one-error messages, with N_{cm2} of two-error messages and so on it results N_{cm}. For n-bits length messages, we can write:

$$N_{cm} = \sum_{i=1}^{n} N_{cmi}. \tag{8}$$

We can estimate that:

$$N_{cm1} > N_{cm3} > ... > N_{cmn}, \quad \text{or even} \quad N_{cm1} \gg N_{cm3} \gg ... \gg N_{cmn}. \tag{9}$$

A possible latency characteristic, depending on the corruption ratio, is represented in Fig. 4. In these figure, C_{rk} represents the corruption rate for up to k-errors messages:

$$C_{rk} = \frac{\sum_{j=1}^{k} N_{cmj}}{N_m}. \tag{10}$$

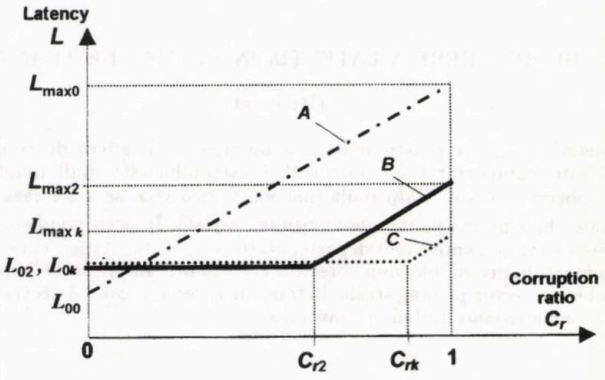

Fig. 4

The curve A represents the latency distribution if no correction block is used. So, the latency will increase when the corruption ratio increases. In the curve B, corresponding to a two-error correction block, we can observe that the latency increases latter, because the system corrects many corrupted messages and transmit them farther. The point in which the curve B begins to increase corresponds to up to two-error corruption ratio. In the curve C, corresponding to a k-error correction block, the latency begins to increase only for up to k-errors corruption ratio.

3. Conclusions

It is obviously that using a correction block on the communication channel, the total systems's latency may be reduced. With a multiplexed bus for system's communication, all messages pass through correction block. Only the corrupted messages

are corrected, which are retransmitted on the bus after the correction is made. Usually, this correction is effected without any trouble, with an appropriate corrector code. The latency has a smaller value using this method, so that the real time system responds better to the timing constraints and its solutions are faster and correctly obtained.

Received, May 14, 1999

Technical University "Gh.Asachi", Jassy,
Department of Applied Electronics

REFERENCES

1. Goddard S., Jeffay K., *Analyzing the Real-Time Properties of a Dataflow Execution Paradigm using a Synthetic Aperture Radar Application.* Proc. of the IEEE Real-Time Technol. and Appl. Symp., Montreal, Canada, June 1997, 60-71.
2. Jeffay K., *On Latency Management in the Time-Shared Operating Systems.* Proc. of the 11th IEEE Workshop on Real-Time Operating Systems and Software, Seattle, WA, May 1994, 86-90.
3. Vornicu L., Dimitriu L., *An Individual Transmission Protocol.* Proc. of the Internat. Symp. on Signals Circuits and Systems SCS'99, Jassy, Romania, July 3-6, 1999 (in print).

O METODĂ DE REDUCERE A LATENŢEI ÎN SISTEME DE TRANSMISIE SERIALE

(Rezumat)

Folosind metoda propusă pentru reducerea latenţei unui sistem de timp real cu transmisii seriale multiplexate, comportarea de timp real a sistemului este mult îmbunătăţită. Răspunsul sistemului este obţinut într-un timp mult mai scurt, deoarece se realizează detecţia şi corecţia mesajelor eronate chiar pe magistrala de transmisie serială. În acest mod sunt corectate mesajele eronate, care apoi sunt transmise mai departe, către receptoare. Astfel, chiar dacă se introduce o latenţă suplimentară, la nivelul blocului corector, aceasta este incomparabil mai mică decât latenţa sistemului fără bloc corector pe magistrala de transmisie serială, când detecţia erorilor se realizează la recepţie şi mesajele eronate trebuie retransmise.

BULETINUL INSTITUTULUI POLITEHNIC DIN IAŞI
Tomul XLVII (LI), Fasc. 1–2, 2001
ELECTROTEHNICĂ. ENERGETICĂ. ELECTRONICĂ

D.C. 621.389

THE ANALYTICAL EVALUATION OF THE DISCONNECTING TIME FOR THE DC ELECTROMAGNETIC COMMUTATION APPARATUS WITH CONTACTS

BY

RADU BURLICĂ, EUGEN HNATIUC and *BOGDAN HNATIUC

An analytical method for the disconnecting time evaluation of the commutation electrical apparatus with contacts (EAC), acted with DC electromegnets, is presented, in order to optimize the contacts movement time with the evolution of the commutation electric arc.

Starting from the differential equation which describes the transient disconnecting state of the electromechanical system can be find a mathematical relation for the approximation of the EAC disconnecting time.

The proposed method permits to adjust the electromechanical parameters, even from the EAC design stage, in order to obtain an optimum for the time movement of the electrical contacts.

1. Introduction

In what follows an analytical method for the evaluation of the disconnecting time of the commutation electromechanical apparatus with contacts (EAC), acted by DC electromagnets, is proposed.

The communication and protection of the electrical circuits by the EAC with contacts requires the disconnecting time optimization, in order to minimize the communication transient over-voltage and the effects of the electric arc on the contacts.

It is known that the EAC transient state duration can be determined solving the non-linear differential equations system, which describe the EAC behaviour in the dynamic state. The non-linear equations system has no exact analytical solutions, therefore it is necessary to apply a numerical method to approximate the solution, method that imposed a great volume of calculus.

The proposed analytical method provide an approximation of the disconnecting time of the EAC without solving the non-linear differential equations and can offer the possibility to optimize the movement duration of the contacts by adjusting the EAC parameters, even from the design stage of the electromagnet.

2. The Analytical Evaluation of the Disconnecting Time of the EAC

In order to determine a mathematical relation for the disconnecting time of the EAC is necessary to establish the differential equation, which describe the electrical behaviour of the EAC during the transient state.

A general scheme of an EAC is represented in Fig. 1.

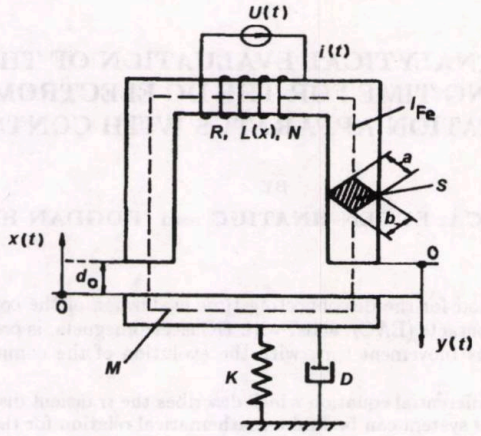

Fig. 1.– The scheme of an electrical commutation apparatus with contacts.

The EAC parameters, represented in Fig. 1, are: R – the electromagnet coil resistance, L – the electromagnet inductance, N – the coil number of turns, d_0 – the maximum air gap of the electromagnet, M – the weight of the electromagnet armature, K – the elastic constant of the antagonistic spring, $u(t)$ – the coil supply voltage.

The differential equation that describes the EAC behaviour from the electric point of view is:

$$\frac{\mathrm{d}\varphi}{\mathrm{d}t} + \frac{R}{L(x)}\varphi = 0, \tag{1}$$

where $\varphi(t)$ is the magnetic flux in the electromagnet magnetic core.

Multiplying both terms of equation (1) with the value of the magnetic flux through the electromagnet air gap, $\varphi(t)$, the equation (1) became:

$$\frac{\mathrm{d}\varphi}{\mathrm{d}t}\varphi + \frac{R}{L(x)}\varphi^2 = 0, \tag{2}$$

or:

$$\frac{1}{2}\cdot\frac{\mathrm{d}\varphi^2}{\mathrm{d}t} + \frac{R}{L(x)}\varphi^2 = 0. \tag{3}$$

Equation (3) can be written also:

$$\mathrm{d}\varphi^2 + 2R\frac{\varphi^2}{L(x)}\,\mathrm{d}t = 0. \tag{4}$$

After the integration of equation (4), taking in account that the integral:

$$A = \int_0^{t_d} \frac{\varphi^2}{L(x)}\,\mathrm{d}t \tag{5}$$

represents the magnetic field energy developed during the disconnecting dynamic state, these integral can be approximated with the difference between the maximum and the minimum of the magnetic field energy as follows:

$$\int_0^{t_d} \frac{\varphi^2}{L(x)}\,\mathrm{d}t \approx \left(\frac{\varphi_1^2}{L_1} - \frac{\varphi_0^2}{L_0}\right) t_d, \tag{6}$$

where: L_1, φ_1 are the electromagnet's inductance and, respectively, the magnetic flux at the minimum air gap; L_0, φ_0 – the electromagnet's inductance and, respectively, the magnetic flux at the maximum air gap (d_0); t_d – the duration of the disconnecting transient state.

The relation (4), considering the approximation (6), became:

$$\varphi_1^2 - \varphi_0^2 + 2R\left(\frac{\varphi_1^2}{L_1} - \frac{\varphi_0^2}{L_0}\right) t_d = 0. \tag{7}$$

From equation (7) it is possible to deduce an analytical expression for the disconnecting time:

$$t_d = \frac{\varphi_1^2 - \varphi_0^2}{2R\left(\frac{\varphi_1^2}{L_1} - \frac{\varphi_0^2}{L_0}\right)}. \tag{8}$$

The relation (8) permits to evaluate the disconnecting time of the EAC with the condition of a correct approximation of the electromagnet's magnetic field at the end of the transient dynamic state (φ_0), when the electromagnet's armature reach the maximum air gap.

The approximation of the magnetic flux, φ_0, is possible if we consider the evolution of the magnetic force comparative with the resistant characteristic of the EAC shown in Fig. 2.

It is possible to approximate the magnetic flux, φ_0, having in view the condition of a successful disconnection of the AEC. This condition imposes that the electromagnetic force, created by the magnetic flux, φ_0, at the end of the disconnection transient state, must be smaller than the precomprimation force of the acting spring,

$F_{\min}$ (Fig. 2). In this case, the values of the magnetic flux, φ_0, are situated in the domain $[0, \sqrt{2\mu_0 S F_{\min}}]$.

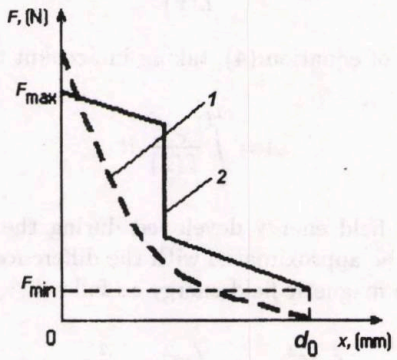

Fig. 2.– *1* – the electromagnet force; *2* – the resistant characteristic.

The magnetic flux, φ_1, at the minimum air gap of the electromagnet, is known and can be calculated with the relation:

$$\varphi_1 = \sqrt{2\mu_0 S F_M}, \tag{9}$$

F_M being the maximum of the electromagnet's force.

The relative difference between the values of the disconnecting time estimated with the relation (8) and the values directly measured can be emphazised with the relation:

$$\varepsilon(t) = \left(1 - \frac{t_d}{t_{dm}}\right) \cdot 100, \quad [\%], \tag{10}$$

where: t_d is the disconnecting time estimated with the relation (8) and t_{dm} – the disconnecting time directly measured.

The evolution of the relative difference of the disconnecting time, $\varepsilon(t)$, can be evaluated if we represent the function $\varepsilon(\varphi_0)$.

3. Experimental Results

The relation (8) was experimentally verified for different electromechanical commutation systems. The values of the disconnecting time evaluated with the relation (8) have been compared with those measured directly for each EAC.

For example, for a DC contactor of 63 A, with the initial data: $F_{\min} = 4$ N, $\varphi_1 = 12 \times 10^{-4}$ Wb, the measured disconneting time is $t_{dm} = 0.18$ s.

In Fig. 3 is represented the evolution of the relative difference of the disconnecting time, $\varepsilon(\varphi_0)/100$, for $\varphi_0 \in [0, \sqrt{2\mu_0 S F_{\min}}]$.

The diagram $\varepsilon(\varphi_0)$ (Fig. 3) shows that for the magnetic flux φ_0 variation in the domain $[0, \sqrt{2\mu_0 SF_{\min}}]$, the relative difference of the disconnecting time do not surpass the value 0.3, (30%), a value acceptable for an analytical method of approximation. Also, if we consider that the magnetic flux of the electromagnet has the value zero at the end of the disconnecting transient state the relative time difference is about 10%.

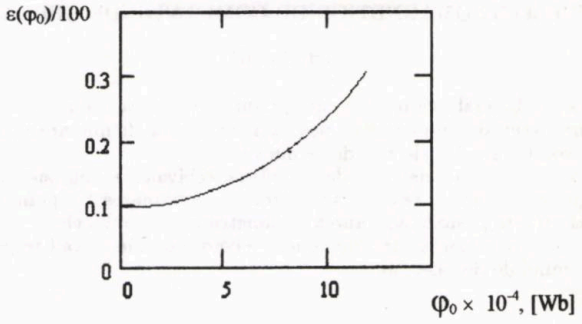

Fig. 3.– The evolution of the relative time diference $\varepsilon(\varphi_0)/100$.

4. Conclusions

The analytical method for the approximation of the disconnecting time, proposed in this paper, offer the possibility to evaluate the transient state duration of the EAC, without solving the non-linear differential equations, which describe the electromechanical dynamic state behaviour. In the same time, it emphazises the influence of the electrical and mechanical parameters of the EAC on the disconnecting time, even from the EAC design stage, and permits to adapt them at the imposed functioning condition in the electrical circuit.

The correlation of the electromechanical parameters, in order to obtain the minimum for the disconnecting time, is an important problem for the ultra-fast DC circuit breakers, which have, also, the role of an electrical circuit protection. Finally, the minimization of the EAC contacts moving time has a positive influence of the effects of the commutation electric arc on the apparatus.

Received, November 6, 2000

Technical University "Gh.Asachi", Jassy,
Department of Energetics
and
**Department of Electrical Engineering*

REFERENCES

1. B u r l i c ă R., *Acţionările cu electromagneţi ale aparatelor electrice.* Ph. D. Diss., Techn. Univ. "Gh. Asachi", Jassy, 1999.

2. Hnatiuc E., *Studiul regimului de vibraţii la electromagneţii de curent continuu şi alternativ. Regimul dinamic al electromagneţilor.* Ph. D. Diss., Polyt. Inst., Jassy, 1983.
3. Fitzgerald A.E., Kingsley Ch., *Electric Machinery. The Dynamics and Statics of Electromechanical Energy Conversion.* 3-nd Edition, McGraw-Hill Book Co. Inc., New York, 1971.
4. Vasilievici Al., Andea P., *Aparate şi echipamente electrice.* Ed. Orizonturi Universitare, Timişoara, 2000.

EVALUAREA ANALITICĂ A TIMPULUI DE DECONECTARE PENTRU APARATELE ELECTROMAGNETICE DE COMUTAŢIE DE CURENT CONTINUU

(Rezumat)

Se propune o metodă analitică inedită care permite evaluarea timpului de deconectare pentru aparatele electromagnetice de comutaţie şi optimizarea timpului de mişcare a contactelor lor mobile ţinând seama de evoluţia arcului electric de comutaţie.

Considerând aceste aparate electrice de comutaţie echivalente unui sistem electromecanic de conversie a energiei se deduce o relaţie care permite aproximarea timpului de deconectare. Cu ajutorul acestei relaţii este posibilă adaptarea parametrilor sistemului electromecanic, chiar pentru etapa de proiectare a aparatelor electromagnetice de comutaţie, în scopul respectării unor condiţii de optim pentru timpul de deconectare.

BULETINUL INSTITUTULUI POLITEHNIC DIN IAŞI
Tomul XLVII (LI), Fasc. 1–2, 2001
ELECTROTEHNICĂ. ENERGETICĂ. ELECTRONICĂ

D.C. 621.316.313; 621.3.025.018.3

DUTY ANALYSE AND SUPPLEMENTARY POWER LOSSES IN DISTRIBUTION ELECTRICAL NETWORKS RUNNING UNDER NON-SINUSOIDAL STEADY STATE

BY

VIOREL VARVARA and *GH. GEORGESCU

A three-phase network is designed to operate under a sinusoidal and balanced steady state. Because of a lot of reasons the real operating duty is non-symmetrical and non-sinusoidal. The main cause of the non-sinusoidal state of a three-phase network is the non-linearity of the load.

A 20 kV distribution network is considered, in which with the help of ALPHA-meter, some parameters of the non-sinusoidal voltage and current are recorded. Parameters, described by PE 143/94 – Normative For Limitation the Distorting State – to define the non-sinusoidal state are calculated, conclusions being taken regarding the main cause of the existence of the non-sinusoidal steady state in this kind of networks. It is presented the powers flow in networks running under non-sinusoidal symmetrical steady state, supplementary active and reactive powers losses being calculated.

1. Introduction

In power electrotechnics the real operating duty is a non-sinusoidal one, voltage and current waveforms being deviated from the sinusoidal shape, usually expressed as harmonic components. Referring to the three-phase networks because it can't be ensured for a long time a balanced charge on the phases, the steady state is non-symmetrical.

Non-sinusoidal state appearance is inevitable in our days technological conditions because every non-linear or parametric device represents a harmonics generator, its response being non-sinusoidal [6].

Low power converters, through their increasing number and diversity of placement in the network, start to become a problem in harmonic flow control. The main problem is represented by the random harmonic appearance and manifestation due to the moments of switching on, the operating time and especially the simultaneously operation of a large number of this kind of devices, with current flow implications.

2. Non-sinusoidal Steady State Analysis in Distribution Networks

By way of an example the non-sinusoidal state of a 20 kV urban distribution network from our country, feeding 11 substations, is considered. The consumers are diverse: domestic, public lighting, small, medium and large business places, hotels, restaurants, a.s.o.

In present, being available ALPHA-meters which can be placed on the 0.4 kV side on every phase in substation, at every 15 min., r.m.s. voltages and currents values, the harmonic levels up to the 15-th, can be measured (Fig. 1).

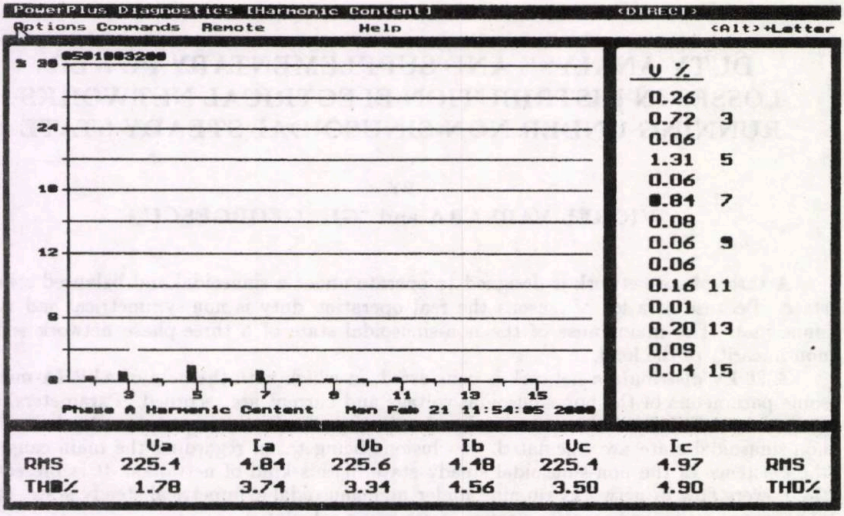

Fig. 1.– Example of record made with an ALPHA-meter.

The harmonic levels are appreciated through γ_u and γ_i coefficients calculated for each phase and defined by expressions:

$$(1) \qquad \gamma_u = \frac{U_k}{U_1} \cdot 100, \quad [\%], \qquad \gamma_i = \frac{I_k}{I_1} \cdot 100, \quad [\%],$$

where U_k, I_k are the voltage and current of k harmonic order; U_1, I_1 – voltage and current first harmonic order (fundamental).

Voltage and current total harmonic distortion (THD – depict as δ in PE 143/94), calculated for each phase, is defined by expressions:

$$(2) \qquad \mathrm{THD}_u = \frac{\sqrt{\sum_{k=2}^{\infty} U_k^2}}{U_1} \cdot 100, \quad [\%], \qquad \mathrm{THD}_i = \frac{\sqrt{\sum_{k=2}^{\infty} I_k^2}}{I_1} \cdot 100, \quad [\%].$$

Voltage and current root mean square values for non-sinusoidal signals are defined by expressions:

$$(3) \qquad U = \sqrt{\sum_{k=0}^{\infty} U_k^2}, \quad [\mathrm{V}], \qquad I = \sqrt{\sum_{k=0}^{\infty} I_k^2}, \quad [\mathrm{A}].$$

Being known, after measuring the voltages and currents harmonic levels, γ_{umk} and γ_{imk}, (m – index for the phase ($m = a, b, c$)) and the r.m.s. values, one can

determine the fundamental magnitudes:

$$(4) \qquad U_{1m} = \frac{100U_m}{\sqrt{100^2 + \sum_{k=2}^{15} \gamma_{umk}^2}}, \ [\mathrm{V}], \qquad I_{1m} = \frac{100I_m}{\sqrt{100^2 + \sum_{k=2}^{15} \gamma_{imk}^2}}, \ [\mathrm{A}],$$

r.m.s. values for each harmonic component:

$$(5) \qquad U_{km} = \gamma_{ukm} U_{1m}, \ [\mathrm{V}], \qquad I_{km} = \gamma_{ikm} U_{1m}, \ [\mathrm{A}],$$

and the distortion residuum:

$$(6) \qquad U_d = \sqrt{\sum_{k=2}^{15} U_k^2}, \ [\mathrm{V}], \qquad I_d = \sqrt{\sum_{k=2}^{15} I_k^2}, \ [\mathrm{A}].$$

With the help of these information the distortion state can be characterized, limits being specified by PE 143/94 normative. In the analysed network it was determined the existence of a powerful distortion regime installed on most of the harmonics. Time evolution study of the distortion state in several substations with diverse consumers focus that the regime is must powerful corresponding to the night period (example 10 p.m.) when most of the non-sinusoidal devices are switched on (public lighting, colour TV sets, personal computers). The operating duty is improving corresponding to the night period (example 4 a.m.) when, probably, only lighting is working. Corresponding to the period of day (example 10 a.m.), when public lighting is switched off, the distortion regime is the lowest. But, in all the situations the prescriptions are exceeded, showing that the non-sinusoidal steady state in the analysed urban distribution network is not a matter of combination of circumstances but a structure one. The main distortion load, in this case, is the lighting. The non-sinusoidal state is conspicuous on two phases, showing the non-symmetry influence. A global improvement can be eventually riced by installing a 5-th harmonic filter on the main busbars. An other one, which doesn't take into account the cause of appearance of the duty, is the increasing of the short-circuit power on the substation busbars, solution which demands supplementary investments. In this way only a delay in confronting with the same problems in the future is obtained.

3. Power Flow in Three-Phase Networks Running under Non-sinusoidal Steady State

For focusing the powers flow it is considered a symmetrical network having ideal sinusoidal generators feeding, through a linear electrical line both three-phase linear and non-linear loads.

In Fig. 2 the following notations are used: P_{g1} – active power on fundamental delivered by the symmetrical generator; P_{l1} – active power on fundamental injected to the line; P_{L1} – active power on fundamental supplied to the linear load; P_{N1} –

active power on fundamental supplied to the non-linear load; P_{Na} – harmonic active power generated by the non-linear element and reinjected to the network; P_{la} – harmonic active power injected to the line, l, by the element N; P_{La} – harmonic active power injected to the linear element, L, by the element N.

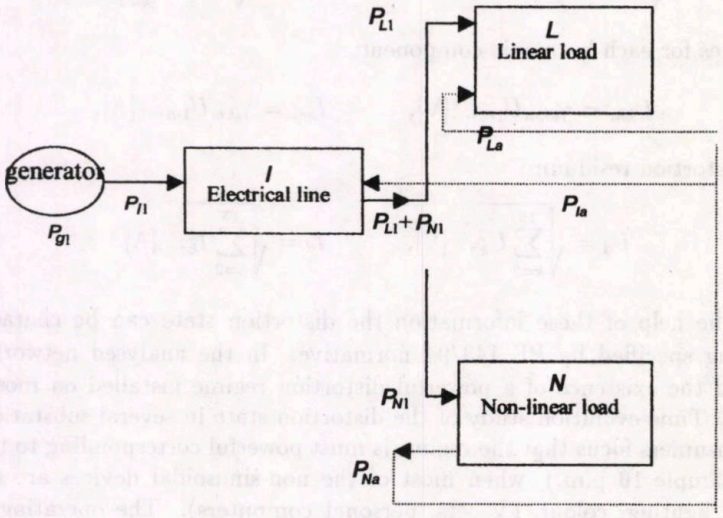

Fig. 2.– Active powers flow in a symmetrical three phase network running under a non-sinusoidal steady state.

In the symmetrical network currents are flowing on fundamental and harmonic components, active and reactive powers being conservative both on fundamental and on every harmonic. Currents flow determine non-sinusoidal voltages, excepting the generators, at their busbars voltages remaining sinusoidal.

The meanings of notations used in the followings expressions are: g – generator; l – electrical line; L – linear load; N – non-linear load; index 1 is reffering to the fundamental; k – harmonics order.

The balance of these powers on fundamental and on every harmonic is expressed as:

$$P_g = P_{l1} + P_{L1} + P_{N1}, \qquad 0 = P_{lk} + P_{Lk} + P_{Nk}. \tag{7}$$

Even if the generator is supplying power exclusively on fundamental, on line, l, at the linear load, L, and at the non-linear one, N, the active power is founded both on fundamental and on every k harmonics.

The line and the linear load absorbs active power on fundamental and on every harmonic, these powers being always positive:

$$P_{l1} > 0, \quad P_{lk} > 0, \quad P_{L1} > 0, \quad P_{Lk} > 0. \tag{8}$$

Regarding the non-linear load this is a receiver for active power on fundamental and a generator for active powers on every k harmonic:

$$P_{N1} > 0, \quad P_{Nk} < 0. \tag{9}$$

Generally, powers balance may be expressed as:

$$P_g = P_{g1} = P_l + P_L + P_N, \quad P_l = P_{l1} + P_{la}, \quad P_L = P_{L1} + P_{La}, \quad P_N = P_{N1} + P_{Na}. \tag{10}$$

Supplementary total active power losses because of the non-sinusoidal duty are:

$$P_{Na} = P_{la} + P_{La}. \tag{11}$$

4. Supplementary Active Power Losses in a Distribution Network Because of the Distortion Duty

Information concerning r.m.s. voltages and currents, phase displacement between signals, active and apparent powers, are obtained measuring in the substations (Fig. 3). Three-phase active and reactive powers are calculated with following expressions:

$$P = \sum_{k=0}^{\infty} U_{ka} I_{ka} \cos \varphi_{ka} + \sum_{k=0}^{\infty} U_{kb} I_{kb} \cos \varphi_{kb} + \sum_{k=0}^{\infty} U_{kc} I_{kc} \cos \varphi_{kc}, \tag{12}$$

and respectively

$$Q = \sum_{k=1}^{\infty} U_{ka} I_{ka} \sin \varphi_{ka} + \sum_{k=1}^{\infty} U_{kb} I_{kb} \sin \varphi_{kb} + \sum_{k=1}^{\infty} U_{kc} I_{kc} \sin \varphi_{kc}, \tag{13}$$

where φ_{km} is the phase displacement between voltage and current phasors on the k harmonic, on the m phase.

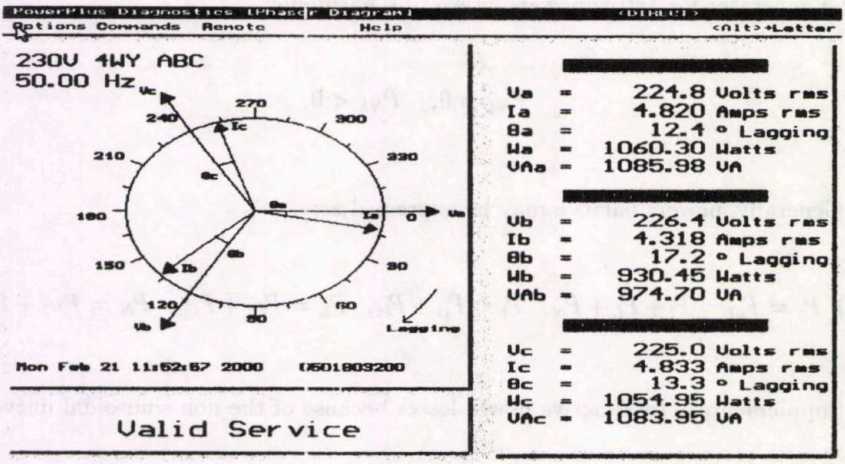

Fig. 3.– Record made in substations for getting information concerning powers, voltage and current phasors attached to the non-sinusoidal signals.

Supplementary total power losses generated by the non-sinusoidal and non-symmetrical duty, are:

$$(14) \qquad \Delta P = P - \sum_{m=a,b,c} U_{1m} I_{1m} \cos \varphi_{1km}, \quad \Delta Q = Q - \sum_{m=a,b,c} U_{1m} I_{1m} \sin \varphi_{1km},$$

where P and Q are the active and reactive three-phase powers.

Generally, voltage and current phase displacements are different on the three phases for all the harmonics. Practically and in concordance with the records made on several distribution networks, phase displacements on fundamental are to a great extent equal on the three phases. Using the records and the calculated quantities one can determine the supplementary power losses generated by the distortion duty, from the load till the transformer. These appreciations were made corresponding to a particular energetic situation, but, by percentage, the losses don't suffer significant deviation under other working conditions. It was found that these losses don't have a significant weight, being 0.52% for active and 0.57% for reactive of the total transmited power (1,354.7 kW and 774.7 kVAr).

Supplementary active power losses in transformers generated by the distortion duty, ΔP_{trafo}, can be evaluated taking into account the equivalent resistance on a phase of the transformer R_T and the harmonic spectrum, with the help of the expression:

$$(15) \qquad \Delta P_{\text{trafo}} = R_{Ta} I_{da}^2 + R_{Tb} I_{db}^2 + R_{Tc} I_{dc}^2 = R_T (I_{da}^2 + I_{db}^2 + I_{dc}^2).$$

For the analysed network, in which the transformers run under a medium charge of 22.6% of their nominal one, these losses represent 0.04% of the total transmited active power.

5. Conclusions

a) In the present structure of the low voltage distribution networks, the main distortion load is represented by the public lighting, generally named as fluorescence type, an important sourse of harmonics being also the colour TV sets and personal computers.

b) The existance of an important number of low power non-linear loads which act as harmonic generators, connected in varied points of the network, produces the dependence of the distortion state magnitude on the load curve.

c) Even the network is running under a powerful non-sinusoidal steady state, supplementary power losses because of this duty aren't important (under 0.6% of the total transited power) and additional active power losses in transformers running at a medium charge of 25% are negligible (under 0.04% of the total transmited power).

Received, November 17, 2000

Technical University "Gh.Asachi", Jassy,
Department of Electrotechnics
and
**Department of Energetics*

REFERENCES

1. Gretsch R., *Harmonics in Low and Medium Voltage Systems Analysis of Disturbing Sources and Measures for a Limitation of the Emission.* 11th Internat. Conf. on Electricity Distribution, 1991, 1732-1739.
2. Deflandre T., Courty S., Greiveldinger C., Javerzac J.L., *Impact of Harmonics on French Public Networks: State of Play, Studies, Future Trends.* Electr. de France, Direction des Etudes et Recherches, Paris, 15-23 (1995).
3. Deflandre T., Arson S., Rioual P., *Working Out a Rule for Connecting Industrial Costumers Generating Harmonics.* Elctr. de France, Direction des Etudes et Recherches, Paris, 12-17 (1994).
4. Kaendler G., *Voltage Distortion in High Voltage Networks Caused by Switched Mode Power Supplies.* Power Quality Conference, Bremen, 1995, 117-125.
5. Mielczarski W., *Quality of Electricity Supply.* 4-th Internat. Conf. on Electrical Power Quality and Utilization, Cracow, 1997, 15-23.
6. Rosman H., Savin Gh., *Circuite electrice liniare.* Inst. polit., Iaşi, 1974.
7. Ţugulea A., *Consideraţii privind efectele energetice în regimuri nesimetrice ale sistemelor trifazate.* Energetica, **XXXIV**, *3*, 121-129 (1986).

ANALIZA REGIMULUI ŞI CALCULUL PIERDERILOR SUPLIMENTARE DE PUTERE ÎN REŢELELE DE DISTRIBUŢIE URBANE FUNCŢIONÂND ÎN REGIM PERMANENT NESINUSOIDAL

(Rezumat)

O reţea trifazată este proiectată să funcţioneze într-un regim permanent sinusoidal echilibrat. Din mai multe motive, regimul real de funcţionare este nesimetric şi nesinusoidal. Cauza principală a apariţiei regimului nesinusoidal în reţea o reprezintă neliniaritatea sarcinii.

Se consideră o reţea de distribuţie de 20 kV în care sunt măsurate cu ajutorul contoarelor ALPHA tensiunile şi curenţii nesinusoidali. Sunt calculate mărimile care definesc regimul nesinusoidal conform Normativului pentru limitarea regimului deformant PE 143/94, fiind precizate concluziile cu privire la principala cauză a apariţiei regimului în aceste tipuri de reţele electrice. Este prezentată circulaţia puterilor în reţele funcţionând în regim permanent nesinusoidal echilibrat, fiind calculate pierderile suplimentare de putere activă şi reactivă.

BULETINUL INSTITUTULUI POLITEHNIC DIN IAŞI
Tomul XLVII (LI), Fasc. 1–2, 2001
ELECTROTEHNICĂ. ENERGETICĂ. ELECTRONICĂ

D.C. 621.365.33

THE INDIVIDUAL HEATING BOILER – MORE EFFICIENT, MORE ECONOMIC

BY

C. ASAFTEI and *DORIN GROZA

Some aspects related to a category of modern heating boilers – *the calorific capacity boilers* – are presented. There are revealed some of the manufacturing and operating principles, the efficiency evaluation criteria and from this point of view, a comparision with the conventional heating boilers.

1. Introduction

The market success of the modern heating boilers is indebted to their economic and technical parameters, on one hand, and to the heating facilities offered by these units to the customers, on the other hand.

Some of the methods and the materials used by the boilers manufacturers, to improve the efficiency and operating conditions, are presented in [1].

The designing and manufacturing experience, have indicated that the boilers efficiency improving is possible by using, among others: a) the recuperation of condensation heat from the water vapours included in the burned gases; b) the preponderant use of low and middle temperature system, 50°/40°and 40°/30°C.

The heating boilers that recover the heat generated by the superior calorific capacity and, particularly, the condensation heat of water vapours, are called *calorific capacity boilers.*

The possibility to render profitable the superior calorific capacity makes this boiler one of the most efficient. That is why we consider that a more detailed presentation of the manufacturing and operating principles, along with this type of heating boiler's efficiency calculation, is of an real interest.

2. Manufacturing and Operating Principles of the *Calorific Capacity Boilers*. The Efficiency Evaluation

To evaluate the efficiency of such a boiler it is used the mathematical relation of efficaciousness [1],...,[3]:

$$\eta = 1 - \frac{q_A + q_B}{100} + \frac{H_0 - H_u}{H_u}\alpha,$$

where: q_A, q_B represents the heat losses, [%], $q_A = (t_{ga} - t_a)(k_1/100 + k)$, [%] – the heat losses from the burned gases, evacuated by the chimney in the atmospheric environment, t_{ga} – the temperature of the evacuated burned gases, that have no limit for *the calorific capacity boilers*, [°C], t_a – the environment temperature, [°C], CO_2 – the carbon dioxide, in the burned gases, influenced by the burner technical evolution, [%], k, k_1 – calculation coefficients, q_B – the heat losses by radiation, [%], $[(H_0 - H_u)/H_u]\alpha$ represents the water heat, recovered from condensation, H_0, H_u, [kWh/m^3] – superior respectively inferior calorific power of the combustible, α – condensation coefficient.

The α coefficient value is determined by the ratio of condensation water quantity produced by the boiler and the theoretical condensation water quantity that could be produced. The efficiency of *the calorific capacity boilers* is better if the recovered condensation heat quantity is greater; this implies a greater value for α.

The condensation water heat is specific for every type of combustible, as results from Table 1.

Table 1

Fuel	Inferior calorific power kWh/m^3	Superior calorific power kWh/m^3	The calorific power ratio	The calorific power difference kWh/m^3	Condensation water quantity kg/m^3
Gaseous fuel LL	9.78	8.83	1.11	0.95	1.53
Gaseous fuel E	11.46	10.35	1.11	1.11	1.63
Propane	28.02	25.80	1.09	2.22	3.37
Butane	37.19	34.35	1.08	2.84	4.29
Oil fuel	10.68	10.08	1.06	0.60	0.88

The difference between the superior, respectively inferior calorific power value is a combustible feature, that depends on carbon/water quantity ratio. But it is clear that if the burning generates more water vapours, the supplementary heat gain is greater. For example, for the gaseous fuel, this gain is of 11% and for oil fuel it is of 6%.

The boiler's efficiency depends on many factors namely:

1. The convection heating surfaces geometry, that could determine more burned gases that means more CO_2 and as a consequence a higher *water vapours condensation temperature*, as presented in the Fig. 1.

It results that, for the oil fuel, *the water condensation temperature* is lower than that for the gaseous fuel.

The operating conditions used by *the calorific capacity boilers* are, as rule, opposite to those used in the classic low temperature boilers: the last boilers must remain dry, but for *the calorific capacity boilers*, the water vapours contained in the burned gases have to condense as much as possible.

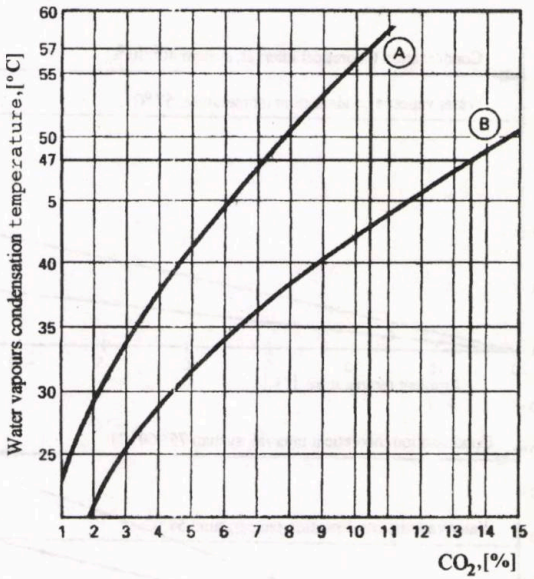

Fig. 1.– The relation between the water condensation vapours temperature and the carbon dioxide concentration, for : Ⓐ – gaseous fuel (95% CH_4); Ⓑ – oil fuel.

As a consequence, in the burned gases flows there can be identified two types of condensation, depending of the heating surfaces:

a) the condensation in the burned gases steam flow, when the temperature in the chimney is lower than the water vapours condensation point;

b) the direct condensation on the heating surfaces (humide steam deposits), when the water temperature is lower than the water vapours condensation point.

The condensation on the heating surfaces suppose for *the capacity caloric boilers* using an optimally design.

To realize a more intense condensation it is necessary, for the burned gases, to be refrigerated in the highest degree. From this point of view, the best solution is to dispose the heating surfaces in vertical sheets manufactured of unoxidable steel.

The condensed water, poor in salts, flows in the opposite direction of the burned gases, washing the heating surfaces and, as a consequence, a self cleaning effect results.

All these factors assure a high condensation rate, that can be maintained at the lowest exterior temperatures, which means almost all the heating period (the cold season).

2. The hydraulic link between the heated area and the heat generator avoiding the devices that are generating a higher temperature of the water in the return line.

The efficient recovery of condensing heat is possible when the water temperature, on the return line, is lower than *the water vapours condensation point*, as illustrated in Fig. 2.

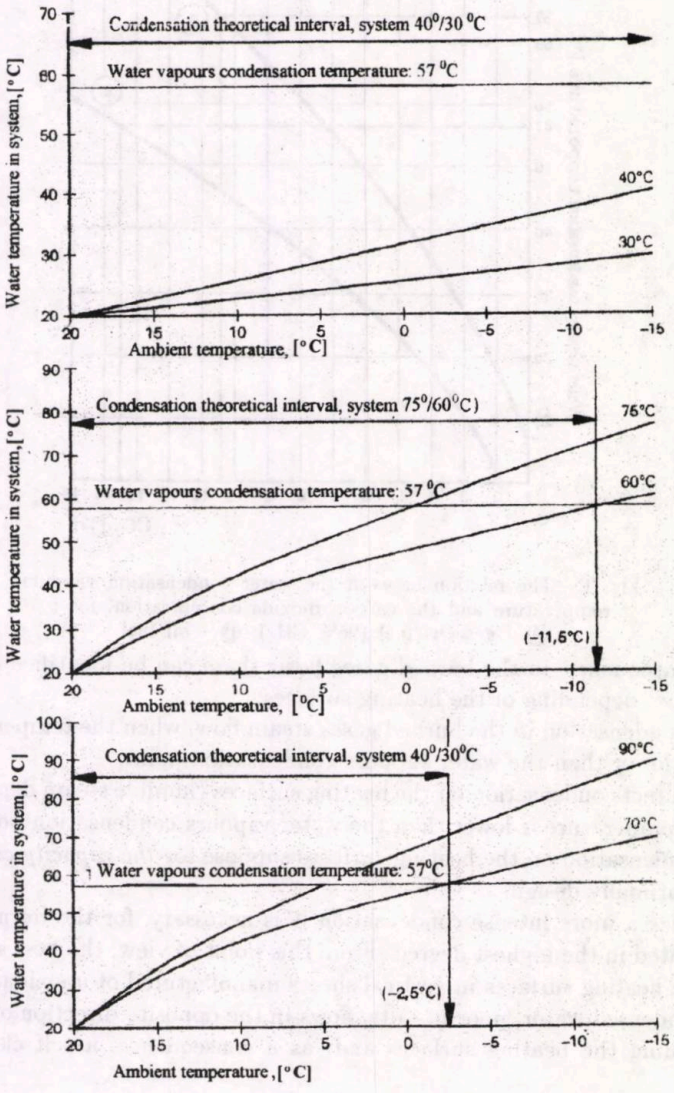

Fig. 2.– The relation between the condensation interval and the heating system's temperature.

It is clear that for a heating system 75°/60°C, an operation with condensation is possible to appear for ambient temperatures higher than –10°C because the return water's temperature gets lower than *the water vapours condensation point*; for a heating unit 90°/70°C, the condensation is possible when the ambient temperature is higher than –2°C.

Ideal conditions for such a heating unit are offered by a heating system 40°/30°C, that can assure, in the highest possible manner, the use of condensation operation, practically all the heating interval.

The lower the burned gases temperature, the greater is the condensed water quantity and respectively the condensation coefficient, α, as represented in Fig. 3.

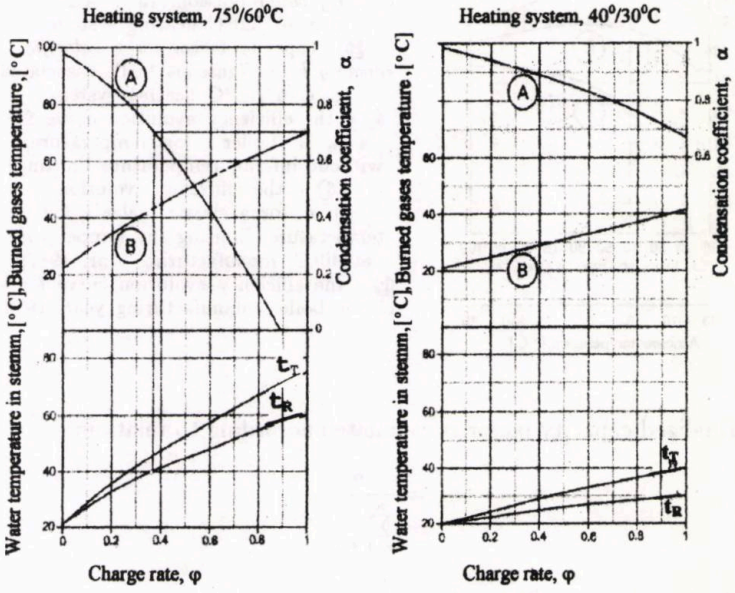

Fig. 3.– The relation between the condensation coefficient α (curve Ⓐ), the burned gases temperature (curve Ⓑ) and respectively the water heating system's temperature (turn/return, t_T/t_R) with modulation burning flame.

Because the burned gases temperature in a *caloric capacity boiler* is inferior, comparatively with the classic heaters, the heat losses in the burned gases are more reduced. This means that *caloric capacity boiler* have two advantages: a) the heat gain obtained from condensation; b) a better using of sensible heat, generated by more reduced losses.

To illustrate this fact, in Fig. 4 is represented, comparatively, the efficaciousness evaluation for the two types of heaters – *caloric capacity* and classic boilers.

Taking into account that, for the heaters, the operation at rated charge, is an exception not a rule, the evaluation of efficiency is performed using the coefficient prescribed in [3].

For examplification, it is considered the operation of a heater, at different thermal charges, having heating parameters 75°/60°C [4]. The calculation rule, taking into account five different operation manners, is presented in Table 2.

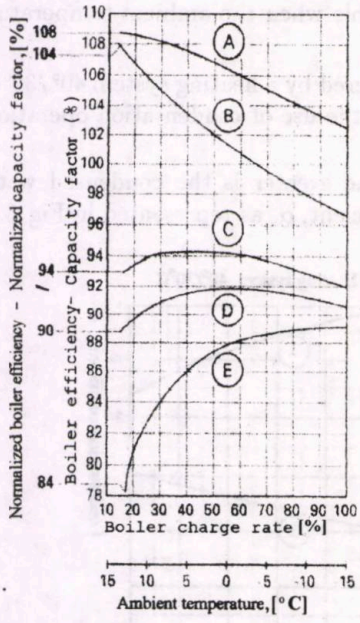

Fig. 4.– The dependence relation between the boiler efficiency, respective capacity factor (normalized and operation values) and the boiler charge, respectively ambient temperature:
Ⓐ – capacity factor for a *calorific capacity boiler* (gaseous fuel), associated to a 40°/30°C heating system;
Ⓑ – capacity factor for a *calorific capacity boiler* (gaseous fuel), associated to a 75°/60°C heating system;
Ⓒ – the efficiency evolution curve for a classic boiler – low temperature, without inferior temperature limiting;
Ⓓ – the efficiency evolution curve, for a classic boiler – low temperature, limiting the temperature at 40°C, manufacturing year, 1987;
Ⓔ – the efficiency evolution curve for a classic boiler, manufacturing year, 1975.

The normalized capacity factor is calculated according to relation:

$$\eta_N = \frac{n}{\sum_{i=1}^{n} \frac{1}{\eta_{d,i}}},$$

where n is the number of calculation points.

For the considered example, $n = 5$ and $\eta_N = 103.5$, [%].

Table 2

Charge ratio %	Water temperature, turn/return, [°C]	Capacity factor, $\eta_{d,i}$ %	Inverse value of capacity factor
20	36/33.3	106.7	0.009372
30	42.5/37.5	105	0.009523
40	47.5/41.7	103.3	0.009680
50	52.5/45	102	0.009803
58	57/47	100.9	0.009910
			$\Sigma = 0.048288$

In Fig. 4 there are presented the variation curves of the efficaciousness and the capacity factor, normal, respectively normalized, for some heaters types.

It must be mentioned that the using rate doesn't have the physical signification of efficaciousness, being able to have values over 100%, fact that could suggest the possibility of a *perpetuum mobile*. But, this value is appreciated, only, as a coefficient that allows a compression of the efficiency, between a classic and a *calorific capacity boiler*; this coefficient could be converted in a factor expressing the efficaciousness when, in the determining calculation, condensation heat is reported to the superior calorific capacity not to the inferior one.

3. Conclusions

Calorific capacity boilers represent the most advanced category of thermal equipment who's real efficaciousness, in heat generation, is nearest to theoretical one.

This thing is possible, for these heaters, because it is, also, taken in consideration the recover of a greater part from the condensation heat. It was indebted to the use, in the manufacturing process, of a special material, resistant to water and acids action.

The efficiency of such a heater is greater as the temperature of the heating system is lower. The best system has proved to be the system 40°/30°C.

Received, October 5, 2000

Technical University "Gh.Asachi", Jassy,
Department of Energetics
and
**Research Institute for*
Electrotechnics, Jassy

REFERENCES

1. A s a f t e i C., G r o z a D., *Some Aspects Regarding the Solutions Applied for the Efficiency Improving of Small Power Heating Units.* Bul. Inst. polit., Iaşi, **XLV (IL)**, *5B*, s.III, 355-359 (1999).
2. A s a f t e i C., G r o z a D., *The Individual Heating Boilers – Economic and Ecologic Heat Supply.* Bul. Inst. polit., Iaşi, **XLV (IL)**, *5B*, s.III, 359-363 (1999).
3. . * . *Heating Boilers*, Prospects Wissman.

CAZANELE CU PUTERE CALORICĂ – MAI EFICIENTE, MAI ECONOMICE

(Rezumat)

Se abordează aspecte din problematica unei categorii aparte de cazane moderne de încălzire şi anume, cazanele cu putere calorică. Sunt prezentate, cu această ocazie, câteva din principiile de realizare şi funcţionare, modul de apreciere a eficienţei şi din acest punct de vedere, în final, o comparaţie cu cazanele convenţionale de încălzire.

BULETINUL INSTITUTULUI POLITEHNIC DIN IAŞI
Tomul XLVII (LI), Fasc. 1–2, 2001
ELECTROTEHNICĂ. ENERGETICĂ. ELECTRONICĂ

D.C. 621.316.13.016.313

THE NON-SYMMETRICAL STEADY STATE OF A THREE-PHASE DISTRIBUTION NETWORK

BY

VIOREL VARVARA

A three-phase network real operating state is a non-symmetrical one, the main cause being the non-symmetry of the three-phases loads. A three-phase network working in sinusoidal steady state, star connection with neutral insulated, is considered, in which the generator is symmetric, having an infinite power and the distribution line is symmetric too. The load has equal impedances on two phases, the unbalance appreciation being made with the help of a factor, α, which modifies the resistance of the third impedance. Power circulation on symmetrical sequences, supplementary losses on the distribution line, voltage and currents, non-symmetry factors and global power factor variation are determined. Network critical duty situations are observed, remarks concerning possibilities of decreasing the losses and increasing the global power factor being made.

1. Introduction

In the assembly generator, line and load, the main cause of the appearance of a non-symmetrical state is the non-symmetry of the load which has different impedances on the phases. Usually, the generator (index g) is considered ideal, symmetrical, having the EMF E, supplying active and reactive power only on the positive sequence and the line is symmetrical, of total impedance $\underline{Z}_1 = R_1 + \mathrm{j}X_1$. In our case the load has equal impedances, $\underline{Z} = R + \mathrm{j}X$, on two phases, the non-symmetry being spotlighted by the unbalance coefficient α (real and positive number) which affects the resistance of the third impedance ($\underline{Z}' = \alpha R + \mathrm{j}X$). This is a common situation, taking into account that the total requested reactive power has approximatively constant values and only the active power changes in large domains. The load is star connected with neutral insulated. The analysis method is that based on considering the state as sinusoidal and decomposing the signals into symmetrical sequences (positive, negative and zero), the non-symmetrical operation being considered as a superposition of these three symmetrical operations. For each one of these three operations the active and reactive powers are separately conservative [4].

2. The Symmetrical Powers Flow

The symmetrical values – positive (direct), negative (inverse) and zero (homopolar), respectively, A_d, A_i, A_0 of three non-symmetrical signals A_1, A_2, A_3 – may be determined with the formula:

$$\begin{bmatrix} A_0 \\ A_d \\ A_i \end{bmatrix} = \frac{1}{3}\begin{bmatrix} 1 & 1 & 1 \\ 1 & a & a^2 \\ 1 & a^2 & a \end{bmatrix}\begin{bmatrix} \underline{A}_1 \\ \underline{A}_2 \\ \underline{A}_3 \end{bmatrix}, \tag{1}$$

where

$$a = e^{j\frac{2\pi}{3}} = -\frac{1}{2} + j\frac{\sqrt{3}}{2} \tag{2}$$

is the rotation operator.

The apparent power for the symmetrical sequences at the load, on the line (index l) and at the generator are calculated with the relations:

$$\underline{S}_m = 3\underline{U}_m\underline{I}_m^*, \quad \underline{S}_{lm} = 3\underline{Z}_1\underline{I}_m^2, \quad \underline{S}_{gm} = 3\underline{E}\underline{I}_m^*, \quad (m = d, i, 0). \tag{3}$$

$\underline{U}_m$ is the voltage referring to the neutral point of the star connected generator, expressed in symmetrical sequences at the load and $\underline{I}_m$ is the current in symmetrical sequences.

Remarking that all the components of zero sequences and the components of apparent power on inverse sequence at the generator are permanently null, the expressions are the followings:

a) at the load:

$$P_d = 3E^2\left\{\frac{3R(R_1^2+X_1^2)(\alpha+2)+R_1R^2(\alpha+2)(\alpha+5)}{[(R+R_1)^2+(X+X_1)^2]\left\{[3R_1+R(2\alpha+1)]^2+9(X+X_1)^2\right\}}+\right. \tag{4}$$

$$\left.+\frac{18RXX_1+R^3(2\alpha+1)(\alpha+2)+9RX^2}{[(R+R_1)^2+(X+X_1)^2]\left\{[3R_1+R(2\alpha+1)]^2+9(X+X_1)^2\right\}}\right\},$$

$$Q_d = 3E^2\frac{3X(R_1^2+X_1^2)+X_1[18X^2+R^2(\alpha-1)^2]+18RR_1X+3R^2X(\alpha+2)+9X^3}{[(R+R_1)^2+(X+X_1)^2]\left\{[3R_1+R(2\alpha+1)]^2+9(X+X_1)^2\right\}}, \tag{5}$$

$$P_i = -3E^2\frac{R_1R^2(\alpha-1)^2}{[(R+R_1)^2+(X+X_1)^2]\left\{[3R_1+R(2\alpha+1)]^2+9(X+X_1)^2\right\}}, \quad Q_i = \frac{X_1}{R_1}P_i; \tag{6}$$

b) on the line the positive components of the active and reactive powers are:

$$P_{ld} = 3R_1E^2\frac{9(R_1^2+X_1^2)+6R_1R(\alpha+2)+18XX_1+R^2(\alpha+2)^2+9X^2}{[(R+R_1)^2+(X+X_1)^2]\left\{[3R_1+R(2\alpha+1)]^2+9(X+X_1)^2\right\}}, \quad Q_{ld} = \frac{X_1}{R_1}P_{ld}. \tag{7}$$

The equations which express the circulation and the conservation of the powers, written in symmetrical sequences, are the followings:

$$P_{gm} = P_{lm} + P_m, \quad Q_{gm} = Q_{lm} + Q_m, \quad (m = d, i, 0). \tag{8}$$

The powers corresponding to each element of the network are:

$$P_g = P_{gd}, \quad Q_g = Q_{gd}; \tag{9}$$

$$P_l = P_{ld} + P_{li} = P_{ld} + \Delta P_l > P_{ld}, \quad Q_l = Q_{ld} + Q_{li} = Q_{ld} + \Delta Q_l > Q_{ld}; \tag{10}$$

$$P = P_d + P_i = P_d - |\Delta P_n| < P_d, \quad Q = Q_d + Q_i = Q_d - |\Delta Q_n| < Q_d. \tag{11}$$

Supplementary losses on the line results as:

$$\Delta P_l = P_{li} = |\Delta P_n| = |P_i| > 0, \quad \Delta Q_l = Q_{li} = |\Delta Q_n| = |Q_i| > 0. \tag{12}$$

Because its non-symmetry the load demands from the generator more power (P_d, Q_d) than it needs (P, Q). It receives it on positive sequence and transforms a part into negative sequence and injects it to the line. This ($|\Delta P_n|$, $|\Delta Q_n|$) represents an additional power which flows in the network and which determines additional losses (ΔP_l, ΔQ_l). The line isn't responsible for this kind of losses (even through its parameters, R_1 and X_1, influences their values), representing only the element of the circuit on which the non-symmetrical load manifests its capacity of generating negative sequence active and reactive powers. Thus the effects of the non-symmetry of an element of the circuit isn't concentrated only locally but these ones are propagated to the whole network. The generator, being of infinite power, is not effected by the injection of the non-symmetrical powers. In the hypothesis that there are more symmetrical receivers connected at the same distribution bars, the negative sequence powers will spread in the whole network.

3. The Influence of the Non-symmetry Coefficient on the Active Power Flow

In the followings, the behaviour of the positive sequence active power at the load, P_d, *versus* the α coefficient, is taken into account, for common values of the network's elements, under different values for X/R ratio. The quantity to which P_d and further ΔP_l are divided to obtain the relative units (r.u.) is E^2/R.

In Fig. 1 is represented this dependence for $X_1/R_1 = 10$ and in Fig. 2 for $X_1/R_1 = 5$.

It is possible to observe that, if the active charge on the third phase is small, the total positive sequence active power transferred to the load decreases. The biggest power is find if the α coefficient is small, close to zero, the third impedance being reduced to its reactance. If X/R ratio decreases more active power is find at the load. The influence of α in the interval $(0.001; 0.5)$ isn't significant for P_d variation. If the

electrical parameters of the line lead to a smaller value for X_1/R_1 (for example, 5 instead of 10), P_d increases but not in a significant way (for $X/R = 1.33$ the increase is approximately of 5% and for $X/R = 0.48$ is approximately of 7...10%).

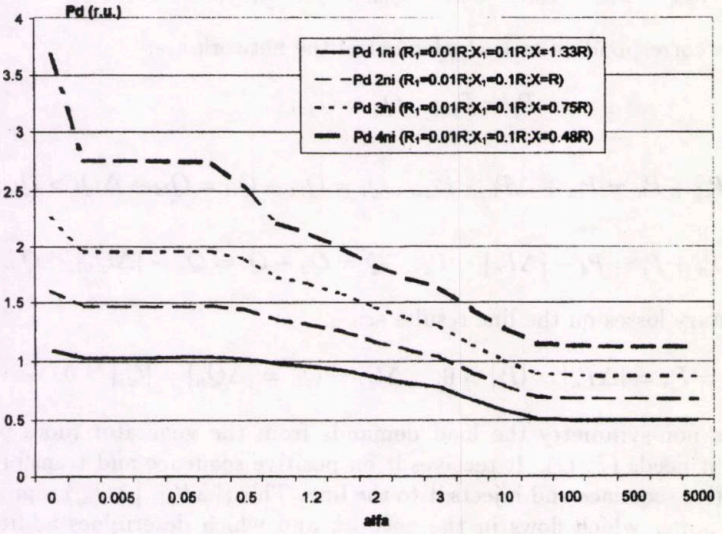

Fig. 1.– The influence of the non-symmetry on the positive sequence active power transferred to the load for different values of X/R ratio.

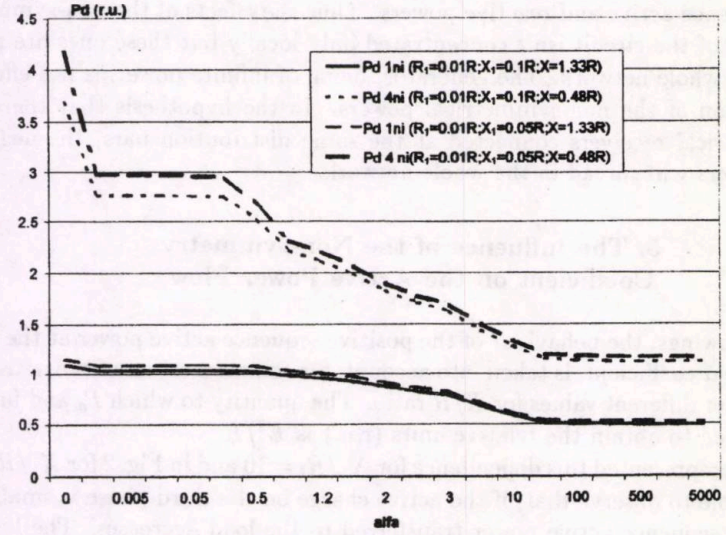

Fig. 2.– The influence of the non-symmetry and of the X_1/R_1 ratio on the positive sequence active power transferred to the load, for different values of X/R ratio.

4. The Additional Active Power Losses on the Line

Through the transmission lines runs negatives sequences of active and reactive power, injected by the non-symmetrical load, named as power of non-symmetry,

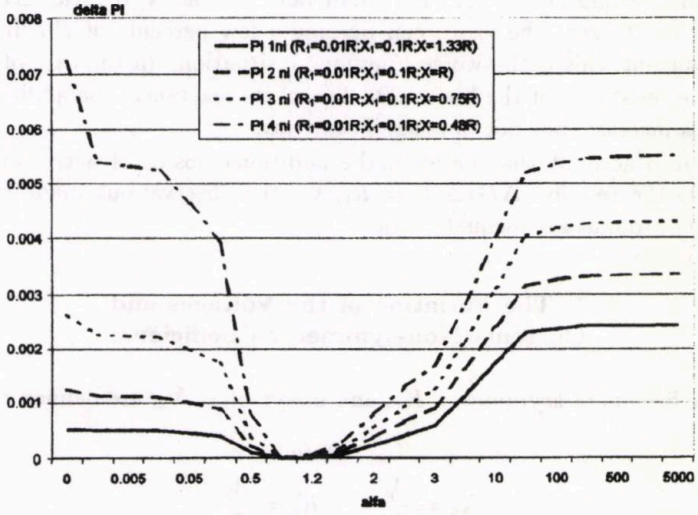

Fig. 3.– The influence of the non-symmetry on the additional active losses for different values of the X/R ratio.

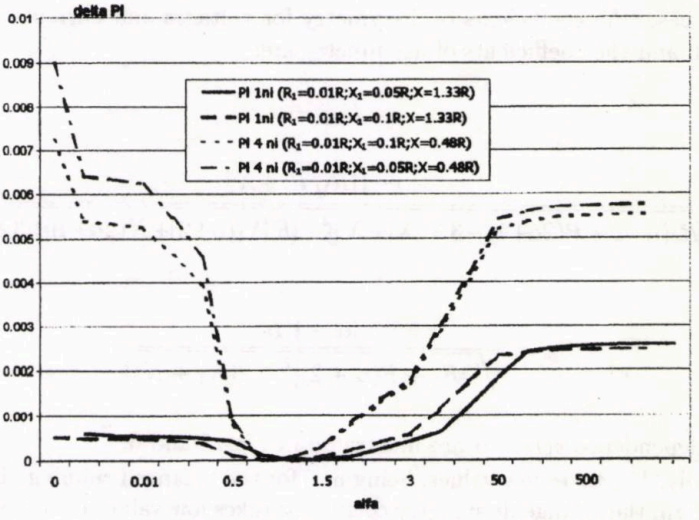

Fig. 4.– The influence of the non-symmetry and of the X_1/R_1 ratio on the additional active power losses for different values of X/R ratio.

which leads to additional losses, ΔP_l. In Fig. 3 it is represented the dependence of this power *versus* α coefficient and in Fig. 4 the influence of X_1/R_1 on it.

Related to P_d, ΔP_l takes values under 0.5% for common values of α, being zero in the case of a balanced load. Obviously, a balanced load can't be a generator of non-symmetrical power. If the active load decreases very much on the third phase the additional active power losses increase, this situation being the most undesirable one, if R takes values close to X. For small values of the X/R ratio, ΔP_l increases and for α close to zero the losses can become a few percents of P_d. If the active load is important, this is the worse functioning situation. In the case of a network in which the resistance of the line is 20...30% of its reactance, the additional active power losses increase, but not in a significant way.

Taking into account that between the additional losses of active and reactive power exists the relation $\Delta P_l/\Delta Q_l = R_1/X_1$, the observations made for ΔP_l are valid for ΔQ_l, too, at an adequate ratio.

5. The Variation of the Voltages and Currents Non-symmetry Coefficients

The coefficients of asymmetry, K_a, and dissymetry, K_d, are defined by the relations:

$$K_a = \frac{A_i}{A_d}, \qquad K_d = \frac{A_0}{A_d}, \tag{13}$$

where A_i, A_0, A_d are the negative, zero and positive sequences of the signal.

In this case, the coefficients of dissymetry for voltages and currents are permanently null, and the coefficients of asymmetry are:

$$K_{du} = \frac{|\alpha-1|R\sqrt{R_1^2+X_1^2}}{\sqrt{\{R[R_1(\alpha+2)+R(2\alpha+1)]-3X(X_1+X)\}^2+\{R[X_1(\alpha+2)+X(2\alpha+1)]+3X(R_1+R)\}^2}}, \tag{14}$$

$$K_{di} = \frac{|\alpha-1|R}{\sqrt{[3R_1+R(\alpha+2)]^2+9(X_1+X)^2}}. \tag{15}$$

Their dependence *versus* α are illustrated in Figs. 5 and 6.

Generally, K_{du} takes low values, being null for the balanced running. If the active charge is high, the voltage dissymetry coefficient takes low values in comparison with the situation when the reactive charge is dominant. If the X/R ratio increases, better values for K_{du} are obtained, for the same value of the non-symmetry coefficient, α.

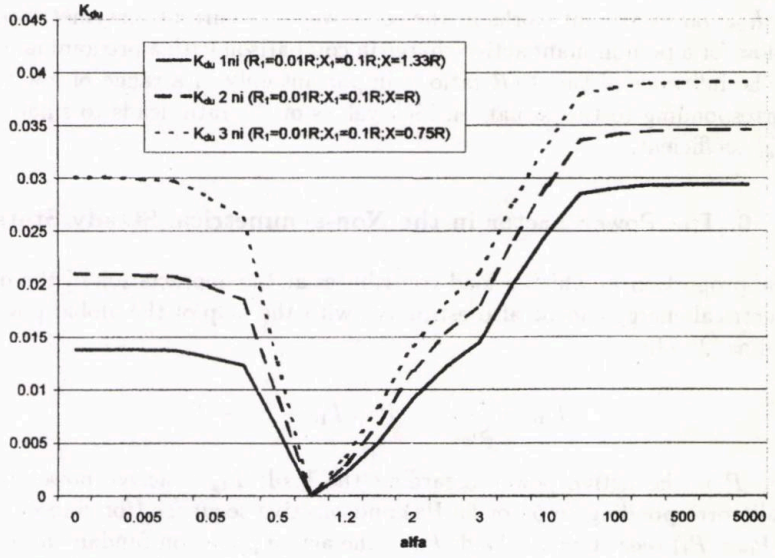

Fig. 5.– The variation of the voltage dissymetry coefficient *versus* the non-symmetry coefficient of the load.

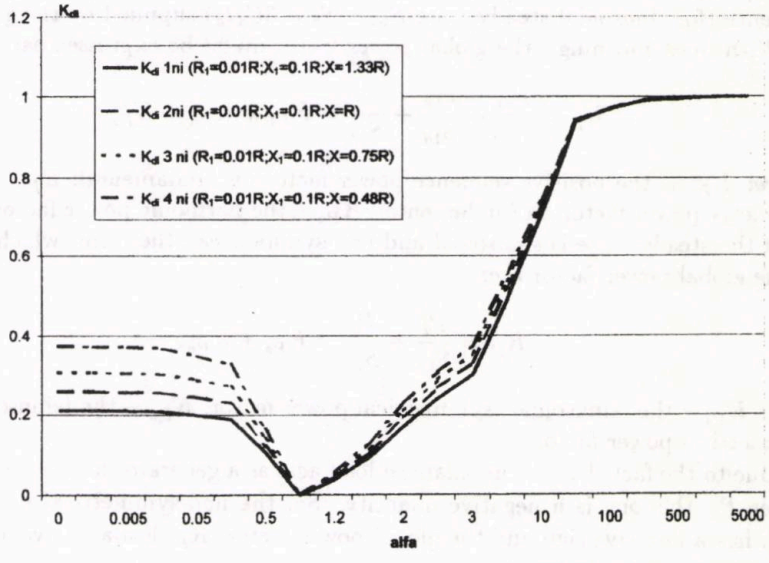

Fig. 6.– The variation of the current dissymetry coefficient *versus* the non-symmetry coefficient of the load.

The current dissymetry coefficient, K_{di}, takes higher values than K_{du} in the same running condition. The influence of the charge is more important than in the case of the K_{du} variation, but works in the same way, the current dissymetry coefficient being low for a predominant active charge in comparison with a predominant reactive one. The influence of the X/R ratio is important only in a range of low values for α. Corresponding to this situation, high values of the ratio leads to small values of the K_{di} coefficient.

6. The Power Factor in the Non-symmetrical Steady State

The proportion in which a load contributes at the depreciation of the quality of the electrical energy can be also estimated with the help of the global power factor defined as [2], [3]:

$$K_P = \frac{P}{S_{1d}}, \qquad P = P_{1d} + P_{1n} + P_a, \tag{16}$$

where: P is the active power regarding the load; P_{1d} – active power on fundamental (corresponding to 50 or 60 Hz) and positive sequence (for sinusoidal steady state $P_{1d} = P_d$) regarding the load; P_{1n} – the active power on fundamental and non-symmetrical components (for sinusoidal steady state, $P_{1n} = P_n = P_i + P_0$) regarding the load; for networks with the neutral insulated, $P_{1n} = P_n = P_i$; P_a – the harmonic (integer multiple of fundamental frequency) active power (for sinusoidal steady state, $P_a = 0$) regarding the load; S_{1d} – the apparent power on fundamental and positive sequence (for sinusoidal steady state $S_{1d} = S_d = 3U_d I_d$) supplied by the generator.

With these meanings, the global power factor might be expressed as:

$$K_P = \frac{P_{1d}}{S_{1d}} + \frac{P_{1n}}{S_{1d}} + \frac{P_a}{S_{1d}} = K_{P1} + K_{Pn} + K_{Pa}, \tag{17}$$

where: K_{P1} is the positive sequence power factor on fundamental; K_{Pn} – the non-symmetry power factor on fundamental; K_{Pa} – the harmonic power factor.

If the steady state is sinusoidal and non-symmetrical, the terms which are parts of the global power factor are:

$$K_P = \frac{P_d}{S_{1d}} + \frac{P_n}{S_{1d}} = K_{Ps} + K_{Pn}, \tag{18}$$

with: K_{Ps} – the (sinusoidal) symmetrical power factor; K_{Pn} – the (sinusoidal) non-symmetrical power factor.

Due to the fact that the unbalanced load acts as a generator for non-symmetrical power P_1, this one is a negative quantity. So, the non-symmetrical power factor, K_{Pn}, has a negative sign and the global power factor, K_P, has a less value than the symmetrical power factor, K_{Ps}.

The dependences of the power factors K_{Ps} and K_{Pn} *versus* α coefficient are represented in Figs. 7 and 8.

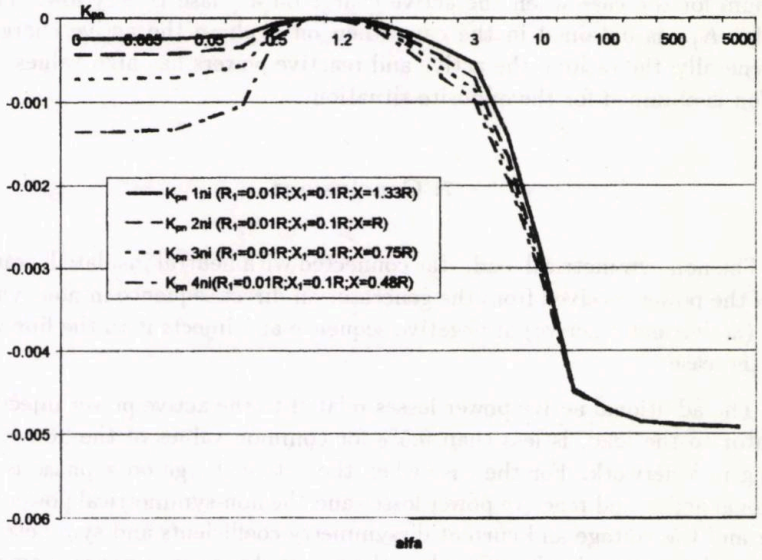

Fig. 7.– The variation of the non-symmetrical power factor *versus* the non-symmetry coefficient.

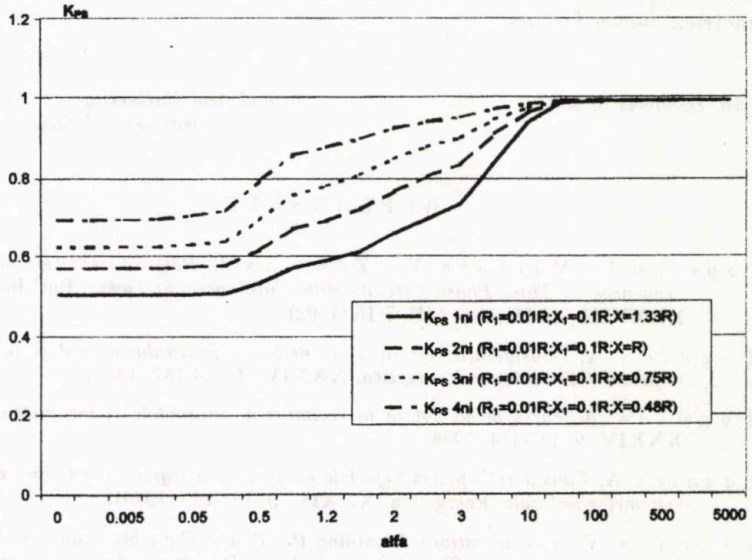

Fig. 8.– The variation of the symmetrical power factor *versus* the non-symmetry coefficient.

The non-symmetrical power factor, K_{Pn}, has values less than 0.005 when α takes high values, in rest being almost negligible. The symmetrical power factor, K_{Ps}, is maximum for the case when the active charge on a phase is very low. The lowest value for K_{Ps} is obtained in the case when on a phase the active charge is high and, generally, the ratio of the active and reactive powers has high values. The best situation is obtained for the opposite situation.

7. Conclusions

a) The non-symmetrical load, star connected with neutral insulated, transforms a part of the power received from the generator on direct sequence in non-symmetrical power (active and reactive) of negative sequence and injects it to the line where the losses increase.

b) The additional active power losses related to the active power injected by the generator to the load, is less than 0.5% for common values of the non-symmetries existing in a network. For the case when the active charge on a phase is high, the additional active and reactive power losses and the non-symmetrical power factor are higher and the voltage and current dissymmetry coefficients and symmetrical power factor are lower than in the case when the active charge on a phase is small.

c) For a given coefficient of non-symmetry, common values of the X/R ratio, up than unit, leads to better values for the additional active and reactive power losses, for the voltage and current dissymetry coefficients and for the non-symmetrical and symmetrical power factors.

Received, December 4, 2000

Technical University "Gh.Asachi", Jassy,
Department of Electrotechnics

REFERENCES

1. P o p e s c u I., V a r v a r a V., Z a h a r i a I., *Power Circulation on Symmetrical Sequences in Three-Phase Circuits with Unbalanced Receivers.* Bul. Inst. polit., Iaşi, **XXXVIII (XLII)**, *1-4*, s.III, 7-16 (1992).

2. Ţ u g u l e a A, *Consideraţii referitoare la definirea factorului de putere pentru sistemele trifazate dezechilibrate.* Energetica, **XXXIV**, *4*, 164-167 (1986).

3. Ţ u g u l e a A, *Factorul de putere în regimuri nesinusoidale şi nesimetrice.* Energetica, **XXXIV**, *9*, 407-414 (1986).

4. Ţ u g u l e a A, *Consideraţii privind efectele energetice în regimuri armonice nesimetrice ale sistemelor trifazate.* Energetica, **XXXIV**, *3*, 121-129 (1986).

5. V a r v a r a V., *Considerations Regarding the Power Circulation and the Calculation of the Non-symmetry Coefficients for a Network Running under a Permanent Periodical Sinusoidal and Non-symmetrical State.* Internat. Conf. on Appl. a. Theoret. Electr., ICATE'2000, Craiova, 229-233.

REGIMURI DE FUNCŢIONARE NESIMETRICE ALE UNEI REŢELE ELECTRICE DE DISTRIBUŢIE

(Rezumat)

Regimul real de funcţionare al unei reţele electrice este nesimetric, principala cauză constituind-o nesimetria receptoarelor trifazate. Se consideră o reţea trifazată funcţionând în regim permanent sinusoidal, cu conexiunea în stea, cu neutrul izolat, în care generatorul este simetric şi de putere infinită iar linia este simetrică. Receptorul are impedanţele a două faze identice, aprecierea dezechilibrului realizându-se prin intermediul unui coeficient, α, care modifică rezistenţa celei de-a treia impedanţe. Se analizează circulaţia puterilor pe componente simetrice, pierderile suplimentare de putere pe linia de distribuţie, coeficienţii de nesimetrie ai tensiunilor şi curenţilor şi factorul de putere global. Se pun în evidenţă situaţii de funcţionare critice, făcându-se aprecieri cu privire la posibilităţile de micşorare a pierderilor suplimentare şi de creştere a factorului de putere global.

BULETINUL INSTITUTULUI POLITEHNIC DIN IAŞI
Tomul XLVII (LI), Fasc. 1–2, 2001
ELECTROTEHNICĂ. ENERGETICĂ. ELECTRONICĂ

RECENZII

BOOK REVIEWS

ROUSSEAU P., APOSTOL T., *Valeur environnementale de l'énergie*. Presses Polytechniques et Universitaires Romandes, Lausanne, 1998, 200 pp., 210.00 FF, ISBN 2-88074-437-7.

Cet ouvrage complète l'évaluation classique des procédés et des systèmes industriels. Son premier objectif est *pédagogique*: il expose l'évaluation environnementale des systèmes énergétiques à partir d'une nouvelle méthodologie: l'Analyse du Cycle de Vie (ACV). Le second objectif est *opérationnel* et consiste à fournir des informations permettant de réaliser l'évaluation environnementale de certaines systèmes énergétiques.

Le premier chapitre établit une terminologie et présente les différents impacts environnementaux ainsi que leurs moyens d'évaluation. Une présentation du cycle de vie des systèmes énergétiques et des bilans matière–énergie de ces cycles est proposée dans les chapitres suivants et détaillée en annexe. On distingue les énergies fossiles, l'énergie nucléaire, les énergies renouvelables et valorisation énergétique des déchets. Les impacts environnementaux des filières énergétiques sont analysés au cours du dernier chapitre. S'inspirant des méthodes d'analyse multicritère, les auteurs montrent comment la valeur environnementale globale des systèmes énergétiques peut être déterminée dans le but de comparaison, illustrant leur propos par deux exemples d'application.

Complétant les connaissances enseignées dans les filières scientifiques et techniques dans le domaine de l'énergie, cet ouvrage s'adresse aux élèves ingénieurs ou ingénieurs énergéticiens, aux étudiants (maîtrise, DEA, DESS), ainsi qu'aux environnementalistes et à certains professionnels de l'énergie.

* * *

Docteur de l'Institut National des Sciences Appliquées (INSA) de Lyon, Patrik Rousseau a soutenu sa thèse (*Evaluation comparative de l'impact environnemental global (ECIEG) du cycle de vie des produits*) en 1993, dans la spécialité „sciences et techniques du déchet". Depuis, il développe des recherches sur les méthodes d'évaluation des impacts environnementaux et des risques d'accident (étude d'impact, étude de danger, observatoire de l'environnement, système de management environnemental en Analyse du Cycle de Vie). Patrik Rousseau est actuellement maître de conférences à l'INSA de Lyon, rattaché au Laboratoire d'Analyse Environnementale des Procédés et des Systèmes Industriels (LAEPSI).

Docteur de l'Université Polytechnique de Bucarest (Roumanie), Tiberiu Apostol a soutenu sa thèse en 1998 (*Evaluation des impacts environnementaux de différentes filières de traitement des ordures ménagères avec récupération d'énergie*). Il est actuellement maître assistant dans cette université et rattaché au Département Génie Energétique. Ses travaux de recherche portent sur l'évaluation environnementale des systèmes énergétiques.

Table de matières: Préface; Remerciements: Département Génie Enérgétique et Environnement; 1. Définition de la valeur environnementale de l'énergie et objectifs de l'ouvrage; 2. Evaluation de la valeur environnementale des systèmes; 3. Présentation des filières énergétiques; 4. Méthodologie d'évaluation de la valeur environnementale globale des systèmes énergétiques; Conclusion générale; Annexe: Banque de données sur les systèmes énergétiques.

Data aparitiei: SEPTEMBRIE 2003
Comanda nr. 110, Tiraj: 175
Coli tipar: 13,25

UNIVERSITATEA TEHNICĂ "GH. ASACHI"
IAŞI
TIPOGRAFIA

Str. Lascăr Catargi nr. 38
Tel./Fax: 0232- 21 59 49

ISSN 0258-9109

BULETINUL INSTITUTULUI POLITEHNIC DIN IAŞI

OF 1503/3.
FF
8 000001 780484

Editat de
UNIVERSITATEA TEHNICĂ „GH. ASACHI", IAŞI

Tomul XLVII (LI)

Fasc. 3 – 4

ELECTROTEHNICĂ
ENERGETICĂ
ELECTRONICĂ

2001

BULETINUL INSTITUTULUI POLITEHNIC DIN IAŞI

BUDAPESTI MŰSZAKI ÉS GAZDASÁGTUDOMÁNYI EGYETEM
Műszaki Információs Központi és Könyvtár
2001

Tomul XLVII (LI)
Fasc. 3– 4

ELECTROTEHNICĂ. ENERGETICĂ. ELECTRONICĂ

2001

EDITORIAL STAFF

Prof. Dr. Eng. **MIHAI CREŢU** (President)
Prof. Dr. Eng. **VICTOR BULACOVSCHI** (Vice-President)
Prof. Dr. Eng. **ION GIURMA** (Vice-President)
Prof. Dr. Eng. **GHEORGHE ZET** (Secretary)
Prof. Dr. Doc. Eng. **ALFRED BRAIER** (Editor)
Prof. Dr. Eng. **HUGO ROSMAN** (Editor)
Prof. Dr. Eng. **MIHAIL VOICU** (Head of the Exchange Service)
Prof. Dr. Eng. **IOSIF BARTHA**
Prof. Dr. Eng. **ROMEN BUTNARU**
Prof. Dr. **ADRIAN CORDUNEANU**
Prof. Dr. Eng. **MIRCEA COZMÎNCĂ**
Prof. Dr. Eng. **ADRIAN DIMA**
Prof. Dr. Eng. **AURELIA GRIGORIU**
Prof. Dr. Eng. **MIRCEA GUŞĂ**
Prof. Dr. Eng. **DOREL LEON**
Prof. Dr. Eng. **MIHAI LUCANU**
Prof. Dr. Eng. **VALENTIN I. POPA**
Prof. Dr. Eng. **PAULICĂ RĂILEANU**

The **Bulletin of the Polytechnic Institute of Jassy** is edited by
the **Technical University "Gh.Asachi"** (the former Polytechnic Institute), Jassy.

TEXredaction:
Cristina Vasiliu, Adrian Rotaru
Technical University of Jassy

BULETINUL INSTITUTULUI POLITEHNIC DIN IAŞI
BULLETIN OF THE POLYTECHNIC INSTITUTE OF JASSY
Tomul XLVII (LI), Fasc. 3–4 2001

BUDAPESTI MŰSZAKI ÉS GAZDASÁGTUDOMÁNYI EGYETEM Műszaki Információs Központ és Könyvtár Olvasóterme 2001

ELECTROTEHNICĂ. ENERGETICĂ. ELECTRONICĂ

SUMAR

Pag.

HUGO ROSMAN, Vectorul lui Hertz în medii disipative (franc., rez. rom.) 7

VALERIU MUNTEANU şi DANIELA TĂRNICERIU, Un algoritm pentru maximizarea funcţiilor raţionale peste domenii liniare (engl., rez. rom.) 13

HUGO ROSMAN, Câteva aplicaţii ale unor identităţi şi inegalităţi algebrice în teoria circuitelor electrice (franc., rez. rom.) 21

DORIN BELAUS, Determinarea parametrilor matricei fundamentale pentru un tranzistor bipolar reprezentat printr-un cuadripol general liniarizat, în regim permanent armonic (engl., rez. rom.) 29

ILIE POPESCU, IUSTINA ZAHARIA şi CAMELIA PETRESCU, Modelarea elementelor cu comutaţie folosite în comanda motoarelor electrice (engl., rez. rom.) 35

DANIELA TĂRNICERIU şi VALERIU MUNTEANU, O metodă de proiectare a bancurilor de filtre cu răspuns infinit la impuls, biortogonale, cu reconstrucţie perfectă (engl., rez. rom.) 43

AL.-M. AVASILOAIE, Forma hipercomplexă a răspunsului în tensiune şi curent caracteristic liniilor electrice omogene lungi, excitate cu semnale de intrare armonice, în regim permanent (engl., rez. rom.) 51

LUMINIŢA SCRIPCARIU şi PETRUŢ DUMA, Algoritm de compresie a imaginilor digitale folosind metoda drumului minim dintr-un graf (engl., rez. rom.) 59

EMIL VREMERĂ şi N. DAMEAN, Metodă nouă pentru determinarea difuzivităţii termice a materialelor solide utilizând măsurări de timp. II. Partea experimentală (engl., rez. rom.) 65

LAURENŢIU DIMITRIU şi LILIANA VORNICU, Transfer serial de date cu control de timp în sisteme de control în timp real (engl., rez. rom.) 73

IULIAN RĂDUCANU, LILIANA VORNICU şi LAURENŢIU DIMITRIU, Strategie pentru simplificarea implementării controlerelor cu logică fuzzy pe suport digital (engl., rez. rom.) 79

PETRUŢ DUMA, Asupra unei posibilităţi de reducere a tranziţiilor identice la realizarea prin *soft* a structurilor logice secvenţiale cu metoda tabloului stărilor următoare (engl., rez. rom.) 89

DĂNUŢ BURDIA, O metodă de reducere a unui lanţ de tranzistoare cu canal scurt la un tranzistor MOS echivalent (engl., rez. rom.) 97

Pag.

IRINEL-VALENTIN PLETEA, Eliminarea armonicilor de curent (engl., rez. rom.) 109

I. ANDRONE şi ADRIANA PRISĂCARU, O nouă abordare a teoriei maşinii de inducţie trifazate nesimetrice (engl., rez. rom.) 121

GH. GRIGORAŞ şi GH. CĂRŢINĂ, Aspecte privind planificarea reţelelor electrice cu o considerare particulară a fiabilităţii (engl., rez. rom.) 127

GH. GEORGESCU şi DANIELA RĂDĂŞANU, Analiza statistico-probabilistică a sarcinilor din nodurile reţelelor de distribuţie. Baza de date (engl., rez. rom.) 135

VIOREL VARVARA, Regimuri de funcţionare permanente armonice în reţelele electrice de medie tensiune (engl., rez. rom.) 143

GH. GEORGESCU, DANIELA RĂDĂŞANU şi VIOREL VARVARA, Produse software pentru analiza şi optimizarea regimurilor de funcţionare ale reţelelor de distribuţie (engl., rez. rom.) 151

C. ASAFTEI şi DORIN GROZA, Creşterea eficienţei cazanelor moderne de încălzire prin îmbunătăţirea performanţelor sistemelor de evacuare a gazelor de ardere (engl., rez. rom.) 159

RECENZII 167

BULETINUL INSTITUTULUI POLITEHNIC DIN IAŞI
BULLETIN OF THE POLYTECHNIC INSTITUTE OF JASSY
Tome XLVII (LI), Fasc. 3–4 2001

BUDAPESTI MŰSZAKI ÉS GAZDASÁGTUDOMÁNYI EGYETEM Országos Műszaki Információs Központ és Könyvtár 2001

ELECTROTECHNICS. ENERGETICS. ELECTRONICS

CONTENTS

Pp.

HUGO ROSMAN, Le vecteur de Hertz en milieux dissipatifs (French, Romanian summary) 7

VALERIU MUNTEANU and DANIELA TĂRNICERIU, An Algorithm for the Maximization of Rational Functions Over Linear Domains (English, Romanian summary) 13

HUGO ROSMAN, Quelques applications de certaines identités et inégalités algébriques dans la théorie des circuits électriques (French, Romanian summary) 21

DORIN BELAUS, Parameters Determination of the Fundamental Matrix, for a Bipolar Transistor Represented by a General Linear Four-terminal, in the Harmonic Steady State (English, Romanian summary) 29

ILIE POPESCU, IUSTINA ZAHARIA and CAMELIA PETRESCU, Modelling of Switching Elements Used in Electric Motors Control (English, Romanian summary) 35

DANIELA TĂRNICERIU and VALERIU MUNTEANU, A Method to Design Biorthogonal Perfect Reconstruction Infinite Impulse Response Filter Banks Weight Distribution of Binary Cyclic Codes (English, Romanian summary) 43

AL.-M. AVASILOAIE, Hypercomplex Form of Voltage Response of the Electrical Homogenous Long Lines, Excited by Harmonical Signals, in Steady-State (English, Romanian summary) 51

LUMINIŢA SCRIPCARIU and PETRUŢ DUMA, Digital Image Compression Algorithm Using Spanning Trees (English, Romanian summary) 59

EMIL VREMERĂ and N. DAMEAN, New Measurement Method of the Thermal Diffusivity in Solids Using Time Measurements. II. Experimental Approach (English, Romanian summary) 65

LAURENŢIU DIMITRIU and LILIANA VORNICU, Timed Serial Data Transfer in Real-Time Control Systems (English, Romanian summary) 73

IULIAN RĂDUCANU, LILIANA VORNICU and LAURENŢIU DIMITRIU, Strategy for Simplifying the Implementation of Fuzzy Logic Controllers on Digital Support (English, Romanian summary) 79

PETRUŢ DUMA, On a Possibility of Reducing Identical Transitions in Software Emulation of Sequential Logical Structures Using the Method of the Next-state Table (English, Romanian summary) 89

DĂNUŢ BURDIA, A Method for the Reduction of the Short Channel Transistor Chain to an Equivalent MOSFET (English, Romanian summary) 97

Pp.

IRINEL-VALENTIN PLETEA, The Elimination of Line-Current Harmonics (English, Romanian summary) 109

I. ANDRONE and ADRIANA PRISĂCARU, A New Approach of the Three-phase Unsymmetrical Induction Machine Theory (English, Romanian summary) 121

GH. GRIGORAŞ and GH. CÂRŢINĂ, Electric Network Planning Aspects with Special Regard to Reliability (English, Romanian summary) 127

GH. GEORGESCU and DANIELA RĂDĂŞANU, Statistical-Probabilistic Analysis of Loads from the Distribution Network Nodes. Database (English, Romanian summary) 135

VIOREL VARVARA, Harmonic Steady-States in medium Voltage Networks (English, Romanian summary) 143

GH. GEORGESCU, DANIELA RĂDĂŞANU and VIOREL VARVARA, Soltware Application Package for the Analysis and the Optimization of Distribution Networks Characteristic Regimes (English, Romanian summary) 151

C. ASAFTEI and DORIN GROZA, Higher Efficiency for Modern Boilers by Improving the Burned Gases Evacuating Systems Performances (English, Romanian summary) 159

BOOK REVIEWS 167

BULETINUL INSTITUTULUI POLITEHNIC DIN IAŞI
Tomul XLVII (LI), Fasc. 3–4, 2001
ELECTROTEHNICĂ. ENERGETICĂ. ELECTRONICĂ

C.D. 538.3

LE VECTEUR DE HERTZ EN MILIEUX DISSIPATIFS

PAR
HUGO ROSMAN

On définit le vecteur de Hertz attaché aux potentiels électromagnétiques retardés, dans le cas des milieux dissipatifs, en deux variantes distinctes et on établit les relations de calcul des vecteurs d'état du champ électromagnetique, **E** et **B**, en fonction du vecteur de Hertz.

1. Introduction

C'est bien connu le fait (par ex. [1]) que, dans le cas le plus général, les relations qui permettent à calculer l'intensité du champ électrique, **E** et l'induction magnétique, **B**, en régime nonstationnaire, implique la nécessité de la connaissance des potentiels retardés **A**, V et des antipotentiels retardés **A**′, V':

$$\mathbf{E} = -\text{grad}\, V - \frac{\partial \mathbf{A}}{\partial t} + \frac{1}{\varepsilon}\text{rot}\, \mathbf{A}', \quad \mathbf{B} = -\mu \text{grad}\, V' - \mu \frac{\partial \mathbf{A}'}{\partial t} + \text{rot}\, \mathbf{A}, \tag{1}$$

où ε est la permittivité et μ – la perméabilité du milieu, considéré isotrope, homogène, nonpolarisé et nonmagnétisé permanent et, en outre, imobile.

Compte tenu de leur caractère complexe, ces relations s'avèrent assez difficiles pour la détermination des vecteurs **E**, **B**. Il est, toutefois, possible, que soit les antipotentiels retardés soient considérés nuls, la connaissance rien que des potentiels retardés **A**, V, permettant à déduire l'effet des sources du champ, les équations (1) se réduisant à

$$\mathbf{E} = -\text{grad}\, V - \frac{\partial \mathbf{A}}{\partial t}, \quad \mathbf{B} = \text{rot}\, \mathbf{A}, \tag{2}$$

soit, au contraire, les potentiels retardés soient nuls, de sorte que seulement la connaissance des antipotentiels retardés **A**′, V', permet à déterminer l'effet des sources du champ. Dans ce dernier cas les équations (1) deviennent:

$$\mathbf{E} = \frac{1}{\varepsilon}\text{rot}\, \mathbf{A}', \qquad \mathbf{B} = -\mu \text{grad}\, V' - \mu \frac{\partial \mathbf{A}'}{\partial t}. \tag{3}$$

Si on utilise, dans la première variante, les équations de Maxwell:

$$\text{rot}\, \mathbf{H} = \mathbf{J} + \frac{\partial \mathbf{D}}{\partial t}, \quad \text{div}\, \mathbf{D} = \rho_v, \quad \mathbf{D} = \varepsilon \mathbf{E} \tag{4}$$

et dans la deuxième, les équations:

$$\text{rot}\,\mathbf{E} = -\frac{\partial \mathbf{B}}{\partial t}, \quad \text{div}\,\mathbf{B} = 0, \quad \mathbf{B} = \mu\mathbf{H}, \tag{5}$$

le milieu ayant les propriétés mentionnées ci-dessus, les relations (2) et (3) conduisent aux systèmes d'équations différentielles à dérivées partielles:

$$\begin{cases} \Delta\mathbf{A} - \dfrac{1}{\varepsilon\mu} \cdot \dfrac{\partial^2 \mathbf{A}}{\partial t^2} = \mu\mathbf{J} + \text{grad}\left(\text{div}\,\mathbf{A} + \varepsilon\mu \dfrac{\partial V}{\partial t}\right), \\ \Delta V - \dfrac{1}{\varepsilon\mu} \cdot \dfrac{\partial^2 V}{\partial t^2} = -\dfrac{1}{\varepsilon}\rho_v - \dfrac{\partial}{\partial t}\left(\text{div}\,\mathbf{A} + \varepsilon\mu \dfrac{\partial V}{\partial t}\right), \end{cases} \tag{6}$$

satisfaits par les potentiels retardés, respectivement

$$\begin{cases} \Delta\mathbf{A}' - \dfrac{1}{\varepsilon\mu} \cdot \dfrac{\partial^2 \mathbf{A}'}{\partial t^2} = \text{grad}\left(\text{div}\,\mathbf{A}' + \varepsilon\mu \dfrac{\partial V'}{\partial t}\right), \\ \Delta V - \dfrac{1}{\varepsilon\mu} \cdot \dfrac{\partial^2 V'}{\partial t^2} = -\dfrac{\partial}{\partial t}\left(\text{div}\,\mathbf{A}' + \varepsilon\mu \dfrac{\partial V'}{\partial t}\right), \end{cases} \tag{7}$$

vérifiés par les antipotentiels retardés.

Ayant en vue que les potentiels scalaires retardés V , V' sont définis jusqu'à une constante scalaire active arbitraire tandis que les potentiells vectoriels retardés $\mathbf{A}$, $\mathbf{A}'$, jusqu'à un gradient aditif arbitraire, on adopte, en vue de l'intégration des équations (6) et (7), la condition de Lorentz [1]:

$$\text{div}\,\mathbf{A} + \varepsilon\mu \frac{\partial V}{\partial t} = 0, \tag{8}$$

en ce qui regarde les potentiels $\mathbf{A}$, V et

$$\text{div}\,\mathbf{A}' + \varepsilon\mu \frac{\partial V'}{\partial t} = 0, \tag{9}$$

concernant les antipotentiels $\mathbf{A}'$, V'.

De l'analyse des conditions de Lorentz (8) et (9) il ressort la possibilité d'exprimer les potentiels $\mathbf{A}$, V d'une part et des potentiels retardés $\mathbf{A}'$, V', de l'autre part, en fonction d'un seul vecteur, denommé le vecteur de Hertz à savoir

$$\mathbf{A} = \varepsilon\mu \frac{\partial \mathbf{Z}}{\partial t}, \qquad V = -\text{div}\,\mathbf{Z}, \tag{10}$$

respectivement

$$\mathbf{A}' = \varepsilon\mu \frac{\partial \mathbf{Z}'}{\partial t}, \qquad V = -\text{div}\,\mathbf{Z}', \tag{11}$$

où $\mathbf{Z}$ représent le vecteur de Hertz attaché aux potentiels retardés et $\mathbf{Z}'$, le vecteur de Hertz attaché aux antipotentiels retardés.

Si on dispose des expressions (10) et (11) des potentiels et, respectivement, des antipotentiels retardés on peut déterminer, à l'aide des relations (2) et (3), les vecteurs **E**, **B**, à savoir:

$$\mathbf{E} = \text{grad div } \mathbf{Z} - \varepsilon\mu\frac{\partial^2\mathbf{Z}}{\partial t^2}, \qquad \mathbf{B} = \varepsilon\mu\frac{\partial(\text{rot } \mathbf{Z})}{\partial t}, \tag{12}$$

respectivement

$$\mathbf{E} = \mu\frac{\partial(\text{rot } \mathbf{Z}')}{\partial t}, \qquad \mathbf{B} = \mu\left(\text{grad div } \mathbf{Z}' - \varepsilon\mu\frac{\partial^2\mathbf{Z}'}{\partial t^2}\right). \tag{13}$$

Les vecteurs de Hertz ainsi définis satisfont les équations différentielles à dérivées partielles:

$$\Delta\mathbf{Z} - \varepsilon\mu\frac{\partial^2\mathbf{Z}}{\partial t^2} = -\frac{\mathbf{P}}{\varepsilon_0}, \qquad \Delta\mathbf{Z}' - \varepsilon\mu\frac{\partial^2\mathbf{Z}'}{\partial t^2} = -\mathbf{M}, \tag{14}$$

où **P** est la polarisation et **M** – la magnétisation du milieu.

Les relations ci-dessus sont valables pour des milieux *nondisipatifs* ($\sigma = 0$) tandis que si le milieu est *dissipatif* ($\sigma \neq 0$) les équations (6) deviennent [1]:

$$\begin{cases} \Delta\mathbf{A} - \varepsilon\mu\dfrac{\partial^2\mathbf{Z}}{\partial t^2} - \sigma\mu\dfrac{\partial\mathbf{A}}{\partial t} = \text{grad}\left(\text{div } \mathbf{A} + \varepsilon\mu\dfrac{\partial V}{\partial t} + \sigma\mu V\right), \\ \Delta V - \varepsilon\mu\dfrac{\partial^2 V}{\partial t^2} - \sigma\mu\dfrac{\partial V}{\partial t} = \dfrac{\partial}{\partial t}\left(\text{div } \mathbf{A} + \varepsilon\mu\dfrac{\partial V}{\partial t} + \sigma\mu V\right), \end{cases} \tag{15}$$

tandis que les équations (7) restent inchangées. Ici σ représente la conductibilité électrique du milieu.

Par conséquent, en ce qui concerne les potentiels retardés **A**, V, la condition de Lorentz (8) se modifie, en devenant:

$$\text{div } \mathbf{A} + \varepsilon\mu\frac{\partial V}{\partial t} + \sigma\mu V = 0, \tag{16}$$

tandis que, la condition de Lorentz (9), relative aux antipotentiels retardés **A'**, V', reste inchangée. Dans ce contexte on peut poser le problème de déterminer les potentiels retardés **A**, V, en fonction du vecteur de Hertz, lorsque le milieu est dissipatif.

2. Le vecteur de Hertz en milieux dissipatifs

Si on maintient l'analogie avec le procédé utilisé dans le cas des milieux nondissipatifs, on peut définir, en se basant sur la condition de Lorentz (18), un vecteur de Hertz, **Z**, au moins dans les deux variantes ci-dessous, qui semblent les plus simples.

2.1. Variante I

Dans cette première variante on considère qu'on peut exprimer les potentiels retardés en fonction du vecteur de Hertz à l'aide des relations:

$$V = -\operatorname{div} \mathbf{Z}_{\mathrm{I}}, \qquad \mathbf{A} = \varepsilon\mu \frac{\partial \mathbf{Z}_{\mathrm{I}}}{\partial t} + \sigma\mu \mathbf{Z}_{\mathrm{I}}. \tag{17}$$

Compte tenu des expressions (2) on peut écrire, dans ce cas, les relations:

$$\begin{cases} \mathbf{E} = \operatorname{grad} \operatorname{div} \mathbf{Z}_{\mathrm{I}} - \varepsilon\mu \dfrac{\partial^2 \mathbf{Z}_{\mathrm{I}}}{\partial t^2} + \sigma\mu \dfrac{\partial \mathbf{Z}_{\mathrm{I}}}{\partial t}, \\ \mathbf{B} = \varepsilon\mu \dfrac{\partial (\operatorname{rot} \mathbf{Z}_{\mathrm{I}})}{\partial t} + \sigma\mu \operatorname{rot} \mathbf{Z}_{\mathrm{I}}. \end{cases} \tag{18}$$

Evidemment, pour $\sigma = 0$ en retrouve les relations (12) valables dans les milieux nondissipatifs.

2.2. Variantte II

Dans cette deuxième variante on admet que

$$\mathbf{A} = \varepsilon\mu \frac{\partial \mathbf{Z}_{\mathrm{II}}}{\partial t}, \tag{19}$$

de sorte que si on tient compte de (16), on peut écrire l'équation:

$$\varepsilon\mu \frac{\partial V}{\partial t} + \sigma\mu V + \varepsilon\mu \frac{\partial (\operatorname{div} \mathbf{Z}_{\mathrm{II}})}{\partial t} = 0, \tag{20}$$

ou, sous une forme équivalente:

$$\frac{\mathrm{d}V}{\mathrm{d}t} + \frac{1}{\tau} V + \frac{\mathrm{d}(\operatorname{div} \mathbf{Z}_{\mathrm{II}})}{\mathrm{d}t} = 0, \tag{21}$$

avec

$$\tau = \frac{\varepsilon}{\sigma} \tag{22}$$

– la constante de relaxation du milieu conducteur. On a pu substituer le symbole de dérivée partielle par celui de dérivée totale, compte tenu que dans l'équation (21) n'intervient pas, d'une manière explicite, que la variable t.

L'expression (21) représente une équation différentielle linéaire, à coefficients constants, du première ordre, dont la solution générale est [2]:

$$V = \mathrm{e}^{-\frac{t}{\tau}} \left[C - \int \mathrm{e}^{-\frac{t}{\tau}} \frac{\mathrm{d}(\operatorname{div} \mathbf{Z}_{\mathrm{II}})}{\mathrm{d}t} \mathrm{d}t \right], \tag{23}$$

ou C est une constante d'intégration. En intégrant par parties on obtient finalement l'expression

$$V = \mathrm{e}^{-\frac{t}{\tau}} \left[C - \mathrm{e}^{-\frac{t}{\tau}} \operatorname{div} \mathbf{Z}_{\mathrm{II}} + \frac{t}{\tau} \int \mathrm{e}^{-\frac{t}{\tau}} \operatorname{div} \mathbf{Z}_{\mathrm{II}} \, \mathrm{d}t \right]. \tag{24}$$

À l'aide des relations (2) on peut déterminer les expressions des vecteurs du champ:

$$(25)\qquad \begin{cases} \mathbf{E} = \operatorname{grad}\operatorname{div}\mathbf{Z}_{\mathrm{II}} - \varepsilon\mu\dfrac{\partial^2\mathbf{Z}_{\mathrm{II}}}{\partial t^2} - \dfrac{1}{\tau}\mathrm{e}^{-\frac{t}{\tau}}\displaystyle\int \mathrm{e}^{-\frac{t}{\tau}}\operatorname{grad}\operatorname{div}\mathbf{Z}_{\mathrm{II}}\,\mathrm{d}t, \\ \mathbf{B} = \varepsilon\mu\dfrac{\partial(\operatorname{rot}\mathbf{Z}_{\mathrm{II}})}{\partial t}. \end{cases}$$

Si le milieu est nondissipatif ($\sigma = 0$) on retrouve les expressions (13).

3. Les équations differentielles à dérivées partielles satisfaites par le vecteur de Hertz en milieux dissipatifs

Pour établir ces équations on exprime les vecteurs du champ électromagnétique, $\mathbf{E}$ et $\mathbf{B}$, en tant que sommes de leurs expressions écrites en fonction du vecteur de Hertz attaché aux potentiels retardés et, respectivement, en fonction du vecteur de Hertz attaché aux antipotentiels retardés. Compte tenu des relations (13), (18) et (25) on peut aboutir aux expressions:

$$(26)\qquad \begin{cases} \mathbf{E} = \operatorname{grad}\operatorname{div}\mathbf{Z}_{\mathrm{I}} - \varepsilon\mu\dfrac{\partial^2\mathbf{Z}_{\mathrm{I}}}{\partial t^2} - \sigma\mu\dfrac{\partial\mathbf{Z}_{\mathrm{I}}}{\partial t} - \mu\dfrac{\partial(\operatorname{rot}\mathbf{Z}')}{\partial t}, \\ \mathbf{B} = \varepsilon\mu\dfrac{\partial(\operatorname{rot}\mathbf{Z}_{\mathrm{I}})}{\partial t} + \mu\sigma\operatorname{rot}\mathbf{Z}_{\mathrm{I}} + \mu\left(\operatorname{grad}\operatorname{div}\mathbf{Z}' - \varepsilon\mu\dfrac{\partial^2\mathbf{Z}'}{\partial t^2}\right), \end{cases}$$

respectivement

$$(27)\qquad \begin{cases} \mathbf{E} = \operatorname{grad}\operatorname{div}\mathbf{Z}_{\mathrm{II}} - \varepsilon\mu\dfrac{\partial^2\mathbf{Z}_{\mathrm{II}}}{\partial t^2} - \dfrac{1}{\tau}\mathrm{e}^{-\frac{t}{\tau}}\displaystyle\int \mathrm{e}^{\frac{t}{\tau}}\operatorname{grad}\operatorname{div}\mathbf{Z}_{\mathrm{II}}\,\mathrm{d}t - \mu\dfrac{\partial(\operatorname{rot}\mathbf{Z}')}{\partial t}, \\ \mathbf{B} = \varepsilon\mu\dfrac{\partial(\operatorname{rot}\mathbf{Z}_{\mathrm{I}})}{\partial t} + \mu\left(\operatorname{grad}\operatorname{div}\mathbf{Z}' - \varepsilon\mu\dfrac{\partial^2\mathbf{Z}'}{\partial t^2}\right). \end{cases}$$

On substitue, successivement, les paires de relations (26), (27) dans les équations d'état:

$$(28)\qquad \operatorname{div}\mathbf{D} = \rho_v; \qquad \operatorname{div}\mathbf{B} = 0$$

du champ électromagnétique. Au préalable on tient compte et des équations de liaison entre les vecteurs $\mathbf{E}$, $\mathbf{D}$, $\mathbf{P}$, respectivement $\mathbf{H}$, $\mathbf{B}$, $\mathbf{M}$:

$$(29)\qquad \mathbf{D} = \varepsilon_0\mathbf{E} + \mathbf{P}, \qquad \mathbf{B} = \mu_0(\mathbf{H} + \mathbf{M}).$$

Tous calculs effectués et compte tenu des identités vectorielles [3]:

$$\operatorname{div}\operatorname{rot} \equiv 0, \qquad \operatorname{rot}\operatorname{rot} \equiv \operatorname{grad}\operatorname{div} - \Delta,$$

on obtient, finalement, les équations différentielles à dérivées partielles satisfaites par les vecteurs de Hertz $\mathbf{Z}_{\mathrm{I}}$, $\mathbf{Z}_{\mathrm{II}}$ et $\mathbf{Z}'$:

$$(30)\qquad \Delta\mathbf{Z}_{\mathrm{I}} - \varepsilon\mu\frac{\partial^2\mathbf{Z}_{\mathrm{I}}}{\partial t^2} - \sigma\mu\frac{\partial\mathbf{Z}_{\mathrm{I}}}{\partial t} = -\frac{\mathbf{P}}{\varepsilon_0}, \qquad \Delta\mathbf{Z}' - \varepsilon\mu\frac{\partial^2\mathbf{Z}'}{\partial t^2} = -\mathbf{M},$$

respectivement

$$(31)\qquad \begin{cases} \Delta \mathbf{Z}_{\mathrm{II}} - \varepsilon\mu \dfrac{\partial^2 \mathbf{Z}_{\mathrm{II}}}{\partial t^2} - \dfrac{1}{\tau} e^{-\frac{t}{\tau}} \displaystyle\int e^{-\frac{t}{\tau}} \Delta \mathbf{Z}_{\mathrm{II}}\, dt = -\frac{\mathbf{P}}{\varepsilon_0}, \\ \Delta \mathbf{Z}' - \varepsilon\mu \dfrac{\partial^2 \mathbf{Z}'}{\partial t^2} = -\mathbf{M}. \end{cases}$$

On a utilisé d'une telle manière les équations du champ électromagnétique de sorte que la contribution de la densité du courant de conduction soit inclue dans la magnétisations et celle de la densité volumétrique de la charge électrique libre, dans la polarisation.

On doit observer que l'équation satisfaite par $\mathbf{Z}'$ est la même tant dans le cas des milieux dissipatifs que dans celui des milieux nondissipatifs, ce qui représente la conséquence du fait que la condition de Lorentz est la même dans les deux variantes étudiées ci-dessus.

Pour $\sigma = 0$ $(\tau \to \infty)$ on retrouve les équations différentielles à dérivées partielles (14) satisfaites par les vecteurs de Hertz, $\mathbf{Z}$, $\mathbf{Z}'$, dans le cas des milieux nondissipatifs.

4. Conclusions

1. On définit les vecteur de Hertz $\mathbf{Z}$, $\mathbf{Z}'$ attachés, respectivement, aux potentiels et antipotentiels électromagnétiques retardés, dans le cas des milieux dissipatifs, en deux variantes distinctes ($\mathbf{Z}_{\mathrm{I}}$, $\mathbf{Z}'$; $\mathbf{Z}_{\mathrm{II}}$, $\mathbf{Z}'$) et on établit, les relations de calcul des vecteurs d'état du champ électromagnétique, $\mathbf{E}$ et $\mathbf{B}$, en fonction des vecteurs $\mathbf{Z}_{\mathrm{I}}$ (ou $\mathbf{Z}_{\mathrm{II}}$) et $\mathbf{Z}'$.

2. On prouve que le vecteur de Hertz attaché aux antipotentiels retardés a la même expression tant en milieux dissipatifs qu'en ceux nondissipatifs.

3. On établit les équations différentielles à dérivées partielles satisfaites par les vecteurs de Hertz $\mathbf{Z}_{\mathrm{I}}$, $\mathbf{Z}_{\mathrm{II}}$ et $\mathbf{Z}'$, dans le cas des milieux dissipatifs.

Reçue le 9 décembre 1998
Revisée le 7 janvier 2001

Université Technique „Gh. Asachi", Jassy,
Chaire d'Electrotechnique

BIBLIOGRAPHIE

1. Nicolau Edm., *Propagarea undelor electromagnetice.* Vol.**I**, Ed. Acad., Bucureşti, 1960.
2. Cordunea'nu A., *Ecuaţii diferenţiale cu aplicaţii în electrotehnică.* Ed. Facla, Timişoara, 1981.
3. Beju I., Sobs E., Teodorescu P.P., *Tehnici de calcul vectorial cu aplicaţii.* Ed. Tehnică, Bucureşti, 1976.

VECTORUL LUI HERTZ ÎN MEDII DISIPATIVE

(Rezumat)

Se definesc vectorii lui Hertz, $\mathbf{Z}$ şi $\mathbf{Z}'$, ataşaţi, respectiv, potenţialelor şi antipotenţialelor electromagnetice întârziate, în cazul mediilor disipative, în două variante ($\mathbf{Z}_{\mathrm{I}}$, $\mathbf{Z}'$; $\mathbf{Z}_{\mathrm{II}}$, $\mathbf{Z}'$) şi se stabilesc relaţiile de calcul ale vectorilor de stare ai câmpului electromagnetic, $\mathbf{E}$, $\mathbf{B}$, în funcţie de vectorii $\mathbf{Z}_{\mathrm{I}}$ (sau $\mathbf{Z}_{\mathrm{II}}$) şi $\mathbf{Z}'$.

În acelaşi timp se stabilesc ecuaţiile diferenţiale cu derivate parţiale satisfăcute de vectorii $\mathbf{Z}_{\mathrm{I}}$, $\mathbf{Z}_{\mathrm{II}}$ şi $\mathbf{Z}'$, în cazul unor medii disipative.

BULETINUL INSTITUTULUI POLITEHNIC DIN IAŞI
Tomul XLVII (LI), Fasc. 3–4, 2001
ELECTROTEHNICĂ. ENERGETICĂ. ELECTRONICĂ

D.C. 512

AN ALGORITHM FOR THE MAXIMIZATION OF RATIONAL FUNCTIONS OVER LINEAR DOMAINS

BY

VALERIU MUNTEANU and DANIELA TĂRNICERIU

The well-known B a u m – E a g o n inequality [1] provides an effective iterative scheme for finding a local maximum for homogeneous polynomials with positive coefficients over a domain of probability values. However, in many applications we are interested in maximizing a general rational function. We try to extend the Baum–Eagon inequality to rational functions. We briefly describe some of the applications of this inequality to statistical estimation problems.

1. Introduction

In this paper we design an algorithm for the maximization of rational functions over linear domains. The algorithm we develop is an extension of the well-known inequality that was derived by B a u m and E a g o n [1] for an arbitrary homogeneous polynomial $P(X) = P(\{X_{ij}\})$ with nonnegative coefficients of degree n in variables X_{ij}, $(i = 1, ..., p;\ j = 1, ..., q_i)$. Assuming that this polynomial is defined over a domain of probability values, $D : x_{ij} \geq 0,\ \sum_{j=1}^{q_i} x_{ij} = 1$, they showed how to construct a transformation $T : U \to D$ for some $U \subseteq D$ such that the following property holds:

P r o p e r t y 1. *For any* $x \in U$ *and* $y = T(x)$, $P(y) > P(x)$, *unless* $y = x$.

Polynomials of this type appear in various statistical problems dealing with the estimation of probabilistic functions of Markov processes *via* the maximum likelihood technique. In certain statistical problems estimation of parameters was done *via* some other criteria that use conditional likelihood and mutual information [2]. These problems require finding local maxima for rational functions over domains of probability values.

Let the domain D (previously defined) and a rational function $R(X) = P_1(x)/P_2(X)$, where $P_1(X)$, $P_2(X)$ are polynomials with real coefficients in variables $X = \{X_{ij}\}$ and $P_2(X)$ has only positive values in D. We provide a way for constructing a large class of transformations $T : D \to D$ such that the analog of the Property 1 (with $R(X)$ instead of $P(X)$) holds.

P r o p e r t y 2. *For any* $x \in D$ *and* $y = T(x)$, $R(y) > R(x)$, *unless* $y = x$.

If a transformation $T : D \to D$ satisfies Property 1 we will say that T is a growth transformation of D for $R(X)$.

2. The Case of Rational Functions

In this section we show how to find growth transformations for rational functions. Recall that $R(X) = P_1(x)/P_2(X)$ is a ratio of two polynomials $P_1(X)$, $P_2(X)$, in variables $X = \{X_{ij}\}$, $(i = 1, ..., p; j = 1, ..., q_i)$ defined over a domain

$$D : x_{ij} \geq 0, \qquad \sum_{j=1}^{q_i} x_{ij} = 1. \tag{1}$$

For simplicity we assume throughout this paper that $P_2(x) > 0$ for any $x \in D$. We are looking for a growth transformation $T : D \to D$, such that the Property 2 holds.

First we show that for any $x \in D$ there exists a polynomial $P_x(X)$ such that if $P_x(y) > P_x(x)$, $y \in D$, then $R(y) > R(x)$. With that end in view it is enough to set $P_x(X) = P_1(X) - R(x)P_2(X)$. Indeed, it is easy to see that $P_x(x) = 0$ and, therefore, if $P_x(y) > P_x(x) = 0$, then $R(y) > R(x)$.

Now suppose that for each polynomial $P_x(X)$, $x \in D$, we could construct a growth transformation T_x of D, such that $P_x(T_x(y)) > P_x(y)$ for any $y \in D$ unless $y = T_x(y)$. Then we could define a growth transformation T of D for $R(X)$ as follows:

$$T(y) = T_y(y), \tag{2}$$

for any $y \in D$. The fact that T is a growth transformation would follow from the fact that $R(T(y)) > R(y)$ if $P_y(T_y(y)) > P_y(y)$. Thus we see that we can construct growth transformations for rational functions if we could do so for an arbitrary polynomial.

We mean to prove that for any polynomial $P_y(X)$, there exists a polynomial $P'_y(X)$ with nonnegative coefficients such that any growth transformation of D for the $P'_y(X)$ is also a growth transformation for $P_y(X)$. This statement results in the following

P r o p o s i t i o n 1. *Let* $P(X) = P(\{X_{ij}\})$ *be a polynomial with real coefficients in variables* X_{ij}, $(i = 1, ..., p; j = 1, ..., q_i)$. *Let be a domain* D *with* $x_{ij} \geq 0$, $\sum_{j=1}^{q_i} x_{ij} = 1$. *Then*

a) *There exists a polynomial* $C(X)$ *such that the polynomial* $P'(X) = P(X) + C(X)$ *has only nonnegative coefficients, such that the value* $C(X)$ *at any* $x \in D$ *is a constant (independent of* x*).*

b) *The set of growth transformation of* D *for* $P(X)$ *coincides with the set of growth transformations for* $P'(X)$.

P r o o f.

a) Let n be the degree of $P(X)$ and a its minimal negative coefficient ($a=0$ if no negative coefficient exists). Then a polynomial

$$C(X) = -a\left(\sum_{i=1,\,j=1}^{p,q_i} X_{ij} + 1\right)^n \tag{3}$$

is constant in D (its value in D is equal to $-a(p+1)^n$ since $\sum_{j=1}^{q_i} x_{ij} = 1$). Now, every possible monomial in $P(X)$ also occurs in $C(X)$. Since $a \neq 0$ is the smallest negative coefficient in $P(X)$, it is easily to see that the sum of the coefficients of corresponding monomials in $P(X)$ and $C(X)$ is nonnegative.

b) Since $P'(X)$ and $P(X)$ differ only by a constant in D, it is clear that $P'(y) > P'(x)$ for any $y, x \in D$, if and only if $P(y) > P(x)$.

Now, in order to be able to apply the Baum–Eagon inequality, it remains to show that the problem of finding a growth transformation for a polynomial with nonnegative coefficients can be reduced to the same problem for a homogeneous polynomial with nonnegative coefficients. With that end in view we proceed as follows. Let $P'(X)$ be as before, let n be the degree of $P'(X)$ and let us consider the homogeneous polynomial

$$P''(Y) = P''(\{Y_{km}\}) = Y_{p+1,1}^n P'(\{Y_{ij}/Y_{p+1,1}\}) \tag{4}$$

in variables Y_{km}, $(k = 1,...,p+1;\ m = 1,...,q_i)$, where $q_{p+1} = 1$. In other words $P''(Y)$ is obtained from $P'(X)$ by substituting $X_{ij} = Y_{ij}/Y_{p+1,1}$ and multiplying $P'(\{Y_{ij}/Y_{p+1,1}\})$ by $Y_{p+1,1}^n$. Since the new polynomial, $P''(Y)$, has one more variable than P' growth transformation for P'' will be considered in the following domain:

$$D' : \sum_{j=1}^{q_i} y_{ij} = 1, \quad y_{ij} \geq 0, \quad (i = 1,...,p+1;\ j = 1,...,q_i). \tag{5}$$

The additional variable $Y_{p+1,1}$ is equal to 1 in Y'. Therefore, in fact, the pair $(P''(X), D')$ is an equivalent representation of the pair $(P''(X), D)$ in the sense that there is the bijection $f : D \to D'$, mapping $x = \{x_{ij}\} \in D$ into $x' = \{y_{km}\}$, such that $x_{ij} = y_{ij}$ for $(i,j) \neq (p+1,1)$ and such that for any $x \in D$, $P'(x) = P''(f(x))$. Thus, if T is a growth transformation for P'', then the composition of the maps $f^{-1}Tf$ is a growth transformation for P'.

Summarizing, we see that for a rational function, $R(X)$, over domain D, one can construct a family of homogeneous polynomials with nonnegative coefficients parametrized by points x in D such that a growth transformation of D for $R(X)$ can be reconstructed from a family of growth transformations for these polynomials.

3. Growth Transformation for Rational Functions

In this section we keep the notation of § **2** and in addition we give some new definitions. Given a rational function, $R(X)$, and a real number, C, let

$$\Gamma_{ij}(x;C) = x_{ij}\left(\frac{\partial P_x}{\partial X_{ij}}(x) + C\right) \tag{6}$$

and

$$\Gamma_i(x;C) = \sum_{j=1}^{q_i} \Gamma_{ij}(x;C). \tag{7}$$

We call C *admissible* (for $R(X)$) if for any i, j and $x \in D, \Gamma_{ij}(x;C) \geq 0$, and $\Gamma_i(x;C) > 0$. For any admissible C we consider the transformation T^C of D whose ij coordinate is defined as

$$(T^C(x))_{ij} = \frac{\Gamma_{ij}(x;C)}{\Gamma_i(x;C)}. \tag{8}$$

(It is easy to see that this definition is correct, *i.e.*, T^C maps D into itself). Now we can describe some growth transformations of $R(X)$.

P r o p o s i t i o n 2. *Let $R(X)$ be a rational function in variables X_{ij}. There exists a constant, N_R, such that any $C \geq N_R$ is admissible for $R(X)$ and for any C a map T^C is a growth transformation of D for $R(X)$.*

P r o o f. In the proof of this proposition we will follow the same steps as those from § **2**. Thus, it follows that for any $x \in D$, there exists a constant N_x such that the following polynomial has only nonnegative coefficients $P_x(X) + C_x(X)$, where

$$C_x(X) = N_x\left(\sum_{i=1,j=1}^{p,q_i} X_{ij} + 1\right)^n \tag{9}$$

and n is the degree of P_x. Since, by assumption, $R(X)$ has no poles in the compact set D, one can find $N \geq N_x$ for all $x \in D$, such that for any $C \geq N$ multiplied by a factor (that will be derived below), the transformation T_x^C of D constructed from the polynomial $P_x(X) + C_x(X)$ is a growth transformation for it. For this C a family of growth transformations for $R(X)$ can be constructed following (2):

$$T^C(x) = T_x^C(x), \tag{10}$$

for all $x \in D$.

In order to compute explicitly these growth transformations, let us note that the polynomial

$$\frac{\partial\left(\sum\limits_{i=1,j=1}^{p,q_i} X_{ij} + 1\right)^n}{\partial X_{ij}} = n\left(\sum_{i=1,j=1}^{p,q_i} X_{ij} + 1\right)^{n-1} \tag{11}$$

is equal to $n(p+1)^{n-1}$ at any point in D. Combining this remark with (10), we have

$$\left(T^C(x)\right)_{ij} = \left(T_x^C(x)\right)_{ij} = \frac{x_{ij}\left(\frac{\partial P_x(x)}{\partial X_{ij}} + C\right)}{\sum\limits_{j=1}^{q_i} x_{ij}\left(\frac{\partial P_x(x)}{\partial X_{ij}} + C\right)}, \tag{12}$$

where $C \geq N_R = Nn(p+1)^{n-1}$ and $N = \max_x N_x$.

The class of growth transformations T_R^C, that was considered in Proposition 2, was derived from certain family of polynomials $C_x(X)$. The following extension of Proposition 2 illustrates this point.

Let $\hat{C} = \{C_i\}$, $(i = 1, ..., p)$, be a vector in p-dimensional real space and let

$$\Gamma_{ij}(x; \hat{C}) = x_{ij}\left(\frac{\partial P_x(x)}{\partial X_{ij}} + C_i\right), \tag{13}$$

$$\Gamma_i(x; \hat{C}) = \sum_{j=1}^{q_i} \Gamma_{ij}(x; \hat{C}). \tag{14}$$

As we did before, we call a vector $\hat{C}$ admissible for $R(X)$ if for any i, j and $x \in D$, $\Gamma_{ij}(x; \hat{C}) \geq 0$ and $\Gamma_i(x; \hat{C}) > 0$. For any admissible vector, $\hat{C}$, we consider the transformation of D that is defined as

$$(T^{\hat{C}}(x))_{ij} = \frac{\Gamma_{ij}(x; \hat{C})}{\Gamma_i(x; \hat{C})}. \tag{15}$$

With this notation, we have the following

P r o p o s i t i o n 3. *Let $R(X)$ be a rational function in variables X_{ij}. There exists a constant, N_R, such that any p-dimensional vector, $\hat{C}$, with all its components $C_i \geq N_R$ is admissible for $R(X)$ and for any such a vector $\hat{C}$, a map $T^{\hat{C}}$ is a growth transformation of D for $R(X)$.*

P r o o f. In fact, the constant N_R in the formulation of this proposition can be taken the same as the one in the proof of Proposition 2. It is easy to see that if we take the admissible polynomials that were considered in the proof of Proposition 2 and add to them the polynomial

$$\sum_{i=1}^{p}(C_i - N_R)\left(\sum_{j=1}^{q_i} X_{ij}\right), \tag{16}$$

then, the new family of polynomials will be admissible for $R(X)$. Repeating the computations similar to (12), we come to the formula (15).

It makes sense also to give the general description of growth transformations attached to arbitrary polynomials that were considered in Proposition 1. Let $\Theta = \{C_x(X), x \in D\}$ be a family of polynomials in variables X_{ij}. Let

$$\Gamma_{ij}(x;\Theta) = x_{ij}\left(\frac{\partial P_x(x)}{\partial X_{ij}} + \frac{\partial C_x(x)}{\partial X_{ij}}\right), \tag{17}$$

$$\Gamma_i(x;\Theta) = \sum_{j=1}^{q_i} \Gamma(x;\Theta). \tag{18}$$

We say that this family of polynomials Θ is admissible for $R(X)$, if for any i, j and $x \in D$, $\Gamma_{ij}(x;\Theta) \geq 0$ and $\Gamma_i(x;\Theta) > 0$. These admissible polynomial families give rise to the following set of transformations of D:

$$(T(x))_{ij} = \frac{\Gamma_{ij}(x;\Theta)}{\Gamma_i(x;\Theta)}. \tag{19}$$

Under the previous notation, we have the following

P r o p o s i t i o n 4. *Let $R(X)$ be a rational function in variables X_{ij}. Let $\Theta = \{C_x(X), x \in D\}$ be an admissible family of polynomials for $R(X)$, such that for any $x \in D$, $P_x(X) + C_x(X)$ has nonnegative coefficients and the polynomial $C_x(X)$ is constant in D. Then T, defined by (19), is a growth transformation of D.*

P r o o f. The proof is similar to those for the Propositions 2 and 3.

4. Conclusions

We presented an algorithm for the maximization of certain rational functions defined over domains of probability values. This algorithm is an extension of a method presented first by B a u m and E a g o n [1] and then by others [3], [4]. Our algorithm find applications in several areas including problems arising in statistics.

Received, June 15, 2001

Technical University "Gh.Asachi", Jassy,
Department of Telecommunications

REFERENCES

1. B a u m L.E., E a g o n J.A., *An Inequality with Applications to Statistical Prediction for Functions of Markov Processes and to a Model of Ecology.* Bull. Amer. Math. Soc., **73**, 360–363 (1967).
2. B a h l L.R., J e l i n e k F., M e r c e r R.L., *A Maximum Likelihood Approach to Continuous Speech Recognition.* IEEE Trans., Pattern Anal. Machine Intell., **5**, 79–190 (1983).
3. B a u m L.E., S e l l G., *Growth Transformations for Functions on Manifolds.* Pacific J. Math., **27**, 211–227 (1968).
4. B a u m L.E., P e t r i e T., S o u l e s G., W e i s s N., *A Maximization Technique Occuring in the Statistical Analysis of Probabilistic Functions of Markov Chains.* Ann. Math. Statist., **41**, 164–171 (1970).

UN ALGORITM PENTRU MAXIMIZAREA FUNCŢIILOR RAŢIONALE PESTE DOMENII LINIARE

(Rezumat)

Se stabileşte o extindere a inegalităţii Baum-Eagon la funcţii raţionale definite peste domenii de valori probabilistice. Se specifică succint aplicaţiile posibile ale acestui algoritm în probleme de estimări statistice.

BULETINUL INSTITUTULUI POLITEHNIC DIN IAŞI
Tomul XLVII (LI), Fasc. 3–4, 2001
ELECTROTEHNICĂ. ENERGETICĂ. ELECTRONICĂ

C.D. 621.392.5

QUELQUES APPLICATIONS DE CERTAINES IDENTITÉS ET INÉGALITÉS ALGÉBRIQUES DANS LA THÉORIE DES CIRCUITS ÉLECTRIQUES

PAR
HUGO ROSMAN

L'idée de base utilisée dans ce travail est celle de valorifier certaines identités et inégalités algébriques, assimilant les grandeurs qui y interviennent à des signaux ou paramètres rencontrés dans la théorie des circuits électriques. Si on associe aux identités et inégalités algébriques mentionnées certaines lois, théorèmes et relations de calcul spécifiques, on peut aboutir à des conséquences de celles-ci, présentant un certain intérêt dans la théorie des circuits électriques.

1. Introduction

Les identités algébriques et, quelquefois, les inégalités algébriques ont prouvé leurs utilité dans l'étude des circuits électriques, permettant à obtenir parfois des résultats remarquables. Un exemple dans ce sens est celui de l'utilisation extrèmement bénéfique de l'identité de Lagrange, par C.I. B u d e a n u [1] en vue d'établir la relation de calcul de la puissance déformante dans un circuit linéaire monophasé, en régime permanent périodique nonharmonique.

Elargissant le cadre, dans ce qui suit, on a eu en vue l'utilisation de certaines identités et inégalités algébriques, connues, dans le but d'établir une série de conséquences inédites d'un nombre de lois et théorèmes appartenant à la théorie des circuits électriques. Il est question, en premier lieu, d'exprimer les identités et les inégalités se trouvant dans la littérature de spécialité, ayant un profil algébrique, dans un language adéquat, utilisant des grandeurs représentant des signaux ou des paramètres électriques et deuxièmement de combiner d'une façon avantageuse les identités et inegalités algébriques ainsi obtenues avec des lois et théorèmes connus de la théorie des circuits électriques. On peut obtenir, par cette voie, nombre de conséquences de ces lois et théorèmes qui élargissent leur sphère d'application.

2. Quelques identités et inégalités algébriques

Dès le début on doit préciser que, dans ce qui suit, on utilise, dans le but proposé, seulement quelques identités et inégalités algébriques; il s'agit de

a) l'identité (par ex. [2]):

$$(1)\quad \left(\sum_{i=1}^{n} a_i c_i\right)\left(\sum_{i=1}^{n} b_i d_i\right) - \left(\sum_{i=1}^{n} a_i d_i\right)\left(\sum_{i=1}^{n} b_i c_i\right) = \sum_{\substack{j=1\\ j<k}}^{n}\sum_{k=1}^{n} (a_j b_k - a_k b_j)(c_j d_k - c_k d_j),$$

où $a_i, b_i, c_i, d_i \in \mathbb{R}$, $(i = \overline{1,n})$;

b) l'identité de Lagrange:

$$(2)\quad \left(\sum_{i=1}^{n} a_i^2\right)\left(\sum_{i=1}^{n} b_i^2\right) - \left(\sum_{i=1}^{n} a_i b_i\right)^2 = \sum_{\substack{j=1\\ j<k}}^{n}\sum_{k=1}^{n} (a_j b_k - a_k b_j)^2,$$

qui représente un cas particulier de l'identité (1), si $a_i = c_i$, $b_i = d_i$, $(i = \overline{1,n})$;

c) les inégalités:

$$(3)\quad \left(\sum_{i=1}^{n} a_i^2\right)\left(\sum_{i=1}^{n} b_i^2\right) \geq \left(\sum_{i=1}^{n} a_i b_i\right)^2,$$

$$(4)\quad \left(\sum_{i=1}^{n} a_i^2\right)\left(\sum_{i=1}^{n} b_i^2\right) = \sum_{\substack{j=1\\ j<k}}^{n}\sum_{k=1}^{n} (a_j b_k - a_k b_j)^2,$$

qui découlent de l'identité (2), la première de celles-ci étant connue sous le nom de l'inégalité de S c h w a r t z - B u n i a k o v s k y (par ex. [3]);

d) l'inégalité

$$(5)\quad \int_{t_1}^{t_2} a^2(t)\,\mathrm{d}t \int_{t_1}^{t_2} b^2(t)\,\mathrm{d}t \geq \left[\int_{t_1}^{t_2} a(t)b(t)\,\mathrm{d}t\right]^2,$$

qui représente la forme intégrale de l'inegalité (3).

Certains cas particuliers, comme, par exemple, ceux où $c_i = 1/a_i$, $d_i = 1/b_i$, seront envisagés dans une recherche ultérieure. Avec la même occasion on utilisera aussi d'autres inégalités, comme, par exemple, celles de C a u c h y - H ö l d e r, M i n k o w s k y, J e n s e n (par ex. [4]).

3. Exemples d'utilisation des identités et des inégalités algébriques dans la théorie des circuits électriques

Dans ce paragraphe on se propose d'illustrer par une série d'exemples, le mode d'association des identités et inégalités mentionnés dans le § **2**, avec certaines lois, théorèmes et relations de calcul appartenant à la théorie des circuits électriques, avec des conséquences avantageuses.

3.1. Loi d'Ohm pour des circuits linéaires fonctionnant en régime stationnaire

Si on considère une branche active d'un circuit linéaire en régime stationnaire, la loi d'Ohm est donnée par la relation bien connue:

$$E_{ei} \pm U_i = R_i I_i, \quad (i = \overline{1, B}), \tag{6}$$

où B représente le nombre des branches du circuit considéré, le reste des notations étant celles usuelles. Avec les substitutions $a_i = R_i$, $b_i = I_i$ et tenant compte de (6), l'identité (2) et les inégalités (3), (4) deviennent:

$$\sum_{i=1}^{B} R_i^2 \sum_{i=1}^{B} I_i^2 - \sum_{\substack{j=1 \\ j<k}}^{B} \sum_{k=1}^{B} (R_j I_k - R_k I_j)^2 = \left[\sum_{i=1}^{B} (E_{ei} \pm U_i)\right]^2, \tag{7}$$

respectivement

$$\sum_{i=1}^{B} R_i^2 \sum_{i=1}^{B} I_i^2 \geq \left[\sum_{i=1}^{B} (E_{ei} \pm U_i)\right]^2, \tag{8}$$

$$\sum_{i=1}^{B} R_i^2 \sum_{i=1}^{B} I_i^2 \geq \sum_{\substack{j=1 \\ j<k}}^{B} \sum_{k=1}^{B} (R_j I_k - R_k I_j)^2. \tag{9}$$

3.2. Le théorème des tensions, établi par Kirchhoff, pour les circuits linéaires fonctionnant en régime stationnaire

Soit une boucle, B_p (indépendente ou pas), d'un circuit linéaire en régime stationnaire et une branche, i, supposée à être incidente à cette boucle. Si on utilise les notations usuelles, le théorème des tensions, établi par Kirchhoff, appliqué à cette boucle permet à écrire la relation connue:

$$\sum_{i \in B_p} E_{ei} = \sum_{i \in B_p} R_i I_i, \quad (p = \overline{1, N_b}), \tag{10}$$

où N_b représente le nombre de boucles. Si on utilise cette même fois les notations $a_i = R_i$, $b_i = I_i$, l'identité (2) et les inégalités (3), (4) deviennent, compte tenu de (10):

$$\left(\sum_{i \in B_p} R_i^2\right)\left(\sum_{i \in B_p} I_i^2\right) - \left(\sum_{i \in B_p} E_{ei}\right)^2 = \sum_{\substack{j \in B_p \\ j<k}} \sum_{k \in B_p} (R_j I_k - R_k I_j)^2, \tag{11}$$

$$\left(\sum_{i \in B_p} R_i^2\right)\left(\sum_{i \in B_p} I_i^2\right) \geq \left(\sum_{i \in B_p} E_{ei}\right)^2, \tag{12}$$

$$\left(\sum_{i\in B_p} R_i^2\right)\left(\sum_{i\in B_p} I_i^2\right) \geq \sum_{j\in B_p}\sum_{\substack{k\in B_p \\ j<k}} (R_jI_k - R_kI_j)^2, \tag{13}$$

La dernière inégalité devient une identité dans le cas d'une boucle passive.

3.3. La puissance dans les circuits monophasés fonctionnant en régime permanent harmonique

On considère un circuit monophasé, isolé, fonctionnant dans un régime quasistationnaire, de type magnétique, ayant B branches parcourues par les courants i_j et les tensions de branche u_j, $(j = \overline{1, B})$. La puissance instantanée échangée entre les branches du circuit, par les bornes de celles-ci, est, dans ce cas, nulle:

$$\sum_{i=1}^{B} u_i i_i = 0. \tag{14}$$

Si on effectue, dans l'identité (2) et l'inégalité (5), les substitutions $a_i = u_i$, $b_i = i_i$, on obtient

$$\sum_{i=1}^{B} u_i^2 \sum_{i=1}^{B} i_i^2 \geq \sum_{j=1}^{B}\sum_{\substack{k=1 \\ j<k}}^{B} (u_ji_k - u_ki_j)^2, \tag{15}$$

respectivement

$$\int_{t_1}^{t_2} u_i^2(t)\,\mathrm{d}t \int_{t_1}^{t_2} i_i^2(t)\,\mathrm{d}t \geq \left[\int_{t_1}^{t_2} u_i(t)i_i(t)\,\mathrm{d}t\right]^2, \quad (i = \overline{1, B}), \tag{16}$$

valables pour n'importe quelle forme de variation en fonction du temps des tensions $u_i(t)$ et des courants $i_i(t)$. Si le régime du circuit est permanent périodique et $t_1 = 0$, $t_2 = T$, avec T – la période des signaux, l'inégalité (16) devient

$$S_i^2 > P_i^2, \quad (i = \overline{1, B}),$$

ce qui représente, évidement, une banalité.

3.4. Les puissances dans les circuits linéaires triphasés

Une première application des identités et des inégalités algébriques mentionnées dans le § **2**, concernant le domaine des circuits triphasés, est possible si dans l'identité (2) on effectue les substitutions $a_i = u_i$, $b_i = i_i$, $(i = 1, 2, 3)$, et on note avec $p = \sum_{i=1}^{3} u_i i_i$ la puissance instantanée totale dans le circuit triphasé considéré; on obtient:

$$p = \sum_{i=1}^{3} u_i^2 \sum_{i=1}^{3} i_i^2 - \sum_{j=1}^{3}\sum_{\substack{k=1 \\ j<k}}^{3} (u_ji_k - u_ki_j)^2 \tag{17}$$

et, évidemment, l'inégalité

$$p \geq \sum_{i=1}^{3} u_i^2 \sum_{i=1}^{3} i_i^2. \tag{18}$$

On peut obtenir d'autres applications utilisant, dans la même identité (2), les substitutions $a_i = U_i$, $b_i = I_i \cos\varphi_i$ ou $a_i = U_i \cos\varphi_i$, $b_i = I_i$, qui permettent à établir de nouveaux relations de calcul de la puissance active à savoir:

$$P^2 = \sum_{i=1}^{3} U_i^2 \sum_{i=1}^{3} I_i^2 \cos^2\varphi_i - \sum_{\substack{j=1 \\ j<k}}^{3} \sum_{k=1}^{3} (U_j I_k \cos\varphi_k - U_k I_j \cos\varphi_j)^2, \tag{19}$$

respectivement

$$P^2 = \sum_{i=1}^{3} U_i^2 \cos^2\varphi_i \sum_{i=1}^{3} I_i^2 - \sum_{\substack{j=1 \\ j<k}}^{3} \sum_{k=1}^{3} (U_j I_k \cos\varphi_j - U_k I_j \cos\varphi_k)^2. \tag{20}$$

D'une façon analogue, si on effectue, dans l'identité (2), les substitutions $a_i = U_i$, $b_i = I_i \sin\varphi_i$ ou $a_i = U_i \sin\varphi_i$, $b_i = I_i$ on obtient une paire de nouvelles relations de calcul de la puissance réactive

$$Q^2 = \sum_{i=1}^{3} U_i^2 \sum_{i=1}^{3} I_i^2 \sin^2\varphi_i - \sum_{\substack{j=1 \\ j<k}}^{3} \sum_{k=1}^{3} (U_j I_k \sin\varphi_k - U_k I_j \sin\varphi_j)^2, \tag{21}$$

respectivement

$$Q^2 = \sum_{i=1}^{3} U_i^2 \sin^2\varphi_i \sum_{i=1}^{3} I_i^2 - \sum_{\substack{j=1 \\ j<k}}^{3} \sum_{k=1}^{3} (U_j I_k \sin\varphi_j - U_k I_j \sin\varphi_k)^2. \tag{22}$$

On peut ajouter aux relations (19),...,(22) les inégalités évidentes:

$$P^2 \leq \sum_{i=1}^{3} U_i^2 \sum_{i=1}^{3} I_i^2 \cos^2\varphi_i, \quad P^2 \leq \sum_{i=1}^{3} U_i^2 \cos^2\varphi_i \sum_{i=1}^{3} I_i^2, \tag{23}$$

respectivement

$$Q^2 \leq \sum_{i=1}^{3} U_i^2 \sum_{i=1}^{3} I_i^2 \sin^2\varphi_i, \quad Q^2 \leq \sum_{i=1}^{3} U_i^2 \sin^2\varphi_i \sum_{i=1}^{3} I_i^2. \tag{24}$$

O b s e r v a t i o n s.

1° Les relations (17) et (18) sont valables pour des circuits triphasés symétriques ou non-symétriques, fonctionnant en régime variable quelconque, mais quasistationnaire, de type magnétique.

2° Les relations (19),...,(24) correspondent au cas où le régime de fonctionnement du circuit triphasé considéré (symétrique ou non-symétrique) est permanent harmonique.

3.5. Le théorème de Tellegen

Soient deux circuits électriques ayant les mêmes graphes topologique orientés. Les tensions de branche et les courants dans les branches de ces circuits satisfont les relations:

$$\sum_{k=1}^{B} u_i^{(I)}(t')i_i^{(II)}(t'') = 0, \quad \sum_{k=1}^{B} u_i^{(II)}(t')i_i^{(I)}(t'') = 0, \tag{25}$$

où: I et II représentent chacun des deux circuits, $u_i^{(I)}(t')$ – la tension aux bornes de la branche i, $(i = \overline{1,B})$, du circuit I, dans le moment t', $u_i^{(II)}(t')$ – la tension aux bornes de la branche i du circuit II, au moment t', $i_i^{(I)}(t'')$ – le courant circulant par la branche i du circuit I, dans le moment t'', $i_i^{(II)}(t'')$ – le courant qui circule par la branche i du circuit II, au moment t''. En général les moments t' et t'' sont différents $(t' \neq t'')$ mais il y a aussi la possibilité qu'ils coïncident $(t' = t'')$. Les relations (24) sont conues dans la littérature de spécialité comme représentant l'enoncé du théorème de T e l l e g e n [5].

Si, dans l'identité (1), on utilise les substitutions $a_i = u_i^{(I)}(t')$, $b_i = u_i^{(II)}(t')$, $c_i = i_i^{(II)}(t'')$, $d_i = i_i^{(I)}(t'')$ ou $a_i = u_i^{(I)}(t')$, $b_i = u_i^{(II)}(t')$, $c_i = i_i^{(I)}(t'')$, $d_i = i_i^{(II)}(t'')$ et on tient compte des relations (25) on obtient l'expression:

$$\left[\sum_{i=1}^{B} u_i^{(I)}(t')i_i^{(I)}(t'')\right]\left[\sum_{i=1}^{B} u_i^{(II)}(t')i_i^{(II)}(t'')\right] =$$

$$= \sum_{\substack{j=1 \\ j<k}}^{B}\sum_{k=1}^{B}\left[u_j^{(I)}(t')u_k^{(II)}(t') - u_k^{(I)}(t')u_j^{(II)}(t')\right]\left[i_j^{(I)}(t'')i_k^{(II)}(t'') - i_k^{(I)}(t')i_j^{(II)}(t'')\right], \tag{26}$$

que l'on peut considérer comme une généralisation du théorème de Tellegen.

On peut obtenir une autre généralisation du même théorème si on utilise, dans l'identité (2), les substitutions: $a_i = u_i^{(I)}(t')$, $b_i = i_i^{(II)}(T'')$, en résultant la relation:

$$\sum_{i=1}^{B} u_i^{(I)^2}(t')\sum_{i=1}^{B} i_i^{(II)^2}(t'') = \sum_{\substack{j=1 \\ j<k}}^{B}\sum_{k=1}^{B}\left[u_j^{(I)}(t')i_k^{(II)}(t'') - u_k^{(I)}(t')i_j^{(II)}(t'')\right]^2. \tag{27}$$

4. Conclusions

On essaye à valorifier les identités algébriques (1), (2) et les inégalités (3),...,(5), en attribuant aux grandeurs qui y interviennent les significations de certains signaux

rencontrés fréquemment dans les circuits électriques ou de certains paramètres de ceux-ci. Si on associe aux identités et aux inégalités ainsi obtenues certaines lois et théorèmes de la théorie des circuits électriques ou certaines relations de calcul du même domaine, on parvient à obtenir des conséquences importantes de ces lois, théorèmes et relations qu'on ne trouve pas dans la littérature. Il est question de nombre de conséquences de la loi d'Ohm ou du théorème des tension, de Kirchhoff, pour les circuits linéaires fonctionnant en régime stationnaire, des relations de calcul des puissances soit dans les circuits monophasés, soit dans ceux triphasés, en régime permanent harmonique et du théorème de Tellegen.

Le procédé proposé peut être élargi utilisant d'autres lois et théorèmes appartenant à la théorie des circuits électriques ainsi que d'autres identités et inégalités algébriques.

Reçue le 28 février 2000

Université Technique „Gh. Asachi", Jassy,
Chaire d'Electrotechnique

BIBLIOGRAPHIE

1. Budeanu C.I., *Puissances réactive et fictives.* Inst. Roumain de l'Energie, Bucarest, 1927.
2. Leonte A., Vraciu G., *Elemente de calcul matriceal cu aplicaţii.* Ed. Tehnică, Bucureşti, 1975, 75.
3. Courant R., *Vorlesungen über Differential- und Integralrechnung.* Dritte Aufl., I/Bd., Springer Verlag, Berlin–New York, 1954.
4. Fikhtengoltz G.M., *Kurs differentzial'nogo i integral'nogo isčislenia.* T.**II**, Fizmatguiz, Moskva, 1959.
5. Tellegen B.D.H., *A General Network Theorem, with Applications.* Phillips Res. Rep., **7**, 259-269 (1952).

CÂTEVA APLICAŢII ALE UNOR IDENTITĂŢI ŞI INEGALITĂŢI ALGEBRICE ÎN TEORIA CIRCUITELOR ELECTRICE

(Rezumat)

Ideea de bază pe care se sprijină lucrarea este aceea de a valorifica unele identităţi şi inegalităţi algebrice, asimilând mărimile care intervin în acestea cu anumite semnale sau anumiţi parametri care sunt întâlniţi în teoria circuitelor electrice. Asociind acestor identităţi şi inegalităţi unele legi, teoreme sau relaţii de calcul specifice se pot obţine consecinţe ale acestora, de vădit interes.

BULETINUL INSTITUTULUI POLITEHNIC DIN IAŞI
Tomul XLVII (LI), Fasc. 3–4, 2001
ELECTROTEHNICĂ. ENERGETICĂ. ELECTRONICĂ

D.C. 621.392.5; 621.396

PARAMETERS DETERMINATION OF THE FUNDAMENTAL MATRIX, FOR A BIPOLAR TRANSISTOR REPRESENTED BY A GENERAL LINEAR FOUR-TERMINAL, IN THE HARMONIC STEADY STATE

BY
DORIN BELAUS

The transistors running at high frequencies are better represented by the *general four-terminals* (GF), or in *a broad sense four-terminals* (BSF), whose fundamental parameters, $\underline{A}_{ij}$, are determined in this paper. It is proved that the fundamental parameters depend on the transistors parameters reported to terminal, or external currents.

1. Introduction

In the theory of electronic schemes with transistors, these ones are represented by in *restricted sense four-terminals* (RSF) and their matrices are expressed in $\underline{Z}$, $\underline{Y}$ or $\underline{H}$ parameters.

In the harmonic steady state, at high frequency, it must be considered the parasite capacitors between the terminals of the transistor or to ground (Fig. 1 *a*).

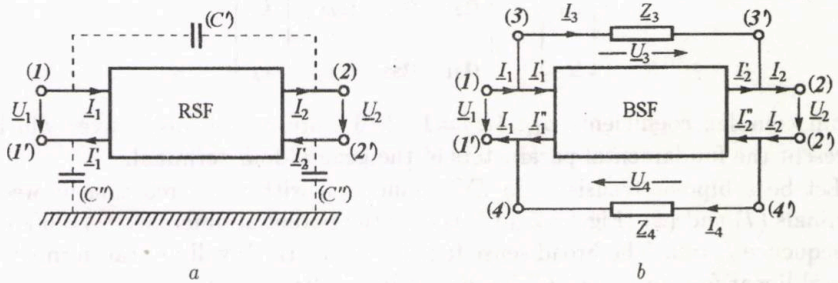

a *b*

Fig. 1

Usually, for schemes at high frequency, the RSF transistor is connected in parallel with RSF parasite capacitors (C') and (C''). In this case, the Bode's condition is neglected, because usually the currents are different, $\underline{I}_1 \neq \underline{I}_1'$, $\underline{I}_2 \neq \underline{I}_2'$.

This situation oblige to require at the theory of general four-terminals [2] or to a broad sense four-terminals theory [3], [4].

In the Fig. 1 *b* is represented a such four-terminal, the impedances $\underline{Z}_3$, $\underline{Z}_4$ being considered as reactions of any type of transistor.

2. The Equations and the Matrix of Fundamental Parameters $\underline{A}_{ij}$, $(i,j=1,2,3)$

Usually, the electronic schemes contain transistors, which are connected in cascade (amplifiers) and this case impose to calculate the fundamental parameters of $\underline{A}$-matrix. In case when the matrix $[\underline{A}]$ would be linear, it must to consider that the variables signals (tension and current) have a small magnitude w.r.t the values in the run static point.

For any four-terminal, there are four currents to terminals, three of them being independent, and six tensions between terminals, three being independent too [1]. For writing the equations, it must to select the input signals u_1, i_1', u_3 which are nonlinear functions of the output signals u_2, i_2', i_2''.

A linear system is obtained if the input signals are developed in Taylor's series and the first terms are kept:

$$(1)\qquad \begin{cases} u_1 = \dfrac{\partial u_1}{\partial u_2}u_2 + \dfrac{\partial u_1}{\partial i_2'}i_2' + \dfrac{\partial u_1}{\partial i_2''}i_2'', \\ i_1' = \dfrac{\partial i_1'}{\partial u_2}u_2 + \dfrac{\partial i_1'}{\partial i_2'}i_2' + \dfrac{\partial i_1'}{\partial i_2''}i_2'', \\ u_3 = \dfrac{\partial u_3}{\partial u_2}u_2 + \dfrac{\partial u_3}{\partial i_2'}i_2' + \dfrac{\partial u_3}{\partial i_2''}i_2'', \end{cases}$$

or in complex values:

$$(2)\qquad \begin{bmatrix} \underline{U}_1 \\ \underline{I}_1' \\ \underline{U}_3 \end{bmatrix} = \begin{bmatrix} \underline{\alpha}_{11} & \underline{\alpha}_{12} & \underline{\alpha}_{13} \\ \underline{\alpha}_{21} & \underline{\alpha}_{22} & \underline{\alpha}_{23} \\ \underline{\alpha}_{31} & \underline{\alpha}_{32} & \underline{\alpha}_{33} \end{bmatrix} \begin{bmatrix} \underline{U}_2 \\ \underline{I}_2' \\ \underline{I}_2'' \end{bmatrix},$$

within complex coefficients $\underline{\alpha}_{ij}$, $(i,j=1,\ 2,\ 3)$, are partial derivatives which will represent the fundamental parameters of the general four-terminal.

Let be a bipolar transistor in *EC* connection with a $\underline{Z}_R$ reaction between the terminals (*1*) and (*2*) (Fig. 2 *a*). In this case the potential difference $\underline{U}_A = 0$ and as a consequence $\underline{I}_A = 0$. The broad sense four-terminal (BSF) will be transformed into a general linear four-terminal (GLF), drawn in Fig. 2 *b*.

The relations between input and output signals from Figs. 2 *a* and 2 *b* will be:

$$(3)\qquad \begin{aligned} &\underline{U}_1 = \underline{U}_{BE},\quad \underline{I}_1' = \underline{I}_B,\quad \underline{U}_3 = -\underline{U}_{CB}, \\ &\underline{U}_2 = -\underline{U}_{CE},\quad \underline{I}_2' = \underline{I}_C,\quad \underline{I}_2'' = -\underline{I}_L. \end{aligned}$$

Having in view that:

$$\underline{I}_E = \underline{I}_B + \underline{I}_C = \underline{I}_S + \underline{I}_L, \quad \underline{I}_S \ll \underline{I}_L, \tag{4}$$

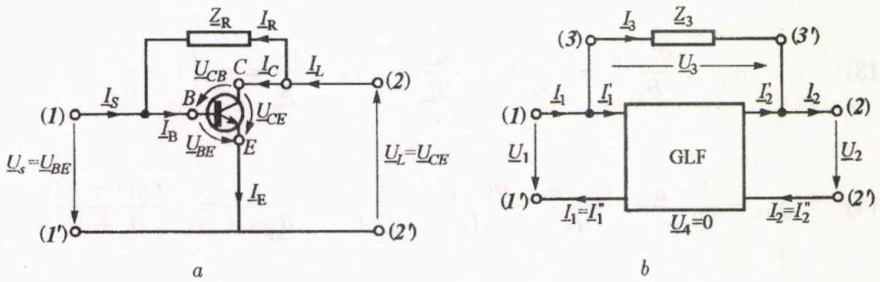

Fig. 2

it may be accepted that $\underline{I}_E \cong \underline{I}_L$ and the equations system (2) can be written as:

$$\begin{bmatrix} \underline{U}_{BE} \\ \underline{I}_B \\ -\underline{U}_{CB} \end{bmatrix} = \left[\underline{\alpha}_{ij}\right] \begin{bmatrix} -\underline{U}_{CE} \\ -\underline{I}_C \\ -\underline{I}_E \end{bmatrix}, \tag{5}$$

where:

$$\underline{\alpha}_{11} = \frac{\partial \underline{U}_{BE}}{\partial \underline{U}_{CE}} = -\frac{1}{\underline{\mu}}; \tag{6}$$

$\underline{\mu}$ is an amplifier complex factor in voltage, the sign "–" being associated with the oppositions of the tensions variations;

$$\underline{\alpha}_{12} = \frac{\partial \underline{U}_{BE}}{\partial \underline{I}_C} = \frac{\partial \underline{U}_{BE}}{\partial \underline{U}_{CE}} \cdot \frac{\partial \underline{U}_{CE}}{\partial \underline{I}_C} = -\frac{r_C}{\underline{\mu}}, \tag{7}$$

where r_C is the dynamic resistance collector–emitter;

$$\underline{\alpha}_{13} = \frac{\partial \underline{U}_{BE}}{\partial \underline{I}_E} = \frac{\partial \underline{U}_{BE}}{(\underline{\beta}+1)\partial \underline{I}_B} = \frac{r_B}{\underline{\beta}_0 + 1}, \tag{8}$$

where r_B is the dynamic resistance base–emitter and $\underline{\beta}_0 = \partial \underline{I}_C / \partial \underline{I}_B$ is a transistor parameter called *base efficiency*;

$$\underline{\alpha}_{21} = \frac{\partial \underline{I}_B}{\partial \underline{U}_{CE}} = \frac{\partial \underline{I}_B}{\partial \underline{U}_{BE}} \cdot \frac{\partial \underline{U}_{BE}}{\partial \underline{U}_{CE}} = -\frac{1}{\underline{\mu} r_B}, \tag{9}$$

where the product $\underline{\mu} r_B = \underline{S}$ is another transistor's parameter called *transistor slope*;

$$\underline{\alpha}_{22} = \frac{\partial \underline{I}_B}{\partial \underline{I}_C} = \frac{1}{\underline{\beta}_0}, \tag{10}$$

$$\underline{\alpha}_{23} = \frac{\partial \underline{I}_B}{\partial \underline{I}_E} = \frac{\partial \underline{I}_B}{\partial \underline{I}_C + \partial \underline{I}_B} = \frac{1}{\underline{\alpha}_0 + 1}, \tag{11}$$

with $\underline{\alpha}_0 = \partial \underline{I}_C / \partial \underline{I}_B = 1/(\underline{\beta}_0 + 1)$ another transistor parameter called *current gain*;

$$\underline{\alpha}_{31} = \frac{\partial \underline{U}_{CB}}{\partial \underline{U}_{CE}} = 1 - \frac{\partial \underline{U}_{BE}}{\partial \underline{U}_{CE}} = 1 + \frac{1}{\underline{\mu}}; \tag{12}$$

$$\underline{\alpha}_{32} = \frac{\partial \underline{U}_{CB}}{\partial \underline{I}_C} = \frac{\partial \underline{U}_{CE}}{\partial \underline{I}_C} - \frac{\partial \underline{U}_{BE}}{\partial \underline{I}_C} = r_C - \frac{r_C}{\underline{\mu}} = r_C \left(1 - \frac{1}{\underline{\mu}}\right); \tag{13}$$

$$\underline{\alpha}_{33} = \frac{\partial \underline{U}_{CB}}{\partial \underline{I}_E} = \frac{\partial \underline{U}_{CE}}{\partial \underline{I}_E} - \frac{\partial \underline{U}_{BE}}{\partial \underline{I}_E} = \frac{\underline{\beta}_0 r_C}{\underline{\beta}_0 + 1} - \frac{r_B}{\underline{\beta}_0 + 1} = -\frac{r_B(1 + \underline{\mu})}{\underline{\beta}_0 + 1}. \tag{14}$$

Consequently, the expression of $[\underline{\alpha}_{ij}]$ matrix is:

$$[\underline{\alpha}_{ij}] = \begin{bmatrix} -\frac{1}{\underline{\mu}} & -\frac{r_C}{\underline{\mu}} & \frac{r_B}{\underline{\beta}_0 + 1} \\ -\frac{1}{\underline{\mu} r_B} & \frac{1}{\underline{\beta}_0} & \frac{1}{\underline{\alpha}_0 + 1} \\ \frac{1}{\underline{\mu}} + 1 & r_C \frac{\underline{\mu} - 1}{\underline{\mu}} & -\frac{r_B(1 + \underline{\mu})}{\underline{\beta}_0 + 1} \end{bmatrix}. \tag{15}$$

In the case when we have in view to write the equations system (5) in function of the output currents of the four-terminal, it must be observed (Fig. 2 *a*) that:

$$\underline{I}_B = \underline{I}_S + \underline{I}_R, \qquad \underline{I}_C = \underline{I}_L - \underline{I}_R, \tag{16}$$

and the system (5) becomes:

$$\begin{bmatrix} \underline{U}_{BE} \\ \underline{I}_S \\ \underline{U}_{CB} \end{bmatrix} = \begin{bmatrix} -\underline{\alpha}_{11} & \underline{\alpha}_{12} - \underline{\alpha}_{13} & -\underline{\alpha}_{12} \\ -\underline{\alpha}_{21} & \underline{\alpha}_{22} - \underline{\alpha}_{23} & -\underline{\alpha}_{22} - 1 \\ \underline{\alpha}_{31} & \underline{\alpha}_{32} + \underline{\alpha}_{33} & -\underline{\alpha}_{32} \end{bmatrix} \begin{bmatrix} \underline{U}_{CE} \\ \underline{I}_L \\ \underline{I}_R \end{bmatrix}. \tag{17}$$

The system (17) corresponds to equations system of the fundamental parameters $\underline{A}_{ij}$, $(i, j = 1, 2, 3)$, of a GLF [2], or of a BSF equations [3], [4] within $\underline{U}_4 = 0$, that is:

$$\begin{bmatrix} \underline{U}_1 \\ \underline{I}_1 \\ \underline{U}_3 \end{bmatrix} = [\underline{A}_{ij}] \begin{bmatrix} \underline{U}_2 \\ \underline{I}_2 \\ \underline{I}_3 \end{bmatrix}, \tag{18}$$

where:

$$\underline{A}_{11} = -\underline{\alpha}_{11} = \frac{1}{\underline{\mu}},\quad \underline{A}_{12} = \underline{\alpha}_{12} - \underline{\alpha}_{13} = -r_C\underline{\mu} - \frac{r_B}{\underline{\beta}_0 + 1},\quad \underline{A}_{13} = -\underline{\alpha}_{12} = \frac{r_c}{\underline{\mu}},$$

$$\underline{A}_{21} = -\underline{\alpha}_{21} = \frac{1}{\underline{\mu} r_B},\quad \underline{A}_{22} = \underline{\alpha}_{22} - \underline{\alpha}_{23} = \frac{1}{\underline{\beta}_0} - \frac{1}{\underline{\alpha}_0 + 1},$$

(19)

$$\underline{A}_{23} = -\underline{\alpha}_{22} - 1 = -\frac{1}{\underline{\beta}_0} - 1,\quad \underline{A}_{31} = \underline{\alpha}_{31} = \frac{1}{\underline{\mu}} + 1,$$

$$\underline{A}_{32} = \underline{\alpha}_{32} + \underline{\alpha}_{33} = \frac{r_C(\underline{\mu} - 1)}{\underline{\mu}} - \frac{r_B(1 + \underline{\mu})}{\underline{\beta}_0 + 1},\quad \underline{A}_{33} = -\underline{\alpha}_{32} = \frac{r_B(1 + \underline{\mu})}{\underline{\beta}_0 + 1}.$$

3. Conclusions

1. At high frequencies schemes with transistors it is necessary to require to broad sense four-terminal theory, or to general four-terminal theory.

2. The linear equations of a bipolar transistor and their fundamental parameters of matrix $\underline{A}_{ij}$, $(i, j = 1, 2, 3)$, were established.

3. The fundamental parameters are functions of transistors parameters $\underline{\alpha}_0$, $\underline{\beta}_0$, $\underline{\mu}$, S, r_C, r_B. The same procedure may be driven to find the parameters of other types of transistors.

Received, June 15, 1999

Technical University "Gh.Asachi", Jassy,
Department of General Electrotechnics
and Electrical Machines

REFERENCES

1. Şora C., *Le quadripôle électrique.* Ed. Masson, Paris, 1969.
2. Sigorsky V.P., *Théorie générale des quadripôles* (en russe). Ed. Acad. Sci. Ukraïne, Kiew, 1955.
3. Rosman H., Belaus D., *Quadripôles linéaires en sens élargi, nonautonomes, en régime permanent harmonique.* Bul. Inst. polit., Iaşi, **XLIII (XLVII)**, *1-2*, s.III, 11-16 (1997).
4. Belaus D., *Contribuţii la studiul diporţilor generalizaţi în regim permanent armonic.* Ph. D. Diss., Techn. Univ. "Gh. Asachi", Jassy, 1998.

DETERMINAREA PARAMETRILOR MATRICEI FUNDAMENTALE PENTRU UN TRANZISTOR BIPOLAR REPREZENTAT PRINTR-UN CUADRIPOL GENERAL LINIARIZAT, ÎN REGIM PERMANENT ARMONIC

(Rezumat)

Se reprezintă un tranzistor bipolar, funcţionând la înaltă frecvenţă (sau cu reacţie), printr-un cuadripol în sens lărgit sau un cuadripol general liniar. Sunt calculaţi parametrii fundamentali ai matricei fundamentale în funcţie de parametrii tranzistorului în raport cu curenţii la bornele tranzistorului şi curenţii exteriori.

BULETINUL INSTITUTULUI POLITEHNIC DIN IAŞI
Tomul XLVII (LI), Fasc. 3–4, 2001
ELECTROTEHNICĂ. ENERGETICĂ. ELECTRONICĂ

D.C. 621.34; 621.313.3-9

MODELLING OF SWITCHING ELEMENTS USED IN ELECTRIC MOTORS CONTROL

BY
ILIE POPESCU, IUSTINA ZAHARIA and CAMELIA PETRESCU

A new method for the determination of non-linear circuit elements parameters (equivalent resistance, firing angle) is proposed. The method is based on the energetic interpretation that can be given to the voltage–current and voltage integral *versus* current characteristics and is illustrated for the switching diode and for the thyristor.

1. Introduction

Semiconductor switching devices have been used during the last decades on a large scale in the command and control of electric motors. Their presence, imposed by the desired operation of the system, modifies the overall active and reactive power consumption.

In this paper a new method for the determination of the non-linear element parameters is proposed. The method is based on the possibility to determine the active and reactive power absorbed by the device in a periodic steady-state using its non-linear voltage–current characteristic. The paper focuses on the most frequently encountered semiconductor devices used in motor control, the switching diode and the thyristor.

The possibility to determine the active and reactive power absorbed by a one-port circuit in non-sinusoidal steady-state has been previously presented by the authors of this paper in [1]. The method is based on the observation that the active power, P, is proportional with the area, A_P, bounded by the characteristic $i\left(\int u(t)\,\mathrm{d}t\right)$:

$$P = \frac{1}{T}\int_0^T i(t)\,\mathrm{d}\left(\int u(t)\,\mathrm{d}t\right) = f A_P\left(\int u(t)\,\mathrm{d}t, i\right), \tag{1}$$

while the reactive power is proportional with the area, A_Q, bounded by the characteristic $u(i(t))$:

$$Q = \frac{1}{2\pi}\int_0^T u(t)\,\mathrm{d}i(t) = \frac{1}{2\pi}A_Q(i,u). \tag{2}$$

In the subsequent sections the method for the non-linear element parameters determination will be presented.

2. Energetic Modelling of the Switching Diode

Fig. 1 presents a simple circuit that contains a diode connected to a resistive load, R. In this simplified model $u(t)$ is sinusoidal ($u(t) = U_m \sin \omega t$) and the DC voltage source, E, establishes the value of the voltage above which the diode opens. Consequently the current in this circuit is:

$$(3) \quad i(t) = \begin{cases} 0, & t \in (0, t_1), \\ \dfrac{u(t) - E}{R}, & t \in \left(t_1, \dfrac{T}{2} - t_1\right), \\ 0, & t \in \left(\dfrac{T}{2} - t_1, T\right), \end{cases}$$

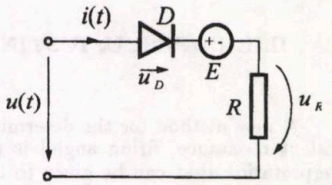

Fig. 1

where $t_1 = \dfrac{1}{\omega} \arcsin \dfrac{E}{U_m}$.

Fig. 2 represents the current–voltage plot for the circuit in Fig. 1, the area A_{Q_1} of the hatched surface being used to determine the reactive power (s. rel. (2)).

Fig. 3 represents the characteristic $i(U)$ where $U = \int u(t)\,dt = \dfrac{U_m}{\omega} \sin\left(\omega t - \dfrac{\pi}{2}\right)$; the area A_P of the hatched surface is used in this case for the calculation of the active power (s. rel. (1)).

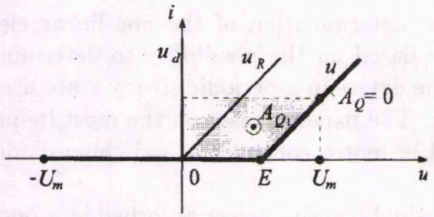

Fig. 2

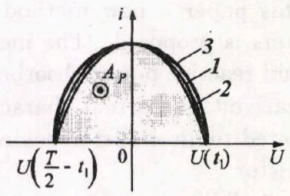

Fig. 3

The characteristic $i(u)$ in Fig. 2 suggests the possibility to redraw the electric circuit as presented in Fig. 4. Here D is an ideal switching diode, R' includes both the resistive load and the direct resistance of the diode, and

$$(4) \quad e(t) = \begin{cases} E = U_m \sin \omega t_1, & t \in \left(0, \dfrac{T}{2}\right), \\ 0, & t \in \left(\dfrac{T}{2}, T\right), \end{cases}$$

where $e(t)$ is a voltage controlled voltage generator.

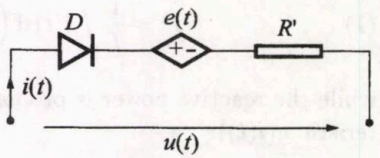

Fig. 4

The parameters E and R may be determined by solving the system of equations (5) established using the expressions for $i(t)$, $u(t)$ and $U(t)$ and eliminating t:

$$(5) \qquad A_P = \frac{T}{R}\left(\frac{U_m^2}{4} - \frac{U_m^2}{2\pi}\arcsin\frac{E}{U_m} - \frac{E\sqrt{U_m^2 - E^2}}{2\pi}\right), \quad A_{Q_1} = \frac{U_m^2 - E^2}{2R},$$

where A_{Q_1} is the area of the characteristic $u(i(t))$, $t \in [0, T/2]$.

An exact solution of the system may be obtained using numerical methods. However analytical solutions may be found if the real characteristic in the (U, i)-plane (plot *1* in Fig. 3) is approximated either by a parabola (plot *2*) or by an ellipse (plot *3*).

The best approximation is given by the parabola. In this case (5) becomes:

$$(6) \qquad A_P = \frac{T}{R}\cdot\frac{2}{3\pi}(U_m - E)\sqrt{U_m^2 - E^2}, \qquad A_{Q_1} = \frac{U_m^2 - E^2}{2R}.$$

The parameters of the circuit are:

$$(7) \qquad R = \frac{U_m^2 - E^2}{2A_{Q_1}} = \frac{2U_m^2 K_P}{A_{Q_1}(1 + K_P)^2}, \qquad E = \frac{U_m(1 + K_P)}{1 + K_P},$$

where

$$K_P = \left(\frac{3\pi}{4}\cdot\frac{1}{T}\cdot\frac{A_P}{A_{Q_1}}\right)^2.$$

If the approximation with an ellipse is used, then system (5) becomes

$$(8) \qquad A_P = \frac{T}{4R}(U_m - E)\sqrt{U_m^2 - E^2}, \qquad A_{Q_1} = \frac{U_m^2 - E^2}{2R}$$

and the parameters E and R are:

$$(9) \qquad R = \frac{U_m^2 - E^2}{2A_{Q_1}} = \frac{2U_m^2 K_{\text{el}}}{A_{Q_1}(1 + K_{\text{el}})^2}, \qquad E = \frac{U_m(1 - K_{\text{el}})}{1 + K_{\text{el}}},$$

where

$$K_{\text{el}} = \left(\frac{2}{T}\cdot\frac{A_P}{A_{Q_1}}\right)^2.$$

A study of the errors introduced by the two approximations was made for $U_m = 100$ V, $R = 100\ \Omega$, $T = 1/50$ s, and a firing angle comprised between 10° and 60°. The results are presented in Table 1.

Table 1

ωt_1 / A_P	Curve *1*	Curve *2*	Curve *3*	Relative error %	Error %
10°	0.3898	0.4094	0.3477	5	10.8
20°	0.2864	0.3125	0.2654	9.1	7.3
30°	0.1954	0.2187	0.1858	11.9	4.9
45°	0.0908	0.10656	0.0905	17.3	0.33
60°	0.0288	0.0355	0.03014	23.26	4.6

As may be seen the approximation of the real characteristic (1) with an ellipse leads to smaller errors for small firing angles while for large values of ωt_1 it is better to approximate the real characteristic with a parabola.

The parameters R and E in the case of the two approximations are calculated for a small angle (10°) and for a large one (60°) (Table 2).

Table 2

	$R=100\ \Omega$		E	
ωt_1 / error	10°	60°	10°	60°
ellipse	99.98; err = 0.02%	107.21; err = 7.2%	17.35; err = 0.08%	86.59; err = 0.01%
parabola	99.98; err = 0.07%	100.03; err = 0.03%	17.5; err = 0.77%	86.6; err = 0.77%

The real values for E are: $E = 17.36$ V for $\omega t_1 = 10°$ and $E = 86.6$ V for $\omega t_1 = 60°$, while $R = 100\ \Omega$.

3. Energetic Modelling of the Thyristor

Fig. 5 presents a thyristor used to control the current in the resistive load, R (representing the overall circuit resistance). The supply voltage, $u(t)$, is sinusoidal. The non-sinusoidal current is given by the relation

$$(10)\quad i(t) = \begin{cases} \dfrac{U_m \sin \omega t}{R}, & t \in \left(t_1, \dfrac{T}{2}\right), \\ 0, & t \in \left(\dfrac{T}{2}, T\right) \cup (0, t_1), \end{cases}$$

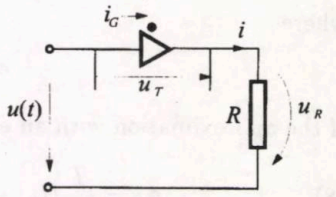

Fig. 5

where $\alpha = \omega t_1$ is determined by the command current, i_G. The real circuit in Fig. 5 and the characteristics $i(U)$ and $i(u)$ enable the determination of a model that corresponds to rel. (10) (Fig. 4). The voltage of the controlled voltage generator, $e(t)$, is:

$$(11)\quad e(t) = \begin{cases} U_m \sin \omega t = E, & t \in (0, t_1), \\ 0, & t \in (t_1, T). \end{cases}$$

The characteristic $i(u)$, represented in Fig. 6 *b*, may be regarded as a superposition of two curves:

a) the hatched triangle, whose area is proportional with the reactive power:

$$(12)\quad Q = \frac{1}{2\pi} A_Q(u, i) = \frac{1}{2\pi} \cdot \frac{u_1 i_1}{2},$$

where $u_1 = u(t_1)$ and $i_1 = i(t_1)$;

b) the straight line OA that may be used to determine the active power if represented in the plane $(U(t), i(t))$:

$$(13)\quad P = f A_P(U, i),$$

where

$$A_P = \frac{TU_m^2}{R}\left(\frac{1}{4} - \frac{t_1}{2T} + \frac{\sin 2\omega t_1}{8\pi}\right), \tag{14}$$

obtained from relations (2), (4) and (10).

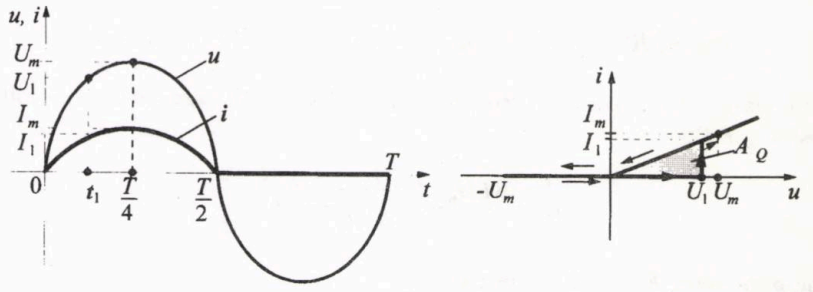

a b

Fig. 6

Relations (12) and (14) enable the determination of the parameters R and t_1 as a solution of the system:

$$\begin{cases} A_Q = \dfrac{U_m^2 \sin^2 \omega t_1}{2R}, \\ A_P = \dfrac{U_m^2 T}{R}\left(\dfrac{1}{4} - \dfrac{t_1}{2T} + \dfrac{\sin 2\omega t_1}{8\pi}\right) = \dfrac{U_m^2}{R} T \left(\dfrac{1}{4} + \dfrac{\sin 2\omega t_1 - 2\omega t_1}{8\pi}\right). \end{cases} \tag{15}$$

The solution may be obtained numerically. In order to obtain an analytical solution, a piece-wise approximation of the characteristic $i(U)$ is proposed (Fig. 7). The following cases may appear:

a) For small angles ($\omega t_1 \in (0, 10°)$) approximating the plot $A_P(U, i)$ with a half of an ellipse, the parameters have the expressions:

$$R = \frac{U_m^2}{4fA_P}, \quad E = U_m\sqrt{\frac{A_Q}{2fA_P}}. \tag{16}$$

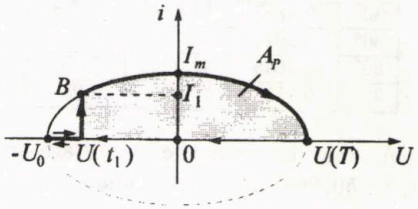

Fig. 7

b) For large values ($\omega t_1 \in (80°, 90°)$) approximating the plot $A_P(U, i)$ with a quarter of an ellipse, the parameters R and E result as:

$$R = \frac{U_m^2}{8fA_P}, \qquad E = U_m\sqrt{\frac{A_Q}{4fA_P}}. \tag{17}$$

c) For intermediate values ($\omega t_1 \in (10°,80°)$) A_P may be approximated with:

$$A_P = \frac{TU_m^2}{8R} + \frac{U_m}{\omega}\cos\omega t_1 \cdot \frac{U_m}{R}\sin\omega t_0, \qquad A_Q = \frac{E^2}{2R}, \tag{18}$$

where ωt_0 is a refference angle that gives minimum errors. In this analysis the value adopted for ωt_0 is 60°.

System (18) gives the following equation in R:

$$64\pi^2 A_P^2 R^2 + 8TU_m^2(TA_Q - 2\pi^2 A_P)R + T^2U_m^2(\pi^2 - 4) = 0.$$

In this equation the constant term may be neglected, thus resulting the following expression for R:

$$R = \frac{8TU_m^2(2\pi^2 A_P - TA_Q)}{64\pi^2 A_P^2}. \tag{19}$$

The parameter E has the expression:

$$E = \sqrt{2RA_Q}. \tag{20}$$

The option for one of the three forementioned cases is made using the characteristic in Fig. 6 *b* and approximating the firing angle ωt_1, since $U_1 = U_m \sin\omega t_1$.

A numerical simulation was conducted in order to verify the proposed model and to determine the errors. The following values were used in computations: $U_m = 100$ V, $R = 100$ Ω, $f = 50$ Hz, $E = U_m \sin\omega t_1$. The obtained results are presented in Table 3.

Table 3

ωt_1	A_P	A_Q	A_P	A_Q	R, [Ω]	E, [V]	ε_R, [%]	ε_E, [%]
	using approx. char.		using real char.					
10°	0.4995	0.4775	0.5	1.5077	100	17.36	0	0
20°	0.4956	5.8378	0.509	5.8489	97.08	33.699	2.9	1.4
30°	0.4855	12.5449	0.4887	12.5	99.66	49.9	0.3	0.2
60°	0.4025	37.4549	0.3878	3.75	116.3	93.39	16.3	7.8
80°	0.3045	48.5215	0.25	48.4923	82.1	89.26	17.9	9.3
90°	0.251	49.999	0.25	50	100	100	0	0

As may be seen the errors are small ($< 3\%$) for $\omega t_1 \in (0, 50°)$. In the case $\omega t_1 \in (50, 90°)$ a reference angle $\omega t_0 = 70°$ is proposed and option b) is disregarded.

4. Conclusions

The energetic models for the non-linear circuit elements studied in this paper are established using the non-sinusoidal input signals in the time domain. The elements involved in the equivalent circuits are determined using the active and the reactive powers calculated with a method proposed by the authors of this paper [5]. This

method avoids signal harmonic analysis and uses the characteristics $i(u)$ and $i(U)$. Both hysteretic and non-hysteretic characteristics $u(i)$ were considered.

The parameters of the equivalent circuits were determined both analytically and numerically. In order to obtain analytical solutions, approximations of the characteristic $i(U)$ with simple curves (such as parabola and ellipse) were necessary. In such cases the errors envolved by the approximations were evaluated for different values of the firing angle ωt_1 resulting a suitable choice of the approximation method.

The method proposed in this paper to determine the energetic parameters of non-linear elements proves to be both simple and efficient.

Received, January 26, 2001

Technical University "Gh.Asachi", Jassy,
Department of Electrotechnics

REFERENCES

1. Popescu I., Zaharia I., Petrescu C., *Power Study in Electrical Circuits under Non-sinusoidal Steady-state Using Representation in the Real Plane.* ISTET'97, IXth Internat. Symp. on Theoretical Electrical Engineering, Palermo, Italy, 1997.
2. Furga G.S., *The Mean Generalized Content: a Conservative Quantity in Periodically-forced Non-linear Networks.* ETEP Eur. Trans. on Electr. Power, *5*, 205-212 (1994).
3. Popescu I., Zaharia I., Petrescu C., *Energetic Aspects in Non-linear Circuits Containing Thiristors.* Modelling, Measurement & Control A, AMSE Press, 1993, **53**, *2*, 11-21 (1993).
4. Popescu I., Zaharia I., Petrescu C., *New Possibilities for Power Measurement in Non-sinusoidal Steady-state.* First European Power Quality Conf., Nürnberg, Germany, 1998.
5. Popescu I., Petrescu C., Zaharia I., Popescu-Lasacco G., *Modelling Non-linear Circuit Elements Using an Energetic Interpretation on Their Characteristics.* Internat. Symp. on Non-linear Electromagnetic Systems, ISEM'99, Pavia, Italy, 1999.

MODELAREA ELEMENTELOR CU COMUTAŢIE FOLOSITE ÎN COMANDA MOTOARELOR ELECTRICE

(Rezumat)

Se propune o nouă metodă de determinare a parametrilor elementelor neliniare de circuit utilizate în comanda motoarelor electrice (rezistenţă echivalentă, tensiune de aprindere).

Metoda se bazează pe interpretarea energetică a caracteristicilor tensiune–curent, respectiv integrala tensiunii–curent şi este ilustrată practic pentru cazul diodei de comutaţie reală şi cel al tiristorului.

BULETINUL INSTITUTULUI POLITEHNIC DIN IAŞI
Tomul XLVII (LI), Fasc. 3–4, 2001
ELECTROTEHNICĂ. ENERGETICĂ. ELECTRONICĂ

D.C. 621.394.9

A METHOD TO DESIGN BIORTHOGONAL PERFECT RECONSTRUCTION INFINITE IMPULSE RESPONSE FILTER BANKS

BY
DANIELA TĂRNICERIU and VALERIU MUNTEANU

On account of lower computational complexity of infinite impulse response (IIR) filters compared to finite impulse response ones, a large number of methods for IIR filter banks have been presented in the recent literature. Some of them restrict the order of the numerator of the transfer function of filters to be odd, fact that has some drawbacks. The proposed method removes this constrain and it is formulated as a generalized eigenvalue problem by using Remez multiple exchange algorithm.

1. Introduction

Various ways to implement efficiently filter banks have been investigated extensively in recent years in order to achieve perfect reconstruction [1]. A variety of techniques are available for the design of perfect reconstruction (PR) filter banks under some constraints, where the system (the analysis and synthesis filters) have to be quadrature mirror, biorthogonal, orthogonal or paraunitary ones [2],...,[4]. Digital filter banks have been studied from various points of view because of their use in applications as speech and image processing, as well communications. It is known that infinite impulse response (IIR) filters have computational efficiency compared to finite impulse response (FIR) ones which meet the same specifications, but unfortunately, they have not linear phase required in image coding. Since linear phase IIR filter banks are generally nonstable or noncausal, it is not appropriate for infinite length signals as in speech applications. However, for finite length signals, such as images, a noncausal filtering is possible. S m i t h *et al.* [5] have proposed PR linear phase IIR filter banks and M a t s u m u r a *et al.* [6] have presented a design method of linear phase IIR filter banks with quasi-power complementary characteristics.

In this paper we propose a design method for two channel biorthogonal IIR PR filter banks that satisfies the causal stable condition. To obtain the optimal solution in the Tchebyshev sense, we apply Remez multiple exchange algorithm and formulate the design problem in term of a generalized eigenvalue problem [1]. The filter coefficients can be computed by solving the eigenvalue problem to get the positive minimum eigenvalue and then the stability is tested.

2. Biorthogonal PR IIR Filter Banks

The structure of a two-channel filter bank is shown in Fig. 1, where $H_0(z)$, $H_1(z)$ are analysis filters and $G_0(z)$ and $G_1(z)$ are synthesis filters. The notations and fundamentals regarding this topic are presented in [1]. The well known perfect reconstruction conditions are:

$$(1)\quad G_0(z) = H_1(-z), \quad G_1(z) = -H_0(z), \quad H_0(z)H_1(-z) - H_1(z)H_0(-z) = z^{-2k-1}.$$

According to polyphase representation, the system in Fig. 1 can be redrawn as in Fig. 2 *a*, which is equivalent to that in Fig. 2 *b*.

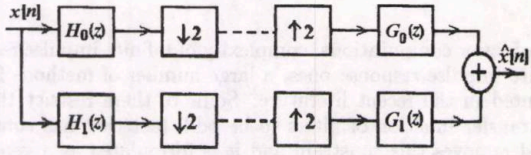

Fig. 1.– Two channel maximally decimated filter bank.

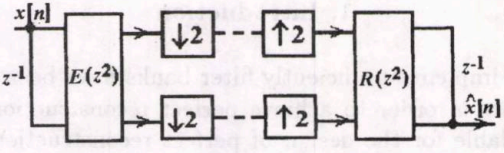

Fig. 2 *a*.– Polyphase representation of two channel maximally decimated filter bank.

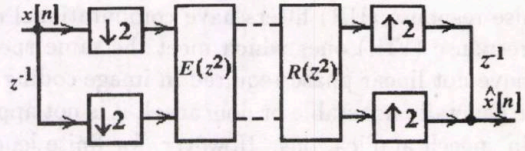

Fig. 2 *b*.– Rearrangement of system in Fig. 2 *a* by using noble identities.

The system is said to be a biorthogonal filter bank if $R(e^{j\omega})E(e^{j\omega}) = I$ for all ω. Since the denominator of filters in Fig. 1 must be functions of z^2, in what follows we deal with the following transfer functions

$$(2)\quad H_0(z) = \frac{E_{00}(z^2) + z^{-1}E_{01}(z^2)}{D_0(z^2)}, \qquad (3)\quad H_1(z) = \frac{E_{10}(z^2) + z^{-1}E_{11}(z^2)}{D_1(z^2)},$$

where $E_{00}(z^2)+z^{-1}E_{01}(z^2)$ and $E_{10}(z^2)+z^{-1}E_{11}(z^2)$ are symmetric or antisymmetric polynomials and $D_0(z^2)$ and $D_1(z^2)$ are symmetric polynomials whose order are multiple of four. When $H_0(z)$ and $H_1(z)$ are specified, the synthesis system $G_0(z)$ and $G_1(z)$, which satisfy perfect reconstruction, can be chosen as:

$$G_0(z) = \frac{2H_1(-z)}{H_0(z)H_1(-z) - H_0(-z)H_1(z)}, \tag{4}$$

$$G_1(z) = \frac{-2H_0(-z)}{H_0(z)H_1(-z) - H_0(-z)H_1(z)}. \tag{5}$$

Another way to design the synthesis filters is to impose quadrature mirror feature to the analysis filters ($H_0(z) = H_1(-z)$) and then

$$G_0(z) = \frac{1}{2}\left[\frac{D_0(z^2)}{E_{00}(z^2)} + \frac{zD_0(z^2)}{E_{01}(z^2)}\right], \tag{6}$$

$$G_1(z) = \frac{1}{2}\left[\frac{D_0(z^2)}{E_{00}(z^2)} - \frac{zD_0(z^2)}{E_{01}(z^2)}\right]. \tag{7}$$

The drawback of this class of filter banks is that the order of the numerator is restricted to be odd. For some applications it is required that $H_0(z)$ and $H_1(z)$ have different number of zeros at $z=1$ and $z=-1$. In order to overcome this problem, we impose the perfect reconstruction condition in (1) on the analysis filters. Using $H_0(z)$ and $H_1(z)$ which satisfy (1), $G_0(z)$ and $G_1(z)$ have the same characteristic as $H_1(-z)$ and $H_0(-z)$.

3. Design Algorithm

In this section we describe the design of IIR PR filter banks based on eigenvalue problem by using Remez multiple exchange algorithm. In this method we suppose that the highpass filter, $H_1(z)$, has already been designed and $H_0(z)$ is designed to satisfy the PR condition (1). We relax the condition on $H_0(z)$ regarding the order of its numerator and denumerator and assume the general IIR filters:

$$H_0(z) = \frac{N(z)}{D(z)} = \frac{\sum_{n=0}^{M} a_n z^{-n}}{\sum_{n=0}^{N} d_n z^{-n}}, \quad \text{with} \quad d_0 = 1. \tag{8}$$

The desired frequency response of $H_0(z)$ is of the form:

$$H_d(\omega) = \begin{cases} e^{-jK\omega}, & 0 \geq \omega \geq \omega_p, \\ 0, & \omega_s \geq \omega \geq \pi, \end{cases} \tag{9}$$

where ω_p, ω_s are the passband and stopband edge frequencies, respectively. We define an error function between the frequency response and the desired response of $H_0(z)$ as

$$\varepsilon(\omega) = \frac{H_0(\omega) - H_d(\omega)}{H_d(\omega)}. \tag{10}$$

To apply Remez multiple exchange algorithm, we first select $J+1$ ($J = \lfloor \frac{1}{2}(M+N+1) \rfloor$) extremal frequencies ω_i, ($\omega_p = \omega_0 > \omega_1 > ... > \omega_J \geq 0$), where $\omega_j > 0$ when $M+N$ is even and $\omega_J = 0$, when $M+N$ is odd. $\lfloor x \rfloor$ denotes the integer part of x. Then, we can formulate $\varepsilon(\omega)$ as follows:

$$\varepsilon(\omega_i) = \delta e^{j\theta(\omega_i)}, \tag{11}$$

where δ (> 0) is the magnitude error to be minimized and $\theta(\omega_i)$ is the phase response at ω_i. Substituting (8),...,(10) into (11), and divide it into the real and imaginary parts, we get:

$$\sum_{n=0}^{M} a_n \cos(K-n)\omega_i - \sum_{n=0}^{N} d_n \cos n\omega_i = \delta \sum_{n=0}^{N} d_n \cos[\theta(\omega_i) - n\omega_i], \quad (i = 0, 1, ..., J), \tag{12}$$

$$\sum_{n=0}^{M} a_n \sin(K-n)\omega_i - \sum_{n=0}^{N} d_n \sin n\omega_i = \delta \sum_{n=0}^{N} d_n \sin[\theta(\omega_i) - n\omega_i], \quad (i = 0, 1, ..., J_1), \tag{13}$$

where $J_1 = J$ when $M+N$ is even and $J_1 = J-1$ when $M+N$ is odd, since Eq. (11) has no imaginary part at $\omega_J = 0$. Eqs. (12) and (13) can be rewritten in a matrix form as:

$$\mathbf{A}\mathbf{v} = \delta \mathbf{Q}\mathbf{v}, \tag{14}$$

where

$$\mathbf{v} = [a_0, a_1, ..., a_M, d_0, d_1, ..., d_N]^T, \tag{15}$$

$$\mathbf{A} = \begin{bmatrix} \cos K\omega_0 & \cos(K-1)\omega_0 & \cdots & \cos(K-M)\omega_0 & -1 & -\cos\omega_0 & \cdots & \cos N\omega_0 \\ \cos K\omega_1 & \cos(K-1)\omega_1 & \cdots & \cos(K-M)\omega_1 & -1 & -\cos\omega_1 & \cdots & \cos N\omega_1 \\ \vdots & \vdots & \cdots & \vdots & \vdots & \vdots & \cdots & \vdots \\ \cos K\omega_J & \cos(K-1)\omega_J & \cdots & \cos(K-M)\omega_J & -1 & -\cos\omega_J & \cdots & \cos N\omega_J \\ \sin K\omega_0 & \sin(K-1)\omega_0 & \cdots & \sin(K-M)\omega_0 & 0 & \sin\omega_0 & \cdots & \sin N\omega_0 \\ \sin K\omega_1 & \cos(K-1)\omega_1 & \cdots & \cos(K-M)\omega_1 & 0 & \sin\omega_1 & \cdots & \sin N\omega_1 \\ \vdots & \vdots & \cdots & \vdots & \vdots & \vdots & \cdots & \vdots \\ \cos K\omega_{J_1} & \cos(K-1)\omega_{J_1} & \cdots & \cos(K-M)\omega_{J_1} & 0 & \sin\omega_{J_1} & \cdots & \cos N\omega_{J_1} \end{bmatrix}, \tag{16}$$

$$
(17)\quad \mathbf{Q} = \begin{bmatrix}
0 & 0 & \cdots & 0 & \cos\theta(\omega_0) & \cos[\theta(\omega_0)-\omega_0] & \cdots & \cos[\theta(\omega_0)-N\omega_0] \\
0 & 0 & \cdots & 0 & \cos\theta(\omega_1) & \cos[\theta(\omega_1)-\omega_1] & \cdots & \cos[\theta(\omega_1)-N\omega_1] \\
\vdots & \vdots & \cdots & \vdots & \vdots & \vdots & \cdots & \vdots \\
0 & 0 & \cdots & 0 & \cos\theta(\omega_J) & \cos[\theta(\omega_J)-\omega_J] & \cdots & \cos[\theta(\omega_J)-N\omega_J] \\
0 & 0 & \cdots & 0 & \sin\theta(\omega_0) & \sin\omega_0 & \cdots & \sin[\theta(\omega_0)-N\omega_0] \\
0 & 0 & \cdots & 0 & \sin\theta(\omega_1) & \sin\omega_1 & \cdots & \sin[\theta(\omega_1)-N\omega_1] \\
\vdots & \vdots & \cdots & \vdots & \vdots & \vdots & \cdots & \vdots \\
0 & 0 & \cdots & 0 & \cos\theta(\omega_{J_1}) & \sin\omega_{J_1} & \cdots & \sin[\theta(\omega_{J_1})-N\omega_{J_1}]
\end{bmatrix}.
$$

Eq. (14) corresponds to a generalized eigenvalue problem, that is, δ is an eigenvalue and $\mathbf{v}$ is a corresponding eigenvector. Therefore, to minimize the maximum error, δ, we have to compute the positive minimum eigenvalue by solving the above eigenvalue problem. By appropriately selecting the initial extremal frequencies, ω_i, and phases, $\theta(\omega_i)$, the procedure is applied iteratively. An arbitrary selection of initial values cannot guarantee the convergence of this algorithm. A possible choice of initial values for ω_i is to pick these frequency points equally spaced in $[0, \omega_p]$ and assuming that there exist $J_1 + 1$ frequency points, $\overline{\omega}_i$, so that

$$
(18)\qquad \varepsilon(\overline{\omega}_i) = 0.
$$

Since $d_0 = 1$, Eq. (18) can be rewritten as:

$$
(19)\qquad \sum_{n=0}^{M} a_n \cos(K-n)\overline{\omega}_i - \sum_{n=0}^{N} d_n \cos n\overline{\omega}_i = 1,
$$

$$
(20)\qquad \sum_{n=0}^{M} a_n \sin(K-n)\overline{\omega}_i - \sum_{n=0}^{N} d_n \sin n\overline{\omega}_i = 0,
$$

which represents a set of linear equations. By solving them, we get an initial solution for filter coefficients. Then, we compute the error function and search for the peak point $|\varepsilon(\omega_i)|$ in the band $[0, \omega_p]$.

To apply this algorithm, the next steps have to be followed:

a) choose M, N, K, ω_p;

b) select $J_1 + 1$ frequency points $\overline{\omega}_i$ equally spaced in the band $[0, \omega_p]$;

c) solve Eqs. (19) and (20) to obtain an initial solution of filter coefficients;

d) compute the error function, $\varepsilon(\omega)$, and search for peak frequencies as extremal ones, Ω_i and compute its phases $\theta(\Omega_i)$;

e) set $\omega_i = \Omega_i$ for $i = 0, 1, ..., J$;

f) find the positive minimum eigenvalue of (14) until the maximum error is smaller then a prescribed small constant;

g) check stability of $H_0(z)$ by finding the pole location.

The proposed method is illustrated by considering the design of an IIR PR filter bank for which the lowpass analysis filter meets the following specification: $M = 6$, $N = 4$, $f_p = 0.15$, $f_s = 0.2$, $\delta = \delta_p = 0.01$. The magnitude response is shown in Figs. 3 *a* and *b*. The FIR filter that meets the same specification in the passband has the order of 27.

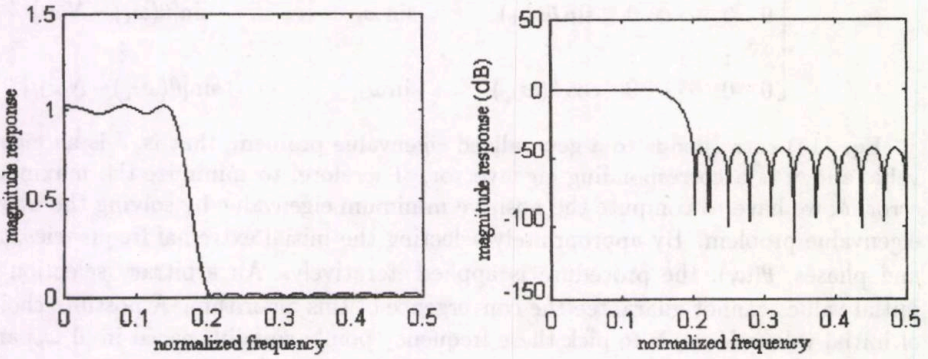

a *b*

Fig. 3.– Magnitude response of $H_0(z)$.

4. Conclusions

In this paper we have proposed a method for designing two channel biorthogonal IIR filter banks which satisfy both the perfect reconstruction and causal stable conditions. The design of the analysis lowpass filter is formulated in the form of a generalized eigenvalue problem by using Remez multiple exchange algorithm. The filter coefficients are obtained as optimal solution in the Tchebyshev sense by computing the minimum positive eigenvalue. The design example demonstrates the effectiveness of the proposed method.

Received, June 15, 2001

Technical University "Gh.Asachi", Jassy,
Department of Telecommunications

REFERENCES

1. Vaidyanathan P.P., *Multirate Systems and Filter Banks.* Englewood Cliffs, Prentice Hall, NJ, 1993.
2. Basu S., Chiang C.H., Choi H.M., *Wavelets and Perfect Reconstruction Subband Coding with Causal Stable IIR Filters.* IEEE Trans. Circuits and Systems – II, **42**, *1* (1995).
3. Phoong S.M., Kim C.W., Vaidyanathan P.P., *A New Class of Two-Channel Biorthogonal Filter Banks and Wavelet Bases.* IEEE Trans. Signal Processing, **43**, *3*, 649-664 (1995).

4. Z h a n g X., I w a k u r a H., *Design of IIR Digital Filters Based on Eigenvalue Problem.* IEEE Trans. Signal Processing, **44**, *6*, 1325-1333 (1996).
5. S m i t h M.J.T., E d d i n s S.L., *Analysis/Synthesis Techniques for Subband Image Coding.* IEEE Trans. Acoustic, Speech and Signal Processing, **38**, *8*, 1446-1456 (1990).
6. M a t s u m u r a S., M u r a t a F., T a k e b e T., *Perfect Reconstruction Two Channel Linear Phase IIR Filter Banks with Quasi Power Complementary Characteristic.* Proc. of ECCTD'97, **3**, 1997, 543-548.

O METODĂ DE PROIECTARE A BANCURILOR DE FILTRE CU RĂSPUNS INFINIT LA IMPULS, BIORTOGONALE, CU RECONSTRUCŢIE PERFECTĂ

(Rezumat)

Datorită complexităţii reduse a calculelor pe care o prezintă filtrele cu răspuns infinit la impuls (IIR) în comparaţie cu cele cu răspuns finit la impuls (FIR), în ultimul timp s-au dezvoltat o multitudine de metode de proiectare a acestora în bancurile de filtre cu reconstrucţie perfectă. Unele metode, atractive din punct de vedere al cauzalităţii şi stabilităţii, impun ca numărătorul funcţiei de transfer a filtrului să fie impar, ceea ce uneori poate reprezenta un dezavantaj. Metoda propusă înlătură această constrângere şi este formulată ca o problemă generalizată în sensul valorilor proprii, folosind algoritmul de schimb a lui Remez.

BULETINUL INSTITUTULUI POLITEHNIC DIN IAŞI
Tomul XLVII (LI), Fasc. 3–4, 2001
ELECTROTEHNICĂ. ENERGETICĂ. ELECTRONICĂ

D.C. 621.315.051

HYPERCOMPLEX FORM OF VOLTAGE RESPONSE OF THE ELECTRICAL HOMOGENEOUS LONG LINES, EXCITED BY HARMONICAL SIGNALS, IN STEADY-STATE

BY

AL.-M. AVASILOAIE

Using a symbolic representation of real functions of many independent variables, by elements of some algebras over the real field [1], it is possible to get the hypercomplex forms of the voltage and current waves response that are occuring in the steady-state of an electrical homogeneous long line, as signals of two independent variables, which may be symbollicaly represented by elements of "$\mathcal{P}$-Polynions Algebra" (PPA).

So, the signal (8) can be symbollicaly represented by elements (30) of "$\mathcal{P}$-Polynions Algebra" (5), using the derivation operators (28), (29).

1. Introduction

In [4] (classical theory of electrical long lines) it is shown that the steady-state voltage and current responses of an electrical homogeneous long line (EHLL) to an harmonic input signal, generally, are each of them, a two independent variables (x – the distance from the end of EHLL, and t – time) signal, namely:

$$u(x,t) = \sqrt{2}U_{d_0}\mathrm{e}^{\alpha x}\sin(\omega t + \beta x + \varphi_1) + \sqrt{2}U_{i_0}\mathrm{e}^{-\alpha x}\sin(\omega t - \beta x + \varphi_2) =$$

$$= u_d(x,t) + u_i(x,t),$$

(1)

$$i(x,t) = \sqrt{2}I_{d_0}\mathrm{e}^{\alpha x}\sin(\omega t + \beta x + \varphi_1 - \varphi_c) - \sqrt{2}I_{i_0}\mathrm{e}^{-\alpha x}\sin(\omega t - \beta x + \varphi_2 - \varphi_c) =$$

$$= i_d(x,t) + i_i(x,t),$$

which represent a composition of two progressive waves, a direct one, $u_d(x,t)$, $i_d(x,t)$, and a reverse one, $u_i(x,t)$, $i_i(x,t)$.

In the present paper we will try to get the *hypercomplex form* for each of these signals, by means of a symbolic method proposed by A. B r a i e r [1], [2], that has established a relation between amplitude modulated signals and elements of some algebras over the real field.

2. Symbolical Method of Representation of Functions of Many Independent Variables

In [1] was introduced a symbolic representation of real functions of many independent variables by means of elements of some algebras over the real field.

Let be $\mathcal{A}$ a n order algebra over $\mathbb{R}$, and it's multiplication table:

$$\varepsilon_i \varepsilon_j = \sum_{k=1}^{n} \gamma_{ijk} \varepsilon_k, \quad (i,j = 1,2,...,n), \tag{2}$$

where $\varepsilon_i \in \mathcal{A}_n$, $(i = 1,2,...,n)$, are the elements of an arbitrary basis and γ_{ijk}, $(i,j,k = 1,2,...,n)$ – the structure constants that characterize $\mathcal{A}_n$.

Let $f(x_1, x_2, ..., x_p)$, $x_q \in \mathbb{R}$, $(q = 1,2,...,p)$, be a function of p real independent variables, and let $\partial f/\partial x_q$, $(q = 1,2,...,p)$, be its partial derivatives.

The symbolic representation makes a correspondence between an element, $\hat{w} \in \mathcal{A}_n$, $\hat{w} = \sum_{i=1}^{n} a_i \varepsilon_i$, $(i = 1,2,...,n)$, and the function f, so that the elements $\hat{w}^{(q)} \in \mathcal{A}_n$, $\hat{w}^{(q)} = \sum_{i=1}^{n} a_i^{(q)} \varepsilon_i$, $(q = 1,2...,p)$, which corresponds to the partial derivatives $\partial f/\partial x_q$, are obtained each one by multiplying one by one $\hat{w}$ with p distinct and fixed elements $\hat{d}^{(q)} = \sum_{i=1}^{n} \delta_i^{(q)} \varepsilon_i \in \mathcal{A}_n$, $(q = 1,2,...,p)$, a_i, $a_i^{(q)}$, $\delta_i^{(q)} \in \mathbb{R}$. That means:

$$\hat{w}^{(q)} = \hat{d}^{(q)} \hat{w}, \quad (q = 1,2,...,p). \tag{3}$$

By using this symbolic representation it was proved, [1], that the usual complex algebra, with its known multiplication table:

$$\varepsilon_1^2 = \varepsilon_1, \quad \varepsilon_1 \varepsilon_2 = \varepsilon_2 \varepsilon_1 = \varepsilon_2, \quad \varepsilon_2^2 = -1,$$

can represent, by an element $\hat{w} = a_1 \varepsilon_1 + a_2 \varepsilon_2$, and with the derivation operators (for $p = 2$, $x_1 = x$, $x_2 = y$),

$$\hat{d}^{(x)} = \delta_1 \varepsilon_1 + \delta_2 \varepsilon_2, \qquad \hat{d}^{(y)} = \mu_1 \varepsilon_1 + \mu_2 \varepsilon_2,$$

the function $f(x,y)$ of two independent real variables:

$$f(x,y) = A e^{\delta_1 x + \mu_1 y} \sin(\delta_2 x + \mu_2 y + \varphi), \tag{4}$$

where $A\cos\varphi = a_1$, $A\sin\varphi = a_2$, $A, \delta_1, \delta_2, \mu_1, \mu_2, \varphi \in \mathbb{R}$.

In [2] it was proved that the sum of two functions, f_1, f_2, each of them symbollicaly represented by elements of $\mathcal{A}_m$, respectively $\mathcal{A}_n$ algebras, can be symbollicaly represented by elements of the direct sum $\mathcal{A}_{m+n} = \mathcal{A}_m \dotplus \mathcal{A}_n$.

In [3] it was introduced an algebra, $\mathcal{A}_4$, characterized by the multiplication table:

$$\begin{cases} \varepsilon_1^2 = \varepsilon_1, \ \varepsilon_2^2 = -\varepsilon_1, \ \varepsilon_3^2 = -\varepsilon_1, \ \varepsilon_4^2 = \varepsilon_1, \\ \\ \varepsilon_1\varepsilon_2 = \varepsilon_2\varepsilon_1 = \varepsilon_2, \ \varepsilon_1\varepsilon_3 = \varepsilon_3\varepsilon_1 = \varepsilon_3, \ \varepsilon_1\varepsilon_4 = \varepsilon_4\varepsilon_1 = \varepsilon_4, \ \varepsilon_2\varepsilon_3 = \varepsilon_3\varepsilon_2 = \varepsilon_1, \end{cases} \tag{5}$$

which is an associative and commutative algebra of IV$^{\text{th}}$ order, with unity element (ε_1), over $\mathbb{R}$. It was proved that this algebra, called "$\mathcal{P}$-Polynions Algebra" (PPA), is the direct sum of two complex algebras.

In this paper, it will be proved that an element of PPA,

$$\hat{w} = \sum_{i=1}^{4} a_i \varepsilon_i, \quad \hat{w} \in \mathcal{A}_4, \tag{6}$$

with two derivation operators:

$$\hat{d}^{(t)} = \sum_{i=1}^{4} \delta_i^{(t)} \varepsilon_i, \qquad \hat{d}^{(x)} = \sum_{i=1}^{4} \delta_i^{(x)} \varepsilon_i, \tag{7}$$

satisfying certain conditions, may symbolically represent a function of similar type to (1), that constitutes the response of an EHLL, in steady-state, to an harmonical input signal, namely:

$$\begin{cases} u(x,t) = [U_1 \sin(\omega t + \beta x + \varphi_1)]\mathrm{e}^{\alpha x} - [U_2 \sin(\omega t - \beta x + \varphi_2)]\mathrm{e}^{-\alpha x}, \\ \\ i(x,t) = [I_1 \sin(\omega t + \beta x + \varphi_1 - \varphi_c)]\mathrm{e}^{\alpha x} - [I_2 \sin(\omega t - \beta x + \varphi_2 - \varphi_c)]\mathrm{e}^{-\alpha x}, \end{cases} \tag{8}$$

where U_1, U_2, I_1, I_2, ω, α, β, φ_1, φ_2, φ_c are real constants.

3. Demonstration of the Symbolical Representation

Because of the simillarity between the voltage (8_1) and the current (8_2) responses of an EHLL to harmonical input signal, we will consider, for demonstration only, the voltage response, that is a sum of two signals.

As it was shown in § **2**, (s. (3),(4)), the first signal (that is a progressive direct wave):

$$u_d(x,t) = U_1 \mathrm{e}^{\alpha x} \sin(\omega t + \beta x + \varphi_1) \tag{9}$$

can be symbollicaly represented by an element of the complex algebra:

$$\hat{w}_1 = a_1' \varepsilon_1' + a_2' \varepsilon_2', \quad (\varepsilon_1')^2 = \varepsilon_1', \quad (\varepsilon_2')^2 = -\varepsilon_1', \quad \varepsilon_1' \varepsilon_2' = \varepsilon_2' \varepsilon_1' = \varepsilon_2', \tag{10}$$

with:

$$a_1' = U_1 \cos\varphi_1, \quad a_2' = U_1 \sin\varphi_1 \quad \text{and} \tag{11}$$

$$\hat{d}^{(t)} = \omega \varepsilon_2', \quad \hat{d}^{(x)} = \alpha \varepsilon_1' + \beta \varepsilon_2'. \tag{12}$$

In a similar way, the second signal (that is a reversing wave):

$$u_i(x,t) = U_2 \mathrm{e}^{-\alpha x} \sin(\omega t - \beta x + \varphi_2), \tag{13}$$

can be symbollicaly represented by an element:

$$\hat{w}_2 = a_1'' \varepsilon_1'' + a_2'' \varepsilon_2'', \quad (\varepsilon_1'')^2 = \varepsilon_1'', \quad (\varepsilon_2'')^2 = -\varepsilon_1'', \quad \varepsilon_1'' \varepsilon_2'' = \varepsilon_2'' \varepsilon_1'' = \varepsilon_2'', \tag{14}$$

with

(15) $a_1'' = U_2 \cos\varphi_2$, $a_2'' = U_2 \sin\varphi_2$ and (16) $\hat{d}^{(t)} = \omega\varepsilon_2''$, $\hat{d}^{(x)} = -\alpha\varepsilon_1'' - \beta\varepsilon_2''$.

Obviously, with respect to (4), here $x = t$, $y = x$ and $\delta_1 = \delta_1' = 0$, $\delta_2 = \delta_2' = \omega$, $\mu_1 = \mu_1' = \alpha$, $\mu_2 = \mu_2' = \beta$, $\varepsilon_1 = \varepsilon_1'$, $\varepsilon_2 = \varepsilon_2'$, respectively $\delta_1 = \delta_1'' = 0$, $\delta_2 = \delta_2'' = \omega$, $\mu_1 = \mu_1'' = -\alpha$, $\mu_2 = \mu_2'' = -\beta$, $\varepsilon_1 = \varepsilon_2''$, $\varepsilon_2 = \varepsilon_2''$.

The function (9) can be expressed as follows:

$$u_d(x,t) = U_1 e^{\alpha x} \sin(\omega t + \beta x)\cos\varphi_1 + U_1 e^{\alpha x}\cos(\omega t + \beta x)\sin\varphi_1. \tag{17}$$

By virtue of the correspondence between (9) and (10_1), and having in mind (11), we can see that the elements ε_1', ε_2' of the basis symbollicaly represent the functions $u_{d_1}(x,t)$, $u_{d_2}(x,t)$:

$$\varepsilon_1' \leftrightarrow u_{d_1}(x,t) = e^{\alpha x}\sin(\omega t + \beta x), \quad \varepsilon_2' \leftrightarrow u_{d_2}(x,t) = e^{\alpha x}\cos(\omega t + \beta x). \tag{18}$$

Similarly, the function (13) can be written as:

$$u_i(x,t) = U_2 e^{-\alpha x}\sin(\omega t - \beta x)\cos\varphi_2 + U_2 e^{-\alpha x}\cos(\omega t - \beta x)\sin\varphi_2 \tag{19}$$

and the elements ε_1', ε_2'', of the basis, symbollicaly represent the functions $u_{i_1}(x,t)$, $u_{i_2}(x,t)$:

$$\varepsilon_1'' \leftrightarrow u_{i_1}(x,t) = e^{-\alpha x}\sin(\omega t - \beta x), \quad \varepsilon_2'' \leftrightarrow u_{i_2}(x,t) = e^{-\alpha x}\cos(\omega t - \beta x). \tag{20}$$

O b s e r v a t i o n. In [1], [2] it was proved that a function u, which is symbollicaly represented by an element $\hat{w} \in \mathcal{A}_n$, with $\hat{w} = \sum_{i=1}^{n} a_i\varepsilon_i$, $a_i \in \mathbb{R}$, can be written as:

$$u = \sum_{i=1}^{n} a_i u_i, \tag{21}$$

where u_i are the functions symbollicaly represented by the ε_i, $(i = 1, 2, ..., n)$, elements of an arbitrary basis of the $\mathcal{A}_n$ algebra.

The direct sum of the algebras (10_2),...,(10_4) and (14_2),...,(14_4) has the multiplication table:

$$\begin{cases} (\varepsilon_1')^2 = \varepsilon_1', \ (\varepsilon_2')^2 = -\varepsilon_1', \ \varepsilon_1'\varepsilon_2' = \varepsilon_2'\varepsilon_1' = \varepsilon_2', \\ (\varepsilon_1'')^2 = \varepsilon_1'', \ (\varepsilon_2'')^2 = -\varepsilon_1'', \ (\varepsilon_1''\varepsilon_2'') = (\varepsilon_2''\varepsilon_1'') = \varepsilon_2'', \\ (\varepsilon_1'\varepsilon_1'') = (\varepsilon_1''\varepsilon_1') = (\varepsilon_1'\varepsilon_2'') = (\varepsilon_2''\varepsilon_1') = (\varepsilon_1''\varepsilon_2') = (\varepsilon_2'\varepsilon_1'') = (\varepsilon_2'\varepsilon_2'') = (\varepsilon_2''\varepsilon_2') = 0. \end{cases} \tag{22}$$

We will make a change of the base of this algebra, as follows:

$$\varepsilon_1' + \varepsilon_1'' = 1, \ \varepsilon_1' - \varepsilon_1'' = \mathrm{ij}, \ -\varepsilon_2' + \varepsilon_2'' = \mathrm{i}, \ \varepsilon_2' + \varepsilon_2'' = \mathrm{j}; \tag{23}$$

the obtained multiplication table is now:

(24)

	1	i	j	ij
1	1	i	j	ij
i	i	−1	ij	−j
j	j	ij	−1	−i
ij	ij	−j	−i	1

We can see that the new obtained algebra is, as it was anticipated in § **1**, the PPA (5), where obviously $\varepsilon_1 = 1$, $\varepsilon_2 = \mathrm{i}$, $\varepsilon_3 = \mathrm{j}$, $\varepsilon_4 = \mathrm{ij}$.

From (23) it results the expressions:

$$\varepsilon_1' = \frac{1+\mathrm{ij}}{2},\quad \varepsilon_2' = \frac{\mathrm{j}-\mathrm{i}}{2},\quad \varepsilon_1'' = \frac{1-\mathrm{ij}}{2},\quad \varepsilon_2'' = \frac{\mathrm{j}+\mathrm{i}}{2}. \tag{25}$$

By virtue of the symbolical representation, the new elements of the base 1, i, j, ij are representing the functions:

$$\begin{aligned} 1 &\leftrightarrow \mathrm{e}^{\alpha x}\sin(\omega t+\beta x)+\mathrm{e}^{-\alpha x}\sin(\omega t-\beta x)=u_1(x,t),\\ \mathrm{i} &\leftrightarrow -\mathrm{e}^{\alpha x}\cos(\omega t+\beta x)+\mathrm{e}^{-\alpha x}\cos(\omega t-\beta x)=u_2(x,t),\\ \mathrm{j} &\leftrightarrow \mathrm{e}^{\alpha x}\cos(\omega t+\beta x)+\mathrm{e}^{-\alpha x}\cos(\omega t-\beta x)=u_3(x,t),\\ \mathrm{ij} &\leftrightarrow \mathrm{e}^{\alpha x}\sin(\omega t+\beta x)-\mathrm{e}^{-\alpha x}\sin(\omega t-\beta x)=u_4(x,t). \end{aligned} \tag{26}$$

As it was shown in § **1**, the steady-state voltage response (8) of an EHLL to an harmonical input signal, which can be written as $u(x,t) = u_d(x,t) + u_i(x,t)$, with $u_d(x,t)$, $u_i(x,t)$ given by (9), (13), can be symbollicaly represented by an element, $\hat{u}$, of the direct sum algebra (22):

$$\begin{aligned} \hat{u} = \hat{w}_1 + \hat{w}_2 &= (U_1\cos\varphi_1)\varepsilon_1' + (U_1\sin\varphi_1)\varepsilon_2' + (U_2\cos\varphi_2)\varepsilon_1'' + (U_2\sin\varphi_2)\varepsilon_2'' = \\ &= 1\frac{(U_1\cos\varphi_1+U_2\cos\varphi_2)}{2} + \mathrm{i}\frac{-U_1\sin\varphi_1+U_2\sin\varphi_2}{2} + \\ &+ \mathrm{j}\frac{U_1\sin\varphi_1+U_2\sin\varphi_2}{2} + \mathrm{ij}\frac{U_1\cos\varphi_1-U_2\cos\varphi_2}{2}, \end{aligned} \tag{27}$$

where there were taken in account relations (23).

The derivation operators are given by the relations:

$$\hat{d}^{(t)} = \delta_1^{(t)}\varepsilon_1' + \delta_2^{(t)}\varepsilon_2' + \delta_3^{(t)}\varepsilon_1'' + \delta_4^{(t)}\varepsilon_2'' = \omega\varepsilon_2' + \omega\varepsilon_2'' = \mathrm{j}\omega, \tag{28}$$

$$\hat{d}^{(x)} = \delta_1^{(x)}\varepsilon_1' + \delta_2^{(x)}\varepsilon_2' + \delta_3^{(x)}\varepsilon_1'' + \delta_4^{(x)}\varepsilon_2'' = \alpha\varepsilon_1' + \beta\varepsilon_2' - \alpha\varepsilon_1'' - \beta\varepsilon_2'' = -\mathrm{i}\beta + \mathrm{ij}\alpha, \tag{29}$$

where there were taken in account relations (7), (12), (16), (23).

By virtue of the symbolical representation, having in mind relations (25), (26), it results that an element

$$\hat{u} = u_1 + \mathrm{i}u_2 + \mathrm{j}u_3 + \mathrm{ij}u_4 \tag{30}$$

of the PPA (24), where:

$$\begin{aligned} u_1 &= \frac{U_1 \cos\varphi_1 + U_2 \cos\varphi_2}{2}, \quad u_2 = \frac{-U_1 \sin\varphi_1 + U_2 \sin\varphi_2}{2}, \\ u_3 &= \frac{U_1 \sin\varphi_1 + U_2 \sin\varphi_2}{2}, \quad u_4 = \frac{U_1 \cos\varphi_1 - U_2 \cos\varphi_2}{2}, \end{aligned} \tag{31}$$

with the two derivation operators (28), (29), may represent the hypercomplex expression of the steady-state voltage response (8_1) of an EHLL to an harmonical input signal; the response may be written as:

$$u(x,t) = u_1 u_1(x,t) + u_2 u_2(x,t) + u_3 u_3(x,t) + u_4 u_4(x,t), \tag{32}$$

where $u_1(x,t), ..., u_4(x,t)$ are given by relations (26_2).

Similarly, the hypercomplex expression of the current response of an EHLL to an harmonical input signal, in steady-state, may be written as:

$$\hat{i} = i_1 + \mathrm{i}i_2 + \mathrm{j}i_3 + \mathrm{ij}i_4, \tag{33}$$

where

$$\begin{aligned} i_1 &= \frac{I_1 \cos(\varphi_1 - \varphi_c) - I_2 \cos(\varphi_2 - \varphi_c)}{2}, \quad i_2 = \frac{-I_1 \sin(\varphi_1 - \varphi_c) - I_2 \sin(\varphi_2 - \varphi_c)}{2}, \\ i_3 &= \frac{I_1 \sin(\varphi_1 - \varphi_c) - I_2 \cos(\varphi_2 - \varphi_c)}{2}, \quad i_4 = \frac{I_1 \cos(\varphi_1 - \varphi_c) + I_2 \cos(\varphi_2 - \varphi_c)}{2}, \end{aligned} \tag{34}$$

the derivation operators being (28), (29).

4. Conclusions

1. An element $\hat{u}$, (30), (31), $\hat{i}$, (33), (34), of the "$\mathcal{P}$-Polynions Algebra", with two elements $\hat{d}^{(x)}$, (28_3), $\hat{d}^{(t)}$, (29_3), of the same algebra, as derivation operators, represents by means of a symbolic calculus, the hypercomplex forms of the steady-state responses (which are a sum of two progressive waves (s. (1)) of an EHLL with an harmonical input signal, the response having the forms similar to (8).

2. The symbolical representation allows to write that the partial derivatives with respect to x, t of the function $u(x,t)$, can be symbollicaly represented by elements $\hat{u}^{(x)}$, $\hat{u}^{(t)}$, $\hat{i}^{(x)}$, $\hat{i}^{(t)}$ of the same algebra, which are given by the relations:

$$\hat{u}^{(x)} = \hat{d}^{(x)}\hat{u}, \quad \hat{u}^{(t)} = \hat{d}^{(t)}\hat{u}, \quad \hat{i}^{(x)} = \hat{d}^{(x)}\hat{i}, \quad \hat{i}^{(t)} = \hat{d}^{(t)}\hat{i}. \tag{35}$$

3. Signals similar to (8) also occurs in the study of the transmission lines, and of the electrical circuits with distributed parameters. The symbolical representation exposed allows to transform the equations with partial derivatives into differential (or algebrical) ordinary ones.

Received, June 4, 2001

Technical University "Gh.Asachi", Jassy,
Department of Electrotechnics

REFERENCES

1. B r a i e r A., *A Symbolic Calculus Using Algebras on the Real Field.* Bul. Inst. polit., Iaşi, **XV (XIX)**, *1-2*, s.I, 129-134 (1969).
2. B r a i e r A., *Utilizarea algebrelor pe corpul real în mecanica vibraţiilor.* Ph. D. Diss., Inst. polit., Iaşi, 1968.
3. B r a i e r A., R o s m a n H., *Utilizarea polinionilor pentru studiul unor mişcări forţate ale sistemelor liniare.* Bul. Inst. polit., Iaşi, **XI (XV)**, *1-2*, 309-320 (1965).
4. P r e d a M., *Bazele electrotehnicii.* Vol.**II**, Ed. Did. şi Pedag., Bucureşti, 1981.

FORMA HIPERCOMPLEXĂ A RĂSPUNSULUI ÎN TENSIUNE ŞI CURENT CARACTERISTIC LINIILOR ELECTRICE OMOGENE LUNGI, EXCITATE CU SEMNALE DE INTRARE ARMONICE, ÎN REGIM PERMANENT

(Rezumat)

Se utilizează reprezentarea simbolică a unor funcţii reale de mai multe variabile, prin elemente ale unor algebre peste câmpul real, [1], pentru obţinerea formelor hipercomplexe ale răspunsului în curent şi tensiune al liniilor electrice omogene lungi, excitate cu semnale de intrare, în regim permanent. Răspunsul este o funcţie de două variabile, reprezentabil simbolic prin elemente ale „Algebrei Polinionilor-$\mathcal{P}$". Astfel, funcţiile de tipul (8), pot fi reprezentate simbolic prin elementele hipercomplexe (30), (31), (33), (34) ale „Algebrei Polinionilor-$\mathcal{P}$", (5), utilizând operatorii de derivare (28), (29).

BULETINUL INSTITUTULUI POLITEHNIC DIN IAŞI
Tomul XLVII (LI), Fasc. 3–4, 2001
ELECTROTEHNICĂ. ENERGETICĂ. ELECTRONICĂ

D.C. 621.394.9

DIGITAL IMAGE COMPRESSION ALGORITHM USING SPANNING TREES

BY

LUMINIŢA SCRIPCARIU and PETRUŢ DUMA

Discrete images could be better compressed if different scanning orders of the image elements are considered [1], [2]. The optimum searching algorithm needs an increased time of image analysis. The proposed method is a near optimum one, with a reduced image processing time. It is based on the spanning tree algorithm for graph searching and Huffman coding algorithm for image compression. The performances of the designed code are deduced and a comparison with other similar algorithms is made.

1. Image Scanning

The discrete image matrix is a 3D one (R, G, B) so three different matrices are processed for the same image.

The Huffman coding algorithm has to be applied on a finite set of image elements so that a block-partition is made [3]. A 4×4 pixels structure is considered:

$$a = \begin{bmatrix} a_{11} & a_{12} & a_{13} & a_{14} \\ a_{21} & a_{22} & a_{23} & a_{24} \\ a_{31} & a_{32} & a_{33} & a_{34} \\ a_{41} & a_{42} & a_{43} & a_{44} \end{bmatrix}. \tag{1}$$

The image redundancy is reduced by a differential compression method, called *decorrelation*. The original image can be exactly recovered from the differential one. Depending on the image element, a different scanning order may give better compression.

Each image element has 8 neighbours:

$$n_i = \begin{bmatrix} n_{1i} & n_{2i} & n_{3i} \\ n_{4i} & a_i & n_{5i} \\ n_{6i} & n_{7i} & n_{8i} \end{bmatrix}, \tag{2}$$

where a_i represents the current pixel.

The optimum *neighbourhood function* or *tree* will be deduced.

For example, let us consider an image element corresponding to the matrix:

$$a = \begin{bmatrix} 12 & 11 & 11 & 12 \\ 10 & 10 & 12 & 13 \\ 11 & 12 & 13 & 14 \\ 12 & 13 & 14 & 14 \end{bmatrix}. \tag{3}$$

The differential image is obtained by *horizontal scanning* (first step) row-by-row, from the left to the right, and *vertical scanning* (second step) for the first element of each row, up-to-down:

$$c = \begin{bmatrix} 12 & -1 & 0 & -1 \\ -2 & 0 & -2 & -1 \\ 1 & 1 & 1 & 1 \\ 1 & 1 & 1 & 0 \end{bmatrix}. \tag{4}$$

Excepting the initial value of the matrix, the others could be coded with a reduced number of bits comparing to the original. So the spatial redundancy is reduced.

This is a graph problem and the spanning tree algorithm could be used in order to minimize the *zero-order entropy* given by [1]:

$$H(\overline{p}) = -\sum_{k=0}^{L-1} p_k \log_2(p_k), \tag{5}$$

where: L represents the number of the vectorial quantizing levels, $\overline{p} = [p_k]_{k=\overline{0,L-1}}$ – the probability array of the image first-order histogram:

$$p_k = P\{a_{ij} = v_k\} \approx \frac{N(k)}{M}, \tag{6}$$

with v_k – the quantified amplitude level for $0 \leq k \leq L-1$, $N(k)$ – the number of pixels of amplitude v_k and M – the total number of pixels of the image matrix.

The probability array and the first-order entropy of the original image matrix a are:

$$\overline{p} = \left\lfloor \tfrac{2}{16} \quad \tfrac{3}{16} \quad \tfrac{5}{16} \quad \tfrac{3}{16} \quad \tfrac{3}{16} \right\rfloor, \qquad H(\overline{p}) = 2.26 \text{ bpp}.$$

An 8-neighbourhood model is used, so all the adjacent pixels are considered.

But there are many different ways of taking differences and probably one of them is optimum. For example, the pixel at (2,3) would have a difference value of zero if the location (1,4) is considered (s. Fig. 1). The minimum spanning tree keeps for every node from the possible 8 input edges, the edge with minimum weigth.

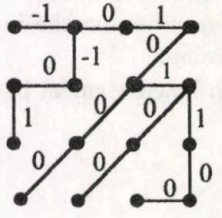

Fig. 1.– Minimum spanning tree.

The *residual matrix* consists of the input values for every node or vertix of the graph. The "spanning tree" must be known in the decoder.

For example, for the case considered before it results the optimal residual matrix:

$$r = \begin{bmatrix} -1 & 0 & 0 & 1 \\ 0 & -1 & 0 & 1 \\ 1 & 0 & 0 & 1 \\ 0 & 0 & 0 & 0 \end{bmatrix}. \tag{7}$$

This matrix has the probability vector:

$$\overline{p}_r = \left\lfloor \frac{10}{16} \quad \frac{4}{16} \quad \frac{2}{16} \right\rfloor \tag{8}$$

and the first-order entropy is:

$$H(\overline{p}_r) = 1.30 \text{ bpp}. \tag{9}$$

Many possible trees could be used for differential image scanning.

For a $M \times N$ matrix there are $C_{MN}^{(M-1)(N-1)}$ trees.

O b s e r v a t i o n. C_N^k represents all combinations of N elements taken k at a time.

A 4×4 matrix has 1,372,800 possible trees. A very large codebook for the spanning trees results and the analysis time is too high. Therefore a near optimum case is considered.

Only 4 spanning trees will be used, namely T_1; T_2; T_3; T_4 (Fig. 2).

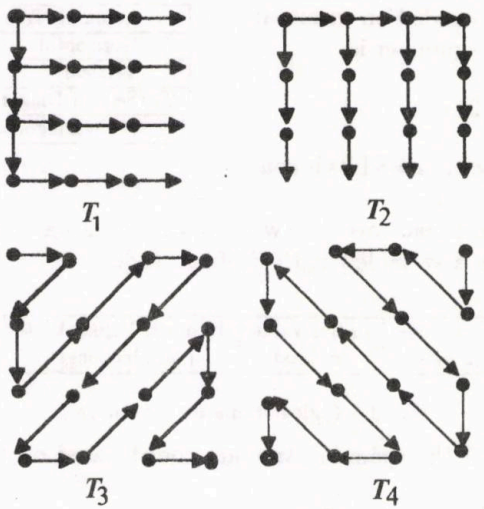

Fig. 2.– 4×4 spanning trees.

2. The Compression Algorithm

The scanning process begin with the discrete image partitioning into matrices. Then each element is scanned based on the four spanning trees. The near optimum tree corresponding to the minimum value of the first-order entropy (computed on the residual matrices) is deduced.

For example, the initial image matrix, a, has the following residual matrices, obtained based on the considered spanning trees with the entropy values given below:

$$(10)\quad r_1=\begin{bmatrix} 0 & -1 & 0 & 1 \\ -2 & 0 & 2 & 1 \\ 1 & 1 & 1 & 1 \\ 1 & 1 & 1 & 0 \end{bmatrix};\ H_1=1.72\,\text{bpp};\quad (11)\quad r_2=\begin{bmatrix} 0 & -1 & 0 & 1 \\ -2 & -1 & 1 & 1 \\ 1 & 2 & 1 & 1 \\ 1 & 1 & 1 & 0 \end{bmatrix};\ H_2=1.80\,\text{bpp};$$

$$(12)\quad r_3=\begin{bmatrix} 0 & -1 & 1 & 1 \\ -1 & -1 & 0 & 0 \\ 1 & 0 & 0 & 1 \\ 0 & 1 & 0 & 0 \end{bmatrix};\ H_3=1.48\,\text{bpp};\quad (13)\quad r_4=\begin{bmatrix} 2 & 0 & -2 & 0 \\ -2 & -3 & 1 & 1 \\ -2 & 2 & -1 & 2 \\ 1 & -1 & 2 & 0 \end{bmatrix};\ H_4=2.48\,\text{bpp}.$$

So the optimal "tree" for this matrix is T_3.

The resulting spanning trees codebook, with 2 bits length of the coded sequences, is given in Table 1. We may denote these trees by H, V, S or M, according to their geometrical orientation.

The "tree" code and the initial value of the (1,1) or (1,4) pixel form the header of the image element codeword (Fig. 3).

The initial value is coded on m bits if the quantization levels number is:

$$(14)\qquad L=2^m.$$

The particular case of $m=8$ bits is considered.

Table 1
Spanning Tree Codebook

Spanning Tree	Codeword
T_1 (Horizontal)	00
T_2 (Vertical)	01
T_3 (Second Diagonal)	10
T_4 (Main Diagonal)	11

The residual matrix read row-by-row is converted into a vector and coded with less than m bits using a variable length Huffman code.

Tree Code (2 bits)	Initial Value (m bits)	Residual Values Vector (variable length)

Fig. 3.– Coded frame for an image.

The label values of the spanning tree are coded based on the Huffman coding algorithm.

The maximum absolute value of the tree depends on the correlation degree of the original image.

The proposed Huffman code could be designed on a reduced number of values (N) instead of $2^m = 256$.

For $N = 8$ the character set is:

$$V = \{0; 1; -1; 2; -2; 3; -3; 4; -4; \text{others}\}. \tag{15}$$

Other values of the tree, which are not included in the Huffman set, are coded using a binary prefix added to their value coded on m bits (one bit is the sign and the others represents the absolute value of the number).

The elements weights are:

$$W = \{16; 4; 4; 2; 2; 1; 1; 4\}. \tag{16}$$

The Huffman codewords are given in Table 2.

Table 2
Huffman Code

Label value	Weight	Codeword	Coding length, [bits]
0	16	0	1
1	4	100	3
-1	4	101	3
2	2	1100	4
-2	2	1101	4
3	1	11100	5
-3	1	11101	5
Prefix	4	1111xxxxxxxxx	12

The estimated mean length of a binary coded value is:

$$\bar{l}_0 = 2.42 \text{ bpc}. \tag{17}$$

The mean value of the coded frame associated with an image element with 16 pixels is:

$$\bar{l} = 2 + 8 + 16 \times 2.42 = 48.72 \text{ bps} = 3.045 \text{ bpp}. \tag{18}$$

So, instead of $16 \times 8 = 128$ bits transmitted for the uncoded matrix of 16 pixels, the proposed algorithm gives a coded frame with an average length of 48.72 bits and the compression rate is about 62% or 2.62 : 1.

Different codebook sizes could be considered and other dimensions of the image element could be used (8×8; 16×16). The coding performances are sensitive to the size of the codebook.

Test values were obtained for a coloured image with three matrice, r, g, b, corresponding to three color planes – red, green and blue. These matrices are partitioned into 4×4 pixels elements and scanned with four spanning trees (T_1; T_2; T_3; T_4).

Some experimental results are given in Table 3. The near-optimum trees are used. The image first-order entropy is deduced for the original matrix and for the residual matrices obtained with these spanning trees: H, V, S and M. The optimal case is also analysed.

Table 3
First-Order Entropy,[bpp], *of the (Un)Coded Image Matrix*

Image Matrix	Original	H-Coded	V-Coded	S-Coded	M-Coded	Optimal code	Spanning tree
$g(1{:}4,1{:}4)$	2.61	2.84	2.49	2.41	2.20*	1.77	M
$g(31{:}34,61{:}64)$	3.19	2.60*	2.66	2.90	3.09	2.95	H
$r(5{:}8,1{:}4)$	2.95	3.25	2.23*	3.17	3.42	2.53	V
$b(21{:}24,56{:}60)$	3.92	3.61	3.55	2.85*	3.46	2.16	S

The proposed compression algorithm is a loseless one. The processing time and complexity are reduced in comparison with the optimal code.

3. Conclusions

The proposed method for discrete colour image scanning and compression is based on the spanning trees algorithm for graphs analysis and the Huffman coding algorithm in order to reduce the image redundancy and to increase the compression rate. The coding performances are tested and a comparison with other compression algorithms is made. This is a near optimum method with a decreased analysis time comparing to the optimum method proposed by N.D. M e m o n *et al.* [2].

Received, May 5, 2001

Technical University "Gh.Asachi", Jassy,
Department of Telecommunications

REFERENCES

1. P r a t t W.K., *Digital Image Processing.* John Wiley & Sons Inc., NY, 1991.
2. M e m o n N.D., S a y o o d K., M a g l i v e r a s S.S., *Loseless Image Compression with a Codebook of Block Scans.* IEEE J. on Selected Areas in Commun., **13**, 24-30 (1995).
3. S c r i p c a r i u L., A l e x a n d r u N.D., *Binary Image Compression Based on Huffman Coding.* Proc. of Intern. Conf., D & AS, Suceava, May 1998, Vol.**10**, 97-102.

ALGORITM DE COMPRESIE A IMAGINILOR DIGITALE
FOLOSIND METODA DRUMULUI MINIM DINTR-UN GRAF

(Rezumat)

Se propune o metodă suboptimă de căutare a „drumului minim" într-un graf obţinut prin scanarea elementelor unei imagini discrete. Imaginea este partiţionată în submatrici pătratice de dimensiuni reduse (4×4 pixeli). Se utilizează doar patru arbori pentru scanarea elementelor de imagine în vederea reducerii timpului necesar analizei, comparativ cu algoritmul optim de scanare pe toate direcţiile posibile. Se proiectează codul Huffman de codare a imaginilor color discrete şi se testează performanţele acestuia comparativ cu alte metode de compresie cunoscute.

BULETINUL INSTITUTULUI POLITEHNIC DIN IAŞI
Tomul XLVII (LI), Fasc. 3–4, 2001
ELECTROTEHNICĂ. ENERGETICĂ. ELECTRONICĂ

D.C. 621.317

NEW MEASUREMENT METHOD OF THE THERMAL DIFFUSIVITY IN SOLIDS USING TIME MEASUREMENTS
II. EXPERIMENTAL APPROACH

BY

EMIL VREMERĂ and N. DAMEAN

A measurement system for the thermal properties of the solids materials is presented. This paper is a practical application of the theoretical developments from [1]. The measuring system is based on semiconductor temperature sensors, a Data Acquisition Board and an adequate software package. The virtual instrument achieved allows a graphical representation for temperature variation and table format for data carried out for a later processing. The virtual instrument can be used for both testing of the system performances when the physical properties of the material are known and for diffusivity measurement of unknown solids.

1. Introduction

In [1] is proposed a measurement method of the thermal diffusivity in solids using transient conditions. This method uses the Seebeck effect for measuring the time dependence of temperature. The method does not involve accurate absolute temperature measurement but a high-resolution and high-stability of the relative measurement is necessary. This method uses only electrical tools for carry out non-electrical parameter values. In this paper, we develop a measurement system based on this method.

The measurement system was designed such as a virtual instrument [2] because the described method involves data acquisition at precise moments from multiple points disposed along of the test sample. We used other temperature sensors than those described in [1] because we needed a high resolution for small temperature changes.

From the temperature acquisitions data the graphical dependence *versus* time of these quantities can be draw and the delay time for the peak value can be computed. After that the parameters β, η and α are computed with Eqs. (5), (7) and (8) from [1].

2. The Virtual Instrument

For realising a virtual instrument the following elements are required: temperature sensors, data acquisition board, control and execution devices and a PC. For data acquisition, we used a DAQ with analogue channels inputs and digital outputs suitable for measurement and control. The whole process is controlled by means of a PC. From the above mentioned elements only rectangular pulse heat generator and temperature sensors are placed outside PC as shown in Fig. 1.

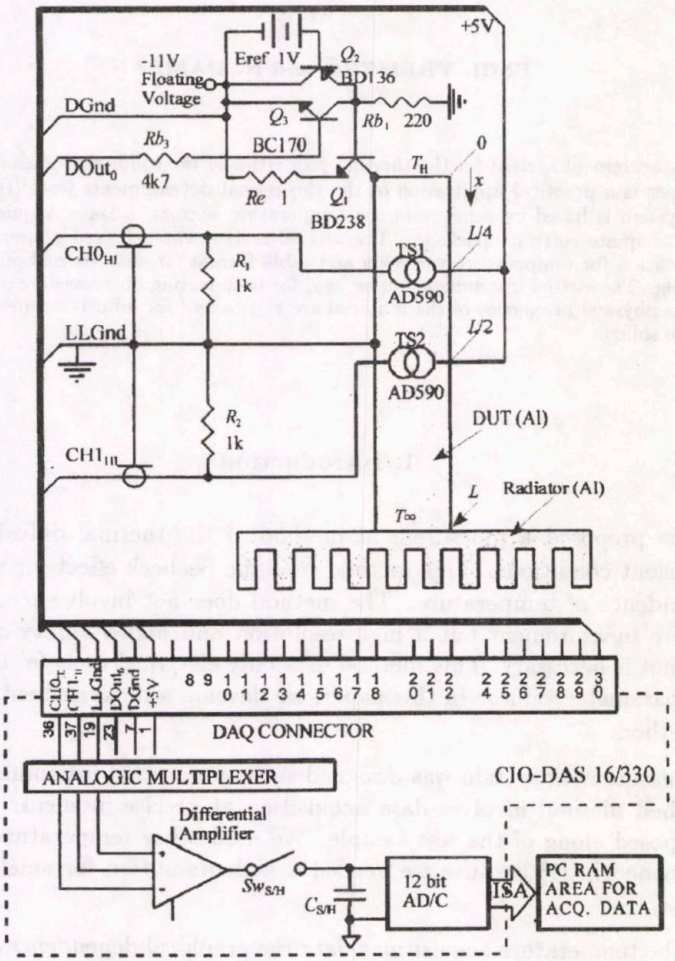

Fig. 1.– Simplified diagram of the measuring system.

2.1. Hardware Considerations

The device under test (named DUT), is an Aluminium rode-shaped probe heaving physical size of $L = 140$ mm and $d = 12$ mm and thermal diffusivity $\alpha = 0.97$ mm·s^{-1}. Therefore, the probe satisfies the condition for the one-dimensional thermal model developed in [1]. The edges of DUT are perfectly coupled at heater and fan cooled aluminium heat sink as Fig. 1 shows. A good polystyrene thermal insulator (not figured) covers the lateral surface. The electric heater, such as in [3], is designed based on power transistor in constant dissipated power configuration. Constant voltage supply and constant current configuration for Q_1 perform this request. The whole dissipated power is converted in an unidirectional thermal constant flux because the transistor is direct mounted (without an insulator) on the DUT edge surface. The mass and the thermal time constant of Q_1 are insignificant. The constant power heater is thermally compensated by means of Q_2 and electronic switched on/off by means of Q_3.

The temperature transducers are two AD590. They are of semiconductor type with current as output signal (1 μA·K^{-1}), have small dimensions, fast response and linear transfer function. They were implanted in DUT at precise points at a quarter ($L/4$) and at a half ($L/2$) length from the heated edge. The voltage drops across R_1 and R_2 resistors are 1 mV·K^{-1} and correspond to 0.3 V voltage range for normal testing conditions.

The acquisition board DAQ is a CIO-DAS 16/330 type from Computer Boards Inc. It is an internal PC connected board (ISA), having 16 asymmetric input channels 12-bit resolution, 1.25 V minimum measurement domain (0.3 mV maximum resolution) and 300 kilo samples per second maximum conversion rate. This voltage resolution corresponds at 0.3 K temperature resolution and can be increased by averaging procedures. The voltages across R_1 and R_2 are applied at two analog single ended input channels ($CH0_{HI}$ and $CH1_{HI}$). One of digital outputs of the DAQ, $DOUT_0$, is connected at input of electronic switch Q_3 for automatic turn on/off of the heater. This connection will allow the perfectly synchronization between heat process and measurement one. The data from both channels are internally PC memorized in a RAM area allocated by Windows program.

2.2. Software Considerations

The necessary software for developing own programs is based on Computer Boards Universal Library DAQ board. The library is universal in two ways: contains high level functions for all of the common operations for all boards and provides the identical set of functions and arguments for BASIC, C and Pascal. Languages supported, in both 16 bit and 32 bit, are: Microsoft Windows and DOS languages, Borland Windows and DOS languages, Watcom C^{++}, Hewlett Packard HP-VEE and National Instruments Lab View. From these, we chose Visual Basic Library and we used Microsoft Visual Basic 3.0 package to write the program, [4].

The virtual instrument must perform some important duties such as:

a) start the measurement of the time and turn-on the heater at the start moment;

b) start the temperature measurement and the results filtering by averaging procedures;

c) turn-off the heater after precise elapsed time;

d) stop the temperature and time measurement, records and organizes measurement data;

e) graphical representation for temperature and heater state *versus* time.

The simplified logical diagram shown in Fig. 2 describes the work of the measurement system.

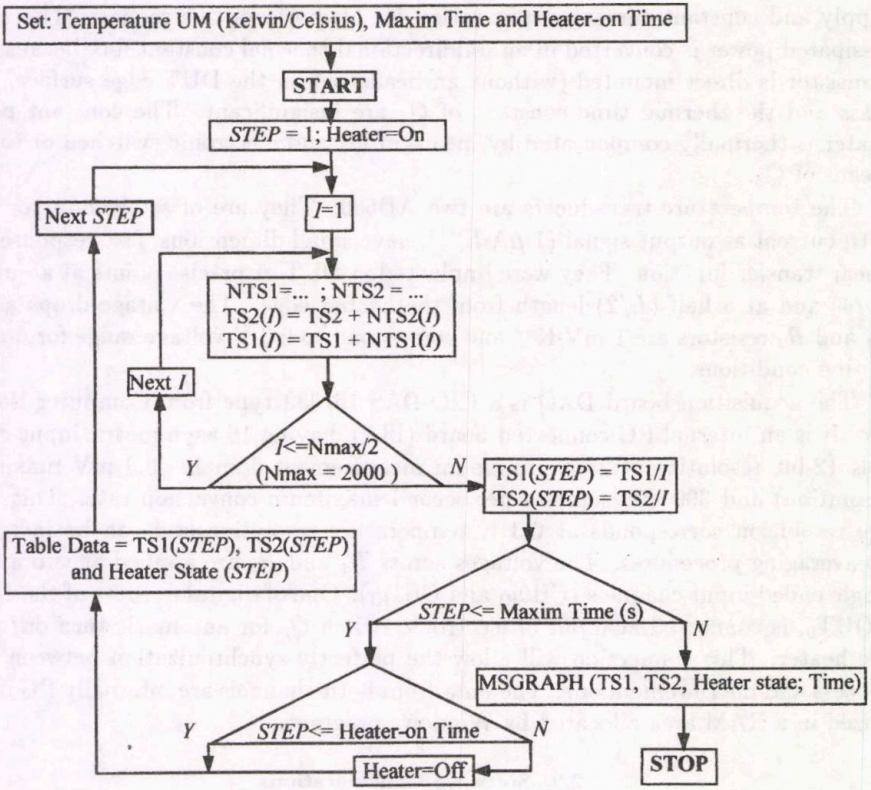

Fig. 2.– Simplified logical diagram followed by the measuring system.

The time resolution (STEP) was chosen 1 s. With acquisition rate of 5 kHz and 1,000 results per channel, the time interval taken in account for average computation is 400 ms, that is suitable for a good rejection at 50 Hz common mode signal. A time correction of 0.8 s (=1–0.4/2) will be necessary in this situation.

The panel of the virtual instrument is represented in Fig. 3.

In this picture, we can observe the possibilities of command, adjustment and display of this virtual instrument. The graphical representation is obtained with MSGraph software as an OLE application. The data from table in MSGraph can be

easily transferred in Excel table for manifold processing. For a maximum measurement time, t_m, of 60 s and 90 s and a heater-on rate between 20% and 50% from t_m, the measurements get results like in Fig. 3. We observe the delay between heater-off moment and the reach of maximum temperature moments of both temperature sensors.

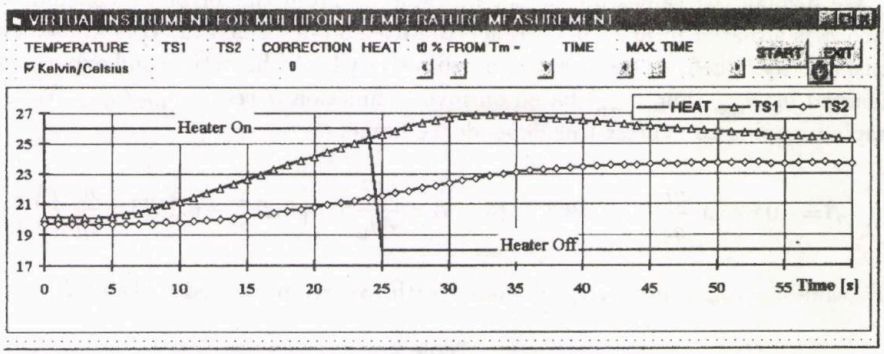

Fig. 3.– The panel of the virtual instrument for $t_m = 60$ s and $t_P = 25$ s.

3. Experimental Results

From the two temperature curves we carry out the elapsed time, τ, until temperature reach the pick value. The right values for parameters β, η and α are obtained after the curves are fitted and 0.8 s delay value is applied. The delay time due to finite time constant of the temperature sensors is much difficult to eliminate, but the ratio $\eta_{L/2}/\eta_{L/4}$ does not depend on this quantity. The indices $L/2$ and $L/4$, included in η and τ, specify the measurement points. The ratio $\eta_{L/2}/\eta_{L/4}$ is computed using initial parameters and those measured. The results are done in Table 1.

Table 1

t_m s	t_P $\%t_m$	t_0 s	β	$\tau_{L/4}$ s	$\tau_{L/2}$ s	$\eta_{L/4}$	$\eta_{L/2}$	$\eta_{L/2}/\eta_{L/4}$
60	20	12	0.147	21.2	39.2	1.7667	3.2667	1.8491
Interpolation value			0.150					1.8276
60	30	18	0.220	27.2	44.2	1.5111	2.4556	1.6250
60	40	24	0.293	32.2	47.2	1.3417	1.9667	1.4658
90	30	27	0.330	35.2	49.2	1.3037	1.8222	1.3977
90	40	36	0.440	43.2	59.2	1.2000	1.6444	1.3704
Interpolation value			0.500					1.3355
90	50	45	0.550	51.2	67.2	1.1378	1.4933	1.3125

Besides the experimental data we obtained, we considered in Table 1 two interpolation values when β is 0.15 and 0.5. These values are necessary to fit theoretical range with experimental one for β.

We compute $\eta_{L/2}/\eta_{L/4}$ ratio for both theoretical and experimental data and the relative error of this ratio, denoted by:

$$(1) \qquad \varepsilon_{\text{RATIO}} = 100\frac{(\eta_{L/2}/\eta_{L/4})_{\text{theor}} - (\eta_{L/2}/\eta_{L/4})_{\text{exp}}}{(\eta_{L/2}/\eta_{L/4})_{\text{theor}}}, \ [\%].$$

We display the values for $\varepsilon_{\text{RATIO}}$ in Table 2. From this error we conclude that when β is situated in $[0.22, 0.33]$ range the method described in [1] is implemented satisfactorily. Then, we get the thermal diffusivity both theoretical and experimental (denoted by α_{theor} and α_{exp}) based on inverse function β *versus* $\eta_{L/2}/\eta_{L/4}$. We set a simple mapping to express this dependence namely:

$$(2) \quad \beta = -0.625 \ln\frac{\eta_{L/2}}{\eta_{L/4}} + 0.5368, \quad (3) \quad \alpha = \frac{4L^2}{\pi^2 t_0}\beta = \left(0.2175 - 0.2533 \ln\frac{\eta_{L/2}}{\eta_{L/4}}\right)\frac{L^2}{t_0}.$$

The values of α_{theor} and α_{exp}, calculated with (3), are presented in Table 2.

Table 2

β	$\eta_{L/2}$	$\eta_{L/4}$	$\varepsilon_{\text{RATIO}}$ %	α_{theor} $\text{mm}^2\cdot\text{s}^{-1}$	α_{exp} $\text{mm}^2\cdot\text{s}^{-1}$
0.150	2.427	1.227	-7.60	71.72	103.79
0.220	1.867	1.124	-2.08	97.21	103.01
0.293	1.582	1.078	-0.11	98.35	98.58
0.330	1.489	1.064	-0.15	96.11	96.37
0.440	1.317	1.039	8.17	85.84	75.01
0.500	1.259	1.031	9.38	80.01	69.14

We consider the two sets of α values, namely α_{theor} and α_{exp}. We compare these values with the known value of α for Aluminium (wich is the tested material). The relative errors are presented in Fig. 4. The measurement error increases at the ends of β range because the delay times, $\tau_{L/2}$, is less accurate for small values of β and the temperature of the heat sink increases at high values of β.

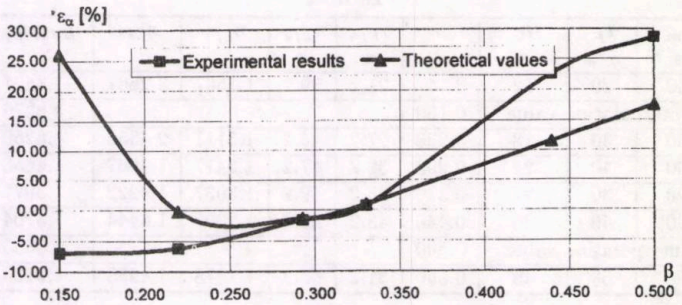

Fig. 4.– The errors of α calculated with relation (3) for theoretical and practical η ratio.

4. Conclusions

The experimental results presented in this paper prove the validity of the theoretical model developed in [1]. Based on this model we propose a procedure to determine the thermal diffusivity of the solids materials. This procedure is implemented like an automatic measurement system using a virtual instrument.

The practical implementation of this system is very flexible because various kinds of temperature sensors can be used. The effect of the delay time of the temperature sensors is eliminated using the ratio of two quantities instead of these quantities.

Another advantage of this virtual instrument is that many perturbative factors, such as power source variations and non-ideal radiator of cold edge, can be simply tested by power time-on adjustment.

The overall error of the thermal diffusivity determination with this virtual instrument is smaller than 2% for β in the range $[0.22, 0.33]$. Improvement of the overall experimental results is possible by increasing the temperature and time resolution [3].

Notations

α – thermal diffusivity, $[m^2 \cdot s^{-1}]$;
β – parameter;
η – parameter;
ρ – density, $[kg \cdot m^{-3}]$;
τ – time to reach maximum temperature, [s];
d – probe diameter, [m];
L – probe length, [m];
n – integer;
t – time, [s];
t_0 – operating time of thermal load, [s];
t_m – measurement time interval, [s];
t_P – heater-on time interval, [s];
x – axial coordinate, [m];
T_H – temperature at the heater edge, [K];
T_∞ – temperature at the sink edge, [K];
PC – Personal Computer;
OLE – Object Linking and Embedding;
DAQ – Data Acquisition Board;
TS1, TS2 – temperature sensors.

Received, December 30, 2000

Technical University "Gh.Asachi", Jassy,
Department of Electrical
Measurements and Materials

REFERENCES

1. Damean N., Vremeră E., *New Measurement Method of the Thermal Diffusivity in Solids Using Time Measurements* (I). Bul. Inst. polit., Iaşi, **XLVII (LI)**, *1-2*, s. Electrot., Energ., Electron. (2001).
2. Taner A.H., White N.M., *Virtual Instrumentation: A Solution to the Problem of Design Complexity in Intelligent Instruments.* Measurement and Control, **29**, 165-171 (1996).
3. Dowding K.J., Blackwell B.F., *Joint Experimental/Computational Techniques to Measure Thermal Properties of Solids.* Measurement Sci. Technol., UK, *9*, 877-887 (1998).
4. Vlasiu L., *Visual Basic 3.0.* Ed. Tehnică, Bucureşti, 1996.

METODĂ NOUĂ PENTRU DETERMINAREA DIFUZIVITĂŢII TERMICE A MATERIALELOR SOLIDE UTILIZÂND MĂSURĂRI DE TIMP

II. Partea experimentală

(Rezumat)

Se prezintă un sistem de măsurare a difuzivităţii termice ca aplicaţie a metodei şi traductorului descrise în [1]. Sistemul descris se bazează pe senzori de temperatură de tip semiconductor şi un sistem de achiziţie de date programat în Visual Basic. Instrumentul virtual astfel obţinut permite reprezentări grafice ale variaţiei temperaturii, obţinerea datelor în format tabel pentru o prelucrare ulterioară şi controlul procesului investigat. Aplicaţia sistemului descris este destinată atât pentru verificarea teoriei, în cazul în care materialul utilizat în traductor este cunoscut ca puritate, cât şi pentru determinarea difuzivităţii termice pentru materiale necunoscute.

BULETINUL INSTITUTULUI POLITEHNIC DIN IAŞI
Tomul XLVII (LI), Fasc. 3–4, 2001
ELECTROTEHNICĂ. ENERGETICĂ. ELECTRONICĂ

D.C. 621.391.5

TIMED SERIAL DATA TRANSFER IN REAL-TIME CONTROL SYSTEMS

BY

LAURENŢIU DIMITRIU and LILIANA VORNICU

In many situations, in the complex systems, and not only for real-time ones, a difficult problem is to valorize in useful time the information provided of a large number of sources, *e.g.* sensors. Using polling strategy or a usual prioritized system does not assure a facile arrangement of events with time criteria. We have proposed a solution for CAN (Controller Area Network) serial communication protocol in which a special station "time reference" introduces in the data field a unique reference for all station linked *via* CAN multiplexed bus [1]. The above-mentioned problems could be easily solved using certain particularities of multiplexed bus serial communication CAN protocol.

1. Introduction

To understand the implementation of our method we present first some particularities of CAN protocol. Concerning the frame format, there are two different formats, which differ in the length of the *identifier* field. Frame with the number of 11 bit identifier are denoted *Standard Frames.* In contrast, frames containing 29 bit identifier are denoted *Extended Frames* [2].

A data frame, as is presented in the Fig. 1, is composed of seven different bit fields: *Start of Frame, Arbitration Field, Control Field, Data Field, CRC Field, ACK Field* and *End of Frame.*

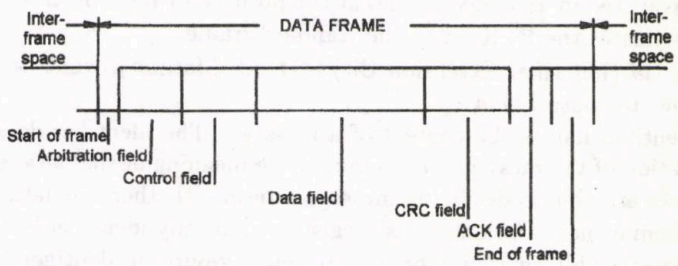

Fig. 1

For the goal of our researches is important to detailed discuss the format of *arbitration field.* This is different for standard format and extended format frames, namely:

a) In standard format the arbitration field consists of the 11 bit identifier and the *RTR-bit.*

b) In extended format the arbitration field consists of the 29 bit identifier, the *SRR-bit*, the *IDE-bit* and the *RTR-bit.*

In the Fig. 2 the structure of *arbitration field* both in standard and extended format frames is presented.

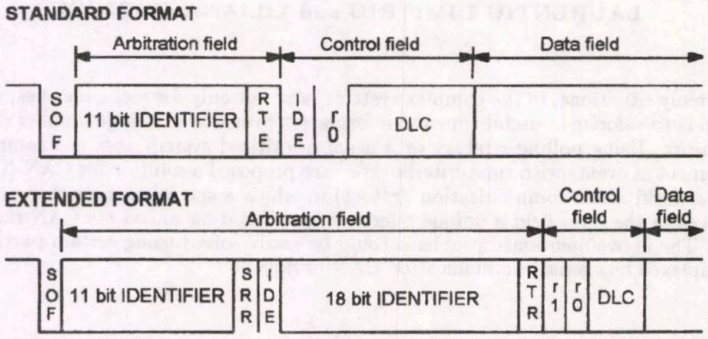

Fig. 2

Inside of this field there are the following parts:

1. *Identifier* – standard format, with a length of 11 bits corresponds to the *Base ID* in extended format.

2. *Identifier* – extended format, with a length of 29 bits, comprising two sections: *Base ID*, with 11 bits and *Extended ID* with 18 bits. The base ID defines the extended frame's base priority.

3. *RTR Bit* (Remote Transmission Request Bit) (standard format as well as extended format).

4. *SRR Bit* (Substitute Remote Request Bit) (extended format) is a recessive bit and is transmitted in extended frames at the position of RTR bit in standard frames and so substitutes the RTR bit in the standard frame.

5. *IDE Bit* (Identifier Extension Bit) (extended format), which in standard format, belongs to control field.

The identifier names the content of a message. The identifier does not indicate the destination of the message, but describe the meaning of the data, so all nodes in the networks are able to decide by message filtering whether the data is to be acted upon by them or not. Optional mask registers allow any identifier bit to set "dont't care" for message filtering, may be used to select groups of identifiers to be mapped into the attached receive buffers. The length of the mask register can comprise the whole identifier or only a part of it.

2. System with Time Reference and Timed Priorities

Let consider a serial multiplexed system with linear bus and with time reference, as is shown in the Fig. 3.

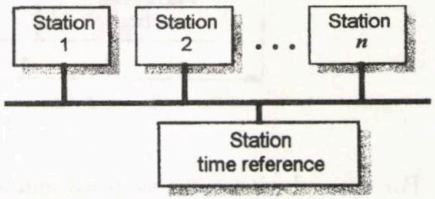

Fig. 3

We analyse the situation of standard CAN format using. The 11 bits of identifier will be used to achieve a timed priority structure of the messages. We take into the consideration that different system's stations could be grouped on distinct priority levels. Let be k the number or distinct priority level. Consequently, we can consider the system's structure as in the Fig. 4.

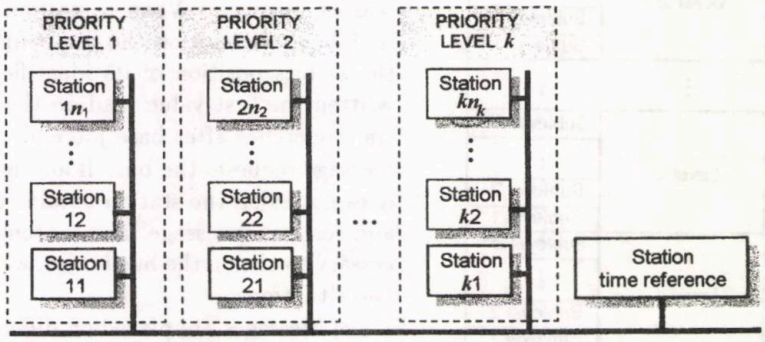

Fig. 4

The 11 bits of the *identifier* will be divided into two groups: p bits to indicate the station's priority group and st bits for system's timing. We can write:

$$p + st = 11, \quad 2^{p-1} < k \leq 2^p. \tag{1}$$

The $st = 11 - p$ bits assigned to time information can code $2^{st} = 2^{11-p}$ distinct states. If the complex system contains n stations, then:

$$n = \sum_{i=1}^{k} n_i, \tag{2}$$

where n_i represents the station's number on every priority level.

The *station time reference* is implemented with a clock generator and a counter. If T_{CLK} denotes the clock period of time reference the period which can be monitored is:

$$T_{\mathrm{mon}} = 2^{st} T_{\mathrm{CLK}}. \tag{3}$$

The way of using the bits *identifier field* is shown in the Fig. 5.

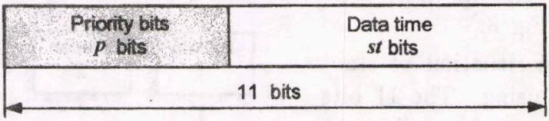

Fig. 5

For example, if we choose $p=3$ and $st=11-3=8$, it results a system with $2^p = 2^3=8$ priority levels, and every of them containing $2^{st}=2^8=256$ timed prioritized sublevels. The system's priority structure is graphically represented in the Fig. 6.

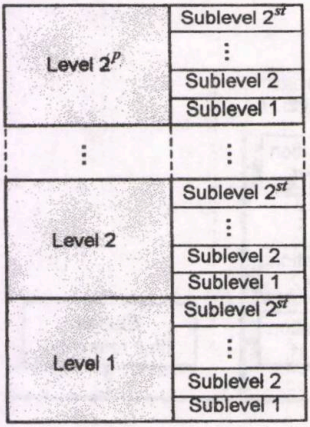

Fig. 6

Considering a time reference, which counts up the clock generator pulses, it results a higher priority level of lower counter values (earlier events). When a station, finishing its job, must send on the bus some data, in the *st* bits position of its identifier, will be written the first value read on the bus from time reference after base job end. Then the message requests the bus. If another request does not exist, the station obtains the access and sends its message. If a contention is necessary to obtain the bus access, we can meet two situations:

a) Messages are placed on different priority levels (fixed by the first p bits of identifier) – when the higher priority level message wins the contention (having the first a dominant bit).

b) Messages are placed on the same priority level – when the contention's winner depends on message priority sublevel, fixed by the last *st* bits identifier. Taking into consideration the significance of these bits, it results that an older message has a higher priority. In this way the information "does not become old".

We can imagine many other solutions. An example could be a system with priority fixed only by time, when all the 11 bits of *identifier* will be set by *time reference*. Sometimes only for some stations (less then n) the timed priority is necessary. Only these stations will use the *time reference* data, the others stations having the *st* bits group data fixed from others considerations.

The receiver can not extract the identifier bits from message, though have a certain information level (implicit) about the time. Sometimes is necessary that time information to be explicitly. In this case we can use the above-mentioned method by introducing q bits data time in the data field. To have a sufficient precision of system's time reference it is necessary to satisfy the condition $q > st$. We can obtain a very rigorous timing of complex system if we use the *station time reference* as

unique source, both for *st* bits of the identifier and q bits of *data time* in *data field.* In the condition above-mentioned ($q > st$), the solution is to achieve the station *time reference* using a q bits counter and a clock generator with T_{ref} period. The *station time reference* is placed on the highest priority level to be able to send the time information immediately after the counter has incremented. All (interested) system's stations receive the time message and use it to build the own messages. The first *st* bits of time reference message are introduced in *identifier* and just to q bits (depending on necessities) in the *data field.* In the Fig. 7 is presented the way to introduce the time information in the *data frame* (both in *identifier field* and *data field*).

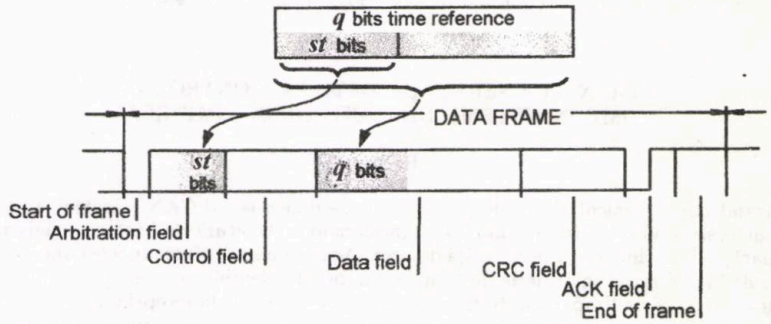

Fig. 7

To exemplify let consider a system with $q = 16$ and $st = 8$, and the time reference $T_{\text{ref}} = 300$ μs (considering 300 bit time of 1 Mbits/s bit rate). In this way, one of three messages on the bus will be a time message (a message has 111 in standard and 131 in extended format – bit times). For $q = 16$ bits we obtain a time loop $T_{\text{LOOP}} = 2^q T_{\text{CLK}} \times 300 = 2^{16} \times 10^{-6} \times 300 = 19.6608$ s. Because $st = 8$, it results that the time markers used in timed priority have a period:

$$T_{\text{TP}} = (2^q/2^{st}) T_{\text{CLK}} \times 300 = 2^{q-st} T_{\text{CLK}} \times 300 = 2^8 \times 10^{-6} \times 300 = 0.0768 \text{ s} = 76.8 \text{ ms}.$$

The system's timing is described as it follows:

a) The full time control period (time loop) in the system, $T_{\text{LOOP}} = 19.6608$ s.
b) Clock resolution (binary), $q = 16$ bits.
c) Time reference in CAN bus clock, $T_{\text{ref}} = 300$ μs.
d) Serial transfer clock period, $T_{\text{CLK}} = 1$ μs (1 MHz).
e) Period of time markers used in the system's timed priority, $T_{\text{TP}} = 76.8$ ms.

3. Conclusions

Using the method presented above, the system's timing has an increased quality. In many real-time applications this could be a helpful and useful feature. We can fix

time markers and to build a priority system which significantly improve the control and diagnosis of real-time systems.

The numerical example supports the theoretical conclusions, suggesting a useful method for the timing of real-time systems.

Received, February 28, 2000

Technical University "Gh.Asachi", Jassy,
Department of Applied Electronics

REFERENCES

1. Dimitriu L., Vornicu L., Răducanu I., *Serial Multiplexed Communication System with Time Reference.* Internat. Symp. on Signals, Circuits and Systems, SCS'99, Iaşi, Romania, July 6–7, 1999, 219-222.
2. * * * *CAN Specification, Version 2.0.* Robert Bosch GmbH, Stuttgart 1991.

TRANSFER SERIAL DE DATE CU CONTROL DE TIMP ÎN SISTEME DE CONTROL ÎN TIMP REAL

(Rezumat)

Utilizând unele particularităţi ale protocolului de dialog serial CAN (Control Area Network) se propune o structură de sistem complex. Considerând o structură de bază cu magistrală serială CAN liniară, se introduce o staţie referinţă de timp. Aceasta permite introducerea unui număr corespunzător de biţi purtând informaţia de timp în câmpul de identificare, configurând o structură de priorităţi controlată de timp. Cum biţii din identificator se pierd la recepţie, în câmpul de date se introduce referinţa de timp preluată de pe magistrala serială. Staţia referinţă de timp are cea mai înaltă prioritate în sistemul complex, astfel încât informaţia de timp apare ritmic şi fără întârzieri semnificative.

BULETINUL INSTITUTULUI POLITEHNIC DIN IAŞI
Tomul XLVII (LI), Fasc. 3–4, 2001
ELECTROTEHNICĂ. ENERGETICĂ. ELECTRONICĂ

D.C. 621.391.5

STRATEGY FOR SIMPLIFYING THE IMPLEMENTATION OF FUZZY LOGIC CONTROLLERS ON DIGITAL SUPPORT

BY

IULIAN RĂDUCANU, LILIANA VORNICU and LAURENŢIU DIMITRIU

This paper introduces a strategy for simplifying the digital FLC (Fuzzy Logic Controller) implementation based on the Fuzzy Functional Equivalent System (FFS) and direct analog–crisp to digital–fuzzy conversion using. An off-line procedure is used to carry out the consequence of the equivalent FFS, while the A/D converter quantifier determines the antecedent structure of this equivalent FFS. The direct fuzzification and the simplified software structure of the on-line inference are presented. A comparison between the control surface and the response time, of the original and equivalent systems, is presented.

1. Introduction

The capability to process information within uncertainty environment recommends the fuzzy logic as a very appropriate approach for solving the complex control plants. Despite the research effort, the theoretical performance of this control method is somewhat jeopardized by the limited implementation possibilities as well as the lack of clear design algorithms.

Most of the applications relies on pure software implementation of the control algorithm and this introduces a large computational burden. This paper proposes a new design strategy for digital implementation of a Fuzzy Logic Controller (FLC), which simplifies the computational effort. In this respect it must to follow two steps:

a) first – the fuzzy partition of the antecedents are designed for direct analog–crisp to digital–fuzzy conversion;

b) second – the deterministic consequence of the Functional Equivalent Systems (FFS) is tuned so that the control surface carryout by them approximates enough that of original system.

Thus, the FLC regular cascade of A/D conversion and digital fuzzification is replaced by a unique stage of defining the digital fuzzy variables directly based on the analog input. When implemented in a low cost microcontroller, the response time is also improved since the numerical reconstruction is lacking and the implementation of algorithm for minimizing the number of rules [4] is implicitly done.

First section is destined to define the basics of the analog–crisp to digital–fuzzy direct conversion method and the next one, to give the off-line procedure for the FFS equivalent determination. Comparative results are finally included too.

2. Analog–Crisp to Digital–Fuzzy Conversion

Generally, a fuzzy logic based control system needs an A/D acquisition of the inputs followed up by fuzzification. Thus, the inputs would be defined as fuzzy variables in a digital form. In [1] a new method of direct conversion from analogic–crisp to digital–fuzzy is proposed.

A uniform fuzzy partition with triangular membership functions, which have 100% overlapping (Fig. 1), is considered in order to simplify the presentation.

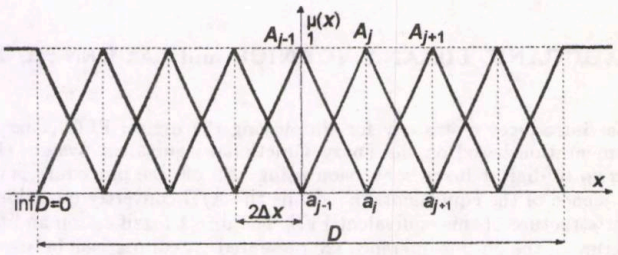

Fig. 1

If the universe of discourse (D) equals the tuning fork of one uniform A/D converter (n bits resolution) then the numeric reconstruction process, expressed by:

$$x_q = k(x)\Delta x + \frac{\Delta x}{2} + x_0, \qquad a_j = k(a_j)\Delta x + \frac{\Delta x}{2} + x_0, \quad j \in \mathbb{Z}, \tag{1}$$

yields:

$$\mu_{A_j}(x) = \begin{cases} \dfrac{k(x) - k(a_{j-1})}{k(a_j) - k(a_{j-1})}, & a_{j-1} \le x_q < a_j; \\ \dfrac{k(a_{j+1}) - k(x)}{k(a_{j+1}) - k(a_j)}, & a_j \le x_q \le a_{j+1}, \end{cases} \tag{2}$$

for the membership function definition:

$$\mu_{A_j}(x) = \begin{cases} \dfrac{x_q - a_{j-1}}{a_j - a_{j-1}}, & a_{j-1} \le x_q < a_j, \\ \dfrac{a_{j+1} - x_q}{a_{j+1} - a_j}, & a_j \le x_q \le a_{j+1}. \end{cases} \tag{3}$$

So, it can be observed that the nominator $k(x) - k(a_{j-1})$ may be written as

$$k(x) - k(a_{j-1}) = E\left[\frac{x - a_{j-1}}{\Delta x}\right], \tag{4}$$

where $E[...]$ denote the best approximation for the argument, and Δx is the quantifier step. Eq. (4) is equivalent to

$$k(x) = k(a_{j-1}) + E\left[\frac{x - a_{j-1}}{\Delta x}\right]. \tag{5}$$

If the lower bound of universe D is $\inf D$, it yields:

$$k(a_{j-1}) = E\left[\frac{a_{j-1} - \inf D}{\Delta x}\right]. \tag{6}$$

From this equation the following corollary results: *if every limit* a_j, $j \in N$, *is an integer of* 2^p *quantifier steps* Δx, *then*:

$$E\left[\frac{a_{j-1} - \inf D}{\Delta x}\right] = \frac{a_{j-1} - \inf D}{\Delta x} = (j-1) \times 2^p, \tag{7}$$

in the assumption that $\inf D \equiv a_0$.

Consequently the decimal equivalent, $k(x)$, becomes:

$$k(x) = (j-1) \times 2^p + E\left[\frac{x - a_{j-1}}{\Delta x}\right] = (j-1) \times 2^p + k(x) - k(a_{j-1}). \tag{8}$$

It can be concluded that the group of the most significant $n - p$ bits of the binary word provided by the A/D conversion of the analog–crisp value, x, may be regarded as a fuzzy set identifier and the group of the less significant p bits leads to the corresponding real membership value. Thus, this approach can be schematized as follows:

$$x \xrightarrow{\substack{A-C/D-F \\ \text{conversion}}} \left[\begin{array}{c|c} (n-p) \text{ bits} & p \text{ bits} \\ \text{fuzzy set} & \text{membership} \\ \text{identificator} & \text{value} \end{array}\right].$$

3. Off-Line Procedure for FFS Equivalent Determination

Let consider one Mamdani Fuzzy Logic Controller, having the canonic form:

$$R(k_1, ..., k_n; h): \text{ if } x_1 \text{ is } A^1_{k_1} \,\&...\&\, x_n \text{ is } A^n_{k_n}, \text{ then } y \text{ is } C_h.$$

In control applications the ranges of the inputs $x_1, ..., x_n$ are well known so that the above system will provide a hypersurface, $y = \mathcal{F}(x_1, ..., x_n)$. Our goal is to obtain an equivalent system having the rules form:

$$R(k_1, ..., k_n; h): \text{ if } x_1 \approx A'^1_{k_1} \,\&...\&\, x_n \approx A'^n_{k_n}, \text{ then } y \approx \alpha_h,$$

with α_h deterministic values and which generates about the same surface. The output of this equivalent system is defined in [3] as:

$$y = \sum_{r=1}^{N} w_r \alpha_r, \tag{9}$$

where w_h signifies the activation degree of the h-th rule, (s. Eq. (10)), $N = q_1 q_2 ... q_n$ and q_i, $(i = 1, 2, ..., n)$, is the fuzzy sets number associated to each input x_i:

$$w_h = \mu_1(x_1 - a^1_{k_1,h}) \wedge \mu_2(x_2 - a^2_{k_2,h}) \wedge ... \wedge \mu_n(x_n - a^n_{k_n,h}). \tag{10}$$

Note that the fuzzy sets, $A_{k_i}^{'i}$, defined by Eq. (3), have its number and distribution fixed by the quantifier structure of the A/D conversion. Consequently, only α_h may be tuning parameters. From Eq. (9) yields following LMS algorithm [3]:

$$\alpha_h[m+1] = \alpha_h[m] + \beta(m)e[m]w_h[m], \tag{11}$$

where the gradient of square error between real and desired output is estimated by the gradient of current square error:

$$e^2(x_1, ..., x_n) = \mathcal{F}(x_1, ..., x_n) - y(x_1, ..., x_n). \tag{12}$$

Fig. 2 represents the scheme used for α_h generation.

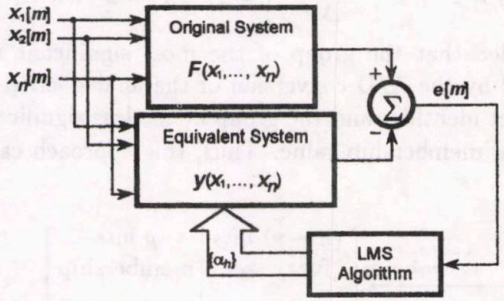

Fig. 2

The inputs $x_1[m], ..., x_n[m]$ are provided by a noise generator with uniform distribution in the definition range of the model function $\mathcal{F}(x_1, ..., x_n)$.

In Eq. (11) $\beta(m)$ is an adaptive constant having the expression:

$$\beta(m) = \frac{0.5}{E_{in}[m]}, \tag{13}$$

where

$$E_{in}[m] = \gamma E_{in}[m-1] + (1-\gamma)\sum_{h=1}^{N} w_h^2[m], \tag{14}$$

with γ a sub-unitary constant ($\gamma = 0.15$).

The performances of modeling are evaluated with normalized RMS (RMSN),

$$\mathrm{RMSN} = \frac{\sqrt{\sum_{m=1}^{M} e^2[m]}}{M \max\{d[m]\}}, \tag{15}$$

where $\max\{d[m]\}$ is the maximum of $\mathcal{F}(...)$ for all M inputs sets.

4. On-Line Software Development

This section presents the on-line software for fuzzy inference solving. For practical implementation we had considered that the equivalent FFS, determined on previous off-line procedure, has two inputs and one output. Also, in order to provide direct fuzzification [1], the input fuzzy partitions was correlated with the quantifier structure of one 8-bits A/D converter. Taking into account § **2** of this paper, if the fuzzy set identifier has 3 bits length, then $2^3 + 1$ fuzzy sets can be assigned for each

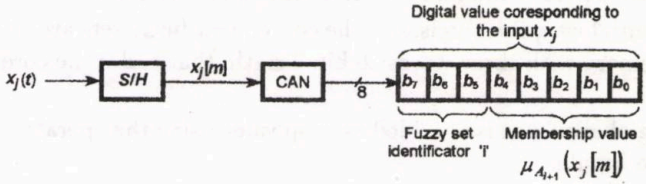

Fig. 3

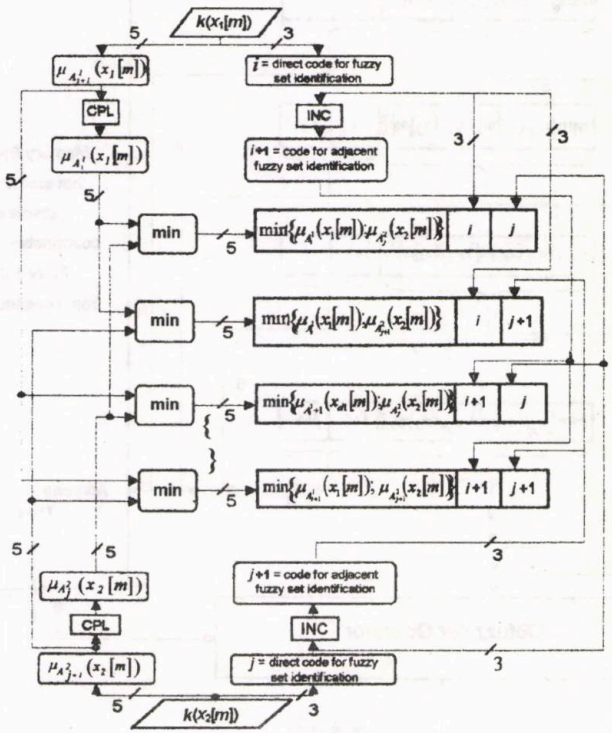

Fig. 4

input. Consequently, the membership values will be represented by 5 bits length words. So, the simple A/D conversion of one input x_j, $(j = \{1,2\})$, provides more information (s. Fig. 3).

Due to the novel interpretation on groups of bits, the software that provides the fuzzification and the active rules identification yields very simply. In Fig. 4 it could be shown the flowchart for antecedents determination.

The groups of most significant 3 bits (b_7 b_6 b_5) are used for carry out four words that will indicate the active rules. The groups of less significant 5 bits (b_4 b_3 b_2 b_1 b_0), will be used for determining the activation degree of correspondent rules.

The global result of fuzzy inference involves the following steps:

a) into a sequential way, the abscissa of the consequent fuzzy sets are obtained by addressing the memory with those words: 6 bits length, that codes the corespondent rules;

b) finally, the global output is provided as crisp value using the operator described by Eq. (9) for two inputs.

Fig. 5 show the logical scheme followed for carry out the crisp output value.

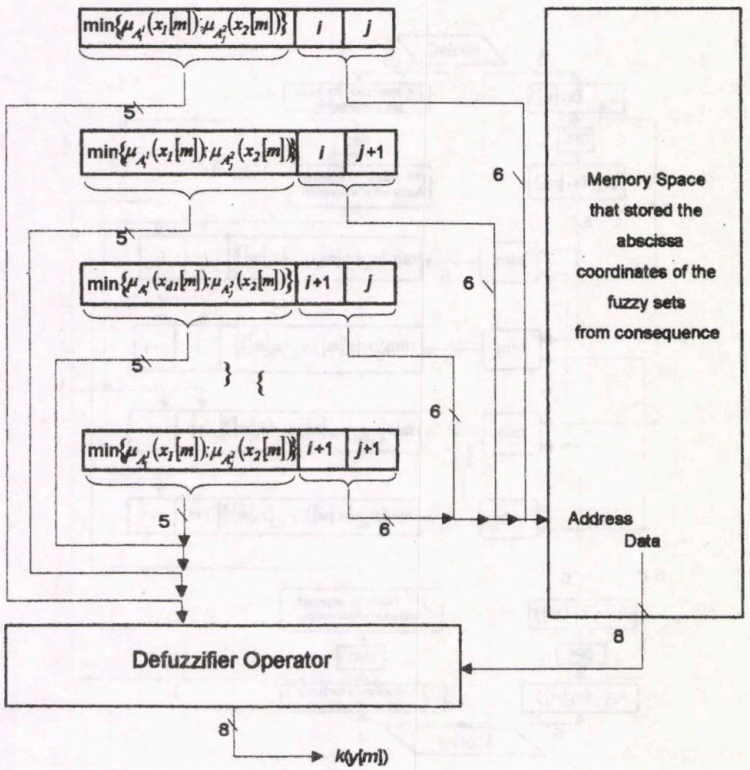

Fig. 5

5. Results

The proposed strategy was applied for fuzzy logic controller defined in [2] and presented in Fig. 6. Fig. 7 shows the two corespondent control surfaces.

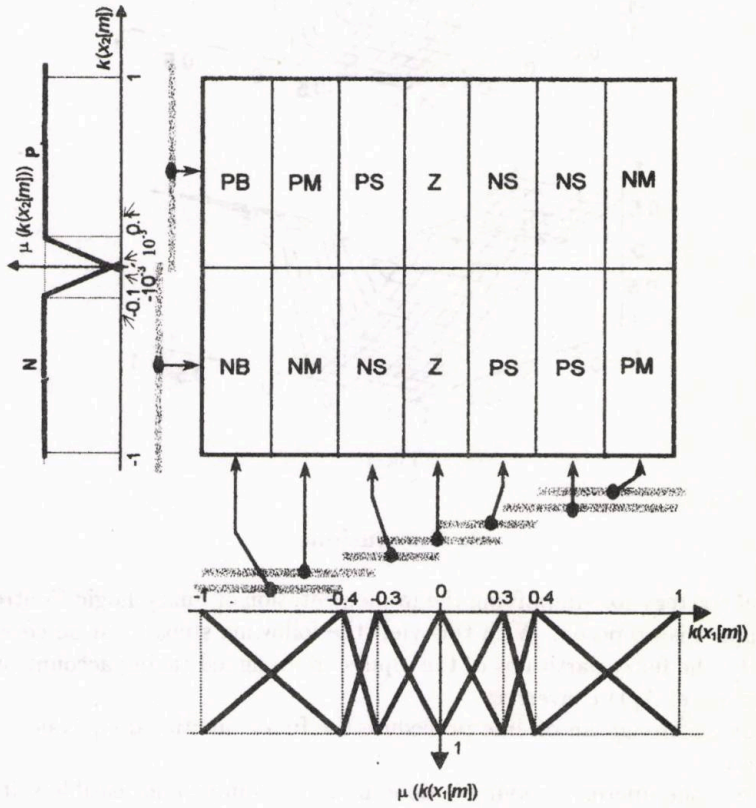

Fig. 6

The response time requested by an implementation on 80C552 support was $\tau \approx 150$ μs. Table 1 contains the performances of the off-line procedure.

Table 1

RMSN	Rules Number	Number of LMS cycles
0.02809	81	10,000

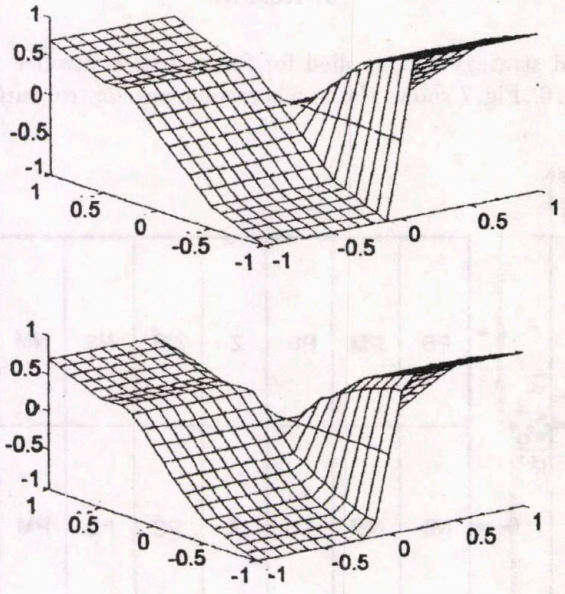

Fig. 7

6. Conclusions

A novel strategy for simplifying the implementation of Fuzzy Logic Controller on digital support is proposed. With this view the following steps must be covered:

a) firstly, the fuzzy partitions of the inputs are designed taking account by quantifier structure of A/D converter;

b) secondly, trough an off-line procedure the fuzzy functional equivalent system is determined;

c) thirdly, the inference solving is done into very simple and feasible software in a regular microcontroller.

Simulation results including the two control surfaces and the response time for an implementation with regular 80C552 microcontroller (12 MHz clock) are presented.

We have used the following notations: RL(...) – left rotation of the binary word; INC – binary increment operation; CPL – complement by the unit.

Received, July 8, 1999

Technical University "Gh.Asachi", Jassy,
Department of Applied Electronics

REFERENCES

1. Răducanu I., Dimitriu L., *The Principle of Analog-Crisp to Digital-Fuzzy*

Conversion. 6th Internat. Symp. on Automatic Control and Computer Sci. SACS'98, Iaşi, Romania, November 20–21, 1998, **I**, 232-237.

2. S o u s a G.C.D., B o s e B.K., C l e l a n d J.G., *Fuzzy Logic Based On-line Efficiency Optimization Control of an Indirect Vector-controlled Induction Motor Drive.* IEEE Trans. on Ind. Electronics, **42**, *2*, 192-198 (1995).
3. C h e l a r u M., B u h u s C., *Functional Fuzzy Systems.* Proc. Int. Conf. on Fuzzy Systems, Trabzon, Turkey, 1992.
4. T e o d o r e s c u H.N., *Minimization of Rule-Chips in Fuzzy Control and Fuzzy Inference Systems.* Proc. of the 2nd Internat. Conf. on Fuzzy Logic and Neural Networks, Iizuka, Japan, 1992, 441-444.

STRATEGIE PENTRU SIMPLIFICAREA IMPLEMENTĂRII CONTROLERELOR CU LOGICĂ FUZZY PE SUPORT DIGITAL

(Rezumat)

Se introduce o strategie pentru simplificarea implementării controlerelor cu logică fuzzy (FLC) bazată pe sistem funcţional fuzzy (FFS) echivalent şi folosirea conversiei analog–digital-fuzzy. Se foloseşte o procedură *off-line* pentru a realiza sistemul funcţional fuzzy echivalent sistemului cu logică fuzzy original. Cuantificatorul convertor A/D determină structura antecedentă a sistemului funcţional fuzzy. Se prezintă fuzzificarea directă şi structura simplificată software a inferenţei *on-line*. Se compară suprafeţele şi timpii de răspuns ale sistemelor original şi echivalent.

BULETINUL INSTITUTULUI POLITEHNIC DIN IAŞI
Tomul XLVII (LI), Fasc. 3–4, 2001
ELECTROTEHNICĂ. ENERGETICĂ. ELECTRONICĂ

D.C. 681.142.33

ON A POSSIBILITY OF REDUCING IDENTICAL TRANSITIONS IN SOFTWARE EMULATION OF SEQUENTIAL LOGICAL STRUCTURES USING THE METHOD OF THE NEXT-STATE TABLE

BY
PETRUŢ DUMA

The software emulation of sequential logical structures based on the method of the next-state table is described concisely. The author proposes a variant of this method that eliminates the identical transitions from next-state table, introducing the notion of "unique signal".

The advantage of the solution is the significant reduction of the data volume corresponding to the next-state table for numerous purposes.

1. Introduction

Assume a random sequential logical structure (SLS) as depicted in Fig. 1, having a n-bit input signal X, a m-bit output signal Y, while the number of states (S) is p.

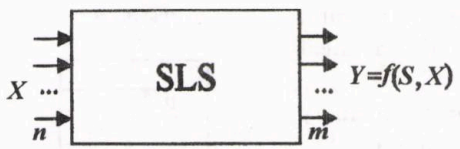

Fig. 1

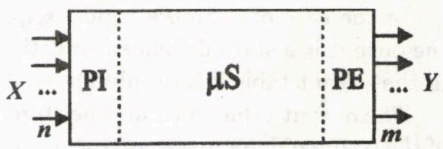

Fig. 2

The software emulation of logical sequential structures requires a microprocessor or microcontroller-based command microsystem (μS) including input ports, PI, where the X signal is to be applied and output ports, PE, where the computed Y signal is loaded (Fig. 2).

The evolution of the logical sequential structures from one state into another is made based on the clock signal, T, which is part of the input signal, X. The software detection of the clock signal, either active on ascending or on descending edge, can be performed by program loops or by converting the edge into levels. In the latter case, the clock signal may be tested in the program or may be outlined in the data structure. The processing of the clock signal, T, generates the processed input signal, XP.

2. Software Emulation of the Logical Sequential Structures Using the Method of the Next-state Table

The evolution between states of a sequential logical structure is described by a data structure called the next-state table TSU (Table 1). Assume that the sequential logical structure has p different states numbered from 0 to $p-1$, while the processed n-bit input signal XP has values from 0 to $2^n - 1$.

Table 1
TSU

S	XP					
	0	1	...	j	...	2^n-1
0	S_{00}	S_{01}	...	S_{0j}	...	S_{02^n-1}
1	S_{10}	S_{11}	...	S_{1j}	...	S_{12^n-1}
...	...	...	...	...	...	...
i	S_{i0}	S_{i1}	...	S_{ij}	...	S_{i2^n-1}
...	...	...	...	...	...	...
$p-1$	S_{p-10}	S_{p-11}	...	S_{p-1j}	...	S_{p-12^n-1}

If, at a certain moment, the sequential logical structure is in state i and the processed input signal has the value j, then the next state is S_{ij}. From the symbolic address TSU, the command microsystem memory is loaded successively with the lines of the next-state table:

$$\begin{aligned} \text{TSU}: \quad & S_{00}, S_{01}, ..., S_{02^n-1}, && \text{line 0 from TSU;} \\ & S_{10}, S_{11}, ..., S_{12^n-1}, && \text{line 1 from TSU;} \\ & \ldots\ldots\ldots\ldots\ldots\ldots\ldots\ldots\ldots\ldots\ldots\ldots\ldots\ldots\ldots\ldots \\ & S_{p-10}, S_{p-11}, ..., S_{p-12^n-1}, && \text{line } p-1 \text{ from TSU.} \end{aligned}$$

In the case of a Moore logical sequential structure, the output is a state-dependent function and is detailed in the output table TE (Table 2).

Table 2
TE

S	Y
0	Y_0
1	Y_1
...	...
$p-1$	Y_{p-1}

The output table must also be stored in the memory of the command microsystem from symbolic address TE:

$$\text{TE}: \ Y_0, \ Y_1, ..., Y_{p-1}.$$

The actual processing performed by the system in order to emulate through software a Moore sequential logical structure consists of processing the clock signal and of transferring from TSU the next state, using the processed input and the previous state. The address of the next state results from the addition of starting address of TSU table to the relative address $2^nS + XP$. Once the next state is determined, the output table TE is used for transferring the output value (from address $\text{TE} + S$) into the output port.

In the case of a Mealy logical sequential structure, the output is a function of state and input and is described in the output table TE (Table 3).

Table 3
TE

S	X					
	0	1	...	k	...	2^n-1
0	Y_{00}	Y_{01}	...	Y_{0k}	...	Y_{02^n-1}
1	Y_{10}	Y_{11}	...	Y_{1k}	...	Y_{12^n-1}
...	...	...	...	...	...	...
i	Y_{i0}	Y_{i1}	...	Y_{ik}	...	Y_{i2^n-1}
...	...	...	...	...	...	...
$p-1$	Y_{p-10}	Y_{p-11}	...	Y_{p-1k}	...	Y_{p-12^n-1}

In the same way as TSU, the output table is stored line by line in the command microsystem's memory starting from symbolic address TE:

TE : $Y_{00}, Y_{01}, ..., Y_{02^n-1}$, line 0 from TE;
$Y_{10}, Y_{11}, ..., Y_{12^n-1}$, line 1 from TE;
.....
$Y_{p-10}, Y_{p-11}, ..., Y_{p-12^n-1}$, line $p-1$ from TE.

The processing performed by the system in order to emulate through software a Mealy sequential logical structure are similar to those described above, with the necessary adjustments required by the particular manner of computing the output value.

The duration of the processing cycle is constant and has a minimal value, while the structure of the processing does not depend on the data and insures the software emulation of any sequential logical structure inserting the adequate contents into tables TSU and TE.

3. The Method of the Next-state Table with Reducing the Identical Transitions

Logical sequential structures used in practical applications have, in many cases, identical transitions for different processed input signals. Using the transformation of the groups of processed input signals that determine identical transitions for all the states into "unique signals" (XU) the dimension of TSU tables can be reduced.

The "unique signals" have consecutive numeric values starting from value 00 and perform the same operation for all the states of the logical sequential structure.

In order to transform the processed input signals which determine identical transitions for all the states into "unique signals", the direct method used for software emulation of logical combinational structures can be applied. In this case, it is necessary to define a data table which transforms the processed input signals into "unique signals". The data table (Table 4) starts from symbolic address TDT and includes the values of the "unique signals" corresponding to all the consecutive binary values of the processed input signal.

The groups of the input signals 0,1,...,i($i+1, i+2, ..., j$ or $j+1, j+2, ..., k$) determine identical transitions for all the states of the structure and they are transformed

Table 4

XP	0	...	i	$i+1$	...	j	$j+1$	...	k	...
XU	XU_n	...	XU_n	XU_p	...	XU_p	XU_m	...	XU_m	...

into the "unique signal" XU_n (XU_p, XU_m respectively), etc. The "unique signals" XU_n, XU_m, XU_p,... have values belonging to the class $\{0, 1, 2...\}$, while their number is significantly smaller than the one of processed input signals.

Assume the sequential logical structure in Fig. 1 with p states, having a n-bit processed input signal and determining numerous identical transitions. The analysis of the groups of processed input signals, which determine identical transitions, produces the "unique signals" 0, 1,...,$L-1$ (from 2^n processed input signals, L "unique signals" result, $L \ll 2^n$).

The evolution of the sequential logical structure is described by the next-state table wich reduces the identical transitions based on "unique signals" (Table 5).

If, at a certain moment, the sequential logical structure is in state i and the processed input signal XP is, in fact, "unique signal" j, then the next state is S_{ij}.

Table 5

TSU

S	XU					
	0	1	...	j	...	$L-1$
0	$S_{0\,0}$	$S_{0\,1}$	...	$S_{0\,j}$	...	$S_{0\,L-1}$
1	$S_{1\,0}$	$S_{1\,1}$	...	$S_{1\,j}$	...	$S_{1\,L-1}$
...	...	...	...	...	...	...
i	$S_{i\,0}$	$S_{i\,1}$	...	$S_{i\,j}$	...	$S_{i\,L-1}$
...	...	...	...	...	...	...
$p-1$	$S_{p-1\,0}$	$S_{p-1\,1}$	...	$S_{p-1\,j}$	...	$S_{p-1\,L-1}$

The basic logical scheme for software emulation of a Moore sequential logical structure is, in this case, as follows:

(START)	
|	
Prog. CP	Peripheral circuitry programming.
S ← 0	State initialization.
Z ← TI	Anterior clock initialization.
PE ← Y_0	Output initialization.
(SA1) ——————|	
X ← PI	Input is loaded.
Processed clock	Clock signal T is processed in order to obtain the processed input XP.
XU ← (TDT + XP)	The value of the processed input signal XP is converted into the "unique signal" XU, based on the data table TDT.
V ← S · L + XU	The relative address of the next state from TSU is computed.
S ← (TSU + V)	The next state is transferred from TSU.
Y ← (TE + S)	The output value is transferred from TE.
PE ← Y	The output is updated.
|	The algorithm is replayed.
(SA1)	

As an example, assume a 2-bit resettable register, with serial left/right shifting and parallel load, represented in Fig. 3.

The notations have the following meanings: T – clock input; D – data input for serial shifting; $L/\overline{R}$ – input the left/right shifting sense; a and b – data inputs for parallel loading; $\overline{R}$ – initialization input; Q_A, $\overline{Q}_A$, Q_B, $\overline{Q}_B$ – register outputs.

The register's input and output are assigned to the input port $P1$ and output port $P4$, respectively, of the microcontroller (μC) INTEL 80C451, as depicted in Fig. 4. Input line $P1.7$ is not used, as are the output lines $P4.2...P4.5$, which are set in logical 1.

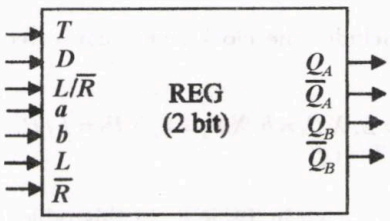

Fig. 3

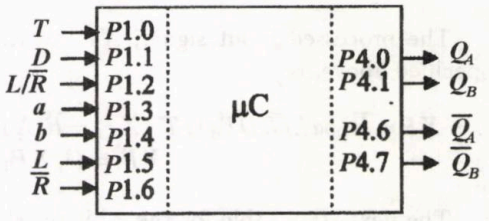

Fig. 4

The descending edge active clock input, T, is outlined in the data structure by converting the edge into logical level; the register's input for the shifting sense, $L/\overline{R}$, determines a right shifting if $L/\overline{R}=0$ and a left shifting if $L/\overline{R}=1$; the parallel load input, L, synchronous with the clock signal, is active on logical "1" and prioritary compared to the shifting sense input; the reset input, $\overline{R}$ (asynchronous), is active on logical "0" and prioritary compared to any other input.

The 2-bit register has four states, numbered from 0 to 3; the evolution between states is described in Table 6 (x – irrelevant binary logical value).

Table 6

$\overline{R}$	L	b	a	$L/\overline{R}$	D	T	State
0	x	x	x	x	x	x	$S \leftarrow 0$
1	x	x	x	x	x		$S \leftarrow S$
1	1	b	a	x	x		$S \leftarrow ba$
1	0	x	x	0	d		$S \leftarrow S/2 + 2d$
1	0	x	x	1	d		$S \leftarrow 2S + d$

The input signal, X, has the form:

$$X = \overline{R}Lba L/\overline{R}DT \ (X_6 = \overline{R}, X_5 = L, X_4 = b, X_3 = a, X_2 = L/\overline{R}, X_1 = D, X_0 = T).$$

The descending edge of the clock signal, T, is converted in logical "0" level using the logical operation $\overline{T}a \cup T$ (Ta – anterior clock) and is included in the data structure. In this case, the register's evolution between states is described in Table 7.

Table 7

$\overline{R}$	L	b	a	$L/\overline{R}$	D	$\overline{T}_a \cup T$	State
0	x	x	x	x	x	x	$S \leftarrow 0$
1	x	x	x	x	x	1	$S \leftarrow S$
1	1	b	a	x	x	0	$S \leftarrow ba$
1	0	x	x	0	d	0	$S \leftarrow S/2 + 2d$
1	0	x	x	1	d	0	$S \leftarrow 2S + d$

The processed input signal, XP, which includes the clock signal converted as specified above, is:

$$XP = \overline{R}LbaL/\overline{R}D\overline{T}_a \cup T \ (XP_6 = \overline{R}, XP_5 = L, XP_4 = b, XP_3 = a, XP_2 = L/\overline{R}, XP_1 = D, XP_0 = \overline{T}_a \cup T).$$

The next-state table for the 2-bit register is shown in Table 8. In this table, the processed input signals that determine identical transition are grouped. If the input signals are not grouped, than the 128 distinct values of the processed input signal imply a 128-column table, which is uncomfortable to fill.

Table 8

TSU

	XP								
S	$0xxxxxx$, $1100xx0$	$1xxxxx1$	$1101xx0$	$1110xx0$	$1111xx0$	$10xx000$	$10xx010$	$10xx100$	$11xx110$
0	0	0	1	2	3	0	2	0	1
1	0	1	1	2	3	0	2	2	3
2	0	2	1	2	3	1	3	0	1
3	0	3	1	2	3	1	3	2	3

For this application, the following "unique signals" should be defined:

0 – for the processed input signals group 00-$3FH$, $60H$, $62H$, $64H$, $66H$;
1 – for the processed input signals group $41H$-$7FH$ odd ($41H, 43H, 45H$,...,$7FH$);
2 – for the processed input signals group $68H$, $6AH$, $6CH$, $6EH$;
3 – for the processed input signals group $70H$, $72H$, $74H$, $76H$;
4 – for the processed input signals group $78H$, $7AH$, $7CH$, $7EH$;
5 – for the processed input signals group $40H$, $48H$, $50H$, $58H$;
6 – for the processed input signals group $42H$, $4AH$, $52H$, $5AH$;
7 – for the processed input signals group $44H$, $4CH$, $54H$, $5CH$;
8 – for the processed input signals group $66H$, $6EH$, $76H$, $7EH$.

The data table that converts the processed input signals XP into "unique signals" XU is stored into the memory of the command microsystem, starting from address TDT:

TDT: 0,0,0,0,0,0,0,0,0,0,0,0,0,0,0,0,0,0,0,0,0,0,0,0,0,0,0,0,0,0,0,0,
0,0,0,0,0,0,0,0,0,0,0,0,0,0,0,0,0,0,0,0,0,0,0,0,0,0,0,0,0,0,0,0,
5,1,6,1,7,1,8,1,5,1,6,1,7,1,8,1,5,1,6,1,7,1,8,1,5,1,6,1,7,1,8,1,
0,1,0,1,0,1,0,1,2,1,2,1,2,1,2,1,3,1,3,1,3,1,3,1,4,1,4,1,4,1,4,1.

Another possibility of defining the "unique signals" is to mask the processed input signal and to adequately test it. This solution eliminates the TDT table, but implies a program sequence to mask and test the input signals. Therefore, a longer time interval is required in order to determine the "unique signal" XU.

The next-state table that reduces identical transitions for the 2-bit resettable register with left/right shifting and parallel loading is depicted in Table 9 *a*. The output is a function of state (Moore) and is shown in Table 9 *b*.

Table 9 *a*

TSU

S	XU								
	0	1	2	3	4	5	6	7	8
0	0	0	1	2	3	0	2	0	1
1	0	1	1	2	3	0	2	2	3
2	0	2	1	2	3	1	3	0	1
3	0	3	1	2	3	1	3	2	3

Table 9 *b*

TE

Y
FC
BD
$7E$
$3F$

4. Conclusions

The proposed method significantly reduces the data structure in the case of sequential logical structures with identical transitions; for the example assumed (2-bit resettable register with left/right shifting and parallel loading), the next-state table TSU is reduced from a data volume of 128×4 bytes for the processed input signals, to 9×4 bytes for the "unique signals".

The time interval needed for the determination of the numerical output value remains the same, regardless the input signal, X, and the state, S, of the sequential logical structure.

The method is applicable even if the structure has impossible or irrelevant transitions. In this particular case, the input signals that determine these transitions can be either grouped in a distinct "unique signal" or they can be associated to other input signals.

For a Mealy sequential logical structure, the method can be applied as well, but, in addition, the adequate processing for computing the output values is also required. If, for different input signals, identical output values are obtained, then the algorithm used on the next-state table can also be performed for the output table.

Received, June 3, 2001

Technical University "Gh.Asachi", Jassy,
Department of Telecommunications

REFERENCES

1. Căpăţînă O., *Proiectarea cu microcalculatoare integrate*. Ed. Dacia, Cluj-Napoca, 1992.
2. Leventhal A., *Programmation en language assembleur*. Ed. Radio, Paris, 1989.
3. Rony R., Larsen D.G., Titus A., *Microcomputer Interfacing and Programming*. Howard W. Sams & Co.Inc., NY, 1987.
4. Somnea D., Vlăduţ T., *Programarea în Assembler*. Ed. Tehn., Bucureşti, 1992.
5. Sztojanov I., Borcoci E., Tomescu N., Bulik D., Petrec M., Petrec C., *De la poarta TTL la microprocesor*. Ed. Tehn., Bucureşti, 1987.
6. Toacşe Gh., *Introducere în microprocesoare*. Ed. Ştiinţ. şi Encicl., Bucureşti, 1985.
7. * * * *INTEL 8051 Microcontroller*. Data Book, 1990.

ASUPRA UNEI POSIBILITĂŢI DE REDUCERE A TRANZIŢIILOR IDENTICE LA REALIZAREA PRIN *SOFT* A STRUCTURILOR LOGICE SECVENŢIALE CU METODA TABLOULUI STĂRILOR URMĂTOARE

(Rezumat)

Se descrie pe scurt realizarea prin *soft* a structurilor logice secvenţiale cu metoda tabloului stărilor următoare. Pe baza acestei metode este propusă de autor o variantă care elimină tranziţiile identice din tabelul TSU prin introducerea noţiunii de „semnal unic".

Avantajul soluţiei este acela de a reduce considerabil volumul de date din tabelul stărilor următoare pentru numeroase aplicaţii.

BULETINUL INSTITUTULUI POLITEHNIC DIN IAŞI
Tomul XLVII (LI), Fasc. 3–4, 2001
ELECTROTEHNICĂ. ENERGETICĂ. ELECTRONICĂ

D.C. 621.396

A METHOD FOR THE REDUCTION OF THE SHORT CHANNEL TRANSISTOR CHAIN TO AN EQUIVALENT MOSFET

BY
DĂNUŢ BURDIA

A modeling technique for the reduction of series-connected MOSFETs to a simple equivalent transistor with the same behavior is studied. The proposed method takes into account the short-channel effects, the influence of body effect and coupling capacitance and is developed for nonzero transition time input. The effective width of the equivalent transistor is calculated considering the operating conditions of each transistor in the chain. The case when all transistors are switching together, which is the worst scenario, is analyzed. The results produced by the proposed model for a 0.8 μm CMOS process technology show very good agreement with SPICE simulations.

1. Introduction

In the last years, many different techniques for timing modeling of the digital integrated circuits have been proposed in order to improve the speed of circuit simulators. The reliability of these approaches depends on the accuracy with which the transient response of basic circuits can be evaluated. Circuit simulators, such as SPICE, that can provide a detailed and accurate analysis, are based on numerical methods and, therefore, are prohibitively slow for large designs. The alternative is to use analytical expressions which take into account the most critical factors that influence the system behavior and are with orders of magnitude faster than SPICE. During recent years much research effort has been devoted to the modeling of the CMOS inverter behavior [1],...,[4]. More complicated gates, such as NAND/NOR structures, are difficult to model, mainly because of the multinodal circuitry and multiple inputs of the transistor chain. Therefore, many reduction techniques of multiple-input gates to equivalent inverters have been proposed in the literature [5],...,[8].

Traditionally, a single transistor, that has the equivalent width approximated by W/N, is used to model the transistor chain (W – channel width of one transistor, N – number of series-connected transistors from chain) [7], without taking into account the effects of the load and the input transition time. This is the main reason of inaccuracy, because it is valid only for step input waveforms, or when all transistors operate in the linear region. Several attempts have also been made in order to model the transistor chain trying to exploit the fact that all transistors in the chain except for the top one, operate always in linear mode [6], [8]. These previous works used simplifying assumptions for the operation of the chain, such as step inputs, resistive behaviour, long channel models and negligible body effect.

Some of the secondary effects which are present in the operation of the transistor chain have been mentioned in [9], [10], where a chain collapsing technique based on a nonlinear macromodel is proposed, but it extracts parameters from dc analysis and applies them on transient phenomena resulting in inaccuracies.

In what follows, a reduction-technique based on the dynamic behavior of series-connected MOSFETs, is presented. The equivalent transistor's width is calculated taking into account the mode of operation of the transistors in the chain, the influences of the output load, the input transition time and the body effect. Also, the additional effects due to the internal and coupling capacitances are included. For the transistor currents, the α-power MOS model [11] is used, in order to take into account the velocity saturation effect of short-channel devices.

2. Transistor Chain Analysis and Equivalent Width

In the following let us consider the discharging of an output load by the NMOS transistor chain shown in Fig. 1 *a*. The analysis of a PMOS charging chain is symmetrical. The case when a common rising input ramp is applied to all transistor gates, is analysed. The waveform of input voltages is given by

$$V_{\text{in}} = \begin{cases} 0, & t \leq 0, \\ \dfrac{V_{DD}}{\tau} t, & 0 < t \leq \tau, \\ V_{DD}, & t > \tau, \end{cases} \tag{1}$$

where τ is the input rise time.

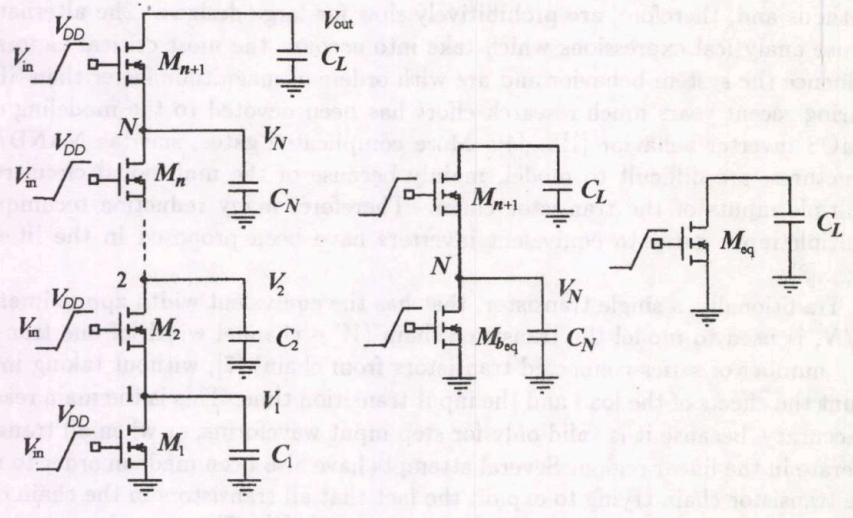

Fig. 1.– *a* – Complete NMOS transistor chain; *b* – two transistor equivalent circuit; *c* – single equivalent transistor model.

For the transistor drain currents, the expressions of the α-power law MOSFET model [1], which takes into account the carrier velocity saturation effect of short channel devices, is used:

$$(2) \qquad I_D = \begin{cases} 0, & V_{GS} \leq V_{TH}, \quad \text{cutoff region,} \\ P_S \dfrac{W}{L}(V_{GS} - V_{TH})^{\alpha}, & V_{DS} \geq V'_{DO}, \quad \text{saturation region,} \\ P_L \dfrac{W}{L}(V_{GS} - V_{TH})^{\alpha/2} V_{DS}, & V_{DS} < V'_{DO}, \quad \text{linear region,} \end{cases}$$

where $V'_{DO} = P_D(V_{GS} - V_{TH})^{\alpha/2}$ is the drain saturation voltage and $P_L = P_S/P_D$. The parameters α (velocity saturation index), P_S and P_D are extracted from the I–V static characteristics of the transistor:

$$P_S = \frac{I_{DO1}}{(V_{DD} - V_{TH})^{\alpha}}, \quad P_D = \frac{V_{DO1}}{(V_{DD} - V_{TH})^{\alpha/2}}.$$

I_{DO1} is the drain current of the transistor with the ratio $W/L = 1$ observed when $V_{GS} = V_{DS} = V_{DD}$ (Fig. 2). V_{TH} is the threshold voltage which is expressed by its first-order Taylor approximation around $V_{SB} = 0.2V_{DD}$:

$$(3) \qquad \tilde{V}_{TH} = V_{TH}\Big|_{V_{SB}=0.2V_{DD}} + \frac{\mathrm{d}V_{TH}}{\mathrm{d}V_{SB}}\Big|_{V_{SB}=0.2V_{DD}} (V_{SB} - 0.2V_{DD}) = \theta + \delta V_{SB},$$

where V_{SB} is the source-to-substrate voltage.

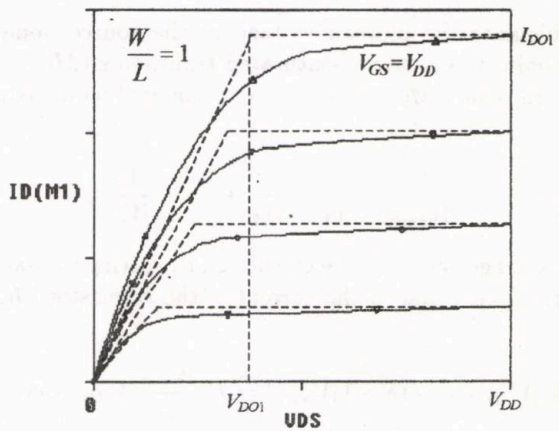

Fig. 2.– Determination of the α-power law model parameters (broken lines).

Assuming that the internal node capacitances are initially discharged, while the input is applied, the top-most transistor in the chain (M_{n+1}) begins its operation in saturation mode and then enters the linear region when $V_{DS} = V'_{DO}$. The rest

of the transistors in the chain $(M_1, ..., M_n)$ operate in the linear region without ever leaving this region [12]. In the case of the fast input ramp the top-most transistor is still saturated after the end of input transition, and its source node is charged up to a plateau voltage [12], [13]. This voltage level is maintained constant until the top-most transistor exits saturation (Fig. 3). Also, during this time interval all internal node voltages remain constant. Thus, the parasitic currents due to drain/source node capacitances and gate-to-drain/source coupling capacitances are eliminated because the voltages at the corresponding nodes remain constant. Therefore, during this state, the same current flows through all transistor in the chain.

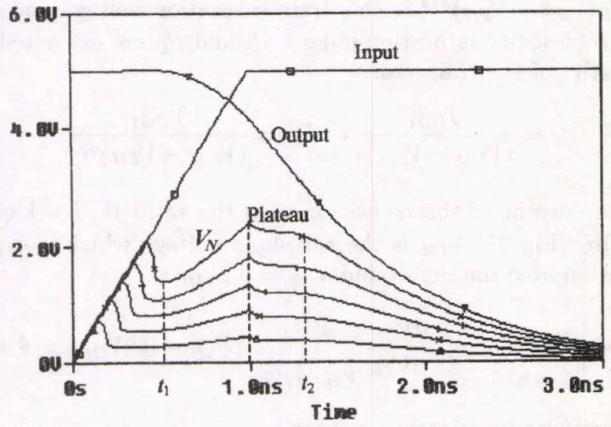

Fig. 3.– Output and intermediate node voltage waveforms of the transistor chain.

In order to calculate the plateau voltage at the source node of the top-most transistor of the chain, V_{PN}, the non-saturated transistors $(M_1, ..., M_n)$ are replaced by an equivalent transistor $M_{b\,\mathrm{eq}}$ (Fig. 1 *b*) with channel width equal to $W_{b\,\mathrm{eq}}$ given by

$$\frac{1}{W_{b\,\mathrm{eq}}} = \frac{1}{W_1} + \frac{1}{W_2} + \cdots + \frac{1}{W_n}. \tag{4}$$

Thus, the plateau voltage, V_{NP}, can be calculated by setting the saturation current of the top transistor, M_{n+1}, equal to the current of the transistor $M_{b\,\mathrm{eq}}$ which operates in linear mode:

$$P_{S_{n+1}} \frac{W_{n+1}}{L} [V_{DD} - \theta - (\delta + 1)V_{NP}]^{\alpha} = P_L \frac{W_{b\,\mathrm{eq}}}{L} (V_{DD} - V_{T_{b\,\mathrm{eq}}})^{\alpha_b/2} V_{NP}, \tag{5}$$

where

$$V_{T_{b\,\mathrm{eq}}} = \theta + \delta \frac{V_{NP}}{N}. \tag{6}$$

The parameter α_b is extracted using the channel width $W_{b\,\mathrm{eq}}$ because it depends on the transistor width as in the Fig. 4.

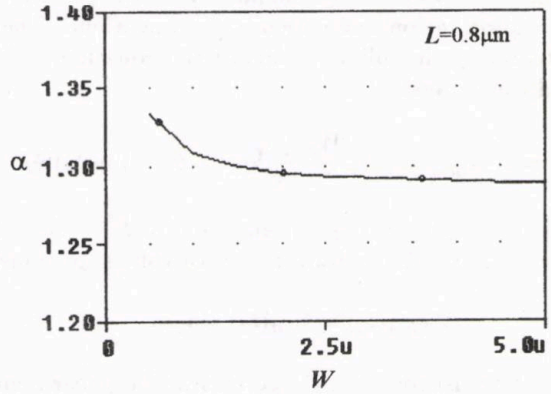

Fig. 4.– The dependence of parameter α *vs.* the channel width.

The equation (5) can be solved using some Newton-Raphson iterations with the initial point $V_{NP}^{(0)} = V_{DD}/2$.

In the following, the source voltage (V_N) of the top transistor in the chain is considered linear for the interval between time t_1, when the chain starts conducting, and time τ, when the input reaches V_{DD}. This observation is based on SPICE simulations (Fig. 3) and leads to highly accurate results. The time point t_1 is calculated in the next section by analysing the influence of the gate-to-drain and gate-to-source capacitances on the chain operation. After the calculation of the time t_1 and the value of V_N at that time ($V_N(t_1) = [V_{\mathrm{in}}(t_1) - \theta]/(1+\delta)$), the expression of the voltage waveform at the node N is given by

$$V_N(t) = \frac{V_{NP} - V_N(t_1)}{\tau - t_1} t + \frac{V_N(t_1)\tau - V_{NP} t_1}{\tau - t_1}. \tag{7}$$

In order to obtain the width (W_{eq}) of the single equivalent transistor (M_{eq}) (Fig. 1 *c*) the currents through transistor M_{n+1} of the complete chain and transistor M_{eq} should be set equal. When the transistor M_{n+1} is saturated we have:

$$P_{S_{n+1}} \frac{W_{n+1}}{L} [V_{\mathrm{in}} - \theta - (\delta+1)V_N]^{\alpha} = P_L \frac{W_{\mathrm{e}}}{L} \left(V_{\mathrm{in}} - \theta - \delta \frac{V_N}{N}\right)^{\alpha_b/2} V_N. \tag{8}$$

From the above equation it results the expression:

$$W_{\mathrm{eq}} = W_{n+1} \frac{P_{S_{n+1}}}{P_L} \cdot \frac{[V_{\mathrm{in}} - \theta - (1+\delta)V_N]^{\alpha_{n+1}}}{V_N \left[V_{\mathrm{in}} - \theta - \delta \dfrac{V_N}{N}\right]^{\alpha_b/2}}. \tag{9}$$

Note that the expression of W_{eq} depends on time. Therefore, an average value has to be considered. Thus, for the time interval $[t_1, \tau]$ the equivalent width is calculated with equation (9) at the time $t = (t_1+\tau)/2$. For the next time interval, (τ, t_2), which corresponds to the plateau voltage, the equivalent width is calculated with equation (9) for $V_{in} = V_{DD}$ and $V_N = V_{NP}$. The time point t_2 is the one when the transistor M_{n+1} leaves the saturation region and enters in the linear one. The value of t_2 can be calculated by integrating the following differential equation which describes the discharge of the load capacitance:

$$C_L \frac{dV_{out}}{dt} = -I_{M_{n+1}} = -P_S \frac{W_{n+1}}{L} [V_{DD} - \theta - (1+\delta)V_{NP}]^{\alpha_{n+1}}, \tag{10}$$

with the initial condition $V_{out}(t_1) = V_{DD}$. Then, the time t_2 is calculated by equating the drain saturation voltage and the drain-to-source voltage of transistor M_{n+1}:

$$V_{DSsat}(t_2) = V_{out}(t_2) - V_{NP}. \tag{11}$$

When the top-most transistor (M_{n+1}) operates in the linear region ($t \leq t_2$), the transistor chain can be considered as a voltage divider with a uniform distribution of the output voltage among all drain/source nodes. Thus, the voltage at the source of the top-most transistor is given by

$$V_N = \frac{N}{N+1} V_{out}. \tag{12}$$

Then, the equivalent width for the linear region can be obtained in a similar way as in the saturation region:

$$W_{eq} = \frac{W_{n+1}}{N+1} \left[\frac{V_{DD} - \theta - (1+\delta)\dfrac{NV_{out}}{N+1}}{V_{in} - \theta - \delta \dfrac{V_{out}}{N+1}} \right]^{\alpha_{n+1}}. \tag{13}$$

Since W_{eq} depends on V_{out}, the average between the value calculated with Eq. (13) for $t = t_2$ and that calculated for $V_{out} = 0$ is considered:

$$W_{eq} = \frac{W_{eq}(t_2) + W_{eq}\big|_{V_{out}=0}}{2}. \tag{14}$$

3. Evaluation of the Starting Point of Conduction

In order to model efficiently the chain by an equivalent transistor, the starting point of conduction of the chain has to be estimated. In a transistor chain with the same input applied to the gates of all transistors, the closer to the top of the chain starts conducting later because of a gradual increase in their source and threshold

voltage. Therefore, the starting point of conduction of the chain is that of the top-most transistor, M_{n+1}.

In order to estimate this starting time consider the example of a six transistor chain with the same input applied to all transistors. In Fig. 5 are shown the piece-wise linear representation of the drain voltages of the five lower transistors together with the common input. Because of coupling capacitances between transistors gates and the drain/source nodes, the drain voltages tend to follow the input ramp until all lower transistors start conducting. Initially the transistors are in the cutoff region and the coupling capacitance is calculated as the sum of the gate-to-source and gate-to-drain overlap capacitances of the upper and lower transistors respectively, in each node. Thus, the overlap capacitances are given by $C_{\text{overlap}} = W(C_{gd0} + C_{gs0})$. Until the time where the transistor below a node starts conducting, the voltage waveform of that node is derived by equating the current due to the coupling capacitance of the node, $I_{C_{M_i}}$, with the charging current of the parasitic node capacitance, I_{C_i}:

$$I_{C_{M_i}} = I_{C_i},$$

that is

$$C_{M_i} \frac{\mathrm{d}(V_{\text{in}} - V_i)}{\mathrm{d}t} = C_i \frac{\mathrm{d}V_i}{\mathrm{d}t}$$

and finally

$$V_i(t) = \frac{C_{M_i}}{C_{M_i} + C_i} V_{\text{in}}(t), \quad (i = 1, 2, ..., n). \tag{15}$$

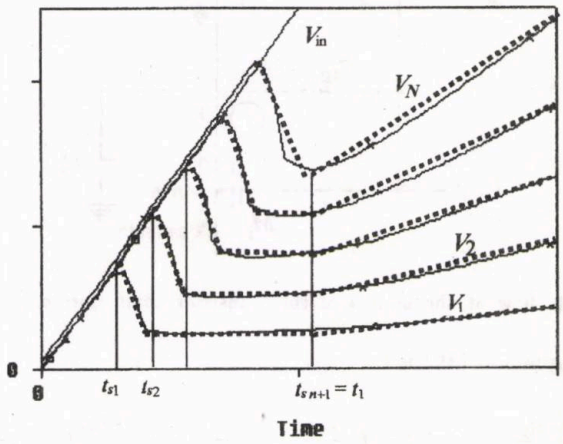

Fig. 5.– Intermediate node voltage waveforms approximation until the transistor chain starts conducting.

When a transistor starts to conduct, *e.g.*, transistor M_i, at the time t_{s_i}, it operates initially in saturation. Since its gate-to-drain coupling capacitance is very small, the voltage, V_i, at the drain of M_i decreases because of the discharging currents through

all lower transistors. This continues until time $t_{S_{i+1}}$ when transistor M_{i+1} starts conducting and enters in saturation. On the other hand, because of increasing the gate-to-source voltage of transistor M_i while its V_{DS} decreases, the transistor M_i will enter in the linear region close to point $t_{S_{i+1}}$. From this point on, the gate-to-source coupling capacitance of transistor M_{i+1} increases by $2/3C_{0x}WL$ and the gate-to-drain coupling capacitance of transistor M_i increases by $1/2C_{0x}WL$. Because of this increased coupling capacitance at the node i, the node voltage, V_i, will become almost constant and equal to its value at $t_{S_{i+1}}$. This observation has also been verified by SPICE simulations. The node voltages start to rise again when the complete chain starts conducting at time t_1. Also, during the time interval $[t_{S_i}, t_{S_{i+1}}]$ the slope of voltage waveform V_i is considered the same for each node.

The voltage expression of node 1 during the time interval $[t_{S_1}, t_{S_2}]$ can be calculated by integrating the differential equation which results from the application of Kirchhoff's current law at node 1 (Fig. 6 for $i=1$):

$$i_{C_{M_1}} = i_{C_1} + i_{D_1}$$

i.e.

$$C_{M_1}\left(\frac{\mathrm{d}V_{\mathrm{in}}}{\mathrm{d}t} - \frac{\mathrm{d}V_1}{\mathrm{d}t}\right) = C_1\frac{\mathrm{d}V_1}{\mathrm{d}t} + P_S\frac{W_1}{L}(V_{\mathrm{in}} - V_{TO})^{\alpha_1}. \tag{16}$$

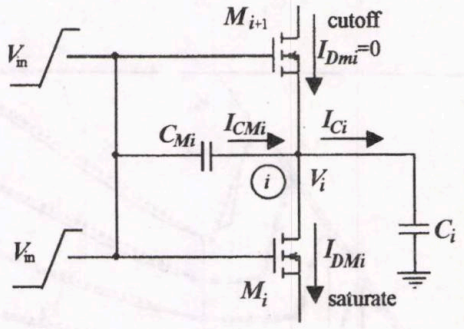

Fig. 6.– Currents flow at the node i of the transistor chain during $[t_{S_i}, t_{S_{i+1}}]$ interval.

The solution of equation (16) is

$$V_1(t) = \frac{C_{M_1}}{C_{M_1}+C_1}\cdot\frac{V_{DD}}{\tau}t - P_S\frac{W_1}{L}\cdot\frac{\tau}{(\alpha+1)V_{DD}}\left(\frac{V_{DD}}{\tau}t - V_{TO}\right)^{\alpha+1} + V_1(t_{S_1}), \tag{17}$$

where

$$V_1(t_{S_1}) = \frac{C_{M_1}}{C_{M_1}+C_1}\cdot\frac{V_{DD}}{\tau}t_{S_1} \quad \text{and} \quad t_{S_1} = \frac{V_{TO}}{V_{DD}}\tau.$$

In what follows the expression of $V_1(t)$ given by Eq. (17) is approximated by the first term of Taylor series around the point $t = 2t_{S_1}$ and then can be used in order to calculate the time when the next transistor further up starts conducting. Thus, the time t_{S_2}, when the transistor M_2 starts conducting represents the solution of the linear equation:

$$V_{GS_2}(t_{S_2}) - V_{TH_2}(t_{S_2}) = 0. \tag{18}$$

Now, knowing time points t_{S_1}, t_{S_2}, and the corresponding voltage drain values of the bottom transistor, $V_1(t_{S_1})$ and $V_1(t_{S_2})$, the average slope, m, of the waveform voltage, $V_1(t)$, in the time interval $[t_{S_1}, t_{S_2}]$, can be easily obtained. Also, this value of the slope is considered for each node voltage waveform during the interval $[t_{S_i}, t_{S_{i+1}}]$.

According to the above analysis, the time point at which the M_{i+1} transistor in the chain starts conducting can be found by solving the following equation:

$$V_{GS_{i+1}}(t_{S_{i+1}}) - V_{TH_{1+1}}(t_{S_{1+1}}) = 0$$

i.e.

$$V_{\text{in}}(t_{S_{i+1}}) - \theta - (1+\delta)\left[\frac{C_{M_i}}{C_{M_i}+C_i}\cdot\frac{V_{DD}}{\tau}t_{S_i} + m(t_{S_{i+1}} - t_{S_i})\right] = 0, \tag{19}$$

so that the following recursive expression:

$$t_{S_{i+1}} = \frac{\theta + (1+\delta)\left(\dfrac{C_{M_i}}{C_{M_i}+C_i}\cdot\dfrac{V_{DD}}{\tau} - m\right)t_{S_i}}{V_{DD} - (1+\delta)m\tau}\tau, \quad (i = 2, ..., N), \tag{20}$$

is obtained.

From the above expression, the time at which the chain starts conducting, $t_{S_n} = t_1$, can be easily obtained.

4. Results and Conclusions

The accuracy of the reduction method presented in this paper were validated by comparison of the output voltage of the complete transistor chain and that of the single equivalent transistor. The CMOS process technology assumed is 0.8 μm. A supply voltage of 5 V and an output load of 0.1 pF have been used. The model parameters of the α-power law model used in calculations are $I_{DO_1} = 557$ μA,

$V_{DO_1} = 1.8$ V, $V_{TH} = 0.65$ V, $\alpha = 1.29$. In Fig. 7 the output voltage waveforms of the complete chain (six transistors) and the single equivalent transistor for some typical

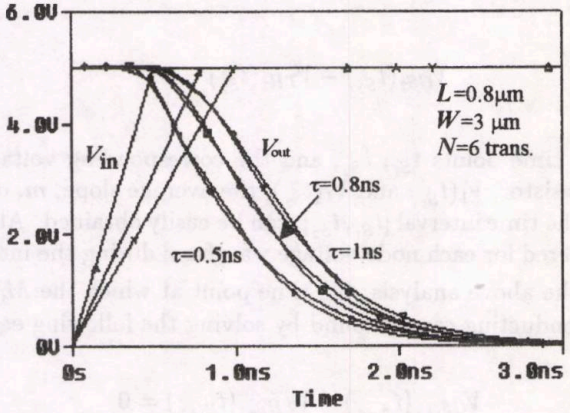

Fig. 7.– Output waveforms of the complete chain and the nonlinear equivalent transistor for a six transistor chain and some typical values of input rise time, τ.

values of the input rise time, are represented. It can be observed that the analytical waveforms are very close to those produced by SPICE simulations. This occurs because the presented model for the reduction of series-connected MOSFETs include the influences of the input transition time, the coupling, parasitic and load capacitances, and the body effect.

Received, June 4, 2001

Technical University "Gh.Asachi", Jassy,
Department of Telecommunications

REFERENCES

1. Hedenstierna N., Jeppson K.O., *CMOS Circuit Speed and Buffer Optimization.* IEEE Trans. on Computer-Aided Design, **6**, *3*, 270-281 (1987).
2. Kayssi A.I., Sakallah K.A., Burks T.M., *Analytical Transient Response of CMOS Inverters.* IEEE Trans. on Circ. a. Syst.-I, **39**, *1*, 42-45 (1992).
3. Jeppson K.O., *Modeling the Influence of the Transistor Gain Ratio, and the Input-to-Output Coupling Capacitance on the CMOS Inverter Delay.* IEEE J. of Solid-State Circ., **29**, *6*, 646-654 (1994).
4. Bisdounis L., Nikolaidis S., Koufopavlou O., *Analytical Transient Response and Propagation Delay Evaluation of the CMOS Inverter for Short-channel Devices.* IEEE J. of Solid-State Circuits, **33**, *2*, 302-306 (1998).
5. Nabavi-Lishi A., Rumin N.C., *Inverters Models of CMOS Gates for Supply Current and Delay Evaluation.* IEEE Trans. on CAD, **13**, 1271-1279 (1994).
6. Sakurai T., Newton A.R., *Delay Analysis of Series-connected MOSFET Circuits.* IEEE J. of Solid-State Circuits, **26**, *2*, 122-131 (1991).
7. Shih Y.H., Leblebici Y., Kang S.M., *ILLIADS: A Fast Timing and Reliability Simulator for Digital MOS Circuits.* IEEE Trans. on CAD, **12**, 1387-1402 (1993).
8. Kang S.M., Chen H.Y., *A Global Delay Model for Domino CMOS Circuits with Application to Transistor Sizing.* Int. J. of Circ. Theory a. Appl., **18**, 289-306 (1990).

9. Kong J.-T., Overhauser D., *Methods to Improve Digital MOS Macromodel Accuracy.* IEEE Trans. on CAD, **14**, 868-881 (1995).
10. Kong J.-T., Hussain S.Z., Overshauser D., *Performance Estimation of Complex MOS Gates.* IEEE Trans. on CAS-I, **44**, *9*, 785-795 (1997).
11. Sakurai T., Newton A.R., *Alpha-power Law MOSFET Model and its Applications to CMOS Inverter Delay and other Formulas.* IEEE J. of Solid-State Circ., **25**, *4*, 584-594 (1990).
12. Bisdounis L., Koufopavlou O., *Modeling the Dynamic Behavior of Series-connected MOSFETs for Delay Analysis of Multiple-input CMOS Gates.* IEEE Int. Symp. on Circ. a. Syst., June 1998, **6**, 342-345.
13. Catzigeorgiou A., Nikolaidis S., Tsoukalas I., *A Modeling Technique for CMOS Gates.* IEEE Trans. on CAD, **18**, 557-575 (1999).

O METODĂ DE REDUCERE A UNUI LANŢ DE TRANZISTOARE CU CANAL SCURT LA UN TRANZISTOR MOS ECHIVALENT

(Rezumat)

Se propune o tehnică de modelare pentru reducerea unui lanţ de tranzistoare conectate în serie la un simplu tranzistor echivalent, având aceeaşi comportare în regim dinamic. Metoda propusă ia în consideraţie efectele de canal-scurt din cadrul tranzistoarelor submicronice, influenţele variaţiei tensiunii de prag, a capacităţilor de sarcină, de cuplaj şi parazite, precum şi a timpului de tranziţie a formei de undă a tensiunii de la intrare. În cadrul metodei este calculată lăţimea efectivă a tranzistorului echivalent în funcţie de condiţiile de funcţionare a fiecărui tranzistor din cadrul lanţului. În lucrare este prezentat cazul cel mai defavorabil când forma de undă de la intrare este aplicată simultan pe terminalele de poartă ale tuturor tranzistoarelor. Modelul propus a fost testat pentru cazul tranzistoarelor CMOS conectate în serie, realizate în tehnologie de 0.8 μm, iar rezultatele obţinute indică o foarte bună concordanţă cu simulările efectuate cu ajutorul programului SPICE.

BULETINUL INSTITUTULUI POLITEHNIC DIN IAŞI
Tomul XLVII (LI), Fasc. 3–4, 2001
ELECTROTEHNICĂ. ENERGETICĂ. ELECTRONICĂ

D.C. 621.316.94

THE ELIMINATION OF LINE-CURRENT HARMONICS

BY
IRINEL-VALENTIN PLETEA

A particular single-stage power-factor-correction (PFC) switching regulator is studied employing a discontinuous-conduction-mode (DCM) boost-input cell and a continuous-current-mode (CCM) forward output cell. Although this single-stage (PFC regulator can provide a reasonably high power factor when its PFC stage is operating in discontinuous mode, substantial reduction in line-current harmonics is possible by applying a suitable frequency-modulation scheme. This paper derives a frequency-modulation scheme and proposes a practical implementation using a simple translinear analog circuit.

1. Introduction

Due to the increased awareness of the many undesirable consequences of harmonic distortions in line currents drawn by switch-mode power supplies (SMPS's), *high power factor* and *low line-current harmonic distortion* are expected to be mandatory requirements for SMPS's in coming years. A common approach to satisfy these requirements is to incorporate an additional power-factor-correction (PFC) stage preceding the normal switching converter one. In this approach, the switching converter maintains a regulated output voltage while the preceding PFC stage ensures a high-input power factor. Thus, the combined circuit usually has a lower efficiency and is less cost effective, especially for low-power applications, due to the use of two separate power stages. R e d l *et al.* [1] proposed a family of topologies for single-stage power-factor-corrected power supplies, which amalgamates a PFC cell with a swithching regulator one to form a single power stage. In this paper, a particular type of the single-stage power-factor-corrected power supplies proposed by R e d l *et al.* [1] is proposed in which a DCM boost cell and continuous-current-mode (CCM) forward cell are used. We will derive an appropriate model for the single-stage PFC power supply under investigation, based on which a novel frequency-modulation scheme for achieving unity power factor is developed, *i.e.*, a harmonic-free line current [2].

2. Principle of the Proposed Single-stage PFC Regulator

The simplified schematic of a single-stage PFC regulator, comprising a cascade connection of a boost cell and forward cell, is shown in Fig. 1.

The two constituent cells share the same switch, S_1. Nodes A and B serve as both the output terminals of the boost cell and the input terminals of the forward cell. The presence of diode D_1 prevents the primary current of transformer T_1 from circulating through diode D_2.

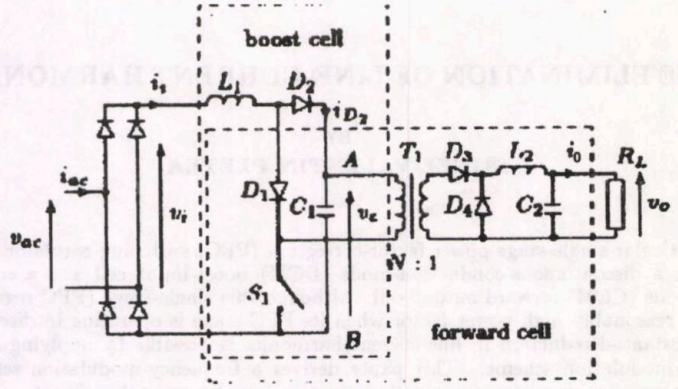

Fig. 1.– A single-stage PFC regulator using boost-input cell.

The charging current, i_{D_2}, of capacitor C_1, is a rectified sinusoid, which causes a ripple voltage to appear on the output voltage, v_C, of the boost cell. The amplitude of the ripple voltage would depend on the value of C_1 and the input current of the forward cell. With a sufficiently large C_1, the ripple voltage can be kept to a small value compared to the dc component of v_C. As a compulsory requirement of any PFC power supply, a storage element is needed to buffer the difference between the instantaneous input power (square of sine) and the instantaneous output power (constant value). In this particular case, capacitor C_1 serves the purpose, presenting itself as the load for the boost cell and as the source for the forward cell. In this particular single-stage PFC regulator, the duty cycle of switch S_1 is used to regulate output voltage v_0 *via* a voltage feedback loop. Under this condition, it can be shown that the shape of the averaged input current, I_i, of the boost cell is not an ideal rectified sinusoid.

3. Derivation of Averaged Model for the Single-stage PFC Regulator

In what follows it is assumed that the boost cell is operating in discontinuous mode, whereas the forward cell is in continuous mode. The waveforms of input current, i_i, of the boost cell and charging current, i_{D_2}, of C_1 are shown in Fig. 2, where T denotes the switching period, DT – the on-time of switch S_1, and DT – the on-time of diode D_2. For the boost cell operating in discontinuous mode, we have:

$$D' = \frac{v_i}{v_C - v_i} D < 1 - D. \tag{1}$$

By inspection of the waveform shown in Fig. 2, the averaged input current and the averaged charging current of C_1 are given by:

$$(2)\quad \bar{i}_i = \frac{T}{2L_1} D(D+D')v_i = \frac{TD^2}{2L_1} \cdot \frac{1}{1-\frac{v_i}{v_C}} v_i, \quad \text{respectively} \quad \bar{i}_{D_2} = \frac{TD^2}{2L_1} \cdot \frac{v_i}{\frac{v_C}{v_i} - 1}.$$

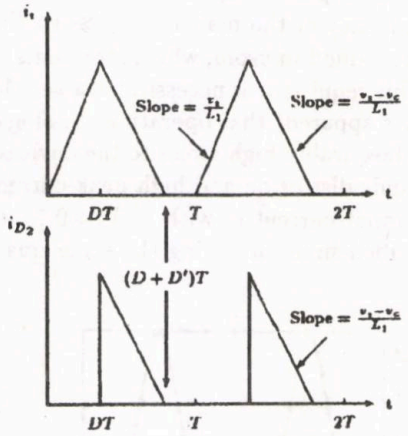

Fig. 2.– Waveforms of i_i and i_{D_2}.

Furthermore, with the forward cell operating in continuous mode, the averaged voltage driving the output filter is equal to Dv_C/N, and the averaged current discharging C_1 is Di_{L_2}/N.

Thus, a complete averaged model [3] for the single-stage PFC regulator can be obtained as shown in Fig. 3.

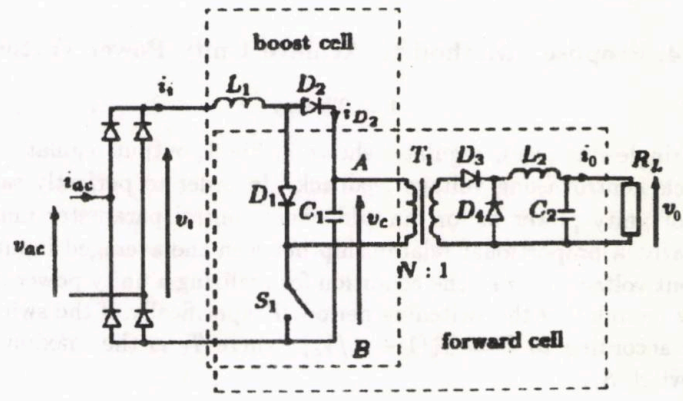

Fig. 3.– Averaged behavior model of the single-stage PFC regulator.

To facilitate steady-state analysis, the following conditions will be assumed, whose validity can be readily verified:

1° v_C is essentially a dc voltage by virtue that C_1 is sufficiently large. We shall denote this voltage by V_c in the analysis that follows.

2° The output voltage is well regulated, which implies that the duty cycle, D, of switch S_1 is constant because V_c is approximately a dc voltage.

For off-line operation, the input voltage is a rectified sinusoid, $v_i = \hat{V}_i|\sin\omega t|$, where ω is the angular frequency of the mains. If $V_c \gg \hat{V}_i$, then the averaged input current, $\bar{i}_i$, becomes a pure rectified sinusoid, which represents the condition for unity-power-factor operation. This requirement necessitates a very large V_c, relative to the mains peak voltage, $\hat{V}_i$. It is apparent that operating the single-stage PFC regulator with a large V_c imposes unfavourably high stress to the devices, while operating with a small V_c results in harmonic distortion and high peak-current stress. In Fig. 4, the waveform of the averaged input current $\bar{i}_i$, with $\hat{V}_i/V_c = 0.75$, is represented, and the dotted curve is a pure rectified sinusoid having the same rms value.

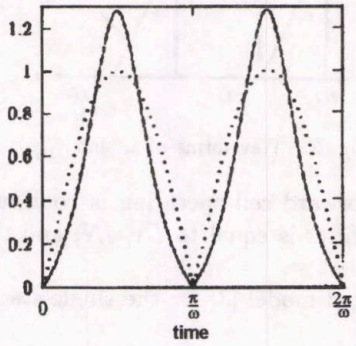

Fig. 4.– Averaged input current $\bar{i}_i$ waveform with $\hat{V}_i/V_c = 0.75$.

4. Proposed Method to Achieve Unity Power Factor

4.1. Theory

For the single-stage PFC regulator shown in Fig. 1, output regulation is achieved by duty-cycle control using voltage feedback. In order to perfectly satisfy the requirement of unity power factor, an additional control parameter must be established. Clearly, a proportional relationship between the averaged input current, $\bar{i}_i$, and the input voltage, v_i, *i.e.*, the condition for realizing a unity power factor can be achieved by modulating the switching period, T, specifically, if the switching period is adjusted according to $T = T_0(1 - v_i/V_c)$, where T_0 is the maximum switching period of switch S_1,

$$\bar{i}_i = \frac{T_0 D^2}{2L_1} v_i. \tag{3}$$

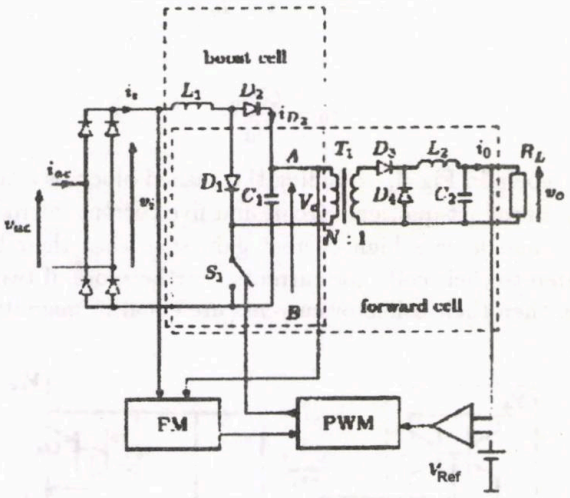

Fig. 5.– Block diagram of a single-stage PFC regulator with a feedforward frequency control scheme.

Consequently, the extra control equation is done by $T = T_0(1 - v_i/V_c)$, which represents a continuous adjustment of the switching frequency according to v_i and V_c, *i.e.*, a feedforward control. The block diagram of a single-stage PFC regulator with such a feedforward frequency control scheme is shown in Fig. 5. In order to arrive at a viable scheme that can be applied to practical systems, the following conditions must be taken in consideration:

1° The circuit required to implement the frequency control scheme should be simple enough to allow either a custom IC realization or a circuit implementation involving a relatively few discrete components.

2° The required amount of frequency deviation for a given ratio $\hat{V}_i/V_c$ must not be excessively large to complicate magnetic design and electromagnetic interference (EMI) considerations.

4.2. Implementation of the Frequency Control Using an Analog Translinear Circuit

Referring to Fig. 6, the dashed block represents the oscillator circuit of a pulse-width-modulation (PWM) controller chip in which a current mirror provides a current i to charge up capacitor C. The value of i is usually adjusted with an external resistor. When the capacitor voltage is equal to a thresshold voltage, say v_{th}, switch S_V turns on and capacitor C is discharged.

Immediately after the discharge, switch S_V turns off and capacitor C is charged up by current i again. The circuit oscillates with a constant period determined by the duration of the charging interval, specifically, if current is controlled according

to

$$T = \frac{Cv_{\text{th}}}{i}, \qquad i = I_0 \frac{V_c}{V_c - v_i}, \tag{4}$$

$$T_0 = \frac{Cv_{\text{th}}}{I_0}. \tag{5}$$

The diagram shown in Fig. 6, excluding the dashed block, is a translinear circuit, which consists of a product-quotient circuit and five current mirrors. All transistors used are identical and have a high current gain such that their base currents are negligible compared to their collector currents. Furthermore, if two transistors have the same voltage, then their collector currents are equal in magnitude.

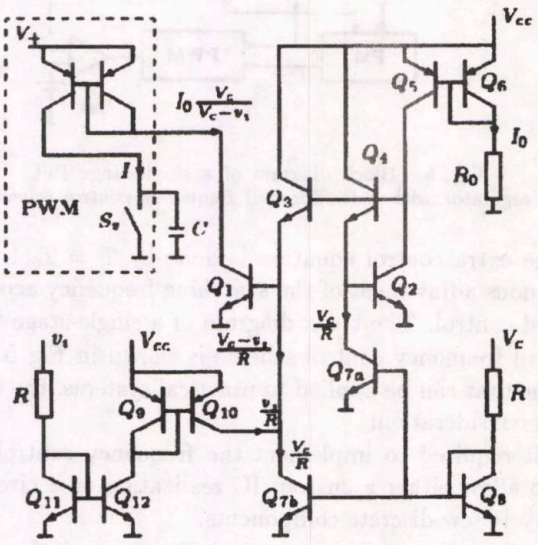

Fig. 6.– Translinear circuit for the frequency control of the charging interval.

Refering to Fig. 6, Q_5 and Q_6 are connected as a current mirror to provide Q_2 with a collector current of I_0, where

$$I_0 \approx \frac{V_{\text{cc}}}{R_0}. \tag{6}$$

In addition, Q_{7a} and Q_8 are connected as a current mirror to provide Q_4 with a collector current of V_c/R. Similarly, Q_{11} and Q_{12}, Q_9 and Q_{10}, and Q_{7b} and Q_8 are connected as current mirrors to provide with a collector current of $(V_c - v_i)/R$. The product-quotient circuit is constructed with $Q_1, ..., Q_4$ so that

$$v_{BE_1} + v_{BE_3} = v_{BE_2} + v_{BE_4}. \tag{7}$$

Based on the translinear circuit principle [4]:

$$i_{C_1} i_{C_3} = i_{C_2} i_{C_4}$$

it results

$$i_{C_1} = \frac{i_{C_2} i_{C_4}}{i_{C_3}}. \tag{8}$$

Hence, putting $i_{C_2} = I_0$, $i_{C_4} = V_c/R$ and $i_{C_3} = (V_c - v_i)/R$ we obtain

$$i_{C_1} = I_0 \frac{V_c}{V_c - v_i}.$$

Finally, the required frequency control can be realized easily by mirroring to the charging current, i, in the PWM block, as shown in Fig. 6.

5. Performance Analysis

5.1. Calculation of Power Factor

Referring to the averaged behavior model of the single-stage PFC regulator shown in Fig. 3, the averaged input current, $\bar{i}_i$, and the rms value of the averaged input current are given by

$$\bar{i}_i = \frac{TD^2}{2L_1} \cdot \frac{v_i}{1 - v_i/V_c}, \quad \text{respectively} \quad \bar{I}_i = \frac{D^2 \hat{V}_i}{2\sqrt{\pi L_1}} \sqrt{\int_0^{\pi} \frac{T^2 \sin^2\theta}{\left[1 - (\hat{V}_i \sin\theta)/V_c\right]^2} \, \mathrm{d}\theta}, \tag{9}$$

where $v_i = \hat{V}_i |\sin \omega t|$ and t has been substituted by θ/ω for algebraic reasons.

Under steady-state operation, V_c can be considered as a dc voltage. Hence, for the purpose of maintaining a regulated output voltage, the duty cycle D can be assumed constant.

The input power is

$$P_i = \frac{\omega}{\pi} \int_0^{\frac{\pi}{\omega}} v_i(t) \bar{i}_i(t) \, \mathrm{d}t = \frac{1}{\pi} \int_0^{\pi} \hat{V}_i \sin\theta \frac{TD^2}{2L_1} \cdot \frac{\hat{V}_i \sin\theta}{1 - \dfrac{\hat{V}_i \sin\theta}{V_c}} \, \mathrm{d}\theta. \tag{10}$$

Hence, the power factor of the single-stage PFC regulator is

$$\text{p.f.} = \frac{P_i}{V_i \bar{I}_i} = \sqrt{\frac{2}{\pi}} \cdot \frac{\displaystyle\int_0^{\pi} \frac{T \sin^2\theta}{1 - (\hat{V}_i \sin\theta)/V_c} \, \mathrm{d}\theta}{\sqrt{\displaystyle\int_0^{\pi} \frac{T^2 \sin^2\theta}{\left[1 - (\hat{V}_i \sin\theta)/V_c\right]^2} \, \mathrm{d}\theta}}. \tag{11}$$

We shall study two cases separately for $T = \text{const.}$ and for T variable according to the proposed feedforward control scheme.

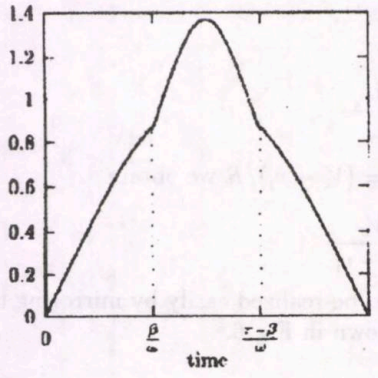

Fig. 7.– Waveform of averaged input current with limited frequency deviation.

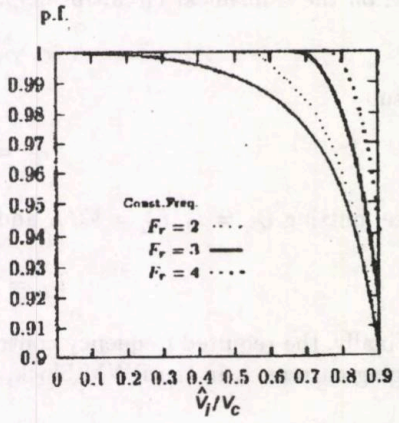

Fig. 8.– Power factor *versus* $\hat{V}_i/V_c$ with different values of F_r.

a) *Constant Frequency Operation.* When $T = T_0$, *i.e.* at constant frequency, the single-stage PFC regulator operates with nonunity power factor. From (11), the power factor results

$$\text{(12)} \qquad \text{p.f.}_{\text{const. freq.}} = \sqrt{\frac{2}{\pi}} \cdot \frac{\displaystyle\int_0^{\pi} \frac{\sin^2\theta}{1-(\hat{V}_i \sin\theta)/V_c}\,\mathrm{d}\theta}{\sqrt{\displaystyle\int_0^{\pi} \frac{\sin^2\theta}{\left[1-(\hat{V}_i \sin\theta)/V_c\right]^2}\,\mathrm{d}\theta}}.$$

b) *Feedforward Frequency Control.* Since the input voltage is a rectified sinusoid, *i.e.* $v_i = \hat{V}_i|\sin\omega t|$, where ω is the angular frequency of the mains, the feedforward frequency control can be rewritten as

$$\text{(13)} \qquad T = T_0\left(1 - \frac{\hat{V}_i|\sin\omega t|}{V_c}\right), \quad \text{with} \quad F_{\max} = F_{\min}\frac{1}{1-\hat{V}_i/V_c},$$

where $F_{\max}$ is the maximum acceptable frequency and $F_{\min}$ – the minimum one. Thus, we observe that minimizing would unfavourably call for a large range of operating frequency if unity power factor is imposed to be maintained.

Fig. 7 illustrates the case when $F_r < \dfrac{1}{1-\hat{V}_i/V_c}$, where F_r determines the extent to which input current waveform deflects from the ideal rectified sinusoid. Here, distortion near the peak of the waveform is apparent.

Fig. 8 represents the dependence of power factor *versus* $\hat{V}_i/V_c$ ratio, corresponding to different values of F_r. It is clear that for a given ratio $\hat{V}_i/V_c$, the single-stage PFC regulator, with the proposed frequency-modulation control scheme, can achieve higher power factor.

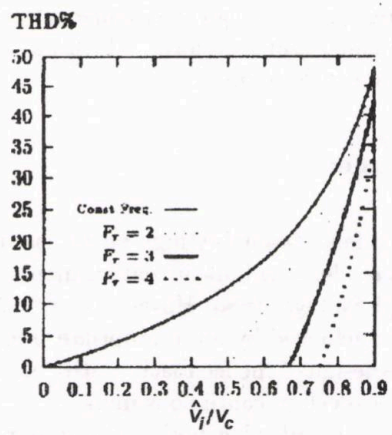

Fig. 9.– THD *versus* $\hat{V}_i/V_c$ dependence for different F_r values.

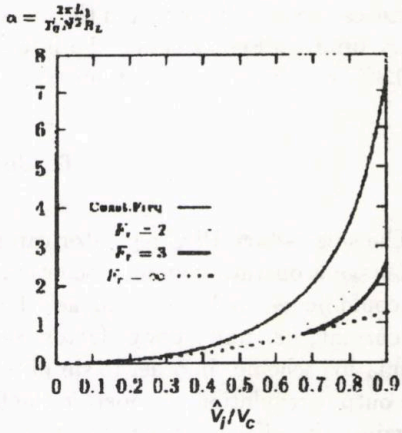

Fig. 10.– α *versus* $\hat{V}_i/V_c$ dependence for different F_r values.

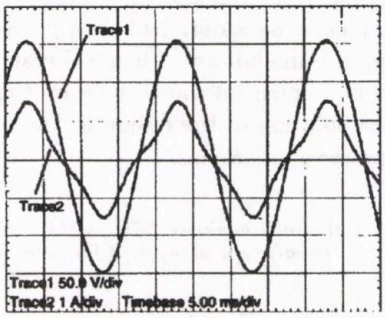

Fig. 11.– Filtered line-current waveform with constant frequency: $\hat{V}_i/V_c = 0.66$, p.f. $= 0.984$, THD $= 15.6\%$.

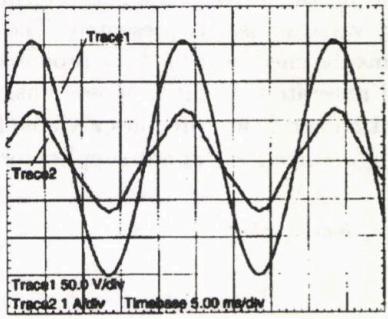

Fig. 12.– Filtered line-current waveform with constant frequency: $\hat{V}_i/V_c = 0.55$, p.f. $= 0.991$, THD $= 10.8\%$.

5.2. Calculation of the Total Harmonics Distortion

In general, the total harmonics distortion (THD) can be expressed as

$$\text{THD} = \sqrt{\frac{1}{(\text{p.f.}/\cos\varphi)^2 - 1}}, \tag{14}$$

where φ is the phase angle between the line voltage and line current. In the case of the single-stage PFC regulator $\cos\varphi = 1$. Fig. 9 represents the dependence of THD *versus* $\hat{V}_i/V_c$ ratio with different F_r values.

Fig. 10 provides a means to estimate the voltage-stress variation under various loading conditions. Fig. 11 renders evident that the proposed frequency-modulation scheme can reduce distortion in the line current, even though the frequency excursion is very limited. Fig. 12 shows the filtered line-current waveform, which has a THD of 10.8%, which is more less than that of the previous case.

6. Conclusions

The single-stage PFC regulator can provide a reasonably high power factor if its PFC stage is operating under discontinuous mode. The line-current harmonic distortion could be reduced at the expense of a high voltage stress. However, harmonic-free line current, *i.e.* unity power factor, can be achieved by an appropriate frequency-modulation scheme. In order to simplify the design of the feedback control associated with output regulation, we operate the forward cell in continuous mode, immunizing it against the effect of frequency variation, thus allowing both unity power factor and output regulation to be achieved independently on frequency modulation and duty-cycle modulation. This paper derives a frequency-modulation scheme with a practical implementation based on the translinear circuit principle. A quantitative analysis on the THD of the line current with respect to the allowable range of frequency variation is also presented. The experimental data obtained on a prototype confirms the effectiveness of the proposed frequency-modulation scheme. Finally, we should reiterate that the proposed analog circuit implementation allows custom IC realization and hence provides a viable low-cost solution to the design of harmonic-free single-stage PFC power supplies for low-power applications.

Received, June 4, 2001

Technical University "Gh.Asachi", Jassy,
Department of Applied Electronics

REFERENCES

1. Redl R., Balogh L., Sokal N.O., *A New Family of Single-stage Isolated Power-factor-correctors with Fast Regulation of the Output Voltage.* IEEE PESC Rec., 1137-44 (1994).

2. Lee Y.S., Siu K.W., *Single-switch Fast-response Switching Regulators with Unity Power Factor.* Proc. APEC'96, San Jose, CA, 791-796.

3. Middlebrook R.D., Cuk S., *A General Unified Approach to Modeling Switching-converter Power Stages.* IEEE PESC Rec., 18-34 (1976).

4. Toumazou C., Fidgey F.J., Haigh D.G., *Analogue IC Design: The Current-mode Approach.* Ch. **2**, Peregrinus, London, 1990.

5. Jovanovic M.M., Tsang D.M.C., Lee F.C., *Reduction of Voltage Stress in Integrated High-frequency Rectifier-regulators by Variable-frequency Control.* Proc. APEC'94, Orlando, Florida, 596-575.

6. Severn R.P., Bloom G.E., *Modern DC/DC Switchmode Power Converter Circuits.* Ch. **3**, Van Nostrand Reinhold, NY, 1985.

ELIMINAREA ARMONICILOR DE CURENT

(Rezumat)

Se studiază un caz particular a reducerii factorului de putere pentru regulatoare în mod discontinuu de lucru pentru o celulă Boost la intrare şi în mod continuu de lucru pentru o celulă Forward la ieşire. Acest regulator al factorului de putere are o comportare rezonabilă în putere când funcţionează în mod discontinuu, iar reducerea substanţială a armonicilor în curent este posibilă aplicând o frecvenţă de modulaţie convenabilă schemei. Se imaginează o schemă de modulaţie în frecvenţă şi se propune o implementare practică a sa utilizând un circuit analogic transliniar simplu.

BULETINUL INSTITUTULUI POLITEHNIC DIN IAŞI
Tomul XLVII (LI), Fasc. 3–4, 2001
ELECTROTEHNICĂ. ENERGETICĂ. ELECTRONICĂ

D.C. 621.313.333.021.3

A NEW APPROACH OF THE THREE-PHASE UNSYMMETRICAL INDUCTION MACHINE THEORY

BY
I. ANDRONE and ADRIANA PRISĂCARU

There are many reasons for the three-phase induction machines to be or to become unsymmetrical. To avoid the difficulties in the treatment of these unsymmetrical machines the "equivalent numbers of the stator phases" concept is proposed. These numbers are global coefficients which take into account the difference between magnitudes, phase angles and space angles of the three magnetic inductions of the unsymmetrical three-phase induction machines.

1. Introduction

The main reasons of a three-phase induction machine to be unsymmetrical are: the three magnetic flux densities set up by the three-phase induction machine windings are of different magnitudes; the three-phase windings are space-around the periphery by angles different from 120 electrical degrees and the phase-shifts of the magnetic inductions are diferent from 120 degrees.

Let us consider such an unsymmetrical three-phase induction machine, having three different windings (u, v, and w – Fig. 1), spaced-around the stator periphery by different angles and setting up magnetic inductions of different magnitudes. The phase-shifts between the three-stator currents are assumed to be different from 120 electrical degrees.

The product of number of turns and winding factor, for each winding, are: $w_u k_{uyq}$, $w_v k_{vyq}$ and $w_w k_{wyq}$. The space angles between stator windings are: α_{1uv}, α_{1vw} and α_{1wu} electrical degrees.

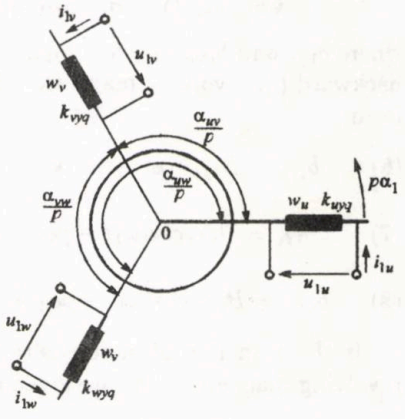

Fig. 1

The rotor, ignored here, is not excited ($i_2 = 0$) and is of symmetrical type, squirrel-cage for example.

The main goal of the paper is to define the *equivalent number of stator phases* of unsymmetrical three-phase induction machine, as in [1],...,[3] was done for two-phase unsymmetrical machine.

2. Magnetic Inductions

The stator voltages are of form:

$$u_{1k} = \sqrt{2}U_{1k}\cos(\omega_1 t + \theta_{1k}), \tag{1}$$

where $k = u, v, w$.

If the phase-shifts are defined as differences between initial phase angles:

$$\theta_{1uv} = \theta_{1u} - \theta_{1v}, \quad \theta_{1uw} = \theta_{1u} - \theta_{1w}, \quad \theta_{1vw} = \theta_{1v} - \theta_{1w} \tag{2}$$

and if the value $\theta_{1u} = 0$ is chosen, then the stator voltages are:

$$u_{1u} = \sqrt{2}U_{1u}\cos\omega_1 t,\ u_{1v} = \sqrt{2}U_{1v}\cos(\omega_1 t - \theta_{1uv}),\ u_{1w} = \sqrt{2}U_{1w}\cos(\omega_1 t - \theta_{1uw}). \tag{3}$$

The corresponding currents, in no load regime, are:

$$i_{1k0} = \sqrt{2}I_{1k0}\cos(\omega_1 t + \gamma_{1k}), \tag{4}$$

where $k = u, v, w$.

The magnetic flux densities set up by the currents (4), flowing through the three different windings (u, v and w), are:

$$\begin{cases} b_{1u}(\alpha_1, t) = B_{1u}\cos(\omega_1 t + \gamma_{1u})\cos p\alpha_1 = b_{1fu} + b_{1bu}, \\ b_{1v}(\alpha_1, t) = B_{1v}\cos(\omega_1 t + \gamma_{1v})\cos(p\alpha_1 - \alpha_{1uv}) = b_{1fv} + b_{1bv}, \\ b_{1w}(\alpha_1, t) = B_{1w}\cos(\omega_1 t + \gamma_{1w})\cos(p\alpha_1 - \alpha_{1uw}) = b_{1fw} + b_{1bw}, \end{cases} \tag{5}$$

where b_{1fu} and b_{1bu}, b_{1fv} and b_{1bv}, b_{1fw} and b_{1bw} are the forward (f) and respectively backward (b) revolving magnetic field of each stator phase, having, respectively, the form:

$$b_{1fu} = B_{1fu}\cos(\omega_1 t - p\alpha_1 + \beta_{1fu}), \quad b_{1bu} = B_{1bu}\cos(\omega_1 t + p\alpha_1 + \beta_{1bu}), \tag{6}$$

$$b_{1fv} = B_{1fv}\cos(\omega_1 t - p\alpha_1 + \beta_{1fv}), \quad b_{1bv} = B_{1bv}\cos(\omega_1 t + p\alpha_1 + \beta_{1bv}), \tag{7}$$

$$b_{1fw} = B_{1fw}\cos(\omega_1 t - p\alpha_1 + \beta_{1fw}), \quad b_{1bw} = B_{1bw}\cos(\omega_1 t + p\alpha_1 + \beta_{1bw}). \tag{8}$$

If the principle of superposition is assumed, then the resulting two counter-revolving magnetic fields are given by:

$$\begin{cases} b_{1f} = b_{1fu} + b_{1fv} + b_{1fw} = B_{1f}\cos(\omega_1 t - p\alpha_1 + \beta_{1f}), \\ b_{1b} = b_{1bu} + b_{1bv} + b_{1bw} = B_{1b}\cos(\omega_1 t + p\alpha_1 + \beta_{1b}), \end{cases} \tag{9}$$

where the magnitudes B_{1f}, B_{1b} and the phase shifts β_{1f} and β_{1b} must to be determined by an identification process.

3. The Revolving Magnetic Fields

Through an identification process for the forward magnetic fields it follows that:

$$B_{1f} = \Big[B_{1fu}^2 + B_{1fv}^2 + B_{1fw}^2 + 2B_{1fu}B_{1fv}\cos(\beta_{1fu} - \beta_{1fv}) + \tag{10}$$
$$+2B_{1fu}B_{1fw}\cos(\beta_{1fu} - \beta_{1fw}) + 2B_{1fv}B_{1fw}\cos(\beta_{1fv} - \beta_{1fw})\Big]^{1/2}$$

and

$$\operatorname{tg}\beta_{1f} = \frac{B_{1fu}\sin\beta_{1fu} + B_{1fv}\sin\beta_{1fv} + B_{1fw}\sin\beta_{1fw}}{B_{1fu}\cos\beta_{1fu} + B_{1fv}\cos\beta_{1fv} + B_{1fw}\cos\beta_{1fw}}. \tag{11}$$

If the following notations are made:

$$k_{1uv} = \frac{B_{1fu}}{B_{1fv}} = \frac{B_{1u}}{B_{1v}} = \frac{w_u k_{uyq} I_{1u0}}{w_v k_{vyq} I_{1v0}} = \frac{1}{k_{1vu}}, \tag{12}$$

$$k_{1vw} = \frac{B_{1fv}}{B_{1fw}} = \frac{B_{1v}}{B_{1w}} = \frac{w_v k_{vyq} I_{1v0}}{w_w k_{wyq} I_{1w0}} = \frac{1}{k_{1wv}}, \tag{13}$$

$$k_{1wu} = \frac{B_{1fw}}{B_{1fu}} = \frac{B_{1w}}{B_{1u}} = \frac{w_w k_{wyq} I_{1w0}}{w_u k_{uyq} I_{1u0}} = \frac{1}{k_{1uw}}, \tag{14}$$

and the following relationships are taking into account:

$$\beta_{1fu} - \beta_{1fv} = \gamma_{1uv} - \alpha_{1uv},\ \beta_{1fu} - \beta_{1fw} = \gamma_{1uw} - \alpha_{1uw},\ \beta_{1fv} - \beta_{1fw} = \gamma_{1vw} - \alpha_{1vw}, \tag{15}$$

the relationship for the equivalent number of three-phase unsymmetrical stator machine corresponding to the forward revolving magnetic field are obtained:

$$k_{fu} = [1 + k_{1vu}^2 + k_{1wu}^2 + 2k_{1vu}\cos(\gamma_{1uv} - \alpha_{1uv}) + \tag{16}$$
$$+2k_{1wu}\cos(\gamma_{1uw} - \alpha_{1uw}) + 2k_{1vu}k_{1wu}\cos(\gamma_{1vw} - \alpha_{1vw})]^{1/2},$$

$$k_{fv} = [1 + k_{1uv}^2 + k_{1wv}^2 + 2k_{1uv}\cos(\gamma_{1uv} - \alpha_{1uv}) + \tag{17}$$
$$+2k_{1wv}\cos(\gamma_{1vw} - \alpha_{1vw}) + 2k_{1uv}k_{1wv}\cos(\gamma_{1uw} - \alpha_{1vw})]^{1/2},$$

$$k_{fw} = [1 + k_{1uw}^2 + k_{1vw}^2 + 2k_{1uw}\cos(\gamma_{1uw} - \alpha_{1uw}) + \tag{18}$$
$$+2k_{1vw}\cos(\gamma_{1vw} - \alpha_{1vw}) + 2k_{1uw}k_{1vw}\cos(\gamma_{1uv} - \alpha_{1uv})]^{1/2}.$$

The main conclusion is that these equivalent numbers of stator phases, corresponding to the forward revolving magnetic field, are functions of ratios between magnetic inductions magnitudes and of differences between phase angles and space angles of these magnetic inductions, set up by the three different windings.

The "*phase angle*" of the forward revolving magnetic field given in (11), becomes:

$$\operatorname{tg}\beta_{1f} = \frac{\sin\gamma_{1u} + k_{1vu}\sin(\gamma_{1v} + \alpha_{1uv}) + k_{1wu}\sin(\gamma_{1w} + \alpha_{1uw})}{\cos\gamma_{1u} + k_{1vu}\cos(\gamma_{1v} + \alpha_{1uv}) + k_{1wu}\cos(\gamma_{1w} + \alpha_{1uw})}. \tag{19}$$

In a similar manner the magnitude and the phase angle of the backward revolving field are obtained:

$$B_{1b} = [B_{1bu}^2 + B_{1bv}^2 + B_{1bw}^2 + 2B_{1bu}B_{1bv}\cos(\beta_{1bu} - \beta_{1bv}) + 2B_{1bu}B_{1bw}\cos(\beta_{1bu} - \beta_{1bw}) + 2B_{1bv}B_{1bw}\cos(\beta_{1bv} - \beta_{1bw})]^{1/2}, \tag{20}$$

$$\operatorname{tg}\beta_{1b} = \frac{B_{1bu}\sin\beta_{1bu} + B_{1bv}\sin\beta_{1bv} + B_{1bw}\sin\beta_{1bw}}{B_{1bu}\cos\beta_{1bu} + B_{1bv}\cos\beta_{1bv} + B_{1bw}\cos\beta_{1bw}}. \tag{21}$$

The equivalent numbers of phases and the *phase angle* corresponding to the backward revolving magnetic field become:

$$k_{bu} = [1 + k_{1vu}^2 + k_{1wu}^2 + 2k_{1vw}\cos(\gamma_{1uv} - \alpha_{1uv}) + 2k_{1uw}\cos(\gamma_{1uw} - \alpha_{1uw}) + 2k_{1vu}k_{1wu}\cos(\gamma_{1vw} - \alpha_{1vw})]^{1/2}, \tag{22}$$

$$k_{bv} = [1 + k_{1uv}^2 + k_{1wv}^2 + 2k_{1uv}\cos(\gamma_{1uv} + \alpha_{1uv}) + 2k_{1vw}\cos(\gamma_{1vw} + \alpha_{1uw}) + 2k_{1uv}k_{1wv}\cos(\gamma_{1uw} + \alpha_{1uw})]^{1/2}, \tag{23}$$

$$k_{bw} = [1 + k_{1uw}^2 + k_{1vw}^2 + 2k_{1uw}\cos(\gamma_{1uw} + \alpha_{1uw}) + 2k_{1vw}\cos(\gamma_{1vw} + \alpha_{1vw}) + 2k_{1uw}k_{1vw}\cos(\gamma_{1uv} + \alpha_{1uv})]^{1/2}, \tag{24}$$

$$\operatorname{tg}\beta_{1b} = \frac{\sin\gamma_{1u} + k_{1vu}\sin(\gamma_{1v} - \alpha_{1uv}) + k_{1wu}\sin(\gamma_{1w} - \alpha_{1uw})}{\cos\gamma_{1u} + k_{1vu}\cos(\gamma_{1v} - \alpha_{1uv}) + k_{1wu}\cos(\gamma_{1w} - \alpha_{1uw})}. \tag{25}$$

It is to notice that the equivalent numbers of phases corresponding to the backward revolving magnetic field are functions of ratios between magnetic induction magnitudes and of sum of phase angles and space angles of these inductions set up by three different windings.

4. The Magnetizing Reactances

The three phase windings have different magnetizing reactances, corresponding to the forward and backward revolving magnetic field [1],...,[3].

The magnetizing reactances corresponding to the revolving magnetic fields, forward and backward, are of following types:

$$X_{mfk} = \frac{k_{fk}}{2} X_{mk}^{(p)}; \quad X_{mbk} = \frac{k_{bk}}{2} X_{mk}^{(p)}, \tag{26}$$

where $X_{mk}^{(p)}$ is the magnetizing reactance corresponding to the pulsating magnetic field, and, again, $k = u, v, w$; k_{fk} and k_{bk} are the equivalent numbers of stator phases. For example, for u phase and for forward and, respectively, backward revolving magnetic fields, the magnetizing reactances are:

$$X_{wfu} = \frac{k_{fu}}{2} \cdot \frac{8}{\pi} \mu_0 f_1 \frac{\tau L}{p\delta'} w_u^2 k_{uyq}^2; \quad X_{wbu} = \frac{k_{bu}}{2} \cdot \frac{8}{\pi} \mu_0 f_1 \frac{\tau L}{p\delta'} w_u^2 k_{uyq}^2. \tag{27}$$

In relations (27) k_{fu} is the equivalent number of stator phases of u type and corresponding to the forward magnetic field; k_{bu} are the same equivalent numbers but corresponding to the backward revolving magnetic field.

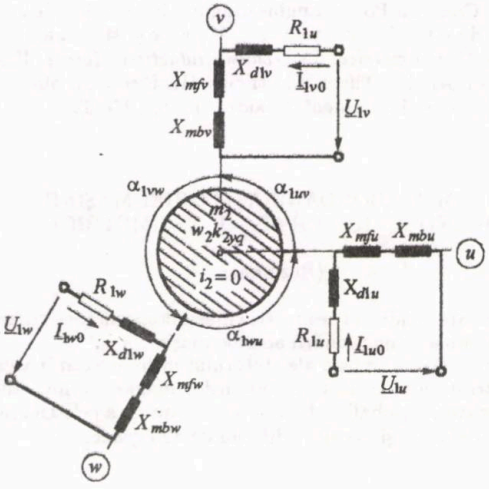

Fig. 2

The voltage equations in no load regime, (the subscript 0), in complex quantities, are of the type

$$\underline{U}_{1k} = (R_{1k} + \mathrm{j}X_{1dk})\underline{I}_{1k0} + \mathrm{j}(X_{mfk} + X_{mbk})\underline{I}_{1k0}, \tag{28}$$

where $k = u, v, w$.

The corresponding equivalent circuits diagrams of the equations of type (28) are drawing in Fig. 2.

5. Conclusions

The equivalent numbers of stator phases of the unsymmetrical induction machine are defined. They are global coefficients which take into account the main reasons for a three-phase induction machine to be or to become unsymmetrical.

The magnetizing reactances of the unsymmetrical induction machine are close functions of the equivalent numbers of phases. Also the no load currents and equivalent circuit diagram can be examined with the help of the equivalent numbers of phases.

Received, April 11, 2001

Technical University "Gh.Asachi", Jassy,
Department of General Electrotechnics
and Electrical Machines

REFERENCES

1. Androne I., Prisăcaru A., *On the Equivalent Circuits Diagram of the Two-phase Unsymmetrical Induction Motors.* Bul. Inst. polit., Iaşi, **XLII (XLIV)**, *1-2*, s.III, 95-104 (1996).
2. Androne I., Prisăcaru A., Pavel V., Verdeş M., Lozonschi T.L., *Voltages Equations of the Unsymmetrical Two-phase Electrical Induction Motors.* Proc. of the Internat. Conf. on Power Engineering'97, ICOPE'97, Tokyo, **2**, 1997, 297-300.
3. Prisăcaru A., Androne I., Pavel V., Verdeş M., Radu G., *The Magnetizing Currents of the Unsymmetrical Two-phase Induction Motors.* ICATE'98, Proc. of the Internat. Conf. on Appl. a Theor. Electricity, III, Electrical Machines, Electrical Drives and Electromechanical Equipment, Craiova, 1998, 127-132.

O NOUĂ ABORDARE A TEORIEI MAŞINII DE INDUCŢIE TRIFAZATE NESIMETRICE

(Rezumat)

Există numeroase cauze care conduc la nesimetria maşinilor asincrone trifazate, generând, astfel, dificultăţi în tratarea sistematică a funcţionării acestor maşini.

Se definesc numerele echivalente de fază ale statorului utile în examinarea funcţionării maşinii asincrone trifazate nesimetrice pe baza teoriei câmpurilor magnetice învârtitoare. Aceste numere echivalente de faze sunt coeficienţi globali ce ţin seama de faptul că cele trei inducţii magnetice pot avea amplitudini diferite şi defazaje şi decalaje diferite de 120 grade.

BULETINUL INSTITUTULUI POLITEHNIC DIN IAŞI
Tomul XLVII (LI), Fasc. 3–4, 2001
ELECTROTEHNICĂ. ENERGETICĂ. ELECTRONICĂ

D.C. 621.316.13

ELECTRIC NETWORK PLANNING ASPECTS WITH SPECIAL REGARD TO RELIABILITY

BY

GH. GRIGORAŞ and GH. CÂRŢINĂ

Evaluating the reliability of a distribution network is a complex process and the methods used are difficult to work with. Reliability studies require information about the history of the network components' behavior, about the economic consequences of outages, etc. Today, heuristic or empiric methods are used in planning networks. The $n-1$ principle is also a factor in the process of designing the network architecture. The input data for these methods are the reliability coefficients in the perspective of the long time behavior of the system. This general framework is now enhanced as one can use the uncertainties in failure and repair rates and can find supply unavailability, as fuzzy variable. In this paper we propose to use input data obtained by fuzzy techniques, instead of the statistical reliability indices. Test results on real distribution networks show that the performance of this method is very good.

1. Introduction

A main constraint when planning electrical power systems is the reliable supply of the consumers. Utilities are required to provide reliable power to customers. In the design stages, utilities need to plan ahead for participated future load growth under different possible scenarios. The service reliability of electric power systems is determined by the availability of the components. It is a function of the load, generation, and the redundancy of the system, [7]. However, utilities do not want to overbuild their system because they need to bear the unnecessary cost. In the ideal situations, utilities will build a reliable power system, with just enough capacity (with proper reliability borders) to support their customers, [3]. Network configurations are compared in terms of the resulting quality as experienced by the consumer, and evaluated in relation to national goals, which the company may have to envisage for the year 2015, for example, [5], [8]. In this order minimum and average thresholds for the number of long/short failures, and for cut off periods sustained by consumers are defined [5].

In the present era of information technology, we can access much more information than a few years ago. However, we also face the information explosion problem, in which we have so much information that humans alone cannot handle the huge amount of data without help from other appropriate technologies such as fuzzy logic,

neural networks, expert systems, distributed data base. These have been developed to menage the large amount of data available and to best utilize the information provided in the data. Heuristic, intuition, expert knowledge, and linguistic descriptions are often used by engineers in planning and reliability of distribution networks [3].

In recent years, the fuzzy techniques started to be used to model the uncertainties in reliability evaluation. The qualitative assessments as *Failure/repair rate is around/between...* can be mathematically translated into membership functions and thus integrated in several methodologies used for planning or operation purpose [6]. This paper proposes a general method to use input data obtained by fuzzy techniques instead of the statistical reliability indices.

2. Membership Functions and Fuzzification

Since its first presentation in 1965 by L.A. Z a d e h, the Fuzzy Techniques (FT) have had an unexpected growth and success. The board development of mathematical theory, especially in areas of Possibility Theory, Fuzzy Control, Neural Networks, and Pattern Recognition, provided the basis for different applications. They finally became the driving force of FT that today is reflected in many different software and hardware products [7].

The basic idea of FT is to model and to be able to calculate with uncertainty. Mathematical models and algorithms in electric power system theory aim to be as close to reality as possible. The required human observations, descriptions during the modelling process, are always a source of imprecision. A way to classify this imprecision is depicted in Fig. 1 [7].

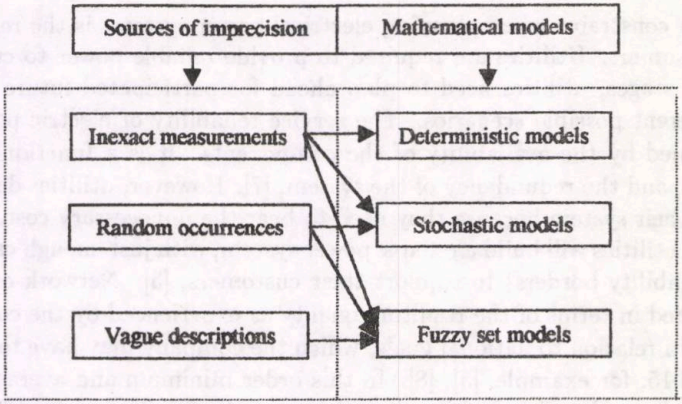

Fig. 1.– Mathematical models for imprecision.

While the first two sources of imprecision have led to suitable mathematical models, the last one came in our mind only a few decades ago, although we use it instinctively in our everyday life, *e.g.*: *The reliability of this component is very*

high. Most of linguistic descriptions such as *Small, Medium, High* are in nature fuzzy [3]. These vague descriptions are as well part of modelling process and the algorithm. The system analyzer has to differ between classes, *e.g.*, when classifying system operation states according to certain operational aspects [7].

Uncertainty in fuzzy logic is a measure of nonspecificity that is characterized by possibility distributions. This is, somewhat, similar to the use of probability distributions, which characterize uncertainty in probability theory. Linguistic terms used in our daily conversation can be easily captured by fuzzy sets for computer implementations. A fuzzy set is an one containing elements that have varying degrees of membership in the set. Elements of fuzzy set are mapped to a universe of a membership function. Fuzzy sets and membership functions are often used interchangeably. There are different ways to derive membership functions. Subjective judgment, intuition and export knowledge are commonly used in constructing membership function. Even though the choices of membership function are subjective, there are some rules *for* membership function selection that can produce good results, [3]. The membership values of each function are normalized between 0 and 1.

The uncertainty of the reliability indices will be represented in this paper as fuzzy numbers, with membership functions over the real domain $\mathbb{R}$. A fuzzy number can have different forms but, generally, this is represented as trapezoidal or triangular fuzzy number. In the case of triangular representation, a fuzzy number, $\tilde{A}$, is usually represented by its breaking points [7] (Fig. 2):

$$\tilde{A} \Leftrightarrow (x_1, x_2, x_3) = [m, a, b]. \tag{1}$$

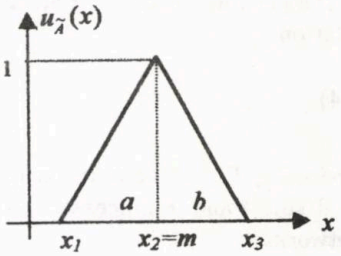

Fig. 2.– Triangular fuzzy number.

The usual algebraic operations with numbers can be extended to fuzzy sets, as following [2]:

$$\tilde{A} = \left\{\left(x_1, u_{\tilde{A}}(x_1)\right), x_1 \in X\right\}, \tag{2}$$

$$\tilde{B} = \left\{\left(y_1, u_{\tilde{A}}(y_1)\right), y_1 \in X\right\}, \tag{3}$$

$$\tilde{A}+\tilde{B} = \left\{\left(z_1, u_{\tilde{A}+\tilde{B}}(z_1)\right), z_1 \in X\right\}, \tag{4}$$

$$u_{\tilde{A}+\tilde{B}}(z_1) = \max_{z_1=x_1+y_1}\left\{\min[u_{\tilde{A}}(x_1), u_{\tilde{B}}(y_1)]\right\}, \tag{5}$$

$$\tilde{A}\cdot\tilde{B} = \left\{\left(z_1, u_{\tilde{A}\cdot\tilde{B}}(z_1)\right), z_1 \in X\right\}, \tag{6}$$

$$u_{\tilde{A}\cdot\tilde{B}}(z_1) = \max_{z_1=x_1\cdot y_1}\left\{\min[u_{\tilde{A}}(x_1), u_{\tilde{B}}(y_1)]\right\}, \tag{7}$$

$$c\cdot\tilde{A} = \left\{\left(x_1, u_{c\cdot\tilde{A}}(x_1)\right), x_1 \in X\right\}, \tag{8}$$

$$u_{c\cdot\tilde{A}}(x) = u_{\tilde{A}}(c\cdot x). \tag{9}$$

For three factors, $\tilde{A}$, $\tilde{B}$, $\tilde{C}$, defined as fuzzy variables (Fig. 2):

$$\tilde{A} = [m_1, a_1, b_1], \quad \tilde{B} = [m_2, a_2, b_2], \quad \tilde{C} = [m_3, a_3, b_3], \tag{10}$$

the resulting expression for the multiplication (s. (6), (7), (10)) is [7]:

$$\tilde{A} = [m_1, a_1, b_1] = \tilde{B} \cdot \tilde{C} = [m_2 m_3,\ m_2 a_3 + m_3 a_2 - a_2 a_3,\ m_2 b_3 + m_3 b_2 + b_2 b_3]. \tag{11}$$

For reliability evaluation of distribution networks by fuzzy techniques it is necessary to define the division operation with the fuzzy numbers. Using the relations (10), (11), we have:

$$m_3 = \frac{m_1}{m_2}, \qquad a_3 = \frac{a_1 - \dfrac{m_1}{m_2} a_2}{m_2 - a_2}, \qquad b_3 = \frac{b_1 - \dfrac{m_1}{m_2} b_2}{m_2 + b_2}; \tag{12}$$

$$\frac{a_1}{a_2} > \frac{m_1}{m_2}, \qquad \frac{b_1}{b_2} > \frac{m_1}{m_2}. \tag{13}$$

3. Methodology for Calculation of Indices λ and μ

The calculation of indices λ (failure rate) and μ (repair rate), for each element of the network (cables, circuit breakers, disconnectors, bus bars), uses the following relations:

$$\lambda = \frac{1}{T_f}, \qquad \mu = \frac{1}{T_r}, \tag{14}$$

where T_f, T_r are the uninterrupted function, respectively, reparation duration, [h].

Using λ and μ indices we can calculate following reliability indices for distribution networks:

$$P_s = \frac{\mu}{\lambda + \mu}, \qquad Q_s = \frac{\lambda}{\lambda + \mu}; \tag{15}$$

$$M[\alpha(T)] = \frac{\mu}{\lambda + \mu} T, \ \text{[h]}; \tag{16}$$

$$M[\beta(T)] = \frac{\lambda}{\lambda + \mu} T, \ \text{[h]}; \tag{17}$$

$$\text{SAIDI} = \frac{\sum M[\beta(T)]_i N_i}{\sum N_i}, \ \text{[h]}, \tag{18}$$

where: P_s is the function probability; Q_s – failure probability; $M[\alpha(t)]$ – total duration of the function; $M[\beta(t)]$ – total duration of the failure; SAIDI – system average interruption duration; T – study duration (1 year = 8,760 h); N_i – number of supply customers from the i distribution substation (DS).

Let us assume that the failure and repair rates of a component are described as triangular fuzzy numbers. From the upper/lower limits for statistical reliability

indices, with expert knowledge, it is possible to settle the linguistic variables and membership functions for each of these.

With the upper/lower limits given in [4], the Figs. 3 and 4, Tables 1 and 2, present the membership functions of three linguistic variables: Small (**S**), Medium (**M**), and Large (**L**), used to describe the values of the failure rate (λ) and repair rate (μ), for the MV (20 kV) cables. The characteristic values (breaking points, Fig. 2) of the indices λ and μ are presented in Tables 1 and 2.

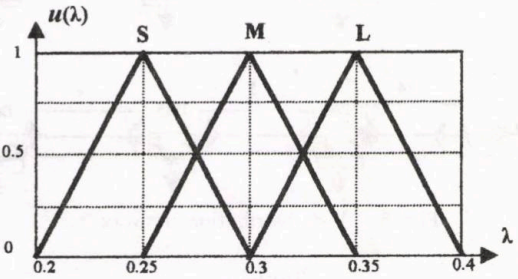

Fig. 3.– $u(\lambda)$ membership functions.

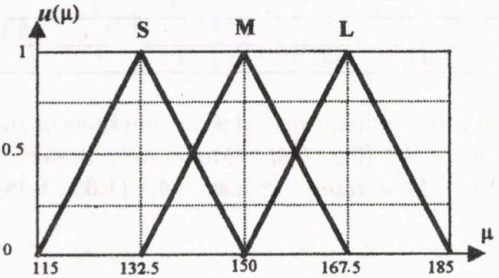

Fig. 4.– $u(\mu)$ membership functions.

Table 1
Characteristic Values for λ, $[10^{-4}/\text{h·km}]$

S	M	L
$m\lambda_S = 0.25$	$m\lambda_M = 0.3$	$m\lambda_L = 0.35$
$a\lambda_S = 0.05$	$a\lambda_M = 0.05$	$a\lambda_L = 0.05$
$b\lambda_S = 0.05$	$b\lambda_M = 0.05$	$b\lambda_L = 0.05$

Table 2
Characteristic Values for μ, $[10^{-4}/\text{h}]$

S	M	L
$m\mu_S = 132.5$	$m\mu_M = 150$	$m\mu_L = 167.5$
$a\mu_S = 17.5$	$a\mu_M = 17.5$	$a\mu_L = 17.5$
$b\mu_S = 17.5$	$b\mu_M = 17.5$	$m\mu_L = 17.5$

4. Case Study

Due to the general and basic idea of FT, these offer a variety of different possible applications. The proposed technique has been applied to several cases. Using the relations for calculation of the reliability indices and the characteristic values (breaking points) of λ and μ indices, the supply unavailability of the test network

was calculated. Therefore, because supply unavailability is assumed to be increased by an increased length of the cable, two cases for the different lengths of the cable were considered (Table 3).

The results for a test distribution network (Fig. 5) are presented in the Tables 4 and 5.

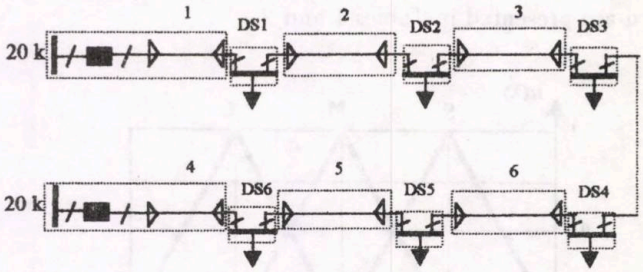

Fig. 5.– Test distribution network.

Table 3
The Lengths of the Cable, [km]

Case	Section I		Section II		Section III	
	1	4	2	5	3	6
I	0.5	0.5	0.1	0.1	0.1	0.1
II	1.5	1.5	1	1	1	1

We have considered five linguistic variables, as functions of supply unavailability (Fig. 6): Strongly Prefer – **SP** (0.3...0.45); Moderately Prefer – **MP** (0.45...0.75); Neutral – **NT** (0.75...1.05); Moderately Against – **MA** (1.05...1.35); Strongly Against – **SA** (1.35...1.5).

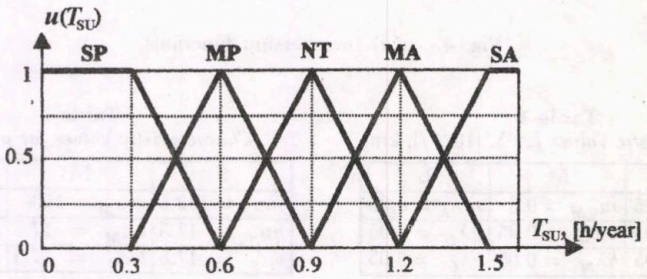

Fig. 6.– $u(T_{SU})$ membership functions.

Since there are two inputs (λ, μ) and one output (supply unavailability), the fuzzy rules can be represented by a Fuzzy Matrix (FM). Using the $n-1$ principle, in the Tables 4 and 5, the possible rules, with respect to the linguistic description of two inputs (λ, μ), for the supply unavailability, [h/year], are considered.

The proposed method allow finding the supply unavailability for different structures and dimensions of the MT networks.

Table 4

FM for Supply Unavailability for the First Case, [h/year]

μ		λ = S	λ = M	λ = L
	L	m = 0.3546 a = 0.00196 b = 0.00174 crisp = 0.3545 **SP**	m = 0.5069 a = 0.00189 b = 0.00167 crisp = 0.5068 **MP**	m = 0.6601 a = 0.0016 b = 0.00135 crisp = 0.66009 **MP**
	M	m = 0.3966 a = 0.00218 b = 0.0018 crisp = 0.3959 **SP**	m = 0.5661 a = 0.00193 b = 0.0016 crisp = 0.566 **MP**	m = 0.7373 a = 0.00140 b = 0.00113 crisp = 0.7372 **MP**
	S	m = 0.4490 a = 0.00234 b = 0.00191 crisp = 0.4488 **SP**	m = 0.6419 a = 0.00175 b = 0.00189 crisp = 0.6418 **MP**	m = 0.8363 a = 0.0007 b = 0.00058 crisp = 0.8362 **NT**

Table 5

FM for Supply Unavailability for the Second Case, [h/year]

μ		λ = S	λ = M	λ = L
	L	m = 0.5577 a = 0.04256 b = 0.03797 crisp = 0.5562 **MP**	m = 0.7977 a = 0.0406 b = 0.0351 crisp = 0.7981 **NT**	m = 1.0593 a = 0.0346 b = 0.03797 crisp = 1.05755 **MA**
	M	m = 0.6492 a = 0.04721 b = 0.04060 crisp = 0.6470 **MP**	m = 0.9313 a = 0.0416 b = 0.0345 crisp = 0.9289 **NT**	m = 1.2348 a = 0.03006 b = 0.0244 crisp = 1.2329 **MA**
	S	m = 0.7734 a = 0.05058 b = 0.04151 crisp = 0.7703 **NT**	m = 1.1097 a = 0.0378 b = 0.03002 crisp = 1.10716 **MA**	m = 1.4735 a = 0.01626 b = 0.0126 crisp = 1.4723 **SA**

From the Tables 4 and 5 is possible to observe that the increase of the length of the feeder sections assume an increase of the supply unavailability. At the same time, the tables give the results for the optimist case (λ – low values, μ – large values) and pessimist one (λ – low values, μ – large values).

5. Conclusions

The paper presents a possible field of application for the Fuzzy Techniques in the area of reliability analysis of power distribution system. In this order the failure and repair rates are modeled by linguistic variables and fuzzy numbers.

1. The proposed method uses for input the failure and repair data and the triangular form representation of the linguistic variables. The method can find the supply unavailability in the fuzzy manner.

2. Simulations carried out on several tests models shows that the proposed method is efficient and robust.

Received, May 18, 2001

Technical University "Gh.Asachi", Jassy,
Department of Energetics

REFERENCES

1. Carer P., Martin F., Pinget A., Hamet T., Journet T., *Dependability Approach Applied to Digital Protection and Control–Command Systems of EdF HV/MV Substations.* EdF-DER, 97NR00027, Janvier 1997.
2. Cârţină Gh., Alexandrescu V., Bonciu Cr., Voinea E., *Multiobjective Optimization Using Fuzzy Logic.* Proc. of the 6th Internat. Symp. on Automatic Control and Computer Sci., SACCS'98, Jassy, Romania, November 20-21, 1998, **I**, 202-207.
3. Chow M.-Y., Tram H., *Application of Fuzzy Logic Technology for Spatial Load Forecasting.* IEEE Trans. on Power Systems, **12**, *3*, 1360-1365 (1997).
4. *** *The Normative for the Calculation Tools and Methods of the Power Equipments Reliability* (in Romanian). Regia autonomă de electricitate – RENEL PE013/1994.
5. Romanello E., *Development of Medium Voltage Network Structures in Rural Field.* EdF-DER, 95NR00096, 1995.
6. Saraiava J.T., Sousa A.V., *New Advances in Integrating Fuzzy Data in Monte-Carlo Simulation to Evaluate Reliability Indices of Composite Power Systems.* Proc. of the MELECON'98, **II**, Tel-Aviv, 1998, 1084-1089.
7. Setz Ph., Hubrich H.-J., Bovy A., *Reability Evaluation of Power Distribution Systems with Local Generation Using Fuzzy Sets.* Proc. of the 11the PSCC, Avignon, 30 Aug.–3 Sept. 1993, **I**, 39-45.
8. Sinius R., *Structure d'alimentation des grandes agglomérations en France et à l'étranger.* REE, *1*, 29-40 (1999).

ASPECTE PRIVIND PLANIFICAREA REŢELELOR ELECTRICE CU O CONSIDERARE PARTICULARĂ A FIABILITĂŢII

(Rezumat)

Se propune o metodă pentru analiza fiabilităţii sistemelor de distribuţie bazată pe tehnicile fuzzy. Aceasta foloseşte, pentru calculul duratei de întrerupere, date de intrare descrise ca variabile lingvistice.

BULETINUL INSTITUTULUI POLITEHNIC DIN IAŞI
Tomul XLVII (LI), Fasc. 3–4, 2001
ELECTROTEHNICĂ. ENERGETICĂ. ELECTRONICĂ

D.C. 621.316.13

STATISTICAL-PROBABILISTIC ANALYSIS OF LOADS FROM THE DISTRIBUTION NETWORK NODES DATABASE

BY
GH. GEORGESCU and DANIELA RĂDĂŞANU

Taking into account the electric loads from the nodes of medium and low voltage distribution system as random variables, the paper presents the typical load curves modeling, based on a statistical-probabilistic analysis for different consumer categories, in four standard days, for every month of the year. The active and reactive load curves from the nodes of the distribution systems are computed using the typical load curves, maintained in the application database, the complex structure of the consumer and a limited number of direct measurements in the system.

The adopted model is simple and leads to an important increase of results accuracy supplied by majority of software application packages used for the optimal planning of the running and structure regimes of the electrical distribution systems.

1. Introduction

Current trends of power market deregulation and the necessity of carefully planning of acquisition and energetic resources stocks will have as result the growing of complexity for the planning, operation and management of transport and distribution electric networks.

For optimal operation of distribution networks and a rational economical-financial administration of the electric power distribution utilities, one of the most important problems, which have to be solved with a good precision, is the knowing of power and energy necessary: where, how and when.

The obtaining of this information is more simply when it uses a suitable model for load representation. If, for every consumer supplied from electric distribution networks, it is known the active and reactive load curves for a certain time interval (for example a day, a month, a season or a year), these can be used to solve some typical problems, as the followings: regime operation analysis of distribution networks, structure optimization, by determining the optimal sectionalizing points, optimal placement of compensators for improving the electric power quality and the power and energy losses reduction on distribution network components.

Having this information, the service staff can adopt suitable decisions concerning the national planning and development of installations.

There are specialized and very good software application packages, which allow solving all the above problems, and which assure a good precision, too. The major problem is represented by the input data used in these programs, active and reactive loads from the medium and low voltage distribution network nodes, which are not recorded, usually.

In this context, for taking into account more accurate the loads required by the consumers and their variations in time, we adopt a simply and precisely representation model of loads. This model is usually used in our country [1], [5], [8] and abroad [2],...,[4], [10]. It is based on a model of active and reactive load curves from the electric distribution system nodes that use the consumer structure from the nodes, a database including typical load curves for every consumer category and a small number of direct measurements made on the network.

2. Typical Load Curves Elaboration

Loads from the distribution network nodes are random functions depending on many parameters, which have also random nature. So, the correct analysis of load curves and their main indicators are possible only on the basis of mathematical-statistical methods and the probabilities calculus.

Active and reactive loads from the distribution system nodes are random functions of time and daily past variations of load represents their concrete realizations.

To obtain the statistical series of random variable, X (active or reactive load from a network node), at a fixed moment, the whole variation pitch of this measure, comprised between maximum value, $X_{\max}$, and minimum value, $X_{\min}$, is divided into n intervals depending on the desired precision. On every interval it is determined the n_k number of values for X measure, which fulfill the condition:

$$X_{k-1} < X < X_k,$$

where X_{k-1} and X_k represent the values at the extremities of k interval.

For every interval, statistical frequency, which characterizes the random values of active and reactive load, results from the equation:

$$f_k(X) = \frac{n_k}{n}, \quad (k = \overline{1,m}),$$

where: n is the total number of values obtained for X measure, at the considered moment; n_k – the number of values for X included in k interval; m – the intervals number.

Fig. 1 presents the statistical series of X random variable distribution and the normal distribution density curve. For a relative big number of measurements (over 100) one can consider that the statistical series coincides with probabilities distribution series of X random measure. In the case of electric distribution systems these observations justify the adoption of hypothesis, sufficiently precise for the practical calculus, that the active and reactive loads are submitted in every moment of the day to normal distribution law.

Normal distribution law is characterized by two measures: the medium value (also named mathematical confidence), M_x, and the dispersion, D_x, which are determined using the following relations:

$$(1) \qquad M_x = \frac{1}{n}\sum_{i=1}^{n} X_i, \qquad (2) \qquad D_x = \frac{n}{n-1}\left(\frac{\sum_{i=1}^{n} X_i^2}{n} - M_x^2\right),$$

where X_i is the random measure value obtained or measured in i experiment and n – the total number of experiments.

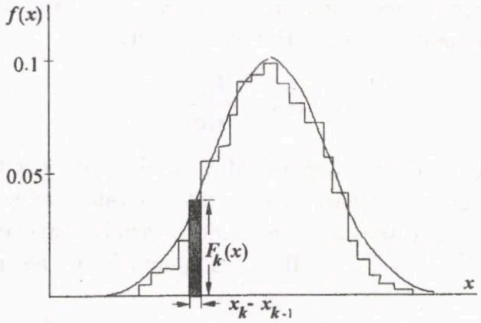

Fig. 1.– Statistical series of x random variable distribution.

Maximum value, $X_{\max}$, of random variable, is calculated using the equation:

$$(3) \qquad X_{\max} = M_x + t\sigma_x,$$

where $\sigma_x = \sqrt{D_x}$ represents the standard deviation and t is a parameter of normal distribution law.

If, after the measurements at the same moment, we obtained values for more random variables (for example, active and reactive loads for certain distribution system nodes from where are supplied consumers of the same category), then we can determine the numerical characteristics of probabilities distribution for the system of these variables.

Medium value of random measure of the system with m variables can be expressed as the sum of medium values of the components:

$$(4) \qquad M = \sum_{k=1}^{m} M_k.$$

To determine the system dispersion of m variables, it is necessary to take into account the probabilistic dependence between every pair of variables. This can be

expressed by correlation moment which, for the pair of variables X_k and X_l, is given by the equation:

$$K_{kl} = \frac{n}{n-1}\left(\frac{\sum_{i=1}^{n} X_{ki}X_{li}}{n} - M_k M_l\right). \tag{5}$$

In the case of algebraic sum of m variables, dispersion is calculated using relation:

$$D = \sum_{k=1}^{m} D_k \pm 2\sum_{k=1}^{m-1}\sum_{l=k+1}^{m} K_{kl}, \tag{6}$$

where D_k is the dispersion for X_k.

Stochastically dependence measure between two random variables can be expressed more convenient by correlation coefficient:

$$R_{kl} = \frac{K_{kl}}{\sigma_k \sigma_l}. \tag{7}$$

In the case of two random independent variables, this coefficient takes the zero value and for linear dependent variables, it takes a value between $+1$ and -1. Correlation coefficients for a system with m random variables are arranged into a square matrix $[R_{kl}]$, $(k = \overline{1,m};\ l = \overline{1,n})$, all the elements from the main diagonal having the value 1.

Typical load curves are build for the consumer categories, which have common characteristics. Also, into one category the load curves shape are influenced by the social-economical factors as the endowment with electrical apparatus, installations and equipment at suppliers and by the temperature variations from one day to another and seasonal cycle, mirrored in the length of the day.

Based on the above fundamentals, we have made a software application, which allows to establish the typical active and reactive load curves for different consumer categories supplied from the distribution networks, by the automatic analyse of obtained information from the direct measurement on the network [1], [8], [9].

Typical load curves represent the probable variation of load (active/reactive), on a given time interval, usually 24 h. These curves are drawn up using a 30 or 60 min level pattern, the loads being expressed in relative units, by division at medium value of loads from the recorded and processed curves.

A small database, containing typical load curves on every consumer categories (domestic, hotel, hospital, polyclinic, school, shop, post office a.s.o.), for winter/summer regimes, working and weekend days, was accomplished for the first time in our country between 1980-1985, using recording apparatus type WATT REG [1], [5], [6].

With a view to develop and to update this database that can be used with a higher precision for modeling the loads on distribution network nodes, we take into account the ANRE prescriptions [10], which stipulate the following consumer categories supplied from distribution networks:

a) A – domestic consumers;

b) B – commercial companies which can be: industrial consumers, public services, agricultural consumers, tertiary or temporary consumers;

c) C – atypical consumers, usually assimilated with domestic consumers.

According to the same prescriptions, the typical load curves have to be worked out for every month of the year and the following standard days: Monday and Friday; Tuesday, Wednesday and Thursday; Saturday; Sunday and legally holidays.

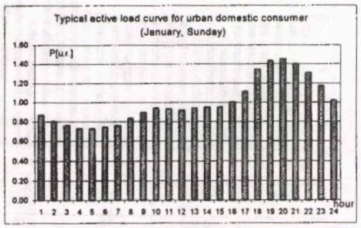

hour	P[u.r.]	hour	P[u.r.]
1	0.869	13	0.941
2	0.804	14	0.951
3	0.760	15	0.954
4	0.732	16	1.005
5	0.728	17	1.112
6	0.744	18	1.340
7	0.762	19	1.436
8	0.835	20	1.453
9	0.892	21	1.401
10	0.942	22	1.309
11	0.932	23	1.172
12	0.919	24	1.021

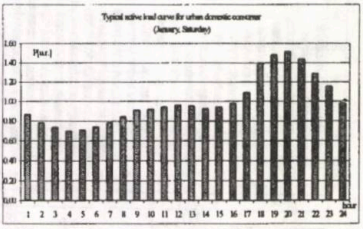

hour	P[u.r.]	hour	P[u.r]
1	0.866	13	0.952
2	0.776	14	0.925
3	0.733	15	0.943
4	0.698	16	0.977
5	0.707	17	1.091
6	0.738	18	1.395
7	0.776	19	1.478
8	0.842	20	1.518
9	0.910	21	1.435
10	0.917	22	1.291
11	0.940	23	1.151
12	0.962	24	0.980

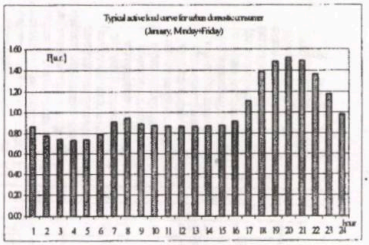

hour	P[u.r.]	hour	P[u.r.]
1	0.864	13	0.868
2	0.773	14	0.867
3	0.741	15	0.875
4	0.727	16	0.909
5	0.738	17	1.108
6	0.786	18	1.388
7	0.906	19	1.486
8	0.943	20	1.524
9	0.887	21	1.489
10	0.871	22	1.363
11	0.866	23	1.177
12	0.864	24	0.980

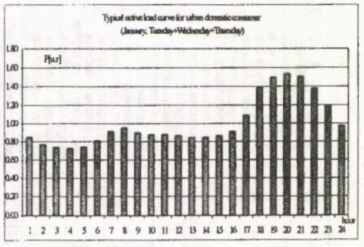

hour	P[u.r.]	hour	P[u.r]
1	0.849	13	0.842
2	0.768	14	0.842
3	0.736	15	0.867
4	0.723	16	0.907
5	0.741	17	1.084
6	0.805	18	1.385
7	0.909	19	1.497
8	0.950	20	1.533
9	0.897	21	1.506
10	0.876	22	1.375
11	0.880	23	1.189
12	0.867	24	0.973

Fig. 2.– Typical active load curves for urban domestic consumer, in January, for standard days.

To achieve this aim, together with electric utilities staff from Jassy, Bacău, Suceava, Neamţ, Galaţi, Constanţa, we have been started a recording action of active and reactive load curves on different nodes of distribution networks having a fixed and known structure of consumers. The recording of load curves is fulfilled using ALPHA/meters, for each month of the years 2000 and 2001.

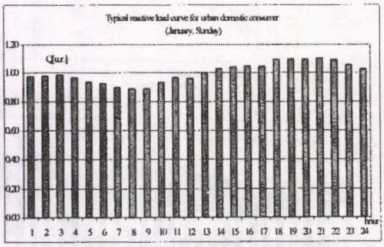

hour	Q[u.r.]	hour	Q[u.r.]
1	0.973	13	1.000
2	0.978	14	1.029
3	0.983	15	1.039
4	0.967	16	1.045
5	0.937	17	1.042
6	0.925	18	1.092
7	0.896	19	1.095
8	0.888	20	1.096
9	0.887	21	1.102
10	0.933	22	1.090
11	0.965	23	1.055
12	0.960	24	1.026

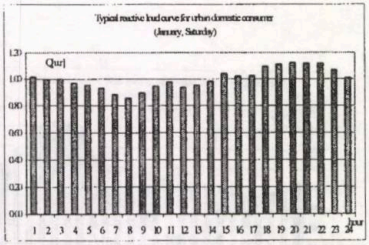

hour	Q[u.r.]	hour	Q[u.r.]
1	1.014	13	0.953
2	0.996	14	0.981
3	0.997	15	1.040
4	0.968	16	1.018
5	0.952	17	1.024
6	0.930	18	1.094
7	0.884	19	1.107
8	0.856	20	1.121
9	0.896	21	1.119
10	0.946	22	1.118
11	0.979	23	1.068
12	0.937	24	1.007

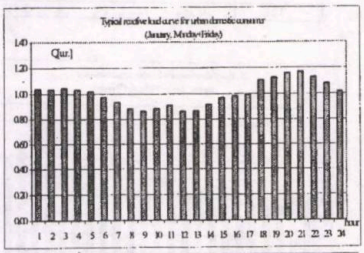

hour	Q[u.r.]	hour	Q[u.r.]
1	1.038	13	0.866
2	1.032	14	0.916
3	1.047	15	0.970
4	1.032	16	0.982
5	1.020	17	0.994
6	0.974	18	1.105
7	0.934	19	1.127
8	0.884	20	1.159
9	0.865	21	1.171
10	0.884	22	1.131
11	0.910	23	1.080
12	0.864	24	1.015

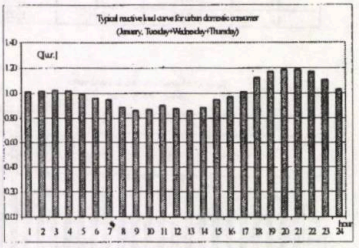

hour	Q[u.r.]	hour	Q[u.r.]
1	1.013	13	0.859
2	1.017	14	0.884
3	1.024	15	0.949
4	1.019	16	0.972
5	0.992	17	1.008
6	0.958	18	1.124
7	0.949	19	1.170
8	0.886	20	1.186
9	0.858	21	1.186
10	0.871	22	1.169
11	0.899	23	1.106
12	0.872	24	1.029

Fig. 3.– Typical reactive load curves for urban domestic consumer, in January, for standard days.

By statistical processing of recorded active and reactive load curves using the software application, we have been determined typical load curves for different categories of consumers, for every month of the year and for standard days. Figs. 2 and 3 illustrate the typical load curves for domestic consumer on January.

3. Modeling of Load Curves from the Nodes of Distribution Networks

The above database can be used for modeling the active and reactive consumption from the nodes of distribution networks, for every month by association to the typical load curves of some measurements in the system [4], [5], [6].

3.1. Measured Current in Every Node at Certain Hour of the Day

In this case, the active and reactive load at hour t can be calculated using the following equations:

$$P_{n,j}(t) = \sqrt{3} U_n I_{n,j}(k) \cos\varphi_j^T(k) \frac{P_j^T(t)}{P_j^T(k)},$$

(8)

$$Q_{n,j}(t) = \sqrt{3} U_n I_{n,j}(k) \sqrt{1 - \cos^2\varphi_j^T(k)} \frac{Q_j^T(t)}{Q_j^T(k)}, \quad (t = \overline{1,24}),$$

where: $P_{n,j}(t)$, $Q_{n,j}(t)$ are the active and, respectively, reactive power for node n, regime j, hour t; $I_{n,j}(k)$ – measured current in node n, regime j, hour k; $P_j^T(t)$, $P_j^T(k)$, $Q_j^T(t)$, $Q_j^T(k)$ – medium value of active and reactive powers from typical curves, for regime j, hour t, respectively k; $\cos\varphi_j^T(k)$ – power factor for regime j, hour k; U_n – nominal voltage of the network.

3.2. The Energy which Circulates over 24 Hours through the Node n

The active and reactive powers are

$$P_{n,j}(t) = \frac{W_{n,j}}{24} P_n^T(t), \quad Q_{n,j}(t) = P_{n,j}(t) \sqrt{\frac{1}{\cos\varphi_j^T(t)} - 1}, \quad (t = \overline{1,24}), \tag{9}$$

where: $W_{n,j}$ is the active energy which circulates through the node n over 24 hours, in regime j; $\cos\varphi_j^T(t)$ – power factor for regime j, hour t.

In the case of nodes with a mixed structure of consumer, their associated typical load curves are established on the basis of the typical load curves of the supplied consumers and their weight in the consumption structure.

To improve the accuracy of the results, the modeled curves can be corrected for balancing the hourly powers on certain sections of networks or on the whole network [6],...,[9].

4. Conclusions

The database is formed by typical active and reactive load curves for different consumer categories, in four standard categories of days and for each month of the year.

Using this database, we efficiently can model the load curves from the nodes of distribution systems during a year, with a high precision.

The adopted model is simply and leads to an important increase of results accuracy supplied by majority of software application packages used for the optimal planning of the running and structure regimes of the electrical distribution systems.

Received, April 15, 2001

Technical University "Gh.Asachi", Jassy, Department of Energetics

REFERENCES

1. Poeată Al., Georgescu Gh., Poeată N., *Posibilităţi de utilizare a graficelor tip de sarcină ale consumatorilor în studiile de dezvoltare şi pentru exploatarea raţională a reţelelor de distribuţie urbană.* Energetica, *2* (1985).
2. Codiasse A.M., Guillevic M., Giraud D., *Connaissance des charges moyenne tension en vue de leur prise en compte dans les études de planification.* R.G.E., *7-8* (1982).
3. Potrebiči A.A., *Rasčet poteri energhii električeskikh setiakh s učetam grafikov nagruzov.* Električestvo, *6* (1990).
4. Marcusheviči N.S., *Avtomatizirovannoe upravlenie rezhimami elektrosetei 6-20 kV.* Izd. Energhia, Moskva, 1980.
5. Georgescu Gh., Poeată Al., Poeată N., *Contribuţii la modelarea reţelelor electrice de distribuţie urbană.* Bul. Inst. polit., Iaşi, **XXIX (XXXIII)**, *1-4*, s.III (1983).
6. Georgescu Gh., *Transportul şi distribuţia energiei electrice.* Inst. polit., Iaşi, 1989.
7. Georgescu Gh., Gavrilaş M., Rădăşanu D., *Calculul şi reducerea pierderilor de putere şi energie în reţelele electrice.* Ed. Spectrum, Iaşi, 1997.
8. Georgescu Gh., Rădăşanu D., *Transportul şi distribuţia energiei electrice.* Vol.**I**, Ed. „Gh. Asachi", Iaşi, 2000.
9. Georgescu Gh., Gavrilaş M., Cârţină Gh., *Aspects Concerning Power Distribution Networks Planning Using Artificial Intelligence.* 14th Internat. Conf. on Electricity Distribution, CIRED '97, Birmingham, 1997.
10. * * * *Metodologie de încadrare pe categorii a consumatorilor captivi de energie electrică.* ANRE, Bucureşti, 2000.

ANALIZA STATISTICO-PROBABILISTICĂ A SARCINILOR DIN NODURILE REŢELELOR DE DISTRIBUŢIE
Baza de date

(Rezumat)

Considerând sarcinile din nodurile reţelelor de distribuţie de medie şi joasă tensiune ca mărimi aleatoare, pe baza unei analize statistico-probabilistice, se prezintă modul de întocmire a graficelor tip de sarcină, pe categorii de consumatori, în cele patru zile standard, pentru fiecare lună a anului. Graficele tip de sarcină astfel obţinute constituie o bază de date, cu ajutorul căreia precum şi a unui număr relativ redus de informaţii obţinute prin măsurători directe în reţea se pot modela, cu o precizie ridicată, graficele de sarcină activă şi reactivă din nodurile reţelelor de distribuţie.

Adoptarea unui astfel de model simplu conduce la creşterea semnificativă a preciziei rezultatelor furnizate de majoritatea produselor software utilizate în practica curentă pentru planificarea optimală a structurii şi regimurilor de funcţionare ale reţelelor de distribuţie.

BULETINUL INSTITUTULUI POLITEHNIC DIN IAŞI
Tomul XLVII (LI), Fasc. 3–4, 2001
ELECTROTEHNICĂ. ENERGETICĂ. ELECTRONICĂ

D.C. 621.316.13

HARMONIC STEADY-STATES IN MEDIUM VOLTAGE NETWORKS

BY

VIOREL VARVARA

The real operation state of the electrical systems is a non-sinusoidal and non-symmetrical one. The appearance of the non-sinusoidal state is mainly on account of the medium and high power non-linear loads. Electrically, they are operating as concentrated circuit elements installed on medium voltage, a concrete case being represented by the electrical railway traction. A medium voltage electrical network, provided with power factor capacitor banks, feeding several linear loads and a railway substation, is considered. For diverse energetic situations in which the network might be, the varied circuit elements behaviour under the non-sinusoidal state is determined.

1. Introduction

The sizes and the non-sinusoidal electrical states present a special importance in the design, construction and operation of the electrical machines, mechanisms, devices and, generally, of the various electrical equipments. The measure of the harmonic voltages and the determination of the harmonic currents flow in electrical networks represent an essential element in the non-sinusoidal steady state analysis [1]. Usually, is estimated the harmonic content of the currents and voltages waveforms at the coupling point to the energetic system and the way in which this depends on the charge curve and on the electrical characteristics of the network. On the base of these information measures for placing the sizes inside the normative are choosen.

Large power converters (MW order) represent the most important harmonic source in the system [1], [2], [4]. Concentrated distortion elements can be considered: the electrical traction, factories which have arc furnaces, cement plants, a.s.o.

The study of the frequency characteristic of the impedance seen from the harmonic generator bars, the behaviour of each of the network's branch at the interception of the harmonic current and their contribution to the eventually amplifications of the voltages, represent decisive elements in harmonic current flow control in an electrical network [1], [2].

2. Harmonic Current Flow

In the electrical traction, the supply from the electric system is realized in accordance to the scheme represented in Fig. 1. From the same 110 kV bars, equipped with an equivalent power factor capacitor bank, is also fed an equivalent linear load. In real operation states, for a given point of the network, if the harmonic source is far away, it works as an ideal harmonic voltage generator and if it is close, as a current one [3]. In the analysed case, the electrical equipment of the locomotive – the main non-linear element of the circuit – is replaced with an ideal harmonic current generator, the other circuit's elements being replaced with their harmonic impedances namely: $\underline{Z}_1$ – the system impedance seen from the 110 kV bars; $\underline{Z}_l$ – the 110 kV line impedance which feeds the substation; $\underline{Z}_T$ – the impedance of the feeding transformer 110/27.5 kV; $\underline{Z}_{T1}$ – the impedance of the transformer from the locomotive 27.5/1 kV; $\underline{Z}_B$ – the impedance of the capacitor bank installed on the locomotive; $\underline{Z}_L$ – the impedance of the linear equivalent load fed from the same 110 kV bars as the substation; $\underline{Z}_D$ – the impedance of the equivalent power factor capacitor bank.

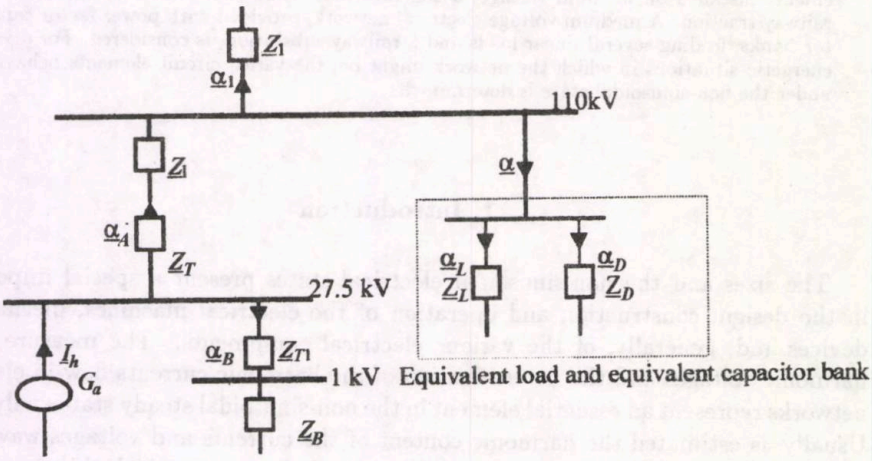

Fig. 1.– Electrical network supplying a railway substation.

The harmonic current on each of the network's branches, $\underline{I}_m$, may be estimated, depending on the harmonic current injected by the harmonic generator, I_h, with the help of some complex quantities, $\underline{\alpha}_m$, defined as follows:

$$\underline{I}_m = \underline{\alpha}_m I_h, \quad (m = A, B, 1, L, D), \tag{1}$$

where:

$$\underline{\alpha}_B = \frac{\underline{Z}_T + \underline{Z}_l + \underline{Z}_N}{\underline{Z}_{T1} + \underline{Z}_B + \underline{Z}_T + \underline{Z}_l + \underline{Z}_N}, \quad \underline{\alpha}_A = \frac{\underline{Z}_{T1} + \underline{Z}_B}{\underline{Z}_{T1} + \underline{Z}_B + \underline{Z}_T + \underline{Z}_l + \underline{Z}_N}, \tag{2}$$

$$\underline{\alpha}_1 = \underline{\alpha}'_1 \underline{\alpha}_A, \quad \underline{\alpha}'_1 = \frac{\dfrac{\underline{Z}_L \underline{Z}_D}{\underline{Z}_L + \underline{Z}_D}}{\underline{Z}_1 + \dfrac{\underline{Z}_L \underline{Z}_D}{\underline{Z}_L + \underline{Z}_D}}, \tag{3}$$

$$\underline{\alpha} = \underline{\alpha}' \underline{\alpha}_A, \quad \underline{\alpha}' = \frac{\underline{Z}_1}{\underline{Z}_1 + \dfrac{\underline{Z}_L \underline{Z}_D}{\underline{Z}_L + \underline{Z}_D}}, \tag{4}$$

$$\underline{\alpha}_L = \underline{\alpha}'_L \underline{\alpha} = \underline{\alpha}'_L \underline{\alpha}' \underline{\alpha}_A, \quad \underline{\alpha}'_L = \frac{\underline{Z}_D}{\underline{Z}_L + \underline{Z}_D}, \tag{5}$$

$$\underline{\alpha}_D = \underline{\alpha}'_D \underline{\alpha} = \underline{\alpha}'_D \underline{\alpha}' \underline{\alpha}_A, \quad \underline{\alpha}'_D = \frac{\underline{Z}_L}{\underline{Z}_L + \underline{Z}_D}. \tag{6}$$

Here $\underline{\alpha}_A$ represents harmonic current relative units (r.u.) which runs on the A branch; $\underline{\alpha}_B$ – harmonic current (r.u.) absorbed by the capacitor bank installed on the B branch; $\underline{\alpha}$ – harmonic current (r.u.) which runs to the L and D branches; $\underline{\alpha}_1$ – harmonic current (r.u.) which runs to system; $\underline{\alpha}_L$ – harmonic current (r.u.) which runs on the L branch (to the linear load); $\underline{\alpha}_D$ – harmonic current (r.u.) absorbed by the equivalent power factor capacitor bank.

These quantities satisfy the following relations:

$$\underline{\alpha}_A + \underline{\alpha}_B = 1, \quad \underline{\alpha}'_1 + \underline{\alpha}' = 1, \quad \underline{\alpha}'_L + \underline{\alpha}'_D = 1. \tag{7}$$

Following the dependence of this quantities *versus* frequency, one may establish the availability of each branch in absorbing the harmonic current and the behaviour of the network on the resonant frequencies. In the considered network, the first resonance which can appear is a current one, the other possible resonant states alternate, after a voltage resonance following a current one a.s.o. The type (parallel or series) and the place of the resonance (near by or far away the harmonic generator) can be estimated following the phasorial relationship which is established between the harmonic currents of the network's branches. The comportment of the $\underline{\alpha}_m$, $(m = A, B, 1, L, D)$, coefficients is synthesized in Table 1, where f_{1P}, f_{2P} are the first and the second parallel resonant frequencies and f_{1S} is the series one.

Table 1

The $\underline{\alpha}_m$ Coefficients Behaviour in the Harmonic Steady-State

Frequency	α_B	arg α_B	α_A	arg α_A	α_1	arg α_1	α_L	arg α_L	α_D	arg α_D
$f < f_{1P}$	$\uparrow$	$\in 2 \approx 180°$	$\uparrow$	$\in 4 \approx 0°$	$\uparrow$	$\in 4 \approx 0°$	$\uparrow$	$\in 1 \approx 0°$	$\uparrow$	$\in 2$
$f = f_{1P}$	max	$2 \to 1 \approx 0°$	max	$4 \to 3 \approx 180°$	max	$4 \to 3$	max	$1 \to 4 \approx 0°$	max	$2 \to 1 \approx 0°$
$f_{1P} < f < f_{1S}$	$\downarrow$	$\in 1$	$\downarrow$	$\in 3$	$\downarrow$	$\in 3$	$\downarrow$	$\in 4$	$\downarrow$	$\in 1$
$f = f_{1S}$	$\downarrow$	$\in 1$	min	$3 \to 4 \approx 0°$	min	$3 \to 4 \approx 0°$	min	$4 \to 1 \approx 0°$	min	$1 \to 2$
$f_{1S} < f < f_{2P}$	$\downarrow$	$\in 1$	$\uparrow$	$\in 4$	$\uparrow$	$\in 4$	$\uparrow$	$\in 1$	$\uparrow$	$\in 2$
$f = f_{2P}$	$\downarrow$	$1 \to 4 \approx 0°$	$\uparrow$	$4 \to 1 \approx 0°$	max	$4 \to 3$	max	$1 \to 4 \approx 0°$	max	$2 \to 1 \approx 0°$
$f > f_{2P}$		$\in 4$		$\in 1$	$\downarrow$	$\in 3$	$\downarrow$	$\in 4$	$\downarrow$	$\in 1$

L e g e n d: $\uparrow$ increases; $\downarrow$: decreases; $1 \to 4$; $0°$: the argument turns from 1-st quadrant to the 4-th one, having values close to 0 degrees; $\in j$: the argument is in the j-rd quadrant, $(j = \overline{1,4})$.

The dependence of $\underline{\alpha}_A$ and $\underline{\alpha}_B$ *versus* frequency can be also pointed out with the $\Im m\,\alpha = f(\Re e\,\alpha)$ plotting (Figs. 2 and 3). The $\arg\underline{\alpha}_A$ and $\arg\underline{\alpha}_B$ quantities are in a such relation so that the sum of their imaginary components be null. If the phase difference is 180°, the quantities being in 1-st and 3-rd quadrant, the two currents are in opposition. Corresponding to the situation when $|\sin\arg(\underline{\alpha}_A)| = |\sin\arg(\underline{\alpha}_B)|$ the modulus satisfy the relation $\alpha_A = \alpha_B = \max$ and an energy oscillation between the inductive, A, branch (which mainly includes the system) and the capacitive one, B, is established, the equivalent impedance getting a maximum value. A parallel

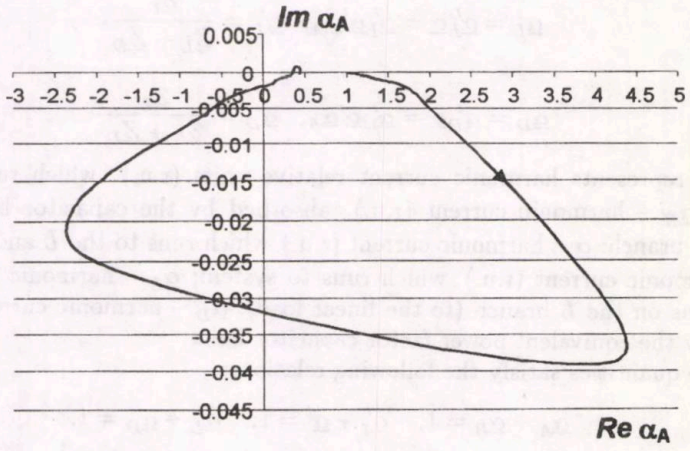

Fig. 2.– The behaviour of the $\underline{\alpha}_A$ quantities *versus* frequency.

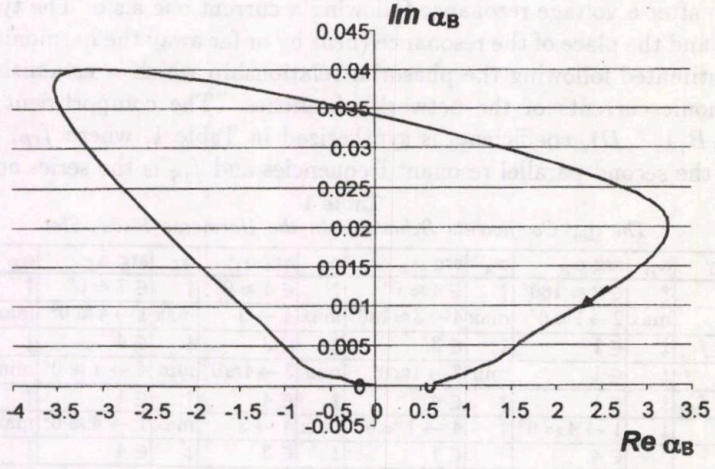

Fig. 3.– The behaviour of the $\underline{\alpha}_B$ quantities *versus* frequency.

resonance is established on that frequency and if this is close to a low harmonic order, the current which flows to the B branch can rich a higher value than the admissible one for capacitors. The parallel resonant frequency shift can be obtained by changing the capacitive power connected on the B bar, an increased value leading to a lower resonant frequency.

When both branches have simultaneously the real components of the current of positive sign, the phase difference of the two quantities tends to 90°, when we are close to a series resonance. When the two phasors, $\underline{\alpha}_A$ and $\underline{\alpha}_B$, are in quadrature and α_A has a very small value and α_B is close to unit, a series resonance is realized, the equivalent impedance becoming minimum. A filter near the harmonic generator is realized.

When the voltage resonance takes place far away the generator, the two quantities are in phase concordance and approximately equal. A current oscillation between the two branches doesn't take place. The frequency on which this resonance is realized isn't determined by the capacitive power on the 1 kV bar.

Referring to the other phasors, they simultaneously satisfy the relations:

$$\alpha_A \cos(\arg\underline{\alpha}_A) = \alpha_1 \cos(\arg\underline{\alpha}_1) + \alpha_L \cos(\arg\underline{\alpha}_L) + \alpha_D \cos(\arg\underline{\alpha}_D), \tag{8}$$

$$\alpha_A \sin(\arg\underline{\alpha}_A) = \alpha_1 \sin(\arg\underline{\alpha}_1) + \alpha_L \sin(\arg\underline{\alpha}_L) + \alpha_D \sin(\arg\underline{\alpha}_D). \tag{9}$$

The behaviour of the $\underline{\alpha}_1$, $\underline{\alpha}_D$, $\underline{\alpha}_L$ phasors *versus* frequency may be also followed with the help of quantities plotted in Figs. 4 and 5.

The positions of the two phasors are identically in conditions when the first voltage and current resonance conditions are satisfied. This show that the phenomenon appears mainly on account of the relations which are established between the quantities of the circuit's elements placed close to the harmonic generator. The same observation is valid also for frequencies $f < f_{1P}$ or $f_{1S} < f < f_{2P}$. The α_L and α_D coefficients have low values, showing the negligible participation of the respective branches at the harmonic current absorbtion. Practically, the whole current which runs through the substation's transformer is absorbed by the system, $\underline{\alpha}_A$ and $\underline{\alpha}_1$ phasors being in phases concordance and approximately equal. For the series resonance frequency, $\underline{\alpha}_D$ and $\underline{\alpha}_L$ are dephased with $\pi/2$, as $\underline{\alpha}_A$ and $\underline{\alpha}_B$ also are, corresponding to the same conditions.

Corresponding to the conditions in which a parallel resonance far away the harmonic generator takes place, the differences of phases between phasors modify substantially. The branch which has the power factor capacitors becomes an important flow path for the harmonic current. Between the system and this branch a current oscillation takes place, phenomenon pointed out by the two phasors approximately equal in modulus and in oppposition of phase. The current which runs through the substation's transformer will approximately entirely flow to the linear load branch, the two corresponding phasors being almost equal. For higher frequencies than f_{2P}, one can observe the substantially contribution of the D capacitive branch at the harmonic current distribution on the circuit branches.

If the following conditions are fulfilled, a series resonance, far away the harmonic generator, is realized namely: the equivalent impedance of the network seen from the harmonic generator bars is minimum; the capability of harmonic current absorption of the A branch and of the capacitor bank connected in the electrical vicinity of the harmonic generator to have a local minimum; the capability of harmonic current absorption of the system, of the equivalent linear load and of the power factor capacitor bank to be maximum. Frequency on which this resonance takes place can be controlled with help of the capacitive power of the power factor capacitor bank.

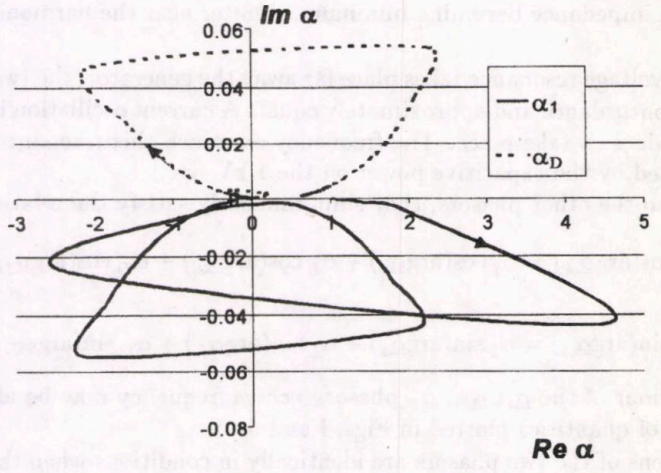

Fig. 4.– The behaviour of $\underline{\alpha}_1$ and $\underline{\alpha}_D$ quantities *versus* frequency.

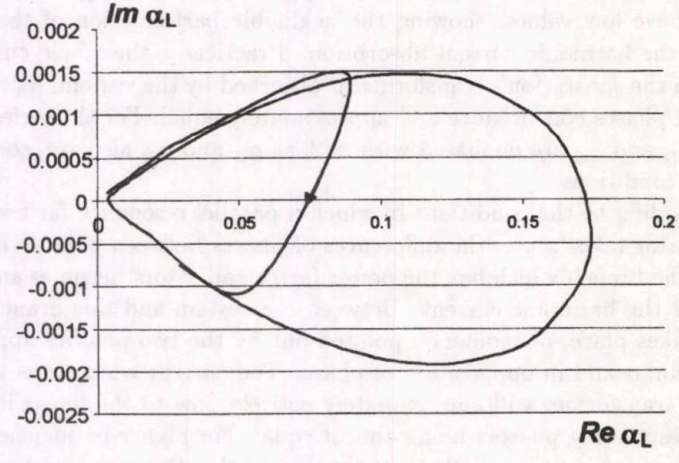

Fig. 5.– The behaviour of $\underline{\alpha}_L$ quantity *versus* frequency.

3. Conclusions

1. In a network feeding the railway electrical traction, the first resonance which may appear is a current one, the other possible resonance states alternating, after a voltage resonance following a current one.

2. Harmonic currents on all the branches, out of the resonant frequencies, are in phase or in opposition with the current injected by the harmonic generator; on the resonant frequencies, the current which flows to the power factor capacitor bank is in phase opposition with the one which runs to system and in quadrature with that runs to the linear load.

3. The type (parallel or series) and the place of the resonance (near by or far away from the harmonic generator) can be estimated following the phasorial relationship which may be established between the harmonic currents of the network's branches.

Received, December 4, 2000

Technical University "Gh.Asachi", Jassy,
Department of Electrotechnics

REFERENCES

1. Arie A., Neguş C., Golovanov C., Golovanov N., *Poluarea cu armonici a sistemelor electroenergetice funcţionând în regim permanent simetric.* Ed. Acad., Bucureşti, 1994.
2. Arrilaga J., *Power System Harmonics.* John Wiley & Sons, New York, 1985.
3. Popescu I., Zaharia I., Petrescu C., Varvara V., *Determination of Harmonic Active Losses Produced by the A.C. Networks Supplying Railway.* Bul. Inst. polit., Iaşi, **XXXV (XXXIX)**, *3-4*, s.III, 73-78 (1989).
4. Puşcaşu S., Marcovici J., *Mărimi şi regimuri electrice nesinusoidale.* Ed. Scrisul Românesc, Craiova, 1974.

REGIMURI DE FUNCŢIONARE PERMANENTE ARMONICE ÎN REŢELELE ELECTRICE DE MEDIE TENSIUNE

(Rezumat)

Regimul real de funcţionare a sistemelor electrice este permanent nesinusoidal şi nesimetric. Apariţia regimului nesinusoidal se datorează în primul rând existenţei elementelor neliniare de circuit de putere medie şi mare. Din punct de vedere electric ele se comportă ca elemente de circuit concentrate instalate pe medie tensiune, un caz concret reprezentându-l tracţiunea electrică feroviară.

Se consideră o reţea electrică de medie tensiune prevăzută cu baterii de condensatoare pentru îmbunătăţirea factorului de putere care alimentează diverşi consumatori liniari şi o substaţie de tracţiune, urmărindu-se circulaţia curentului armonic injectat de elementul neliniar – instalaţia electrică de alimentare a locomotivei. În funcţie de conjuncturile energetice în care se poate găsi reţeaua se determină comportarea diferitelor elemente de circuit în regim nesinusoidal.

BULETINUL INSTITUTULUI POLITEHNIC DIN IAŞI
Tomul XLVII (LI), Fasc. 3–4, 2001
ELECTROTEHNICĂ. ENERGETICĂ. ELECTRONICĂ

D.C. 621.316.13

SOFTWARE APPLICATION PACKAGE FOR THE ANALYSIS AND THE OPTIMIZATION OF DISTRIBUTION NETWORKS CHARACTERISTIC REGIMES

BY
GH. GEORGESCU, DANIELA RĂDĂŞANU and *VIOREL VARVARA

A software application package for the complex analysis of power distribution networks characteristic regimes during a year and possibilities of their optimization are presented. The analysed aspects are studied using classical methods and methods based on the evolutionary algorithms, too. The nodal loads are modelled using a database, which contains typical load curves for different consumer categories, on every month and standard days, the complex structure of the consumer from each node and a limited number of measurements in the network.

The obtained results may be useful in the operation and management process and in adopting decisions concerning the planning and the development of distribution networks.

1. Introduction

The actual trends of energy market deregulation and the necessity of carefully planning the acquisition and energetic resources stock will have as result the development of the running and leading planning activities of the distribution networks. The new problems which must be solved by the companies of electricity are multiple, the mains being: the assurance of consumers power supply at contractual parameters, the growth of delivered quality of the energy, the decrease of the investments/running costs, technological losses and costs of delivered kWh, the reasonable planning of the maintenance, the decrease of the installations and technological routines impact on environment, a.s.o.

For the achievement of these objectives and reasonable development of the distribution networks, the people who works with these equipment must precisely know the electrical quantities for their equipment, during the whole year. Having performance software, which certifies a high precision of the results, the main problem is the accuracy of the input data, such as the active and reactive nodal loads in distribution networks, which generally are not recorded.

2. The Modelling of the Nodal Load Curves

On the base of the papers [1],...,[4], the low and medium voltage nodal loads can be modelled using typical load curves, the nodal load structure and, at least, one measurement in each node of the network. For using this methodology, one

must have at his disposal a large and permanently up-to-date data base, which must contain active and reactive typical load models for different categories of consumers supplied from the distribution network (urban and rural domestic, urbanistic – hospital, school, hotel, shop, railway station a.s.o.) in different characteristic seasons and days of the year. Since 2000, according to our actual prescriptions of The National Regulation Authority on the Electrical and Thermal Energy (ANRE), the data base used for modelling must contain active and reactive typical load curves for different consumer categories, for every month of the year and four standard days of the week (Monday and Friday / Tuesday, Wednesday and Thursday / Saturday / Sunday and legal holidays).

By statistical processing of the recorded active and reactive load curves using ALPHA/meters, between 1999, June – 2000, June, have been determined typical load curves for different categories of consumers, for every month of the year and for standard days. The obtained active and reactive typical load curves, with 24 hourly levels, are given in relative units, related to the medium load of the recorded load curves [4], [5].

This database can be easily and efficiently used for modelling active and reactive consumption from the nodes of power distribution systems [3], [4]. This model needs two kinds of information: firstly, the nodal load structure and secondly, at least one measurement (for instance, a current) in each node of the network. To increase the precision of the results concerning the modelling of the load curves, these can be corrected, for balancing the active and reactive powers, depending on the powers injected in different nodes or for the whole network.

3. Classical Methods for Characteristic Regimes Analysis of the Distribution Networks

For the characteristic regimes analysis and structure optimization of the distribution networks by establishing the optimal points of division into sections in an open-loop radial distribution systems, the optimal placement of the compensation sources, the optimal power transformer sizing depending on the real annual loads, the authors made a software application package which provides useful informations for the maintenance and management process. The software package includes classical methods and genetic algorithms based methods, being written in Delphi under Windows.

The input data are:

a) general network data – the rated voltage, the number of feeders, the number of nodes, the hour voltage values of the power supply points;

b) branch data – for each branch: the node indexes at the both ends of the branch, the resistance, reactance and capacitive susceptance of the branch, the maximum admissible current of the branch;

c) nodal data – for each node: the loads structure, direct measurements (the current measured at a moment or the transferred energy through the node in 24 h).

The active and reactive load curves are modelled using typical load curves from the database, as it was presented in § **2**. Using the **Run** menu of the software package, the user may choose one of the analysis options, as we can see in Fig. 1.

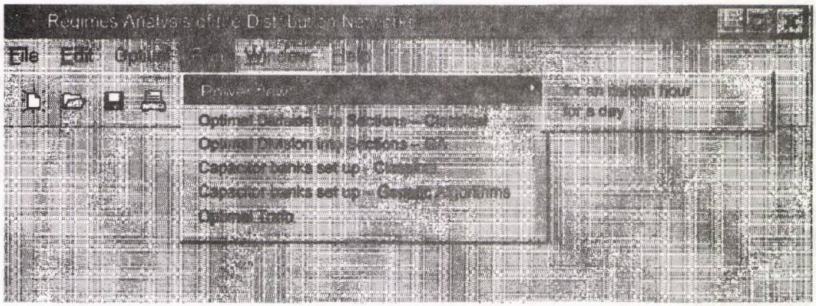

Fig. 1.– The analysis options of the software package.

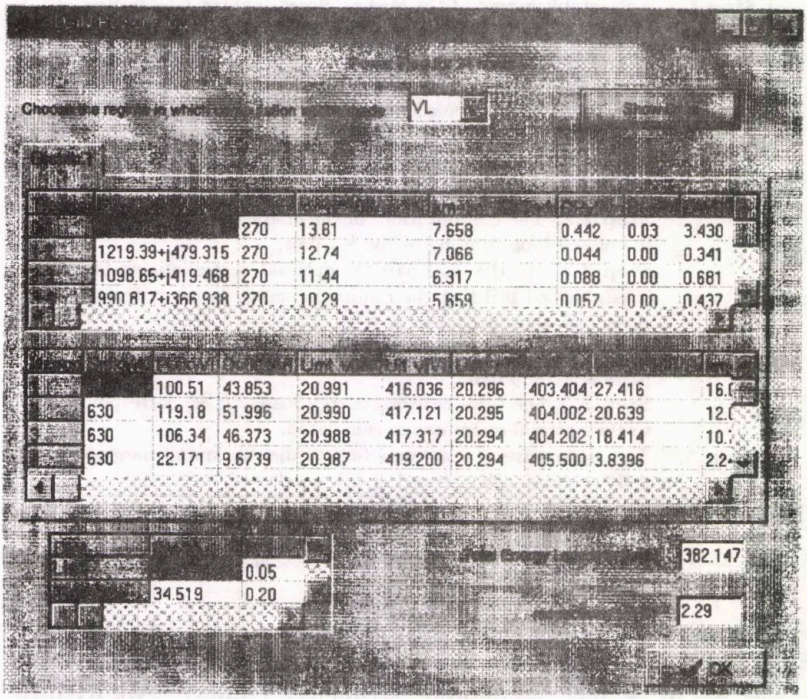

Fig. 2.– The results of power-flow analysis.

Choosing **Power Flow (Calcul de regim)** the analysis may be made for 1 h or for the whole day (24 h) corresponding to a certain characteristic regime and offers information concerning the peak load coefficients, the voltage levels on the low and medium voltage bars of the substation for peak and valley loads, integral indicators of the power quality analysis, the active power losses on peak load on each branches or for the whole network, the energy losses on each branches and for the whole network. In Fig. 2 it is presented the window illustrating this option.

For the optimal selection of sectionalizing points in an open-loop radial distribution network, the user has to choose from the **Run** menu the **Optimal Sectionalizing – Classical (Secţionare optimă – clasic)** or **Optimal Sectionalizing – Genetic Algorithms (Secţionare optimă – Algoritmi genetici)** submenu. For the classical option, there are sequentially analysed all the possible ways of looping the feeders on medium, respectively on low voltage, depending on the real existing conditions in the distribution network. For finding the sectionalizing points which certify minimum energy losses for the whole network the steps indicated in Fig. 3 must be covered.

Step 1.	The establishment of the feeders closed-looping possibilities set: $V = \{v_i\}$, $i = 1, 2, ...$; one possibility is the set of the pairs of feeders which may be looped: $v_i = \{b_{kj}\}$, $(k, j = 1, ..., ND;$ $k \neq j$, ND – the number of feeders from the analysed network).
Step 2.	Each possibility is considered v_i, $(i = 1, 2, ...)$, the following steps being covered:
	Step 2.1. A pair of feeders $b_{kj} \in v_i$ is choosen for which the closed-loop is made by activating the reserve branch.
	Step 2.2. The computation of the characteristic regimes for the closed-loop running of the b_{kj} pair.
	Step 2.3. For the b_{kj} pair the optimal sectionalizing branch is established utilizing the minimum energy losses criterion and these losses are memorized, ΔW_{kj}.
	Step 2.4. Step 2.1 is again actualized until all the $b_{kj} \in v_i$ pairs are computed.
	Step 2.5. The total network energy losses, ΔW, corresponding to the optimal open-loop is calculated.
Step 3.	The alternative v^* corresponding to the minimum energy losses $\Delta W^* = \min\{\Delta W_i\}$, $(i = 1, 2, ...)$, is selected.

Fig. 3.– Classical method steps for optimal selection of sectionalizing points.

For large distribution networks, with many possibilities of closed-looping, the sequential loading of the problem has negative implications on the computational time. The use of parallel computation techniques **Genetic Algorithms – GA (Algoritmi genetici – AG)** represents a viable alternative by replacing the serial search with the parallel one [6], [8], [9].

For a given network configuration and number of power supply points, the number of sectionalizing points, which certify the open-loop of the network and the power supply of all consumers, is a constant:

$$N_{\text{sec}} = NS + NC - 1,$$

where: N_{sec} is the number of sectionalizing points; NS – the number of the power supply sources; NC – the number of independent cycles from the network graph.

Using **GA**, the solution is represented by the meaning of a double chain of strings (chromosomes) of $2N_{\text{sec}}$ length, where first N_{sec} elements indicating the feeders on which sectionalizing is made and the last N_{sec} elements indicating the branch of each feeders on which the sectionalizing is made, in fact. The crossover of "parent" chromosomes must be done in two points corresponding to the feeder, respectively the branch where the sectionalizing is carried out. If the "offspring" chromosomes doesn't represent a viable solution, in the next generation will pass to the "parent" chromosomes [5], [7].

The software application package permits choosing of the following specific parameters of the genetic algorithms: the population dimension, the crossover rate, the mutation rate; these parameters influence the evolution of the energy losses associated to the dominant and optimal chromosomes. The dominant chromosome is that which is most frequently find in the actual generation and the optimal one is that to whom corresponds the minimum energy losses, being, in the same time, the solution of the optimal sectionalizing points of the distribution network.

At the end of the computation, both methods (**Classical** or **GA**) present the list with the optimal sectionalizing points of the network and the decrease of the energy losses in the new network configuration.

For an optimal compensation of the reactive loads, to minimize the losses and to increase the quality of the delivered energy, in the **Run** menu there are two more options: a classic one based on simulation techniques and one based on genetic algorithms and evolutionary strategies. Simulation techniques are methods of successive search, which eliminate one by one the capacitors until the global minimum of objective function is reached. The method has two steps: first set up the maximum possible number of capacitor banks in all buses of the network, taking into account the technical restrictions; the second is the iterative process of elimination of the banks until the global function (energy losses or up-date total cost) reaches a global minimum [4], [5].

The **GA** method is based on a combination between the principles of the genetics algorithms and the evolutionary strategies as is described in Fig. 4 [6].

Both methods provide the results of the optimal placement of the reactive sources (capacitor banks) and information concerning the evolution of iterative process (total capacitor banks number, the energy losses and up-date total cost) (Fig. 5).

Step 1. **GENERATION** $= 1$.

Step 2. *Solution evaluation*: m admissible chromosomes are randomly generated and the values of the fitness function of this generation are calculated $f_i = 1/\mathrm{UTC}_i$, $(i = \overline{1,m})$.

Step 3. *Selection* of "parent" chromosomes for crossover according to the "roulette wheel" method.

Step 4. *Crossover*: each pair of "parent" chromosomes are crossover under a certain probability given by the crossover rate and produce the offsprings.

Step 5. *Mutation*: the mutation modify at random one gene of the offsprings chromosomes with a probabilistic mutation rate.

Step 6. *Competition*: each individual in the combined population ($2m$ chromosomes – the old generation and the offsprings after crossover and mutation) participates at a competition with all others for surviving and to be transcribed to the next generation. All chromosomes are ordered in descending order of their corresponding fitness function. The first m chromosomes are transcribed together with their fitness function. They are the new generation.

Step 7. *Etlitism*: The best chromosome (the one with the best fitness function) replaces the worse one.

Step 8. **GENERATION** $=$ **GENERATION** $+ 1$.

Step 9. *Stop condition* (maximum number of iterations): if it is not fulfiled, steps 3...8 are covered again, else the (sub)optimal solution is the chromosome with the best fitness function in the last generation.

Fig. 4.– The algorithm based on genetic algorithms and evolutionary strategies.

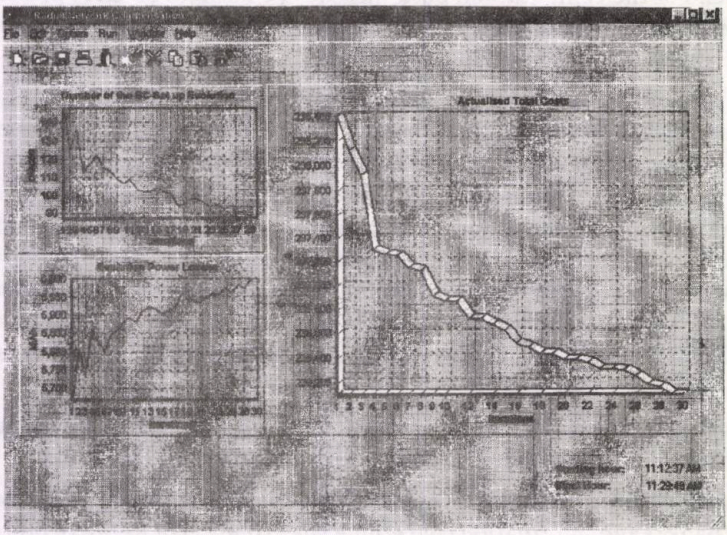

Fig. 5.– Results window after running an example.

If the user of the software wants to determine the optimal sizing of power transformers from the substation, he must choose the **Optimal Trafo (Trafo optim)** option from the **Run** menu. Depending on the real charges of the analysed transformer during a year, the software application chooses, from its database, the one that leads to minimum energy losses.

4. Conclusion

The proposed software allows a complex analysis of the distribution networks concerning the characteristic regimes during a year and possibilities of their optimization using classical methods and evolutionary computation based methods. The results may be useful in the operation and management process and in adopting decisions concerning the planning and development of the distribution networks.

The optimal solution concerning the placement of the capacitor banks in the distribution networks, using as objective function the minimum energy losses or the up-date total cost criteria, must be correlated with the placement of filters in varied nodes for decreasing the effects of the non-sinusoidal state.

Received, December 4, 2000

Technical University "Gh.Asachi", Jassy,
Department of Energetics
and
**Department of Electrotechnics*

REFERENCES

1. Codiasse A.M., Guillevic M., Giraud D., *Connaissance des charges moyenne tension en vue de leur prise en compte dans les études de planification.* R.G.E., *7-8*, 481-486 (1982).
2. Georgescu Gh., Gavrilaş M., Cârţină Gh.,*Aspects Concerning Power Distribution Networks Planning Using Artificial Intelligence.* 14th Internat. Conf. on Electricity Distribution, CIRED '97, Birmingham, 1997.
3. Poeată A., Georgescu Gh., Ţăranu V. *et al., Posibilităţi de utilizare a graficelor tip de sarcină ale consumatorilor în studiile de dezvoltare şi pentru exploatarea raţională a reţelelor electrice urbane.* Energetica, *2*, 60-64 (1985).
4. Georgescu Gh., Rădăşanu D., *Transportul şi distribuţia energiei electrice.* Vol.**I**, Ed. Spectrum, Iaşi, 2000.
5. Georgescu Gh., Gavrilaş M., Rădăşanu D., *Calculul şi reducerea pierderilor de putere şi energie în reţelele electrice.* Ed. Spectum, Iaşi, 1997.
6. Lee K.Y., Bai X., Park Y.M., *Optimization Method for Reactive Power Planning by Using a Modified Simple Genetic Algorithm.* IEEE Trans. on Power Systems, **10**, *4*, 1843-1850 (1995).
7. Gavrilaş M., Georgescu Gh., *Utilizarea algoritmilor genetici pentru determinarea schemei optime de funcţionare a reţelelor de distribuţie urbană.* Energetica, Seria B, *6*, 249-256 (1996).
8. Goldberg D.E., *Genetic Algorithms and Rule Learning in Dynamic System Control.* Proc. of the First Internat. Conf. on Genetic Algorithms and Their Appl., Pittsburgh, 1985, 8-15.
9. Grefenstette J.J., *Optimization of Control Parameters for Genetic Algorithms.* IEEE Trans. on Systems, Man and Cybernetics, **16**, *1*, 122-128 (1986).

PRODUSE SOFTWARE PENTRU ANALIZA ŞI OPTIMIZAREA REGIMURILOR DE FUNCŢIONARE ALE REŢELELOR DE DISTRIBUŢIE

(Rezumat)

Se propune un produs software pentru analiza complexă a regimurilor de funcţionare ale reţelelor de distribuţie, pe parcursul unui an şi se indică posibilităţile de optimizare ale acestora. Problemele analizate sunt studiate atât prin metode clasice cât şi prin metode bazate pe calculul evolutiv. Sarcinile nodale sunt modelate în cadrul programului cu ajutorul unei baze de date care conţine grafice tip de sarcină pe categorii de consumatori, pe fiecare lună şi zi standard, a structurii de consum din noduri şi a unui număr redus de măsurători efectuate direct în reţea.

Rezultatele furnizate pot fi utilizate de personalul de exploatare şi de conducere în vederea adoptării deciziilor privind planificarea şi dezvoltarea reţelelor de distribuţie.

BULETINUL INSTITUTULUI POLITEHNIC DIN IAŞI
Tomul XLVII (LI), Fasc. 3–4, 2001
ELECTROTEHNICĂ. ENERGETICĂ. ELECTRONICĂ

D.C. 621.181.646

HIGHER EFFICIENCY FOR MODERN BOILERS BY IMPROVING THE BURNED GASES EVACUATING SYSTEMS PERFORMANCES

BY
C. ASAFTEI and *DORIN GROZA

There are presented some sonsiderations regarding the stage and the performances of burned gases evacuating systems, performances correlated with the progresses made in modern boilers designing and manufacturing. From this point of view an important aspect represents the improving of working efficiency and fiability. There are mentioned the operating conditions and dimensioning criteria.

1. Introduction

The optimal operating of boilers depends of many factors, one of these being the burned gases evacuating systems.

A performant system must to assure the fiable operating and the improved efficiency of the boiler. The design and manufacturing of burned gases evacuating systems has always considered these two features as an important objective. The modern burned gas evacuation systems, as result of researching efforts, have as principal features the operating fiability and the high stability in difficult environmental conditions (moisture, chemicals, fire, earthquakes, etc.).

These features have generated the development of improved boilers like classic ones (at low temperatures) and the most advanced type, namely power calorific boilers [1].

In what follows there are presented some considerations referring to the operating and dimensioning conditions; in the same time are mentioned the technical performances regarding the level of the burned gas evacuation systems.

2. The Actual Level and the Performances in the Manufacturing and Operating of the Burned Gas Evacuation Systems

The main request in the operating of burned gas evacuation systems is to assure a better flue, for facilitate the burned gas evacuation from the burned area and an optimum of the burning and heat exchange processes. The safe evacuation of the burned gases is made through gas flue effect; the necessary gas flue may be natural or forced [2].

The natural flue result as a consequence of the difference between the environmental air and the burned gases densities, difference generated by the higher temperature of burned gases, comparatively with the environmental air.

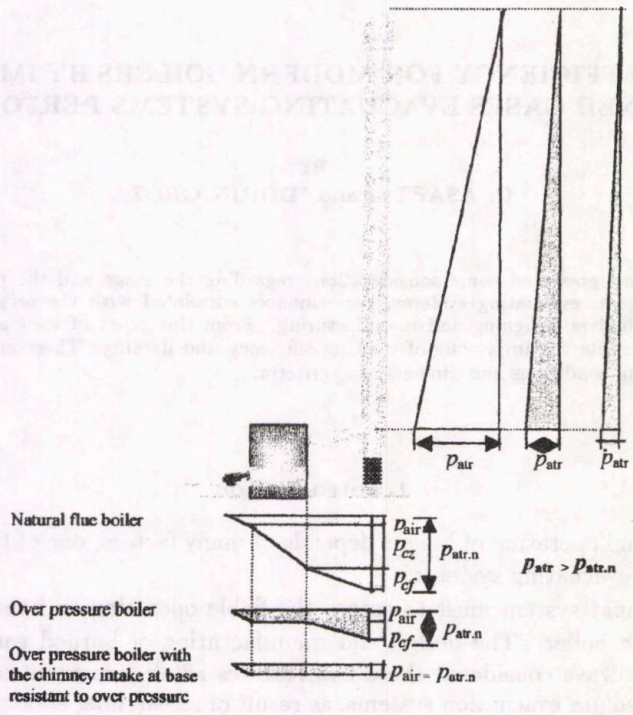

Fig. 1.– Pressure ratio's inside the boiler and the chimney, for different boilers types.

As a result, the condition to obtain the natural flue, for an ideal system, is:

$$p_{at} > 0, \quad T_{ga} > T_a, \tag{1}$$

with

$$p_{at} = (\rho_a - \rho_{ga})gH, \tag{2}$$

where: p_{at} represents the natural flue fro ideal system, [bar]; ρ_a, ρ_{ga} – the air and burned gas density, [kg/m^3]; H – chimney stack height, [m]; T_{ga}, T_a – the burned gases and air temperature, [K], respectively. For the real operating installations it is necessary to take into account the losses in charge generated on the chimney between the air aspiration and the burned gases evacuating; as consequence the inequality:

$$p_{atr} > p_{air} + p_{cz} + p_{cf} = p_{atr.n} \tag{3}$$

must be satisfied, where: p_{atr} represents the flue draft; $p_{atr.n}$ – the natural flue, minimum necessary for real system; p_{air} – the losses of charge, on air flue; p_{cz} – the losses of charge in boiler area (burner, burned gases way); p_{cf} – the losses of charge, on the chimney's base.

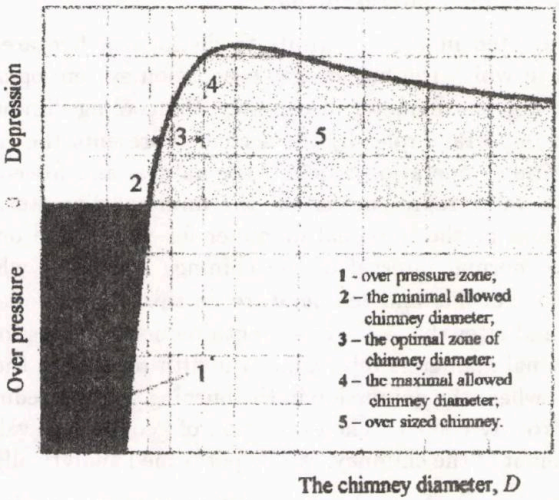

Fig. 2.– The dependence between the pressure status and the diameter of the chimney.

The chimney stack configuration and geometrical features, the surfaces quality, the velocity and density of burned gases, influence the losses of charge.

An efficient flue involves the maximal reduction of the losses of charge and a greater height of the chimney, respectively a bigger difference between air and burned gases densities, situation that is fulfilled by the condition:

$$T_{ga} > T_a. \tag{4}$$

It is seen that a maximal reduction of losses implies a minimal difference between the two temperature values.

For the natural flue it is possible to find two situations: a) the environmental air is *aspirated* and introduced in the furnace by the flue effect, the burners operating with "*self aspired*" air; b) the air is *insufflated* in the fire box chamber by a ventilator, to compensate the losses in charge on the air way.

When it is not possible to build a chimney stack with natural flue, it is used the forced circulation in three variants: a) the air is *insufflated* in the fire box chamber by a ventilator which generates a small over-pressure that allows the burned gases to be evacuated through the chimney stack; b) the air is *aspired* using an exhauster blower which generates, on one hand, the necessary depression in the fire box for air aspiration and the over-pressure in the chimney to evacuate the burned gases, on the other hand; c) the air is *introduced* in the fire box by an air exhauster and the burned gases are *evacuated* by a gas exhauster.

In Fig. 1 it is represented the fluctuation of pressure variation for a modern boiler in some specific situations.

To assure a sufficient ascension motion in the burned gases link area, it is necessary to take into consideration the chimney diameter.

In Fig. 2 is represented the dependence of pressure level in the evacuating link area reported to the chimney interior diameter.

The curve represented in Fig. 2 permits to distinguish five areas: a) the first represents the area in which the burned gas evacuation system operates with overpressure, when, for a given diameter of chimney, the cooling diminution of burned gases does play an important role; b) the second represents the interference area between the two chimney operation modes – the natural and forced flue operation; in other words, this value represents either the minimal diameter, which permits natural flue operation, or the maximal diameter for forced flue operation; c) the third represents the normal interval of the chimney diameters when are fulfilled the optimal conditions of flue and temperature; in this area the diameter reducing implies first a slow and after that a faster strength reducing depression; d) the fourth represents the maximal diameters interval; e) the fifth represents the interval of the very high diameters where the depression in the burning space is reduced because the burned gases are strongly cooled. The evaluation of geometrical values and mainly the diameter and height of the chimney, can be performed analytically or graphically.

In the latest situation, the burned gas evacuation systems manufacturers [3] offer, to users, the graphics that allows an operative evaluation of the diameter and height of the chimney, in correlation with: heating charge, combustion air type, number of boilers linked to the chimney, burner type, necessary flue. As example is considered, in Fig. 3, a boiler linked to the chimney type QUADRO.

The optimal operation condition of the burned gas evacuation systems is strongly correlated with the temperature condition (4), which must be fulfilled on all the chimney way.

In Fig. 4 it is represented the evolution of burned gases temperature and interior walls on all chimney space.

The installation operation is more efficient if the burned gases temperature is higher and the environmental air temperature is lower.

In this situation it is necessary that the temperature losses, on the chimney altitude, to be as reduced as possible, being dependent of: thermal conductivity of dumreg thermal insulation, chimney altitude, chimney internal surface, burned gases flow velocity, etc.

From this point of view, it results that the fire brick chimney are more efficient that the metal chimneys.

It is necessary to consider that T_{ga} depends on: the boiler and burner type, the water temperature in the heating system, especially the return water temperature.

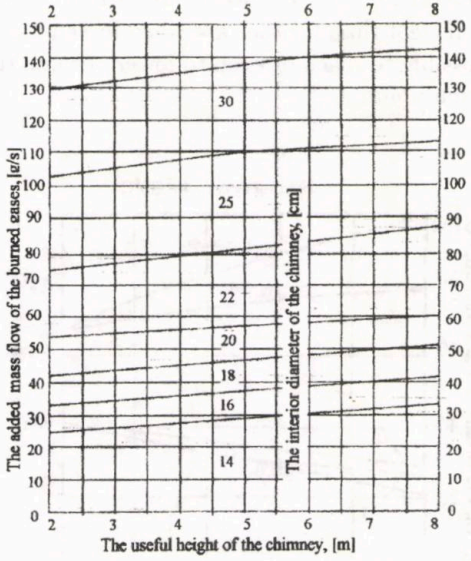

Fig. 3.– The dimensioning diagram of a chimney, type QUADRO, linked to boilers with different powers.

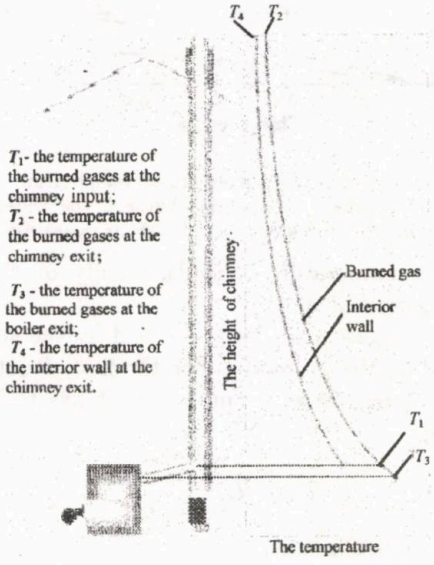

Fig. 4.– The variation of the burned gases temperature and the interior wall temperature, inside the chimney.

From Fig. 5 it results that for the low temperature heating system T_{ga} is smaller than for the high temperature one, fact which implies that, on one hand, for the natural flue to be less efficient than for the case when forced flue is preferred and, on the other hand, it is possible to reach or even to lower become that the temperature level of acid condensation point.

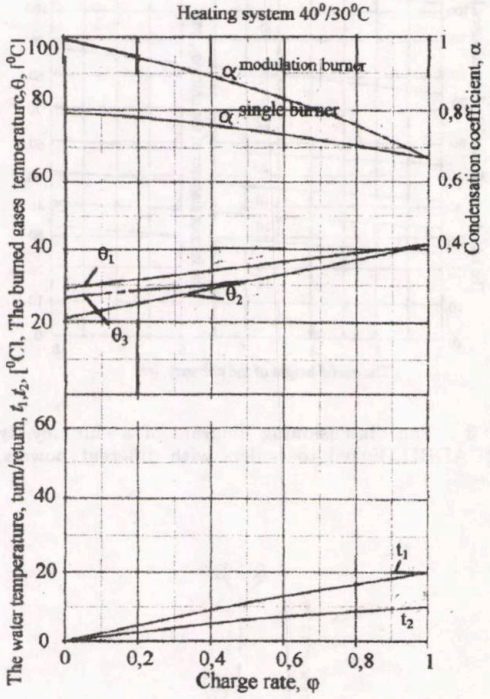

Fig. 5.– The relation between the burned gases temperature (θ_1 – single burner, θ_2 – modulation burner, θ_3 – double burner), the water temperature of the heating system, the charge rate and the condensation coefficient.

The condensation point temperature depends, mainly, on the fuel type and air flow coefficient, as results from Fig. 6.

The evacuation of burned gases can be performed by the sensible, respectively insensible chimneys regarding the humidity. For the first situation (sensible chimney), the burned gases temperature at chimney output has to be greater than the condensation temperature:

$$T_{ga} \geq T_{\text{cond}}, \tag{5}$$

and for the humidity insensible chimney:

$$T_{ga} \geq 213 \text{ K}, \quad T_4 \geq 273 \text{ K}. \tag{6}$$

From this point of view, the humidity insensible chimney, manufactured from stainless steel, synthetic materials, refractory brick, etc., allows the greatest impeovement of the efficiency, as it results from the analysis of its expression:

$$\eta = 1 - \frac{q}{100} + \alpha \Delta H, \tag{7}$$

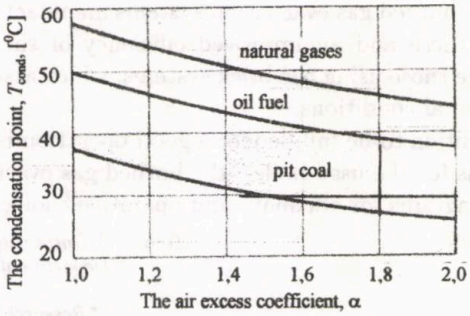

Fig. 6.– The dependence between the condensation point temperature, the type of fuel and the air excess coefficient.

where: q represents the heat losses, from the burned gases, evacuated by the chimney in the atmospheric environment and respectively by radiation, [%]; ΔH – the relative water heat, possible to recovered from condensation; α – the condensation coefficient.

So, if using the humidity insensible chimney is possible the recovery of almost all of the generated heat. This type of chimney is recommended, particularly, in case when low temperatures and calorific capacity boilers are utilized. While the low temperature boiler doesn't allow the recovery of the condensation latent heat, the power calorific boilers can recover almost all of the sensible heat, and also, a part of the condensation latent heat, who depends on the condensation coefficient, α (Fig. 5) [1].

The α coefficient value is determined by the ratio of condensation water quantity produced by the boiler and the theoretical condensation water quantity that could be produced. The efficiency of *the calorific capacity boilers* is better if the recovered condensation heat quantity is greater; this implies a greater value for α.

For the humidity sensible chimneys, the high temperature of the burned gases generates more heat lost, and, as a consequence, the efficiency of the boiler is smaller.

A chimney type manufactured in fire brick by Schiedel–Kaminwerke is represented in Fig. 7 [3].

The brick duct is insulated, in exterior, to reduce the temperature losses, facilitating the optimal flue. The air circulation in the ring conduit space is favourable to maintain dry the insulation.

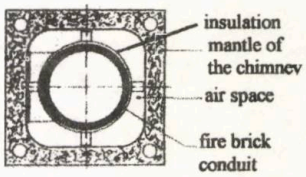

Fig. 7.– Section throught the chimney, type Schiedel.

The humidity insensible chimney allows the most advanced recovering of heat from burned gases, facilitating the preliminary heating of the combustion air; so, the combustion air is aspirated through the ring conduit space and it is heated in contact with the fire brick duct wall, circulated by burned gases.

3. Conclusions

The progress in the burned gas evacuation systems manufacturing have generated a greater fiability of these and an improved efficiency of the boilers. The most performant systems are those using the brick systems, which assure a good operation in different environmental conditions.

An important condition to be fulfilled for a good operation is the colerate burned gas evacuation systems for the used boiler; the burned gas evacuation systems manufacturers offer the diagrams for adequate and operative choice.

Received, February 28, 2001

Technical University "Gh.Asachi", Jassy,
Department of Energetics
and
**Research Institute for*
Electrotechnics, Jassy

REFERENCES

1. A s a f t e i C., G r o z a D., *Some Aspects Regarding the Solutions Applicated for the Efficiency Improving of Small Power Heatings Units.* Bul. Inst. polit., Iaşi, **XLV (IL)**, 5B, s. Electrot., Energ., Electron., 355-359 (1999).
2. P ă n o i u N., *Cazane de abur.* Ed. Did. şi Pedag., Bucureşti, 1982.
3. * * * *Manualul proiectantului. Coşuri de fum tip Schiedel.* Ed. BreStar, Braşov, 1999.

CREŞTEREA EFICIENŢEI CAZANELOR MODERNE DE ÎNCĂLZIRE PRIN ÎMBUNĂTĂŢIREA PERFORMANŢELOR SISTEMELOR DE EVACUARE A GAZELOR DE ARDERE

(Rezumat)

Evoluţiile spectaculoase, din ultimii ani, în domeniul cazanelor moderne de încălzire, au fost posibile şi datorită perfecţionării sistemelor de evacuare a gazelor de ardere şi, respectiv, de introducere a aerului necesar combustiei. În acest sens se abordează câteva aspecte teoretice şi practice vizând construcţia şi dimensionarea sistemelor de evacuare a gazelor de ardere, precum şi interdependenţa care există în raport cu cazanul de încălzire propriu-zis.

BULETINUL INSTITUTULUI POLITEHNIC DIN IAŞI
Tomul XLVII (LI), Fasc. 3–4, 2001
ELECTROTEHNICĂ. ENERGETICĂ. ELECTRONICĂ

RECENZII BOOK REVIEWS

WESTON D.A., *Electromagnetic Compatibility. Principles and Applications.* Sec. Ed., Marcel Dekker, Inc., New York, 2001, 864 pp., $ 195.00, ISBN 0-8247-8889-3.

This second, revised and updatet edition of the book contains approximately 65% more information than the first edition. This includes a review of computer modeling programs, a new chapter on PCB layout, and additional commercial and military EMI test methods. New data on cable radiation and coupling to cables is included, extending out to 12 GHz, and on EMI enclosure shielding.

All electronic and electrical equipment is a potential source of electromagnetic interference (EMI). Similarly, such equipment will not function as designed at some level electromagnetic ambient. The problems associated with EMI can range from simple annoyance (*e.g.* static on telecommunications equipment or increased bit error rates on digital equipment) to catastrophe (*e.g.* inadvertent detonation of explosive devices).

Electromagnetic compatibility (EMC) can be achieved by evaluating the electromagnetic environment (often characterized by standards or requirements) to which equipment/systems is exposed and then designing and building equipment/systems to function correctly in the operational environment without itself creating EMI.

Containing updated data on EMI diagnostic verification measurements, as well as over 900 drawings, photographs, tables, and equations – 500 more than the previous edition – the Second Edition of *Electromagnetic Compatibility*:

a) explores the *latest* verification/certification testing procedures;
b) discusses inaccuracies in current EMI test and EMC prediction methods;
c) furnishes a new chapter on "good" printed circuit board layout techniques;
d) describes essential approaches to computational electromagnetic modeling.

Effectively demonstrating innovative techniques for on-the-job use, troubleshooting, and time conservation, the Second Edition of *Electromagnetic Compatibility* is an authoritative reference for electrical and electronics, circuit/system design, and radio and telecommunications engineers, technicians, and technologists, and an ideal text for upper-level undergraduate students in these disciplines.

* * *

David A. W e s t o n is an EMC consultant and Certified National Association of Radio and Telecommunications Engineers (NARTE) EMC engineer and EMC Consulting Inc., Merrickville, Ontario, Canada. A member of the Institute of Electrical and Electronics Engineers and NARTE, Mr. Weston has worked in electronic design for 30 years, specializing in the control, prediction, problem solving, and design aspects of EMC for the last 20 years. Mr. Weston studied at Croydon Technical College from 1960 to 1965, and in 1965 received the Radio and Television certificate from the City and Guilds of the London Institute, both in England.

* * *

C o n t e n t s: Introduction to EMI and the Electromagnetic Environment. Introduction to **E** and **H**, Near and Far Fields, Radiators, Receptors, and Antennas; Typical Sources and Characteristics of Radiated and Conducted Emissions; Crosstalk and Electromagnetic Coupling between PCB Tracks, Wires and Cables; Components, Emission Reduction Techniques, and Noise Immunity; Electromagnetic Shielding; Cable Shielding, Coupling from **E** and **H** Fields, and Cable Emissions;

Grounding and Bonding; EMI Measurements, Control Requirements, and Test Methods; Systems EMC and Antenna Coupling; Printed Circuit Boards; EMI and EMC Control, Case Studies, EMC Prediction Techniques, and Computational Electromagnetic Modeling; A p p e n d i x 1: Characteristic Impedance of Conductors, Wires, and Cables; A p p e n d i x 2: Units and Conversions Factors; A p p e n d i x 3: Electric Field Strength to Magnetic Field to Power Density Conversions; A p p e n d i x 4: Commonly used Related Formulae; A p p e n d i x 5: Data on Bare Solid Copper Wire (Dimensions, Weight and Resistance).

WILLIS H.L., WELCH G.V., *Aging Power Delivery Infrastructure.* Marcel Dekker, Inc., New York, 2000, 568 pp., $ 165.00, ISBN 0-8247-0539-4.

Illustrating state-of-the-art diagnostic, assesment, planning, design, operational, and managerial methods, *Aging Power Delivery Infrastructures* demonstrates novel approaches to utilizing resources in an aging electric power delivery infrastructure – maximizing system effectiveness and maintaining competitive financial performance while reinforcing good customer service.

Provides new and internationally proven applications for reliability and cost management.

Highlighting monetary and operational requirements in an open retail access environment, *Aging Power Delivery Infrastructures* identifies:

a) factors contributing to aging infrastructure problems;
b) types of delivery system design;
c) "fixes" for outdated system structures;
d) limitations of $N - 1$ methods;
e) flexibility and effectiveness in feeder level planning;
f) Monte Carlo methods to analyse economic risks;
g) diagnosis and evaluation of equipment and insulating oil
h) and more!

Offering practical strategies in both engineering and business management, *Aging Power Delivery Infrastructures* is a definitive reference suitable for power, electrical and electronics, industrial, manufacturing, and mechanical engineers; energy efficiency analysts; and upper-level undergraduate and graduate students in these disciplines.

C o n t e n t s: Aging Power Delivery Infrastructures; Power Delivery Systems; Customer Demand for Power and Reliability of Service; Power System Reliability of Service; Cost and Economic Evaluation; Equipment Inspection, Testing and Diagnostics; Aging Equipment and Its Impacts; Obsolete System Structures; Traditional Reliability Engineering Tools and Their Limitations; Primary Distribution Planning and Engineering Interactions; Equipment Condition Assessment; Prioritization Methods for O&M; Planning Methods for Aging T&D Infrastructures; Reliability Can Be Planned and Engineered; Strategy, Management, and Decision Making; Guidelines and Recommendations.

KASIKCI I., *Kurtzschlußstromberechnung in elektrischen Anlagen.* Expert Verlag GmbH, Renningen, Germany, 2000, 204 S, DM 98, ISBN 3-8169-1835-2.

Jeder Elektroplaner ist heute verpflichtet, die Berechnung des ein- bzw. Dreipoligen Kurzschlußstroms vor und nach der Projektbearbeitung durchzuführen, Schutzmaßnahmen und die Kurzschlußfestigkeit der elektrischen Anlagen zur Auswahl der Geräte zu überprüfen.

Das Buch befaßt sich mit der Berechnung von Kurzschlüssen in elektrischen Anlagen nach neuesten Normen und Vorschriften (DIN VDE 0102-IEC 60 909), ferner mit der Berechnung der einzelnen Kurzschlußströme und ihrer Bedeutung für die Planung und Projektierung elektrischer Anlagen.

Die stufenweise Darstellung der Vorschrift ist beibehalten und möglichst einfach und verständlich zusammengefaßt, damit der Leser seine Arbeit ohne große Mühe erledigen kann.

Das Buch gibt zahlreiche praxisbezogene Beispiele und Projektierungshinweise. Eine CD-ROM zur Berechnung elektrischer Anlagen mit dem Programm KUBS plus der Firma Siemens ist dem Buch beigelegt. Das Programm unterstützt die Fachleute bei der Kurzschlußstromberechnung, der Auswahl der Schutzeinrichtungen und der Leiterdimensionierung. Dabei werden die Selektivität, der Back-up- Schutz und der Spannungsfall berücksichtigt und angezeigt.

I n h a l t:

Begriffe und Definitionen – Allgemeines zu DIN VDE 0102 – Bedeutung von DIN VDE 0102 – Versorgungsnetze – Netzformen bei der Kurzschlußberechnung – Systeme bei 1kV – Sternpunktbehandlung in Drehstromnetzen – Impedanzen von Drehstrom – Betriebsmitteln – Impedanzkorrekturen – Methode der symmetrischen Komponenten – Berechnung der Kurzschlußströme – Vorbereitung der Berechnung – Berücksichtigung von Motoren in DS-Netzen – Mechanische und thermische Kurzschlußstromfestigkeit – Berechnungsgrößen für die Kurzschlußstromfestigkeit – Überstrom-Schutzeinrichtungen – Software – Programm KUBS plus – Beispiele aus der Praxis.

D i e I n t e r e s s e n t e n:

a) Planer, Errichter und Betreiber elektrischer Anlagen;

b) Meister, Techniker und Ingenieure;

c) Planungsbüros in den Bereichen der Energieanlagen und der Installationstechnik;

d) Studenten und Berufsschulen.

DATA A.K., ANANTHESWARAN R.C., *Handbook of Microwave Technology for Food Applications*. Marcel Dekker Inc., New York, 2001, 536 pp., $ 185.00, ISBN 0-8247-0490-8.

This interdisciplinary volume integrates principles of electromagnetics, dielectric properties, heat and moisture transfer, microwave system design, packaging, product development, and food safety, chemistry, and microbiology to provide a comprehensive overview of microwave processing in *a single accessible source*.

Featuring over 1 200 references, equations, illustrations, photographs, and tables, the *Handbook of Microwave Technology for Food Applications*: a) outlines the component hardware of a microwave system as well as instrumentation and measurement techniques;

b) describes temperature and moisture changes and their effect on microwave absorbtion;

c) clarifies guiding principles for heating complex food systems in specially developed packages;

d) details cavity heating and flavor, microbial, and enzymatic changes that occur during microwave heating;

e) presents strategies for product development of microwaveable foods;

f) discusses industrial microwave processes and effective home use of microwave ovens.

Drawn from the profesional experience of more than 15 experts industry, academia, and government, the *Handbook of Microwave Technology for Food Applications* is a benchmark reference for food scientists, technologists, and engineers; agricultural, biological, and chemical engineers; product and process developers; quality control personnel; biochemists; microbiologists; nutritionists; and upper-level undergraduate and graduate students in these disciplines.

C o n t e n t s: *Fundamental Physical Aspects of Microwave Absorbtion and Heating*: Electromagnetics: Fundamental Aspects and Numerical Modeling; Electromagnetics of Microwave Heating: Magnitude and Uniformity of Energy Absorption in an Oven; Dielectric Properties of Food Materials and Electric Field Interactions; Fundamentals of Heat and Moisture Transport for Microwaveable Food Product and Process Development; *Chemical and Biological Changes due to Heating*: Generation and Release of Food Aromas Under Microwave Heating; Bacterial Destruction and Enzyme Inactivation During Microwave Heating; *Processing Systems and Instrumentation*: Consumer, Commercial, and Industrial Microwave Ovens and Heating Systems; Measurement and Instrumentation; *Processes at Industry and Home*: Microwave Processes for the Food Industry; Basic Principles for Using a Home Microwave Oven; *Product and Process Development*: Ingredient Interactions and Product Development for Microwave Heating; Packaging Techniques for Microwaveable Foods; *Safety*: Safety in Microwave Processing.

KIEHNE H.-A., *Gerätebatterien*. Expert Verlag GmbH, Renningen, 2001, 164 S., DM 69, EURO 35.28, ISBN 3-8169-1470-5.

Dieser Themenband gibt einen umfassenden Überblick über den aktuellen technischen Stand von Primärbatterien und wartungsfreien Sekundärbatterien. Neue Anforderungsprofile verlangen eine besondere Anpassung vorhandener Systeme oder gar die Einführung bisher marktüblicher Systeme, wie z.B. Lithium-Batterien.

Batterieelektrische Energie ist sicher und umweltfreundlich. Es gibt kaum einen technischen Bereich, in dem man ohne Grundwissen und Verständnis über die Einsatzmöglichkeiten auskommen kann. Der Leser erhält Hinweise für die zweckmäßige und wirtschftliche Anwendung.

Die Interessenten: Ingenieure, Physiker, Techniker aus den Entwicklungsbereichen der Elektronik, Uhren- und Geräteindustrie sowie der Nachrichtentechnik.

WEINFURTNER W.W., *Licht schreibt Beschriften mit dem Laser in der Industrie.* Expert Verlag GmbH, Renningen, 2000, 64 S., DM 29, EURO 14.83, ISBN 3-8169-1758-5.

Der Laser ist in vielen Bereichen der Industrie zum „Beschriftungswerzeug Nummer 1" geworden. Das Buch zeigt die sinnvollen Einsatzgebiete des Beschriftungslasers, gibt eine Grundlage für die Kostenberechnung und hilft, das Prinzip der Laserbeschriftung anhand detaillierter Beschreibungen der eingesetzten Bauteile, der Softwaremöglichkeiten und der einstellbaren Prozeßparameter besser zu verstehen.

Anhand vieler Applikationsphotos werden die einzelnen Beweggründe aufgezeit, die zur Anschaffung eines Laserbeschrifters für die jeweilige Application geführt haben. Eine Checkliste und eine Liste von Ansprechtpartnern runden das Bild ab.

Inhalt: Einführung – Entstehung und Eigenschaft von Laserlicht-Laserschutzklassen – Qualifikation des Lasertyps – Excimer Laser – CO_2-Laser – Nd:YAG Laser – Betriebsarten – Prinzip des Laserbeschrifters – Verschiedene Beschriftungsmethoden – Wann setze ich den Laser ein? – Möglichkeiten der Markiersoftware – Möglichkeiten der Graphikgestaltung – Graphikformate – Vorgang beim Erstellen eines Logos – Geeignete Materialien – Realistische Beschriftungsgeschwindigkeiten – Beschaffung eines Lasersystems – Beschriftung mittels Gradienten-index – Glasfaser – Strahlführungssysteme – Ermittlung der Betriebskosten – Bereitstellung des Kunden – Beispiele aus der Industrie – Andere Anwendungsgebiete – Kurtz und bündig-Kontakte – Checkliste – Quelenverzeichnis und Bildernachweis.

Die Interessenten: Führungskräfte, Organisatoren, Mitarbeiter im Einkauf, der Produktion und Arbeitsvorbereitung, die mit der Beschriftung oder Kennzeichnung von Teilen in der industriellen Fertigung befaßt sind.

BUDAPESTI MŰSZAKI ÉS GAZDASÁGTUDOMÁNYI EGYETEM Műszaki Információs Központ és Könyvtár Országos
2001

BUDAPESTI MŰSZAKI ÉS GAZDASÁGTUDOMÁNYI EGYETEM
Műszaki Információs Központ és Könyvtár
2001

Data aparitiei: noiembrie 2003
Comanda nr.170, Tiraj 175
Coli de tipar: 10,75

UNIVERSITATEA TEHNICA "GH. ASACHI" IASI
TIPOGRAFIA

Str. Lascăr Catargi nr.38
Tel./Fax: 0232/21 59 49

ISSN 0258 - 9109